COLLEGE OF EXTENDED STUDIES
PROFESSIONAL DEVELOPMENT
SAN DIEGO STATE UNIVERSITY
SAN DIEGO CA 92182

(619) 265-6190

Lecture Notes for

Applied Sedimentation and River Engineering

January 17 - 20, 1984

by

Joseph C. Hill

Leonard J. Lane

V. Miguel Ponce

Vito A. Vanoni

Howard H. Chang, Coordinator

THE CALIFORNIA STATE UNIVERSITY

TABLE OF CONTENTS

I. Joseph C. Hill

An Application of River Engineering-Flood Plain Management

II. Leonard J. Lane

Introduction

Watershed Process

Development of Models

Example Applications

Summary

Future Directions in Research & Technology

Acknowledgements

References

III. V. Miguel Ponce

Kinematic, Dynamic and Inertial Waves

Overview of Flood Routing Methods

Stream Channel Routing

The Muskingum-Cunge Method

Properties of Numerical Solutions

Choice of Models in Engineering Practice

Digital Simulation of Hydrologic Systems

IV. Vito A. Vanoni

River Sedimentation

Velocity-Depth Relations for Alluvial Streams

Stability of Granular Sediments

V. Howard H. Chang

Overview of Design Methods for Alluvial Streams

Stable Alluvial Canal Design

River Morphology and Thresholds

A Mathematical Model for Erodible Channels

Modeling of River Channel Changes Using Energy Approach

Input/Output Descriptions for Fluvial Programs

AN APPLICATION OF RIVER ENGINEERING - FLOOD PLAIN MANAGEMENT

by

Joseph C. Hill

OUTLINE

I. Examples and Problems

A. San Diego River - Erosion Undermined Structure
B. San Dieguito River - Bank Erosion
C. San Luis Rey River - Sedimentation at Highway Crossing
D. San Luis Rey River - Sedimentation and Erosion at Bends
E. San Diego River - Erosion at Bridge Piers
F. San Vicente Creek - Erosion, Sedimentation

II. Flood Plain Management - Overview

A. Flood Plain Mapping Program
B. Mapping Procedures
   Survey Basis
   Survey Contractor
   Hydraulic Analysis
   Erosion Analysis
   Floodway Analysis
   Administration
C. Federal Programs
   National Flood Insurance Program
   Insurance Rates - Requirements for Local Government
D. American Society of Civil Engineers Award for San Diego

III. Flood Plain Computations

A. Topography & Cross Sections
B. Flow Characteristics, Typical Cross Section
C. Typical Values, Manning N & Eddy Loss Coefficients
D. Water Surface Profile Computations
E. Pressure Flow, Bridge or Culvert
F. Flow Over Roads
G. Alluvial-River Models, National Academy of Sciences Report

I. EXAMPLES AND PROBLEMS

Examples of flood plain maps and a cross-section showing typical development allowed outside the floodway are provided in Appendix A. The primary use of these flood plain studies, done as part of the National Flood Insurance Program, is to regulate land development. Once a flood plain study is put into use by a local government, houses and other structures can be constructed outside the floodway if they are elevated above the level of the floodway. The following examples illustrate the need for a comprehensive erosion and sedimentation analysis. Failure to adequately evaluate these factors can result in loss of life and structures.

A. San Diego River. The structure and road in Figure A were determined to be outside the 100-year flood plain and floodway by a fixed boundary flood plain study (HEC-2). A 10-year flood eroded the bank of the river, causing the road to be washed out and a corner of the structure to collapse.

Figure A

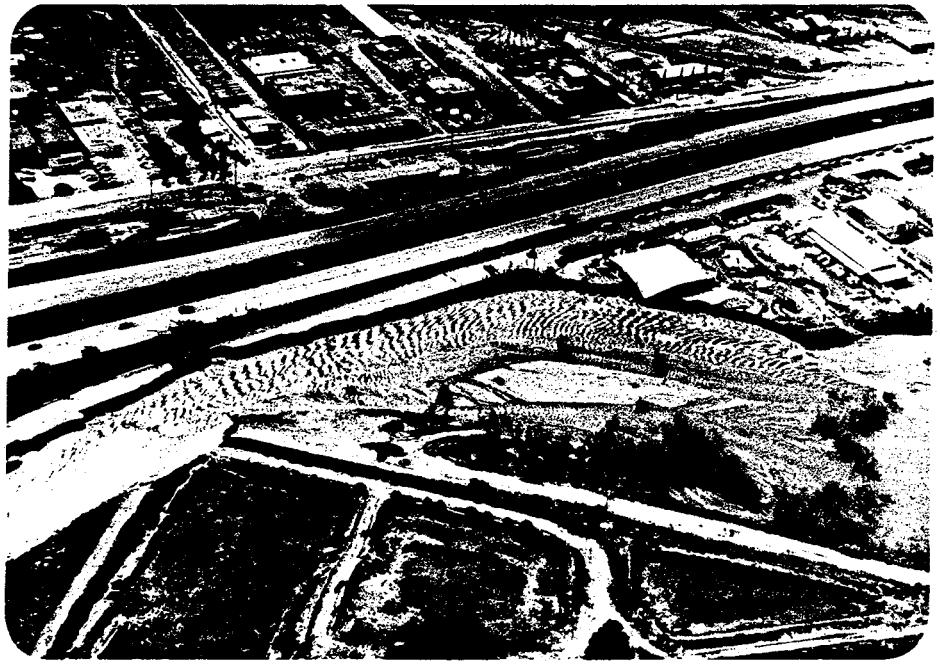

B. San Dieguito River. A fixed boundary study showed the floodway at the outside of a bend. Houses and other structures could be built outside the floodway boundary if raised above the floodway elevation. Floods eroded 200 feet beyond the established floodway line.

C. San Luis Rey River. Figure B shows a picture of a culvert crossing the San Luis Rey River. The culvert design was based on a HEC-2 flood plain study. Floods of 1978 and 1980 caused more than six feet of deposition in the river bed. Not only was the culvert completely covered, making it unusable for many months, but the 100-year flood plain width and elevation would be much greater than determined with the fixed boundary analysis.

D. San Luis Rey River. Bank erosion and sedimentation at bends is shown in Figure C. ⟶

FIGURE B

SAN LUIS REY RIVER AT OLIVE HILL ROAD

(Sedimentation)

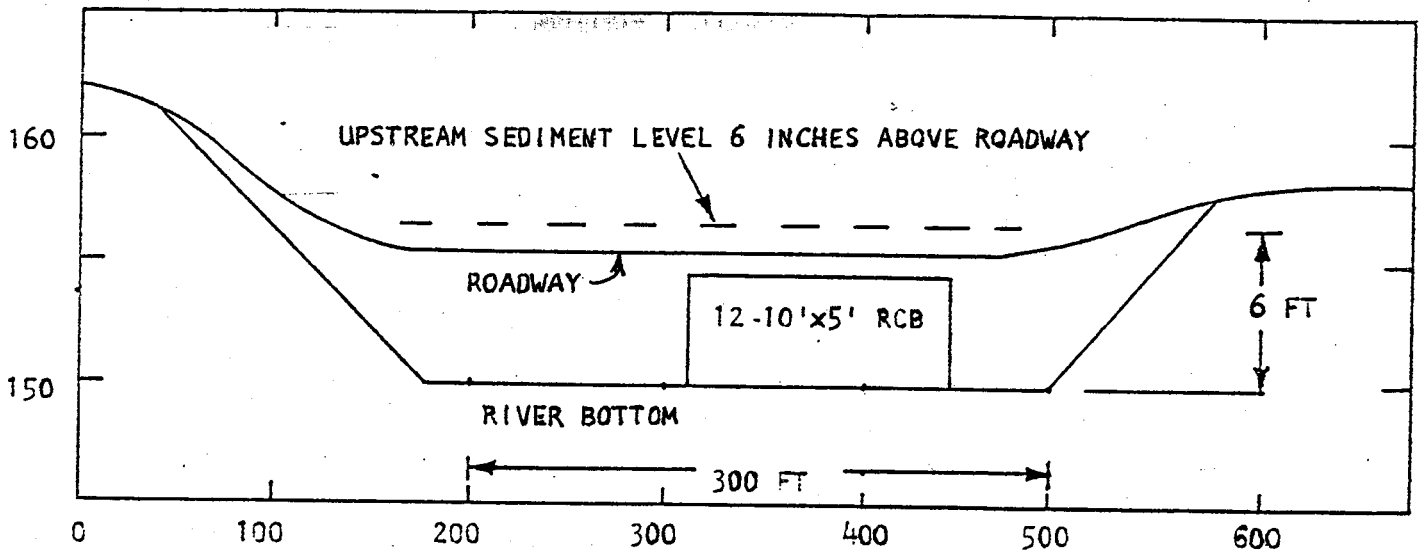

CROSS SECTION

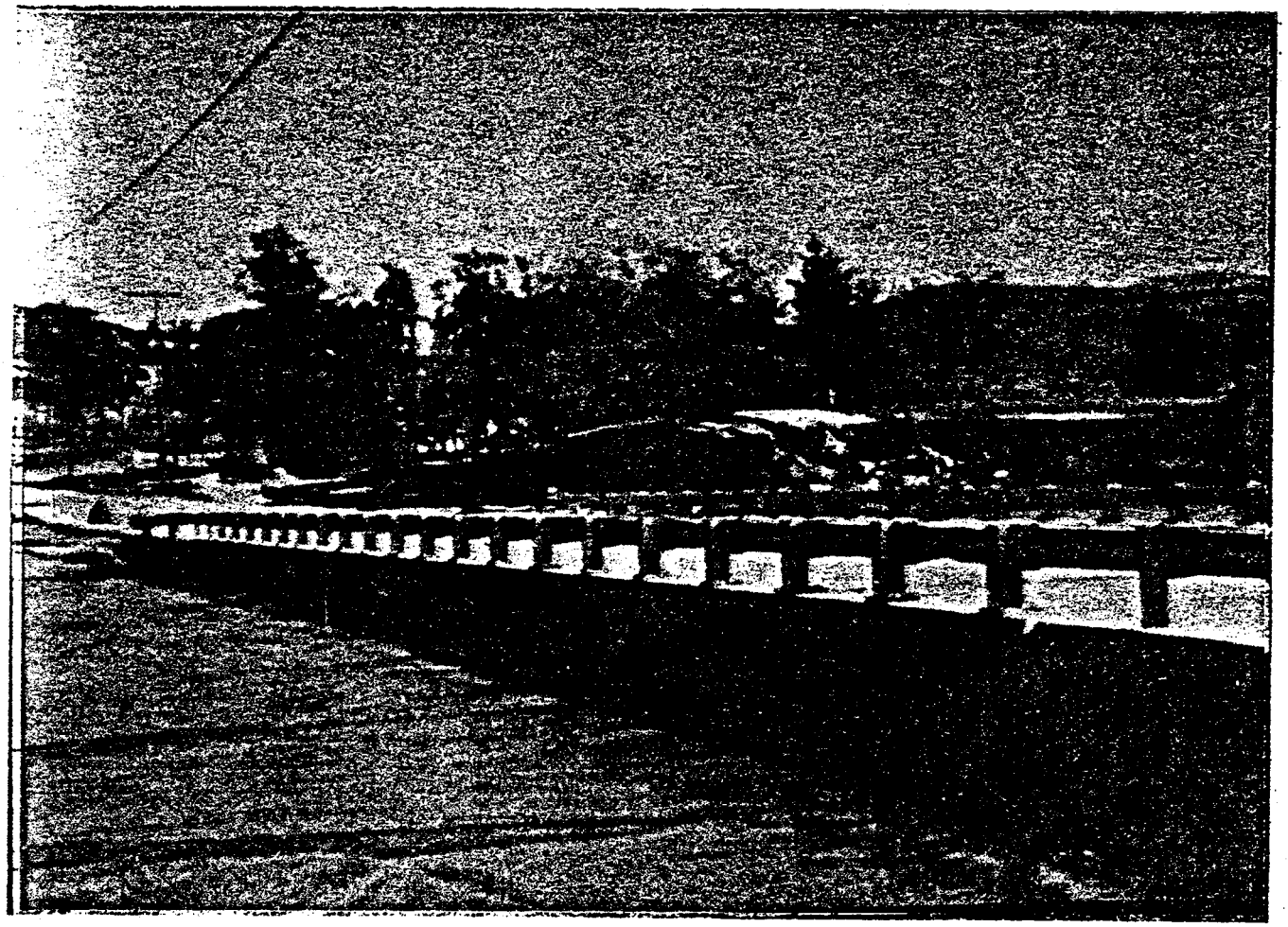

PHOTOGRAPH Before Sediment

E. San Diego River. Design of the bridge at Magnolia Avenue was based upon a flood insurance study. The pile caps were placed 10 feet below the existing ground level. However, 15 feet of erosion occurred during the 1978 floods (about 10-year frequency) exposing the piles.

F. San Vicente Creek. The house shown in Figure D was constructed on the top of the stream bank. High velocity during the peak of the flood eroded the earth from under the foundation of the house. The side of the house dropped about 10 feet and was partially covered by silt as the flood receded. Cars in the same area were completely buried by silt.

Figure D

II FLOOD PLAIN MANAGEMENT--SAN DIEGO COUNTY

Flood plain management is a broad concept. Successful implementation requires a program that includes political, administrative and engineering aspects. In most cases, it involves the consideration of several alternate management possibilities. Many structural methods have been used in the past, including dams, channels, and levees. Other non-structural methods have been used, such as restricting development in the flood plain. A broad information base is necessary before an effective program can be implemented.

Environmental considerations require evaluation of flood plains in their natural or existing condition. This usually means precisely delineating the limits of a major flood. Subsequently, flood hazards can be avoided by restricting development instead of constructing concrete or riprap channels. Natural flood plains provide environmentally desirable natural open-space and avoid large expenditures of funds for channel construction.

The following discussion includes the engineering aspects of flood plain mapping and its relationship to the needs of the public and the National Flood Insurance Program, as implemented by the County of San Diego.

A. FLOOD PLAIN MAPPING PROGRAM

In response to public requests, the San Diego County Board of Supervisors established a flood plain mapping program in 1971, including more than 250 miles of river.

The Program meets the following objectives:

1. Provides precise maps showing the location of the 100-year flood plain.

2. Informs the public of flood hazard areas through zoning and other means.
3. Uses established regulatory means to avoid detrimental construction in flood plains.
4. Provides a basis for environmental analysis and public planning.

The program also conforms to the parallel National Flood Insurance Program.

1. The definition of "floodway" agrees with the Federal definition.
2. Close cooperation with other Agencies such as the Corps of Engineers, the Federal Insurance Administration and the State Department of Water Resources is needed for proper implementation.

B. MAPPING PROCEDURES

A review of procedures for analyzing flood plains shows that the most widely used method of analyzing natural flood plains is the HEC 2 computer program developed by the Corps of Engineers. While this provides a highly sophisticated analysis (including procedures for selecting the floodway location), it has no means of evaluating the effects of erosion and sedimentation in flood plains.

The effect of erosion and sedimentation is extremely important in many flood plains and an engineering analysis is not appropriate without properly analyzing these factors. The need for extensive engineering applications requires appropriate computation procedures. Accordingly, several computer programs have been developed and used for flood plain analysis. All are closely related to the HEC 2 program, so that computer input, variables, and output would be similar. These programs were

developed by Dr. Howard Chang, Professor at San Diego State University. The work was done under contract with the County and included the analysis of several major rivers.

The HEC-2 hydraulic computations provide the location of the floodway. The Federal floodway definition is used--all land required to convey the 100-year flood without increasing the water surface elevation more than one foot. An additional constraint imposed by the County is -- all land required to pass the 10-year flood without structural improvements. The added constraint is usually not controlling, and provides a definition of the low flow area in some locations. The floodway deflection points are plotted and the coordinates may be obtained. With this information, a precise determination is possible using the California Coordinates System. Important subdivision corners and property lines are also tied into the coordinate system.

Hydrology for flood plain projects, when done by the County, uses Federal criteria with modifications to reflect conditions in San Diego County. Primary reliance is placed upon the U. S. Department of Agriculture, Soil Conservation Service Maps and Procedures, and the related National Weather Service "PRECIPITATION FREQUENCY MAPS FOR CALIFORNIA December 1972". Criteria developed by the Corps of Engineers, Los Angeles District, is also used.

In areas studied by the Corps of Engineers, their hydrology is used. If there are significant differences between the preliminary Corps flood flows and flows developed in previous studies, the hydrologic factors

involved are reviewed and comparisons made with County hydrology. The purpose of review of hydrology with responsible organizations is to provide consistency throughout the County.

Flood mapping is coordinated with the County Surveying and Mapping Division. The County program of updating 200 foot per inch scale maps provides a basis for the flood plain studies. This allows the basic mapping to be used for both purposes. The base maps use the new orthophoto process as a means of showing existing details. This concept provides an excellent basis for flood mapping. The photographic detail provided by the orthophoto process allows an easy determination of features and individual property owners can precisely locate their building and lots and relate that to the flood plain or floodway.

The general process for a flood plain study is outlined below. This occurs after the reach of stream or river has been selected. A flow chart shows the important steps in the process (Figure I). The function performed by the individual organizations is described below.

Survey Basis

The first step is to lay out flight control. This is used as a basis for field work which consists of establishing controls and setting targets. At the completion of field surveys, office calculations are necessary to determine coordinates of the various control points. That information is sent to the survey contractor, and after work by his organization, the basis contour lines are sent back for checking.

The final step is a review of the plotted work and other information, such as notes and quality of the orthophoto. At this point, the base map can be completed.

Survey Contractor

Base Map Work

This is the normal work necessary by the contractor to make a standard 200-foot per inch County topo-map. The first step consists of a flight and the processing of the resulting photos. The next step requires aero-triangulation to complete the horizontal and vertical control necessary to do the contour work. It also includes the processing of the ortho-photo which requires a sophisticated process to produce the photo-like image at the proper horizontal scale. The contour lines and spot elevation points are put on a scribe sheet which is then sent back to the County for checking.

After review by the County, any necessary revisions are made and the notes and other information added. The final step is a completion of the base map.

Flood Plain Work

This process is unique to the hydraulic computation procedure and the resulting location of the flood plain. The first step consisists of taking the selected cross sections as determined by the hydraulic engineer and digitizing points along those sections. The digitizing process consists of starting at one end of the designated cross section and determining horizontal and vertical coordinates of each point

where there is a break in the ground slope. The coordinates are obtained by stereo procedures using the air-photos and related triangulation data. Very sophisticated equipment is used in this process and the accuracies are greater than those obtained by selecting points from the base map. The accuracies are summarized in Table I. Several advantages are inherent in this process. First, a much more accurate cross setion can be obtained for the hydraulic computations. Second, the information is computerized and, therefore, capable of being put directly in format necessary for the HEC-2 program. The information goes to the hydraulic engineer and after some preliminary work, additional cross sections are given to the survey contractor to complete the work necessary for hydraulic computations. This work is returned to the hydraulic engineer who does additional work and then returns the final flood plain elevations to the survey contractor.

TABLE I
SURVEYING ACCURACY
(90% of All Points)

	Vertical (feet)	Horizontal (feet)
Base Map		
1. Photographic Details (Houses, roads, bridges, etc.)		5
2. 6-Foot Contour Lines	2.5	
3. Spot Elevations	1.25	5
Hydraulic Data (Varies with Study)		
1. Cross-Sections	.5 or 1.0	2
2. Flood Lines	1 or 2	5

At this stage, all necessary information is available for final plotting of flood lines and floodways. The flood lines are plotted by taking a computed water surface elevation at each cross section and plotting the horizontal location on the orthophoto map. The plotted flood lines have greater accuracy than the five foot contour lines and are, therefore, more appropriate in depicting the location of the the flood plain. The floodway is plotted directly from the points selected by the hydraulic engineer. This information is returned to the hydraulic engineer for final review. After it comes back to the survey contractor, necessary minor adjustments are made in the floodway and the flood plain-floodway portion of the map can be completed. As a final step, the points of deflection on the floodway are digitized so that floodway boundaries may be accurately defined.

Hydraulic Analysis

The area to be mapped is reviewed in the field. The locations of cross sections for hydraulic computations are determined. In addition, information such as the size of bridge openings and the roughness values of channels and flood plains is obtained. While the schedule in Figure I shows this occurring after the flight, it is better to wait until the base orthophoto maps are complete with contours. This greatly aids in the selection of cross sections and helps in determining the roughness values for the flood plains. The cross sections are sent to the survey contractor for digitizing. On return of the digitized cross sections, they are plotted and preliminary hydraulic computations are done. This requires inputting all the variables

such as Manning Values in the computer and the computations are done using the HEC-2 program. It also includes an analysis of erosion and sedimentation conditions. After the results of the hydraulic computations are reviewed, it is usually found desirable to add cross sections at various locations to improve the analysis. These added cross sections usually average about 10% of the total number of cross sections. The information is sent back to the survey contractor who digitizes the additional sections and returns them to the hydraulic engineer. The hydraulic computations are redone with the new cross sections included.

Erosion Analysis

Additional computations are often necessary where changes to the river bed due to erosion or sedimentation are important. The analysis is done by computer with an input format that is essentially the same as the HEC-2 format. After the configuration of the channel bed has been determined during peak flow conditions, the cross sectional data is reanalyzed using the HEC-2program, but substituting a new channel configuration.

Floodway Analysis

Floodway computations are done using the HEC-2 program. Preliminary floodway computation results are reviewed for the purpose of adjusting the floodway so that it is a relatively smooth line, and in some cases, conforms to existing features such as highways or low flow channels. In some cases, the ten-year flood plain is found to be outside the location of the standard floodway and an adjustment is made so that the

floodway will not infringe into the area necessary to convey a ten-year flood. In addition, floodway encroachment is not continued into areas where the velocity exceeds 6 feet/second. After review of the floodway location, final hydraulic computations are made and the results sent to the survey contractor for plotting.

Upon return of the plotted lines, a final review is made and any minor corrections and adjustments included. Information is sent back to the survey contractor who completes the flood map.

Administration

An Administration review of the floodway is done before final hydraulic computations are completed. This is to review the location of the floodway and make necessary adjustments based upon existing structures, property lines, existing or proposed land use or other special considerations.

The total process for completion of a flood plain mapping project requires a considerable amount of coordination and is complex. However, the results are much better than those obtained from using with five-foot contour intervals as a basis for cross-sections.

More than 250 miles of streams have been mapped this way in the County of San Diego. Figure II shows a map locating the areas which are under study or completed. While this process was developed in San Diego County, it is applicable to most area of the United States.

C. FEDERAL PROGRAMS

The U.S. Army, Corps of Engineers, the Federal Emergency Management Agency (FEMA) and other federal agencies have been directly involved with flood plain management.

National Flood Insurance Program (NFIP)

The NFIP is a Federally-subsidized program authorized by Congress in 1968 to protect property owners who up to that time were unable to get coverage through the private insurance industry. The program, for the first time, made flood insurance available to individuals at affordable rates.

Congress initiated the NFIP because the average annual loss due to flooding in the United States was about $1.5 billion and it is projected that by the year 2000, this figure could reach $13 billion unless land use controls are enacted limiting future construction in areas subjected to flooding.

Requirements for Local Government.

In return for the availability of flood insurance, Federal,State and local governments are required to adopt certain minimum land use measures to reduce or avoid future flood damage within their flood-prone areas. They are also required to use flood plain studies as a basis for review of proposed development. Projects can not restrict flow in floodways. The first floor of houses must be elevated above the flood plain level and protected against flood damage.

Insurance Rates

Citizens can purchase flood insurance from most insurance agents. Rates depend upon whether the community is in the Emergency or Regular Phase of the NFIP. Figure III provides examples of the amount of insurance available and rates.

D. American Society of Civil Engineers Award for San Diego

SAN DIEGO SECTION - AMERICAN SOCIETY OF CIVIL ENGINEERS

Outstanding Civil Engineering Achievement Award for 1981

presented to

San Diego County

Department Of Public Works

for their contribution to public safety

in the implementation of the

San Diego County

Flood Plain Mapping and Management Program

William R. Nothomb, President, 1981-82 — March 23, 1982 Date

Figure I

FLOOD PLAIN MAPPING ENGINEERING SCHEDULE

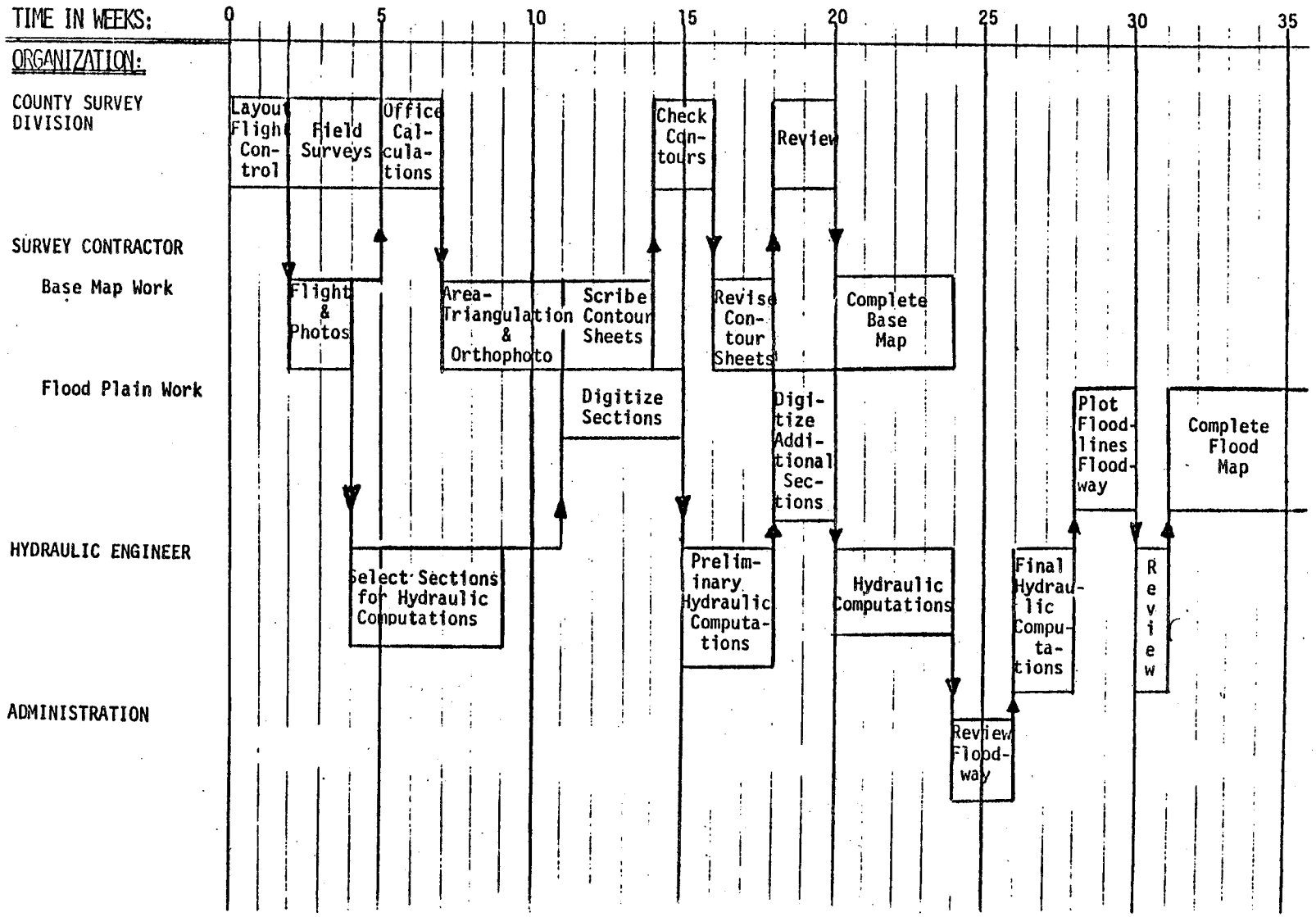

FIGURE II COMPLETED FLOOD PLAIN STUDIES - 1983

Flood Plain Mapping

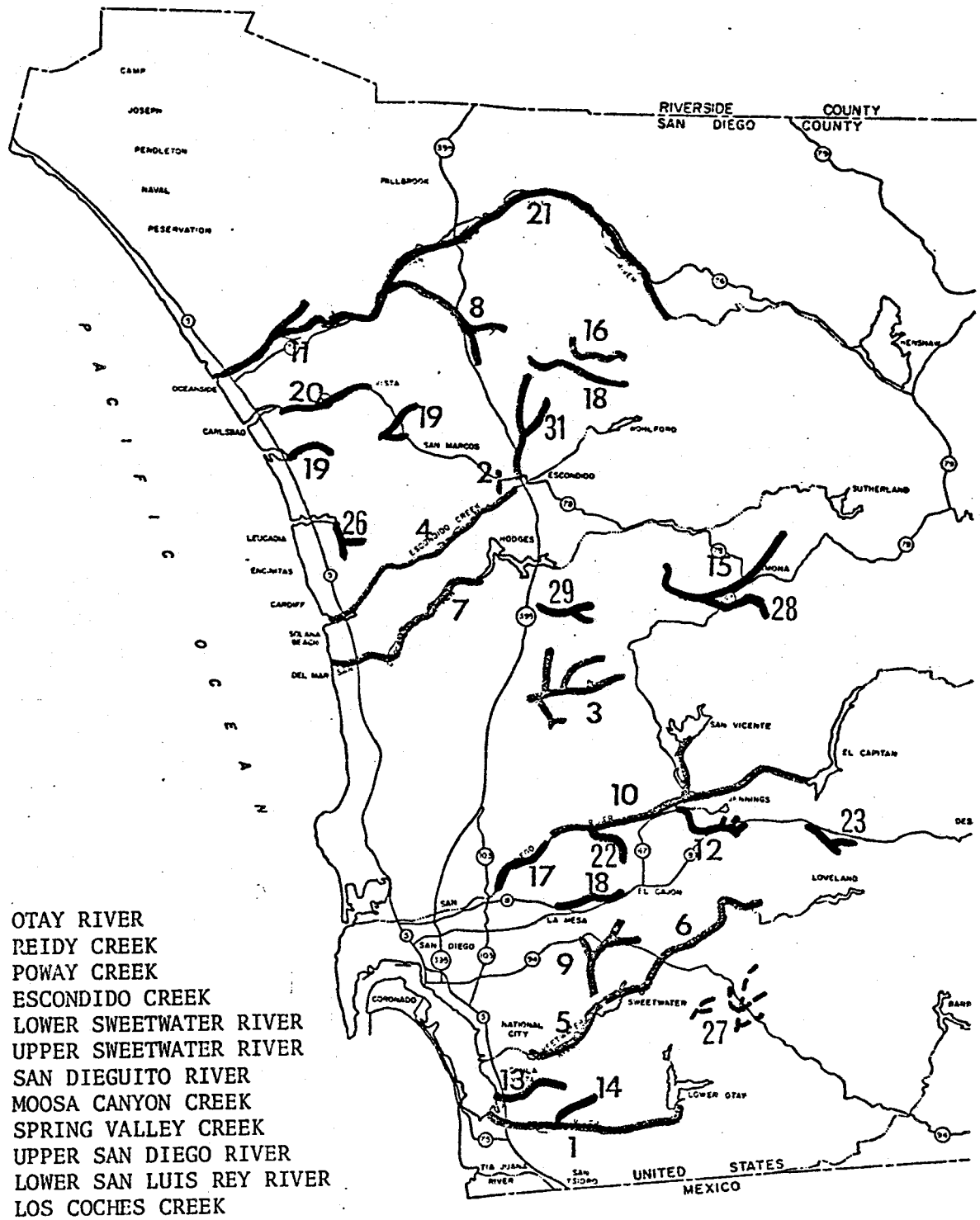

1. OTAY RIVER
2. REIDY CREEK
3. POWAY CREEK
4. ESCONDIDO CREEK
5. LOWER SWEETWATER RIVER
6. UPPER SWEETWATER RIVER
7. SAN DIEGUITO RIVER
8. MOOSA CANYON CREEK
9. SPRING VALLEY CREEK
10. UPPER SAN DIEGO RIVER
11. LOWER SAN LUIS REY RIVER
12. LOS COCHES CREEK
13. TELEGRAPH CANYON CREEK
14. POGGI CANYON CREEK
15. SANTA MARIA CREEK
16. KEYES CANYON CREEK
17. MIDDLE SAN DIEGO RIVER
18. ALVARADO CANYON CREEK
19. AGUA HEDIONDA CREEK
20. BUENA VISTA CREEK
21. UPPER SAN LUIS REY RIVER
22. FORESTER CREEK
23. ALPINE CREEK
24. CAMPO CREEK
25. CAMPO SOUTH
26. ENCINITAS CREEK
27. JAMUL CREEK
28. RAMONA SOUTH
29. GREEN VALLEY
30. PINE VALLEY
31. RINCON TRIBUTARY

COMPLETED FLOOD PLAIN MAPS
(solid lines)

Figure III

NATIONAL FLOOD INSURANCE PROGRAM
Rating Examples
Single Family Dwelling without basement, one floor

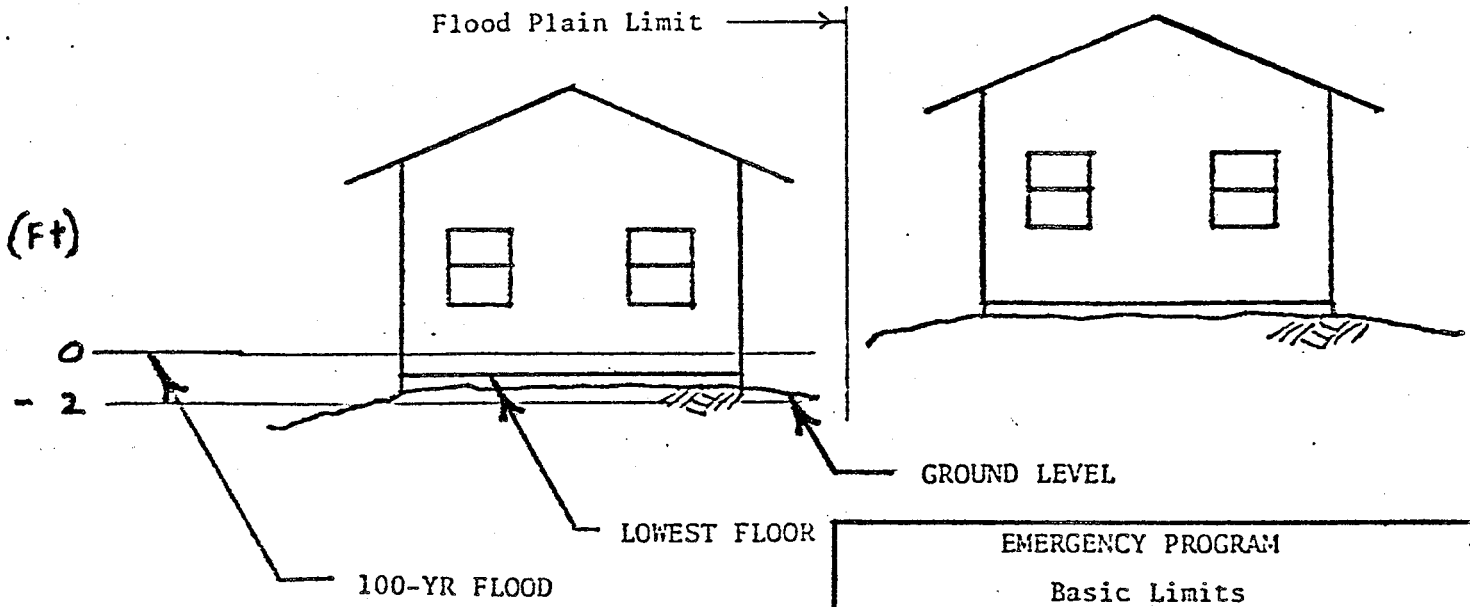

EMERGENCY PROGRAM

Basic Limits

Coverage	Amount of Insurance	Rate	Annual Premium
Building	$35,000*	.45	$ 158
Contents	10,000*	.55	55
	Expense Constant		20
	Tot. Prepaid Premium		$ 233

REGULAR PROGRAM

Pre-FIRM Construction

Zones A1-30
(Elev. - 1 Ft.):

Coverage	Basic Limits: Amount of Insurance	Basic Limits: Rate	Basic Limits: Annual Premium	Additional Limits: Amount of Insurance	Additional Limits: Rate	Additional Limits: Annual Premium	Basic & Additional: Total Amount of Insurance Requested	Total Premium
Building	$35,000*	.45	158	30,000**	.17	51	$65,000	$ 209
Contents	10,000*	.55	55	10,000***	.28	28	20,000	83
							Expense Constant	20
							Tot. Prepaid Premium	$ 312

Zone C
(Elev. - not applicable):

Building	$35,000*	.25	88	30,000**	.06	18	$65,000	$ 106
Contents	10,000*	.40	40	10,000***	.15	15	20,000	55
							Expense Constant	20
							Tot. Prepaid Premium	$ 181

* Maximum amount available.
** " of $150,000 is available.
*** " of $ 50,000 " " .

(October 1983)

III FLOOD PLAIN COMPUTATIONS

A. TOPOGRAPHY & CROSS SECTIONS

PLAN VIEW

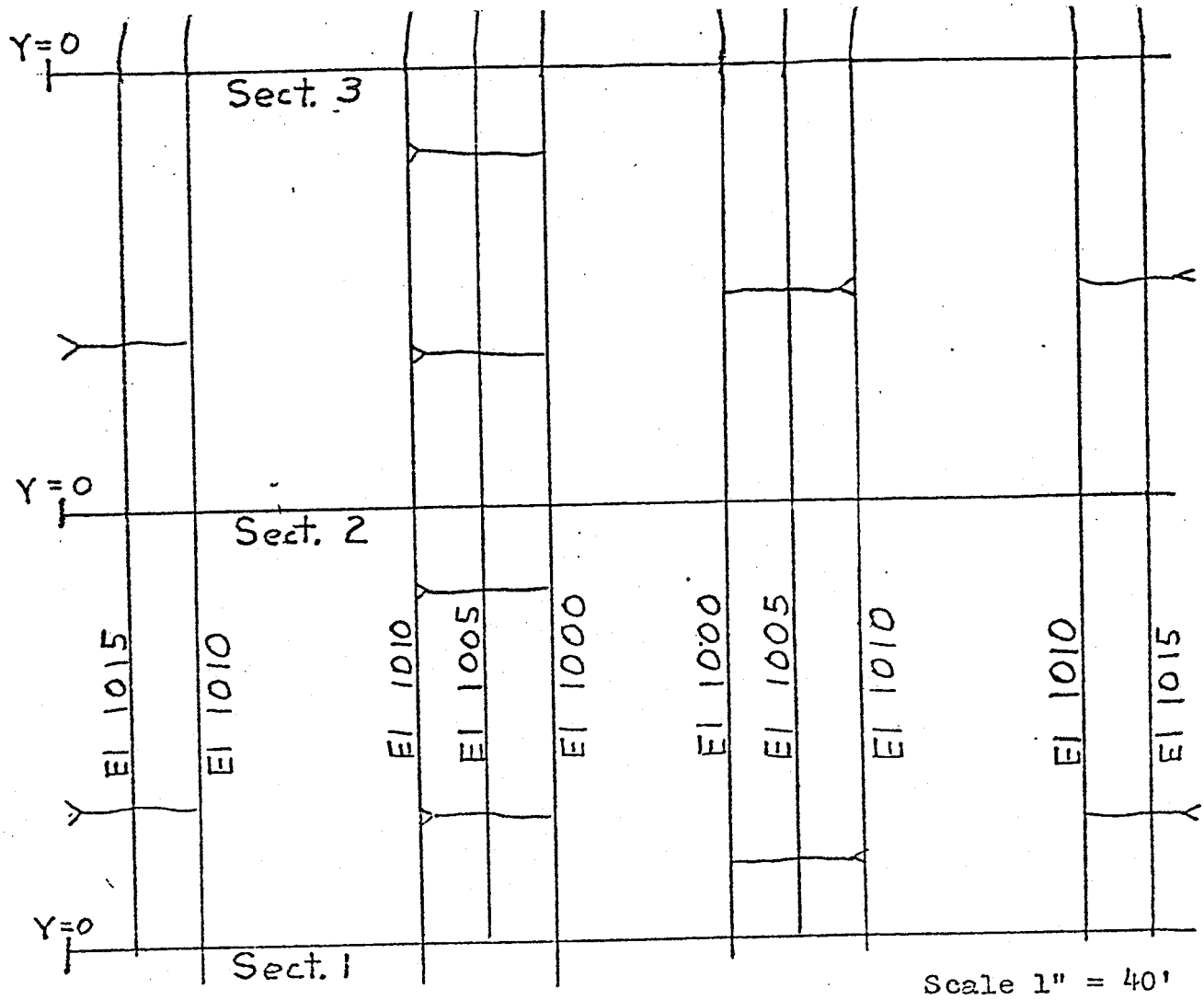

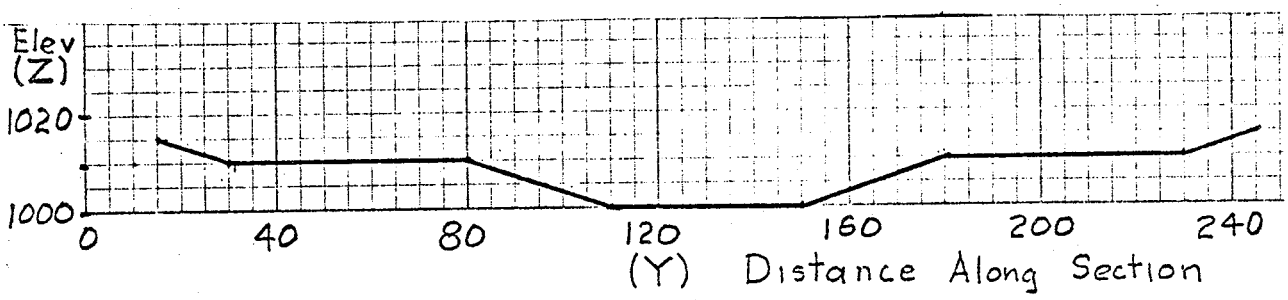

CROSS SECTION

III B FLOW CHARACTERISTICS, TYPICAL CROSS SECTION

TYPICAL CROSS-SECTION

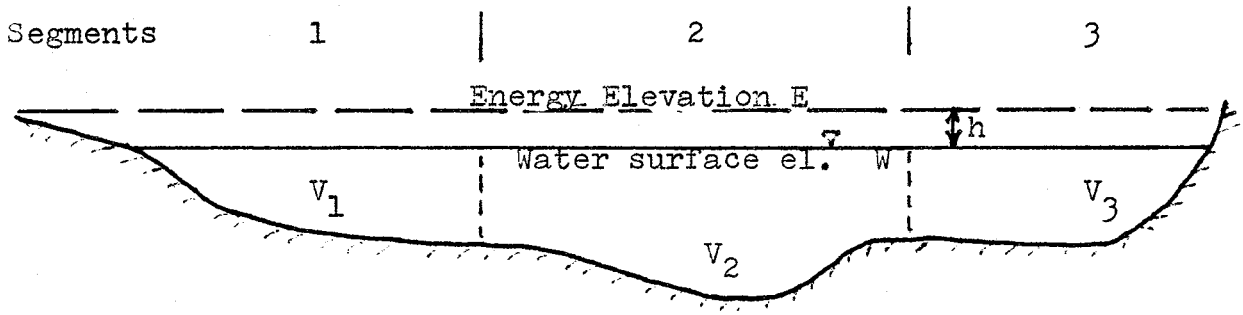

FOR THE TOTAL CROSS-SECTION

Average Velocity $V_A = Q_t/A_t$

Where Q_t is the total flow

A_t is the total cross section area

Manning Equation $Q_t = \left[(1.486/n)\ A\ R^{2/3}\right]\sqrt{S_f}$

(English Units) Where S_f is the Energy slope

SPLITTING THE CROSS-SECTION INTO (I) SEGMENTS

$$Q_t = \left[K_t\right] \sqrt{S_f}$$

$$K_t = \sum_{i=1}^{I} K_i = \sum_{i=1}^{I} = 1.486 \quad (A_i R_i^{2/3} / n_i)$$

Where K is the conveyance

$$S_f = (Q_t / K_t)^2$$

For each segment

$$Q_i = K_i \sqrt{S_f}$$

$$V_i = Q_i / A_i$$

VELOCITY HEAD COEFFICIENT

$$\alpha = \frac{\int V^2\, dQ}{V_A^2 Q_t} \quad \text{or} \quad \alpha = \frac{\sum_{i=1}^{I} V_i^2\, Q_i}{V_A^2\, Q_t}$$

Weighted Velocity Head $h = \alpha\, V_A^2/(2g)$

Water Surface Elev. $+W$

Energy Elev. E

COMPUTATIONS

The cross section is defined by a series of coordinates. Each coordinate consists of an elevation Z (J) and horizontal distance Y(J) for a point (J) on the ground along a cross section. The ground points are selected so that a straight line between them represents the river bed. The cross section from page III-B-1 is shown below with points 3 and 4 labled to illustrate the method. Note that a distorted scale is used.

TYPICAL CROSS-SECTION PLOT

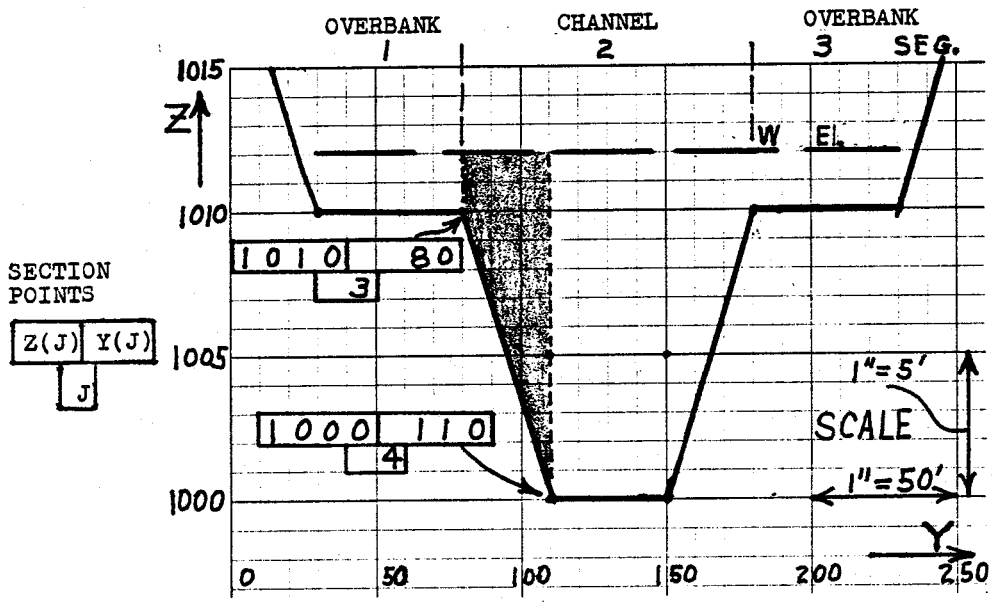

Hydraulic computations proceed by determining the perimeter P(J) and the area A(J) for the portion of a a cross section between point (J) and point (J+1). A straight line between the two points represents the wetted perimeter and the vertical projection between

the line and the water surface represents the flow area. This can be written as :

$$P(J) = \sqrt{(Z(J+1) - Z(J))^2 + (Y(J+1) - Y(J))^2}$$

$$A(J) = (W - (Z(J+1) + Z(J))/2)\ (Y(J+1) - Y(J))$$

(AVERAGE DEPTH) (TRAP. BASE)

The area and perimeter for each segment is determined by summing the perimeter and area between each pair of points within the segment.

Example #1 Hydraulic computations for the cross section with the water surface elevation at 1012.0 feet. The Section is split into three segments, with a value of .035 for each. The flow is 10,000 cubic feet/second.

Segment 2	P	A
Begin with J=3, J+1=4 (Shaded on plot)		
$P(3) = \sqrt{(1010-1000)^2 + (110-80)^2} =$	31.62	
$A(3) = (1012 - (1000+1010)/2)(110-80)$		
$= (\quad 7 \quad)(\quad 30 \quad) =$		210
J = 4 (J+1) =5 (by inspection)		
P(4) =	40	
A(4) = (12) (40) =		480
J=5 (J+1)=6 (same as J=3)		
P(5)=	31.62	
A(5)=		210
Total for Segment 2	103.24	900

$R_2 = 900/103.2 = 8.72$

$K_2 = 1.486\ 900\ 8.72^{2/3}/.035$

$K_2 = 161848$

Segment 3	P	A
J= (6) (J+1)=7 (by inspection)		
P(6)=	50	
A(6)= (2)(50)=		100
J= (7) to water surface		
P(7)= $\sqrt{2^2 + 6^2}$ =	6.32	
A(7)= (1) (6)=		6
Total for Segment 3	56.32	106

$R_3 = 106/56.32 = 1.88$

$K_3 = 1.486\ 106\ 1.88^{2/3}/.035$

$K_3 = 6860$

Segment 1

Since the cross section is symetrical, Segment 1 is the same as Segment 3

For the total Section (with Q_t = 10000cfs)

$K_t = K_1 + K_2 + K_3 =$	175568
$A_t = A_1 + A_2 + A_3 =$	1112 ft^2
$S_f = (Q_t/K_t)^2 =$	.00324
$V_A = Q_t/A_t$	9.0 ft/sec

For each Segment

$$Q_1 = Q_3 = K_1 \sqrt{S_f} = K_3 \sqrt{S_f}$$

$$= \quad = 6860 \sqrt{.00324} = \qquad 391$$

$$V_1 = V_3 = Q_1/A_1$$

$$= 391/106 = \qquad 3.7$$

$$Q_2 = K_2 \sqrt{S_f}$$

$$= 161848 \sqrt{.00324} = \qquad 9213$$

$$V_2 = Q_2/A_2 = \qquad 10.2$$

Computation for the Velocity Head Coefficient

$$\alpha = (\Sigma V_i^2 \, Q_i) / (V_A^2 Q_t)$$

$$\alpha = (3.7^2 \; 391 + 10.2^2 \; 9213 + 3.7^2 \; 391)/(9.0^2 \; 10000)$$

$$\alpha = 1.20$$

The Energy Elevation E

Water Surface Elevation $W = 1012.0$

$\alpha V_A^2/(2g) = 1.2 \; 9^2/(64.3) = \underline{+1.5}$

$E = 1013.5$

Compare thse computations with the computer output for SECT.3 on page III-B-18

Example #2 Analysis of the same cross section as one unit.

For comparison, hydraulic characteristics for the same cross section can be determined considering it as one segment instead of three. The same n = .035, water surface elevation and flow are used.

From previous computations

Velocity V_A = 9.0 ft/sec.

Since there is only one sequent, α =1.0

Velocity Head $h= V_A^2/(2g)=$ 1.26

Water Surface Elevation W = +1012.
Energy Elevation 1013.26

Hydraulic Radius

$R=A/P = 1112/(103.2+56.3+56.3) =$ 5.15

Friction Slope S_f

$S_f= (Q/K)^2 =(Q/((1.486/n)A\ R^{2/3}))^2$

$S_f=(10000/((1.486/.035)1112\ 5.15^{2/3}))^2$

$S_f= .00504$

Compare thses computations with the Computer output for SECT. 2 on page III-B-17

Computer Analysis

The computation proceedure outlined in Examples #1 and #2 has been incorporated into a computer program. The program is simular to HEC 2, the computer program developed at the Corps of Engineers, Hydrologic Engineering Center at Davis, California. Typical computer output is provided on page III-B-16. The cross section input data, the number of

segment and data for each segment are echoed. Average hydraulic characteristics for each water surface elevation are provided. Segment information is printed.

A comparison of analyzing the section as three segments verses one segment is given below:

Three Segments, Example #1 (Designate as Section 3)

Segment	#1	#2	#3
n value	.035	.035	.035
Q	391	9213	391
V	3.7	10.2	3.7

One Segment, Example #2 (Designate as Section 2)

N=.035 Q=10000 V=9.0

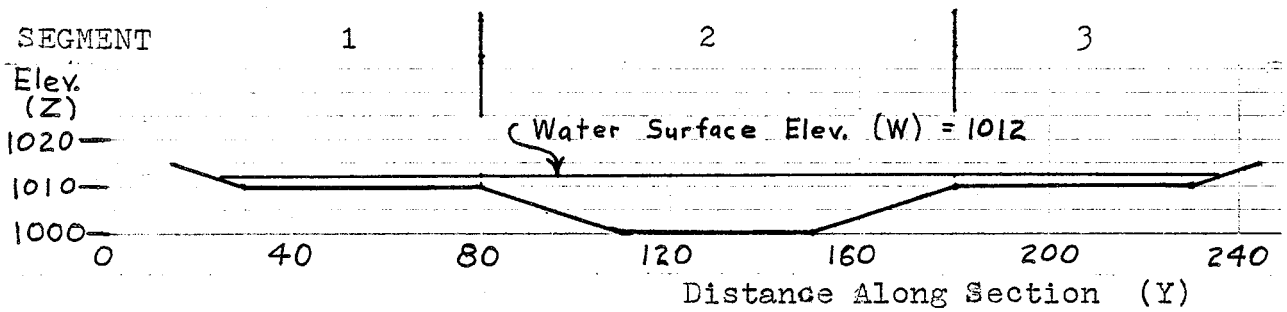

For additional comparison, the results of additional computations (by computer) for different Manning n values are given below:

Three Segments (Designate as Section 1)

Segment	#1	#2	#3
N values	.06	.02	.05
Q	137	9699	164
V	1.3	10.8	1.6

Computer analysis (pages III-B-17 and III-B-18) provide a basis for the following two figures. The effect of using one verses three segments in the same cross section used in the previous examples is illustrated for a range of water surface elevations. A Manning n of .035 is used in all computations.

COMPARISON OF ONE VERSES THREE SEGMENTS
Q= 10000 n= .035

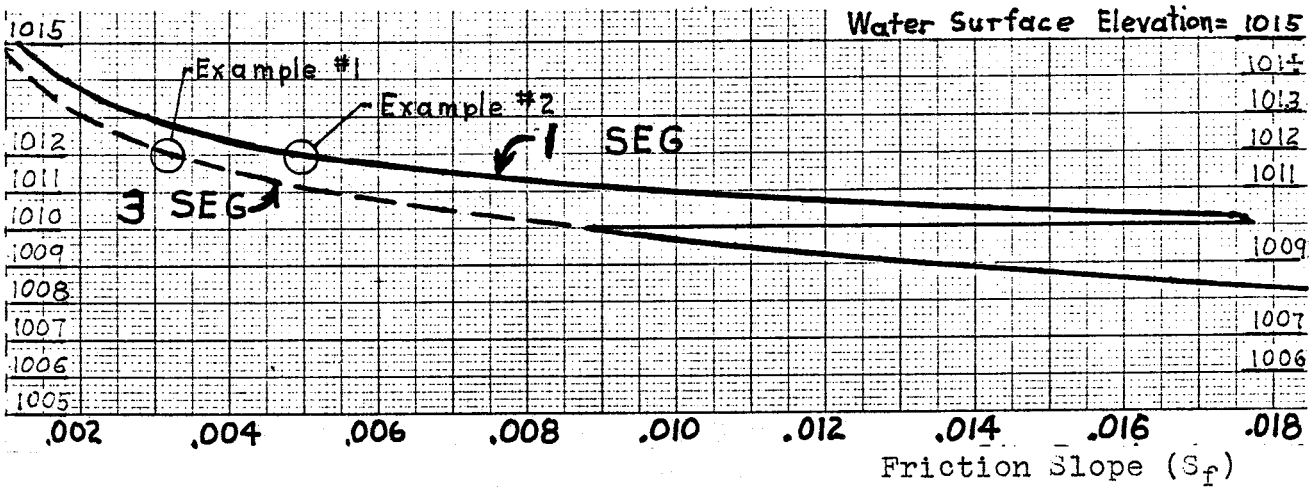

Note that there is a major discontinuity in S_f for water surface elevations above elevation 1010 when only one segment is used in the analysis. The large increase in the wetted preimeter as the water surface increases above the level of the higher trapezoid causes the jump in the friction slope.

The second figure shows the energy elevation and velocities for a range of water surface elevations.

ENERGY & VELOCITY VS. WATER SURFACE ELEVATION

MANNING N = .035

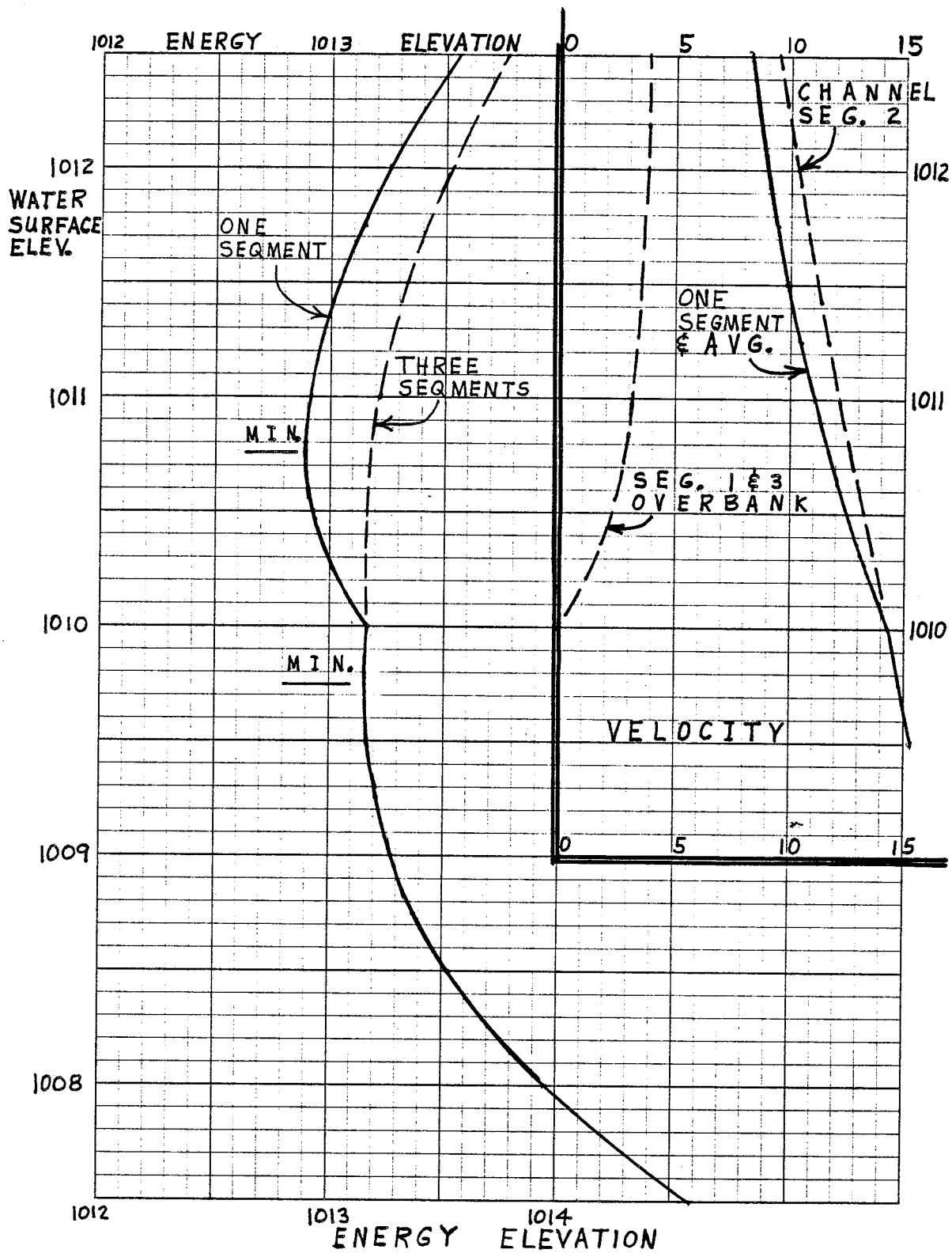

A review of the figure on page III-B-9 provides several significant factors to be considered when performing hydraulic analysis.

A. Energy Considerations.

1. Selecting 1 vs. 3 Segments makes a significant difference in the energy curve.
2. The cross section analyzed as one segment has two local minimums.
3. Near the minimum energy elevation, a minor change in energy elevation can make a large change in water surface elevation.

Water Surface Elevation	Energy Elevation
(1 Seg.) 1012.1	1013.3
(3 Seg.) 1011.4	1013.3
1009.8	1013.2

B. Velocity Considerations

1. Using one segment does not give reasonable overbank velocities.
2. The velocity head in the overbank is significantly different from the channel.

Natural channels are usually not symetrical, as the channel which has been considered. The plot below represents a natural cross section which may be encountered. The cross section is taken from the plan view on page III-D-2 .

A computer analysis is provided on page III-B-19

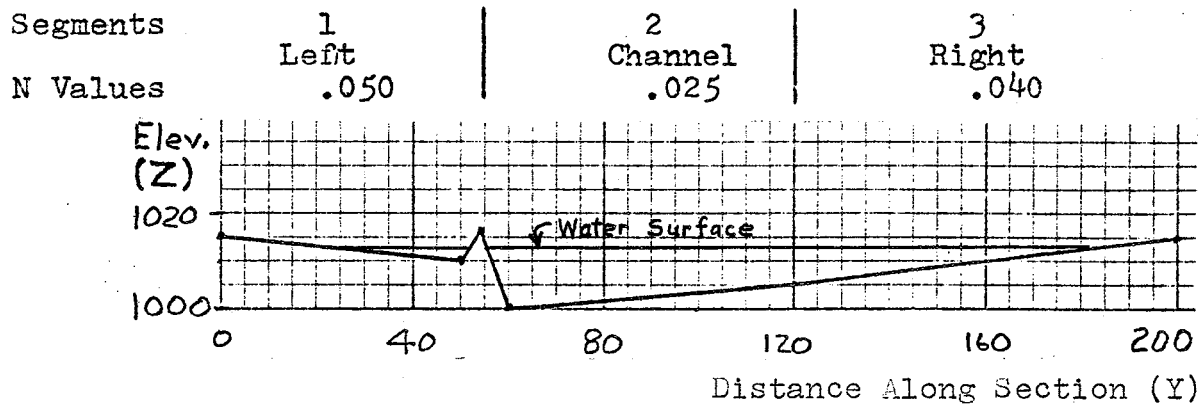

Computer plotted cross sections from the Santa Maria Flood Plain are included on page III-B-12,13,14. The dashed lines show the 100 and 10 year flood water surface elevations. The solid horizontal lines show the floodway. Note that Sections 11.533 and 12.569 show overbank flow and flow under a bridge. Section 12.219 shows a structure (Y=900) in the flood plain.

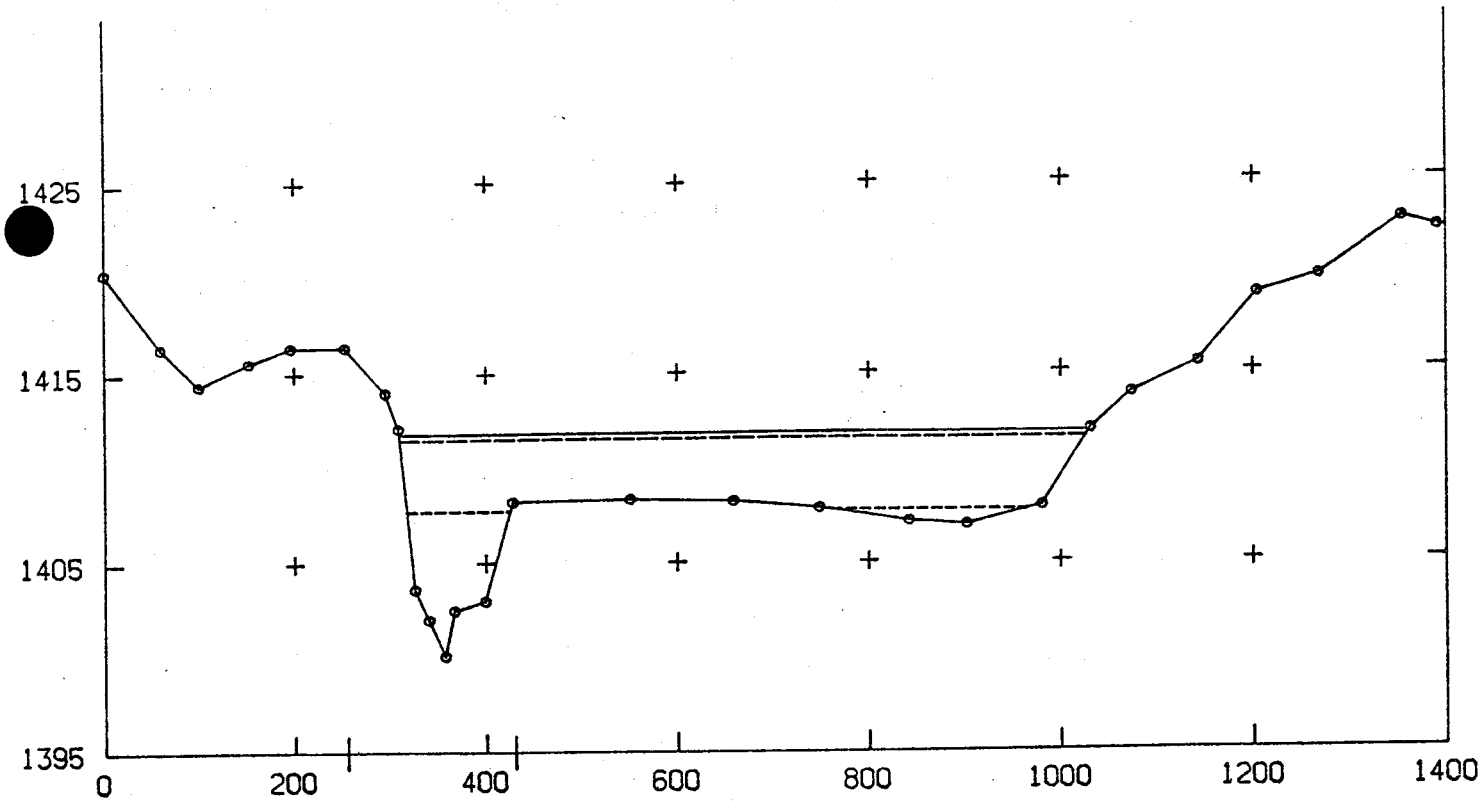

11.781

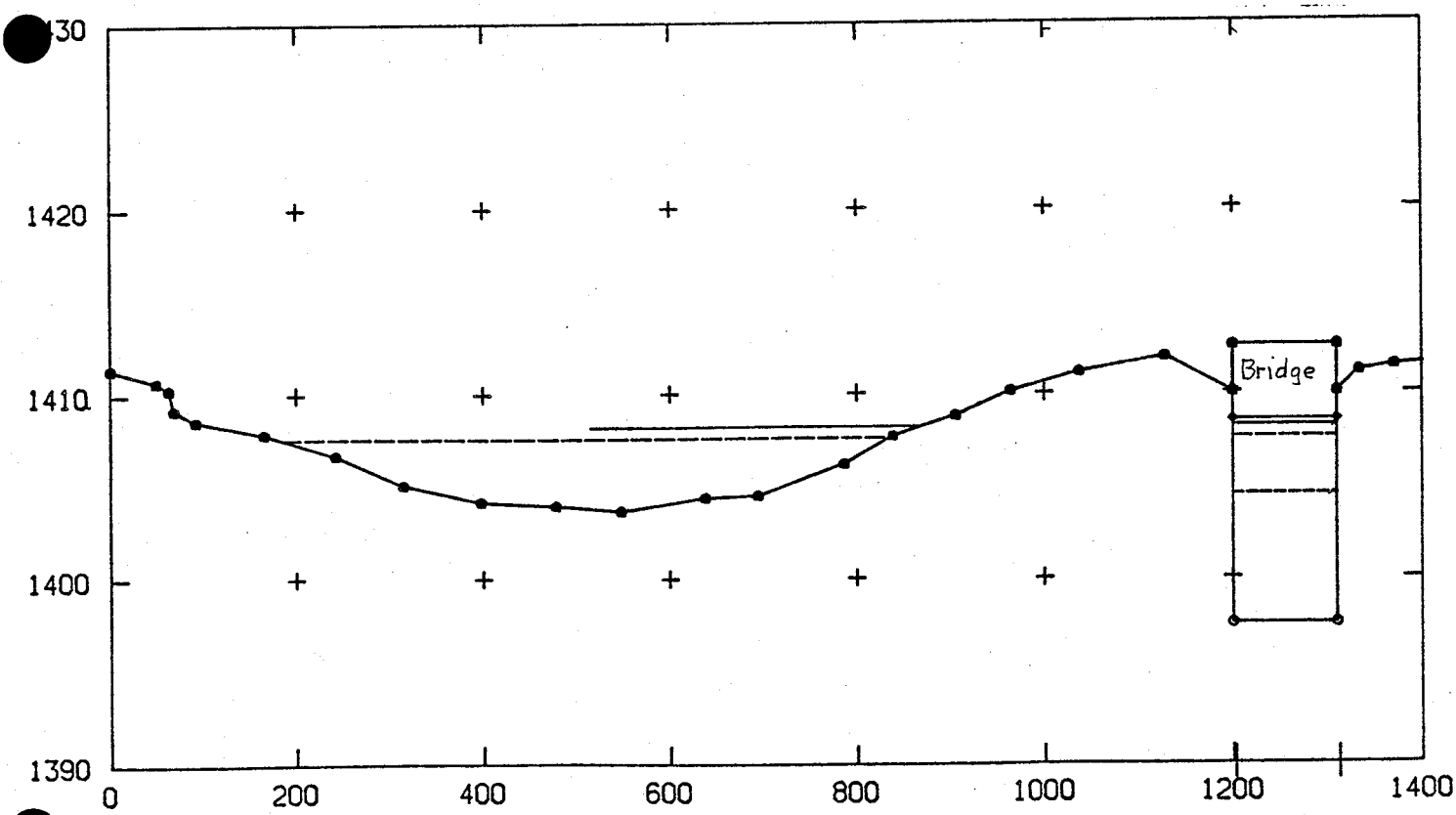

11.533

COUNTY OF SAN DIEGO
DEPARTMENT OF PUBLIC WORKS
HYDROLOGY SECTION
28-DEC-81

SCALES VERTICAL 1"=10' HORIZONTAL 1"=200

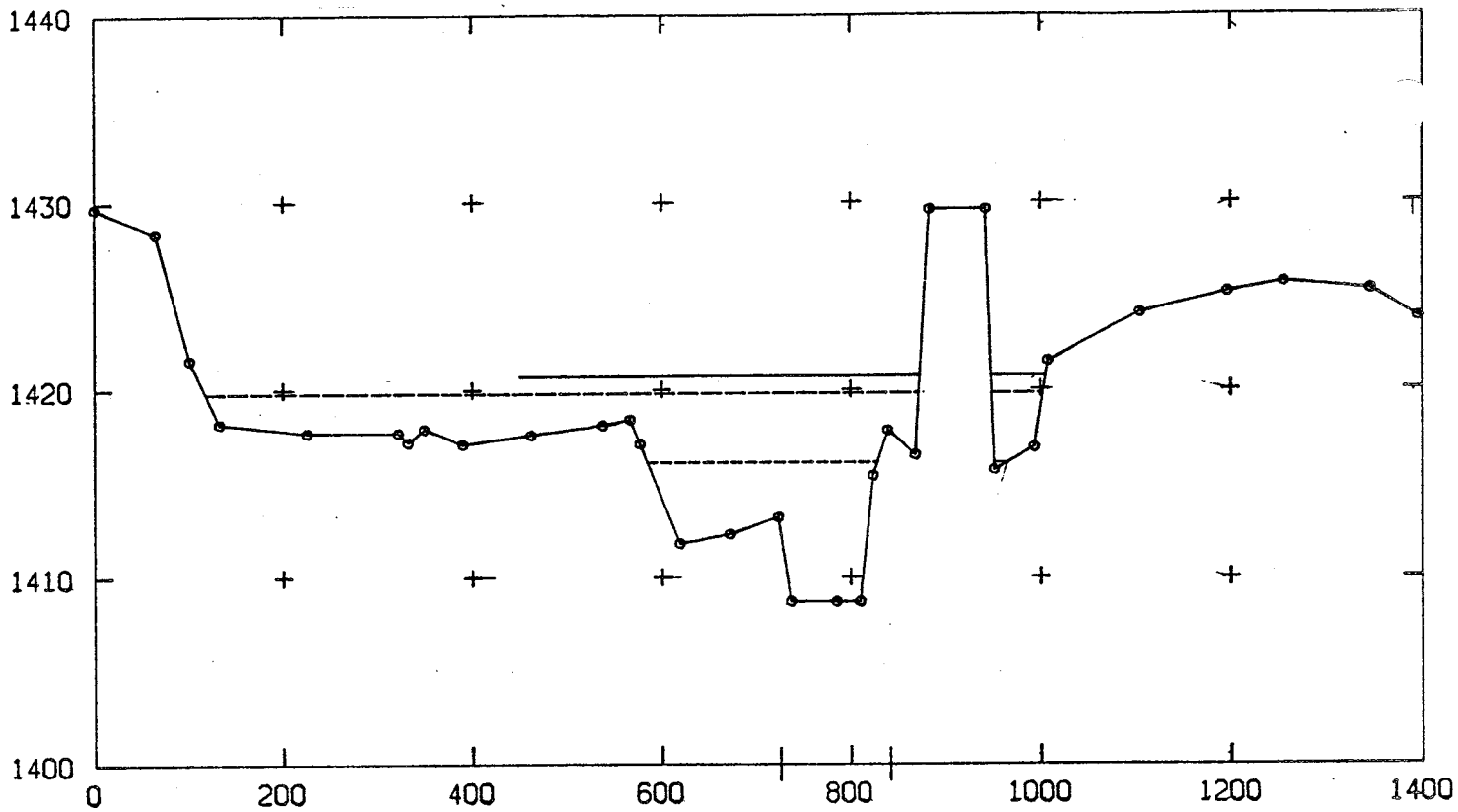
1440
1430
1420
1410
1400
0
200
400
600
800
1000
1200
1400

12.219

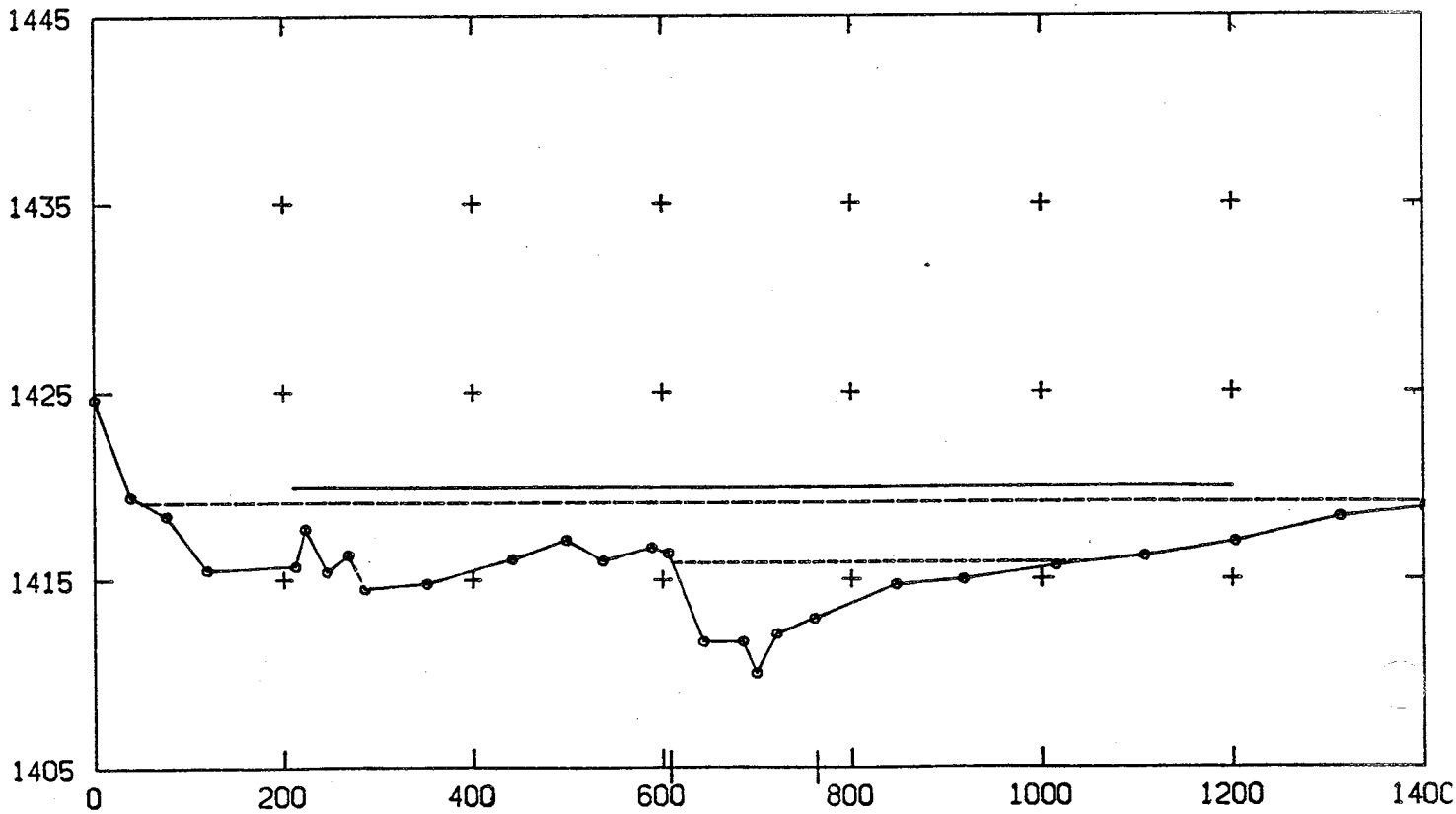
1445
1435
1425
1415
1405
0
200
400
600
800
1000
1200
1400

12.126

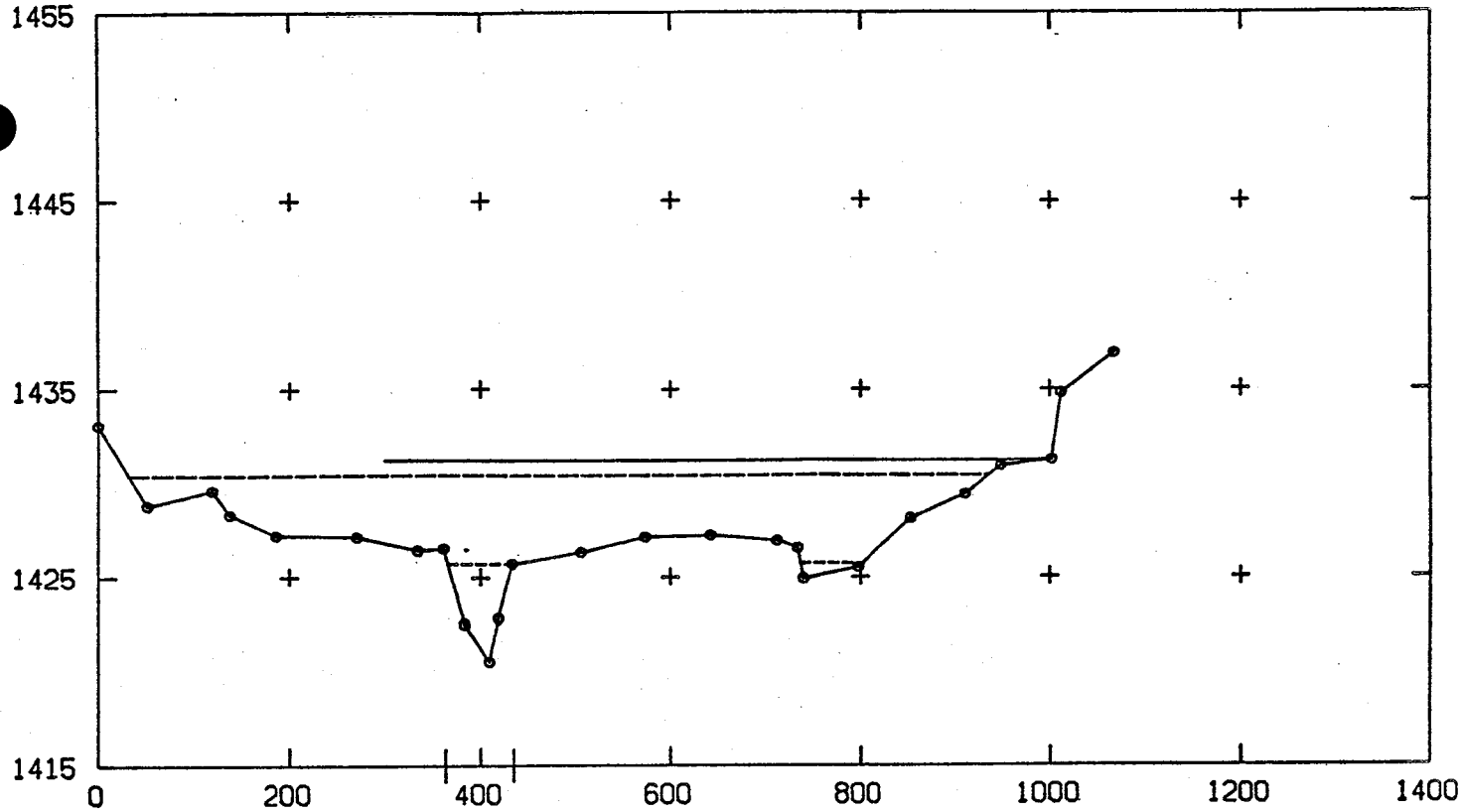

12.691

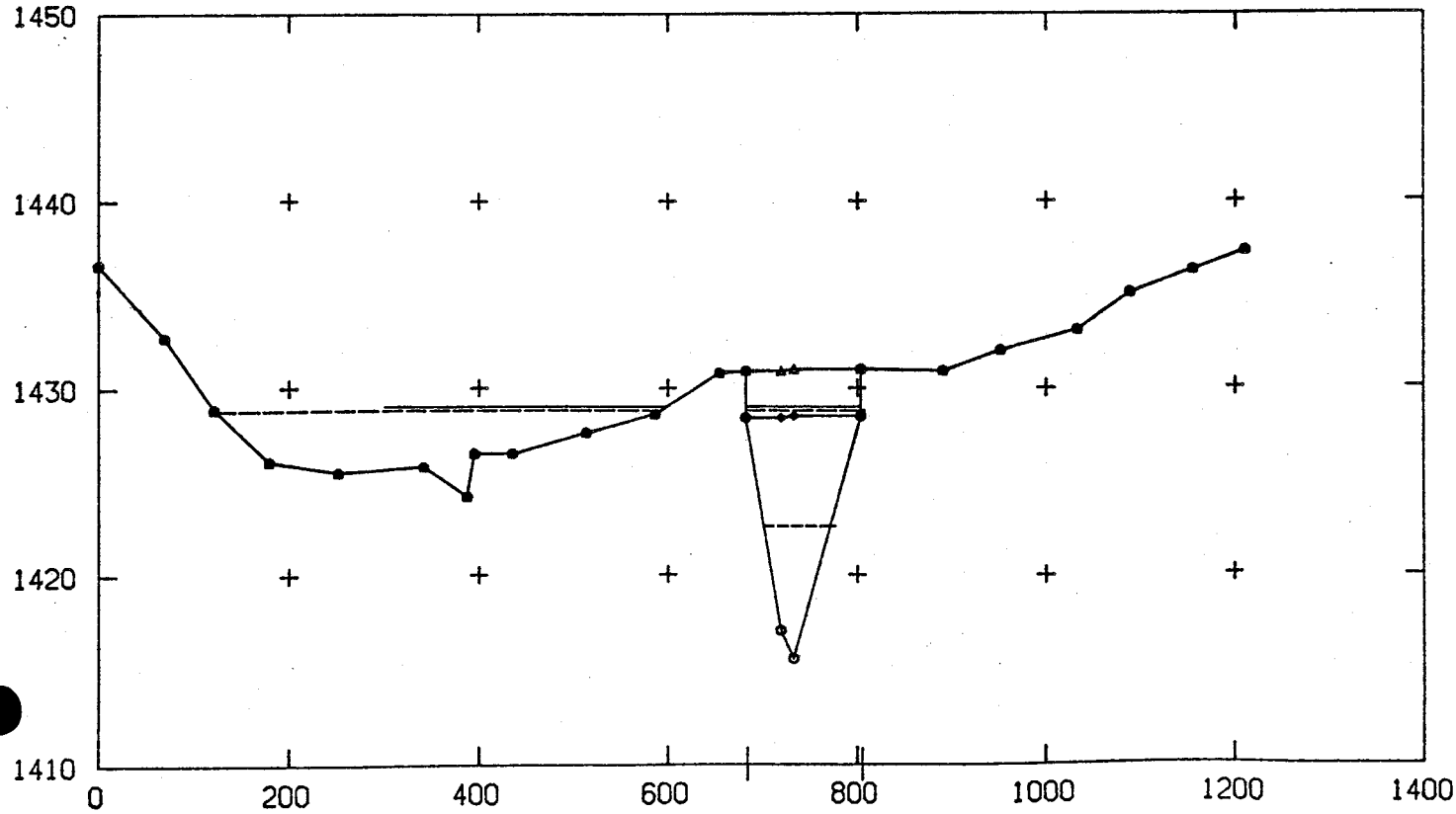

12.569

SANTA M

Copy of Cross-section Plot
on CRT Terminal. Used by
Hydraulic Engineer in
Flood Plain Analysis.

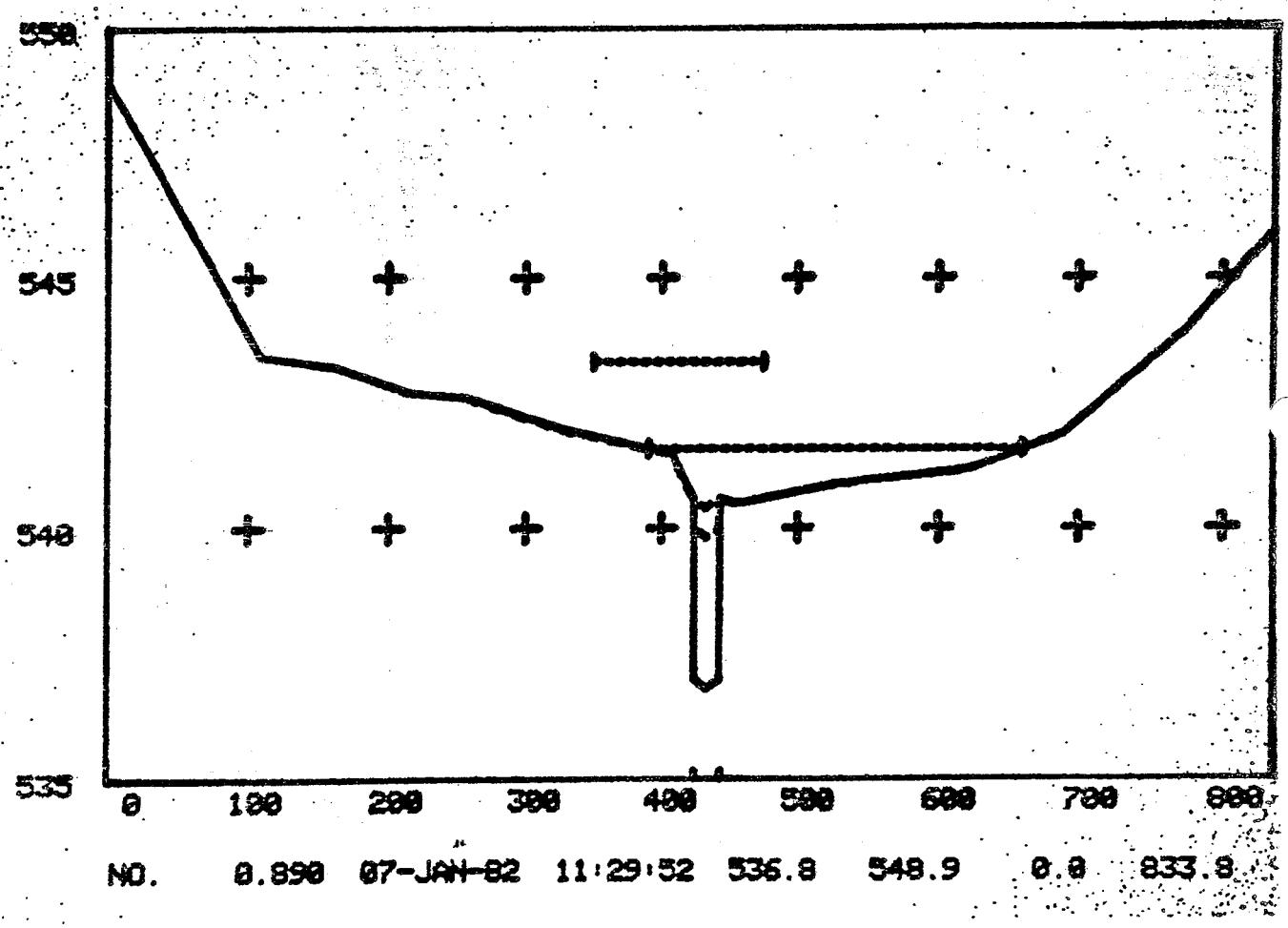

ELEVATION VS ENERGY AND FRICTION SLOPE

NATURAL CHANNEL PROGRAM, SECTION CHARACTERISTICS

SECT. 1

SECT DESC= TEST 3 N VALUES NO PT= 8

Z 1	Y 1	Z 2	Y 2	Z 3	Y 3	Z 4	Y 4	Z 5	Y 5
Z 6	Y 6	Z 7	Y 7	Z 8	Y 8	Z 9	Y 9	Z10	Y10
1012.0	24.0	1010.0	30.0	1010.0	80.0	1000.0	110.0	1000.0	150.0
1010.0	180.0	1010.0	230.0	1012.0	236.0				

GR ELEV, MIN= 1000.0 MAX INTERIOR= 1010.0 LOWEST END= 1012.0

FLOW = 10000. NO OF SEGMENTS = 3

SEG = 1 2 3

PT NO = 3 6

STA = 80. 180.

N = .0600 .0200 .0500

AVG HYD CHARACTERISTICS FOR SECTION

W S EL	T WD	W PER	H RAD	VEL	V HD	ALPHA	E ELV	M E SL	TOT CONV
1012.00	212.	216.	5.15	8.99	1.26	1.39	1013.75	.001173	292036.
1011.00	206.	210.	4.31	11.07	1.91	1.23	1013.35	.001803	235497.
1010.00	100.	103.	6.78	14.29	3.17	1.00	1013.17	.002881	186310.
1009.00	94.	97.	6.22	16.58	4.28	1.00	1013.28	.004354	151555.
1008.00	88.	91.	5.65	19.53	5.93	1.00	1013.93	.006865	120697.
1007.00	82.	84.	5.07	23.42	8.53	1.00	1015.53	.011416	93593.

SEGMENT DATA

1 VS	QS	KS	2 VS	QS	KS	3 VS	QS	KS
WSEL = 1012.00								
1.29	137.	4002.	10.78	9699.	283232.	1.55	164.	4802.
WSEL = 1011.00								
1.03	53.	1249.	12.35	9883.	232749.	1.24	64.	1498.
WSEL = 1010.00								
.00	0.	0.	14.29	10000.	186310.	.00	0.	0.
WSEL = 1009.00								
.00	0.	0.	16.58	10000.	151555.	.00	0.	0.

SECT. 2

SECT DESC= TEST ONLY 1 SEGMENT NO PT= 8

Z 1	Y 1	Z 2	Y 2	Z 3	Y 3	Z 4	Y 4	Z 5	Y 5
Z 6	Y 6	Z 7	Y 7	Z 8	Y 8	Z 9	Y 9	Z10	Y10
1012.0	24.0	1010.0	30.0	1010.0	80.0	1000.0	110.0	1000.0	150.0
1010.0	180.0	1010.0	230.0	1012.0	236.0				

GR ELEV, MIN= 1000.0 MAX INTERIOR= 1010.0 LOWEST END= 1012.0

FLOW = 10000. NO OF SEGMENTS = 1

SEG = 1

PT NO = 8

STA = 236.

N = .0350

AVG HYD CHARACTERISTICS FOR SECTION

W S EL	T WD	W PER	H RAD	VEL	V HD	ALPHA	E ELV	M E SL	TOT CONV
1012.00	212.	216.	5.15	8.99	1.26	1.00	1013.26	.005044	140809.
1011.75	211.	214.	4.94	9.44	1.39	1.00	1013.14	.005874	130478.
1011.50	209.	213.	4.73	9.93	1.53	1.00	1013.03	.006889	120484.
1011.25	208.	211.	4.52	10.47	1.71	1.00	1012.96	.008141	110830.
1011.00	206.	210.	4.31	11.07	1.91	1.00	1012.91	.009703	101518.
1010.75	205.	208.	4.09	11.74	2.14	1.00	1012.89	.011674	92553.
1010.50	203.	206.	3.88	12.49	2.42	1.00	1012.92	.014193	83938.
1010.25	202.	205.	3.66	13.33	2.76	1.00	1013.01	.017460	75679.
1010.00	100.	103.	6.78	14.29	3.17	1.00	1013.17	.008823	106463.
1009.75	99.	102.	6.64	14.81	3.41	1.00	1013.16	.009748	101284.
1009.50	97.	100.	6.50	15.37	3.67	1.00	1013.17	.010795	96249.
1009.25	96.	99.	6.36	15.96	3.96	1.00	1013.21	.011982	91356.
1009.00	94.	97.	6.22	16.58	4.28	1.00	1013.28	.013333	86603.
1008.75	93.	95.	6.08	17.25	4.63	1.00	1013.38	.014876	81989.
1008.50	91.	94.	5.94	17.96	5.02	1.00	1013.52	.016644	77513.

SECT 3

SECT DESC= TEST ALL 3.N VALUES THE SAME NO PT= 8

Z 1	Y 1	Z 2	Y 2	Z 3	Y 3	Z 4	Y 4	Z 5	Y 5
Z 6	Y 6	Z 7	Y 7	Z 8	Y 8	Z 9	Y 9	Z10	Y10
1012.0	24.0	1010.0	30.0	1010.0	80.0	1000.0	110.0	1000.0	150.0
1010.0	180.0	1010.0	230.0	1012.0	236.0				

GR ELEV, MIN= 1000.0 MAX INTERIOR= 1010.0 LOWEST END= 1012.0

FLOW = 10000. NO OF SEGMENTS = 3

SEG = 1 2 3

PT NO = 3 6

STA = 80. 180.

N = .0350 .0350 .0350

AVG HYD CHARACTERISTICS FOR SECTION

W S EL	T WD	W PER	H RAD	VEL	V HD	ALPHA	E ELV	M E SL	TOT CONV
1012.00	212.	216.	5.15	8.99	1.26	1.21	1013.52	.003244	175567.
1011.50	209.	213.	4.73	9.93	1.53	1.19	1013.33	.004131	155594.
1011.00	206.	210.	4.31	11.07	1.91	1.16	1013.21	.005306	137281.
1010.50	203.	206.	3.88	12.49	2.42	1.10	1013.17	.006855	120779.
1010.00	100.	103.	6.78	14.29	3.17	1.00	1013.17	.008823	106463.
1009.50	97.	100.	6.50	15.37	3.67	1.00	1013.17	.010795	96249.
1009.00	94.	97.	6.22	16.58	4.28	1.00	1013.28	.013333	86603.
1008.50	91.	94.	5.94	17.96	5.02	1.00	1013.52	.016644	77513.
1008.00	88.	91.	5.65	19.53	5.93	1.00	1013.93	.021023	68969.
1007.50	85.	87.	5.36	21.33	7.08	1.00	1014.58	.026908	60962.

SEGMENT DATA

1 VS	QS	KS	2 VS	QS	KS	3 VS	QS	KS
WSEL = 1012.00								
3.69	391.	6860.	10.24	9219.	161847.	3.69	391.	6860.
WSEL = 1011.50								
3.47	272.	4227.	11.13	9457.	147140.	3.47	272.	4227.
WSEL = 1011.00								
3.03	156.	2141.	12.11	9688.	133000.	3.03	156.	2141.
WSEL = 1010.50								
2.19	56.	671.	13.19	9889.	119436.	2.19	56.	671.
WSEL = 1010.00								
.01	0.	0.	14.29	10000.	106463.	.01	0.	0.
WSEL = 1009.50								
.01	0.	0.	15.37	10000.	96249.	.01	0.	0.

SECT 4

SECT DESC= NATURAL SECTION NO PT= 6

Z 1	Y 1	Z 2	Y 2	Z 3	Y 3	Z 4	Y 4	Z 5	Y 5
Z 6	Y 6	Z 7	Y 7	Z 8	Y 8	Z 9	Y 9	Z10	Y10
1015.0	0.0	1010.0	50.0	1016.0	54.0	1000.0	60.0	1005.0	120.0
1015.0	200.0								

GR ELEV, MIN= 1000.0 MAX INTERIOR= 1016.0 LOWEST END= 1015.0

FLOW = 10000. NO OF SEGMENTS = 3

SEG = 1 2 3

PT NO = 3 5

STA = 54. 120.

N = .0500 .0250 .0400

AVG HYD CHARACTERISTICS FOR SECTION

W S EL	T WD	W PER	H RAD	VEL	V HD	ALPHA	E ELV	M E SL	TOT CONV
1015.00	199.	213.	6.22	7.54	.88	1.57	1016.39	.001327	274510.
1014.50	189.	203.	6.05	8.14	1.03	1.54	1016.08	.001562	252996.
1014.00	180.	193.	5.89	8.80	1.20	1.50	1015.81	.001849	232585.
1013.50	170.	183.	5.74	9.54	1.41	1.46	1015.57	.002199	213244.
1013.00	161.	172.	5.60	10.36	1.67	1.42	1015.37	.002631	194942.
1012.50	151.	162.	5.47	11.27	1.97	1.38	1015.23	.003169	177645.
1012.00	142.	152.	5.36	12.28	2.34	1.34	1015.15	.003843	161319.
1011.50	132.	142.	5.26	13.41	2.80	1.30	1015.15	.004696	145928.
1011.00	123.	132.	5.18	14.66	3.34	1.27	1015.24	.005789	131435.
1010.50	113.	121.	5.13	16.05	4.01	1.24	1015.46	.007207	117797.
1010.00	104.	111.	5.11	17.58	4.81	1.21	1015.83	.009076	104966.

SEGMENT DATA

1 VS	QS	KS	2 VS	QS	KS	3 VS	QS	KS
WSEL = 1015.00								
1.92	257.	7044.	10.31	8169.	224239.	3.94	1575.	43227.
WSEL = 1014.50								
1.95	210.	5319.	10.93	8300.	209977.	4.13	1490.	37700.
WSEL = 1014.00								
1.96	167.	3885.	11.60	8430.	196061.	4.33	1403.	32639.
WSEL = 1013.50								
1.95	128.	2721.	12.33	8558.	182499.	4.55	1314.	28024.
WSEL = 1013.00								
1.93	93.	1804.	13.12	8684.	169297.	4.78	1223.	23841.
WSEL = 1012.50								
1.87	62.	1109.	14.00	8808.	156464.	5.02	1130.	20071.

III C MANNING N VALUES AND EDDY LOSS COEFFICIENTS

TYPICAL N VALUES - FIXED BOUNDARY ANALYSIS

Natural Streams

a.	Minor streams (surface width at flood stage < 100 ft)		
	(1)	Fairly regular section	
		(a) Some grass and weeds, little or no brush	0.030
		(b) Dense growth of weeds, depth of flow materially greater than weed height	0.040
		(c) Some weeds, light brush on banks	0.040
		(d) Some weeds, heavy brush on banks	0.060
		(e) For trees within channel with branches submerged at high stage, increase all above values by 0.015	
	(2)	Irregular section, with pools, slight channel meander Channels (a) to (e) above, increase all values by 0.015	
	(3)	Mountain streams; no vegetation in channel, banks usually steep, trees and brush along banks submerged at high stage	
		(a) Bottom, gravel, cobbles and few boulders	0.050
		(b) Bottom, cobbles with large boulders	0.060
b.	Flood plains (adjacent to natural streams)		
	(1)	Pasture, no brush	
		(a) Short grass	0.030
		(b) High grass	0.040
	(2)	Cultivated areas	
		(a) No crop	0.040
		(b) Mature row crops	0.040
		(c) Mature field crops	0.050
	(3)	Heavy weeds, scattered brush	0.050
	(4)	Light brush and trees	0.060
	(5)	Medium to dense brush	0.090
	(6)	Dense willows	0.170
	(7)	Cleared land with tree stumps, 100-150 per acre	0.060
	(8)	Heavy stand of timber, little undergrowth	
		(a) Flood depth below branches	0.110
		(b) Flood depth reaches branches	0.140

EDDY COEFFICIENTS

	Contraction	Expansion
Small change in river cross-section (Gradual Transition),	.1	.3
Abrupt change in river cross-section	.6	.9

III D WATER SURFACE PROFILE COMPUTATIONS

BERNOULLI'S EQUATION APPLIED TO FLOOD PLAINS

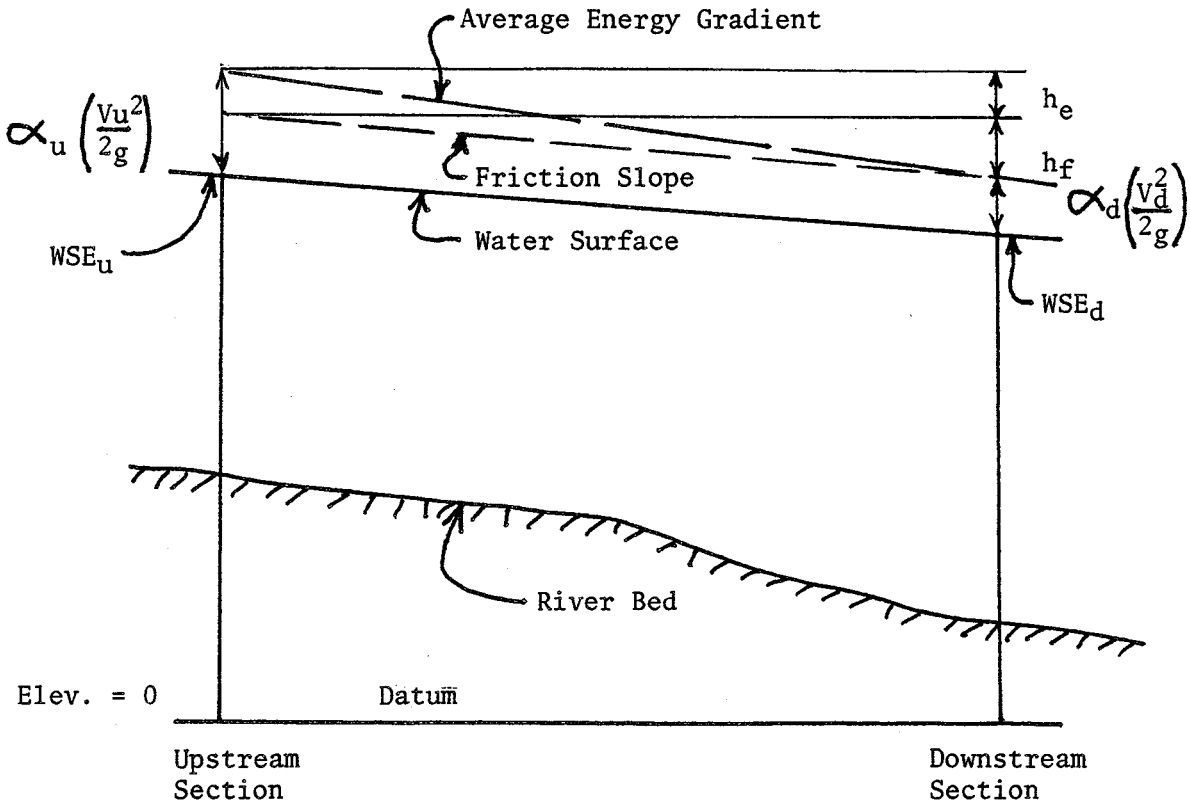

$$WSE_u + \alpha_u \left(\frac{V_u^2}{2g}\right) = WSE_d + \alpha_d \left(\frac{V_d^2}{2g}\right) + h_l$$

Where

WSE	=	Water Surface Elevation
V	=	Average Velocity
α	=	Velocity Head Coefficient
L	=	Effective Flow Length for Reach
S_f	=	Friction Slope for Reach
C	=	Eddy Loss Coefficient
h_l	=	Total Energy Loss, $h_e + h_f$
h_e	=	Eddy (Impact) Loss $= C \left\lvert \alpha_u \left(\frac{V_u^2}{2g}\right) - \alpha_d \left(\frac{V_d^2}{2g}\right) \right\rvert$
h_f	=	Friction Loss $= L \; S_f$

PLAN - TYPICAL FLOOD PLAIN

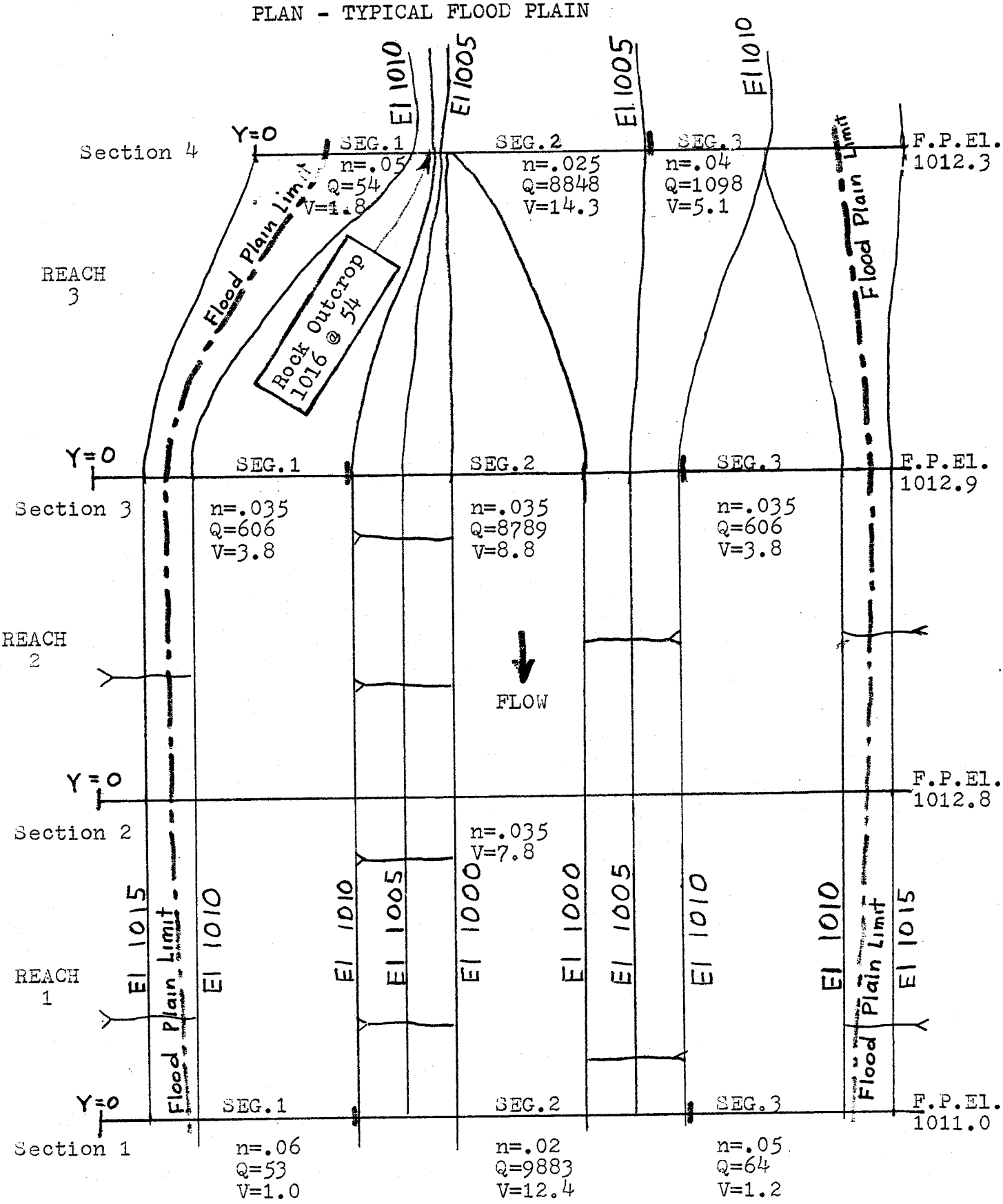

FLOOD PLAIN COMPUTATIONS, NATURAL STREAMS

```
NATURAL CHANNEL PROGRAM, PROFILE COMPUTATION

 ENTER BEGIN W S EL
? 1011.

                                                  SEGMENTS

 W S EL   T WS   A V  ALP  ENG EL   FR S   1 Q   V    2 Q   V    3 Q   V

1011.00  206.0 11.07 1.23 1013.35 .00180    53. 1.0  9883.12.4    64. 1.2

 REACH  1   LENGTH  100.   AVG S.00392   LOSS, F  .25  IMPACT  .14

1012.79  216.7  7.80 1.00 1013.74 .00324 10000. 7.8

 REACH  2   LENGTH  100.   AVG S.00298   LOSS, F  .27  IMPACT  .03

1012.94  217.6  7.61 1.22 1014.04 .00212   606. 3.8  8789. 8.8   606. 3.8

 REACH  3   LENGTH  100.   AVG S.01158   LOSS, F  .27  IMPACT  .88

1012.33  148.1 11.60 1.37 1015.19 .00338    54. 1.8  8848.14.3  1098. 5.1
```

E. PRESSURE FLOW, BRIDGE OR CULVERT

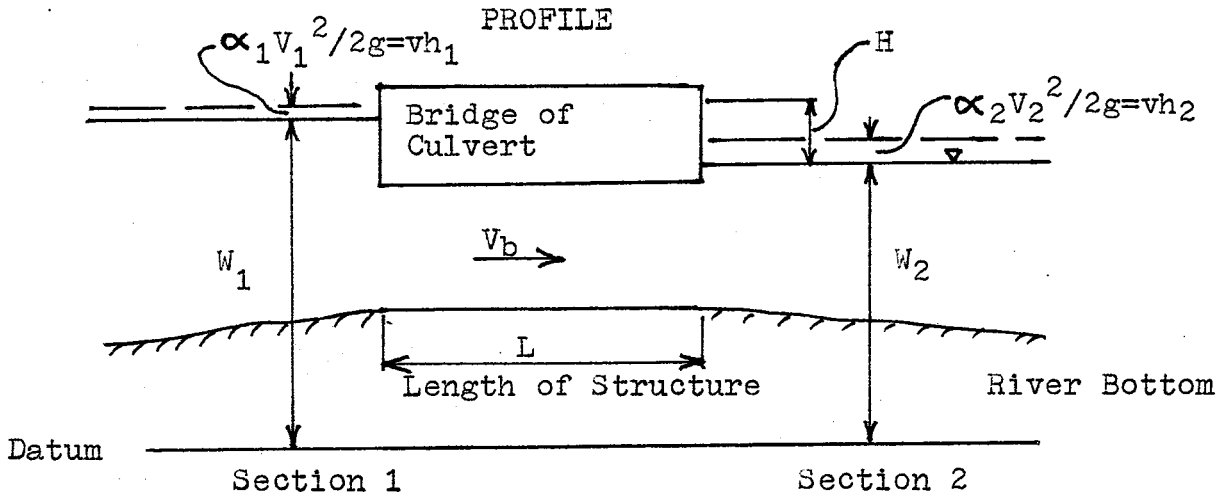

W = Water Surface Elevation

V_b = Average, Velocity in the Bridge (Culvert)

$vh_b = V_b^2/(2g)$ = Velocity head in the Bridge (Culvert)

Applying Bernoulli's Equation

$$W_1 + \alpha_1 V_1^2/(2g) = W_2 + \alpha_2 V_2^2/(2g) + h_L$$

$$W_1 + vh_1 = W_2 + vh_2 + h_L$$

Hydraulic Losses h_L

Transition Losses

Loss at structure entrance

$$h_1 = K_c\,(vh_b - \cancel{vh_1})$$

K_c is the contraction loss coefficient

The upstream velocity head is usually small compared to the bridge velocity head, and neglecting it results in a slightly higher computed water surface elevation.

Loss at structure exit

$$h_2 = K_e\,(vh_b - vh_2)$$

K_e is usually 1.0 (expansion loss coefficient)

Friction Loss - Manning Equation, Flow in Structure

$$h_f = L\ S_f = L\ (n^2 V_b^2)/(2.22\ r^{4/3})$$

$$= L[2g](n^2 V_b^2/[2g])/\ (2.22\ r^{4/3})$$

$$= L(29\ n^2\ /\ r^{4/3}\ )\ V_b^2/(2g)$$

$$= \quad K_f \qquad V_b^2/(2g)$$

where $K_f = 29\ n^2\ /r^{4/3}$

$$h_L = h_1 + h_2 + h_f$$
$$= K_c(vh_b) + 1.0(vh_b - vh_2) + K_f(vh_b)$$

Substituting into the Bernoulli Equation

$$W_1 + vh_1 = W_2 + \cancel{vh_2} + K_c(vh_b) + vh_b - \cancel{vh_2} + K_f\ vh_b$$

$$W_1 + vh_1 - W_2 = H = (K_c + 1 + K_f)\ vh_b$$

$$H = (K_c + 1 + K_f)\ vh_b = K_x\ V_b^2/(2g)$$

Pressure flow of this type is often evalutated using the orifice equation: $Q = CA\sqrt{2gH}$

Dividing both sides by the area A gives

$$V_b = C\sqrt{2gH}$$

$$H = \frac{1}{C^2}\ V^2{}_b/(2g)$$

Comparison with the previous head loss equation shows the

$$K_x = 1/C^2$$

C is frequently given the value of .8

$$K_x = 1/.8^2 = 1.56$$

III. F. FLOW OVER ROADS

Reference: HYDRAULICS OF BRIDGE WATERWAYS, U. S. Department of Transportation

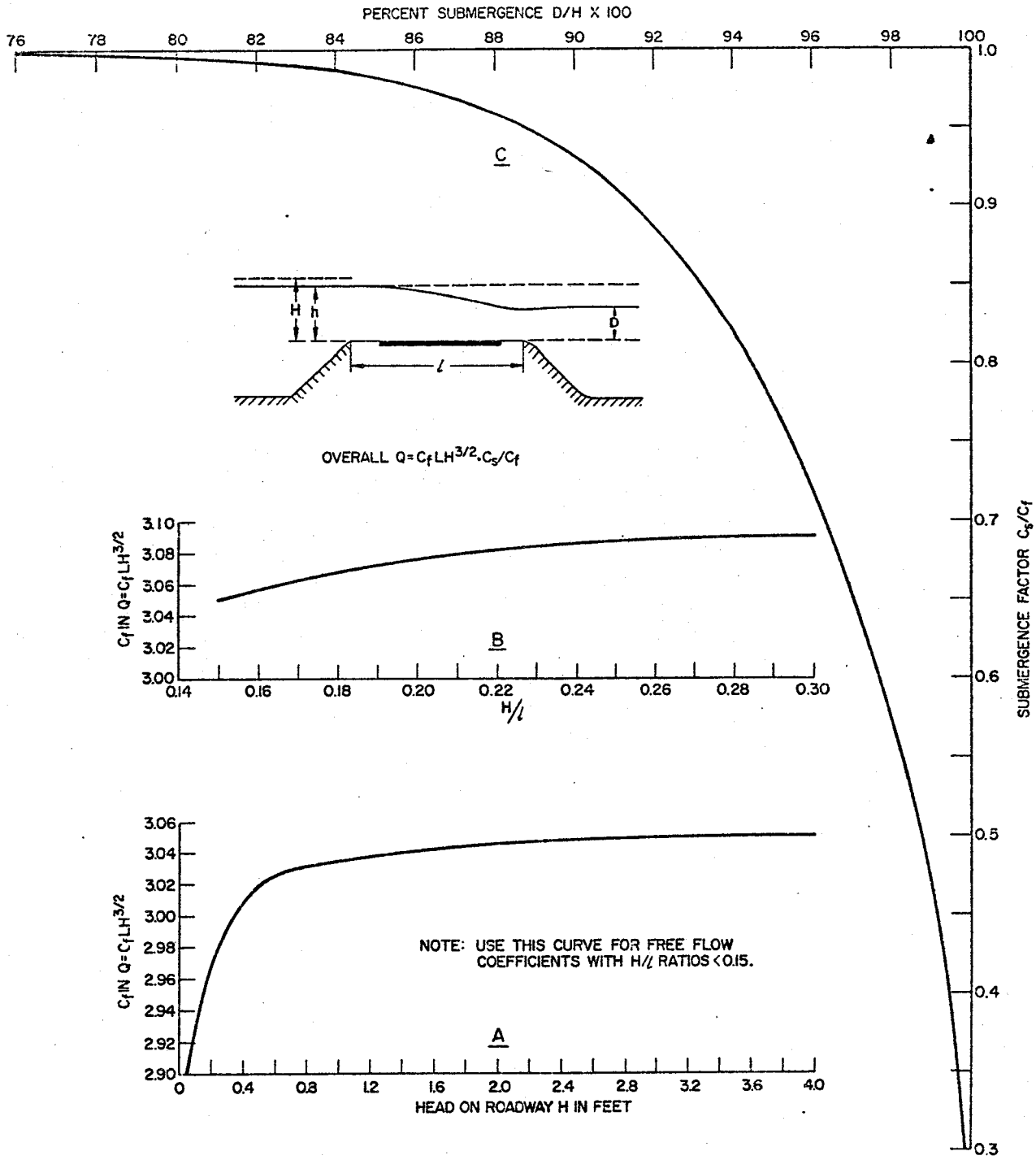

Figure 24.—Discharge coefficients for flow over roadway embankments.

Free Flow Conditions

$Q = C_f \; L \; H^{3/2}$

$q_f = C_f \; H^{3/2}$ Flow per foot of Length

For rectangular open channel hydraulics

$q = 3.087 \; Hm^{3/2}$ at minimum energy condions (Dc)

Using $C = 3.087$

Solving for H

$H = (q_f / C_f)^{2/3}$

$Hm = (q / C)^{2/3}$

Comparison of Minimum Energy Head vs. Roadway Flow

$H / Hm = ((q_f / C_f) / (q / C))^{2/3}$

Since $q_f = q$

$H / Hm = (C / C_f)^{2/3}$

TABULATION - H VS. Hm, C_f from Fig. A

H	C_f	C/C_f	$(C/C_f)^{2/3}$	Hm
4.0	3.05	1.012	1.008	4.03
1.0	3.03	1.019	1.013	1.01
.4	3.00	1.029	1.019	.41

The effect of varying the coefficient C_f is minor (compare H vs. Hm in table). Therefore, free flow over roads can be evaluated by using the cross section analysis method with minimum energy flow conditions.

Submerged Flow Conditions

Downstream conditions affect the depth, velocity and energy at a roadway embankment cross section when a submerged flow condition exists. This can be analyzed using a typical backwater computation as described previously. The computation can be checked by using the method provided in Figure 24.

AN EVALUATION OF FLOOD-LEVEL PREDICTION USING ALLUVIAL-RIVER MODELS

National Research Coundil
National Academy of Sciences

Background

At the request of the Federal Insurance Administration the National Academy of Sciences reviewed the methods and models used for evaluation of erosion and sedimentation in rivers. Three test sites were selected to test models that had been developed by four organizations.

Results of Tests

Upon evaluation of the test results it was found that different models produced significantly different results. Limitations of models include:

I. The procedure for analysis consists of using the existing condition of the riverbed and evaluating the effect of a 100-year flood. However, it is probable that many smaller floods will occur before the 100-year flood. Since it is not possible to determine the sequence of floods, and since the floods that precede the 100-year flood will make major changes in the riverbed, it is difficult to adequately define the initial riverbed conditions that will exist prior to a 100-year flood.

II. The models compute the amount of erosion or sedimentation by sub-reaches of the river. Generally speaking, erosions occur when sediment out-flow for the sub-reach exceeds the in-flow. Sedimentation occurs when this condition is reversed. The predicted sediment discharges varied greatly between models. Related variables, bed armoring and the roughness values also showed considerable differences when the results of models were compared. It was concluded that these processes are not well understood.

III. Other limitations were found in the evaluation of boundary conditions (i.e. sediment input to the river at the upstream and of the study reach and at large tributaries), bank erosion, and changing riverbed width.

Principal Conclusions

Except in cases of severely disturbed rivers which have experienced extreme local degradation or aggradation through man's intervention, utilization of

erodible-bed models instead of fixed-bed models cannot be justified in flood-insurance studies. The added cost of utilizing movable-bed rather than fixed-bed models is not justified in most cases.

An exception to the recommendation set forth above, arises in the case of severely disturbed rivers (e.g. by channel straightening or aggregate mining), or channels in very unstable conditions. If adequate input and calibration data are available, erodible-bed models should be utilized in these cases, because the large-scale geometry changes occurring during a flood can have significant flood-stage effects.

It is unlikely that a model will be forthcoming which will be applicable to all types of rivers. There is a need to classify rivers so an appropriate model can be selected.

Recommendations

I. To instill more confidence in fixed-bed models, a sensitivity analysis is needed to better understand the effects of channel roughness and shape.

II. Future modeling efforts should be directed toward channel width changes and channel-pattern migration. Large-scale tributary-sediment input needs to be better understood.

APPLIED SEDIMENTATION AND RIVER ENGINEERING
Watershed Erosion and Sediment Yield

By
Leonard J. Lane
Environmental Science Group
Los Alamos National Laboratory

CONTENTS

PAGE
INTRODUCTION.....1
WATERSHED PROCESSES.....3
DEVELOPMENT OF MODELS.....11
EXAMPLE APPLICATIONS.....22
SUMMARY.....26
FUTURE DIRECTIONS IN RESEARCH AND TECHNOLOGY.....27
ACKNOWLEDGMENTS.....33
REFERENCES.....34

INTRODUCTION

Watershed erosion and sediment yield are the primary focus of this paper. The terms watershed or watershed processes connote consideration of distributed systems with processes which are neither uniform in space nor constant in time. Watershed processes also suggest processes such as mass flux (water or sediment) relative to a specified contributing area. This contributing area is called the watershed, the drainage basin or area, or the catchment.

If one examines the landscape, and this is easier in arid and semiarid areas where geologic and geomorphic features are more readily apparent, a striking feature is that stream channels combine in complex patterns to form the channel network and the interchannel areas. The term watershed means a drainage area above a specified point on a stream enclosed by the watershed boundary or perimeter. Thus, watershed connotes a physical entity for which statements of continuity can be made.

It is often convenient to visualize a watershed as consisting of the channel network and the contributing or interchannel areas. The contributing areas can further be described as upland or upstream areas and adjacent or lateral areas. Sometimes it is convenient to further characterize the watershed as consisting of the stream channel and the upland and lateral overland flow areas. The reasonableness of this characterization varies depending upon the hydrologic systems under consideration (e.g. more accurate in agricultural and urban areas and much less so in forest environments) and upon the scale of consideration (e.g. micro vs. macro topographic features).

Background Discussion

The emphasis of our discussions is on erosion and sedimentation by water. These are the processes by which soil particles are detached, transported and deposited by raindrop impacts, runoff on the soil surface, and runoff in rills, concentrated flow areas, and stream channels (see Foster, 1982, for additional discussions).

Erosion on farm fields reduces potential crop production and sediment which leaves the field can result in subsequent sedimentation problems which in turn can cause off-site environmental problems (e.g. ASCE, 1975, 1982). Erosion on other upland areas such as construction sites, urban areas, mine developments, or other disturbed areas can also cause on-site and off-site problems (e.g. AGU, 1977; ASCE, 1975).

Channel erosion or deposition processes can cause further problems inasmuch as the stream channels are components of the watershed system (ASCE, 1975, 1982). Because we are concerned with interactive processes linking upland areas with stream channel networks and ultimately with large river systems, we are

concerned with hydrologic and hydraulic processes in their own right and because they provide the driving force for erosion and sedimentation processes.

Objectives

The purpose of this short paper, and the related classroom activity, is to:

1) Provide a background on erosion and sedimentation processes on watersheds,
2) Outline methods used to develop prediction equations and models,
3) Provide knowledge to use and interpret erosion and sediment yield models, and
4) To provide a brief assessment or forecast of some future directions in research and technology applied to watershed erosion and sediment yield.

Scope and Limitations

We will review selected existing techniques and procedures rather than seek to develop new technology. The primary emphasis is on erosion, transportation, and deposition of sediment on upland areas, in small stream channels and thus on small watersheds.

The example applications will be limited to a few specific equations and will be applied to a few specific problems. In this way, we can develop application techniques which are model and problem specific for detailed examination and discussion but which are more general with respect to problem formulation, model selection, application, and evaluation. Rather than producing many examples lacking sufficient details for understanding, we will concentrate on more thorough investigation of a few examples.

Form and Structure of Erosion/Sediment Yield Models

Just as there are an infinite number of objectives, uses, and applications for description, explanation, investigation, understanding, and prediction of erosion and sedimentation processes, there are infinite possibilities for models. These models can be conceptual, descriptive and/or quantitative. If they are not structured, organized, and "written down" or documented they cannot be passed easily from one individual to another. This does not mean they are not models. My concept of how erosion "works" is just as much a model as your mathematical equation describing a process. The concept of modeling or nonmodeling approaches in science and engineering is nonsense and a useless anachronism.

Erosion and sediment yield models can, however, be classified with respect to a large number of characteristics. Some of the most apparent and useful classifications appear in

the following discussion.

A somewhat artificial distinction can be made between component and systems models. An example might be a model of watershed systems with upland and stream channel components. One can consider index vs. quantitative models which could consider erosion as "moderate" on a verbal index or as averaging 10 g/m*m/yr on a quantitative basis. Another useful distinction is stochastic (random processes in time) vs. deterministic models. A very useful distinction is between event models and continuous simulation models. An event model might be a set of equations to predict upland erosion given a parameter set, initial conditions, and a particular rain storm and runoff event. In contrast, a continuous simulation model might maintain a daily water balance throughout the year to specify soil moisture status for runoff and erosion calculations as the result of a given rain storm. An important distinction is between lumped and distributed models. For example, a lumped model might utilize the areal mean rainfall as input (lumped in the sense that a single value is used to represent rainfall over the entire watershed) to compute runoff volume. In contrast, a distributed model might use a three dimensional coordinate system to describe rainfall amount as a function of x, y, and z. Parameters or variables can also be lumped in time as well as space, or both.

The important concept here is that these classifications are important so that a model user can form a picture of how the model is classified and how it is intended to describe processes. This, in turn, can help the user decide if the particular model is appropriate for the intended application. That is, the user can use these classifications to help decide if the model is appropriate for the problem.

WATERSHED PROCESSES

Watershed processes will be described in terms of processes occurring on upland areas, in small stream channels, and over entire watersheds. A basic source document for these concepts is a book entitled THE FLUVIAL SYSTEM, (Schumm, 1977). An idealized fluvial system is described as consisting of: Zone 1, the drainage basin as a sediment and runoff source; Zone 2, the main river channels as a transfer component, and Zone 3, the alluvial fans, deltas, etc. as zones of deposition. Further elaboration on these concepts is given by Schumm (1977) and in an American Society of Civil Engineers Task Committee Report (ASCE, 1982). The emphasis here is on Schumm's Zone 1 as further divided into upland areas and small stream channels. Considered together, they form the watershed.

UPLAND AREAS

Processes considered for upland areas include runoff, sediment detachment, transportation and deposition, and sediment yield. Hydrologic processes such as rainfall amount and

intensity, runoff amount and rate, and hydraulic processes such as flow depth and velocity drive erosion and sedimentation processes.

Runoff

Surface runoff is the result of precipitation and is the amount of water which appears in the stream channel network during and after a precipitation episode. Surface runoff as direct flow of water over the soil surface and in small definable channels is termed overland flow. Overland flow is not necessarily sheet flow, although it may be under idealized conditions and on a sufficiently small enough scale, but consists of flow to and into and in small concentrated flow channels (Foster, 1971, 1982). Overland flow is thus sheet flow on the interrill areas and channel flow in the many small rills. For surface runoff to be classified as overland flow, it must be that the mean flux per unit width of the flow area cross-section is proportional to the storage in an incremental area (e.g. see Lane, Woolhiser, and Yevjevich, 1975, pp. 1-2 for a more detailed description). When surface flow cannot be hydrologically or hydraulically treated as overland flow, it is channel flow. Again, these distinctions are somewhat arbitrary and difficult to quantitatively describe. But they are usefull conceptually and mathematically.

Two general methods are available to compute runoff on small upland areas. The first method is based on Richards' equation (Richards, 1931) or various approximations to it called infiltration equations. This method uses precipitation data as a function of time together with an infiltration equation to separate rainfall rate data (intensity) into the amount entering the soil (infiltration) and the amount which moves over the soil surface (runoff as overland flow). Basic source documents dealing with infiltration include Philip (1969), Morel-Seytoux (1973), and Skaggs and Khaleel (1982).

The second method used to compute runoff on small upland areas is based on rainfall depth alone or rainfall depth and statistics representing rainfall intensity to compute runoff volume. Given runoff volume, other procedures are then used to estimate peak rate of runoff or the runoff hydrograph. The USDA-Soil Conservation Service runoff curve number procedure is the best known and most widely used method of this type (NEH-4, 1972).

Detachment, Transportation, and Deposition

A good description of these processes is given by Foster (1982) and the following brief description follows that outline. Additional detail is given by Foster (1982), by Wischmeier and Smith (1978), by Hjelmfelt, Piest, and Saxton (1975), and by Simons, et.al. (1975).

Soil particles are detached when the impact of raindrops or the erosive force of flowing water are in excess of the ability of the soil to resist erosion. Sediment particles are

transported by raindrop splash and by overland flow. Deposition of soil particles occurs when the weight of the particle exceeds the forces tending to move it. This condition is often expressed as sediment load exceeding sediment transport capacity.

Particles detached in the interrill areas move to the rills by splash mechanisms and as a result of suspension and saltation in overland flow. Thus, their detachment and movement is independent (except for morphological features of rill and channel systems controlling length and slope of interrill areas) of processes in rill and stream channels. This situation is definitely not the case for erosion in rills and channels. The amount and rate of water and sediment delivered to the rills determines rill erosion rates , sediment transport capacity in the rills, and rate of sediment deposition.

The basic relationships between sediment load (QS), transport capacity (TC), erosion rate (E), and deposition rate (D) is

$$\text{Rate (E or D)} = \alpha(TC - QS) \tag{1}$$

where α is a coefficient. The coefficient for erosion is

$$\alpha = EM/TC \tag{2}$$

where EM is the rill erosion detachment capacity rate or the maximum erosion rate when sediment load is zero. Following Foster and Meyer (1972) the rill erosion rate equation can be rewritten as

$$E/EM + QS/TC = 1 \tag{3}$$

where E is the erosion rate. Rewriting this equation in terms of erosion rate means

$$E = EM(1-QS/TC) \tag{4}$$

with the maximum erosion rate given by rearranging Eq. 2

$$EM = \alpha\ TC \tag{5}$$

In a similar manner, the equation for rill deposition rate (D) can be written as

$$D/DM + TC/QS = 1 \tag{6}$$

with DM as the maximum deposition rate when transport capacity is zero. This equation can be rewritten as

$$D = DM\ (1 - TC/QS) \tag{7}$$

with the maximum deposition rate given as

$$DM = -\alpha QS \tag{8}$$

The coefficient α is given (see Einstein, 1968) by the ratio of the particle fall velocity, VS, to the water discharge per unit width, q, as follows

$$\alpha = eVS/q \tag{9}$$

where e = 0.5 for overland flow and e= 1.0 for open channel flow.

To summarize the previous 9 equations and show how sediment load may be different from transport capacity, Eqs. 3 and 7 can be rewritten as

$$E/EM = 1 - QS/TC \tag{10}$$

for erosion and

$$D/DM = 1 - TC/QS \tag{11}$$

which in terms of relative sediment load (QS/TC) can be written as

$$D/DM = 1 - 1/(QS/TC) \tag{12}$$

Now, Eq. 10 shows relative erosion rate, E/EM is a linear function of relative sediment load. Equation 12 shows relative deposition rate is proportional to the reciprocal of relative sediment load. These relationships are shown in Fig. 1.

The data shown in Fig. 1 suggest the following: 1) Erosion rate is at its maximum when sediment load is zero such as when clear water is directly introduced into the upstream end of a rill or channel, 2) Erosion rate decreases linearly with increasing sediment load until net erosion ceases when sediment load exactly equals sediment transport capacity, 3) Deposition rate is at its maximum when transport capacity is zero such as when flow velocity is zero in still water, and 4) Deposition rate decreases nonlinearly from its maximum with decreasing sediment load until net deposition ceases when sediment load exactly equals sediment transport capacity.

Transport capacity tends to increase with increasing flow and flow velocity. For the same flow conditions, transport capacity for smaller or lighter particles is greater than it is for larger or heavier particles. Therefore, many factors influence transport capacity and thus sediment yield. For example, the flow transport capacity in a rill or channel may exceed available sediment load. If the detachment capacity (ability to dislodge soil particles) is less than the resistance of the soil to detachment by flow, then rill or channel erosion will not occur and transport capacity will remain in excess of sediment load. This can be accomplished by lining or armoring the channel. On the other hand, if the transport capacity of a channel is less than available sediment supply from interrill erosion then deposition will occur. Consider a short rill near the top of a hillslope. Flow rate increases nearly linearly with distance from the top of the slope (at least at steady state) so that transport capacity increases with increasing slope length x. For a fixed x, increasing the interrill detachment rate can result in direct increases in sediment yield if sufficient transport capacity in the rills exists. If transport capacity in the rills is much less than the sediment suppply from interrill erosion, then increasing the interrill detachment rate may not result in corresponding increases in sediment yield. The

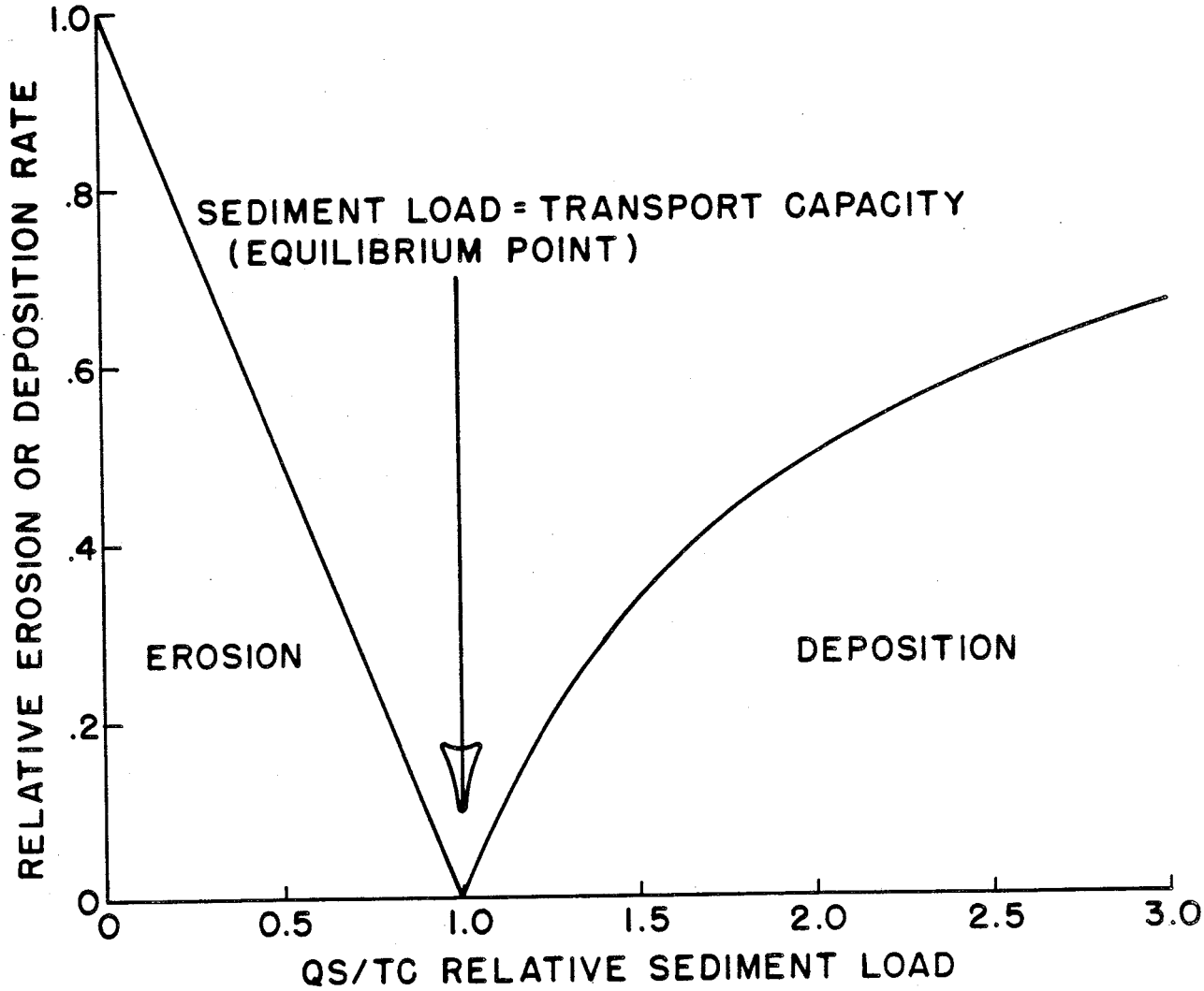

Figure 1. Schematic illustration of relationships between potential erosion rate, transport capacity, and deposition rate.

QS = TC ⇒ EQUILIBRIUM POINT

Sediment load QS can have any value relative to transport capacity.

increased sediment supplied from interrill areas may be deposited in the rills as shown in Fig. 1 and by Eq. 12.

Foster (1982, p. 301) summarizes this latter point by saying, "Most downslope movement of upland sediment is by flow in the rills. Even though excess transport capacity may exist on the interrill areas, this transport capacity does not add to the transport capacity of flow in the rills. This is subtle but a key point in using data from small experimental areas (e.g. 1m by 1m) to estimate parameter values for erosion models. Conversely, excess transport capacity in the rills is not available to transport sediment detached by raindrop impact on interrill areas." This is a key point for practical application of erosion equations and thus merits further elaboration.

Small rainfall simulators (on the order of 1m by 1m plots) are often used to estimate parameters in erosion models and to estimate the erosional impacts of various land use and treatments. These simulators on very small plots can distinguish between various treatments as they affect interrill detachments rates and can be very efficient in estimation of interrill erosion parameters in erosion/sediment yield models. They cannot be used to investigate rill and channel erosion processes nor can they be used to estimate rill and channel erosion, transportation, or deposition parameters.

Erosion data and parameter estimates obtained using these 1m by 1m plots are often found to be in disagreement with data and parameter estimates from larger plots or watersheds. These results are sometimes incorrectly used to question data and models derived from larger plots and small watersheds. While these large plot and watershed derived data and models will, and should, be subject to critical analyses, their applicability and worth should not be judged exclusively in relation to how well they agree with small plot results.

Sediment Yield

Sediment yield from upland areas is simply the final and net result of detachment, transport, and deposition processes occurring from the watershed divide down to the point of interest where sediment yield information is needed. Depending upon the scale of investigation and definition of the problem, this point of interest can be a position on a hillslope, a property boundary at a construction site, the edge of a farm field, delivery point to a stream channel, or some other location dependent upon topography. In any event, sediment yield at the point of interest is determined by the occurrence of physical processes of sediment detachment, transport, and deposition at all positions in the contributing area above the point of interest.

Sediment yield is often discussed (and even computed) based on the use of a delivery ratio defined as the change per unit area from the source to the point of interest. The delivery ratio (D in %) is often expressed as

$$D = 100\ Y/T \tag{13}$$

where Y is the total sediment yield at the downstream point of interest and T is the total material eroded (gross erosion) on the watershed area above the point of interest. Values of Y and T are given in units of mass per unit area per unit time (e.g. T/A/yr). A good description of sediment yield from upland areas is given in Foster (1982, pp 362-369) and from larger watersheds in SEDIMENTATION ENGINEERING, (ASCE, 1975, pp.437-494). The emphasis in this section is on upland areas and the delivery of water and sediment to the stream channel system and ultimately the watershed outlet.

Stream Channels and the Watershed

As interest in erosion and sediment yield extends to progressively larger land areas, the relative importance of stream channels increases. However, there are no rigorous and clear-cut criteria used to set definitive limits to distinguish between rills and small streams or channels. Agricultural definitions focus on size related to tillage. If normal tillage can obliterate the concentrated flow areas they are termed rills. If not, they are termed gullies or channels (Hutchinson, et. al., 1976; Foster, 1982). In a more recent Task Committee Report (ASCE, 1982, p. 1330) a small channel was defined as follows. "Therefore, for this report, we adopt an operational definition of a small stream or channel as a permanent feature of the landscape that conveys water and sediment from the upland areas to the major channels and acts as a sediment source or sink, depending upon the dynamic characteristics of the water-sediment flow system. Central to this definition is the sensitivity of the small channel to upland runoff and erosion processes and to hydraulic and sediment transport processes in the larger downstream channels." Notice this latter definition shares the concept of permanent feature of the landscape with the agricultural definition. As unsatisfactory as these definitions may be, they do reflect the state-of-the-art in hydrology, erosion and sedimentation, and geomorphology.

Individual Channel Segments

Discharge along a single channel segment during a runoff event, and in the absence of significant infiltration losses to the channel bed and banks, can be assumed to vary directly with upstream contributing area. If an initial discharge is allowed at the upper end of a segment to approximate flow from headwater contributing areas, then the channel segment has an upstream inflow and increasing discharge in the downstream direction due to lateral inflow.

Foster, et. al. (1981, p. 1256) described this flow

situation in farm fields as follows.

"Flow in most channels in fields is spatially varied, with discharge increasing along the channel. The model approximates the energy gradeline along the channel assuming a triangular channel section and steady flow at the characteristic peak discharge from a set of polynomial curves fitted to solutions of the normalized spatially varied flow equation (Chow, 1959). This feature approximates either drawdown or backwater at a channel outlet like the edge of a field where vegetation may hinder runoff. As an alternative in the model, the slope of the energy gradeline can be assumed equal to the channel slope. After the slope of the energy gradeline is estimated, a triangular, rectangular, or 'naturally eroded' section is selected at the user's option to compute flow hydraulics and channel erosion and sediment transport."

This description of channel segment representation in the CREAMS model (e.g. Knisel, 1980a) points out several important features of runoff and flow hydraulics in small channels. Of course, flow in these channels is spatially varied and unsteady and various options are available in approximating channel flow. Foster, et. al. (1981) selected a characteristic discharge (the peak discharge) and then assumed spatially varied but steady flow. Others have assumed uniform but unsteady flow. Still others have assumed bed slope equal to friction slope and thus applied the kinematic wave equations. Even application of the dynamic equations requires several simplifying assumptions (e.g., see Chow, 1959) and results in approximate flow calculations. Moreover, the flow perimeter (channel bed and banks) is itself variable and dependent upon flow conditions and is often termed self-formed (ASCE, 1982). Processes of alluvial bed forms and their interaction with flow hydraulics and sediment transport are very important (e.g. Simons and Richardson, 1971).

Relationships between erosion, sediment load, and deposition discussed in the section on rill erosion also apply so upland processes affecting water and sediment supply to the stream channels also affect processes in the channels. Just as localized changes in hydraulic conditions affect erosion, transport, and deposition of sediment in rills, these changes which may occur in channels have similar effects.

Small Watersheds

Upland processes and processes in individual channel segments are combined through the channel network and interchannel areas to influence runoff and sediment yield from watersheds. In addition to the complex relationships on upland areas and in stream channels, processes affecting watershed runoff and sediment yield include interactions (e.g. channel junctions and backwater) as well as land use, soil and cover characteristics, and other factors varying over the drainage area. The state-of-the-art in hydrology is such that runoff and sediment yield from watersheds cannot be adequately described or predicted without resorting to use of indices, coefficients,

fitted parameters, and the application of judgment and experience.

This does not mean that significant progress has not been made or will not be made in the future. For example, the recent publication of the American Society of Agricultural Engineers monograph, HYROLOGIC MODELING OF SMALL WATERSHEDS, (ASAE, 1982), represents a compilation of nearly two decades of significant advances over similar material included in the HANDBOOK OF APPLIED HYDROLOGY (Chow, 1964).

Several factors and trends may serve to slow comparable progress in the next two decades. Short, as opposed to long-term approaches to research and resource conservation may slow progress. Continued evolution and application of "Improved Management Styles and Techniques" wherein appearance, style, micromanagement, bureaucracy, selfishness, and misinformation grow at the expense of research and productivity may overburden science and stifle creativity and individual initiative. On the conceptual level, the incorrect (but surprisingly universal) belief that a good manager need not be competent in any particular area of science to manage research and research scientists, may result in accelerated advancement of incompetent administrators and managers at the expense of scientists and technicians.

Two important factors may tend to oppose or offset these debilitating trends in research and science. First, is the growth and increasing availability of home computers and telecommunications links from the home to major computer centers. This allows the research scientist to escape to the unmanaged and rather free environment of the home. This escape can dramatically increase creativity and productivity. The second factor is the development of artificial intelligence, especially expert systems. These systems will allow compilation and ready access to the expert judgment and experience factors necessary to predict runoff and sediment yield from watersheds. Development of expert systems will be discussed in a later section of this paper.

DEVELOPMENT OF MODELS

Following the previous discussions, the first models examined will deal with soil loss on upland areas. Next, the emphasis will be on simple watersheds. Finally, we will return to a brief discussion of models for runoff and sediment yield from larger and more complex watersheds.

The Universal Soil Loss Equation (USLE)

The most widely used and successful model used to predict soil loss from upland areas is the USLE described by Wischmeier and Smith (1978). Their publication entitled PREDICTING RAINFALL EROSION LOSSES, A GUIDE TO CONSERVATION PLANNING states on page 1, "The procedure is founded on an empirical soil loss equation that is believed to be applicable wherever numerical values of

its factors are available. Research has supplied information from which at least approximate values of the equation's factors can be obtained for specific farm fields or other small land areas throughout most of the United States. Tables and charts presented in this handbook make this information readily available for field use."

Several important points are made in these introductory comments. The phrase "an empirical soil loss equation" suggests the origin and basis of the equation. The equation and its factors are based on observations of erosion and erosion processes rather than theoretically derived relationships. The phrase "research has supplied information" makes reference to a data base consisting of over 10,000 plot-years of data from 37 locations in 21 states used to develop the USLE. Since its development, additional plot data have been collected in many other states and other countries to evaluate USLE factors under a variety of conditions. These efforts will no doubt continue for the foreseeable future. The phrase "for specific farm fields or other small land areas" limits the intended application to upland areas as described earlier and emphasizes agricultural systems, expecialllly farm fields. The phrase "Tables and charts presented..." illustrates the methodology used to prepare the Handbook and its intended level of use as a tabular and graphical handbook. Finally, the Handbook is intended to help in choosing guidelines for selection of erosion control practices on farms and other erosion prone areas.

Wischmeier and Smith (1978, p.3) also state "The USLE is an erosion model designed to predict the longtime average soil losses in runoff from specific field areas in specified cropping and management systems." This comment can be interpreted to mean that the USLE is intended to compute average annual soil loss and the result should be seen as a long-term average annual value.

The USLE was originally derived and presented in English units. Conversion to SI units was accomplished after the fact. Therefore, the presentation herein will follow the original presentation in English units. The USLE is

$$A = R\ K\ L\ S\ C\ P \tag{14}$$

where the terms are described as follows.

The variable A is the computed soil loss per unit area and is most often expressed as an average annual value in tons per acre per year.

Rainfall and Runoff Factor

The R factor is described as a rainfall and runoff factor and is computed as the product of rainfall storm energy (E) and the maximum 30-minute rainfall intensity (I30). The product term (EI) is described by Wischmeier and Smith (1978, p. 5) as "a statistical interaction term that reflects how total energy and

peak intensity are combined in each particular storm. Technically, it indicates how particle detachment is combined with transport capacity." Total energy refers to raindrop detachment and peak intensity refers to the peak rate of runoff. The R factor is often misinterpreted as a rainfall factor only. However, if one conducts regression analyses with data from small upland areas I30 is often most strongly correlated with runoff volume or peak rate of runoff. To the extent that regression equations summarize a data set and result in prediction ability, I30 is a runoff predictor in the R factor.

The energy parameter can be computed from rainfall intensity data using

$$E = 916 + 331 \text{ LOG10 } I \tag{15}$$

where E is kinetic energy in hundreds of foot-tons per acre-inch and I is intensity in inches per hour for a given time period wherein rainfall intensity is constant. Values of E for I greater than 3 inches per hour are assumed to be given as E = 1074 as an upper limit. Equation 15 is applied over each interval in a storm and the sum is rainfall energy. Tabular data for rainfall energy computation are also given in Table 19 on p. 56 of Wischmeier and Smith (1978). However, Eq. 15 and Table 19 give E in terms of hundreds of foot tons per acre so that the cumulative E values (over a storm or over a year) <u>must</u> be divided by 100 before multiplication by I30 to compute EI and thus the annual value of R by summation.

Figures 1 and 2 in Wischmeier and Smith (1978) show average annual values of the rainfall erosion index for the United States. These maps can be used to estimate R for use in the USLE. An approximate equation to estimate R is

$$R = 27.38 \text{ P ** } 2.17 \tag{16}$$

where R is an estimate of the average annual rainfall erosion index in (foot-tons per acre) (in per hr) and P is the 2-yr, 6-hr rainfall amount in inches.

Therefore, if storm rainfall intensity data are available then a value of E can be computed for each storm by summing over uniform intensity periods within each storm. These summed individual storm values are then multiplied by the corresponding I30 values for each storm and then summed over the entire year. This annual value of EI is then divided by 100 as a value of R for that year. If this procedure is repeated over several years an average annual value of R can be estimated. If rainfall intensity data are not available or are unsuitable because of short records, etc., then Figs. 1 and 2 in the USLE Handbook can be used to estimate R. Finally, a rough approximation is given by Eq. 16. Within the continental United States, values of R range from less than 20 to over 550.

Soil Erodibility Factor

The soil erodibility factor, K in units of (tons/acre) (acre/ft.-tons) (hr/in), is the soil loss rate per erosion index unit for a specified soil as measured on a unit plot. A unit plot is defined as a 72.6 ft. length of uniform 9% slope continuously in clean-tilled fallow condition. Note: under these unit plot conditions LS = 1, C = 1, and P = 1 so that LSCP = 1. With these values it must be that A = RK so that if R is plotted on the horizontal axis and A is plotted on the vertical axis, then K is the slope of the line through the origin expressing A as a function of R.

Figure 3 on p.11 of the USLE Handbook (Wischmeier and Smith, 1978) is a nomograph for K as a function of percent sand, silt, clay, and organic matter as well as soil structure code and soil permeability class. Computed values of K range from about 0.02 to 0.70 with most agricultural soils having values in the range 0.10 to 0.40 (e.g. see Table 1, p.9 of the USLE Handbook).

Slope Length and Steepness Factor

The factor LS is dimensionless and is the expected ratio of soil loss per unit area of a field slope to that from a unit plot. A 72.6 ft. uniform slope at 9% would have an LS value of 1.0. Table 3 on p.12 and Fig. 4 on p. 13 of the USLE Handbook give LS values for various combinations of slope length and steepness. For example, a uniform slope length of 25 ft. would have a LS value of 0.06 for 0.2% slope and a value of 2.04 for 20% slope steepness. These estimates are based on data from plots with slopes ranging from 3 to 18% steepness and 30 to 300 feet in length. Within these limits (3 to 18% steepness and 30 to 300 feet length) LS values range from a low of about 0.2 to a high of about 6.

Cover and Management Factor

The cover and management factor C is dimensionless and is the ratio of soil loss from an area with specified cover and management to that from an identical area in tilled and continuous fallow and is a measure of the combined effect of <u>all</u> cover and management variables affecting soil loss. The C factor is the most difficult factor to estimate (under most conditions, except the unit plot) in the USLE. At a particular site, once K, LS and P have been measured or specified then R can be measured or calculated. The C factor is then determined over time (cover and management practices take time to implement and their combined and interactive influences may take months or years to stabilize) and on a mostly empirical basis. Moreover, because vegetative cover develops over time and with the seasons as controlled by plant physiology, climate and weather, management, soil characteristics, etc., it is highly dynamic and highly variable. Therefore, the C factor lumps an enormous

amount of information on biological, chemical, physical, and land use or management induced variability into a single coefficient. Under these conditions, its specification involves a great deal of judgment and subjectivity based upon empirical data and experience. Moreover, the reliability of C factor estimates is a function of all these interactive and ill-defined relationships so that true measures of its variability are impossible in the objective sense or data and judgment based in a heuristic sense.

Within each climatic zone there are periods during the year when highly erosive rainfall episodes are expected (subject to localized and short-term weather patterns) and periods of poor to good plant cover. Therefore, for the some soil, topography, rainfall energy, etc. if the degree of correspondence between rainfall periods and plant growth stages varies between regions, then the value of C for the same cropping system will vary between the regions. Under these conditions, it is necessary to derive C factors for the localized climatic and plant growth relationships.

The USLE Handbook describes various items affecting estimated C factors as follows: 1) Cropstage periods to represent the seasonal changes in effectiveness of plant cover, 2) Crop canopy as a measure of the degree of protection provided by the canopy, 3) Residue mulch as a measure of "on-ground" protection from raindrop impact, 4) Incorporated residues affecting the top few inches of soil, 5) Tillage as it affects the soil, residues, etc., and 6) Land use residuals such as the influence of plant roots, organic matter, and other factors of interseasonal importance.

Table 5 on pp. 22-24 of the USLE Handbook lists several hundred soil loss ratios for croplands. Values in Table 5 range from 1 to 1.40 representing soil loss ratios of from 1% to 140% of the soil loss from a continuous fallow plot. Entries in Table 5 include cover, crop sequence, and management as well as spring residue and % cover after planting, and cropstage from fallow to seedbed preparation, and crop cover from seedbed to complete canopy cover. Tables 6-12 and Figs. 5-9 in the USLE Handbook present additional information on estimating C factors for other cropping practices, for pasture and rangeland sites, and for climatic adjustments for seasonal variations in EI.

Research efforts are underway throughout the United States and in several other countries to determine C factors under a variety of conditions. Two general approaches are used separately and in combination. First is the subfactor approach wherein C for a particular situation is estimated based on the known influence of component processes via a subfactor approach. The second method is to transport portable rainfall simulators to various locations to derive on-site estimates of C factors using simulated rainfall. These efforts are producing additional estimates of C Factors beyond those summarized in the USLE Handbook.

Support Practice Factor

The support practice factor P is a factor used to represent

the ratio of soil loss with a specific support practice to the soil loss on a unit plot. The most important support practices for cropland are contour tillage, stripcropping on the contour, and terrace systems. The P factor is described (for croplands) on pp. 34-39 of the USLE Handbook. Values of P for contouring range from about 0.6 to 0.9, for stripcropping about 0.3 to 0.9, and for contour farmed and terraced fields from about 0.05 to 0.9. Therefore, a reasonable range for P is from 0.05 to 1.0 depending upon the site specific conditions described in the USLE Handbook.

General Comments

The USLE, as an empirically derived and data based model shares the strengths and weaknesses of such procedures. In terms of its main factors (RKLSCP), it is a linear equation but in terms of how physical features and management practices affect the factors, it is nonlinear. For example, LS is a nonlinear function of slope length and steepness and C is a nonlinear function of the % mulch cover.

The USLE is intended to estimate long-term average annual soil loss from upland areas. The emphasis in development of the equation was on agricultural areas of the humid United States. Users and potential users should keep these two facts in mind in application of the USLE.

The USLE has provided a focus and a methodology of conducting erosion and soil conservation research for decades. As a method for focusing research and as a method of summarizing research data representing complex processses and interactions, the USLE has served a very useful purpose. The USLE is the most widely known and accepted method of predicting erosion and of evaluating the influence of erosion control methods. The equation and its associated methodology will probably be used in these ways for the foreseeable future. However, research scientists and users should not see the USLE as a true and final representation of erosion, erosion prediction, and erosion research. The USLE is a step in our continuing efforts to develop understanding and improved models to estimate erosion and sediment yield.

Models for Erosion Dynamics on Upland Areas

A large number of erosion-sediment yield models has been developed. Some of these models use the USLE as a starting point and imporove or elaborate upon particular components or processes. Others begin formulating erosion/sediment yield processes independently of the USLE structure and solve the resulting equations. Foster (1982) summarizes several of these models in tabular format and Knisel (1980b) discusses several models. Although all of these models are in some way related to the USLE, two usefull classifications are whether or not the model is directly related to the USLE.

USLE Modifications

Onstad and Foster (1975) modified the R factor in the USLE to explicitly account for rainfall and runoff separately. This modification was intended to allow individual storm (rather than long term average) estimation of upland soil loss. All other factors in the USLE retained their original interpretation and meaning.

Williams (1975) modified the USLE (called MUSLE for "Modified USLE") to replace the R factor by a runoff factor and to interpret the other USLE factors on a watershed-wide basis. Thus, MUSLE is really a watershed rather than upland sediment yield model and will be discussed in greater detail later.

The ANSWERS model (Beasley, 1977) is a complex and distributed model to estimate erosion and sediment yield in time and over a watershed for individual runoff events. This is a watershed rather than upland model, but is based in part on USLE parameters and factors. The CREAMS model (Knisel, 1980a) estimates erosion and sediment yield on an individual storm basis (not dynamics during or within the storm as in ANSWERS) and incorporates some USLE parameters and factors. The CREAMS model will be discussed in greater detail later.

Other Upland Models

Of all the alternative formulations of erosion dynamics on upland areas, the most useful for the present discussions are those directly coupled with the kinematic wave equations for runoff on a plane. Other formulations or models consisting of a cascade of planes and channels to represent an entire watershed could be considered. But for the present discussions, emphasis will be on a single plane used to represent upland or lateral overland flow areas.

Kinematic wave equations for overland flow on a plane have been shown to apply (with consequent parameter distortions dependent upon the degree of surface irregularity) to many irregular surfaces (e.g. Woolhiser, Hanson, and Kuhlman, 1970). Such surfaces can include topographically simple upland areas on natural watersheds. For these conditions, the one-dimensional kinematic wave equations for a plane are:

$$\partial h/\partial t + \partial q/\partial x = p(t) - f(t) \tag{17}$$

and

$$q = Kh^{m} \tag{18}$$

where h is the local depth of flow per unit width, q is the runoff rate per unit width, p(t) is rainfall rate, f(t) is

infiltration rate, K and m are parameters, t is time, and x is distance down the plane. Equation 17 is the continuity equation and Eq. 18 is a simplified momentum equation wherein the friction slope is assumed equal to the slope of the plane (see Huggins and Burney (1982) as a recent reference describing these equations). In general, p(t) and f(t) are given by complex and numerical rather than analytical functions so that Eqs. 17 and 18 are solved numerically.

The continuity equation for sediment particles traveling with the mean water velocity is given by

$$\partial(ch)/\partial t + \partial qs/\partial x = EI + ER \tag{19}$$

where c is sediment concentration, qs is sediment discharge rate, EI is interrill erosion rate, and ER is rill erosion rate. Notice that EI and ER are complex functions of many factors as described earlier.

Based upon previous work (e.g. Foster, Meyer, and Onstad, 1977; Hjelmfelt, Piest, and Saxton, 1975; Shirley and Lane, 1978; and Lane and Shirley, 1982), several simplifying assumptions for Eqs. 17-19 can be made which allow derivation of analytic solutions. If the difference between rainfall and infiltration rates in Eq. 17 can be approximated as a step function (i.e. p(t) - f(t) = r) then analytic solutions to the runoff equations are available. If we further assume that qs = cq and

$$EI = KIr \tag{20}$$

and

$$ER = KR\ (Bh\ **\ m - qs) \tag{21}$$

where r is rainfall excess rate, KI is an interrill coefficient, KR and B are rill coefficients, and the other variables are as described above. If we further let

$$Bh**m = B/Kq \tag{22}$$

then Eqs. 17-22 form a kinematic wave model for runoff and erosion on a plane.

Foster, Meyer, and Onstad (1977) specified the approximate forms of the erosion equations (Eq. 19-22). Hjelmfelt, Piest, and Saxton (1975) derived an analytic solution to the model (Eqs. 17-22) for the rising portion of the hydrograph but not for the recession. Shirley and Lane (1978) solved the equations for the entire hydrograph and derived a sediment yield equation by integrating the solution to the model. Lane and Shirley (1982)

applied the model to runoff and sediment data from erosion plots and a small watershed to derive parameter values.

The solution to the model (Eqs. 17-22) is runoff rate $q(x,t)$, sediment concentration $c(x,t)$, and thus sediment discharge rate $qs(x,t) = c(x,t)\ q(x,t)$, as functions of distance (x) and time (t). These solutions are integrated with respect to time to produce a sediment yield equation $QS(x)$ as

$$QS(x) = Q(x)\ (B/K + (KI - B/K)\ F(x)\ ) \tag{23}$$

where $QS(x)$ is sediment yield as a function of distance down the plane, $Q(x)$ is runoff volume at x, the other variables are as described above, and $F(x)$ is a function of x. The function F is given as

$$F(x) = (1-\exp(-KRx))/(KRx) \tag{24}$$

Now if both sides of Eq. 23 are divided by the total runoff volume, $Q(x)$, then Eq. 23 becomes an equation for the time average sediment concentration as a function of distance. That is,

$$CBAR\ (x) = B/K + (KI - B/K)\ F\ (x) \tag{25}$$

is an equation for the time average sediment concentration during a runoff event and at a particular x.

The limit of $F(x)$ as x approaches zero is 1.0 so that in the limit

$$CBAR\ (0) = C0 = KI \tag{26}$$

is an expression for the initial concentration as runoff begins. Notice that $C0 = KI$ is a statement that the initial concentration (at $x = 0$ and $t = 0$, and in fact, at $t = 0$ for all x) is equal to the interrill detachment rate.

The limit of $F(x)$ as x approaches infinity is zero so that in the limit

$$CBAR\ (\infty) = B/K \tag{27}$$

is an expression for the time average sediment concentration for infinite distances down the plane. Notice that Eq. 27 can be interpreted as a limiting case where sediment concentration

appproaches the sediment concentration corresponding to transport capacity in the rills.

Therefore, the quantity (KI -B/K) can be used as a measure of how this upland model deals with detachment capacity, transport capacity, and sediment load. If B/K is less than KI, then interrill detachment rate is always in excess of rill transport capacity. Under these conditions then 1) at any particular time, sediment concentration will decrease with distance down the plane and 2) at any particular distance, sediment concentration will decrease with time during the period of runoff. If B/K is exactly equal to KI, then sediment concentration is constant with time and uniform with space during runoff because interrill detachment rate is exactly equal to rill transport capacity. If B/K is greater than KI, then rill transport capacity is always in excess of interrill detachment rate. Under these conditions then 1) At any particular time, sediment concentration will increase with distance down the plane and 2) At any particular distance, sediment concentration will increase with time during runoff.

In the first case (B/K < KI) sediment yield will be limited by transport capacity in the rills. The second case (B/K = KI) is a steady-state and uniform case and is highly unlikely. In the third case (B/K > KI) sediment yield will be limited by interrill detachment if net rill erosion is limited or by rill erosion rate is significant rill erosion occurs.

In terms of the USLE parameters, case 1 (B/K < KI) is likely to occur on shallow slopes with erodible soils and little cover protection (low LS, high K, and high C factors). Case 3 is likely to occur on steep slopes and some cover protection (high LS, moderate to low K, and low to moderate C factors).

A very approximate, but useful, rule-of-thumb for field observations is as follows. Case 1 (B/K < KI, tranport capacity limited) look for: 1) Rills, if apparent, with trapezoidal cross-sections and flat, sandy bottoms, and 2) Small stones or other mulch elements suspended on columns suggesting they provided protection from raindrop impact. Case 3 (B/K > KI, detachment limited) look for: 1) Rills with incised bottoms in a V-shape, and 2) stair-stepped longnitudual slope in the rills characterized by small headcuts or nick points. Of course, the observer should expect to see all of these conditions during field inspections so interpretation will be a matter of sampling method, sampling frequency, extent, and judgment.

The results summarized above are for simplifying assumptions necessary to obtain analytical solutions to Eqs. 17-19. More realistic assumptions on the infiltration process or more complex geometries consisting of cascades of planes and channels require numerical solution of the basic equations. Foster (1982, pp. 370-372) summarizes several important contributions in this area of modeling and provides comments useful in selecting an appropriate model for a particular application.

Watershed Models

Watershed models used in computation of sediment yield from

watersheds vary in complexity depending primarily upon two considerations. The first consideration is the level of detail represented by the equations comprising the model and is a measure of the conceptual and mathematical complexity. The second consideration, for a particular model, is the size and complexity of the prototype watershed represented by the model. For the present discussion, models for overland flow with sheet and rill erosion are classified as upland models. If channel processes are included in the model representation then it is termed a watershed model. Under these criteria the USLE is an upland model while the CREAMS model (although a field scale as opposed to basin scale model) is a watershed model because it includes channel processes. However, the CREAMS model can only deal directly with watersheds characterized by overland flow contributing to a channel segment. Other models such as ANSWERS can simulate sediment yield from watersheds with complex channel networks. Foster (1982) presents a useful summary of many important models and Knisel (1980b) presents an overview of erosion and sediment yield models.

Selected models which incorporate a lumped or index approach to estimation of sediment yield are summarized in Table 1. The MUSLE (Williams, 1975) approach uses USLE factors (averaged over a watershed area) except that the R factor is replaced by a function of runoff volume and peak rate of runoff. This model is relatively easy to use and has been applied on a large number of watersheds. The PSIAC (1968) model was developed as an index or classification method involving factors representing geology, soils, climate, runoff, topography, ground cover, land use, upland erosion, and channel erosion/sediment transport. These factors are combined to produce a rating factor. Based upon the rating, average annual sediment yield is estimated as being in one of five intervals or ranges. Flaxman's method is based upon a regression equation involving average annual precipitation and temperature, average watershed slope, and soil factors. The last entry in Table 1 does not refer to a specific model but a technique or methodology called the delivery ratio approach. The cited references provide basic information on background and the specific form of the equations used to approximate a delivery ratio.

Selected models which incorporate a simulation approach to estimate runoff and sediment yield from watersheds are summarized in Table 2. The Negev (1967) model is based on an early and successful hydrologic simulation model, the Stanford model, (Crawford and Lindsley, 1962). As such, it represented a method of driving erosion/sediment yield models using a hydrologic model and directly incorporated runoff rates and amounts rather than runoff indices. A comprehensive watershed model was developed at Colorado State University and is called the CSU model in Table 2. The model includes overland and open channel flow, bedload and suspended sediment, and sediment routing by particle size classes. Many of the parameters can be estimated from previous analyses and the number of parameters requiring calibration will probably decrease in the future as the model receives wide use. As for all basin scale models, the amount of parameter distortion caused by lumping as watershed size increases is unknown. The

Table 1. Summary of selected models as lumped, simplified, or index procedures to estimate watershed erosion and sediment yield.

MODEL	REFERENCE	COMMENTS
MUSLE	Williams (1975)	Modification of USLE using runoff volume and peak rate in place of the R factor. Sediment yield equation for individual storms.
PSIAC	PSIAC (1968)	Classification method involving 9 factors (high, moderate, and low) to estimate annual sediment yield in Pacific-Southwest.
Flaxman	Flaxman (1972)	Regression equation for reservoir design in the West. Average annual sediment yield.
Delivery Ratio	ASCE (1975) ARS (1975)	Basic references for delivery ratio approach in estimating sediment yield.

Table 2. Summary of selected models as simulation procedures to estimate watershed erosion and sediment yield.

MODEL	REFERENCE	COMMENTS
Negev	Negev (1967)	Example of a distributed erosion and sediment yield model coupled with a hydrologic model.
CSU	Simons, et.al.(1975) Simons and Li (1976) Li (1979)	Erosion and sediment yield in overland flow and open channel flow. Kinematic cascade model. Has been applied under a variety of conditions. Basin scale model for individual events.
ANSWERS	Beasley (1977)	Incorporates some USLE parameters and is based on a grid network to distribute parameters. Designed as a basin scale model for agricultural areas.
CREAMS	Knisel (1980a)	Erosion and sediment yield model for simple watersheds (field scale). Estimates are for an entire storm event with continuous hydrologic simulation between events. Uses some USLE parameters.

ANSWERS model was developed primarily for agricultural areas and thus makes use of some USLE parameters. It is based on a grid network scheme to segment a watershed so it shares the strengths (repeatability, compatability with remote sensing and map specified parameters, etc.) and the weaknesses (parameter estimates often a function of grid size, grid intersections overlap topographic features, etc.) of grid based procedures. The CREAMS model simulates erosion and sediment yield for individual storms but uses runoff volume and peak discharge. Thus, it does not account for dynamic variations within the runoff hydrograph except in an appproximate sense. The CREAMS model uses some USLE parameters and was designed to be used with a minimum amount of calibration. The CREAMS model (like the USLE and the CSU model) has received wide use and will probably receive extensive use in the future.

Finally, a very useful inventory of currently available hydrologic models is given by Renard, Rawls, and Fogel (1982). They provide references, abstracts, and information on processes simulated, geographic area, and land use for 75 hydrologic models. Of these 75 models, 17 include erosion and sediment yield components. Renard, Rawls, and Fogel (1982, p. 510, Table 2) list 10 references which also summarize and catalog hydrologic models. Therefore, potential model users may benefit from the material presented by Renard, Rawls, and Fogel (1982) in their Appendix A and Table 2.

EXAMPLE APPLICATIONS

This section deals with example applications for models used to estimate erosion and sediment yield. Detailed examples for the USLE are presented to illustrate typical applications. The USLE is simple enough so details can be included in the examples. Next, a series of example problems are presented and suggestions are presented for models thought to be appropriate for each problem. Of course, the more complex models are too detailed to describe herein and they require computer facilities. However, it is possible to suggest why and how they are (or are not) applicable to a certain problem.

Example Applications of the USLE

These examples are intended to illustrate some typical and appropriate applications of the USLE. Refer to the USLE Handbook for figures and tables cited.

Example 1. Bare Soil, Tilled

Given: A uniform hillslope in the Four Corners area with: 1) Slope steepness of about 10% and length of 100 ft, 2) A sandy clay soil and 45% clay, 5% silt, 20% very fine sand, and

30% sand, and 3) cover treatment practices characterized as bare soil tilled up and down slope.

Find: The average annual soil loss expected under these conditions.

Solution: From Fig. 1 of the USLE Handbook estimate an average annual R value of about 20. Given 25% silt and very fine sand, assume 1% organic matter, a fine granular structure, and slow permeability. Enter Fig. 3 and estimate a K value of 0.15. From Fig. 4 estimate the LS factor at about 1.4. As the slope is tilled up and down slope similar to a unit plot, estimate the C factor as 1.0. Finally, as no engineering practices are involved use a value of 1.0 for P. We can now apply the USLE as follows

$$A = RKLSCP$$

which is

$$A = (20)(.15)(1.4)(1.0)(1.0) = 4.2 \quad T/A/yr$$

as the estimated long-term average annual soil loss.

Example 2. Bare Soil, Undisturbed

Given: The conditions in Example 1, except assume no tillage or other disturbances for several years and no vegetation is allowed to grow on the hillslope (chemical fallow).

Find: The average annual soil loss under these conditions and the percent change in soil loss from Example 1.

Solution: The only USLE factor affected by the change in management (tillage to chemical fallow) is the C factor. Table 10 on page 32 of the Handbook lists C factors for permanent pasture, range, idle land, or grazed woodland. Bare soil means no appreciable canopy and zero percent ground cover so enter row 1, column 4 of Table 10 to estimate the C factor as 0.45. Because all other factors remained unchanged the average annual soil loss under these conditions is 45% of the soil loss in Example 1 or A = 1.9 T/A/yr. Therefore, by not disturbing the soil the estimated average annual soil loss was reduced from about 4 to about 2 T/A/yr.

Example 3. Grass Cover, Texas Panhandle

Given: The conditions in Example 1 except the hillslope is in the upper Texas Panhandle and we are able to establish and maintain a good grass cover (say 40% ground cover).

Find: The average annual soil loss.

Solution: From Fig. 1 in the Handbook the average annual R values in the Texas Panhandle range from about 100 to 150. From Table 10 for 40% ground cover with grass and no appreciable canopy the C factor is 0.10. Under these conditions the USLE is

$$A = RKLSCP$$

which for the stated conditions becomes

$$A = (R)\ (.15)\ (1.4)\ (0.1)\ (1.0)$$

or A = 0.021 R. For the given range of 100 to 150 for R, this means that the estimate for A varies from 2.1 to 3.15 T/A/yr.

Example 4. Gravel Mulch, Erosion Pavement

Given: A fifty foot hillslope at 12% steepness near Memphis, TN. The soil is a sandy loam with 10% clay, 20% silt, 20% very fine sand, 50% sand, and about 1% organic matter.

Find: The average annual soil loss from undisturbed bare soil and from bare soil covered with a gravel much at the rate of about 70 tons per acre.

Solution: Gravel with an average diameter of 1 inch and a specific gravity of 165 lb/cu ft has the following particle characteristics: volume = 0.000303 cu ft, weight = 0.05 lb, and cross-sectional area = 0.00545 sg ft. Seventy tons per acre is equivalent to 3.21 lb/sq ft of gravel per sq ft of surface area or about 35% coverage of the soil surface. The USLE factors for the given conditions are: R = 300, K = 0.29, LS = 1.3, and P = 1.0. From Table 10, the C factor for undisturbed bare soil is 0.45. If gravel mulch at 35% ground cover acts the same as vegetative cover, interpolation between 20% and 40% ground cover in the first row of Table 10 produces an estimate for C of about 0.12. Table 9 lists C factors for gravel mulch as 0.05 for 135 T/A and 0.02 for 240 T/A. Extrapolating these data back to a value of 70 T/A on log-log paper produces an estimated C factor of 0.17. Therefore, the estimate of C for 70 T/A of gravel mulch is about 0.12 to 0.17. With the specified values the USLE becomes

$$A = (300)\ (0.29)\ (1.3)\ (C)\ (1.0)$$

or A = 113 C. For C in the range 0.12 to 0.17 the estimated average annual soil loss with gravel mulch is 13.6 to 19.2 T/A/yr. Undisturbed bare soil with C = 0.45 would produce an

estimate of about 51 T/A/yr. Thus, 70 T/A of gravel mulch would probably reduce the average annual soil loss by about a factor of three. If we assumed disturbed soil conditions then this rate of gravel mulch might reduce the average annual soil loss by a factor of about seven.

Example 1 illustrated how the USLE is used to calculate average annual soil loss and how the USLE Handbook is used to estimate R, K, LS, and P. Example 2 illustrated a way to estimate the influence of management practices (tillage vs undisturbed soil in this example) on the C factor. Example 3 illustrated the influence of vegetative cover upon the C factor and Example 4 considered methods to estimate the C factor for a specified rate of gravel mulch as an engineeering practice used to control erosion.

The four USLE examples should provide an understanding of how the USLE and the Handbook can be used to make estimates of expected average annual soil loss rates and how the various factors affect the magnitude of those estimates. Moreover, the examples illustrate the general type of problems for which the USLE provides a quick and easy method of deriving solutions.

Example Problems and More Complex Models

In this section, the emphasis is on problem classification and how this classification is related to model selection. This can be stated another way. If we analyze and classify a particular problem, will this information be of use in selecting the appropriate models to apply in reaching a solution?

Upland Erosion

Given the conditions in Example 1, which models might be appropriate to answer the following questions. 1. Is soil loss, on the average, likely to be limited by detachment processes or transport processes? 2. What is a reasonable range (in % by weight) in expected sediment concentration during a "typical" runoff event? 3. What is the particle size distribution one might expect for eroded sediment in the runoff? 4. What would be the influence on sediment yield if the slope were concave or convex? 5. To meet prespecified design criteria, how would one estimate the volume of runoff and total sediment yield for a 25 year storm?

These questions and the suggested models are summarized in Table 3. Other models could be equally applicable, but of those discussed, the ones listed in Table 3 are thought to be most appropriate. For example, Question 4, influence of slope shape, is particularly suited to the CREAMS model because it was intentionally designed to address this problem. The MUSLE model may be particularly appropriate for Question 5 dealing with sediment yield for a 25-yr storm because it can use runoff peak rate and volume estimates from any source including measured values or estimates from an independent flood frequency analysis. If these runoff estimates are available, MUSLE can be applied

Table 3. Example problems and suggested models for each problem related to Example 1.

QUESTION	SUGGESTED MODELS	COMMENTS
1. Detachment or transport limiting	1. Kinematic wave, erosion model	Eqs. 17-27, and relation of KI to B/K used to estimate limiting factors. Choose a representative storm or storms.
2. Range in expected concentration	1.CREAMS 2.MUSLE	Can be used to compute runoff and sediment yield and thus concentration.
3. Particle size distribution	1.CREAMS 2.CSU	Calculations made by particle size classes and default values available.
4. Slope shape	1.CREAMS	Designed for this type of analysis.
5. Yields for 25-yr storm	1.CREAMS 2.MUSLE and runoff model	CREAMS designed to compute runoff and sediment yield. MUSLE needs runoff estimates.

directly and simply as illustrated by the previous examples.

Sediment Yield from Larger Watersheds

Suppose estimates of total sediment yield are needed for a complex (say on the order of 10 to 100 sq km drainage area) watershed. If average annual estimates were of interest then the USLE could be applied to several typical subareas to estimate a watershed-wide estimate of gross erosion and this estimate would be multiplied by a delivery ratio to estimate sediment yield. This would provide a first estimate of average annual sediment yield. As an alternative approach, a time series of runoff volume and peak rates (sufficiently long to estimate average annual values) could be used with the MUSLE to generate a time series of sediment yield estimates. Under conditions as encountered in the western United States, the PSIAC or Flaxman methods might be used to make estimates independent of the USLE structure and methodology.

If individual storm estimates were required then MUSLE could be used with concurrent runoff estimates. The obvious alternative would be to use a complex simulation model such as the CSU or ANSWERS model. However in any case it may be useful to apply the USLE-delivery ratio, or MUSLE, or one of the regression or index methods to make a preliminary estimate. This preliminary estimate could be used as a reference point or rough order of approximation to compare with comparable estimates from the more complex simulation models. Finally, other procedures are available from the USDA Soil Conservation Service and the US Army Corps of Engineers. In many cases these procedures may be most appropriate for a large number of problems. Therefore, potential model users are urged to consult the material presented by Renard, Rawls, and Fogel (1982) to begin the model selection processes on a broader basis than outlined herein.

SUMMARY

The purpose of this short paper is to provide a background on erosion and sedimentation processes on watersheds, to outline methods used to compute watershed erosion and sediment yield, to provide a starting point for selection of appropriate models for a specific problem, and to consider some future developments.

Watershed processes are discussed in terms of processes occurring on upland areas, in small stream channels, and over entire watersheds. Basic relationships between sediment detachment, transport, and deposition are discussed in terms of upland areas and related to parameter estimation techniques. Processes in interrill areas, rills, and small stream channels are described and discussed through functional relationships.

The Univeral Soil Loss Equation is described briefly and then its individual factors are described in detail. Modifications to the USLE are discussed briefly and then a kinematic overland flow-erosion model is used to describe erosion dynamics on upland areas and to interpret the erosion processes.

Next, more complex models are discussed and basic reference material is presented which describes simulation models for runoff, erosion, and sediment yield from complex watersheds.

Example applications are used to illustrate application of the USLE to a range of problems and a number of other problems are used to illustrate how a potential model user might go about selecting the appropriate model or models for a solution to a specific problem. Significant advances in understanding and modeling erosion and sediment yield have been made in the past few decades. Similar advances are now being made and will probably be made in the future. Unfortunately, the present state-of-the-art in hydrology is such that reliable predictions for runoff and sediment yield from watersheds cannot be made without some use of observed data for model calibration and without the application of judgment and experience. Even if this rather pessimistic assessment remains true, available models (e.g. Tables 1 and 2) can be used to gain a great deal of insight into relative rates of erosion (Examples 1-4), processes controlling sediment yield (Fig. 1), and problem specific criteria useful in selecting appropriate models (Table 3).

FUTURE DIRECTIONS IN RESEARCH AND TECHNOLOGY

Throughout the previous sections, specific comments were made as to the likelihood of continued use of a model in the future. This section expands on these comments in a brief fashion. Next, a brief discussion of existing expert systems in chemistry, medicine, and geology is related to development of similar systems in hydrology. Then a relatively new concept or methodology of expert system development and utilization is discussed.

For our purposes here, forecast means to estimate or calculate in advance based on experience and an assessment of present conditions. In the present context, the intent is to forecast the future use of currently available models, and then to forecast development of new models and techniques.

Of course, predictions for the future or forecasts are based on experience and the limited imaginations of the forecasters. These factors limit the scope of the forecasts. Because of these limitations, predictions for the future are sometimes useless or even deceptive to the extent they involve wishful thinking or attempts to actually influence future developments in some way. Nonetheless, forecasts can be useful as an aid to planning and in preparation for events which may be likely in the future.

Continued Application of Existing Models

As suggested earlier, some class of problems will continue to be solved by application of the USLE. There is a need for simple easy-to-use models with sufficiently simple structure and documented parameter values. Moreover, for a specific application if the same results are obtained by several individuals, then the procedure has the advantage of

repeatability.

If capable and dedicated individuals, assisted by institutions committed to support the models and the individuals, assist in prolonged model development and technology transfer, then their models are likely to become widely accepted. This was the case for the USLE, the Stanford model, the CSU model, the CREAMS model, and others such as the procedures and models maintained by agencies such as the Corps of Engineers and the Soil Conservation Service. Therefore, it seems likely that most of the models identified here (especially those shown in Tables 1 and 2) will continue to be used in the near future.

Development of New Models

No model or group of models will ever be appropriate for all problems. Thus, it would seem reasonable to assume the continued modification of existing models and the development of new ones. A reasonable assumption might be the development of coupled partial differential equations for runoff and erosion (similar to Eqs. 17-27) to derive simple sediment yield equations similar to Eq. 23. Developments such as this, coupled with extensive field research programs may produce somewhat more fundamentally based erosion/sediment yield equations comparable to the USLE in practical applications.

Improved models for simple watersheds may be developed based upon the CREAMS model structure (coupled hydrologic models and erosion/sediment yield models). These efforts may result in improved models which better represent the strong interactions between runoff and erosion and which more directly account for dynamic processes and feedback. For example, improved runoff models which more accurately account for spatial variablility in infiltration may produce better estimates of spatial variabilility in erosion, sediment transport, and deposition. The lack of suitable methods to accurately predict infiltration, and thus runoff, constitute a major limitation in the devlopment of improved erosion/sediment yield models. If current efforts of improve infiltration models are successful, then improvements in erosion/sediment yield models will quickly follow.

A second major limitation is the lack of suitable methods of lumping topographic elements (and thus parameter estimates for the topographic elements) to represent large and complex watersheds in mathematical models. For example, how large an area can be represented as an upland area dominated by interrill and rill erosion? At what point is it necessary to include channel processes? Given that we know the answer to these questions, we then need to know how parameter values are affected as the size of the upland area increases. Another related example is in representing the stream channel network in a watershed model. How much of the detailed channel network in the prototype watershed (and remember the number of channel segments is dependent upon the map scale selected to represent the prototype watershed) should be represented in the mathematical model? If the channel network is truncated in the model so that some of the smaller channels are ignored, then how does this

affect the model performance and parameter estimates? At each stage in representing watershed topography or geometry there are various degrees of smoothing detail and spatial lumping. At present, there are no suitable methods of accomplishing this lumping or predicting its influence on parameter distortions or model performance. If progress is made in this general area of lumping-parameter distortion-model performance, then improvements in watershed runoff, erosion, and sediment yield models will directly follow. Additional details on necessary research to advance our ability to understand and model many of these processes are given in a recent state-of-the-art report (ASCE, 1982).

Unanticipated advances in theory, methodology, or experimental techniques may result in significant improvements in the future. Because these advances are unanticipated, further elaboration is not possible.

Applications of Expert Systems

In this section the concept of an expert system is introduced and a relatively new concept of embedding a mathematical model within an expert system is proposed as a method synthesizing the power of expert systems with computer simulation models.

Definition and Significance of Expert Systems

An expert sytem is a realization of a method to combine the experience and judgment of scientists, engineers, or other specialists with the storage ability and computational efficiency of a digital computer to obtain a solution, partial solution, or method of obtaining a solution to a particular problem.

A better definition of an expert system is given in the first chapter of a recent book on expert systems (see Bramer, 1982, p. 3) as follows. "An important development, arising largely from Artificial Intelligence research, which has crystallized in the past few years is the idea of an expert system. An expert system has been defined as a computing system which embodies organized knowledge concerning some specific area of human expertise, sufficient to perform as a skilful and cost-effective consultant."

The significance of expert systems should be obvious, in that if successful, they should provide a means of obtaining expert opinion based on education, experience, and ability without the necessity of obtaining the experts. Of course, the systems will not approach perfection in the foreseeable future (that means they will not be as good as the actual experts) because in the foreseeable future the human brain will remain superior to any program. Perhaps a better summary of the significance of expert systems is given in the Preface of the previously cited book (Michie, 1982, p. xii) as follows. "I do not believe that there is a more important theme for computer-based industry today than the new craft of knowledge

engineering, nor one whose ramifications reach farther into all corners of intellectual, social and economic life. If one sees, as I do, the computer-based expert system as a common model for knowledge-driven transactions of all kinds, from advising a commercial client to planning the economy, from training a student to instructing an industrial robot, then it should be plain to all that whichever community can first master the new technology can expect to obtain a decisive advantage."

Examples of Expert Systems

Three existing expert systems can serve as useful examples in describing such systems in preparation for consideration of systems development for computing erosion and sediment yields. Bramer (1982, Table 1, pp. 8-11) lists 35 expert systems and classifies them according to area of application while providing references and brief descriptions of each system. Three of these systems are briefly described in Table 4.

The DENDRAL system was the first major system developed at Stanford almost twenty years ago. The program was designed to be used by organic chemists to help in the identification of organic compounds by interpretation of mass spectrograms. The first step is to interpret the spectrograms to suggest which chemical substructures are or are not likely to be present. Next a list of chemical structures which could produce the observed spectrogram is prepared. Spectrograms for each likely structure are then computed and compared with the observed spectrogram to select those which best fit the observations. The result is a list of most likely candidates as the sample compound. According to Bramer, DENDRAL is the best known and most successful of all expert systems.

The MYCIN system was developed to aid in diagnosis and recommend drug treatment for infectious diseases. Significant characteristics of this expert system are that it is designed for interactive use and it has the ability to explain how a conclusion and recommendation was reached. That is, it can retrace and display the steps taken to reach a decision. A subject-independent EMYCIN system was developed from MYCIN and has been used to create other expert systems in medicine and engineering.

The PROSPECTOR expert system was developed to aid in evaluating a site or region for mineral deposts. Output from the program includes probability statements as to the occurrence of a mineral deposit at the site. This system is also interactive and can trace or explain how a particular probability (a decision in this case) was reached. The PROSPECTOR system would appear to have significant potential for applications in mineral exploration. It also may continue to serve as a prototype system in the future.

Expert Systems for Runoff, Erosion, and Sediment Yield

From the examples shown in Table 4 and the previous discussions as to the need for experience and judgment (i.e.

Table 4. Selected examples of expert systems as summarized by Bramer (1982) in a review of expert systems research.

System	References	Comments
DENDRAL (chemistry)	Feigenbaum, et.al. (1971)	An early system (developed at Stanford) to identify organic compounds using data from mass spectrograms.
MYCIN (medicine)	Shortliffe (1976)	Developed to diagnose and recommend appropriate drug treatment for infectious diseases (blood diseases and meningitis). Designed for interactive use. Includes procedures to "explain" how a recommendation was reached.
PROSPECTOR (geology)	Duda, et.al. (1979)	Developed at SRI International to aid in evaluating a site or region for mineral deposits. Designed for interactive use. Also includes explanation features.

experts) in applying and interpreting models for runoff, erosion, and sediment yield, it appears that there may be potential for expert systems applications in these areas. For example, even a model as simple as the USLE requires the application of judgment in selecting appropriate C factors.

A USLE based expert system much like those shown in Table 4 would appear to be possible and should be of benefit for a wide class of users. Such a system could conduct an interactive dialogue with the user to first ascertain if the USLE is appropriate for the problem. Once this was established, then information could be obtained to evaluate the factors including application of expert knowledge in estimation of the C factor. Next, the USLE soil loss estimates could be subject to expert interpretation with respect to the broader aspects of the user's problem (e.g. ranking conservation measures, selecting support practices to meet specified soil loss tolerances, etc.) This proposed application provides a hint of the new application or modification of expert systems proposed herein.

Essential aspects of the USLE based expert system proposed above can be placed in five categories as follows: 1) Interactive dialogue with user to reach a decision on problem characteristics-model applicability (in this case, is the model appropriate for the user's problem or can the problem be reformulated so it does match the USLE while meeting the user's needs). 2) Interactive dialogue with the user to select parameter values and input data. 3) Model implementation which in this example would be to use the USLE to compute average annual soil loss. 4) Interactive dialogue with the user to interpret the model output. 5) Interactive dialogue with the user to utilize the model output in reaching a solution to the problem (in the USLE example, this could mean selection of an appropriate mix of management and cropping practices to meet a specified tolerance value for average annual soil loss).

In the first category, the system could recommend alternative models or procedures if the USLE is not appropriate for the problem. In the second category, the system could inform the user of data gaps, the loss of accuracy if default values were used, or specify what additional measurements or observations are required and how to obtain them. In the third category, model implementation, user interaction might be optional as the explanation options for MYCIN and PROSPECTOR. The fourth category, interpretation of model output, is a challenging area for research and development in that for complex simulation models (e.g. CREAMS) interpretation of simulation results may be difficult. Category 5, application of the model output to the user's problem, again requires interactive dialogue and application of expert judgment and opinion.

The major difference between traditional expert systems such as those summarized in Table 4 and the expert systems proposed here is that rather than building in a fixed number of rules or conditions, a simulation model is embedded within the expert system. The fixed conditions or rules are used to provide input data and parameter values for the model and then to interpret the simulation results or model output. With this type of system, the number of conditions or rules remains fixed at a

relatively small number but there are an infinite number of possible simulations. The addition of simulation capability (including sensitivity analysis and predictive capability) to an expert system would enhance the system's ability to examine a problem using a "What if?" approach.

ACKNOWLEDGEMENTS

The hydrology and erosion/sediment yield information summarized in this paper is derived mainly from work sponsored by the U.S. Department of Agriculture, Agriculture Research Service, from work sponsored by the American Society of Civil Engineers, and from work sponsored by the American Society of Agricultural Engineers. Individuals providing opportunity and encouragement to study and conduct research in these areas include K.G. Renard, W.G. Knisel, and G.R. Foster. I thank them for the opportunites and for for their assistance and guidance. For their help in the area of expert systems, I thank Willard Draisin and Gary White of Los Alamos. I wish to thank San Diego State University and Howard Chang for the opportunity to participate in the Applied Sedimentation and River Engineering course. Finally, a special thanks to Rosemary for her help in all aspects involved in the preparation of this paper.

LJL
White Rock, NM
January 1, 1984

REFERENCES

AGU, 1977. Research needs in erosion and sedimentation. Report of the Committee on Erosion and Sedimentation, Hydrology Section, Transactions, AGU 58(12): 1076-1083.

ARS, 1975. Present and prospective technology for predicting sediment yields and sources. ARS-S-40, USDA-Agricultural Research Service, Washington, D.C.

ASAE, 1982, Hydrologic modeling of small watersheds. ASAE Monograph No. 5, C.T. Haan, H.P. Johnson, and D.L. Brakensiek, eds., ASAE, St. Joseph, MI.

ASCE, 1975. Sedimentation engineering. ASCE manuals and reports on engineering practice, No. 54, V.A. Vanoni, ed. ASCE, New York, NY.

ASCE. 1982. Relationships between morphology of small streams and sediment yield. Report of the Task Committee, Committee on Sedimentation of the Hydraulics Division, J. Hyd. Div., ASCE 108 (HY 11):1328-1365.

Beasley, D.B. 1977. ANSWERS: A mathematical model for simulating the effects of land use and management on water quality. Ph.D. Thesis, Purdue University, West Lafayette, IN, 266 pp.

Bramer, M.A. 1982. A survey and critical review of expert systems research. Chapter 1, pp 3-29. In: Introductory readings in expert systems, D. Michie, ed., Gordon and Breach, Science Publishers, Inc., New York, NY.

Chow, V.T. 1959. Open-channel hydraulics. McGraw-Hill Book Co., New York, NY.

Chow, V.T. ed. 1964. Handbook of applied hydrology. McGraw-Hill Book Co., New York, NY.

Crawford, N.H. and Lindsley, R.K. 1962. The synthesis of continuous streamflow hydrographs on a digital computer. Technical Report No. 12, Dept. of Civil Engineering, Stanford University, Stanford, CA.

Duda, R.O., Gaschnig, J., and Hart, P.E. 1979. Model design in the PROSPECTOR consultant system for mineral exploration., In: Expert systems in the micro-electronic age, D. Michie, ed. Edinburg University Press.

Einstein, H.A. 1968. Deposition of suspended particles in a gravel bed. J. Hyd. Div., ASCE 94 (HY 5): 1197-1205.

Feigenbaum, E.A., Buchanan, B.G., and Lederberg, J. 1971. On generality and problem solving: a case study using the DENDRAL program, pp. 165-190. In: Machine intelligence 6, B. Metzger and D. Michie, eds., Edinburg University Press and Halsted Press (Wiley), New York, NY.

Flaxman, E.M. 1972. Predicting sediment yield in western United States. J. Hyd. Div., ASCE 98 (HY 12): 2073-2085.

Foster, G.R. 1971. The overland flow process under natural conditions, pp. 173-185. In: Biological effects in the hydrological cycle. Proc. Third International Seminar for Hydrology Professors, Purdue University, West Lafayette, IN.

Foster, G.R. 1982. Modeling the erosion process. Chapter 8, pp. 295-380. In: Hydrologic modeling of small watersheds. ASAE monograph No. 5, C.T. Haan, H.P. Johnson, and D.L. Brakensiek, eds., ASAE, St. Joseph, MI.

Foster, G.R. and Meyer, L.D. 1972. A closed-form soil erosion equation for upland areas. In: Sedimentation, Proc. Symposium to Honor Prof. H.A. Einstein, H.W. Shen, ed. and publisher, Colorado State University, Fort Collins, CO.

Foster, G.R., Meyer, L.D., and Onstad, C.A. 1977. An erosion equation derived from basic erosion prinicples. Transactions, ASAE 20(4): 678-682.

Foster, G.R., Lane, L.J., Nowlin, J.D., Laflen, J.M., and Young, R.A. 1981. Estimating erosion and sediment yield on field-sized areas. Transactions ASAE 24(5): 1253-1262.

Hjelmfelt, A.T., Piest, R.F., and Saxton, K.E. 1975. Mathematical modeling of erosion on upland areas. Proc. 16'th Congress International Association for Hydraulic Research, Sao Paulo, Brazil, Vol. 2, 40-47.

Huggins, L.F. and Burney, J.R. 1982. Surface runoff, storage and routing. Chapter 5, pp. 167-225. In: Hydrologic modeling of small watersheds. ASAE Monograph No. 5, C.T. Haan, H.P. Johnson, and D.L. Brakensiek, eds., ASAE, St. Joseph, MI.

Hutchinson, D.E., Pritchard, H.W., and Others. 1976 Resource conservation glossary. In: Journal of Soil and Water Conservation 31(4), 63 pp.

Knisel, W.G., Jr., ed. 1980a. CREAMS: A field scale model for chemicals, runoff, and erosion from agricultural management systems. U.S. Dept. of Agriculture, Conservation Research Report, No. 26, Washington, D.C.

Knisel, W.G., Jr., 1980b. Erosion and sediment yield models - an overview. Proc., ASCE Symposium on Watershed Management, Boise, ID., July, 1980, Vol. 1, 141-150.

Lane, L.J., Woolhiser, D.A., and Yevjevich, V. 1975. Influence of simplifications in watershed geometry in simulation of surface runoff. Hydrology Paper No. 81, Colorado State University, Ft. Collins, CO.

Lane, L.J. and Shirley, E.D. 1982. Modeling erosion in overland flow. Proc. USDA-ARS Workshop on estimating erosion and sediment yield on rangelands, Tucson, AZ., March, 1981, Agricultural Reviews and Manuals, ARM-W-26, June, 1982, pp. 120-128.

Li, R.M. 1979. Water and sediment routing from watersheds. Chapter 9, pp. 9-1 to 9-88. In: Modeling of rivers, H.W. Shen, ed., John Wiley and Sons, New York, NY.

Michie, D., ed. 1982. Introductory readings in expert systems. Gordon and Breach, Science Publishers, Inc., New York, NY.

Morel-Seytoux, H.J. 1973. Two phase flows in porous media, pp. 119-202. In: Advances in hydroscience, Vol. 9.

Negev, M. 1967. A sediment model on a digital computer. Tech. Report No. 76, Stanford University, Dept. of Civil Engineering, Stanford, CA.

NEH-4. 1972. SCS National engineering handbook, Section 4, Hydrology, USDA-SCS, Washington, D.C.

Onstad, C.A. and Foster, G.R. 1975. Erosion modeling on a watershed. Transactions ASAE 18(2): 288-292.

Philip, J.R. 1969. Theory of infiltration. pp. 215-296. In: Advances in Hydroscience, Vol. 5.

PSIAC. 1968. Factors affecting sediment yield and measures for the reduction of erosion and sediment yield. Pacific Southwest Inter-Agency Committee Report, 13 pp.

Renard, K.G., Rawls, W.J., and Fogel, M.M. 1982. Currently available models. Chapter 13, pp. 505-522. In: Hydroloic modeling of small watersheds. ASAE Monograph No. 5. C.T. Haan, H.P. Johnson, and D.L. Brakensiek, eds., ASAE, St. Joseph, MI.

Richards, L.A. 1931. Capillary conduction through porous mediums. Physics, Vol. 1: 313-318.

Schumm, S.A. 1977. The fluvial system. John Wiley and Sons, Inc., New York, NY.

Shirley, E.D. and Lane, L.J. 1978. A sediment yield equation from an erosion simulation model. Hydrology and water resources in Arizona and the Southwest. Vol. 8: 90-96.

Shortliffe, E.H. 1976, Computer-based medical consultations: MYCIN. American Elsevier/North Holland Publishing Co., New York, NY.

Simons, D.B. and Richardson, E.V. 1971. Flow in alluvial sand channels. Vol. 1, pp. 9-1 to 9-89. In: River mechanics, H.W. Shen, ed. and publisher, Colorado State University, Ft. Collins, CO.

Simons, D.B., Li, R.M., and Stevens, M.A. 1975. Development of models for predicting water and sediment yield from storms on small watersheds. U.S. Dept. of Agriculture-Forest Service, Rocky Mountain Forest and Range Experiment Station Report, Aug., 1975.

Simons, D.B. and Li, R.M. 1976. Procedures for estimating model parameters of a mathematical model. U.S. Dept. of Agriculture-Forest Service, Rocky Mountain Forest and Range Experiment Station Report, Apr., 1976.

Skaggs, R.W. and Khaleel, R. 1982. Infiltration. Chapter 4, pp. 119-166. In: Hydrologic modeling of small watersheds. ASAE Monograph No. 5, C.T. Haan, H.P. Johnson, and D.L. Brakensiek, eds., ASAE, St. Joseph, MI.

Williams, J.R. 1975. Sediment-yield prediction with universal equation using runoff energy factor. pp. 244-252. In: Present and prospective technology for predicting sediment yields and sources. ARS-S-40, USDA-Agriculture Research Service, Washington, D.C.

Wischmeier, W.H. and Smith, D.D. 1978. Predicting rainfall erosion losses. A guide to conservation planning. Agriculture Handbook No. 537, USDA-Science and Education Administration, Washington, D.C.

Woolhiser, D.A., Hanson, C.L., and Kuhlman, A.R. 1970. Overland flow on rangeland watersheds. New Zealand Journal of Hydrology, 9(2): 336-356.

KINEMATIC, DYNAMIC AND INERTIAL WAVES

by

V. MIGUEL PONCE

TABLE OF CONTENTS

		Page
2.1	INTRODUCTION	2-1
2.2	SHALLOW WAVE PROPAGATION IN OPEN CHANNEL FLOW	2-1
2.3	KINEMATIC WAVES	2-3
2.4	DIFFUSIVE WAVES	2-5
2.5	INERTIAL WAVES	2-6
2.6	DYNAMIC WAVES	2-7
2.7	SUMMARY	2-9
	APPENDIX I. - REFERENCES	2-10
	APPENDIX II. - NOTATION	2-10

2.1 INTRODUCTION

This chapter presents an overview of wave propagation phenomena in open channel flow. The study of wave propagation is regarded as an effective way of introducing several important concepts of unsteady open channel flow. A theoretical treatment provides the proper framework for the detailed analysis of the various types of open channel flow waves, i.e., kinematic, diffusive, dynamic and inertial waves. The emphasis throughout this chapter is on developing the proper background for a more effective use of the numerical methods to be treated in the following chapters.

2.2 SHALLOW WAVE PROPAGATION IN OPEN CHANNEL FLOW

One of the most interesting and important phenomena in unsteady open channel flow is that of the propagation of shallow waves. Shallow waves are those for which the water depth is small in comparison with the wavelength. Deep waves, on the other hand, are those for which the water depth is much larger than the wavelength. Shallow waves are commonly present in river and canal flow, in which the wave can "feel" the presence of the channel bottom. Deep waves belong more to the realm of the ocean environment. The remainder of this chapter will deal with only the propagation of shallow waves in open channel flow.

Method of Analysis. The propagation of shallow water waves can be studied by using the Saint Venant equations. These equations are expressions of the conservation principles of fluid mechanics, and can be used to describe the unsteady movement of water in open channels. From the mathematical standpoint, they constitute a set of two quasilinear first order partial differential equations for which no complete analytical solution is available to date. However, a particular solution can be obtained by a judicious use of the tools of linear analysis. Such a solution can provide an effective way of assessing the overall characteristics of the motion.

Ponce and Simons [1] have developed a theory of wave propagation based on linear analysis. They took the Saint Venant equations, applied a perturbation technique leading to a linearized form of the equations, and forced a solution in sinusoidal form. This procedure enabled the calculation of the celerity and attenuation characteristics of various types of shallow water waves, while throwing additional light onto the wave mechanics itself. The main conclusions of the Ponce and Simons theory are outlined in the following sections. For a more detailed treatment, reference is made to the original publication [1].

Classification of Shallow Water Waves. Shallow water waves in open channel flow are commonly classified according to the relative magnitude of the various forces responsible for the motion. These forces are of three types: body, surface and inertia forces.

In open channel flow, the body force is the component of gravity resolved along the direction of motion. The surface forces can be either normal (pressure) or tangential (stresses). The normal force is the pressure gradient along the direction of motion. The tangential

forces are the bottom stresses and the water surface stresses. The bottom stresses are caused by friction, while the water surface stresses are normally attributed to wind. The latter are usually neglected in open channel flow calculations. The inertia forces are of two types: 1) convective inertia, and 2) local inertia.

The equation of motion for a unit-width channel with no lateral inflow is:

$$\frac{1}{g}\frac{\partial u}{\partial t} + \frac{u}{g}\frac{\partial u}{\partial x} + \frac{\partial d}{\partial x} + S_f - S_o = 0 \qquad (2\text{-}1)$$

in which u = mean velocity; d = flow depth; g = acceleration of gravity; S_f = friction slope; S_o = bottom slope; t = time variable; and x = space variable. In Equation 2-1, the term $(1/g)(\partial u/\partial t)$ represents the local inertia force; the term $(u/g)(\partial u/\partial x)$ represents the convective inertia force; $(\partial d/\partial x)$ represents the pressure gradient force; S_f represents the friction force along the channel bottom; and S_o represents the gravity force.

A dynamic wave is defined as that wave in which all forces (local inertia, convective inertia, pressure gradient, friction and gravity) interact freely with no one particular force predominating over the others. As such, it is the most general type of shallow water wave, an asset to be certainly recognized. However, its solution is quite elaborate since it takes into consideration the complete equation of motion together with the equation of water continuity.

Strictly speaking, a kinematic wave is defined as that wave in which the inertia terms (both local and convective) are neglected on the grounds of being very small in comparison with the remaining terms. There are two types of kinematic waves: 1) a nondiffusive-kinematic wave, for short, kinematic wave, which neglects not only the inertia terms but also the pressure gradient term; and 2) a diffusive-kinematic wave, for short, diffusive wave, which neglects only the inertia terms.

The reasons for the use of kinematic and diffusive waves are twofold: (1) ease of solution, and (2) applicability. Without the neglected terms, the equations of open channel flow are considerably simplified and more amenable to mathematical treatment. Furthermore, there is a large number of practical cases in which the neglect of terms is indeed justified. Therefore, the proper use of these simplified wave models hinges on their applicability to a particular problem situation.

An inertial wave is defined as that wave in which the friction and gravity components of the motion are either zero or negligible. Therefore, such a wave is governed strictly by the inertia and pressure gradient forces. Inertial waves arise in connection with unsteady open channel flow phenomena involving sudden changes in mean velocity and flow depth.

A summary of the classification of shallow water waves treated here is given in Table 2-1.

TABLE 2-1

CLASSIFICATION OF SHALLOW WATER WAVES

Wave	Forces and Terms				
	Inertia		Surface		Body
	Local	Convective	Pressure Gradient	Friction Slope	Bottom Slope
	$\frac{1}{g}\frac{\partial u}{\partial t}$	$\frac{u}{g}\frac{\partial u}{\partial x}$	$\frac{\partial d}{\partial x}$	S_f	$-S_o$
Kinematic				√	√
Diffusive			√	√	√
Inertial	√	√	√		
Dynamic	√	√	√	√	√

2.3 KINEMATIC WAVES

This section discusses the nondiffusive-kinematic wave, commonly referred to simply as kinematic wave. The following section will cover the diffusive-kinematic wave, referred to as diffusive wave.

The kinematic wave model assumes that the inertia and pressure gradient terms in the equation of motion are negligible compared to the friction and gravity terms. Without the inertia and pressure gradient terms, Eq. 2-1 reduces to:

$$S_f = S_o \quad . \tag{2-2}$$

This equation could be construed as a statement of uniform flow. Therefore, the kinematic wave is something erroneously associated with the uniform flow condition. The wavelike features of the kinematic wave, however, are preserved through the equation of water continuity, which does contain information on the nonuniformity and unsteadiness of the flow.

The behavior of the kinematic wave model is described by the kinematic wave equation. This equation is derived from Eq. 2-2 and the equation of water continuity. The equation of water continuity, expressed in terms of flow area A and water discharge Q, and neglecting lateral inflow, is

$$\frac{\partial A}{\partial t} + \frac{\partial Q}{\partial x} = 0 \tag{2-3}$$

Equation 2-2 can be expressed as a uniform flow resistance formula, for which there is a choice of either Manning's or Chezy's:

$$Q = \frac{1.486}{n} AR^{2/3} S_f^{1/2} \tag{2-4}$$

or

$$Q = CA(R\ S_f)^{1/2} \tag{2-5}$$

in which R = hydraulic radius; n = Manning's coefficient; and C = Chezy's coefficient. By definition, $R = A/P$, in which P is the wetted perimeter. In general, the wetted perimeter is a function of the flow area, and the P-A relationship describes the shape of the cross section. Once this relationship is known at a given cross section, Eqs. 2-4 and 2-5 describe a unique Q-A relationship, since n and C are taken as constants, and $S_f = S_o$ = constant. Thus, the discharge-area relation reduces to:

$$Q = \alpha\ A^{\beta} \tag{2-6}$$

in which α = a coefficient containing information on the resistance factor, the bottom slope and the shape of the cross section; and β = an exponent containing information on the type of resistance formula (Manning or Chezy) and the shape of the cross section.

The kinematic wave equation is derived by multiplying Eq. 2-3 by $\partial Q/\partial A$, leading to:

$$\frac{\partial Q}{\partial t} + \left(\frac{\partial Q}{\partial A}\right) \frac{\partial Q}{\partial x} = 0 \tag{2-7}$$

The term in parenthesis in Eq. 2-7 is the kinematic wave velocity (also referred to as the Kleitz-Seddon celerity), obtained from Eq. 2-6 as

$$\frac{\partial Q}{\partial A} = \left.\frac{dQ}{dA}\right|_{x_o} = \alpha\beta A^{\beta-1} \tag{2-8}$$

from which

$$\frac{\partial Q}{\partial A} = \beta\ \frac{Q}{A} = \beta u\ , \tag{2-9}$$

u being the mean flow velocity.

Equation 2-7 is a quasilinear first order partial differential equation. It is quasilinear because the kinematic wave celerity is a function of the mean flow velocity, which increases with discharge. Since it is a first order equation, it can only describe convection (wave travel) and not diffusion (wave attenuation). Its quasilinear property enables the deformation (wave skewness) of the hydrograph, manifested as a steepening rising limb and flattening receding limb as the wave moves downstream. If left uncontrolled, the wave steepening will eventually develop into the so-called "kinematic shock", which resembles a dynamic shock but in the absence of inertia.

In summary, the neglect of the inertia and pressure gradient terms of the equation of motion leads to the kinematic wave equation. This equation provides for convection (wave travel) and deformation (wave skewness), but does not take into account diffusion (wave attenuation). The diffusive property is lost as part of the neglected terms.

2.4 DIFFUSIVE WAVES

This section covers the diffusive-kinematic wave, commonly referred to as diffusive wave.

The diffusive wave model assumes that the inertia (local and convective) terms of the equation of motion are negligible as compared to the pressure gradient, friction and gravity terms. Without the inertia terms, Eq. 2-1 reduces to:

$$S_f = S_o - \frac{\partial d}{\partial x} \tag{2-10}$$

The behavior of the diffusive wave model is described by the diffusive wave equation. For the sake of simplicity, this equation is derived herein assuming a wide channel governed by Chezy friction. The equation of water continuity is recast as:

$$B \frac{\partial d}{\partial t} + \frac{\partial Q}{\partial x} = 0 \tag{2-11}$$

in which B = channel width. Equation 2-10 is substituted into Eq. 2-5, leading to:

$$Q = CA[R(S_o - \frac{\partial d}{\partial x})]^{1/2} \tag{2-12}$$

Taking into consideration the wide channel assumption, Eq. 2-12 reduces to

$$Q = CBd^{3/2} (S_o - \frac{\partial d}{\partial x})^{1/2} \tag{2-13}$$

Differentiating Eq. 2-13 with respect to x, and substituting $\partial Q/\partial x$ into Eq. 2-11, leads to

$$\frac{\partial d}{\partial t} + c_k \frac{\partial d}{\partial x} = \mu \frac{\partial^2 d}{\partial x^2} \tag{2-14}$$

in which $c_k = 1.5\ u$ is the kinematic wave celerity corresponding to a wide channel with Chezy friction; and $\mu = ud/2S_f$ is the diffusion coefficient (or also, hydraulic diffusivity). Note that unlike Eq. 2-7, Eq. 2-14 contains both a convection and a diffusion term. Diffusive wave equations with discharge or flow area as the dependent variable can also be derived, albeit under some additional assumptions.

The diffusive wave equation is a quasilinear second order partial differential equation. As such, it can account for the convection, diffusion and deformation of the hydrograph. Unlike the kinematic wave, the deformation (steepening of the rising limb) cannot proceed uncontrolled, since the diffusive character of the wave would tend to counteract the steepening tendency. Therefore, the "kinematic shock" phenomenon which often plagues kinematic wave computations is totally absent in computations using the diffusive wave.

In summary, the neglect of the inertia terms in the equation of motion leads to the diffusive wave equation. This equation provides for convection, diffusion and deformation of the hydrograph. The diffusive features of the wave can be linked to the presence of the pressure gradient term.

2.5 INERTIAL WAVES

The inertial wave model assumes that the friction and gravity terms are negligible as compared with the inertia and pressure gradient terms. Without the friction and gravity terms, Eq. 2-1 reduces to

$$\frac{1}{g}\frac{\partial u}{\partial t} + \frac{u}{g}\frac{\partial u}{\partial x} + \frac{\partial d}{\partial x} = 0 \qquad (2\text{-}15)$$

The water continuity equation, expressed in terms of velocity and flow depth, and neglecting lateral inflow, is:

$$\frac{\partial d}{\partial t} + d\,\frac{\partial u}{\partial x} + u\,\frac{\partial d}{\partial x} = 0 \qquad (2\text{-}16)$$

Equations 2-15 and 2-16 constitute a set of two quasilinear first order partial differential equations describing the inertial wave model. Their analytical solution is carried out by linearizing the dependent variables u and d around reference values u_o and d_o. The linearized equations are then used to solve for one dependent variable at a time, leading to a second order partial differential equation describing a wave with velocity c_i defined by

$$c_i = u_o \pm \sqrt{gd_o} \qquad (2\text{-}17)$$

Equation 2-17 is the inertial wave velocity (also referred to as the Lagrangian celerity). It describes the speed of travel of free surface flow waves in the absence of gravity and friction. Notice that the inertial wave has two solutions, unlike the kinematic and diffusive waves which have only one solution (precisely because of their lack of inertia). Depending on the value of the Froude number

$$F_o = \frac{u_o}{\sqrt{gd_o}}\ , \qquad (2\text{-}18)$$

the solutions can either travel one upstream and one downstream ($F_o < 1$), or travel both downstream ($F_o > 1$). For $F_o = 1$, one of the solutions is a stationary (still) wave.

The analytical solution of the one dimensional wave equation describing the inertial wave model does not lead to wave diffusion. Therefore, the inertial wave model cannot account for wave attenuation.

In summary, the neglect of the gravity and friction terms in the equation of motion leads to the inertial wave equation. This equation provides for convection (wave travel) at the well-known inertial wave velocity. It does not take into account diffusion, which is lost as part of the neglected terms.

2.6 DYNAMIC WAVES

A dynamic wave is defined as that wave in which all forces (inertia, surface and body) interact freely with no one particular force predominating over the others. Its solution is based on the complete equation of motion, Eq. 2-1, and the equation of water continuity, Eq. 2-16. These equations constitute a set of two quasilinear first order partial differential equations for which no complete analytical solution is available to date. However, a particular solution derived by using the tools of linear analyis can provide a wealth of information on the characteristics of the dynamic wave.

Following Ponce and Simons [1], Eqs. 2-1 and 2-6 are linearized around reference values. A sinusoidal solution is forced on the linearized system of equations, leading to a homogeneous system of linear algebraic equations. The nontrivial condition for the determinant of the coefficient matrix enables the determination of the celerity and attenuation characteristics of the dynamic wave.

The celerity and attenuation of the dynamic wave are shown to be functions of the reference flow Froude number F_o and a dimensionless wave number $\hat{\sigma}$ defined as

$$\hat{\sigma} = \frac{2\pi}{L} L_o \tag{2-19}$$

in which $L_o = d_o/S_o$ = the length of channel necessary for the reference flow to drop a head equal to its depth. Notice that $\hat{\sigma}$ contains information on the size of the wave phenomena, the bottom slope and the channel friction.

There are three well-defined bands in the spectrum of dimensionless wave numbers $(0 < \hat{\sigma} < \infty)$: 1) a kinematic band, corresponding to the smaller wave numbers, in which the wave celerity is essentially the kinematic wave celerity; 2) an inertial band, corresponding to the larger wave numbers, in which the wave celerity is essentially the inertial wave celerity; and 3) a dynamic band, corresponding to wave numbers in the intermediate range, in which the wave celerity lies in between the kinematic and inertial wave celerity values. Such a trend is depicted in Fig. 2-1, which shows the dimensionless wave number $\hat{\sigma}$ in the abscissas, and the dimensionless relative celerity $\hat{c}_r$ defined as

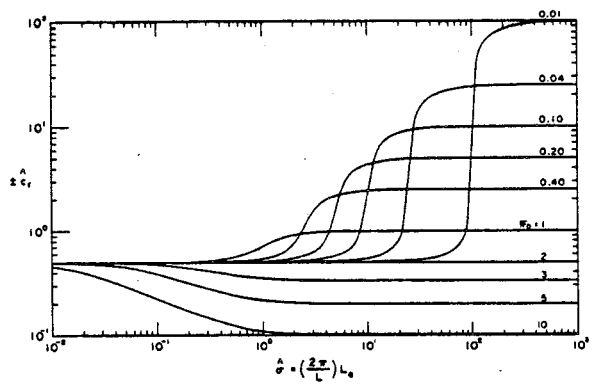

Figure 2-1. Dimensionless relative celerity $\hat{c}_r$, versus dimensionless wave number $\hat{\sigma}$; curve parameter = Froude number F_o , $(0.01 \leq F_o \leq 10)$.

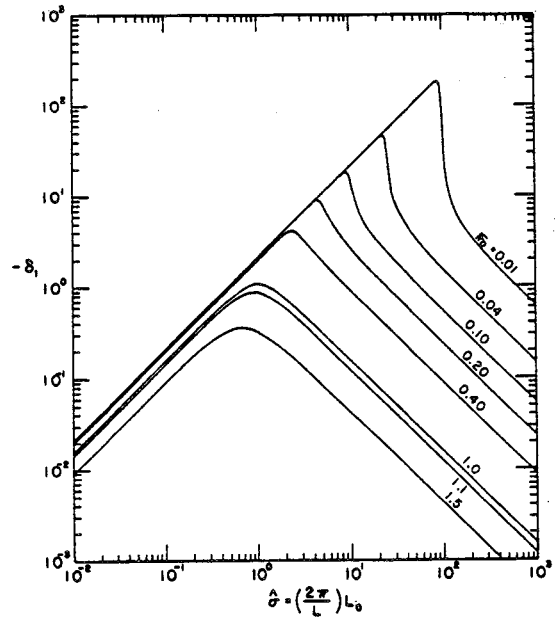

Figure 2-2. Primary wave logarithmic decrement $-\delta_1$, versus dimensionless wave number $\hat{\sigma}$; curve parameter = Froude number F_o , $(F_o < 2)$.

$$\hat{c}_r = \frac{c}{u_o} - 1 \tag{2-20}$$

in the ordinates. Figure 2-1 shows that for small values of $\hat{\sigma}$, the relative celerity $\hat{c}_r$ approaches asymptotically the relative kinematic wave celerity value (0.5 for the case of wide channels with Chezy friction). For large values of $\hat{\sigma}$, the relative celerity $\hat{c}_r$ approaches asymptotically the relative inertial wave celerity value $(1/F_o)$. For intermediate values of $\hat{\sigma}$, the relative dynamic wave celerity is between 0.5 and $1/F_o$.

The attenuation characteristics for the spectrum of dimensionless wave numbers is portrayed in Fig. 2-2. The ordinate is a decay parameter δ referred to as logarithmic decrement, defined in

$$a_1 = a_0 \, e^{\delta} \tag{2-21}$$

in which a_0 = initial wave amplitude, a_1 = wave amplitude after one period of propagation. This figure depicts the variation of the logarithmic decrement of the primary wave (that traveling always in the same direction as the main flow) as a function of $\hat{\sigma}$, and for $F_o < 2$. The decay rate is a minimum at both extremes of the $\hat{\sigma}$ spectrum; $\hat{\sigma} \to 0$ corresponds to the kinematic wave case; $\hat{\sigma} \to \infty$ corresponds to the inertial wave case. In the intermediate $\hat{\sigma}$ range, the decay rate is very high, indicating that the primary dynamic wave has markedly strong dissipative tendencies. For a more detailed discussion on the characteristics of the dynamic wave, reference is made to Ponce and Simons [1].

In summary, the dynamic wave takes into account all forces present in open channel flow: inertia, pressure and body. The dynamic wave model can account for convection, diffusion and deformation. The celerity and attenuation are functions of the reference flow Froude number and a dimensionless wave number characteristic of the unsteady component of the motion and the channel properties. The dynamic wave celerity lies between the kinematic and inertial wave celerity values. The attenuation of the dynamic wave is markedly strong, with a maximum around the midrange values of the dimensionless wave number.

2.7 SUMMARY

The characteristics of various types of shallow water waves are described in this chapter. These waves are: kinematic, diffusive, inertial and dynamic.

Kinematic waves are used to describe wave phenomena under the exclusive action of friction and gravity. They have the property of convection and deformation, but cannot account for wave diffusion. The convection speed is the kinematic wave velocity, defined as $c_k = \beta u$.

Diffusive waves, as their name indicates, can account for convection, diffusion and deformation. The convection speed is very close to that of kinematic waves. The diffusive behavior is due to the added contribution of the pressure gradient term.

Inertial waves are used to describe open channel flow waves under the sole action of inertia and pressure forces. The inertial wave model can account for convection, but does not include diffusion. The convection speed is the inertial wave velocity, defined as $c_i = u_o \pm \sqrt{gd_o}$.

Dynamic waves are the most general type of open channel flow wave. They account for wave convection, diffusion and deformation. The convection speed of the dynamic wave lies in between the kinematic and inertial wave velocities. The attenuation rate is markedly strong compared to that of the other waves treated here.

The foregoing treatment of open channel flow waves is aimed at developing the proper theoretical background for a more effective use of the material to be covered in the following chapters.

APPENDIX I. - REFERENCES

1 Ponce, V. M., and Simons, D. B., "Shallow Wave Propagation in Open Channel Flow, " Journal of the Hydraulics Division, ASCE, Vol. 103, HY12, Proc. Paper 13392, Dec., 1977, pp. 1461-1476.

APPENDIX II. - NOTATION

The following symbols are used in this chapter:

A = flow area;

a = wave amplitude;

B = channel width;

C = Chezy coefficient;

c = wave celerity;

c_i = inertial wave celerity, Eq. 2-17;

c_k = kinematic wave celerity, Eq. 2-9;

$\hat{c}_r$ = dimensionless relative wave celerity, Eq. 2-20;

d = flow depth;

F_o = reference flow Froude number, Eq. 2-18;

g = acceleration of gravity;

L = wavelength;

OVERVIEW OF FLOOD ROUTING METHODS

by

V. MIGUEL PONCE

TABLE OF CONTENTS

		Page
3.1	INTRODUCTION	3-1
3.2	NATURE OF FLOOD WAVES	3-1
3.3	CLASSIFICATION OF FLOOD ROUTING METHODS	3-2
3.4	RESERVOIR ROUTING	3-4
3.5	STREAM CHANNEL ROUTING	3-5
3.6	SUMMARY	3-10
	APPENDIX I. - REFERENCES	3-11
	APPENDIX II. - NOTATION	3-11

3.1 INTRODUCTION

As man continues to build on the flood plain, an increased understanding of the nature of floods remains an ever present challenge. For hydraulic engineers, an assessment of the characteristics of flood waves is the logical starting point at the planning and design stages of flood control works. This chapter presents an overview of flood propagation phenomena in open channels. First, some fundamental concepts on the nature of floods are introduced. This leads naturally into flood routing and a classification of flood routing methods. The remainder of the chapter describes briefly some of the most important methods, emphasizing their major features and giving a rationale for their use. The objective of this chapter is to develop a solid foundation on which to base the more detailed studies to follow.

3.2 NATURE OF FLOOD WAVES

It is perhaps an oddity that the nature of flood waves is most readily grasped by looking at the system rather than at the flood wave itself. The system could be either a channel, a reservoir (or lake), or a channel-reservoir combination. This distinction is of fundamental importance, as will be shown here. The channel case is usually associated with the existence of a finite (nonzero) water surface slope. The reservoir case is normally taken to imply a zero water surface slope.

Flood waves travel downstream in a channel or reservoir and, in general, are subject to attenuation. The rate of travel (flood wave velocity) and the rate of attenuation depend on the system in which the flood wave is moving.

Flood Waves in Stream Channels. Flood waves in stream channels travel at an average velocity closely corresponding to that given by the Kleitz-Seddon law:

$$c = \left.\frac{dQ}{dA}\right|_{x_o} = \left.\frac{1}{B}\frac{dQ}{dy}\right|_{x_o} \tag{3-1}$$

in which c = flood wave velocity; Q = discharge; A = flow area; B = channel width; and y = stage. They attenuate at a rate which is a function of the magnitude of the various forces involved in the motion. Kinematic waves do not attenuate, diffusive waves attenuate at a small to moderate rate, and dynamic waves are subject to very strong attenuation. Strictly speaking, Eq. 3-1 is valid only for flood waves which do not attenuate, i.e., kinematic waves. However, it can also be used as an approximation for flood waves subject to moderate attenuation, i.e., diffusive waves. Figure 3-1 depicts the typical behavior of flood waves in stream channels.

Flood Waves in Lakes and Reservoirs. Flood waves in lakes and reservoirs travel at an infinite velocity, i.e., there is an instantaneous response (outflow hydrograph) to the excitation (inflow hydrograph). However, the system exerts a diffusing effect on the flood wave, with the result that the peak of the outflow hydrograph is

attenuated and delayed. A significant characteristic of flood routing through reservoirs is that when the inflow and outflow coincide, the outflow is a maximum. Figure 3-2 depicts the typical behavior of flood waves in lakes and reservoirs.

Flood Routing. Although flood waves appear to have well-defined properties, in practice it is often necessary to carry out elaborate calculations in order to determine these properties. The reason for this is the variability of the natural environment, manifested in the need to handle large amounts of data. Flood routing is defined as the process of tracing by calculation the movement of a flood wave. The calculations can proceed along one of the following two lines: either by considering only temporal variations (lumped case), or by considering both temporal and spatial variations (distributed case). The lumped case is the classical reservoir routing situation, formulated in terms of one first order ordinary differential equation (the storage equation). The distributed case corresponds to stream channel routing, formulated in terms of two first order partial differential equations. The latter are commonly referred to as the equations of gradually varied unsteady open channel flow, or also, as the Saint Venant equations.

Under certain conditions, the Saint Venant equations with appropriate simplifications can be combined into one second order partial differential equation describing convection and diffusion. This equation can be used to describe flood movement in a large number of practical applications.

3.3 CLASSIFICATION OF FLOOD ROUTING METHODS

A knowledge of the nature of flood waves provides a good basis on which to develop a classification of flood routing methods. The most general classification is that of (1) reservoir (or lake) routing; and (2) stream channel routing. The essential difference between these two is that in the reservoir routing case the water surface slope is zero, while in stream channel routing it has a nonzero value. Several other criteria could be used to classify flood routing methods. Among these, the following are readily identified: (1) the equations used to formulate the problem; (2) the overall approach to data collection; and (3) the approach to obtaining a solution.

Classification Based on Equations Used. According to the equations used to formulate the problem, flood routing methods can be classified as: (1) Mass-balance methods; and (2) Mass-and-momentum-balance methods. The mass-balance methods use the ordinary differential equation of storage plus an auxiliary storage-outflow relationship. The mass-and-momentum-balance methods use the Saint Venant equations or appropriate simplifications. The use of the complete Saint Venant equations leads to the dynamic wave, while the simplified forms lead to kinematic and diffusive waves.

Classification Based on Approach to Data Collection. According to the approach to data collection, flood routing methods can be classified as: (1) hydrologic, in which the parameter estimation is based on hydrologic observations for individual channel reaches; and (2)

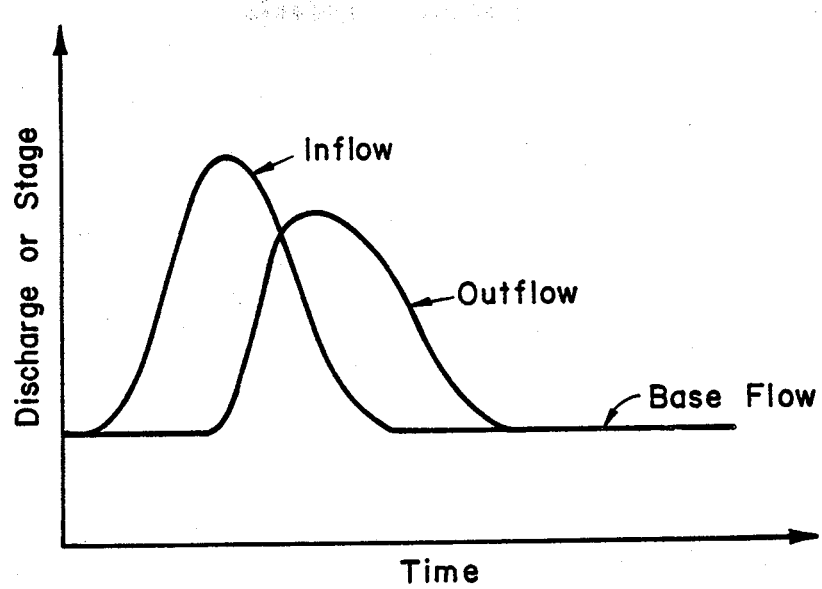

Figure 3-1. Typical inflow and outflow hydrographs for flood waves in stream channels.

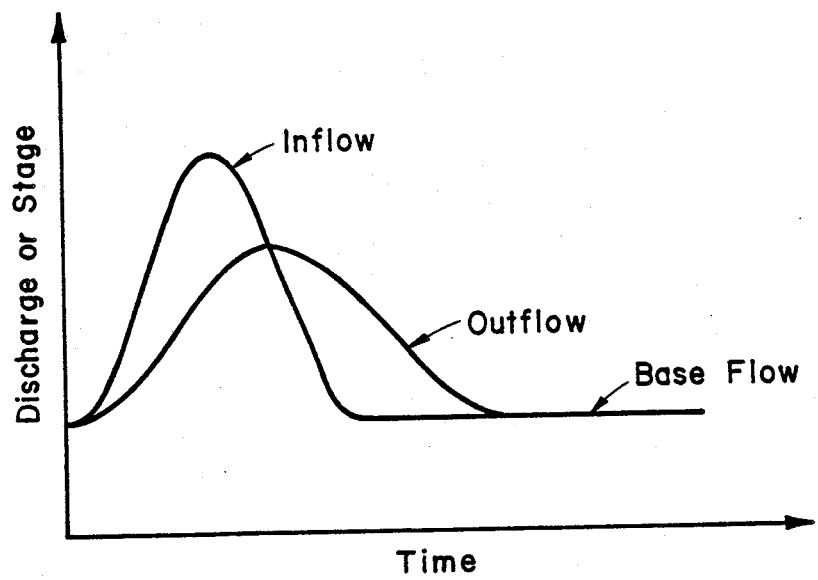

Figure 3-2. Typical inflow and outflow hydrographs for flood waves in lakes and reservoirs.

hydraulic, in which the parameter estimation is based on actual measurements of channel characteristics at individual cross-sections.

Classification Based on the Solution Technique. According to the approach to obtaining a solution, flood routing methods can be classified as: (1) analytical, and (2) numerical. The analytical methods are based on the solution of differential equations specified on a continuous domain of space and time. The numerical methods are based on the solution of algebraic equations on a discrete domain. Analytical solutions use the tools of classical mathematics such as linear analysis and Laplace transforms, while numerical solutions use characteristic or finite difference methods.

Table 3-1 provides a summary of the classification of flood routing methods presented herein.

TABLE 3-1

CLASSIFICATION OF FLOOD ROUTING METHODS

Based on Equations Used	Mass-balance: Storage equation and an auxiliary storage-outflow relationship. Mass-and-momentum-balance: Saint Venant equations (dynamic wave) or appropriate simplifications (kinematic and diffusive waves).
Based on Approach to Data Collection	Hydrologic Routing: Observations for channel reaches. Hydraulic Routing: Measurements of channel characteristics at individual cross-sections.
Based on Solution Technique	Analytical Routing: Differential equations; continuous domain. Numerical Routing: Algebraic equations; discrete domain.

3.4 RESERVOIR ROUTING

The reservoir routing methods follow directly from the differential equation of water storage:

$$I - O = \frac{dV}{dt} \tag{3-2}$$

in which I = inflow; O = outflow; V = volume of storage; and t = time. A significant role is played by the equation relating the outflow rate to the pool level, and therefore, to the volume of storage (V-O relationship).

A widely recognized method of reservoir routing is the level pool (or Puls) technique. Equation 3-2 is discretized over a time interval Δt to yield:

$$\frac{1}{2}(I_1+I_2) - \frac{1}{2}(O_1+O_2) = \frac{1}{\Delta t}(V_2-V_1) \tag{3-3}$$

in which the subscripts 1 and 2 refer to conditions at the start and end of the time interval Δt, respectively. Equation 3-3 is rearranged to:

$$N_2 = N_1 - O_1 + \frac{1}{2}(I_1+I_2) \tag{3-4}$$

in which

$$N_i = \frac{V_i}{\Delta t} + \frac{O_i}{2} \qquad (i=1,2,\ldots) \tag{3-5}$$

is referred to as the storage indication quantity.

The input data consists of the inflow hydrograph and a relationship between storage and outflow (V-O). A suitable Δt is chosen, and the inflow hydrograph is discretized in time, yielding a series of I values. The V-O relationship and Eq. 3-5 are used to derive an N-O relationship. A known initial value of O is used to obtain an initial value of N through the N-O relationship. The calculation proceeds by a sequential application of the following two steps: (1) updating the value of N by using Eq. 3-4; and (2) updating the value of O by using the N-O relationship. The series of O values computed in this way depict the hydrograph attenuation and delay typical of reservoir routing methods.

3.5 STREAM CHANNEL ROUTING

A feature common to all stream channel routing methods is that they consider the balance of mass and momentum, whether this is explicitly stated or not. Historically, stream channel routing methods have developed along three major paths. These are: (1) the classical approach, in which an algebraic inflow-outflow-storage relationship is substituted for the equation of motion; (2) the numerical approach, which relies on the numerical solution of the complete Saint Venant equations; and (3) the simplified approach, which uses a convection-diffusion equation. These three approaches are briefly discussed in the following sections.

The Classical Approach. The classical approach originated in the realization that, unlike reservoir routing, in stream channel routing the reach storage V is a function not only of the outflow O but also of the inflow I. This led naturally into the formulation of several hypothesis for this relationship. One of the most widely recognized of these hypothesis is that of the Muskingum method, which dates back to 1934, and is stated as:

$$V = K[XI+(1-X)O] \tag{3-6}$$

in which K and X = parameters to be determined by calibration using historical flood data for the reach under study.

Equations 3-2 and 3-6 lead to the Muskingum routing equation, stated as:

$$O_2 = C_1 I_1 + C_2 I_2 + C_3 O_1 \tag{3-7}$$

from which the outflow at the new time level O_2 can be calculated from a knowledge of the inflow at the present level I_1, the inflow at the new time level I_2 and the outflow at the present time level O_1. The coefficients C_1, C_2 and C_3 are the Muskingum coefficients, and they are functions of the Muskingum parameters K and X, and the time interval Δt. A more detailed description of the Muskingum method is given in Chapter 5.

The Numerical Approach. The development of the numerical approach to flood routing was triggered by the advent of the electronic computer and the quantum increase in computational power that ensued. Paralleling the availability of the computer, significant progress was made in the field of applied mathematics, particularly with reference to the numerical solution of partial differential equations. Towards the mid-fifties, these advances made possible the early successful attempts to solve the Saint Venant equations by numerical methods with the aid of the computer. Later developments were concentrated on increasing the efficiency and reliability of the numerical approach to flood routing.

The numerical solution of the Saint Venant equations can be carried out by either: (1) the method of characteristics; or (2) finite difference methods. In the method of characteristics, the two partial differential equations (water continuity and motion) are replaced by four ordinary differential equations which are solved numerically on a characteristic grid. The intersections of characteristic lines on the x-t plane define the characteristic grid (see Fig. 3-3).

In the finite difference methods, the functions (e.g., discharge Q, flow area A, stage y) and their derivatives (e.g., $\partial Q/\partial x$, $\partial A/\partial t$) are expressed in terms of their values on a rectangular grid defined on the x-t plane (see Fig. 3-4). A finite difference scheme is a formula expressing a relationship between neighboring values on the rectangular grid. There are two types of finite difference schemes: (1) explicit; and (2) implicit. Explicit schemes are those that advance the solution in time and space by solving for the unknown variables, one grid point at a time. Implicit schemes advance the solution in time by simultaneously solving for the unknown variables at a number of grid points.

Explicit schemes are relatively simple to formulate, but are usually limited to a small time step Δt by considerations of numerical stability. Implicit schemes require the inversion of a matrix, but are not subject to the strict stability criterion of explicit schemes. In general, implicit schemes are more efficient than explicit schemes in their use of computational resources.

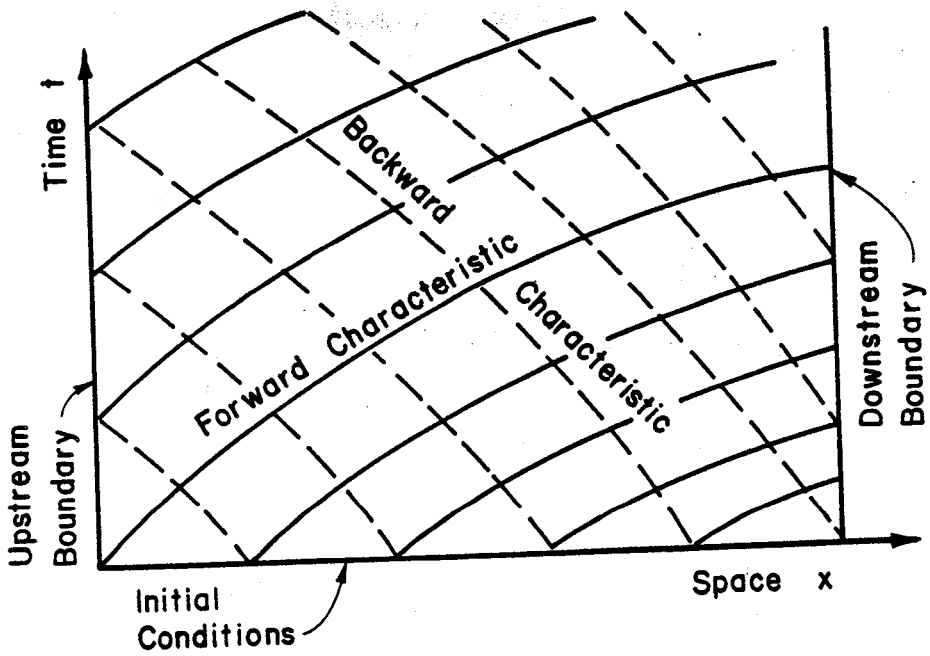

Figure 3-3. Characteristic grid on the x-t plane.

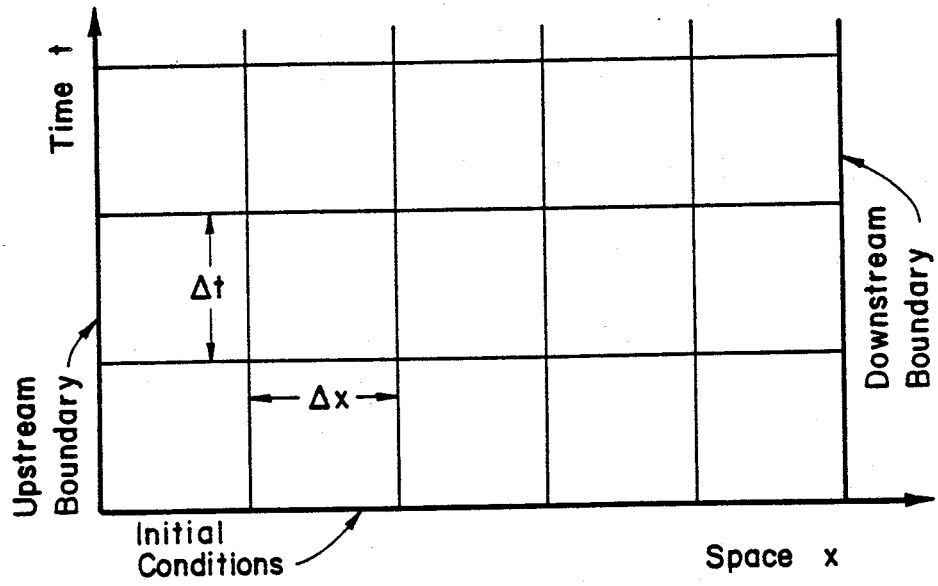

Figure 3-4. Rectangular (finite difference) grid on the x-t plane.

There is a marked difference between the classical and numerical approaches. The latter is based on the complete equations, and therefore, can describe nonlinear effects, looped stage-discharge relationships and other physical details which the classical approach simply cannot consider. On the other hand, the numerical approach represents an altogether higher level of sophistication, demanding not only a thorough understanding of the physical processes, but also a knowledge of numerical mathematics and computer programming. Nevertheless, the increasing use of computers in all aspects of engineering analysis and design guarantees that the numerical approach will continue to play a leading role in the future. The challenge, of course, remains to keep the numerical approach in the proper perspective, making sure that it does not substitute for sound physical reasoning and competent engineering judgment.

The Simplified Approach. The simplified approach to flood routing has its origins in the observations of Hayami, published in 1951 [2]. Hayami pointed out that, given all the irregularities present in natural channels, it is striking that the flow appears steady and nearly uniform in the mean. He reasoned that the disturbances caused by these irregularities quickly damp away as part of a large scale process of longitudinal mixing. This led Hayami to the formulation of a differential equation of flood waves describing convection and diffusion. Later, Lighthill and Whitham [3] used similar physical reasoning to formulate their kinematic wave theory.

In essence, the simplified approach to flood routing is based on the realization that in a large number of practical cases, the inertia terms of the equation of motion play an exceedingly small role. Without these terms, the Saint Venant equations can be combined into one second order partial differential equation describing convection and diffusion. Furthermore, if the pressure gradient term of the equation of motion is also neglected, the resulting equations can be combined into a first order partial differential equation describing only convection. In the terminology introduced in the previous chapter, the convection-diffusion equation forms the basis of the diffusive wave model. Likewise, the convection-only equation is referred to as the kinematic wave model. Both models can be used to describe flood wave movement, provided sufficient care is exercised.

Several comments are necessary regarding the simplified approach to flood routing. First, its solution is based on one partial differential equation; therefore, only one dependent variable (usually discharge Q) can be calculated at a time. The remaining dependent variable (either stage y or flow area A) is calculated from a single-valued rating curve. Strictly speaking, this procedure is correct only as an approximation to the unsteady features of the flood wave which do include a loop in the rating curve (see Fig. 3-5). This apparent limitation can be circumvented in diffusive wave models by belatedly taking into account the nature of this loop (see Chapter 5: Stream Channel Routing Methods).

Second, it is noted that the simplified approach leads to a quasilinear (variable coefficient) partial differential equation. This equation can be solved either in its original form, or linearized

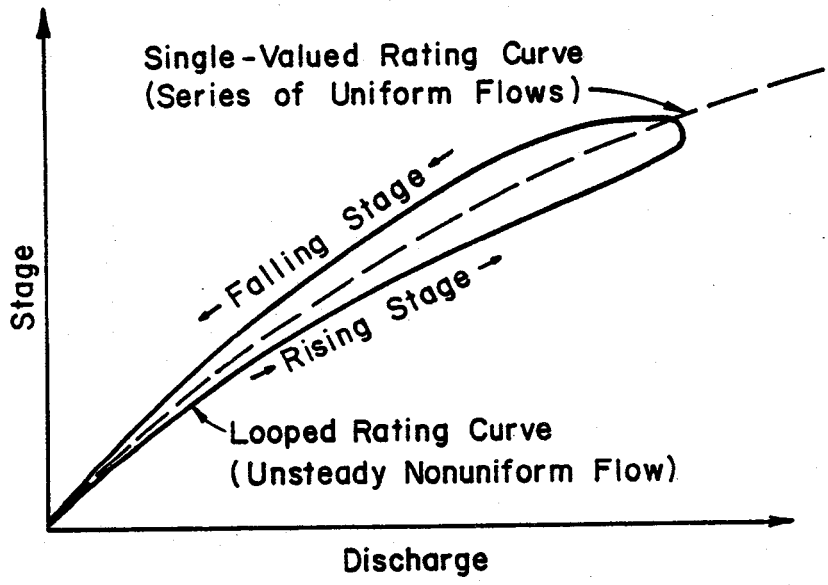

Figure 3-5. Schematic of single-valued and looped rating curves in open channel flow.

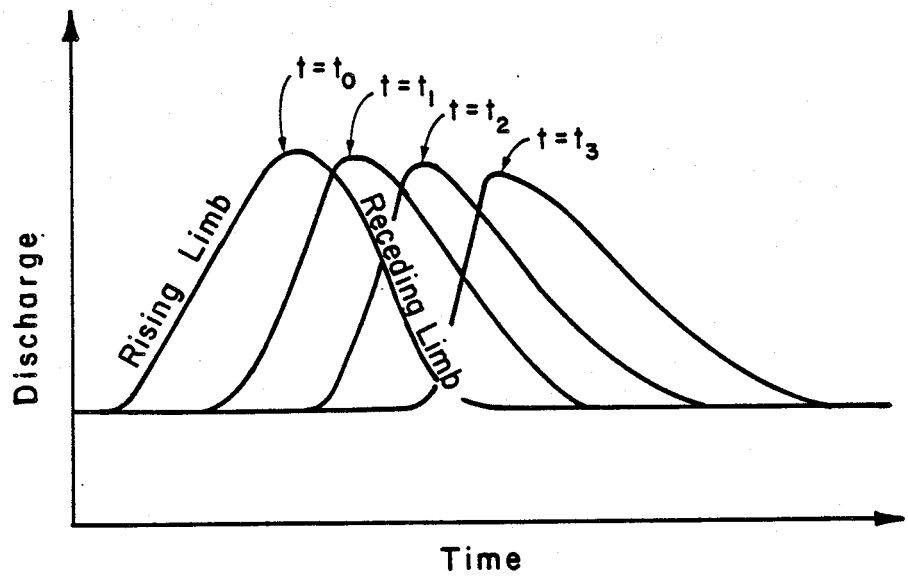

Figure 3-6. Schematic portrayal of the effect of the quasilinear property of a flood wave, manifested as a steepening rising limb and flattening receding limb as the wave moves downstream.

(assuming constant coefficients) in the interest of mathematical expediency. Of course, the quasilinear features of the wave movement are lost in the linearized solution, a situation which can lead to a decrease in the overall accuracy of the simplified approach.

Third, the quasilinear features of the wave movement may lead to physically unrealistic results in a highly simplified model such as the kinematic wave. The quasilinear property is manifested as a steepening rising limb and a flattening receding limb as the wave moves downstream (see Fig. 3-6). If left uncontrolled, the wave steepening will eventually develop into the so-called "kinematic shock," which resembles a dynamic shock but in the absence of inertia. Such problems are altogether avoided in diffusive wave computations. The diffusive wave has its own built-in diffusive properties which tend to counteract the steepening tendency, thus impeding the development of the shock. Therefore, the kinematic shock is totally absent in computations using the diffusive wave.

Relation Between Various Approaches to Stream Channel Routing. Given the apparently widely differing nature of the various approaches to stream channel routing treated here, the question remains: Is there an all-encompassing link? Or stated in other terms: Is there a unifying theory hidden behind the maze of approaches, methods and techniques? The answer to these questions can be found in the work of Cunge [1], who demonstrated the correspondence between the classical approach (e.g., Muskingum method) and the simplified approach (e.g., the convection-diffusion method of Hayami). Since the latter could be construed as a particular case of the numerical approach, the stage was set for a unified theory of flood movement. It is now recognized that all stream channel routing methods can be classified as either kinematic, diffusive or dynamic wave models. The dynamic wave model is the most general, encompassing the other two as particular solutions. While losing somewhat in generality, the diffusive wave model remains widely applicable, encompassing the kinematic wave as a particular solution. The kinematic wave model has a limited range of applicability, being restricted to the cases of very steep bottom slopes (e.g., overland flow) or very long duration (slow-rising) hydrographs.

3.6 SUMMARY

An overview of flood waves and flood routing methods is given in this chapter. Flood routing methods are described as belonging to either one of two classes: (1) reservoir (or lake) routing; and (2) stream channel routing. The notions of flood wave velocity and attenuation for each of these two classes are introduced.

A general classification of flood routing methods is attempted on the basis of the following criteria: (1) the equations used in the formulation; (2) the overall approach to data collection; and (3) the solution technique.

Reservoir and stream channel routing are described in detail, with particular emphasis on the physical processes involved. In stream channel routing, the following three approaches are recognized: (1) the classical approach, of which the Muskingum method is a notable example;

(2) the numerical approach, based on the numerical solution of the complete Saint Venant equations, either by characteristic of finite difference methods; and (3) the simplified approach, which uses a convection-diffusion equation to describe flood wave movement. A closing remark focuses attention on the unified theory of flood wave movement in terms of kinematic, diffusive and dynamic waves.

APPENDIX I. - REFERENCES

1 Cunge, J. A., "On the Subject of a Flood Propagation Computation Method (Muskingum Method)," Journal of Hydraulic Research, Vol. 7, No. 2, 1969, pp. 205-230.

2 Hayami, S., "On the Propagation of Flood Waves," Bulletin No. 1, Disaster Prevention Research Institute, Kyoto University, Kyoto, Japan, December, 1951.

3 Lighthill, M. J. and Whitham, G. B., "On Kinematic Waves, I. Flood Movement in Long Rivers," Proceedings of the Royal Society of London, Vol. A229, May, 1955, pp. 281-316.

APPENDIX II. - NOTATION

The following symbols are used in this chapter:

A = flow area;

B = channel width;

C_1 = Muskingum coefficient;

C_2 = Muskingum coefficient;

C_3 = Muskingum coefficient;

c = flood wave velocity, Eq. 3-1;

I = inflow;

K = parameter of the Muskingum method;

N = storage indication quantity;

O = outflow;

Q = discharge;

t = time variable;

V = volume of storage;

X = parameter of the Muskingum method;

x = space variable;

y = stage; and

Δt = time interval.

STREAM CHANNEL ROUTING

by

V. MIGUEL PONCE

TABLE OF CONTENTS

		Page
5.1	INTRODUCTION	5-1
5.2	CLASSICAL APPROACH	5-1
5.3	SIMPLIFIED APPROACH	5-3
5.4	MUSKINGUM-CUNGE METHOD	5-6
5.5	USE OF CLASSICAL AND SIMPLIFIED APPROACHES	5-10
5.6	SUMMARY	5-11
	APPENDIX I. - THE NUMERICAL DIFFUSION COEFFICIENT OF THE KINEMATIC WAVE EQUATION	5-11
	APPENDIX II. - REFERENCES	5-14
	APPENDIX III. - NOTATION	5-14

5.1 INTRODUCTION

This chapter deals with stream channel routing, its theory, methodologies and practical aspects. The classical and simplified approaches to stream channel routing are treated here in detail. The numerical approach is described in several of the following chapters.

5.2 CLASSICAL APPROACH

The classical approach to stream channel routing is based on the assumption that the storage V in a given channel reach is a function of both inflow I and outflow O. The group of procedures that approximate in some way the relationship between storage, inflow and outflow are referred to here collectively as the classical approach, or also, as coefficient methods of routing. As their name indicates, these methods involve the use of coefficients in a certain type of routing equation. The coefficients as well as the parameters from which they are derived are purely empirical, and are determined by calibration using historical flood records for the reach under study.

The Muskingum Method. Perhaps the best known and most widely used of the coefficient methods is the Muskingum method, developed by the U.S. Army Corps of Engineers in connection with flood control schemes in the Muskingum River Basin, Ohio.

The original Muskingum method was formulated along the following lines. The water continuity equation is expressed in its spatially-integrated form:

$$I - O = \frac{dV}{dt} \tag{5-1}$$

The equation of motion is replaced by a linear storage-inflow-outflow relationship of the following form:

$$V = K[XI + (1-X)O] \tag{5-2}$$

in which K and X are parameters to be determined by calibration using historical flood records on a given reach.

Equation 5-1 can be discretized in time (Fig. 5-1) to yield:

$$\frac{I_{n+1} + I_n}{2} - \frac{O_{n+1} + O_n}{2} = \frac{V_{n+1} - V_n}{\Delta t} \tag{5-3}$$

Likewise, Eq. 5-2 can be expressed at time levels n and $(n+1)$ as:

$$V_n = K[XI_n + (1-X)O_n] \tag{5-4}$$

and

$$V_{n+1} = K[XI_{n+1} + (1-X)O_{n+1}] \tag{5-5}$$

respectively. Substituting Eqs. 5-4 and 5-5 into Eq. 5-3, the following routing equation is obtained:

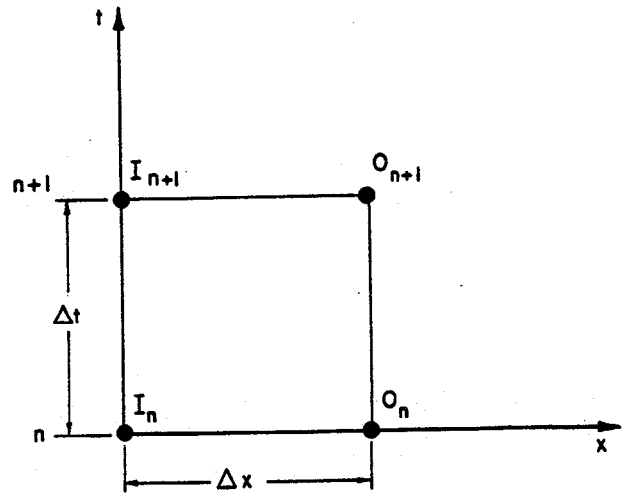

Figure 5-1. Schematic of the Discretization of the Muskingum Method.

$$O_{n+1} = C_1 I_n + C_2 I_{n+1} + C_3 O_n \tag{5-6}$$

in which the coefficients C_1, C_2 and C_3 are defined as:

$$C_0 = \Delta t/K + 2(1-X) \tag{5-7}$$

$$C_1 = (\Delta t/K + 2X)/C_0 \tag{5-8}$$

$$C_2 = (\Delta t/K - 2X)/C_0 \tag{5-9}$$

$$C_3 = [2(1-X) - \Delta t/K]/C_0 \quad . \tag{5-10}$$

Much has been written on the Muskingum method, particularly in reference to the determination of the parameters K and X. The parameter K has the units of time, and has come to be closely associated with the average travel time, i.e., the time it takes the average flood discharge to travel the length of the reach. The parameter X is a weighting factor used for the purpose of matching the attenuation of the calculated hydrograph to that of the observed data. The recommended range for X is $0 \leq X \leq 0.5$. A value of $X = 0$ implies reservoir-type behavior, i.e., storage being only a function of outflow. A value of $X = 0.5$ indicates that the flood hydrograph is not being subject to attenuation. Values of $X > 0.5$ are associated with computational instability.

Discussion. The predictive accuracy of the Muskingum method hinges upon the correct determination of the parameters K and X. These are a function of the flood characteristics, i.e., the hydrograph travel time and attenuation rate, and are usually determined by a process of trial and error calibration. However, since the flood characteristics are likely to vary from one flood to another, it would be rash to assume that the parameters determined from one set of flood records could be used to predict the behavior of an altogether different flood. This, in effect, limits the predictive capability of the method to floods similar to that used in the calibration, and any attempt at extrapolation is unwarranted.

The use of constant parameters in the classical Muskingum method is tantamount to an assumption of linearity, and this is in contradiction with the quasilinear property of flood waves. In addition, the neglect of the looped discharge-stage relations can be justified only as an approximation to the natural phenomena. Nevertheless, the classical Muskingum method remains an expedient way of obtaining approximate answers for a number of practical problems. A comparatively recent improvement, referred to as the Muskingum-Cunge method, considerably enhances the predictive capability of the method, while remaining within the same computational framework. The basic concepts underlying the Muskingum-Cunge method are given later in this chapter.

5.3 SIMPLIFIED APPROACH

The foundations of the simplified approach to stream channel routing are to be found in the work of Hayami [2], Lighthill and Whitham [5], and Cunge [1]. In essence, the simplified approach is based on the realization that the inertia terms in the equation of motion contribute very little to the solution, and can usually be neglected on practical grounds. Without the inertia terms, the Saint Venant equations can be combined into one second order partial differential equation describing the convection and diffusion of a hydraulic quantity, be it either discharge, area or flow depth. Hayami [2] derived a convection-diffusion equation in terms of flow depth (Eq. 2-14). Cunge [1] was able to derive, under some additional assumptions, a convection-diffusion equation in terms of discharge. The latter is particularly useful for stream channel routing applications. For the sake of completeness, this equation is derived here following the approach of Cunge [1].

Derivation of the Convection-Diffusion Equation in Terms of Discharge. The water continuity equation, Eq. 2-11, can be written as:

$$\frac{\partial d}{\partial t} + \frac{1}{B}\frac{\partial Q}{\partial x} = 0 \qquad (5\text{-}11)$$

in which d = flow depth; B = channel width; and Q = discharge. The equation of motion with the neglect of the inertia terms, Eq. 2-10, is expressed as follows:

$$\frac{\partial d}{\partial x} + \frac{Q^2}{k^2} - S_o = 0 \qquad (5\text{-}12)$$

in which Q^2/k^2 = the friction slope; k = channel conveyance ($Q = k\sqrt{S_f}$); and S_o = bottom slope (or alternatively, equilibrium energy slope). For convenience, Eq. 5-12 is expressed as follows:

$$\frac{\partial d}{\partial x} + \eta Q^2 - S_o = 0 \tag{5-13}$$

in which $\eta = 1/k^2$.

A perturbation and linearization technique is used in the derivation of the convection-diffusion equation in terms of discharge. The dependent variables d, η and Q are assumed to be composed of two parts: (1) an equilibrium component; and (2) a transient component; such that

$$d = d_o + d' \tag{5-14}$$

$$\eta = \eta_o + \eta' \tag{5-15}$$

$$Q = Q_o + Q' \tag{5-16}$$

in which the subscripted variables refer to the equilibrium parts, and the superscripted ones to the transient part. The substitution of Eqs. 5-14 to 5-16 into Eqs. 5-11 and 5-13 leads to the following equations of water continuity and motion in terms of superscripted variables:

$$\frac{\partial d'}{\partial t} + \frac{1}{B}\frac{\partial Q'}{\partial x} = 0 \tag{5-17}$$

$$\frac{\partial d'}{\partial x} + 2\eta_o Q_o Q' + Q_o{}^2\eta' = 0 \tag{5-18}$$

in which second and higher order terms in the superscripted variables have been neglected. Experience shows that such a linearization procedure does not compromise the overall accuracy of the analysis.

Differentiating Eq. 5-17 with respect to space, and Eq. 5-18 with respect to time, yields, respectively:

$$\frac{\partial^2 d'}{\partial x \partial t} + \frac{1}{B}\frac{\partial^2 Q'}{\partial x^2} = 0 \tag{5-19}$$

$$\frac{\partial^2 d'}{\partial x \partial t} + 2\eta_o Q_o \frac{\partial Q'}{\partial t} + Q_o{}^2 \frac{\partial \eta'}{\partial t} = 0 \tag{5-20}$$

By using Eq. 5-17 and the chain rule of differentiation:

$$\frac{\partial \eta'}{\partial t} = \frac{\partial \eta'}{\partial d'} \cdot \frac{\partial d'}{\partial t} = -\frac{1}{B} \cdot \frac{\partial \eta'}{\partial d'} \cdot \frac{\partial Q'}{\partial x} \tag{5-21}$$

Substituting Eq. 5-21 into Eq. 5-20:

$$\frac{\partial^2 d'}{\partial x \partial t} + 2\eta_o Q_o \frac{\partial Q'}{\partial t} - \left[\frac{Q_o^{\,2}}{B} \cdot \frac{\partial \eta'}{\partial d'}\right] \frac{\partial Q'}{\partial x} = 0 \qquad (5\text{-}22)$$

Combining Eqs. 5-19 and 5-22, rearranging and dropping the superscripts for simplicity, yields:

$$\frac{\partial Q}{\partial t} + \left[- \frac{Q_o}{2B\eta_o} \cdot \frac{\partial \eta}{\partial d}\right] \frac{\partial Q}{\partial x} = \left[\frac{1}{2B\eta_o Q_o}\right] \frac{\partial^2 Q}{\partial x^2} \qquad (5\text{-}23)$$

which is the convection-diffusion equation with discharge as the dependent variable. The convective celerity c and diffusion coefficient μ are, respectively:

$$c = - \frac{Q_o}{2B\eta_o} \cdot \frac{\partial \eta}{\partial d} \qquad (5\text{-}24)$$

and

$$\mu = \frac{1}{2B\eta_o Q_o} \qquad (5\text{-}25)$$

Equation 5-24 is the kinematic wave celerity as defined by the Kleitz-Seddon law (Eq. 2-8). In order to show this correspondence, recall that

$$Q = \left(\frac{S_f}{\eta}\right)^{1/2} \qquad (5\text{-}26)$$

which leads to:

$$\frac{\partial Q}{\partial \eta} = - \frac{Q_o}{2\eta_o} \qquad (5\text{-}27)$$

around the equilibrium values Q_o and η_o. Substituting Eq. 5-27 into Eq. 5-24, leads to:

$$c = \frac{1}{B} \cdot \frac{\partial Q}{\partial \eta} \cdot \frac{\partial \eta}{\partial d} = \frac{1}{B} \frac{\partial Q}{\partial d} = \frac{\partial Q}{\partial A} = \left.\frac{dQ}{dA}\right|_{x_o} \qquad (5\text{-}28)$$

The diffusion coefficient μ can be alternatively expressed in terms of discharge and slope. In effect, recall that

$$Q_o^{\,2} = k_o^{\,2} S_o = \frac{S_o}{\eta_o} \qquad (5\text{-}29)$$

Therefore, it follows that

$$\mu = \frac{Q_o}{2BS_o} = \frac{q_o}{2S_o} \qquad (5\text{-}30)$$

in which q_o = equilibrium unit-width discharge.

5.4 MUSKINGUM-CUNGE METHOD

The Muskingum-Cunge method of stream channel routing is a variation due to Cunge [1] of the classical Muskingum method. It is based on the realization that a four-point numerical analog of the kinematic wave equation (Eq. 2-7) and the Muskingum storage relationship (Eq. 5-2) lead to the same routing equation (Eq. 5-6). In effect, the kinematic wave equation can be written as follows:

$$\frac{\partial Q}{\partial t} + c\,\frac{\partial Q}{\partial x} = 0 \tag{5-31}$$

in which Q is the flood wave discharge to be convected with the celerity c. In general, c is a function of Q; however, for compatibility with the use of constant parameters K and X, the assumption of constant c is made here.

Equation 5-31 is discretized on the x-t plane as shown in Fig. 5-2 to yield:

$$\frac{X(Q_j^{n+1} - Q_j^n) + (1-X)\,(Q_{j+1}^{n+1} - Q_{j+1}^n)}{\Delta t} + c\,\frac{Y(Q_{j+1}^n - Q_j^n) + (1-Y)\,(Q_{j+1}^{n+1} - Q_j^{n+1})}{\Delta x} = 0 \tag{5-32}$$

in which X and Y = weighting factors; Δx = space interval; Δt = time interval; and c has been taken as constant. Setting $Y = 0.5$, Eq. 5-32 can be expressed as:

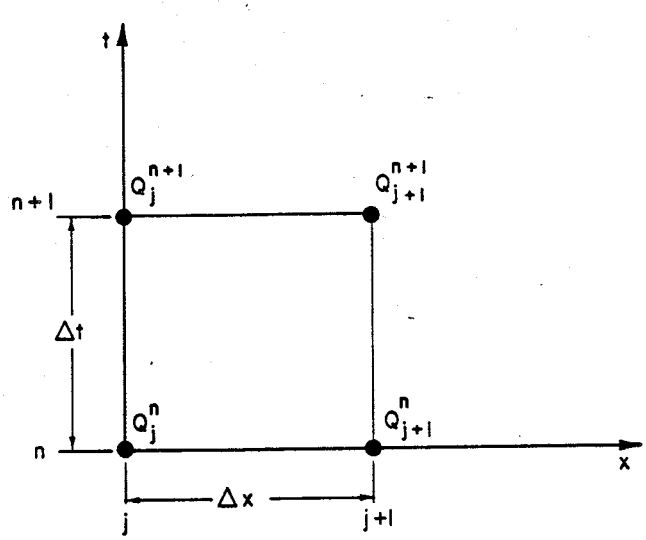

Figure 5-2. Schematic of the Discretization of the Muskingum-Cunge Method.

$$\frac{Q_j^n + Q_j^{n+1}}{2} - \frac{Q_{j+1}^n + Q_{j+1}^{n+1}}{2} =$$

$$\frac{\frac{\Delta x}{c}\left[XQ_j^{n+1} + (1-X)\ Q_{j+1}^{n+1}\right] - \frac{\Delta x}{c}\left[XQ_j^n + (1-X)\ Q_{j+1}^n\right]}{\Delta t} \tag{5-33}$$

In one time increment, the left-hand side of Eq. 5-33 is I-0; the right-hand side is dV/dt if

$$V = \frac{\Delta x}{c}\ [XI + (1-X)0] \tag{5-34}$$

which is recognized as Eq. 5-2, provided $K = \Delta x/c$. Clearly then, the parameter K is the travel time of a representative flood discharge, i.e., the time it takes that discharge to travel the reach length Δx with the celerity c.

The parameter X is recognized as a weighting factor. The use of weighting factors in discrete solutions is ostensibly for the purpose of introducing a certain amount of numerical diffusion, i.e., a diffusion due solely to the finite size of the grid. Cunge [1] was able to use this property of discrete solutions to obtain an estimate of X based on hydraulic quantities. He derived the numerical diffusion coefficient μ_n of the discretized kinematic wave equation (see Appendix I) as:

$$\mu_n = c\Delta x(\tfrac{1}{2} - X) \tag{5-35}$$

By matching this diffusion coefficient with the physical diffusion coefficient (Eq. 5-30) of the convection-diffusion equation, the following expression for X is obtained:

$$X = \frac{1}{2}\left(1 - \frac{q_o}{S_o c\Delta x}\right) \tag{5-36}$$

With $K = \Delta x/c$ and Eq. 5-36, the coefficients C_0 to C_3 (Eqs. 5-7 to 5-10) can be calculated as a function of the flood wave, channel, and grid characteristics. Furthermore, by defining the Courant number C as the following ratio of celerities:

$$C = \frac{c}{\left(\frac{\Delta x}{\Delta t}\right)} = c\ \frac{\Delta t}{\Delta x} \tag{5-37}$$

and the cell Reynolds number D as the following ratio of diffusivities:

$$D = \frac{\left(\frac{q_o}{2S_o}\right)}{\left(\frac{c\Delta x}{2}\right)} = \frac{q_o}{S_o c\Delta x} \tag{5-38}$$

the coefficients C_0 to C_3 can be expressed in the following reduced form:

$$C_0 = 1 + C + D \tag{5-39}$$

$$C_1 = (1 + C - D)/C_0 \tag{5-40}$$

$$C_2 = (-1 + C + D)/C_0 \tag{5-41}$$

$$C_3 = (1 - C + D)/C_0 \tag{5-42}$$

Calculation of the Parameters. Equations 5-39 to 5-42 enable the calculation of the Muskingum coefficients in terms of measurable physical quantities and the characteristics of the grid. These are: 1) the equilibrium (or reference) unit-width discharge q_o; 2) the celerity c corresponding to this discharge; 3) the bottom slope S_o, for channels of regular cross-section (or alternatively, the equilibrium energy slope for channels of irregular cross-section); 4) the time interval Δt; and 5) the space step (or reach length) Δx.

Depending on the modeling needs and resources, the calculation of the parameters in the Muskingum-Cunge method can proceed in one of two ways: either by using (a) constant parameters, or (b) variable parameters. The essential difference between the two is that the use of constant parameters has implicit in it the assumption of linearity, while this is not the case in computations using variable parameters. In the constant parameter method, the linear behavior is associated with a reference value of discharge, the calculation of the parameters being based on this reference value. The accuracy of the computations is shown to be dependent on the choice of reference discharge. For practical purposes, a reference discharge close to the average flood discharge is recommended.

In the variable parameter method, an attempt is made to account for the quasilinear property of flood waves (see Fig. 3-6). This invariably results in an improved definition of certain features of the flood wave, specially in reference to the hydrograph shape and time to peak. Several approaches to the calculation of the variable parameters have been developed, e.g., see Miller and Cunge [6], Price [9], and Ponce and Yevjevich [8]. While there are minor differences in detail between these approaches, that of Ponce and Yevjevich is preferred here due to its simplicity.

Following Ponce and Yevjevich [8], the value of Δt is fixed by considerations of accuracy, the value of Δx is also fixed (reach length), and the value of S_o (equilibrium energy slope) is specified for a given reach. The calculation of variable parameters is based on the variation of the unit-width discharge q and the celerity c. These are defined at grid point (j,n) as:

$$q = \frac{Q}{B}\bigg|_{j,n} \tag{5-43}$$

and

$$c = \frac{dQ}{dA}\bigg|_{j,n} = \frac{1}{B}\frac{dQ}{dy}\bigg|_{j,n} \tag{5-44}$$

in which y = flow stage.

In determining C and D, the values of q and c are calculated either: (1) directly, by using a three-point average of the values of q and c at grid points (j,n), (j+1,n) and (j,n+1); or (2) by iteration, using a four-point average of the values of q and c at grid points (j,n), (j+1,n), (j,n+1) and (j+1, n+1). To improve convergence in the iterative four-point procedure, the results of the three-point procedure can be used as the first guess of the iteration.

Definition of Looped Rating Curves. In the Muskingum-Cunge method, the attenuation of the hydrograph is due to the numerical diffusion effect rather than to the physical process of longitudinal storage. Therefore, the method cannot account for the loop in the rating curve during the passage of the flood, since this loop is a direct consequence of the longitudinal storage. The loop is related to the hydrograph attenuation, larger loops being associated with higher attenuation rates. In certain cases, the definition of the loop may be deemed necessary, especially in connection with hydrographs subject to moderate to high attenuation.

In order to take into account the nature of looped rating curves in the Muskingum method, use is made of the Jones formula and variations of it [3,4,10]. The derivation of this formula is based on the equation for the looped rating curve, expressed in its diffusive wave form:

$$Q = \frac{1}{n} AR^{2/3} \left(S_o - \frac{\partial d}{\partial x}\right)^{1/2} \tag{5-45}$$

in which A = flow area; R = hydraulic radius; n = Manning's friction coefficient; and $(S_o - \partial d/\partial x)$ = friction slope assuming the inertia terms to be negligible. Equation 5-45 can also be expressed as:

$$Q = Q_o \left(1 - \frac{1}{S_o} \frac{\partial d}{\partial x}\right)^{1/2} \tag{5-46}$$

in which Q_o = equilibrium discharge. To derive the Jones formula, the following kinematic argument is resorted to:

$$\frac{\partial d}{\partial x} = - \frac{1}{c} \frac{\partial d}{\partial t} \tag{5-47}$$

Substituting Eq. 5-47 into Eq. 5-46:

$$Q = Q_o \left(1 + \frac{1}{S_o c} \frac{\partial d}{\partial t}\right)^{1/2} \tag{5-48}$$

In addition, by making use of the water continuity and kinematic wave equations, the derivative in Eq. 5-48 can be expressed in terms of discharge, leading to:

$$Q = Q_o \left(1 + \frac{1}{S_o B c^2} \frac{\partial Q}{\partial t}\right)^{1/2} \tag{5-49}$$

Strictly speaking, Eq. 5-47 should not be used in this regard, since it implies the absence of subsidence, which is precisely what is being calculated by the Jones formula. Practical computations, however, serve to reassess the validity of Eq. 5-47, at least as a convenient approximation enabling the calculation of the looped rating curves.

5.5 USE OF CLASSICAL AND SIMPLIFIED APPROACHES

The choice between the classical and simplified approaches on one hand, and the complete numerical models on the other hand, involves considerations of accuracy, ease of application, familiarity with a particular method, and other economic factors. The following advantages of the classical and simplified approaches to stream channel routing are readily recognized: (1) Ease of formulation, manifested in shorter training periods, lower program development costs, lower run costs, and smaller computer size needs; and (2) Applicability for a wide range of practical problems, since the inertia term can be shown to be negligible in a large number of applications.

The major disadvantage is the loss of accuracy resulting from the various assumptions that are made in order to simplify the problem. For instance, upstream wave motions such as those produced in the vicinity of tributary flows or by dams and other control devices, cannot be accounted for in the classical and simplified methods, due primarily to their kinematic formulation. Computational details aside, the simplified methods provide a reasonably good answer to a wide range of problems with a minimum investment of resources. In addition, as shown by Ponce et al. [7] their range of applicability can be clearly delineated in terms of readily identifiable hydraulic quantities.

Criteria for Applicability of Simplified Approach. The criteria for the applicability of kinematic and diffusive wave models is given in detail in Chapter 15. A brief summary is given here.

According to Ponce et al. [7], the error due to the use of the kinematic wave model (error in hydrograph peak accumulated after an elapsed time equal to the hydrograph duration) is within 5%, provided the following inequality is satified:

$$\frac{TS_o u_o}{d_o} \geq 171 \qquad (5\text{-}50)$$

in which T = hydrograph duration; S_o = equilibrium energy slope (or bottom slope, for channels of regular cross-section); u_o = reference mean velocity; and d_o = reference flow depth. When applying Eq. 5-50 to check the validity of the kinematic wave model, the reference values should correspond as closely as possible to the average flow conditions.

The error due to the use of the diffusive wave model (error in hydrograph peak accumulated after an elapsed time equal to the hydrograph duration) is within 5%, provided the following inequality is satisfied:

$$TS_o \left(\frac{g}{d_o}\right)^{1/2} \geq 30 \qquad (5\text{-}51)$$

in which g = acceleration of gravity, and all other terms are as previously defined.

For instance, assume $S_o = 0.001$, $u_o = 3$ fps and $d_o = 10$ ft. The kinematic wave model will apply for hydrographs of duration larger than 6.59 days. Likewise, the diffusive wave model will apply for hydrographs of duration larger than 0.19 days.

5.6 SUMMARY

A description of the theory, methodologies and practical aspects of stream channel routing is given in this chapter. First, the classical approach (Muskingum method) is presented, followed by a discussion on the calculation of the parameters K and X. This leads into the simplified approach based on the convection-diffusion equation. The derivation of this equation with discharge as the dependent variable, allows the calculation of the flood wave celerity and diffusion coefficient in terms of measurable hydraulic quantities.

The Muskingum-Cunge method, in which the parameter K and X are estimated based on Cunge's numerical diffusion theory, is presented. The calculation of the parameters can be carried out either by assuming them constant in space and time, or by varying them throughout the computations. The variable parameter method is shown to preserve the quasilinear property of flood waves, leading to an overall increase in accuracy. The definition of looped rating curves can be belatedly accomplished by using the Jones formula as a convenient approximation to the actual diffusion effect. Finally, several comments are made on the use of the classical and simplified approaches in stream channel routing, and the criteria for the applicability of kinematic and diffusive wave models are briefly described.

APPENDIX I. - THE NUMERICAL DIFFUSION COEFFICIENT OF THE KINEMATIC WAVE EQUATION

The derivation of the numerical diffusion coefficient of the discretized kinematic wave equation (Eq. 5-32) proceeds under the assumption that the grid function $Q\ (j\Delta x,\ n\Delta t)$ can be expanded as a Taylor series about grid point $(j\Delta x,\ n\Delta t)$. This leads to:

$$Q_j^{n+1} - Q_j^n = \left.\frac{\partial Q}{\partial t}\right|_j \Delta t + \frac{1}{2}\left.\frac{\partial^2 Q}{\partial t^2}\right|_j \Delta t^2 + o(\Delta t^3) \qquad (5\text{-}52)$$

$$Q_{j+1}^{n+1} - Q_{j+1}^n = \left.\frac{\partial Q}{\partial t}\right|_{j+1} \Delta t + \frac{1}{2}\left.\frac{\partial^2 Q}{\partial t^2}\right|_{j+1} \Delta t^2 + o(\Delta t^3) \qquad (5\text{-}53)$$

$$Q^n_{j+1} - Q^n_j = \left.\frac{\partial Q}{\partial x}\right|_n \Delta x + \frac{1}{2}\left.\frac{\partial^2 Q}{\partial x^2}\right|_n \Delta x^2 + o(\Delta x^3) \tag{5-54}$$

$$Q^{n+1}_{j+1} - Q^{n+1}_j = \left.\frac{\partial Q}{\partial x}\right|_{n+1} \Delta x + \frac{1}{2}\left.\frac{\partial^2 Q}{\partial x^2}\right|_{n+1} \Delta x^2 + o(\Delta x^3) \tag{5-55}$$

Substituting Eqs. 5-52 to 5-55 into Eq. 5-32, neglecting third order terms, yields:

$$X\left[\left.\frac{\partial Q}{\partial t}\right|_j \Delta t + \frac{1}{2}\left.\frac{\partial^2 Q}{\partial t^2}\right|_j \Delta t^2\right] + (1-X)\left[\left.\frac{\partial Q}{\partial t}\right|_{j+1} \Delta t + \frac{1}{2}\left.\frac{\partial^2 Q}{\partial t^2}\right|_{j+1} \Delta t^2\right]$$

$$+ CY\left[\left.\frac{\partial Q}{\partial x}\right|_n \Delta x + \frac{1}{2}\left.\frac{\partial^2 Q}{\partial x^2}\right|_n \Delta x^2\right] + C(1-Y)\left[\left.\frac{\partial Q}{\partial x}\right|_{n+1} \Delta x + \frac{1}{2}\left.\frac{\partial^2 Q}{\partial x^2}\right|_{n+1} \Delta x^2\right] = 0 \tag{5-56}$$

in which $C = c\,\Delta t/\Delta x$ is the Courant number.

The derivatives at $[(j+1)\Delta x,\ (n+1)\Delta t]$ can be expressed in terms of the derivatives at $(j\Delta x,\ n\Delta t)$ by means of Taylor series:

$$\left.\frac{\partial Q}{\partial t}\right|_{j+1} = \left.\frac{\partial Q}{\partial t}\right|_j + \left.\frac{\partial^2 Q}{\partial x \partial t}\right|_{j,n} \Delta x + o(\Delta x^2) \tag{5-57}$$

$$\left.\frac{\partial Q}{\partial x}\right|_{n+1} = \left.\frac{\partial Q}{\partial x}\right|_n + \left.\frac{\partial^2 Q}{\partial x \partial t}\right|_{j,n} \Delta t + o(\Delta t^2) \tag{5-58}$$

$$\left.\frac{\partial^2 Q}{\partial t^2}\right|_{j+1} = \left.\frac{\partial^2 Q}{\partial t^2}\right|_j + \left.\frac{\partial^3 Q}{\partial t^3}\right|_j \Delta x + o(\Delta x^2) \tag{5-59}$$

$$\left.\frac{\partial^2 Q}{\partial x^2}\right|_{n+1} = \left.\frac{\partial^2 Q}{\partial x^2}\right|_n + \left.\frac{\partial^3 Q}{\partial x^3}\right|_n \Delta t + o(\Delta t^2) \tag{5-60}$$

Substituting Eqs. 5-57 to 5-60 into 5-56, and neglecting third order terms:

$$X\left[\left.\frac{\partial Q}{\partial t}\right|_j \Delta t + \frac{1}{2}\left.\frac{\partial^2 Q}{\partial t^2}\right|_j \Delta t^2\right] + (1-X)\left[\left.\frac{\partial Q}{\partial t}\right|_j \Delta t + \left.\frac{\partial^2 Q}{\partial x \partial t}\right|_{j,n} \Delta x \Delta t + \frac{1}{2}\left.\frac{\partial^2 Q}{\partial t^2}\right|_j \Delta t^2\right]$$

$$+ CY\left[\left.\frac{\partial Q}{\partial x}\right|_n \Delta x + \frac{1}{2}\left.\frac{\partial^2 Q}{\partial x^2}\right|_n \Delta x^2\right] +$$

$$C(1-Y)\left[\left.\frac{\partial Q}{\partial x}\right|_n \Delta x + \left.\frac{\partial^2 Q}{\partial x \partial t}\right|_{j,n} \Delta x \Delta t + \frac{1}{2}\left.\frac{\partial^2 Q}{\partial x^2}\right|_n \Delta x^2\right] = 0 \tag{5-61}$$

Simplifying Eq. 5-61, and dividing by Δt:

$$\left[\left.\frac{\partial Q}{\partial t}\right|_j + c\left.\frac{\partial Q}{\partial x}\right|_n\right] + \frac{\Delta t}{2}\left.\frac{\partial^2 Q}{\partial t^2}\right|_j + \frac{c\Delta x}{2}\left.\frac{\partial^2 Q}{\partial x^2}\right|_n + \Delta x[(1-X) + C(1-Y)]\left.\frac{\partial^2 Q}{\partial x \partial t}\right|_{j,n} = 0 \tag{5-62}$$

In Eq. 5-62, the first term enclosed in brackets is Eq. 5-31. Therefore, the remaining terms constitute the error R of the numerical solution due to the neglect of the second order terms:

$$R = \frac{\Delta t}{2}\left.\frac{\partial^2 Q}{\partial t^2}\right|_j + \frac{c\Delta x}{2}\left.\frac{\partial^2 Q}{\partial x^2}\right|_n + \Delta x[(1-X) + C(1-Y)]\left.\frac{\partial^2 Q}{\partial x \partial t}\right|_{j,n} \tag{5-63}$$

From Eq. 5-31:

$$\frac{\partial Q}{\partial t} = -c\frac{\partial Q}{\partial x} \tag{5-64}$$

therefore:

$$\frac{\partial^2 Q}{\partial t^2} = -c\frac{\partial}{\partial t}\left(\frac{\partial Q}{\partial x}\right) = -c\frac{\partial}{\partial x}\left(\frac{\partial Q}{\partial t}\right) = c^2\frac{\partial^2 Q}{\partial x^2} \tag{5-65}$$

$$\frac{\partial^2 Q}{\partial x \partial t} = -c\frac{\partial^2 Q}{\partial x^2} \tag{5-66}$$

Substituting Eqs. 5-65 and 5-66 into Eq. 5-63, and simplifying:

$$R = c\Delta x[(X - \tfrac{1}{2}) + C(Y - \tfrac{1}{2})]\frac{\partial^2 Q}{\partial x^2} \tag{5-67}$$

Drawing a parallel with the diffusive wave equation:

$$\frac{\partial Q}{\partial t} + c\frac{\partial Q}{\partial x} = \mu\frac{\partial^2 Q}{\partial x^2} \tag{5-68}$$

the numerical diffusion coefficient of the discretized kinematic wave equation is

$$\mu_n = c\Delta x[(\tfrac{1}{2} - X) + C(\tfrac{1}{2} - Y)] \tag{5-69}$$

In the particular case of the Muskingum method, only the weighting factor X is used. Therefore, Y = 0.5, leading to:

$$\mu_n = c\Delta x(\tfrac{1}{2} - X) \tag{5-70}$$

as the numerical diffusion coefficient associated with the Muskingum method.

APPENDIX II. - REFERENCES

1 Cunge, J. A., "On the Subject of a Flood Propagation Computation Method (Muskingum Method)," Journal of Hydraulic Research, Vol. 7, No. 2, 1969, pp. 205-230.

2 Hayami, S., "On the Propagation of Flood Waves," Bulletin No. 1, Disaster Prevention Research Institute, Kyoto University, Kyoto, Japan, December, 1951.

3 Henderson, F. M., "Open Channel Flow," The Macmillan Company, New York, New York, 1966.

4 Koussis, A., "An Approximate Dynamic Flood Routing Method," Paper L1, Proceedings of the International Symposium on Unsteady Flow in Open Channels, Newcastle-upon-Tyne, England, April, 1976.

5 Lighthill, M. J., and Whitham, G. B., "On Kinematic Waves, I. Flood Movement in Long Rivers," Proceedings of the Royal Society of London, Vol. A229, May, 1955, pp. 281-316.

6 Miller, W. A., and Cunge, J. A., "Simplified Equations of Unsteady Flow," Chapter 5 in Unsteady Flow in Open Channels, K. Mahmood and V. Yevjevich, eds., Water Resources Publications, Fort Collins, Colorado, 1975, pp. 183-257.

7 Ponce, V. M., Li, R. M., and Simons, D. B., "Applicability of Kinematic and Diffusion Models," Journal of the Hydraulics Division, ASCE, Vol. 104, HY3, March, 1978, pp. 353-360.

8 Ponce, V. M., and Yevjevich, V., "Muskingum-Cunge Method with Variable Parameters," Journal of the Hydraulics Division, ASCE, Vol. 104, HY12, December, 1978, pp. 1663-1667.

9 Price, R. K., "A River Catchment Flood Model," Proceedings of the Institution of Civil Engineers, Vol. 65, Part 2, September, 1978, pp. 655-668.

10 Weinmann, P. E., and Laurenson, E. M., "Approximate Flood Routing Methods: A Review," Journal of the Hydraulics Division, ASCE, Vol. 105, HY12, Proc. Paper 15057, December, 1979, pp. 1521-1535.

APPENDIX III. - NOTATION

The following symbols are used in this chapter:

A = flow area;

B = channel width;

C = Courant number, Eq. 5-37;

C_0 = coefficient, Eqs. 5-7 and 5-39;

C_1 = Muskingum coefficient, Eqs. 5-8 and 5-40;

C_2 = Muskingum coefficient, Eqs. 5-9 and 5-41;

C_3 = Muskingum coefficient, Eqs. 5-10 and 5-42;

c = convective celerity;

D = cell Reynolds number, Eq. 5-38;

d = flow depth;

g = acceleration of gravity;

I = inflow;

K = Muskingum parameter;

k = channel conveyance;

n = Manning's friction coefficient;

O = outflow;

o = little o function (on the order of);

Q = discharge;

q = unit-width discharge;

R = hydraulic radius, approximation error;

S_f = friction slope;

S_o = bottom slope (alternatively, equilibrium energy slope);

T = flood hydrograph duration;

t = time variable;

u = mean velocity;

V = volume of storage;

X = Muskingum parameter, weighting factor;

x = space variable;

Y = weighting factor;

y = stage;

Δx = space step (reach length);

Δt = time interval;

η = reciprocal of the square of the channel conveyance;

μ = diffusion coefficient (hydraulic diffusivity); and

μ_n = numerical diffusion coefficient.

Subscripts

j = space index

n = time index, and

o = equilibrium value.

Superscripts

' = perturbation; and

n = time index.

THE MUSKINGUM-CUNGE METHOD

by

V. MIGUEL PONCE

TABLE OF CONTENTS

		Page
6.1	INTRODUCTION	6-1
6.2	MUSKINGUM METHOD	6-1
6.3	CALCULATION OF THE VARIABLE PARAMETERS	6-2
6.4	ILLUSTRATIVE EXAMPLE	6-2
6.5	SIMPLIFIED MUSKINGUM ROUTING EQUATION	6-5
6.6	CALCULATION OF SPACE AND TIME INTERVALS FOR SIMPLIFIED ROUTING EQUATION	6-6
6.7	TESTING OF SIMPLIFIED ROUTING EQUATION	6-7
6.8	PARAMETER RANGE AND ACCURACY	6-8
6.9	SUMMARY	6-9
	APPENDIX I. - DERIVATION OF LATERAL INFLOW TERM	6-9
	APPENDIX II. - REFERENCES	6-10
	APPENDIX III. - NOTATIONS	6-11

6.1 INTRODUCTION

This chapter deals with the Muskingum method and its related Muskingum-Cunge version to a greater level of detail than in Chapter 5. Examples are given to illustrate the computational behavior of the constant and variable parameter methods. A simplified routing method is described, applicable to certain specialized cases. Finally, a note is made on the range of parameters in which accuracy is maintained.

6.2 MUSKINGUM METHOD

The formula for the Muskingum Method is (see Fig. 5.2):

$$Q^{n+1}_{j+1} = C_1 Q^n_j + C_2 Q^{n+1}_j + C_3 Q^n_{j+1} \tag{6-1}$$

in which

$$C_1 = \frac{\frac{\Delta t}{K} + 2X}{\frac{\Delta t}{K} + 2(1-X)} \tag{6-2}$$

$$C_2 = \frac{\frac{\Delta t}{K} - 2X}{\frac{\Delta t}{K} + 2(1-X)} \tag{6-3}$$

$$C_3 = \frac{2(1-X) - \frac{\Delta t}{K}}{\frac{\Delta t}{K} + 2(1-X)} \tag{6-4}$$

where Δt is the routing period (time interval). In the Muskingum-Cunge version, the parameters K and X are calculated by (3,4,5,7):

$$K = \frac{\Delta x}{c} \tag{6-5}$$

$$X = \frac{1}{2}\left(1 - \frac{q}{S_o c \Delta x}\right) \tag{6-6}$$

in which Δx = reach length (space interval); c = flood wave celerity; q = unit width discharge; and S_o = equilibrium water surface slope. Substituting Eqs. 6-5 and 6-6 into Eqs. 6-2 to 6-4:

$$C_1 = \frac{1+C-D}{1+C+D} \tag{6-7}$$

$$C_2 = \frac{-1+C+D}{1+C+D} \tag{6-8}$$

$$C_3 = \frac{1-C+D}{1+C+D} \tag{6-9}$$

in which $C = c\Delta t/\Delta x$ is the Courant number; and $D = q/(S_o c\Delta x)$ is a cell Reynolds number. Both C and D have physical and numerical significance, C being a ratio of celerities and D a ratio of diffusivities.

6.3 CALCULATION OF THE VARIABLE PARAMETERS

Usually, Δt is fixed, and Δx and S_o are specified for each computational cell consisting of four grid points. Therefore, it is necessary to determine the flood wave celerity, c, and the unit width discharge, q, for each computational cell. The values of c and q at grid point (j,n) are defined by

$$c = \left.\frac{dQ}{dA}\right|_{j,n} \tag{6-10}$$

$$q = \left.\frac{Q}{B}\right|_{j,n} \tag{6-11}$$

in which Q = discharge; A = flow area; and B = top width. The following ways of determining c and q for use in calculating C and D have been investigated: (1) Directly, by using a two-point average of the values at grid points (j,n) and (j+1,n); (2) directly, by using a three-point average of the values at grid points (j,n), (j+1,n), and (j,n+1); and (3) by iteration, using a four-point average calculation. To improve convergence, the values at (j+1,n+1) obtained by the three-point average method can be used as the first guess of the iteration.

6.4 ILLUSTRATIVE EXAMPLE

The Muskingum-Cunge method with variable parameters has been applied to the problem posed by Thomas in his classical paper on flood routing (9). The problem consists of tracking the travel and subsidence of a flood wave of sinusoidal shape in a unit-width channel with a steady-state rating curve given by:

$$q = 0.688\ d^{5/3} \tag{6-12}$$

The inflow hydrograph is defined by:

$$Q(t) = 125 - 75 \cos\left(\frac{\pi t}{48}\right), \qquad 0 \le t \le 96;$$

$$Q(t) = 50, \qquad t > 96 \tag{6-13}$$

in which t is given in hours.

Thomas applied an approximate method to route the flood wave through a channel 200 miles (322 km) long, using a time interval of Δt = 12 hr. Thomas' approximate method neglects the inertia terms; therefore, his results are directly comparable to those of the Muskingum method (both the Thomas and Muskingum methods can be considered as numerical analogs of the diffusive wave equation).

Figure 6-1 and Table 6-1 summarize the results of computations using the Muskingum-Cunge method with variable parameters. For comparison purposes, the calculations using constant parameters for three reference values of discharge are also shown.

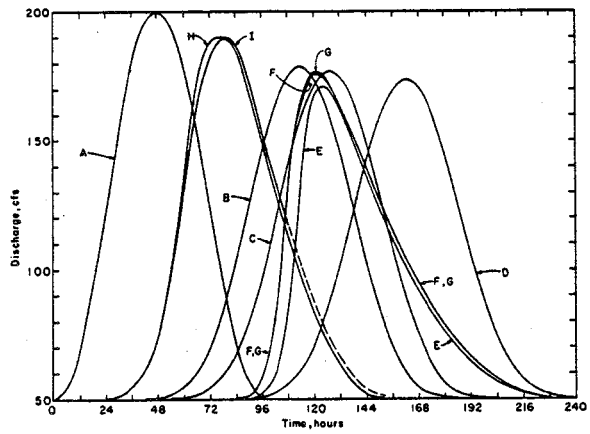

Figure 6-1. Calculated hydrographs as described in Table 6-1.

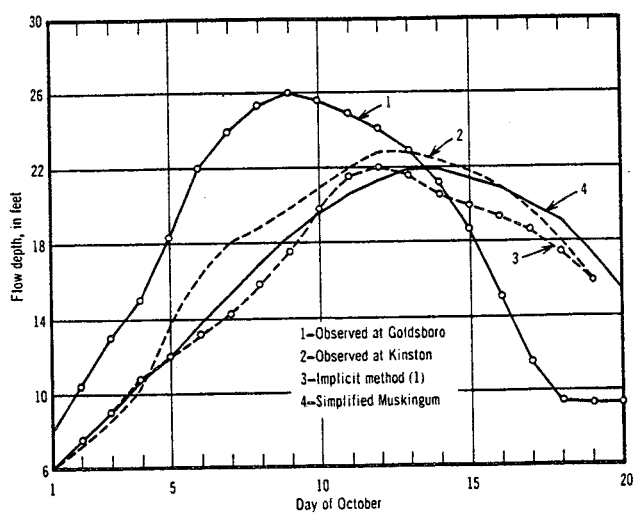

Figure 6-2. Computed and Observed October, 1964 Flood Hydrographs at Goldsboro and Kinston, NC (1 ft = 0.305 m).

TABLE 6-1
SUMMARY OF FLOOD ROUTING COMPUTATIONS
USING CONSTANT AND VARIABLE PARAMETER METHODS

Hydrograph (1)	Station, in miles (2)	Method* (3)	Δx, in miles (4)	Δt, in hours (5)	Peak q, in cubic feet per second (6)	Time to peak in hours (7)	Mass conservation, as a percentage (8)
A	0	-	-	-	200	48	-
B	500	MC/200	25	6	178.5	114	100
C	500	MC/125	25	6	177	128	100
D	500	MC/50	25	6	173.5	162	100
E	500	VPMC2	25	6	171	124	85
F	500	VPMC3	25	6	175.5	121	98
G	500	VPMC4	25	6	176.5	121	99
H	200	VPMC4	25	12	190	77	100
I	200	Thomas(9)	25	12	189	79	-

*MC/200 = constant parameter method, reference discharge 200 cfs (5.66 m^3/s); MC/125 = reference discharge 125 cfs (3.54 m^3/s); MC/50 = reference discharge 50 cfs (1.41 m^3/s); VPMC2 = two-point variable parameter method; VPMC3 = three-point variable parameter method; and VPMC4 = four-point variable parameter method.

TABLE 6-2

COMPARISON OF MEASURED AND CALCULATED HYDROGRAPHS AT KINSTON, NC, FLOOD OF OCTOBER, 1964

Method (1)	Peak flow depth (2)	Date (3)	Lateral inflow, q_L, in cubic feet per second/foot (4)
Measured	22.8	October 13	-[a]
Implicit	22.0	October 12	0.01
Simplified	21.9	October 14	0.01

[a]Unknown, but believed to be within 0.005-0.02 cfs/ft (1).

The examination of Fig. 6-1 enables the following conclusions to be drawn:

1. The Muskingum-Cunge method with constant parameters (hydrographs B, C, and D) shows results that are dependent on the value of reference discharge chosen to evaluate the constant parameters. The higher the reference discharge, the faster the rate of travel and the lesser the subsidence of the flood wave. The calculated outflow hydrographs show negligible distortion from the initially sinusoidal shape, implying that the constant parameter assumption is tantamount to an assumption of linearity.

2. The Muskingum-Cunge method with variable parameters (hydrographs E, F, and G) shows results that fall within the range encompassed by the constant parameter calculations. The noticeable steepening of the rising limb of the calculated outflow hydrographs indicates that the nonlinearity of the phenomenon is being taken into account. The three-point and four-point methods give similar results; however, the two-point method shows a smaller peak and a somewhat slower rate of travel. Furthermore, the two-point method results in a significant loss of mass, as indicated in Col. 8 of Table 6-1.

6.5 SIMPLIFIED MUSKINGUM ROUTING EQUATION

The variable parameter method has an increased accuracy, especially in the definition of the shape of the hydrograph. However, in the cases in which only an estimate of peak flow is desired, it may be sufficient to use the constant parameter method, especially if a good value of reference discharge can be estimated for any one flood wave.

The calculation using constant parameters can proceed in one of two ways. The conventional way is to specify the space and time intervals Δx and Δt, and to calculate K and X (or C and D) therefrom. An alternate way is to specify K and X and to calculate Δx and Δt from them. The proper choice of parameters can result in a considerable simplification in the routing equation, leading to a reasonably accurate solution of the flood rating problem with a minimum of computational effort.

In Eqs. 6-2 to 6-4, if $\Delta t/K$ and X are specified as

$$\frac{\Delta t}{K} = 1 \tag{6-14}$$

and

$$X = 0 \tag{6-15}$$

it follows that

$$C_1 = C_2 = C_3 = \frac{1}{3} \tag{6-16}$$

and the simplified form of the Muskingum routing equation is given as follows:

$$Q_{j+1}^{n+1} = \frac{Q_j^n + Q_j^{n+1} + Q_{j+1}^n}{3} \tag{6-17}$$

The satisfaction of Eqs. 6-14 and 6-15 implies that Δx and Δt are fixed. In effect, K is defined as the time it takes a flood discharge to travel a distance Δx with celerity c:

$$K = \frac{\Delta x}{c} \tag{6-18}$$

Therefore, from Eqs. 6-14 and 6-18:

$$C = \frac{c\Delta t}{\Delta x} = 1 \tag{6-19}$$

Equation 6-19 specifies that the flood wave celerity c be equal to the "grid celerity" $\Delta x/\Delta t$.

The parameter X can be related to the physical problem by the following formula:

$$X = \frac{1}{2}\left(1 - \frac{q}{S_o c\Delta x}\right) \tag{6-20}$$

Equations 6-15 and 6-20 lead to

$$D = \frac{q}{S_o c\Delta x} = 1 \tag{6-21}$$

Equation 6-21 specifies that the channel diffusivity $q/2S_o$ be equal to the "grid diffusivity" $c\Delta x/2$.

Equations 6-19 and 6-21 enable the calculation of Δx and Δt as a function of the flow variables. In this regard, it should be noted that the space interval computed from Eq. 6-21 is the same as the "characteristic length" on which the Kalinin-Milyukov method is based (7). However, the method described here leads to a routing equation (Eq. 6-17) which is much simpler than that of the Kalinin-Milyukov method.

6.6 CALCULATION OF SPACE AND TIME INTERVALS FOR SIMPLIFIED ROUTING EQUATION

From Eqs. 6-19 and 6-21, the space and time intervals are given by

$$\Delta x = \frac{q}{S_o c} \tag{6-22}$$

and

$$\Delta t = \frac{\Delta x}{c} = \frac{q}{S_o c^2} \tag{6-23}$$

For natural (nonprismatic) channels, the channel friction and cross-sectional shape are implicity stated in the following steady-state discharge-area relation:

$$Q = \alpha A^{\beta} \tag{6-24}$$

in which A = cross-sectional flow area; and α and β = a coefficient and exponent, respectively.

The flood wave celerity is the kinematic wave celerity defined as

$$c = \frac{dQ}{dA} = \alpha\beta A^{\beta-1} = \frac{\beta Q}{A} = \frac{\beta Bq}{A} \tag{6-25}$$

in which B = top width. From Eqs. 6-22 and 6-25:

$$\Delta x = \frac{A}{\beta BS_o} \tag{6-26}$$

and

$$\Delta t = \frac{\Delta x}{c} = \frac{A^{2-\beta}}{\alpha\beta^2 BS_o} \tag{6-27}$$

Some judgment is required in the choice of the reference hydraulic variables (i.e., q, A and B in Eqs. 6-25 to 6-27) on which to base the calculations of Δx and Δt. The use of average quantities is usually sufficient from the standpoint of accuracy.

6.7 TESTING OF SIMPLIFIED ROUTING EQUATION

The testing of a mathematical model usually hinges upon whether the model can reproduce measured field data. When discrepancies occur, however, it is very difficult and sometimes impossible to determine whether they are due to errors in the numerical solution, in the estimation of the parameters, or in the measured data. A procedure currently open to question consists of lumping all these errors into one, and adjusting the model parameters to fit the measured data in what has been referred to as "calibration."

A sounder approach consists of isolating the sources of error in order to study their effects separately. This is done by performing both a hypothetical test and a real data test. The hypothetical test is designed to isolate the effects of numerical accuracy on the model results. On the other hand, the real data test is designed to provide information on the accuracy of the parameter estimation. Errors in the measured data can only be assessed from a qualitative standpoint.

Hypothetical Test. A hypothetical test using the classical example of Thomas (9) was set up to test the simplified method described herein. The following two runs were made: (1) A test run using the simplified method; and (2) a control run using the conventional constant parameter method. In the test run, X was made equal to zero and K equal to Δt. Accordingly, the space and time intervals were calculated to be Δx = 13.5 miles (21.7 km) and Δt = 2.16 hr.

In the control run, the space and time intervals were specified to be Δx = 25 miles (40 km) and Δt = 6 hr. This resulted in X = 0.228 and K = $\Delta t/1.5$. The following hydraulic variables were used in both

tests: (1) Base flow = 50 cfs (1.4 m^3/s); (2) peak inflow = 200 cfs (5.7 m^3/s); (3) reference flow = 125 cfs (3.54 m^3/s); (4) channel length = 500 miles (800 km); and (5) channel bed slope = 1 ft/mile (0.19 m/km).

The calculated results for peak outflow = 177 cfs (5.1 m^3/s), travel time = 128 hr, and hydrograph shape were essentially the same for both runs. Therefore, the demonstrated grid-independence of the results can be taken as a measure of the soundness of the simplified method.

Real Data Test. A real data test using flood data measured by the United States Geological Survey in the 45-mile (72 km) reach of the Neuse River, between Goldsboro and Kinston, NC, was set up to further test the simplified routing Eq. 6-17. The details of the data are given in Amein and Fang (1) and Chen (2).

The reference cross-sectional area and top width were chosen to correspond to the average hyraulic depth in the reach: A = 17,900 square ft (1,660 m^2); and B = 2,900 ft (890 m). The average rating curve constants are the following: α = 12, and β = 0.74; and the equilibrium water surface slope is S_o = 0.000133. From Eqs. 6-26 and 6-27, the space and time intervals were calculated to be Δx = 11.9 miles (19 km), and Δt = 25 hr. These values were further adjusted to Δx = 11.25 miles (18 km) and Δt = 24 hr, thus providing an even number of grid points (four computational reaches and 19 time steps). In order to account for the lateral inflow, the discharge calculated by Eq. 6-17 was corrected by adding $Q_L = 2q_L\Delta x/3$ = 396 cfs (11.2 m^3/s) at every computational cell (see Appendix I).

The following general observations are made (Fig. 6-2):

1. None of the methods can reproduce exactly the measured hydrograph at Kinston. The reason for this lies in the uncertainty regarding the amount of lateral inflow which is likely to be space and time dependent. Amein and Fang (1) have documented the sensitivity of the calculated results to the lateral inflow, and have used a constant q_L (lateral inflow) in their model.

2. Table 6-2 shows a comparison of the results for peak flow depth and time of passage for the measured data, implicit method and simplified method. In view of the uncertainties involved in the estimation of the amount of lateral inflow, the results of the simplified method are certainly within reason.

3. The simplified method belongs to the family of diffusive wave models. The applicability of these models has been treated in detail elsewhere (see Chapter 14).

6.8 PARAMETER RANGE AND ACCURACY

The question of what limits to impose on the reach length Δx has puzzled the users of the Muskingum method. Computational experience indicates that for very large values of Δx, the accuracy of the overall

computation may suffer. Weinmann and Laurenson (10) have suggested an upper limit for Δx given by:

$$\Delta x \leq \frac{cT_r}{2X} \tag{6-28}$$

in which c = flood wave celerity; T_r = duration of rise of inflow hydrograph; and X = Muskingum parameter. On the other hand, Koussis (6) recommends a more conservative upper limit for Δx:

$$\Delta x \leq \frac{c\Delta t}{2X} \tag{6-29}$$

in which Δt = time interval. The question of an upper limit on Δx for accuracy considerations has to be answered by considering not only the Courant number C, but also the cell Reynolds number D. If accuracy is to be preserved, the following inequality should hold:

$$CD \geq \xi \tag{6-30}$$

In practice, a value of $\xi = 0.25$ will provide satisfactory results for most cases.

The question of the lower limit for Δx has also led to some confusion. A lower limit for Δx would imply that there is an upper limit for C and D. However, experience shows that values of $C > 1$ do not lead to stability problems. This behavior is explained by recalling that the Muskingum method is a spatially-weighted finite difference formulation of the kinematic wave equation. This feature provides unconditional stability with respect to the Courant condition (8). Furthermore, there appears to be no theoretical upper limit for D. Values of $D > 1$ imply that $X < 0$, a condition which has come to be widely recognized as a physical impossibility. However, values of $D > 1$ can be safely used, and no physical unreality is attached to the results of the computations.

6.9 SUMMARY

The constant and variable parameter Muskingum-Cunge methods are described and compared. The use of the variable parameter method is justified in the cases where a more exact definition of the hydrograph shape is desired. For all other cases, the use of the constant parameter method in which the reference discharge is carefully chosen, will provide sufficient accuracy for practical purposes.

A simplified routing method is described, in which the space and time intervals are specified in such a way that $X = 0$ and $K = \Delta t$. In this case, the routing equation reduces to the computation of a simple average. Testing of this method shows that reasonably accurate results can be obtained with a minimum of computational effort.

Finally, a criterion is given regarding grid size, if accuracy is to be preserved in flood routing computations using the Muskingum-Cunge method. This criterion is readily satisfied in most cases of practical interest.

APPENDIX I.-DERIVATION OF LATERAL INFLOW TERM

The Muskingum routing equation with lateral inflow is:

$$Q^{n+1}_{j+1} = C_1 Q^n_j + C_2 Q^{n+1}_j + C_3 Q^n_{j+1} + Q_L \tag{6-31}$$

in which

$$Q_L = \frac{2cq_L \, \Delta t}{\frac{\Delta t}{K} + 2(1-X)} \tag{6-32}$$

Since $c = \Delta x/K$, and for the condition $K = \Delta t$ and $X = 0$, Eq. 6-32 reduces to

$$Q_L = \frac{2q_L \Delta x}{3} \tag{6-33}$$

APPENDIX II.-REFERENCES

1 Amein, M., and Fang, C. S., "Implicit Flood Routing in Natural Channels," Journal of the Hydraulics Division, ASCE, Vol. 96, No. HY12, Proc. Paper 7773, Dec., 1970, pp. 2481-2500.

2 Chen, Y. H., "Mathematical Modeling of Water and Sediment Routing in Natural Channels," thesis presented to Colorado State University at Fort Collins, Colo. in 1973, in partial fulfillment of the requirement for the degree of Doctor of Philosophy.

3 Cunge J. A., "On the Subject of a Flood Propagation Computation Method (Muskingum Method)," Journal of Hydraulic Research, Vol. 7, No. 2, 1969, pp. 205-230.

4 "Flood Studies Report, Vol. III: Flood Routing Studies," Natural Environment Research Council, London, England, 1975.

5 Koussis, A., "Theoretical Estimation of Flood Routing Parameters," Journal of the Hydraulics Division, ASCE, Vol. 104, No. HY1, Proc. Paper 13456, Jan., 1978, pp. 109-115.

6 Koussis, A., "An Approximate Dynamic Flood Routing Method," Proceedings, International Symposium on Unsteady Flow in Open Channels, Paper L1, Newcastle-Upon-Tyne, England, 1976.

7 Miller, W. A., and Cunge, J. A., "Simplified Equations of Unsteady Flow," Unsteady Flow in Open Channels, K. Mahmood and V. Yevjevich, eds., Water Resources Publications, Fort Collins, Colo., 1975, pp. 183-257.

8 Ponce, V. M., Chen, Y. H., and Simons, D. B., "Unconditional Stability in Convection Computations," Journal of the Hydraulics Division, ASCE, Vol. 105, HY9, Proc. Paper 14807, Sept., 1979, pp. 1079-1086.

10 Thomas, H. A., "The Hydraulics of Flood Movement in Rivers," Engineering Bulletin, Carnegie Institute of Technology, Pittsburgh, Pa., 1934.

11 Weinmann, P. E., and Laurenson, E. M., "Approximate Flood Routing Methods: A Review," Journal of the Hydraulics Division, ASCE, Vol. 105, HY12, Proc. Paper 15057, Dec., 1979, pp. 1521-1535.

APPENDIX III. - NOTATION

The following symbols are used in this chapter:

A = cross-sectional flow area;

B = channel top width;

C = Courant number;

C_1 = coefficient, Eq. 6-7;

C_2 = coefficient, Eq. 6-8;

C_3 = coefficient, Eq. 6-9;

c = flood wave celerity;

d = flow depth;

j = spatial index;

K = Muskingum parameter;

n = temporal index;

Q = discharge;

Q_L = lateral inflow;

q = unit-width discharge;

q_L = lateral inflow per unit of channel length;

T_r = duration of rise of inflow hydrograph;

X = Muskingum parameter;

α = coefficient in Eq. 6-24; and

β = exponent in Eq. 6-24.

PROPERTIES OF NUMERICAL SOLUTIONS

by

V. MIGUEL PONCE

TABLE OF CONTENTS

		Page
9.1	INTRODUCTION	9-1
9.2	FUNDAMENTALS OF THE CALCULUS OF FINITE DIFFERENCES	9-1
9.3	TYPES OF DIFFERENCE SCHEMES	9-5
9.4	STABILITY AND CONVERGENCE	9-8
9.5	SUMMARY	9-13
	APPENDIX I. - GLOSSARY OF TERMS	9-13
	APPENDIX II. - REFERENCES	9-14
	APPENDIX III. - NOTATION	9-14

9.1 INTRODUCTION

The properties of numerical methods, specifically in relation to the use of finite differences for the solution of unsteady open channel flow problems, are presented in this chapter. First, some basic concepts on the calculus of finite differences are given, followed by a classification of finite difference schemes into: (1) explicit; and (2) implicit. Finally, the properties of numerical solutions, i.e., stability, consistency and convergence, are described in relation to the type of difference scheme and the associated differential equation. Appendix I contains a Glossary of Terms designed to help the reader gain familiarity with the terminology in common use in this area.

9.1 FUNDAMENTALS OF THE CALCULUS OF FINITE DIFFERENCES

This section presents several basic concepts regarding the use of finite difference methods in open channel flow computations. The emphasis throughout this section is on developing the proper background for a better understanding of the numerical properties of finite difference solutions.

Difference Equations. A difference equation is an algebraic equation relating the values of one or more dependent variables (say, discharge Q, or stage y) defined on a discrete domain of one or more independent variables (space x or time t). The discrete domain is represented as a grid system on the x-t plane.

The difference equation is obtained by the application of a certain finite difference scheme to the differential equation describing the problem under consideration. This procedure allows the conversion of an analytical statement of the problem (for which a solution may be either difficult or impossible), into an algebraic statement for which a numerical solution can generally be made available.

The properties of numerical solutions are closely associated with the properties of the differential equations from which they derive. Therefore, the study of differential equations is the logical starting point in the understanding of the properties of numerical solutions. Differential equations can be of two types: (1) ordinary (one independent variable); and (2) partial (two or more independent variables). The differential equation which arises most commonly in hydraulic computations is the second order partial differential equation in two independent variables and one dependent variable. Accordingly, this type of equation will be discussed here in more detail.

Differential Equations. The second order partial differential equation can be derived by combining, under the proper assumptions, the two first order partial differential equations of water continuity and motion. In general, the linear form of this equation is:

$$A(x,y)\frac{\partial^2\phi}{\partial x^2} + B(x,y)\frac{\partial^2\phi}{\partial x\partial y} + C(x,y)\frac{\partial^2\phi}{\partial y^2}$$

$$+ D(x,y)\frac{\partial\phi}{\partial x} + E(x,y)\frac{\partial\phi}{\partial y} + F(x,y)\phi + G(x,y) = 0 \qquad (9\text{-}1)$$

in which ϕ = dependent variable; x,y = independent variables; and A, B, C, D, E, F, and G = coefficients. Equation 1 can be classified into the following three types: (1) elliptic; (2) parabolic; and (3) hyperbolic. The value of the discriminant $\Delta = B^2 - 4AC$ determines the type of equation, and with it, the properties of its solution. If $\Delta < 0$, the equation is said to be of elliptic type; if $\Delta = 0$, the equation is parabolic; and if $\Delta > 0$, the equation is of hyperbolic type. As an illustration of these concepts, consider first the Laplace equation for two-dimensional potential flow:

$$\frac{\partial^2\phi}{\partial x^2} + \frac{\partial^2\phi}{\partial y^2} = 0 \tag{9-2}$$

In Eq. 9-2, the values of the coefficients of Eq. 1 are: A = 1; B = 0; and C = 1. Therefore, $\Delta = -4$, and the Laplace equation is of the elliptic type.

Consider another example: that of the convection-diffusion equation which is applicable to flood propagation problems. In its linear form, it is expressed as:

$$\frac{\partial Q}{\partial t} + c\,\frac{\partial Q}{\partial x} - \mu\,\frac{\partial^2 Q}{\partial x^2} = 0 \tag{9-3}$$

Equation 9-3 is parabolic, since $A = -\mu$; B = 0; and C = 0; leading to $\Delta = 0$. Furthermore, the linear wave equation:

$$\frac{\partial^2 u}{\partial t^2} - c^2\,\frac{\partial^2 u}{\partial x^2} = 0 \tag{9-4}$$

is of the hyperbolic type, since $A = -c^2$; B = 0; and C = 1; leading to $\Delta = 4c^2$.

Elliptic equations are generally associated with equilibrium or steady-state problems in two spatial dimensions. For example, the velocity potential for the steady flow of an incompressible inviscid fluid satisfies Laplace's equation, and it is the mathematical way of expressing the fact that the rate at which such fluid enters a given region is equal to the rate at which it leaves it. The analytical solution of an elliptic equation is a function of the space variables x and y which satisfies the differential equation at every point of an area A inside a domain limited by a plane closed curve C (see Fig. 9-1), and satisfies certain conditions at every point of this curve. Those are termed the boundary conditions. Problems associated with elliptic equations are sometimes referred to as "boundary value" or "jury" problems.

Parabolic and hyperbolic equations arise in connection with unsteady problems in one spatial dimension. In contrast to the closed domain typical of the elliptic case, parabolic and hyperbolic problems are characterized by a "open" domain (Fig. 9-2). Therefore, in addition to the differential equations, initial conditions (t = 0) and boundary

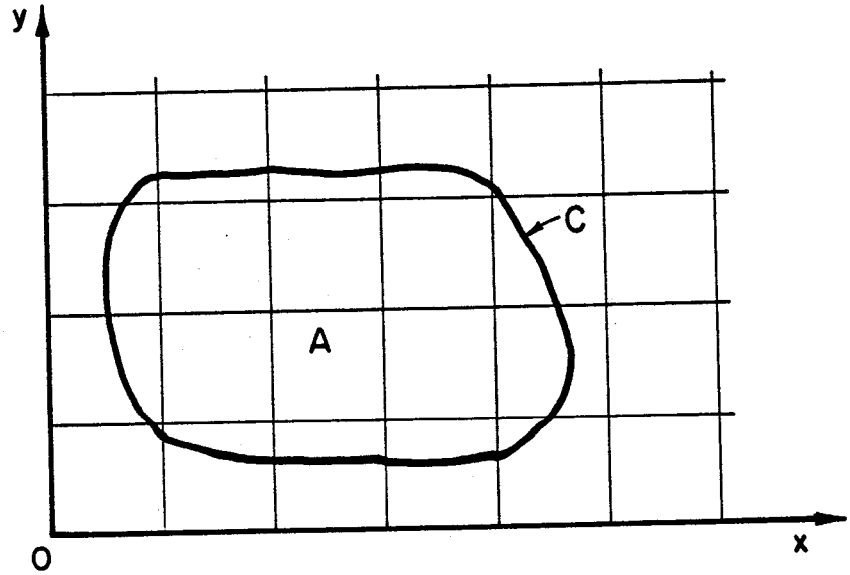

Figure 9-1. Schematic portrayal of the closed domain associated with elliptic equations.

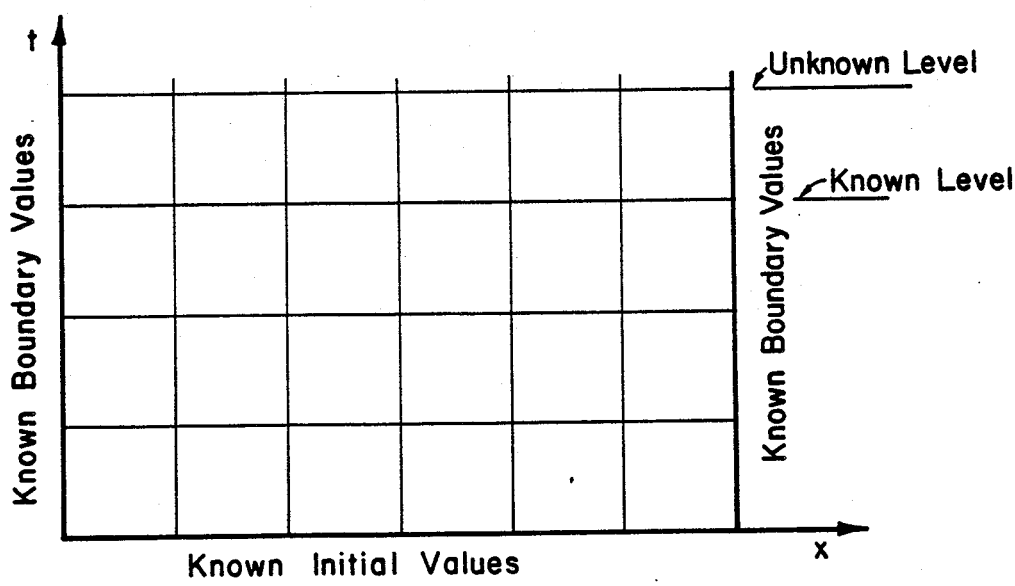

Figure 9-2. Schematic portrayal of the open domain associated with parabolic and hyperbolic equations.

conditions (e.g., x = 0) need to be specified. Problems associated with parabolic and hyperbolic equations are also referred to as "mixed initial-boundary value" or "marching" problems, the latter ostensibly because of the way in which they propagate the solution forward from one time level to the next in a step-by-step fashion.

The essential difference between parabolic and hyperbolic equations is the number of solutions. Parabolic equations possess only one solution, while hyperbolic equations invariably lead to two solutions. The awareness of this difference can be of significant help in the study of the behavior of numerical solutions of parabolic and hyperbolic equations.

Finite Difference Operators. A numerical solution by a finite difference method requires that the domain of the independent variables (space and time) be discretized into a finite number of grid points. The set of grid points within the domain is referred to as the grid system, or grid configuration. The properties of the numerical solution, namely, stability, consistency and convergence, are determined by: (1) the pattern and spacing of grid points; (2) the nature of the problem being solved; and (3) the structure of the finite difference "scheme" being used to solve it.

A finite difference scheme is a computational molecule consisting of one or more finite difference operators. Difference operators can be of the following three types: (1) forward; (2) backward; and (3) central. For instance, the differential operator $\partial\phi/\partial x$ can be discretized on the x domain around grid point j using a forward difference operator $(\phi_{j+1}-\phi_j)/\Delta x$; a backward difference operator $(\phi_j-\phi_{j-1})/\Delta x$; or a central difference operator $(\phi_{j+1}-\phi_{j-1})/2\Delta x$, (see Fig. 9-3).

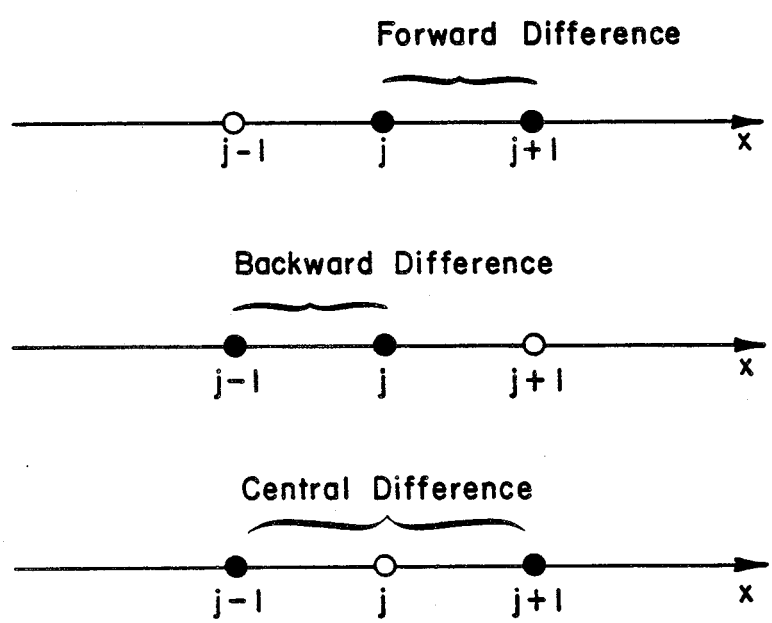

Figure 9-3. Difference operators.

In order to study the properties of difference operators, assume that the function ϕ can be expanded in Taylor series, leading to:

$$\phi_{j+1} = \phi_j + \frac{\partial\phi}{\partial x}\Delta x + \frac{1}{2}\frac{\partial^2\phi}{\partial x^2}\Delta x^2 + \frac{1}{6}\frac{\partial^3\phi}{\partial x^3}\Delta x^3 + o\ (\Delta x^4) \qquad (9\text{-}5)$$

$$\phi_{j-1} = \phi_j - \frac{\partial\phi}{\partial x}\Delta x + \frac{1}{2}\frac{\partial^2\phi}{\partial x^2}\Delta x^2 - \frac{1}{6}\frac{\partial^3\phi}{\partial x^3}\Delta x^3 + o\ (\Delta x^4) \qquad (9\text{-}6)$$

The order of approximation (order of error) of the forward difference operator can be obtained from Eq. 9-5:

$$\frac{\partial\phi}{\partial x} = \frac{\phi_{j+1}-\phi_j}{\Delta x} + o(\Delta x) \qquad (9\text{-}7)$$

in which $o(\Delta x)$ denotes the order of error, given by the exponent of Δx.

Likewise, the order of error of the backward difference operator can be obtained from Eq. 9-6:

$$\frac{\partial\phi}{\partial x} = \frac{\phi_j-\phi_{j-1}}{\Delta x} + o(\Delta x) \qquad (9\text{-}8)$$

Here again, the error is of first order. Finally, substracting Eq. 9-6 from Eq. 9-5:

$$\frac{\partial\phi}{\partial x} = \frac{\phi_{j+1}-\phi_{j-1}}{2\Delta x} + o(\Delta x^2) \qquad (9\text{-}9)$$

which shows that the error of the central difference operator is of second order.

On the basis of the foregoing analysis, it is concluded that the off-centered (forward and backward) difference operators lead to first order errors, while the central operator leads to second order errors. For the same grid spacing (Δx), second order errors are smaller than first order errors. Stated in more general terms, the higher the order of the error, the closer the approximation of the numerical solution to the analytical solution. This fundamental property of difference operators is of significant value in connection with the problem of stability, consistency and convergence to be treated later in this chapter.

9.3 TYPES OF FINITE DIFFERENCE SCHEMES

Finite difference schemes can be either: (1) explicit; or (2) implicit. Explicit schemes lead to a difference equation containing only one unknown variable. For instance, in Fig. 9-4, assume that the

values of ϕ are known at time level n and unknown at time level (n+1). An explicit scheme for the diffusion equation

$$\frac{\partial\phi}{\partial t} = \mu\frac{\partial^2\phi}{\partial x^2} \tag{9-10}$$

is

$$\frac{\phi_j^{n+1}-\phi_j^n}{\Delta t} = \mu\,\frac{\phi_{j+1}^n-2\phi_j^n+\phi_{j-1}^n}{\Delta x^2} \tag{9-11}$$

from which the unknown value of ϕ_j^{n+1} can be calculated directly.

Implicit schemes lead to a difference equation containing more than one unknown variable. An implicit scheme for the diffusion equation is (see Fig. 9-5):

$$\frac{\phi_j^{n+1}-\phi_j^n}{\Delta t} = \mu\,\frac{\phi_{j+1}^{n+1}-2\phi_j^{n+1}+\phi_{j-1}^{n+1}}{\Delta x^2} \tag{9-12}$$

in which the unknowns occur in triads, and the solution requires the inversion of a matrix.

Explicit vs. Implicit Schemes. The choice between explicit and implicit schemes generally involves considerations of the cost of program development vs. the cost of program operation. Explicit schemes are easy to formulate and program for use with a computer, resulting in lower development costs. However, they are usually subject to a strict stability condition, which effectively places are upper limit on the size of the time step that can be used in practice.

Implicit schemes, on the other hand, are free from the stability condition usually imposed on explicit schemes. Therefore, there is no limitation on the size of the time step for stability reasons. The time step, however, cannot be chosen arbitrarily large. Care should be taken to ensure that the continuum problem is being properly discretized. For instance, large errors would result if a hydrograph of 24-hr duration (T=24) is simulated by using a time step of, say, 12 hours (Δt=12).

Not all explicit schemes are subject to a stability condition. For instance, for convection-diffusion problems, unconditionally stable explicit schemes can be formulated. Furthermore, implicit schemes cannot be regarded as altogether free from stability problems. Instability due to nonlinear interaction, roundoff errors, improper boundary conditions, etc., are often present in computations using an implicit scheme. The use of weighting factors (off-centering the temporal or spatial derivatives) is common in this connection, ostensibly to allow the operation of an otherwise unstable numerical scheme.

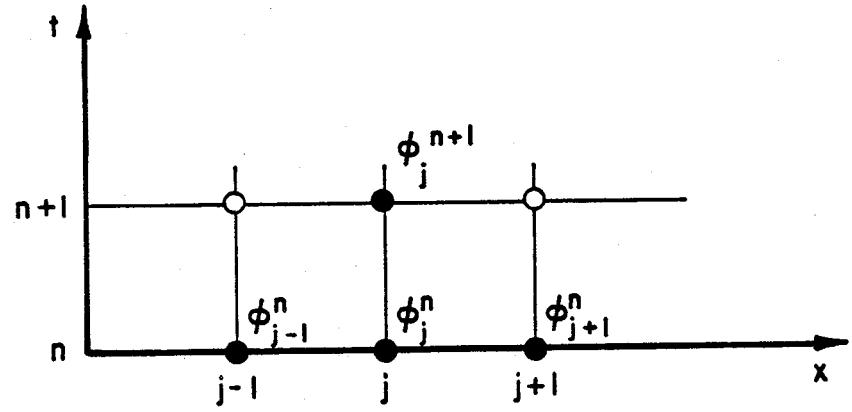

Figure 9-4. Grid configuration for an explicit scheme of the diffusion equation.

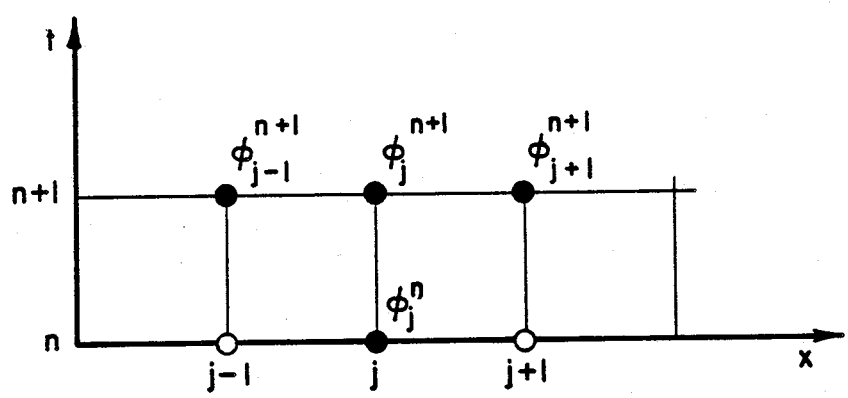

Figure 9-5. Grid configuration for an implicit scheme of the diffusion equation.

The advantage of being able to use a comparatively larger time step with implicit schemes is somewhat offset by the additional complications involved, including the need to solve large sets of simultaneous equations. Still, the choice between explicit and implicit schemes remains primarily one of cost, although convenience and efficiency play a significant role.

9.4 STABILITY AND CONVERGENCE

The properties of numerical solutions are conveniently discussed in terms of the concepts of stability and convergence. In order to illustrate these concepts, the following definitions are introduced [2]. Let D, Δ and N be the solution to the differential equation, the solution to the difference equation, and the numerical (actual) solution, respectively. The quantity (Δ-N) is defined as the roundoff error. It exists because of the inability of the computer to carry out the numerical computations to an infinite number of decimal places. The quantity (D-Δ) is the discretization error due to the finite distance between two neighboring grid points. Stability is associated with conditions such that the roundoff error is small throughout the region of integration. Convergence is related to the size of the discretization error.

Stability. In general, stability refers to the ability of a numerical scheme to inhibit error growth. An unstable scheme is that in which a certain type of numerical error (usually roundoff error) is allowed to grow unbounded until it eventually spoils the calculations. The causes of instability are related to the following: (1) the type of differential equation (e.g., ordinary, partial; first order, second order; linear, nonlinear); (2) the type of continuum system (e.g., elliptic, parabolic or hyperbolic, in the case of linear second partial differential equations); and (3) the type of finite difference scheme (explicit or implicit).

Explicit schemes of hyperbolic systems are subject to the Courant-Friedrichs-Lewy stability criterion. This criterion states that for stability to be maintained, it is necessary that the domain of dependence of the difference equation encompass the domain of dependence of the differential equation (see Fig. 9-6). This leads to:

$$\frac{\Delta x}{\Delta t} \geq c \tag{9-13}$$

in which c = phase velocity of the physical wave. For a given c and Δx, Eq. 9-13 effectively imposes as upper limit on the size of the Δt that can be used in practice. This may often result in an inefficient computation due to the large number of time steps necessary to solve a particular problem.

In implicit schemes, the domain of dependence of the difference equation entirely encompasses the domain of dependence of the solution (see Fig. 9-7). Therefore, implicit schemes are not limited by the Courant-Friedrichs-Lewy criterion. Their unconditional stability allows the use of larger time steps than those usually possible with explicit

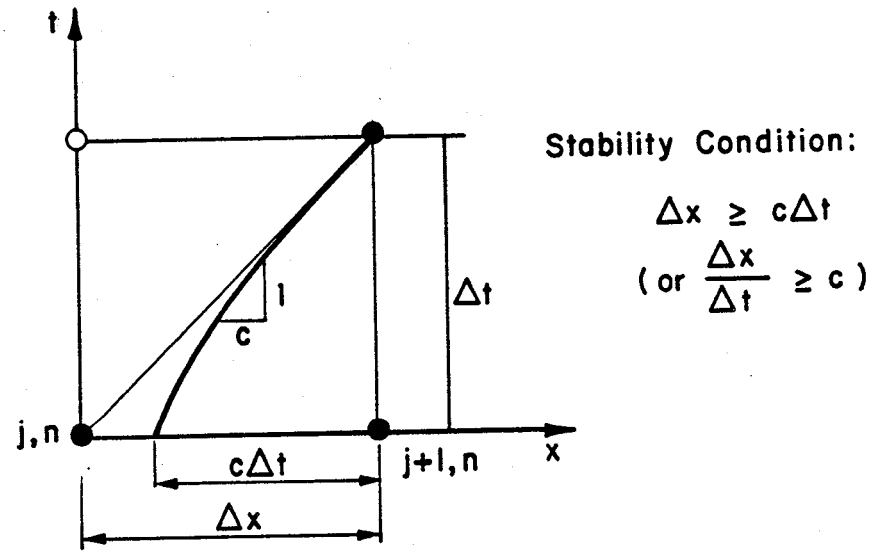

Figure 9-6. Schematic illustrating the stability condition of explicit schemes.

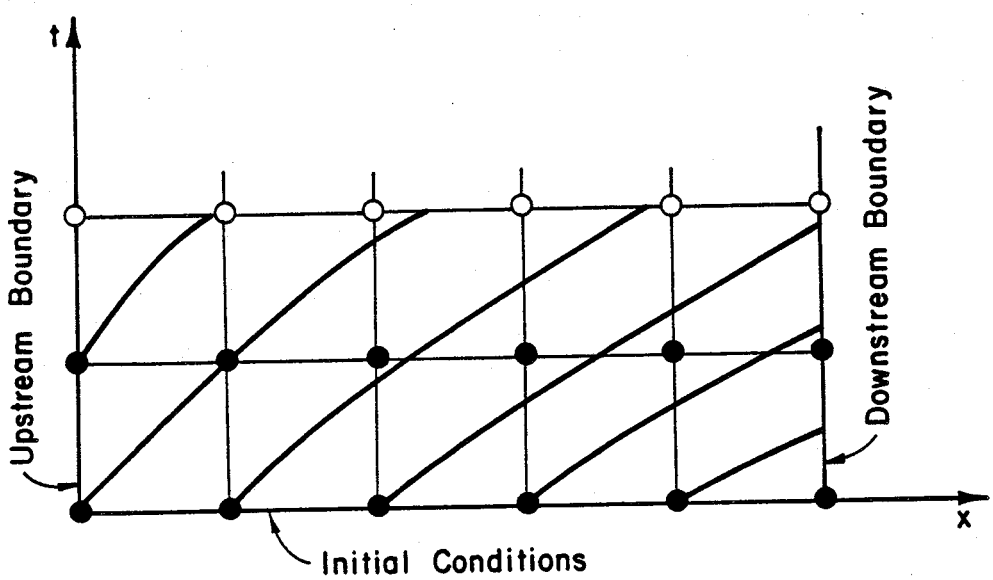

Figure 9-7. Characteristic structure illustrating the unconditional stability of implicit schemes.

schemes. The time step, however, cannot be chosen arbitrarily large. There is a practical limit dictated by the grid resolution above which accuracy would be considerably impaired. In order to remain within reasonable error bounds, experience dictates that the value of $T/\Delta t$ should be greater than 15.

Implicit schemes are not totally free from stability problems. Instabilities of a different nature (e.g., nonlinear interaction, improper boundary conditions) can sometimes plague computations using an implicit scheme. As an illustration of this fact, the Preissmann implicit scheme [1], when used in connection with the Saint Venant equations, can lead to instabilities for certain values of the weighting factor. In the Preissmann scheme, the spatial derivative $\partial\phi/\partial x$ is discretized as:

$$\frac{\partial\phi}{\partial x} = \theta \frac{\phi_{j+1}^{n+1}-\phi_j^{n+1}}{\Delta x} + (1-\theta) \frac{\phi_{j+1}^{n}-\phi_j^{n}}{\Delta x} \tag{9-14}$$

in which θ = weighting factor, restricted in the range $0.5 \leq \theta \leq 1.0$. Within this range, the lower the value of θ, the more the likelihood of instability. In practice, values of $\theta \geq 0.55$ are used to suppress any unstable tendencies which may tend to develop during the computations.

Consistency and Convergence. Consistency refers to the ability of a numerical scheme to produce a solution that approaches the analytical solution as the discretization is made exceedingly small. Convergence is a measure of the size of the discretization errors in any one numerical solution. These concepts are conveniently illustrated by the use of error portraits, as shown in Fig. 9-8. In this figure, the grid resolution (spatial $L/\Delta x$ or temporal $T/\Delta t$) is plotted in the abscissas, and the convergence ratio R, defined as the ratio of numerical to analytical solutions, is plotted in the ordinates. The property of consistency is illustrated by comparing the error portraits of schemes labeled A and B. As the grid resolution increases, scheme A is shown to be consistent with the differential equation; the opposite can be said of scheme B.

The property of convergence is illustrated by comparing the errors portraits of schemes A and C. While both schemes may be in error for low values of grid resolution, it is apparent that for the same accuracy, scheme C requires a much higher value of grid resolution. Scheme A is said to "converge faster" than scheme C.

In explicit schemes, convergence is usually associated with a certain grid configuration which is a function of the properties of the continuum problem. For instance, the convection equation:

$$\frac{\partial C}{\partial t} + u \frac{\partial C}{\partial x} = 0 \tag{9-15}$$

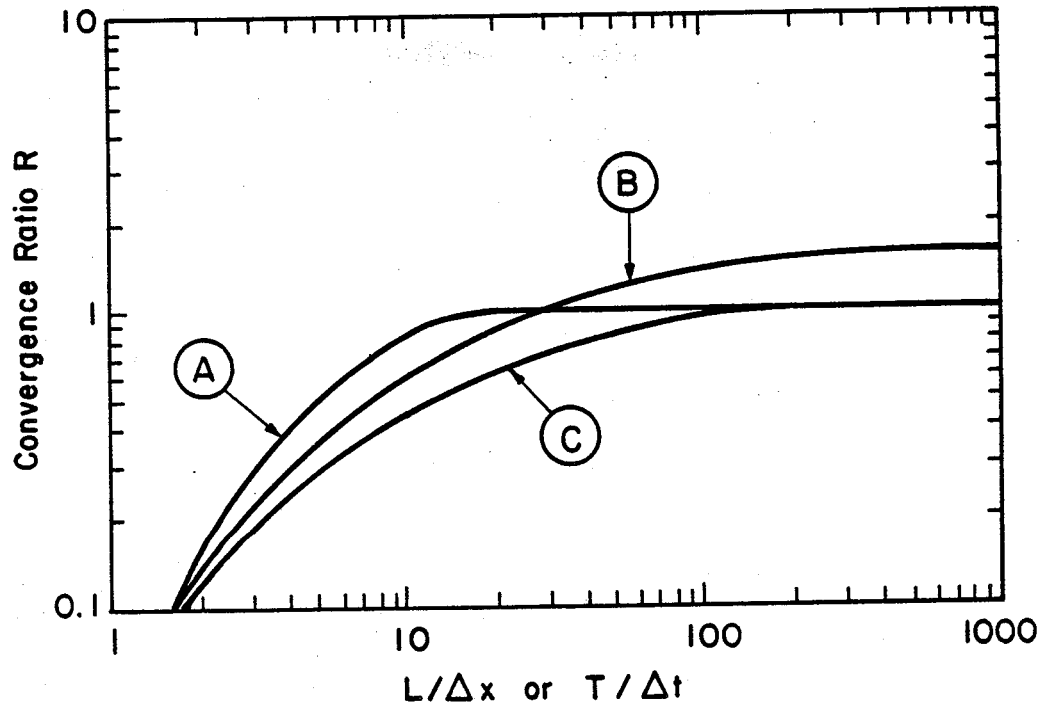

Figure 9-8. Schematic error portraits illustrating the concepts of consistency and convergence.

in which C = concentration, can be discretized using the so-called upstream differencing scheme (Fig. 9-9):

$$\frac{C_j^{n+1}-C_j^n}{\Delta t} + u\,\frac{C_j^n-C_{j-1}^n}{\Delta x} = 0 \qquad (9\text{-}16)$$

In this case, optimum convergence ($R \to 1$) is achieved where the computational time step Δt equals the characteristic time step Δt_c, given as:

$$\Delta t_c = \frac{\Delta x}{u} \qquad (9\text{-}17)$$

Since this is precisely the upper limit from the stability standpoint, it is common practice to set $\Delta t = 0.9\ \Delta t_c$, assuring both stability and adequate convergence.

In implicit schemes, convergence is associated with a certain combination of weighting factor and grid resolution. In general, the closer the weighting factor is to a central value (e.g., $\theta \to 0.5$), the better are the convergence properties of the numerical solution. This behavior is illustrated in Fig. 9-10.

Stability vs. Convergence. Generally speaking, the properties of stability and convergence are at odds in numerical modeling applications, i.e., the more stable the model, the less convergent it is. Therefore, the task is to seek an optimum compromise between the

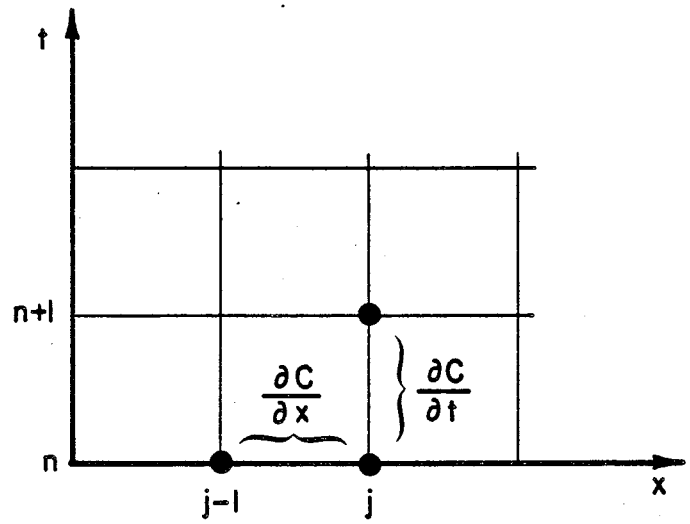

Figure 9-9. Grid configuration for the upstream differencing scheme of the convection equation.

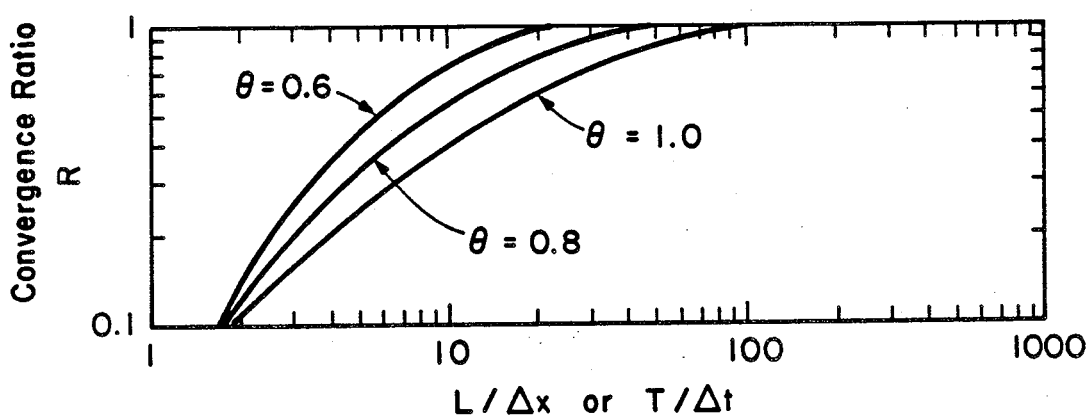

Figure 9-10. Schematic error portraits illustrating the effect of the weighting factor on convergence.

conflicting demands of stability and convergence. To the extent that this can and has been done, numerical modeling remains a powerful tool for the solution of unsteady open channel flow problems.

9.5 SUMMARY

An introductory treatment of the properties of numerical solutions is given in this chapter. Difference equations are discussed in the context of the differential equations from which they derive. The order of error of several finite difference operators of $\partial\phi/\partial x$ is calculated by using Taylor series. A finite difference scheme is defined as a computational molecule consisting of one or more finite difference operators. Difference schemes are classified into: (1) explicit; and (2) implicit.

Stability and convergence are discussed by focusing on the concepts of roundoff errors and discretization errors. Stability is related to roundoff error; convergence, to dicretization error. An overview is given of the stability and convergence properties of finite difference schemes. Emphasis is placed on the difference between explicit and implicit schemes.

APPENDIX I. - GLOSSARY OF TERMS

Analytical Solution: The solution of the differential equation obtained by analytical means.
Characteristic Length: A typical measure of length of the continuum problem (e.g., wavelength L).
Characteristic Time: A typical measure of time of the continuum problem (e.g., wave period T).
Continuum: A differential equation containing physical variables possessing continuous derivatives throughout their domains.
Convergence Ratio: The ratio of numerical and analytical solutions.
Difference Equation: Algebraic equation relating the values of one or more dependent variables defined on a discrete domain of one or more independent variables.
Difference Operator: Algebraic expression representing a function or its derivatives.
Discretization: The process of dividing the continuum domain into a finite number of intervals.
Discretization Error: Error introduced in the numerical solution due to the inability of the grid system to properly resolve the continuum problem.
Discretization Made Exceedingly Small: The process of reducing the discrete intervals, such that $\Delta x \to 0$, and $\Delta t \to 0$.
Domain of Dependence: In the method of characteristics, the spatial domain encompassed within positive and negative characteristics emanating from a given grid point.
Error: Any deviation introduced in the numerical solution which causes it to depart from the analytical solution.
Error Portrait: A plot of the convergence ratio vs. the grid resolution.
Finite Difference Scheme: A computational molecule consisting of one or more finite difference operators.

Grid Resolution: The ratio of a characteristic measure of the continuum system to a characteristic measure of the discrete system (e.g., spatial resolution $L/\Delta x$, or temporal resolution $T/\Delta t$).

Grid System: A discrete representation of the continuum domain with the purpose of identifying the values of dependent variables at specific locations (e.g., nodes).

Numerical Accuracy: A measure of the closeness of the numerical solution to the analytical solution.

Numerical Solution: The solution of the numerical problem, i.e., the solution obtained by the computer using numerical methods.

Order of Error: The exponent of the discrete interval of the leading error term.

Roundoff Errors: Error due to the inability of the computer to carry out the numerical computations to an infinite number of decimal places.

Weighting Factor: A parameter of a numerical scheme used to control stability and convergence.

APPENDIX II. - REFERENCES

1 Liggett, J. A. and Cunge, J. A., "Numerical Methods of Solution of the Unsteady Flow Equations," Chapter 4 in Unsteady Flow in Open Channels, K. Mahmood and V. Yevjevich, eds., Water Resources Publications, Fort Collins, Colorado, 1975, pp. 89-182.

2 O'Brien, G. G., Hyman, M. A., and Kaplan, S., "A Study of the Numerical Solution of Partical Differential Equations," Journal of Mathematics and Physics, Vol. 29, No. 4, 1950, pp. 223-251.

APPENDIX II. - NOTATION

The following symbols are used in this chapter:

A, B, C, D, E, F, G = coefficients, Eq. 9-1;

C = concentration;

c = celerity, phase velocity;

D = solution of the differential equation;

N = numerical solution;

Q = discharge;

t = time variable;

u = velocity;

x = space variable;

y = stage;

Δ = discriminant, solution of the difference equation;

Δt = time step (time interval);

Δt_c = characteristic time step;

Δx = space step (space interval);

θ = weighting factor of a numerical scheme;

μ = diffusion coefficient; and

ϕ = a dependent variable.

Subscripts

j = space index.

Superscripts

n = time index.

CHOICE OF MODELS IN ENGINEERING PRACTICE

by

V. MIGUEL PONCE

TABLE OF CONTENTS

		Page
14.1	INTRODUCTION	14-1
14.2	PHYSICAL vs. MATHEMATICAL MODELS	14-1
14.3	MATHEMATICAL MODELS OF UNSTEADY OPEN CHANNEL FLOW	14-2
14.4	THE CHOICE OF A FLOOD ROUTING METHOD	14-8
14.5	SUMMARY	14-11
	APPENDIX I. - REFERENCES	14-12
	APPENDIX II. - NOTATION	14-12

14.1 INTRODUCTION

The objective of this chapter is to provide the reader with certain basic tools to enable him to make an informed decision regarding the use of models in engineering practice. First, a brief treatment is given on the use of mathematical models, vis-à-vis the physical models. This is followed by a description of several mathematical models of open channel flow, including those used in watershed and channel routing computations. Finally, a systematic way of selecting the routing model most adequate for a particular problem is presented.

14.2 PHYSICAL vs. MATHEMATICAL MODELS

Ever since the digital computer became of widespread use, a large number of problems in hydraulic engineering have been solved by mathematical models. These models utilize the computer to solve by numerical methods an analytical equation which governs the physical process under consideration. Before the advent of the computer, the large amount of calculations usually involved in mathematical models precluded their extensive use. Therefore, in order to solve complex problems for which no analytical solution was available, engineers resorted to the use of reduced-scale replicas referred to as physical models.

The question is often raised as to whether mathematical modeling will one day supersede physical modeling in most routine hydraulic engineering calculations. The answer at the time of this writing is probably a qualified "yes". Provided the computational capabilities of modern digital computers continue to increase as they have in the past, the profession will surely see a gradual trend towards the increased use of mathematical models. In addition, it is also necessary that the users of these models be stepped in the modern concepts of numerical mathematics, so that they are better able to understand and use the models effectively.

For the time being, the question of the choice between physical and mathematical models appears to be dictated primarily by the type of problem at hand, and to some extent, by considerations of cost and convenience. No definitive statement can be made regarding the overall superiority of one of the approaches over the other. However, the capabilities and limitations of both approaches are widely recognized. For one thing, it is known that physical models work best when applied to a specific channel reach or structure, in the search for additional detail on the flow patterns, or on the movements of bed and suspended sediment. For very long reaches, the combined effect of scale distortion and the absence of full dynamic similarity will usually increase the difficulty of interpreting the results of the model. The assessment of an upper limit on the length of reach that can be satisfactorily modeled in a physical laboratory environment is indeed a very subjective matter, but to quote from de Vries, "it can be said that a reach with a maximum length of 10 km is the limit in practice [1]."

While physical models can be used to look at detailed problems and are not very adept at handling large scale problems, mathematical models are altogether different. These models can be formulated in one, two or

three spatial dimensions. The latter is by far the one that best approximates physical reality, but it is still within the realm of research. Two and one-dimensional models are now being used in practice, although the two-dimensional models are significantly more complicated than their one-dimensional counterparts, and therefore, require highly trained and competent staff to develop and run them.

The one-dimensional models of steady and unsteady open channel flow are now within the reach of practicing engineers all over the world. These models are very flexible with regards to problem scale, and they can accommodate small scales as well as large scales. However, it is only in the physical laboratory environment that one-dimensional representations of overall-scale problems can be achieved. For the most part, in the real world, one-dimensional flow representations are possible only in the context of large scale problems, such as flood waves encompassing long river reaches. Therefore, the one-dimensional mathematical model can be applied to precisely the problems that the physical model is unable to handle properly: those involving large scale river processes. To this effect, physical and mathematical models are often used as complementary tools in the analysis of hydraulic and hydrologic problems.

Two- and three-dimensional models are gradually getting established in the research community, and some leading organizations are now beginning to use them on a routine basis. Two significant barriers will need to be overcome if these models are to have a place in engineering practice: (1) the increase in computational speed of present day computers, making possible the operation of two- and three-dimensional models at a cost that would be competitive with that of physical models; and (2) the increase in our understanding of the governing physical processes, since the numerical (computer) model can only be as good as the mathematical theory and equations on which it is based. It can be generally said that the increase in our understanding of the physical process has not kept pace with the accelerated (quantum) increase in our capabilities to develop and run numerical models. If mathematical modeling is to enjoy a period of sustained growth, the current and future effort in both basic and applied research will have to be well balanced.

14.3 MATHEMATICAL MODELS OF UNSTEADY OPEN CHANNEL FLOW

In general, mathematical models of unsteady open channel flow can be classified in the following two broad categories: (1) reservoir routing; and (2) channel routing. The essential difference between the two is that in the reservoir case the water surface slope is assumed equal to zero, while in the channel case is generally has a nonzero value. In addition, the channel routing category can be classified into: (1) kinematic wave routing; (2) diffusive wave routing; and (3) dynamic wave routing. The scope and range of applicability of these routing methods is described below.

Reservoir Routing. The reservoir routing methods are applicable to the cases in which the predominant physical mechanism is that of storage, i.e., those cases that are properly described in terms of the spatially-integrated form of the water contunity equation:

$$I - 0 = \frac{dV}{dt} \tag{14-1}$$

in which I = inflow to the reservoir; 0 = outflow from the reservoir; V = volume of storage; and t = time. Notice that no explicit account is made of the length and width of the reservoir, but rather, the overall size and shape are included in the concept of volume of storage.

Any reservoir routing technique, such as for instance, the level pool (Puls) routing technique described in Chapter 3, can be used to simulate unsteady flows through lakes or reservoirs. The underlying assumption, of course, is that the water surface slope in the reservoir remains equal to zero. In general, this assumption is justified for most cases of practical interest. However, in certain situations, the validity of the assumption may be suspect, especially if the following conditions concur: (1) a sizable backwater effect of the reservoir, primarily due to the small energy slope in the feeder channel; and (2) a small reservoir compared to the feeder stream or channel. In this case, the accuracy of the reservoir routing can be improved by using a routing technique that takes account of the slope of the water surface, i.e., a dynamic wave routing.

Kinematic Wave Routing. The channel routing method known as kinematic wave routing is the most likely simplified of all the channel routing methods. It is based on the neglect of the inertia and pressure forces of the equation of motion, leading to:

$$S_f = S_o \tag{14-1}$$

However, the unsteady chacter of the motion is preserved through the rate-of-rise term of the equation of continuity.

Kinematic wave routing is strictly applicable to kinematic waves, i.e., waves in which the inertia and pressure forces are so small, that they are negligible compared to the terms shown in Eq. 14.1. The criteria to determine whether a wave is kinematic, and thus, subject to kinematic wave analysis, is due to Liggett and Woohliser [3], and to Ponce, et al., [5]. These two criteria are described and compared below.

The Kinematic Flow Number. Liggett and Woolhiser [3] studied the range of applicability of the kinematic wave in connection with overland flow computations. They considered the Saint Venant equations, and showed that through an appropriate normalization of variables, the flow characteristics could be expressed in terms of the following two dimensionless parameters:

$$F_o = \frac{u_o}{\sqrt{gd_o}} \tag{14-2}$$

and

$$k = \frac{S_o L_o}{F_o^2 d_o} \tag{14-3}$$

in which u_o = normalizing mean velocity; d_o = normalizing flow depth; L_o = normalizing length; S_o = channel bed slope; F_o = Froude number; and k = kinematic flow number. The parameters F_o and k are not independent, since k contains F_o^2. An alternative formulation is given by Woolhiser and Liggett [6] as:

$$k' = \frac{S_o L_o}{d_o} \tag{14-4}$$

in which k' is a parameter related to the kinematic flow number by:

$$k^1 = F_o^2 k \tag{14-5}$$

Liggett and Woolhiser [3] found that for values of $k > 20$, the kinematic wave is a very good approximation of the unsteady flow phenomena. For values of $k < 10$, the approximation is a very poor one. In addition, Morris and Woolhiser [4] have recently reported that for low values of F_o, the kinematic wave approximation is valid provided $k' > 5$. For $F_o \cong 0.5$, this condition is compatible with Liggett and Woolhiser's [3] $k > 20$.

In determining the value of k or k', the question remains as to the proper values of the normalizing quantities u_o, d_o and L_o. The quantities u_o and d_o are a typical mean velocity and flow depth, respectively. However, the determination of L_o is not immediately apparent. Woolhiser and Liggett [6] used the length of the overland flow plane in estimating L_o. On the other hand, Liggett [2] refers to L_o as the length of a feature (wavelength) in the direction of flow. Apparently, in overland flow applications the length of a flow feature is of the same order of magnitude as the length of the channel, and the meaning of L_o degenerates accordingly.

In summary, the Liggett and Woolhiser [3] criteria states that for the kinematic wave to apply, the following inequality should hold:

$$k = \frac{S_o L_o}{F_o^2 d_o} > 20 \tag{14-6}$$

where L_o is loosely defined as the length of a flow feature (length of plane in overland flow).

Dimensionless Wave Period. Ponce et al., [5] studied the range of applicability of the kinematic wave in connection with stream channel

routing. They took the Saint Venant equations, applied a perturbation technique and sought a solution in sinusoidal form which led to a system of homogeneous linear equations. The nontrivial condition for the determinant of the coefficient matrix yielded the propagation celerity and logarithmic decrement of small sinusoidal pertubations to the equilibrium flow, in terms of the steady flow Froude number F_o and a dimensionless wave number characteristic of the unsteady component of the motion. By comparing the logarithmic decrement of kinematic and diffusive waves, they were able to determine the range of applicablity of the kinematic wave for stream channel routing computations.

According to Ponce, et al., [5], the kinematic wave will be a good approximation of the unsteady flow phenomena, provided the following inequality is satisfied:

$$\tau = \frac{TS_o u_o}{d_o} > \xi \qquad (14\text{-}7)$$

in which τ = dimensionless wave period; T = wave period of the sinusoidal hydrograph; and ξ = a numerical value which is a function of the specified error tolerance after one period of propagation. Values of ξ are given in Table 14-1.

TABLE 14-1

VALUES OF ξ VS. ERROR

Error*	ξ
1%	873
5%	171
10%	83

*Error computed after one period of propagation.

The values of ξ in Table 14-1 are computed on the basis of the reference hydraulic variables, i.e., values midway between base and peak flow. For practical application, the error expressed in terms of the peak values is likely to be a fraction of that indicated in Table 14-1. Most probably, the error will vary from one-third to one-half of that indicated in Table 14-1. Assuming for illustration purposes, that a 10% error in Table 14-1 leads to a 5% error in peak values after one propagation period, the kinematic wave will apply within this specified tolerance if:

$$\frac{TS_o u_o}{d_o} \geq 83 \qquad (14\text{-}8)$$

A comparison with Liggett and Woolhiser's criterion is possible when it is recognized that:

$$T = \frac{L}{\beta u_o} \tag{14-9}$$

in which L = wavelength; and β = kinematic wave parameter ($\beta \cong 1.5$). Substituting Eq. (14.9) into Eq. (14.8):

$$\frac{LS_o}{d_o} \geq 124 \tag{14-10}$$

which for $L \cong L_o$ is about an order of magnitude larger than Morris and Woolhiser's [4] $k' > 5$. This discrepancy is explained by recalling the essentially different nature of both criteria. Liggett and Woolhiser's was developed for overland flow applications, and accordingly, was based on comparing the performance of the kinematic wave solution "at the basin outlet." Ponce's, et al., criteria is for stream channel routing application, and the performance of the kinematic wave is measured "after one period of propagation." Notwithstanding the differences involved, it is apparent that both criteria can be effectively used to assess the applicability of the kinematic wave.

As an illustration, consider a channel with $S_o = 0.0001$, $d_o =$ 10 ft, and $u_o = 3$ fps. For 95 percent accuracy:

$$\tau = \frac{TS_o u_o}{d_o} > 171 \tag{14-11}$$

which leads to:

$$T > 66 \text{ days} \tag{14-12}$$

for the kinematic wave to apply to this case.

As another example, consider a channel with $S_o = 0.01$, $d_o = 1$ ft, and $u_o = 4$ fps. In this case, the same 95 percent accuracy criteria leads to:

$$T > 1.2 \text{ hours} \tag{14-13}$$

Thus, for mild channel slopes, the hydrograph duration (T) has to be very long for the kinematic wave to apply (very slow using flood waves). For steep slopes, the hydrograph does not have to be very long. The steeper the slope, the shorter the duration of the hydrograph required to satisfy the kinematic wave assumption. The conclusion is that most overland flow problems can be modeled as kinematic flow.

Diffusive Wave Routing. The channel routing method known as diffusive (or diffusion) wave routing differs from the kinematic wave in that it considers the pressure forces, while still neglecting the inertia terms. Thus, in diffusive wave routing, the equation of motion is:

$$S_f = S_o - \frac{\partial d}{\partial x} \tag{14-14}$$

However, the unsteady character of the motion is preserved through the rate-of-rise term of the equation of continuity.

Diffusive wave routing is applicable to diffusive waves, i.e., waves in which the inertia forces are so small that they are negligible compared to the terms shown in Eq. 14-14. The applicability of the diffusive wave is enhanced by the fact that for practical cases of hydrographs, even when the criteria forces are not negligible, the local and convective components are likely to be of the same magnitude but of opposite sign.

The range of applicability of the diffusive wave has been studied in detail by Ponce, et al., [5]. They applied a perturbation technique to determine the celerity and attenuation characteristics of sinusoidal perturbations to the uniform flow. By comparing the celerity and logarithmic decrement of diffusive and dynamic waves, they were able to determine the range of applicability of the diffusive wave for stream channel routing computations.

According to Ponce, et al., [5], the diffusive wave will be a very good approximation of the unsteady flow phenomena, provided the following inequality is satisfied:

$$TS_o \left(\frac{g}{d_o}\right)^{1/2} \geq \xi \tag{14-15}$$

in which T = wave period of the sinusoidal hydrograph (can be taken as the hydrograph duration); S_o = channel bed slope, or equilibrium water surface slope; g = acceleration of gravity; d_o = typical or average flow depth; and ξ = a value which is a function of the Froude number. For practical purposes, a value of $\xi = 30$ was identified by Ponce, et al., for Froude numbers in the subcritical flow regime.

Applying this criterion to the same set of examples uded for the kinematic wave, for $S_o = 0.0001$ and $d_o = 10$ ft:

$$TS_o \left(\frac{g}{d_o}\right)^{1/2} \geq 30 \tag{14-16}$$

therefore:

$$T \geq 1.9 \text{ days} \tag{14-17}$$

In the second example, for $S_o = 0.01$, and $d_o = 1$ ft:

$$T \geq 8.8 \text{ minutes} \tag{14-18}$$

On the basis of these examples, it is concluded that the diffusive wave applies for a wider range of bed slopes and hydrograph durations than the kinematic wave. However, in the cases where inequality 14-16

is not satisfied, only the dynamic wave can properly account for all the physical details of the unsteady flow phenomena.

In practice, inequality 14-16 is readily satisfied for a wide range of hydrograph durations. However, depending on the bed slope, inequality 14-16 may not be satisfied for very flashy hydragraphs. In addition, the criterion breaks down in the case where there is a significant downstream control, i.e., in the flow through reservoirs. In this case, either a dynamic wave routing or a reservoir routing technique will apply. The advantage of the dynamic wave is that it can take into account very small differences in water surface elevation, but if this description is not important, the reservoir routing will suffice.

Dynamic Wave Routing. The channel routing method known as dynamic wave routing is based on the complete equation of motion. As such, it is the most general of all the stream channel routing methods. Since the equations of continuity and motion constitute a set of first order partial differential equations, no complete analytical solution is available. The solution is attempted by numerical means, either by using the method of characteristics or the finite difference methods.

14.4 THE CHOICE OF A FLOOD ROUTING METHOD

Given the variety of existing flood routing methods, the choice of a method best suited for a particular problem could be a bewildering task. In this section, a systematic procedure for choosing a flood routing method is presented. The procedure is based on the careful evaluation of the following four criteria: (1) nature of the problem; (2) input needs; (3) output needs; and (4) utilization of resources (i.e., associated cost).

Nature of the Problem. The nature of a flood routing problem can be identified by looking into: (a) the type of physical system; (b) the type of hydrologic event; and (c) the type of boundary control. The physical system could be a watershed, an overland flow plane, a stream channel reach, a reservoir, or a stream channel-reservoir combination. In general, overland flow and stream channel flow are characterized by a finite water surface slope. On the other hand, in reservoir systems, the water surface slope is reasonably taken equal to zero. At a channel-reservoir confluence, the backwater effect will effectively reduce the water surface slope to a small but nonetheless finite value.

The hydrologic event could be such that it generates a fast rising, a normal rising, or a slow rising flood wave. In general, the rate-of-rise and duration of the hydrograph are directly related to the size and retention characteristics of the contributing watershed. Larger watersheds with longer retention times will result in hydrographs of longer duration.

The boundary control could be either: (a) upstream only; or (b) upstream and downstream. Overland flow planes and most steep stream

channel reaches are subject to upstream control only; i.e., there is no need to specify a downstream boundary condition. Reservoir and channel-reservoir systems are usually subject to both upstream and downstream control. The routing of tributaries through river junctions may also be subject to downstream control (at the junction), depending on the relative magnitude of mainstem and tributary flow.

Input Needs. The input needs for flood routing models can comprise of one or more of the following: (1) upstream inflow discharge or stage hydrograph; (2) hydraulic data at representative cross-sections; (3) geometric and topographic data; and (4) historic discharge and/or stage data for calibration and verification purposes.

The upstream inflow discharge constitutes the upstream boundary condition to the numerical model. When planning the modeling strategy, care should be taken to ensure that the upstream boundary condition is being properly discretized, i.e., that the time step Δt is sufficiently small to account for all the details of the wave phenomena. Otherwise, there will be errors due to insufficient temporal resolution.

The hydraulic data consists of the following: (1) steady-state stage-discharge relations; (2) Manning's n, or alternatively, stage-conveyance functions. To achieve a great level of detail, the hydraulic data can be specified at every cross-section to be used in the computation. Alternatively, average values (composite cross-section) can be used for several cross-sections, albeit at the cost of a reduction in the overall accuracy.

The geometric and topographic data consists of the following: (1) wetted perimeter-area relations; (2) top width-area relations; and (3) stage-area relations. In addition, the distance between adjacent cross-sections is also necessary.

The historic discharge and/or stage data is needed for calibration and verification purposes. This data is used primarily in the "fine tuning" of the resistance parameters, be it either Manning's n or the conveyance functions.

Output Needs. Depending on the problem at hand, the output requirements (information to be obtained from the model) may comprise of one or more of the following: (1) peak discharge and/or peak stage at some or all cross-sections; (2) accurate timings of the travel of the flood wave; (3) hydrograph shape; and (4) definition of the looped rating curves at some or all cross-sections.

Utilization of Resources. An important although sometimes overlooked aspect in choosing a flood routing method is that of the expenditure of resources, i.e., the total cost, including research and development, personnel training, and actual model run costs to achieve a certain objective. In order to adequately estimate the total cost involved in the use of a flood routing model, the following aspects need to be considered: (1) manpower utilization for research and development, training and operation; (2) availability of sufficiently documented commercial or publicly-owned software packages; (3) computer hardware requirements; and (4) actual run costs.

Method Selection. As an example of how to select a method most suited to a particular set of conditions, the following four general approaches are examined here in detail: (1) kinematic wave; (2) diffusive wave; and (4) level-pool routing case. Any flood routing problem of practical importance can be formulated by using at least one of these approaches.

The kinematic wave is particularly suited for channel routing in steep channels, in which there is little or no downstream control. As such, it is used to model overland flow phenomena, since the bed slopes associated with overland flow planes are usually steep to very steep. Over the last two decades, several mathematical models have been developed to simulate the watershed runoff process in a distributed fashion. Invariably, these models use the kinematic wave as a practical alternative to the more complicated dynamic wave. To the extent that the Liggett and Woolhiser [3] criterion is satisfied ($k > 20$), the kinematic wave is an acceptable model of the flow behavior.

A specific input in the kinematic wave is the discharge-area relation at each cross-section, which contains information on the channel geometry and bottom friction. Output is usually given in terms of peak discharge, accurate timing of the hydrograph peak, and hydrograph shape. No looped rating curve can be obtained with the kinematic wave. Furthermore, in discrete (numerical) solutions of the kinematic wave, care must be taken to ensure that the amount of numerical diffusion introduced is minimal. Otherwise, the solution would be essentially a diffusive wave, rather than a kinematic wave.

The diffusive wave is generally well suited for stream channel routing. Its implicit formulation requires the specification of a downstream boundary condition, which can partly account for downstream backwater effects. However, its explicit formulation (Muskingum-Cunge Method) cannot account for a downstream boundary control. To the extent that the Ponce, et al.,[5] criterion is satisfied ($TS_o \sqrt{g/d_o} > 30$), the diffusive wave is an acceptable model of the flow behavior. In practice, a large number of flood waves in stream channels satisfy the Ponce, et al., criterion.

The explicit formulation of the diffusive wave (Muskingum-Cunge Method) requires a discharge-area relation at each cross-section, in order to specify the cannel geometry and bottom friction. The implicit formulation is based on Manning's n values or conveyance functions. In this case, historic discharge and/or stage data are needed in order to "fine tune" the friction coefficients. Output is usually given in terms of peak discharge, accurate timing of the hydrograph peak, and hydrograph shape. In addition, the implicit formulation will take account of the loop in the rating curve.

The dynamic wave is the most general model of unsteady open channel flow. Its advantages are readily seen in connection with a channel-reservoir system for which the average water surface slope may be too small to satisfy the diffusive wave applicability criterion. Furthermore, the dynamic wave can take full account of backwater effects, i.e., it is subject to upstream and downstream control. At the downstream

boundary, either a stage hydrograph, or a single-valued stage-discharge relationship can be used. The latter contradicts the solution at the boundary, but it may be sufficiently adequate if the loop is not too large.

Extensive hydraulic, geometric topographic and historic data are needed to operate a dynamic model. Output is usually given in terms of peak discharge, peak stage, accurate timing of the hydrograph peak, hydrograph shape, and looped rating curve at all cross-sections (excluding the downstream section when a single-valued rating curve is specified).

The level pool routing method is applicable to the cases in which the water surface slope can be taken as horizontal, i.e., in reservoir and lake systems. The input requirements comprise the inflow discharge to stage hydrograph, and a relationship between outflow and volume of reservoir storage. The output consists of the outflow discharge or stage hydrograph.

Cost and Resource Utilization. Once the technical requirements of a particular problem have been determined, the next step is the evaluation of cost and resource utilization. In general, the more precise and elaborate the method, the greater is the investment in research and development, training and operational costs, and data collection requirements. Therefore, the selection of a flood routing method for a particular application is a highly demanding task. Considerable judgement and experience are required in order to make an informed decision regarding this choice. The information presented here is intended to provide an appropriate framework to assist the engineer in such a choice.

14.5 SUMMARY

The subject of the choice of models in engineering practice is treated in detail. A brief comparison is made between mathematical and physical models, emphasizing their applicability as a function of problem scale. Physical models are presently geared for solution of small scale problems, while mathematical models are best suited to the study of large scale phenomena. Nevertheless, the scope of application of mathematical models continues to increase.

A detailed description is given of several mathematical models of unsteady open channel flow, encompassing a wide range of problems likely to be encountered in engineering practice. Kinematic, diffusive and dynamic waves are described, and emphasis is placed on the range of applicability of the approximate waves. In this connection, the criteria of Liggett and Woolhiser [3] and Ponce, et al., [5] are presented.

A systematic appraisal on the way of selecting a routing model is described. Again, kinematic, diffusive, dynamic and level pool routing models are treated. The methodology includes the following: (1) identification of nature of the problem,; (2) assessment of input and output needs; and (3) evaluation of cost.

APPENDIX I. - REFERENCES

1 De Vries, M., 1973, "Application of Physical and Mathematical Models for River Problems," Proceedings, International Symposium on River Mechanics, IAHR, Bangkok, Thailand, pp. 370-393.

2 Liggett, J. A., 1975, "Basic Equations of Unsteady Flow," in Unsteady Flow in Open Channels, K. Mahmood and V. Yevjevich, Eds., Water Resources Publications, Fort Collins, Colorado.

3 Liggett, J. A., and D. A. Woolhiser, 1967, "The Use of Shallow Water Equations in Runoff Computation," Proceedings, Third Annual American Water Resources Conference, San Francisco, Calif., pp. 117-126.

4 Morris, E. M. and D. A. Woolhiser, 1980, "Unsteady One-dimensional Flow Over a Plane: Partial Equilibrium and Recession Hydrographs," Water Resources Research, Vol. 16, No. 2, April, pp. 355-360.

5 Ponce, V. M., R. M. Li and D. B. Simons, 1978, "Applicability of Kinematic and Diffusion Models," Journal of the Hydraulics Division, ASCE, Vol. 104, HY3, Proc. Paper 13635, March, pp. 353-360.

6 Woolhiser, D. A. and J. A. Liggett, 1967, "Unsteady, One-dimensional Flow over a Plane--The Rising Hydrograph," Water Resources Research, Vol. 3, No. 3, Third Quarter, pp. 753-771.

APPENDIX II. - NOTATION

The following symbols are used in this paper:

d_o = normalizing flow depth;

F_o = Froude number, Eq. 14-2;

g = acceleration of gravity;

I = inflow;

k = kinematic flow number, Eq. 14-3;

k' = parameter, Eqs. 14-4 and 14-5;

L = wavelength;

L_o = normalizing length;

O = outflow;

S_f = friction slope;

S_o = channel bed slope;

T = wave period of the sinusoidal hydrograph (hydrograph duration);

t = time;

u_o = normalizing mean velocity;

V = volume of storage;

β = kinematic wave parameter;

ξ = numerical value (tolerance); and

τ = dimensionless wave period.

DIGITAL SIMULATION OF HYDROLOGIC SYSTEMS

by

V. M. Ponce

TABLE OF CONTENTS

		Page
1.	DIGITAL SIMULATION OF SURFACE RUNOFF	1
2.	ELEMENTS OF SIMULATION	2
3.	SUBWATERSHED HYDROGRAPH GENERATION	4
4.	STREAM CHANNEL ROUTING	5
5.	RESERVOIR ROUTING	7
6.	SCS TR-20 MODEL	7
7.	HEC-1 MODEL	8
8.	SUMMARY	9
9.	REFERENCES	9
	APPENDIX .- DATA INVENTORY TOPICS	10

DIGITAL SIMULATION OF HYDROLOGIC SYSTEMS

Hydrologic simulation of all or parts of surface water and groundwater implies the use of digital computational methods to imitate historical events or preview the future response of a hydrologic system (watershed or basin) to a specific plan of action.

Simulation models can be of a deterministic or stochastic nature. Deterministic methods describe the behavior of the hydrologic cycle in terms of mathematical relationships that bear resemblance to the governing physical processes. Stochastic methods seek to simulate hydrologic systems by relying on one or several laws of probability to model the interrelationships between the hydrologic variables. This monograph concentrates exclusively on the digital simulation of surface runoff.

1. DIGITAL SIMULATION OF SURFACE RUNOFF

A simulation model is a set of equations and algorithms that describe a real system and imitate its behavior. In hydrologic modeling, the real system is a watershed or basin, i.e., a surface area with clearly defined boundaries, with the property that water falling above it drains towards one outlet point located along the main stream, and at the lowest point of the watershed/basin. The watershed/basin consists of several physically identifiable features, such as subwatersheds, stream channels, and natural or man-made reservoirs. Rainfall precipitates on individual subwatersheds, and usually only a portion of it (the net rainfall) goes on to constitute direct runoff from the watershed. This runoff is commonly expressed as a discharge or flow hydrograph (a plot of discharge vs time) at the respective subwatershed outlet. From here, runoff travels along defined stream channels, with added contributions of lateral inflow from the subwatersheds along the stream channels. Routing is the process of calculation of the flow as it travels downstream, first along a stream channel, and later through a network of stream channels (with or without reservoirs). This process continues in the downstream direction until a point of interest is reached, i.e., a point where a flow forecast, evaluation or design criteria is called for.

Hydrologic simulation serves different purposes, depending on the application at hand. For instance, if historic flows are being input to the model as they occur, the model would be being used in a flood forecasting mode. If hypothetical design flows are used, the model is being used for analysis of "what if" conditions necessary for design. Other possibilities include the evaluation of hydrologic impact due to urbanization, overgrazing, controlled forest burning, or any other application where man's activities on the land surface are likely to significantly alter the hydrologic response of the watershed to the precipitation input.

Hydrologic simulation is a multiphase activity, encompassing a variety of tasks, to include: 1) Data collection; 2) Model selection; 3) Model calibration; 4) Actual runs; and 5) Analysis of results.

The simulation of all or parts of a watershed or basin requires a thorough appraisal of the relevant data, including geometric data, soil and land use data, rainfall and runoff measurements, and physical characteristics of the various watershed/basin elements. A general list of data inventory topics that encompasses most hydrologic/economic models is given in the Appendix.

2. ELEMENTS OF SIMULATION

Crucial to the task of hydrologic simulation is the selection of a model which will do an adequate job, given the available data. Several models are currently being used in hydrologic practice, most of them either developed or endorsed by federal agencies. Before a description of any of these models is attempted, it is necessary to describe their overall features.

All comprehensive hydrologic simulation models consist of the following elements: 1) a subwatershed hydrograph generation method; 2) a stream channel routing algorithm; and 3) a reservoir routing procedure. In addition, some may include other features such as extent of inundation, snowmelt calculations and flood damage analysis.

The first element, the subwatershed hydrograph generation, is further complicated by the need to abstract the gross precipitation input (to deduct infiltration and other losses) to arrive at a value of net precipitation to be converted to runoff. The hydrograph generation itself is usually based on a "unit hydrograph," i.e., the hydrograph for one unit of runoff lasting for a certain period of time. This unit hydrograph is convoluted with the measured or assumed distribution of net precipitation input, to obtain the composite hydrograph taken as the outflow from the subwatershed.

Stream channel routing can be either hydrologic (storage volumes), or hydraulic (values expressed at cross-sections). Reservoir routing is done by using one of the classic reservoir routing techniques based on storage indication quantities. Both stream channel and reservoir routing are subject to the specification of base flow in one or more of several established ways. Lastly, a snowmelt routine could be incorporated in order to account for runoff due to snowmelt. Table 1 shows five of the major existing hydrologic simulation models supported by the various federal agencies, with indication of their principal features.

ARS = Agricultural Research service

TABLE 1

MAJOR EXISTING HYDROLOGIC SIMULATION MODELS

	HEC-1 (C.of E.)	TR-20 (SCS)	USGS (USGS)	HYMO (ARS)	SWMM (EPA)
ELEMENTS					
Losses					
Runoff Curve Number		X		X	
Variable loss rate	X				
Phillip's equation			X		
Horton's equation					X
Unit Hydrograph					
Input as data	X	X			
Dimensionless		X			
Clark's	X		X		
Snyder's	X				
2-parameter gamma distr.				X	
Stream Channel Routing					
Muskingum	X				
Convex		X			
Translation-only			X		
Variable storage coeff.				X	
Hydraulic					X
Reservoir Routing					
Storage indication	X	X		X	
Base Flow					
Input as data			X		
Constant value		X	X		
Recession equation	X				
Snowmelt Calculation	X				

Source: Viesmann et al.: "Introduction to Hydrology."

3. SUBWATERSHED HYDROGRAPH GENERATION

The subwatershed hydrograph generation consists of two parts: 1) the abstractions; and 2) the hydrograph generation per se. The abstraction is a procedure by which losses due to infiltration, interception, detention storage, etc., are accounted for and subtracted from the total (or gross) rainfall to produce the direct (or net) rainfall. Several methods are in use to calculate the abstractions. As an illustration, the SCS runoff curve number method is described here in detail.

The SCS runoff curve number method is a procedure developed by the USDA Soil Conservation Service for use in their hydrologic calculations, and explained in detail in the SCS National Engineering Handbook, NEH-4. It consists of a function given in the form of a graph, relating total rainfall P, and direct runoff Q, both given in inches. A third parameter in this relationship is given by the runoff curve number CN, a number varying between 0 and 100 which provides a way to obtain Q as a function of P and CN. This generalized rainfall-runoff relation was developed for use with usually available rainfall data (nonrecording rain gages), and therefore the data is based on storms occurring in a calendar day, with no information on the time distribution of such storms. Consequently, it does not take into account rainfall intensities.

The runoff curve numbers to be used for particular applications are determined based on the following features of the land: 1) land use or cover; 2) treatment or practice; 3) hydrologic condition; and 4) hydrologic soil group. Standard tables and assistance from local SCS offices are useful in estimating the values of the runoff curve numbers for use in specific applications. In addition, the method has a provision for accounting for antecedent moisture, by correcting the normal curve numbers upwards for wet conditions, or downwards for dry conditions.

The hydrograph generation consists of three major steps: 1) the selection of a unit hydrograph; 2) the selection of a design hyetograph (based on a chosen temporal distribution of net design rainfall); and 3) the convolution of the unit hydrograph with the design hyetograph. Each one of these steps is briefly explained below.

The unit hydrograph is a procedure found in all major hydrologic models, perhaps due to its simplicity as compared to the more elaborate distributed parameter models which remain still at the research stage. The unit hydrograph is defined as the hydrograph for one unit of runoff lasting for a specified period of time. It can be obtained experimentally based on the analysis of rainfall-runoff data, or synthetically for ungaged watersheds. The synthetic unit hydrographs have been assembled based on large quantities of data, and are considered to represent regional characteristics on the broad mean. As an

illustration of the use of unit hydrographs, the SCS dimensionless unit hydrograph is decribed herein.

The SCS dimensionless unit hydrograph is based on the initial assumption that the unit response form a basin is shaped in the form of a triangle, with a time base equal to 8/3 of the time-to-peak. This leads to a formula for the peak flow as a function of the time-to-peak and the area of the watershed. Once the peak flow is determined, the shape of the dimensionless hydrograph is adjusted to conform more closely with a gamma-type function, with a time base equal to 5 times the time-to-peak. The latter is calculated by lag relationships, i.e., by estimating the time lag of the watershed based on physical characteristics such as length, slope, runoff curve number and area. The time lag is defined as the distance from the centroid of rainfall to the peak of runoff. The rainfall duration is estimated as a percentage of the time of concentration, this being the time it takes an element of water to travel from the watershed divide to the outlet. Alternatively, the time of concentration is defined as the time base minus the rainfall duration.

The above relationships help determine a unit hydrograph for the watershed in question. A suitable temporal distribution of rainfall is chosen, and the design hyetograph calculated based on this distribution. Finally, the unit hydrograph for the subwatershed is convoluted with the design hyetograph. The procedure is based on the incremental application of the unit hydrograph to the design hyetograph, by 1) multiplying ordinates of the unit hydrograph times each increment of rainfall; 2) lagging the resultant hydrographs in time to conform to the time of occurrence of the individual rainfall increments; and 3) superimposing all hydrographs to obtain the composite hydrograph constituting the response of the watershed to the design hyetograph.

4. STREAM CHANNEL ROUTING

Stream channel routing is the process of calculation of the flow as the flood wave travels downstream in time and space. A stream channel routing algorithm consists of the following steps: 1) a connectivity routine, which enables the flows to be routed along a network of channels, usually configured in a tree-like structure; and 2) a reach routing algorithm, either hydrologic (storage oriented) or hydraulic (cross-section oriented).

The connectivity routine is the heart of the network topology, allowing the flow to be routed from tributaries to main branch in a logical and consistent manner. In this regard, the concepts of order, branch and channel reach are important. The network order determines the degree of branching, i.e., the hierarchical arrangement among the various tributaries. Several tributaries to a main stream may be of the same order, and they

are referred to as branches. Within each branch, the distance between confluences is referred to as a channel reach. Order, branch and channel reach determine the topological numbers which configure the stream network in anticipation to the reach routing.

The reach routing can be done in one or more of several ways. The standard procedure is to apply a hydrologic method, i.e., one based on storage relationships. Examples of the hydrologic approach to reach routing are the Muskingum, convex, and other methods. The alternative to these are the hydraulic methods, such as the kinematic wave or dynamic wave. Both hydrologic and hydraulic methods have advantages and disadvantages. The hydrologic methods are simple but may not follow closely the physics of the problem. The hydraulic methods, on the other hand, tend to be more physically based, but in turn may become exceedingly complicated for certain applications.

A third procedure for reach routing which is receiving increased attention is the diffusion method (Muskingum-Cunge). This method remains within the computational framework of the hydrologic methods, but its coefficients are based on physical characteristics of the channel, making it in fact a "hybrid" model. The advantage of the diffusion method is its simplicity, robustness, and relative ease of application to ungaged watersheds, for which extensive historical data for model calibration is not available. Over the past three years, the Soil Conservation Service has funded studies to incorporate the diffusion reach routing methodology into an updated version of their popular TR-20 model, and studies continue to that effect.

The difference between the diffusion method and other established hydrologic reach routing schemes is one of fundamental importance. The classic Muskingum method requires extensive calibration in order to determine the applicable routing parameters K and X, and these can only be guaranteed within a reasonable range of flows. The convex method (and its variation, the Att-Kin) currently used in TR-20 suffers from the problem of inconsistency, i.e., the results are a function of the space interval. This is because the method, as formulated in SCS National Engineering Handbook NEH-4 and implemented in TR-20, is based on coefficients which should be calculated as a function of grid size, instead of determined empirically. These disadvantages of the classic Muskingum and convex methods are overcome by the diffusion method, which can be formulated in either a linear or nonlinear mode to encompass the routing of a wide range of flows and which bases its coefficients on the grid size, making it consistent as well as accurate.

5. RESERVOIR ROUTING

An important feature of digital watershed simulation is the capability for routing flows through reservoirs (either man-made or natural) and other flood retarding structures. For this purpose, individual reaches within the order-branch-reach network are properly identified as reservoir reaches, for which storage-outflow relationships are needed instead of stream channel rating curves. Since the reservoir routing problem is based on the storage equation only, the well known storage indication method is commonly used. In this method, the storage equation is discretized in time and coupled with the storage-outflow data to produce a recursive solution for the outflow hydrograph, given the inflow and base flow values.

6. SCS TR-20 MODEL

This model is currently one of the leading hydrologic models, being fully supported by the Soil Conservation Service. The model is a computer program of methods used by this agency as presented in their National Engineering Handbook NEH-4.

TR-20 was designed to take soil and land use information to determine runoff hydrographs for known storms, and to perform reservoir and channel routing on the generated hydrographs. The program has been used extensively by SCS engineers and others, in applications ranging from flood insurance and flood hazard studies to the design of reservoir and channel projects.

Surface runoff is computed using the runoff curve number approach to abstract losses. The excess rainfall hyetograph is constructed using the effective rain and a given rainfall distribution, and applied incrementally to the SCS dimensionless unit hydrograph to obtain the runoff hydrograph for the subwatershed for the given storm.

TR-20 uses the storage indication method to route hydrographs through reservoirs. For stream channel routing, it uses the convex method, although recent updates include the Att-Kin method (for attenuation-kinematic) and a version of the diffusion method which is being considered on an experimental basis. The program computes the subwatershed hydrographs, routes the flows through stream channels and reservoirs, combines the routed hydrographs with those of other tributaries, and routes the combined hydrograph to the watershed outlet.

Subdivision of the watershed is accomplished by determining the location of control points. Control points are defined as stream locations corresponding to cross-sectional data, reservoir sites, damage centers, diversion points, gaging stations or tributary confluences. Subarea data requirements include drainage area, time of concentration, reach lengths, routing coefficients and cross-sectional data. Applications of TR-20

normally incorporate control points spaced from a few hundred feet to more than 2 miles apart. The resulting subareas that contribute runoff to a control point are usually less that 5 sq mi.

Output from TR-20 can produce any combination of the following:

1) peak discharge rate, timing, and peak water surface elevations;
2) discharge rates for the entire hydrograph in tabular form;
3) water surface elevations as a function of time; and
4) summary tables containing water balance information.

6. HEC-1 MODEL

The HEC-1 Flood Hydrograph Model is a digital computer system developed and supported by the Hydrologic Engineering Center, U.S. Army Corps of Engineers. It consists of a calling program and a number of subroutines. Two of these subroutines determine the optimal unit hydrograph, loss rate (abstractions), and stream channel routing parameters by matching measured and calculated hydrographs. Other routines perform snowmelt computations, unit hydrograph computations, hydrograph routing and combining, and other tasks. As an added feature, HEC-1 will also perform economic analyses of flood damage by numerically integrating areas under damage-frequency curves for existing and proposed conditions. Other capabilities include the recent addition of a dam-breach analysis feature.

In HEC-1, the precipitation for a subarea can be determined by one of the following methods: 1) precipitation station data; 2) basin mean precipitation; or 3) standard project or probable maximum hypothetical precipitation distributions. Either gross or net rainfall amounts may be input, depending on the user's choice. HEC-1 abstracts losses by using the loss rate function, which is easily bypassed if net rain is available for direct input.

The loss rate function is an exponential decay function describing the instantaneous loss rate, given the rainfall intensity and the antecedent losses. For gaged watersheds, HEC-1 allows the user to input rainfall and runoff data from which the loss rate function parameters are optimized to give a best fit to the available data. Estimates of loss rate function parameters for ungaged watersheds are based largely on experience with the model. A constant loss rate is available in HEC-1 as an alternative to the loss rate function.

Unit hydrographs for each subarea are either provided by the user or calculated following Clark's unit hydrograph. The latter is also known as the time-area-curve method of hydrologic watershed routing. If the time-area curves are not available,

the model provides a synthetic time-area curve as an alternative.

The HEC-1 model allows the user a choice of several hydrologic techniques for routing floods through stream channels and reservoirs. The alternative routing procedures include 1) storage-indication reservoir routing; 2) Muskingum; 3) Working R and D; 4) Straddle-stagger; 5) Tatum; and 6) Multiple storage.

Computations of snowmelt by HEC-1 are possible in up to 10 elevation zones. The precipitation in any zone is considered to be snow below a certain base temperature. The snowmelt is computed by degree-day or energy budget methods whenever the temperature is equal to or greater than the base temperature. The elevations zones are usually delineated in increments of 1000 ft, although other equal increments can be used.

Output from HEC-1 includes most relevant data and calculated hydrographs at selected locations. Options are available for graphical and other displays.

7. SUMMARY

An overview of current practice in the field of digital simulation of hydrologic systems, specifically surface runoff, is presented. First, a description is made of the concepts involved in the simulation of surface runoff from watersheds and river basins. The three elements of simulation--subwatershed, stream channel and reservoir routing--are described in some detail. The subwatershed hydrograph generation focuses on the SCS runoff curve number approach and dimensionless unit hydrograph used in the TR-20 model. The stream channel routing segment highlights the physically based diffusion routing methodology, as an effective alternative to the dated channel routing procedures currently used by most models. The reservoir routing segment describes the classic storage-indication method.

Both TR-20 and HEC-1, currently the leading hydrologic simulation models, are described in detail. Data requirements for digital hydrologic simulation are sketched in the Appendix.

8. REFERENCES

Ponce, V. M., "Development of an Algorithm for the Linearized Diffusion Method of Flood Routing," San Diego State University Civil Engineering Series, No. 81148, September, 1981.

USDA Soil Conservation Service, "National Engineering Handbook, Section 4, Hydrology," Revised, August, 1972.

APPENDIX.- DATA INVENTORY TOPICS

A. Subwatershed Characteristics

1. Lag time, time of concentration
2. Contributing area
3. Mean overland flow distance
4. Mean slope
5. Design storm abstractions
6. Land use or cover, treatment, condition, soil type

B. Channel Characteristics

1. Channel bed profiles
2. Normal flow or other applicable rating curves
3. Manning or Chezy coefficients
4. Cross-sectional data
5. Base flow and channel losses to seepage
6. Overbank storage characteristics
7. Sediment loads, bank stability and vegetative growth

C. Streamflow Data

1. Recorded streamflow data, including statistical analyses
2. Flood frequency data
3. Flow duration data
4. Rating curves
5. Extent of inundation
6. Stage vs frequency curves
7. Stage vs flood damage

D. Design Floods and Flood Routing Parameters

1. Design storm, including temporal and spatial distribution
2. Standard project and probable maximum floods
3. Routing parameters, or the means to evaluate them
4. Base flow estimates during design floods
5. Historic floods for calibration purposes

E. Reservoir Data

1. Location data and/or potential sites
2. Elevation-storage data
3. Elevation-area data
4. Normal, minimal and other pool levels
5. Evaporation and seepage loss data
6. Sediment and dead storage requirements
7. Operating policies and rule curves
8. Outflow characteristics, including storage-outflow data

DIGITAL SIMULATION OF HYDROLOGIC SYSTEMS

by

V. M. Ponce

TABLE OF CONTENTS

		Page
1.	DIGITAL SIMULATION OF SURFACE RUNOFF	1
2.	ELEMENTS OF SIMULATION	2
3.	SUBWATERSHED HYDROGRAPH GENERATION	4
4.	STREAM CHANNEL ROUTING	5
5.	RESERVOIR ROUTING	7
6.	SCS TR-20 MODEL	7
7.	HEC-1 MODEL	8
8.	SUMMARY	9
9.	REFERENCES	9
	APPENDIX .- DATA INVENTORY TOPICS	10

DIGITAL SIMULATION OF HYDROLOGIC SYSTEMS

Hydrologic simulation of all or parts of surface water and groundwater implies the use of digital computational methods to imitate historical events or preview the future response of a hydrologic system (watershed or basin) to a specific plan of action.

Simulation models can be of a deterministic or stochastic nature. Deterministic methods describe the behavior of the hydrologic cycle in terms of mathematical relationships that bear resemblance to the governing physical processes. Stochastic methods seek to simulate hydrologic systems by relying on one or several laws of probability to model the interrelationships between the hydrologic variables. This monograph concentrates exclusively on the digital simulation of surface runoff.

1. DIGITAL SIMULATION OF SURFACE RUNOFF

A simulation model is a set of equations and algorithms that describe a real system and imitate its behavior. In hydrologic modeling, the real system is a watershed or basin, i.e., a surface area with clearly defined boundaries, with the property that water falling above it drains towards one outlet point located along the main stream, and at the lowest point of the watershed/basin. The watershed/basin consists of several physically identifiable features, such as subwatersheds, stream channels, and natural or man-made reservoirs. Rainfall precipitates on individual subwatersheds, and usually only a portion of it (the net rainfall) goes on to constitute direct runoff from the watershed. This runoff is commonly expressed as a discharge or flow hydrograph (a plot of discharge vs time) at the respective subwatershed outlet. From here, runoff travels along defined stream channels, with added contributions of lateral inflow from the subwatersheds along the stream channels. Routing is the process of calculation of the flow as it travels downstream, first along a stream channel, and later through a network of stream channels (with or without reservoirs). This process continues in the downstream direction until a point of interest is reached, i.e., a point where a flow forecast, evaluation or design criteria is called for.

Hydrologic simulation serves different purposes, depending on the application at hand. For instance, if historic flows are being input to the model as they occur, the model would be being used in a flood forecasting mode. If hypothetical design flows are used, the model is being used for analysis of "what if" conditions necessary for design. Other possibilities include the evaluation of hydrologic impact due to urbanization, overgrazing, controlled forest burning, or any other application where man's activities on the land surface are likely to significantly alter the hydrologic response of the watershed to the precipitation input.

Hydrologic simulation is a multiphase activity, encompassing a variety of tasks, to include: 1) Data collection; 2) Model selection; 3) Model calibration; 4) Actual runs; and 5) Analysis of results.

The simulation of all or parts of a watershed or basin requires a thorough appraisal of the relevant data, including geometric data, soil and land use data, rainfall and runoff measurements, and physical characteristics of the various watershed/basin elements. A general list of data inventory topics that encompasses most hydrologic/economic models is given in the Appendix.

2. ELEMENTS OF SIMULATION

Crucial to the task of hydrologic simulation is the selection of a model which will do an adequate job, given the available data. Several models are currently being used in hydrologic practice, most of them either developed or endorsed by federal agencies. Before a description of any of these models is attempted, it is necessary to describe their overall features.

All comprehensive hydrologic simulation models consist of the following elements: 1) a subwatershed hydrograph generation method; 2) a stream channel routing algorithm; and 3) a reservoir routing procedure. In addition, some may include other features such as extent of inundation, snowmelt calculations and flood damage analysis.

The first element, the subwatershed hydrograph generation, is further complicated by the need to abstract the gross precipitation input (to deduct infiltration and other losses) to arrive at a value of net precipitation to be converted to runoff. The hydrograph generation itself is usually based on a "unit hydrograph," i.e., the hydrograph for one unit of runoff lasting for a certain period of time. This unit hydrograph is convoluted with the measured or assumed distribution of net precipitation input, to obtain the composite hydrograph taken as the outflow from the subwatershed.

Stream channel routing can be either hydrologic (storage volumes), or hydraulic (values expressed at cross-sections). Reservoir routing is done by using one of the classic reservoir routing techniques based on storage indication quantities. Both stream channel and reservoir routing are subject to the specification of base flow in one or more of several established ways. Lastly, a snowmelt routine could be incorporated in order to account for runoff due to snowmelt. Table 1 shows five of the major existing hydrologic simulation models supported by the various federal agencies, with indication of their principal features.

TABLE 1

MAJOR EXISTING HYDROLOGIC SIMULATION MODELS

	HEC-1 (C.of E.)	TR-20 (SCS)	USGS (USGS)	HYMO (ARS)	SWMM (EPA)
ELEMENTS					
Losses					
Runoff Curve Number		X		X	
Variable loss rate	X				
Phillip's equation			X		
Horton's equation					X
Unit Hydrograph					
Input as data	X	X			
Dimensionless		X			
Clark's	X		X		
Snyder's	X				
2-parameter gamma distr.				X	
Stream Channel Routing					
Muskingum	X				
Convex		X			
Translation-only			X		
Variable storage coeff.				X	
Hydraulic					X
Reservoir Routing					
Storage indication	X	X		X	
Base Flow					
Input as data			X		
Constant value		X	X		
Recession equation	X				
Snowmelt Calculation	X				

Source: Viesmann et al.: "Introduction to Hydrology."

3. SUBWATERSHED HYDROGRAPH GENERATION

The subwatershed hydrograph generation consists of two parts: 1) the abstractions; and 2) the hydrograph generation per se. The abstraction is a procedure by which losses due to infiltration, interception, detention storage, etc., are accounted for and subtracted from the total (or gross) rainfall to produce the direct (or net) rainfall. Several methods are in use to calculate the abstractions. As an illustration, the SCS runoff curve number method is described here in detail.

The SCS runoff curve number method is a procedure developed by the USDA Soil Conservation Service for use in their hydrologic calculations, and explained in detail in the SCS National Engineering Handbook, NEH-4. It consists of a function given in the form of a graph, relating total rainfall P, and direct runoff Q, both given in inches. A third parameter in this relationship is given by the runoff curve number CN, a number varying between 0 and 100 which provides a way to obtain Q as a function of P and CN. This generalized rainfall-runoff relation was developed for use with usually available rainfall data (nonrecording rain gages), and therefore the data is based on storms occurring in a calendar day, with no information on the time distribution of such storms. Consequently, it does not take into account rainfall intensities.

The runoff curve numbers to be used for particular applications are determined based on the following features of the land: 1) land use or cover; 2) treatment or practice; 3) hydrologic condition; and 4) hydrologic soil group. Standard tables and assistance from local SCS offices are useful in estimating the values of the runoff curve numbers for use in specific applications. In addition, the method has a provision for accounting for antecedent moisture, by correcting the normal curve numbers upwards for wet conditions, or downwards for dry conditions.

The hydrograph generation consists of three major steps: 1) the selection of a unit hydrograph; 2) the selection of a design hyetograph (based on a chosen temporal distribution of net design rainfall); and 3) the convolution of the unit hydrograph with the design hyetograph. Each one of these steps is briefly explained below.

The unit hydrograph is a procedure found in all major hydrologic models, perhaps due to its simplicity as compared to the more elaborate distributed parameter models which remain still at the research stage. The unit hydrograph is defined as the hydrograph for one unit of runoff lasting for a specified period of time. It can be obtained experimentally based on the analysis of rainfall-runoff data, or synthetically for ungaged watersheds. The synthetic unit hydrographs have been assembled based on large quantities of data, and are considered to represent regional characteristics on the broad mean. As an

illustration of the use of unit hydrographs, the SCS dimensionless unit hydrograph is decribed herein.

The SCS dimensionless unit hydrograph is based on the initial assumption that the unit response form a basin is shaped in the form of a triangle, with a time base equal to 8/3 of the time-to-peak. This leads to a formula for the peak flow as a function of the time-to-peak and the area of the watershed. Once the peak flow is determined, the shape of the dimensionless hydrograph is adjusted to conform more closely with a gamma-type function, with a time base equal to 5 times the time-to-peak. The latter is calculated by lag relationships, i.e., by estimating the time lag of the watershed based on physical characteristics such as length, slope, runoff curve number and area. The time lag is defined as the distance from the centroid of rainfall to the peak of runoff. The rainfall duration is estimated as a percentage of the time of concentration, this being the time it takes an element of water to travel from the watershed divide to the outlet. Alternatively, the time of concentration is defined as the time base minus the rainfall duration.

The above relationships help determine a unit hydrograph for the watershed in question. A suitable temporal distribution of rainfall is chosen, and the design hyetograph calculated based on this distribution. Finally, the unit hydrograph for the subwatershed is convoluted with the design hyetograph. The procedure is based on the incremental application of the unit hydrograph to the design hyetograph, by 1) multiplying ordinates of the unit hydrograph times each increment of rainfall; 2) lagging the resultant hydrographs in time to conform to the time of occurrence of the individual rainfall increments; and 3) superimposing all hydrographs to obtain the composite hydrograph constituting the response of the watershed to the design hyetograph.

4. STREAM CHANNEL ROUTING

Stream channel routing is the process of calculation of the flow as the flood wave travels downstream in time and space. A stream channel routing algorithm consists of the following steps: 1) a connectivity routine, which enables the flows to be routed along a network of channels, usually configured in a tree-like structure; and 2) a reach routing algorithm, either hydrologic (storage oriented) or hydraulic (cross-section oriented).

The connectivity routine is the heart of the network topology, allowing the flow to be routed from tributaries to main branch in a logical and consistent manner. In this regard, the concepts of order, branch and channel reach are important. The network order determines the degree of branching, i.e., the hierarchical arrangement among the various tributaries. Several tributaries to a main stream may be of the same order, and they

are referred to as branches. Within each branch, the distance between confluences is referred to as a channel reach. Order, branch and channel reach determine the topological numbers which configure the stream network in anticipation to the reach routing.

The reach routing can be done in one or more of several ways. The standard procedure is to apply a hydrologic method, i.e., one based on storage relationships. Examples of the hydrologic approach to reach routing are the Muskingum, convex, and other methods. The alternative to these are the hydraulic methods, such as the kinematic wave or dynamic wave. Both hydrologic and hydraulic methods have advantages and disadvantages. The hydrologic methods are simple but may not follow closely the physics of the problem. The hydraulic methods, on the other hand, tend to be more physically based, but in turn may become exceedingly complicated for certain applications.

A third procedure for reach routing which is receiving increased attention is the diffusion method (Muskingum-Cunge). This method remains within the computational framework of the hydrologic methods, but its coefficients are based on physical characteristics of the channel, making it in fact a "hybrid" model. The advantage of the diffusion method is its simplicity, robustness, and relative ease of application to ungaged watersheds, for which extensive historical data for model calibration is not available. Over the past three years, the Soil Conservation Service has funded studies to incorporate the diffusion reach routing methodology into an updated version of their popular TR-20 model, and studies continue to that effect.

The difference between the diffusion method and other established hydrologic reach routing schemes is one of fundamental importance. The classic Muskingum method requires extensive calibration in order to determine the applicable routing parameters K and X, and these can only be guaranteed within a reasonable range of flows. The convex method (and its variation, the Att-Kin) currently used in TR-20 suffers from the problem of inconsistency, i.e., the results are a function of the space interval. This is because the method, as formulated in SCS National Engineering Handbook NEH-4 and implemented in TR-20, is based on coefficients which should be calculated as a function of grid size, instead of determined empirically. These disadvantages of the classic Muskingum and convex methods are overcome by the diffusion method, which can be formulated in either a linear or nonlinear mode to encompass the routing of a wide range of flows and which bases its coefficients on the grid size, making it consistent as well as accurate.

5. RESERVOIR ROUTING

An important feature of digital watershed simulation is the capability for routing flows through reservoirs (either man-made or natural) and other flood retarding structures. For this purpose, individual reaches within the order-branch-reach network are properly identified as reservoir reaches, for which storage-outflow relationships are needed instead of stream channel rating curves. Since the reservoir routing problem is based on the storage equation only, the well known storage indication method is commonly used. In this method, the storage equation is discretized in time and coupled with the storage-outflow data to produce a recursive solution for the outflow hydrograph, given the inflow and base flow values.

6. SCS TR-20 MODEL

This model is currently one of the leading hydrologic models, being fully supported by the Soil Conservation Service. The model is a computer program of methods used by this agency as presented in their National Engineering Handbook NEH-4.

TR-20 was designed to take soil and land use information to determine runoff hydrographs for known storms, and to perform reservoir and channel routing on the generated hydrographs. The program has been used extensively by SCS engineers and others, in applications ranging from flood insurance and flood hazard studies to the design of reservoir and channel projects.

Surface runoff is computed using the runoff curve number approach to abstract losses. The excess rainfall hyetograph is constructed using the effective rain and a given rainfall distribution, and applied incrementally to the SCS dimensionless unit hydrograph to obtain the runoff hydrograph for the subwatershed for the given storm.

TR-20 uses the storage indication method to route hydrographs through reservoirs. For stream channel routing, it uses the convex method, although recent updates include the Att-Kin method (for attenuation-kinematic) and a version of the diffusion method which is being considered on an experimental basis. The program computes the subwatershed hydrographs, routes the flows through stream channels and reservoirs, combines the routed hydrographs with those of other tributaries, and routes the combined hydrograph to the watershed outlet.

Subdivision of the watershed is accomplished by determining the location of control points. Control points are defined as stream locations corresponding to cross-sectional data, reservoir sites, damage centers, diversion points, gaging stations or tributary confluences. Subarea data requirements include drainage area, time of concentration, reach lengths, routing coefficients and cross-sectional data. Applications of TR-20

normally incorporate control points spaced from a few hundred feet to more than 2 miles apart. The resulting subareas that contribute runoff to a control point are usually less that 5 sq mi.

Output from TR-20 can produce any combination of the following:

1) peak discharge rate, timing, and peak water surface elevations;
2) discharge rates for the entire hydrograph in tabular form;
3) water surface elevations as a function of time; and
4) summary tables containing water balance information.

6. HEC-1 MODEL

The HEC-1 Flood Hydrograph Model is a digital computer system developed and supported by the Hydrologic Engineering Center, U.S. Army Corps of Engineers. It consists of a calling program and a number of subroutines. Two of these subroutines determine the optimal unit hydrograph, loss rate (abstractions), and stream channel routing parameters by matching measured and calculated hydrographs. Other routines perform snowmelt computations, unit hydrograph computations, hydrograph routing and combining, and other tasks. As an added feature, HEC-1 will also perform economic analyses of flood damage by numerically integrating areas under damage-frequency curves for existing and proposed conditions. Other capabilities include the recent addition of a dam-breach analysis feature.

In HEC-1, the precipitation for a subarea can be determined by one of the following methods: 1) precipitation station data; 2) basin mean precipitation; or 3) standard project or probable maximum hypothetical precipitation distributions. Either gross or net rainfall amounts may be input, depending on the user's choice. HEC-1 abstracts losses by using the loss rate function, which is easily bypassed if net rain is available for direct input.

The loss rate function is an exponential decay function describing the instantaneous loss rate, given the rainfall intensity and the antecedent losses. For gaged watersheds, HEC-1 allows the user to input rainfall and runoff data from which the loss rate function parameters are optimized to give a best fit to the available data. Estimates of loss rate function parameters for ungaged watersheds are based largely on experience with the model. A constant loss rate is available in HEC-1 as an alternative to the loss rate function.

Unit hydrographs for each subarea are either provided by the user or calculated following Clark's unit hydrograph. The latter is also known as the time-area-curve method of hydrologic watershed routing. If the time-area curves are not available,

the model provides a synthetic time-area curve as an alternative.

The HEC-1 model allows the user a choice of several hydrologic techniques for routing floods through stream channels and reservoirs. The alternative routing procedures include 1) storage-indication reservoir routing; 2) Muskingum; 3) Working R and D; 4) Straddle-stagger; 5) Tatum; and 6) Multiple storage.

Computations of snowmelt by HEC-1 are possible in up to 10 elevation zones. The precipitation in any zone is considered to be snow below a certain base temperature. The snowmelt is computed by degree-day or energy budget methods whenever the temperature is equal to or greater than the base temperature. The elevations zones are usually delineated in increments of 1000 ft, although other equal increments can be used.

Output from HEC-1 includes most relevant data and calculated hydrographs at selected locations. Options are available for graphical and other displays.

7. SUMMARY

An overview of current practice in the field of digital simulation of hydrologic systems, specifically surface runoff, is presented. First, a description is made of the concepts involved in the simulation of surface runoff from watersheds and river basins. The three elements of simulation--subwatershed, stream channel and reservoir routing--are described in some detail. The subwatershed hydrograph generation focuses on the SCS runoff curve number approach and dimensionless unit hydrograph used in the TR-20 model. The stream channel routing segment highlights the physically based diffusion routing methodology, as an effective alternative to the dated channel routing procedures currently used by most models. The reservoir routing segment describes the classic storage-indication method.

Both TR-20 and HEC-1, currently the leading hydrologic simulation models, are described in detail. Data requirements for digital hydrologic simulation are sketched in the Appendix.

8. REFERENCES

Ponce, V. M., "Development of an Algorithm for the Linearized Diffusion Method of Flood Routing," San Diego State University Civil Engineering Series, No. 81148, September, 1981.

USDA Soil Conservation Service, "National Engineering Handbook, Section 4, Hydrology," Revised, August, 1972.

APPENDIX.- DATA INVENTORY TOPICS

A. Subwatershed Characteristics

1. Lag time, time of concentration
2. Contributing area
3. Mean overland flow distance
4. Mean slope
5. Design storm abstractions
6. Land use or cover, treatment, condition, soil type

B. Channel Characteristics

1. Channel bed profiles
2. Normal flow or other applicable rating curves
3. Manning or Chezy coefficients
4. Cross-sectional data
5. Base flow and channel losses to seepage
6. Overbank storage characteristics
7. Sediment loads, bank stability and vegetative growth

C. Streamflow Data

1. Recorded streamflow data, including statistical analyses
2. Flood frequency data
3. Flow duration data
4. Rating curves
5. Extent of inundation
6. Stage vs frequency curves
7. Stage vs flood damage

D. Design Floods and Flood Routing Parameters

1. Design storm, including temporal and spatial distribution
2. Standard project and probable maximum floods
3. Routing parameters, or the means to evaluate them
4. Base flow estimates during design floods
5. Historic floods for calibration purposes

E. Reservoir Data

1. Location data and/or potential sites
2. Elevation-storage data
3. Elevation-area data
4. Normal, minimal and other pool levels
5. Evaporation and seepage loss data
6. Sediment and dead storage requirements
7. Operating policies and rule curves
8. Outflow characteristics, including storage-outflow data

SEDIMENT TRANSPORTATION

by

Vito A. Vanoni

OUTLINE

I. River Sedimentation
   1. Classification of Sediment Load
   2. Measurement of Sediment Discharge
   3. The Sediment Transport Curve
   4. Factors Affecting Sediment Discharge
   5. Formulas for Sediment Discharge
   6. Evaluation of Formulas
   7. Selection of Formulas

II. Velocity-Depth Relations for Alluvial Streams
   1. Sand Bed Streams
   2. Gravel Bed Streams

III. Stability of Granular Sediments
   1. Granular Sediment on a Stream Bed
   2. Granular Sediment on Bank
   3. Granular Sediment on Sloping Bed

IV. References

Notes on Sediment Transportation

by Vito A. Vanoni

Prepared for: Applied Sedimentation and River Engineering; a Short Course Jan. 17-20, 1983, San Diego State University.

I. River Sedimentation

1. Classification of Sediment Load

The term "load" as used here refers to the sediment that is in motion in a stream. One can say that the load is coarse or fine sand or gravel. Some times load is used to denote the rate at which sediment is being moved, e.g., lbs per sec or tons per day. In these notes the rate of movement of sediment is referred to as the sediment discharge of the stream.

There are two common ways of classifying the load of a stream. The first divides the load into bed load and suspended load and the second classifies the load into wash load and bed sediment load. Bed load is defined as that part of the load moving on or near the bed. The suspended load, as the term denotes, moves in suspension and is that part of the load which is not bed load.

Wash load is fine sediment which makes up a very small part, usually a few percent, of the sediment on the bed. Wash load is commonly taken as the silt and clay fraction of the bed sediment, i.e., that fraction with grain sizes finer than 0.062 mm. The bed sediment load consists of particles that are coarser than the wash load. The transport rate or discharge of wash load tends not to be correlated with water discharge while discharge of bed sediment load is usually correlated with water discharge.

2. Measurement of Sediment Discharge

Suspended sediment discharge

Measurement of sediment discharge is made by samplers (ASCE 1975 p. 374). The suspended load samplers, a diagram of which is shown in Fig. 1, were developed by a group of U.S. government agencies. A number of different models are available but the principle of all models is the same. The samplers are designed so that the velocity into the intake nozzle is always the same as the local stream velocity. It takes in a sample of water and the sediment suspended in it as it is moved from the surface to the bed and returned to the surface at a uniform rate of transit.

When the sampler is touching the bed the inlet nozzle is a small distance, "a" of 0.3 ft to 0.4 ft from the bed. Therefore, the sampler does not sample in the layer of thickness "a" near the bed. The material transported in this layer near the bed and the bed load is called the unmeasured load. That transported above this layer is called the measured load.

Figure 2 is a diagram showing the velocity profile, suspended sediment concentration profile and a suspended sediment sampler in the sampling position. The sampler takes in water at a rate proportional to the velocity "u" at each level with suspended sediment of concentration "c". The suspended sediment discharge G_{ssi} in a section of a stream is:

$$G_{ssi} = 43.2\ C_{mi} V_i d_i b_i \qquad (1)$$

in which G_{ssi} is in T/da, C_{mi} is the concentration in lb/ft^3 in the sample, V_i is the mean velocity at the vertical in ft/sec, d_i is the depth in ft,

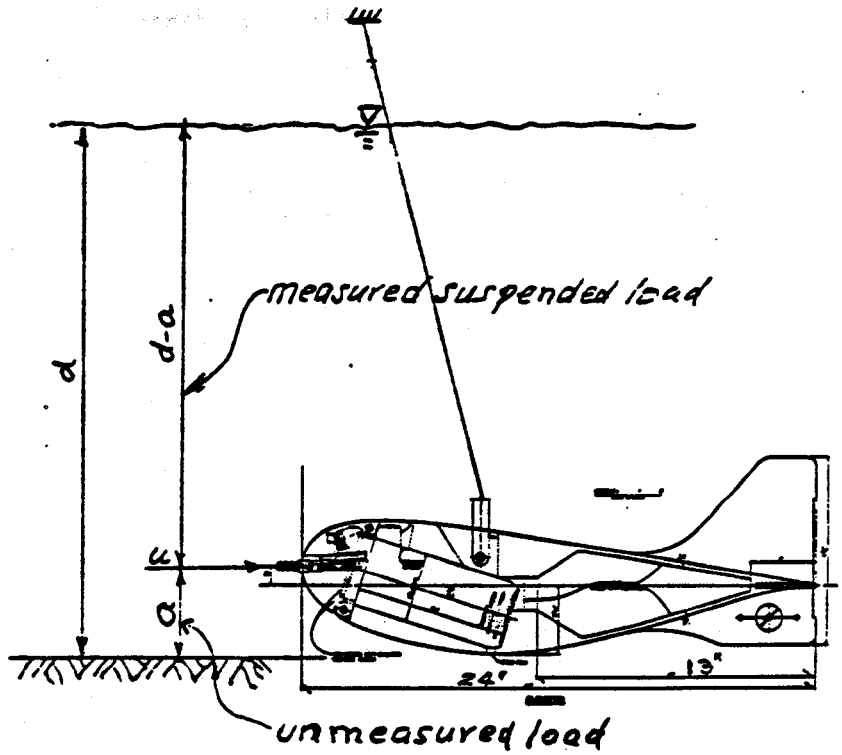

Fig. 1 USD49 Depth Integrating Suspended Sediment Sampler.

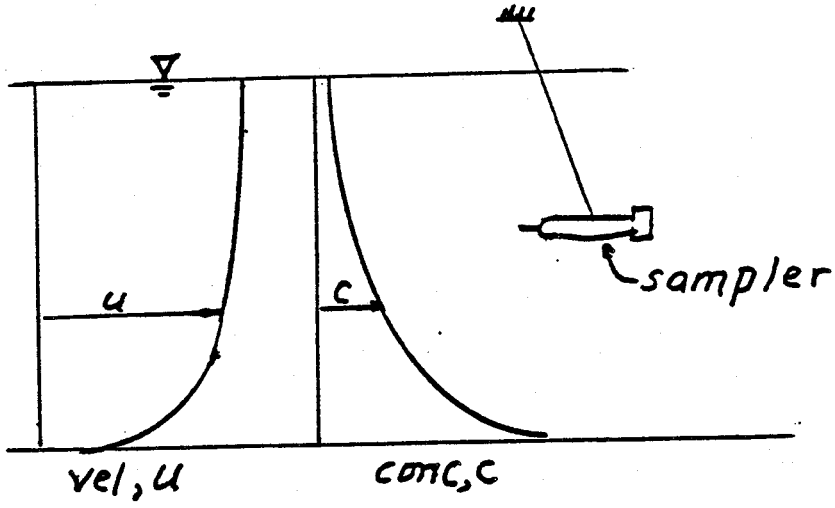

Fig. 2 Schematic of Velocity Profile, Suspended Sediment Profile and Suspended Load Sampler.

b_i is the width in ft of the section of stream over which the measured velocity and concentration are taken to be average values, 43.2 is the factor for converting lbs per sec to tons per day. The suspended sediment discharge, G_{ss} of the entire stream is the sum of the discharges at several selected sections covered the entire width of the stream,

$$G_{ss} = \sum_{c=1}^{N} G_{ssi} \qquad (2)$$

in which N = the number of stream sections at which samples were taken. The mean velocities V_i, depths d_i and section widths b_i are measured when current meter measurements are made to determine the stream discharge.

Bed load discharge

This is measured with samplers which rest on the bed. Figure 3 is a sketch of the Helley-Smith bed load sampler developed by the U.S. Geologica Survey (Emmett, 1979). The opening of this particular model is 3 in. wide by 3 in. high. Sediment carried into the sampler is filtered out and retained by the mesh bag at the rear.

Measurement of bed load with a sampler is not done on a routine basis in the United States. It is a difficult operation and requires experienced operators to obtain reliable results.

Estimating unmeasured sediment discharge

When bed load measurements are not made the unmeasured sediment discharge must be estimated in order to obtain the total sediment discharge. A common method of estimating the unmeasured load is by the Modified Einstein Procedure developed by Colby and Hembree (1955). This method which is described in ASCE 1975 (pp. 214-217) requires some special measurements which are not routinely made.

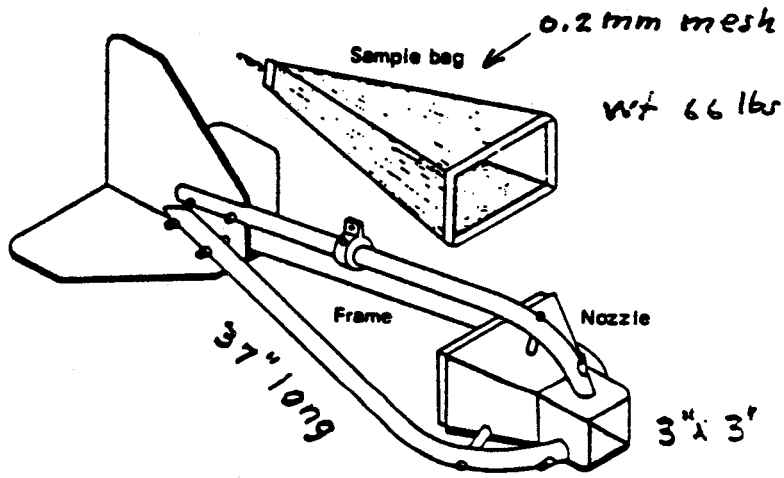

Fig. 3 Helley-Smith Bedload Sampler (Emmett, 1979).

A second method of estimating unmeasured sediment discharge is due to Colby (1957) (see ASCE 1975 pp. 217-220). It requires much less data than the modified Einstein method and the calculations involved are simple.

The unmeasured sediment discharge is often taken as a percentage of the measured suspended sediment discharge. Commonly used percentages are in the 10% to 15% range.

3. The Sediment Transport Curve

The sediment transport curve for a station on a river gives the sediment discharge as a function of water discharge. Figure 4 is suspended sediment transport curve for the Colorado River near Grand Canyon. Although the sediment discharge is given in tons per day it represents an instantaneous rate for the given discharge and is not a daily average. The scatter of the data about the curve in Fig. 4 is typical. The reasons for this scatter are not completely understood but among the causes are sampling errors due to the unsteadiness in the rivers and in the sediment transport phenomena.

An important use of the sediment transport curve is to estimate the sediment yield of a stream during a period of time in which the flow hydrograph is known or can be estimated. From the hydrograph, the duration in days that given flow rates occur is determined. The sediment discharge curve will give the sediment discharge for each flow rate. The total sediment yield is then the sum of the products of sediment discharge for each flow rate and the duration of the flow rate. If one has the flow duration curve and the sediment transport curve one can calculate the mean annual sediment yield.

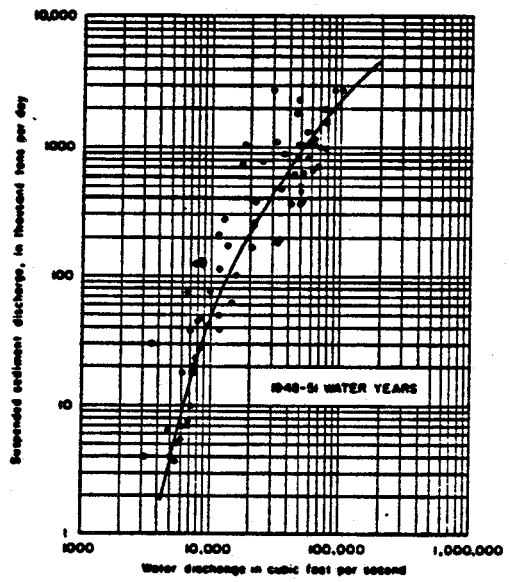

Fig. 4 Suspended Sediment Transport Curve for Colorado River near Grand Canyon. (J. Hyd. Div. ASCE, Sept. 1969, p. 1508)

4. Factors Affecting Sediment Discharge

General relations for sediment discharge

A general relation for sediment discharge can be presented symbolically in terms of the quantities which are affecting the transport phenomena. Such a general relation is:

$$G_s = f_1(V, d, b, d_{50}, \rho_s, \sigma_g, \rho, \nu, g) \tag{3}$$

in which G_s = transport rate in mass per time, V = mean flow velocity, d = flow depth, b = flow width, d_{50} = median size of bed sediment, ρ_s = density of sediment, σ_g = geometric standard deviation of bed sediment sizes, ρ = density of water, ν = kinematic viscosity of water and g = acceleration of gravity. Equation (3) can be expressed in terms of dimensionless quantities as:

$$\frac{G_s}{\rho b d V} = C_m = f_2\left(\frac{V}{\sqrt{gd}}, \frac{d}{d_{50}}, \frac{b}{d}, \frac{\rho_s}{\rho}, \sigma_g, \frac{d_{50}\sqrt{gd_{50}}}{\nu}\right) \tag{4}$$

Normally we assume that flows are two dimensional and omit the terms b/d, also ρ_s is essentially constant and σ_g is assumed not to vary greatly and the terms ρ_s/ρ and σ_g also are ignored. This simplifies Eq. (4) to

$$C_m = f_3\left(\frac{V}{\sqrt{gd}}, \frac{d}{d_{50}}, R_g\right) \tag{5}$$

in which $R_g = d_{50}\sqrt{gd_{50}}\ \nu$. If the relation for slope or friction factor is introduced Eq. (5) can be modified to read

$$C_m = f_4\left(\frac{VS}{\sqrt{gd_{50}}}, \frac{d}{d_{50}}, R_g\right) \tag{6}$$

To illustrate the forms of the functions f_3 and f_4 in Eqs. (5) and (6),

respectively, data by Stein (1965) are plotted according to these equations. Figure 5 shows the data plotted according to Eq. (5). As noted in the figure d_{50} = 0.40 mm, σ_g = 1.50 and R_g varies from 25 to 31 and its effect is probably small. The function f_3 is seen to be too complicated to be of practical significance. Figure 6 shows the Stein data plotted according to Eq. (6). The function f_4 shown on Fig. 5 may be used to develop a sediment discharge relation. The product VS has been used in sediment discharge formulas by Maddock (1970), Shen and Hung (1972) and Yang and Stall (1976).

Effect of water temperature

The effect of water temperature on transport of sand is illustrated in Fig. 7 by Lane et al. (1949) which shows data for the Colorado River at Taylor's Ferry. The discharge varies only moderately, but the temperature varies from 50°F to over 85°F and the sediment discharge varies approximately 2½ fold from summer to winter. The gradual decrease in sediment discharge is due to the coarsening of the bed sediment. The suspended load ranged in size from .044 mm to 0.589 mm. The finer sizes in the range .044 - 0.295 mm were very sensitive to water temperature but particles coarser than 0.295 mm showed negligible temperature effect.

The fall velocity of sediment grains tend to decrease as the water temperature drops so that grains are easier to transport in cold water than in warm water. The fall velocities of sand grains of different size in water at temperatures of 50°F and 85°F are shown in Table 1. The ratio of fall velocity in water at 50°F to that in water at 85°F is seen to increase from 0.68 for very fine sand to 0.81 for coarse sand. The decrease in fall velocity of sand with decrease in temperature can account for a large part of the increase in sediment discharge in the Colorado River. The roughness

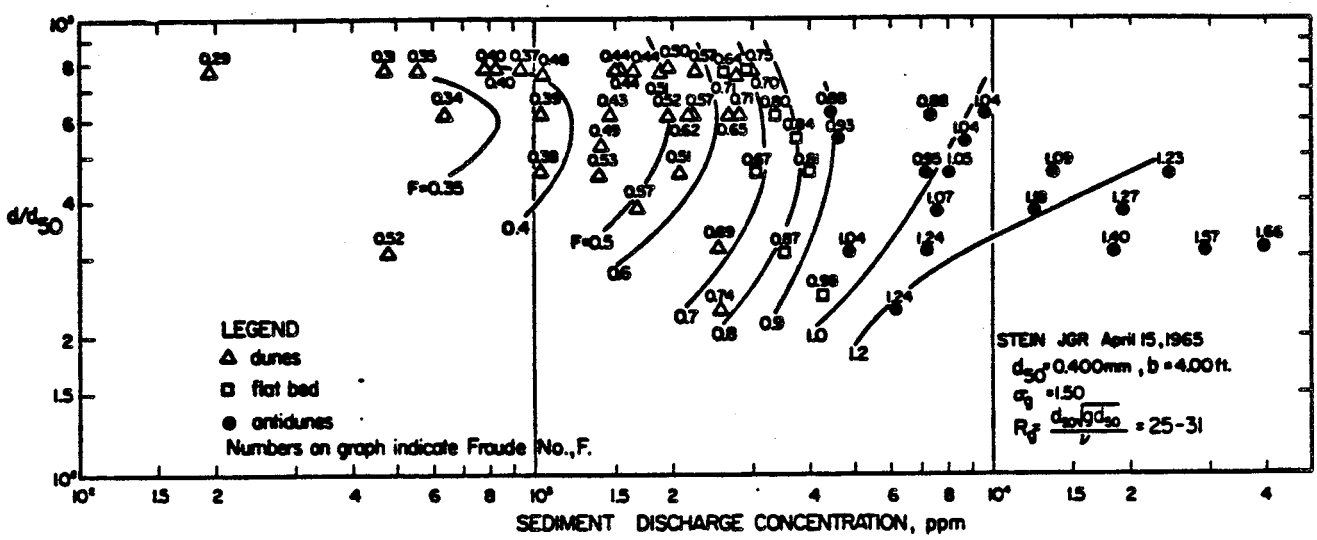

Fig. 5 Plot of Stein (1965) Data as Sediment Discharge Concentration against Froude Number, F, and the ratio of Flow Depth, d to Bed-Sediment Size d_{50} (Vanoni, 1978).

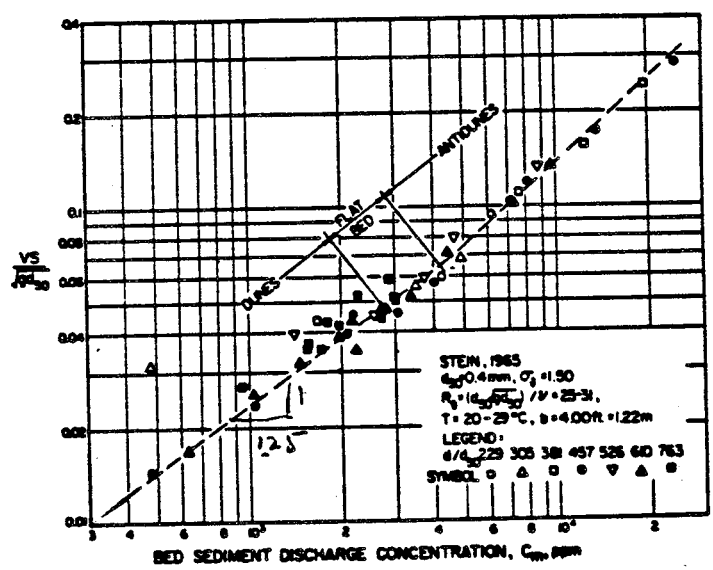

Fig. 6 Plot of Stein (1965) Data as Sediment Discharge Concentration against $VS/\sqrt{gd_{50}}$ (Vanoni, 1978).

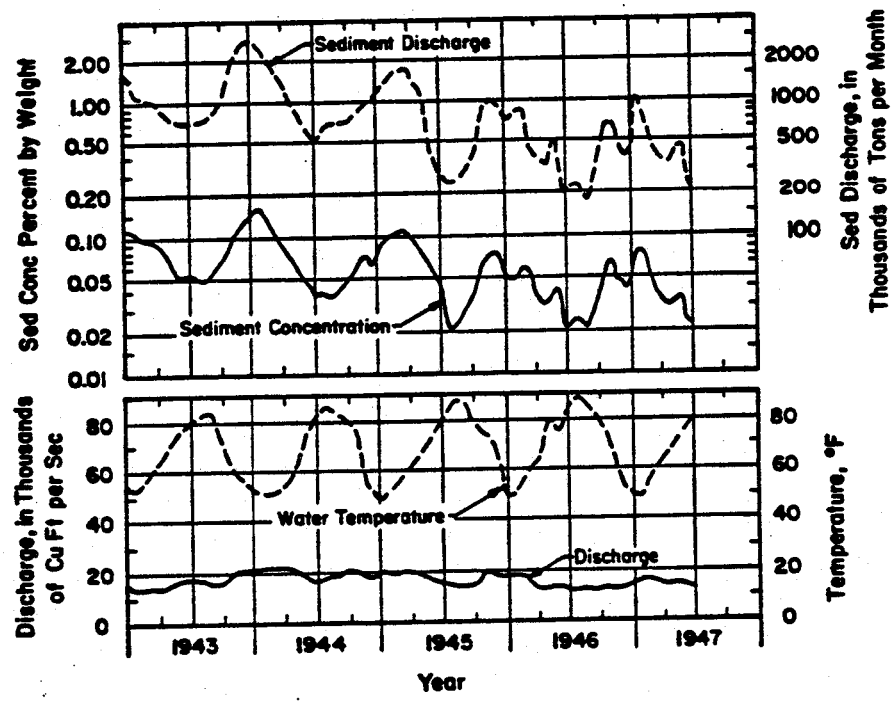

Fig. 7 Plots of Data from the Colorado River Showing the Effect of Water Temperature on Sediment Transport after Lane et al., 1949.

Table 1 Effect of water temperature on fall velocity of sand grains.

Grain Size mm	Very Fine Sand		Fine Sand		Medium Sand		Coarse Sand	
	0.088		0.177		0.354		0.707	
Temp °F	50	85	50	85	50	85	50	85
Fall Vel cm/sec	0.61	0.90	1.8	2.4	4.5	5.5	8.4	10.4
Ratio	0.68		0.75		0.82		0.81	

of the bed has been observed to decrease as temperature drops which causes the velocity to increase (U.S. Army Corps of Engrs., 1969)(ASCE 1975 pp. 186-7). This may account for some of the increase in sediment discharge in the Colorado River as the water temperature drops.

Effect of size gradation of bed sediment

The size gradation of sediment is indicated by the geometric standard deviation of sizes, σ_g, which is often defined by:

$$\sigma_g = \sqrt{d_{84}/d_{16}} \tag{7}$$

in which d_{84} and d_{16} indicate the sizes for which 84% and 16% by weight, respectively, of the particles are finer. Common values of σ_g for river sands are in the neighborhood of 1.5. Some authors define σ_g as:

$$\sigma_g = \frac{1}{2}\left(\frac{d_{84}}{d_{50}} + \frac{d_{16}}{d_{50}}\right) \tag{8}$$

The investigation of the effect of σ_g on sediment transport rate has been carried out in two sets of flume experiments, the results of which were reported by Guy et al. (1966). The median size d_{50} of the bed sediment in

the two sets of experiments were the same (0.33 mm) but σ_g was 1.25 for one set and 2.07 for the other. The depths were held within 0.48 ft and 0.53 ft and water temperature varied between 18.3°C and 21.9°C. The sediment discharge for these two experiments are presented in Fig. 8 as a function of VS, the product of mean flow velocity and slope. The sediment discharge with the highly graded bed sediment (σ_g = 2.07) is higher than for the sorted bed sediment. The median size of the load with the graded sediment was approximately one half that of the bed sediment. With the sorted bed sediment the median size of the load was about the same as that of the bed sediment. The flows were able to entrain large quantities of the fine sediments in the graded bed sediment and thus achieve a higher sediment discharge than flows over the sorted bed sediment in which the fine sediments were present in relatively smaller quantities.

Effect of concentration of wash load

Flows with high concentration of wash load are known to have higher capacity for transporting sands than similar clear water flows. Colby (1964) developed a transport relation in which he accounted for the effect of wash load concentration. This relation indicates that the transport rate of 0.5 mm sand in a flow 5 ft deep with a velocity of 10 ft/sec and a wash load concentration of 100,000 ppm is five times that for clear water.

The presence of high concentrations of wash load reduces the fall velocity of sand grains and makes them easier to transport. This effect is shown in Fig. 9 taken from Nordin (1963). For a concentration of 100,000 ppm which is unusually high the fall velocity for very fine sand (0.062 - 0.125 mm) is 0.15 times that in clear water.

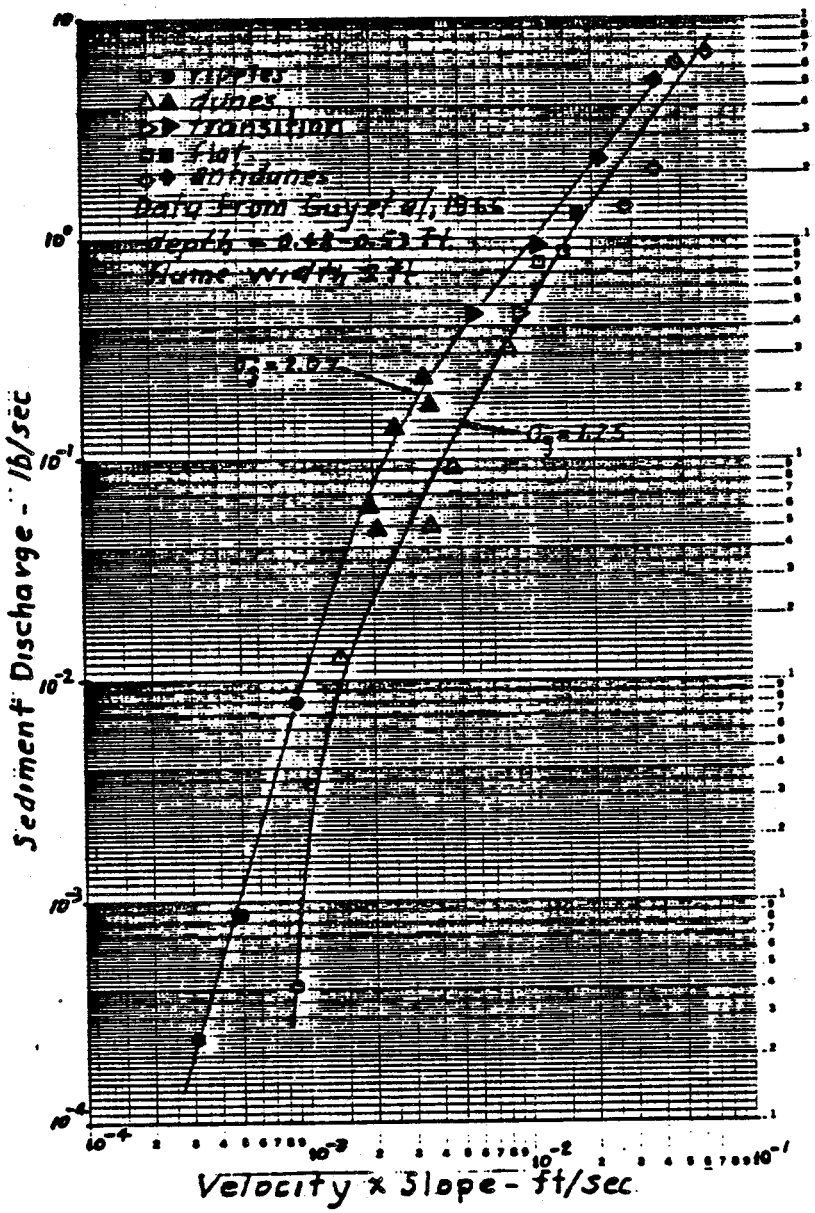

Fig. 8 Plot of Data by Guy et al. (1966) Showing the Effect of Size Gradation of Bed Sediment on Transport Rate.

5. Formulas for Sediment Discharge

Introduction

Many formulas for sediment discharge can be found in the literature and new ones continue to appear. All of the formulas are empirical in that they depend on laboratory and/or field data for the coefficients in the expressions. No truly theoretical formulas have been developed. The main difference between the many formulas stems from the variables selected in their development. Factors in Eqs. (5) and (6) are two of the possible sets of variables that can be used in transport formulas.

A complete discussion of formulas cannot be presented in such a short course. Therefore, rather than discuss each of several formulas, several formulas will be presented along with their evaluation. The evaluation cannot be done on theoretical grounds so it is done by comparing values of sediment discharge or concentration calculated by formula with measured values.

Sediment discharge formulas

All of the formulas listed are presented and discussed in one or more of the following books: ASCE (1975), Raudkivi (1976), and Simons and Senturk (1976). All of the formulas give the total bed sediment discharge which includes the suspended and bed load but does not include the discharge of wash load.

ROTTNER FORMULA (1959)

$$C_m = \frac{s}{F_D}\left\{\left[0.667\left(\frac{d_{50}}{d}\right)^{2/3} + 0.14\right]F_D - 0.778\left(\frac{d_{50}}{d}\right)^{2/3}\right\}^3 \qquad (9)$$

$$F_D = \frac{v}{\sqrt{(s-1)gd}}$$

The relation was based on dimensional analysis and 2500 sets of flume data.

ENGELUND-HANSEN (1967) FORMULA

$$C_m = 0.05\left(\frac{s}{s-1}\right)\left(\frac{vs}{\sqrt{(s-1)\,g\,d_{50}}}\right)\sqrt{\frac{ds}{(s-1)d_{50}}} \qquad (10)$$

The formula was checked against flume data published by Guy, Simons and Richardson (1966).

ACKERS-WHITE (1973) FORMULA

$$C_m = c\rho_s/\rho\left(\frac{d_{50}}{d}\right)\left(\frac{V}{\sqrt{gdS}}\right)^n\left(\frac{F_{gr}}{A} - 1\right)^m \qquad (11)$$

$$F_{gr} = \frac{(gdS)^{n/2}}{\sqrt{gd_{50}(s-1)}}\left[\frac{V}{\sqrt{32}\,\log\left(\frac{10d}{d_{50}}\right)}\right]^{1-n} \qquad (11a)$$

$$D_{gr} = d_{50}\left[\frac{g(s-1)}{\nu^2}\right]^{1/3}$$

	$D_{gr} > 60$	$60 \geq D_{gr} \geq 1$
n	0.0	$1 - 0.56 \text{ Log } D_{gr}$
A	0.170	$0.23/\sqrt{D_{gr}} + 0.14$
m	1.50	$9.66/D_{gr} + 1.34$
c	0.025	$\text{Log } c = 2.86 \text{ Log } D_{gr} - (\text{Log } D_{gr})^{\frac{1}{2}} - 3.53$

The coefficients in this formula were based on almost 1000 sets of flume data. The relation is not expected to apply to flows with Froude numbers in excess of 0.8.

YANG (1973) FORMULA

$$\text{Log } C_m = 5.435 - 0.286 \text{ Log}\frac{wd_{50}}{\nu} - 0.457 \text{ Log } \frac{u_*}{w} +$$

$$\left(1.799 - 0.409 \text{ Log}\frac{wd_{50}}{\nu} 0.314 \text{ Log } \frac{u_*}{w}\right)\text{Log}\left(\frac{VS}{w} - \frac{V_{cr}S}{w}\right) \qquad (12)$$

$$\left.\begin{aligned} \frac{V_{cr}}{w} &= \frac{2.5}{\text{Log}\frac{u_*d_{50}}{\nu} - 0.06} \quad \text{for} \quad 1.2 < \frac{u_*d_{50}}{\nu} < 70 \\ \frac{V_{cr}}{w} &= 2.05 \quad \text{for} \quad \frac{u_*d_{50}}{\nu} \geq 70 \end{aligned}\right] \qquad (12a)$$

The coefficients in the formula were based on 1093 sets of flume data and 65 sets of field data.

BROWNLIE (1982) FORMULA

$$C = 7115\ C_F(F_g - F_{go})^{1.978} S^{0.6601} \left(\frac{r}{D_{50}}\right)^{-0.3301} \qquad (13)$$

$$F_g = \frac{V}{\sqrt{\left(\frac{\rho_s - \rho}{\rho}\right) gD_{50}}} \qquad (13a)$$

$$F_{go} = 4.596\ \tau_{*o}^{0.5293}\ S^{-0.1405}\ \sigma_g^{-0.1606} \qquad (13b)$$

$$\tau_{*o} = 0.22Y + 0.060(10)^{-7.7Y} \qquad (13c)$$

$$Y = \left[\sqrt{\frac{\rho_s - \rho}{\rho} R_g}\right]^{-0.6} \tag{13d}$$

$$R_g = \frac{D_{50}\sqrt{gD_{50}}}{\nu} \tag{13e}$$

C_F = 1.0 for flume flows

C_F = 1.268 for rivers

The symbols used in the relations (Eqs. 9-13) are defined as follows:

C_m = sediment concentration, ppm

w = fall velocity of median size of bed sediment ft/sec

d = flow depth, ft

r = hydraulic radius, ft

D_{50}, d_{50} = median size of bed sediment, ft

ν = kinematic viscosity of water, ft^2/sec

u_* = bed shear velocity, ft/sec

V = mean flow velocity, ft/sec

V_{cr} = critical flow velocity, ft/sec

S = slope of stream

s = ρ_s/ρ

ρ_s = density of sediment $slugs/ft^3$

ρ = density of water $slugs/ft^3$

g = acceleration of gravity ft/sec^2

Relations for unmeasured load:

Modified Einstein method (Colby & Hembree, 1955)

Colby (1957)

The Modified Einstein method of Colby and Hembree (1955) is based on an application of the Einstein (1950) bed load function. To apply it one must first measure flow depth, velocity and suspended load at several verticals. One also needs the size analysis of the suspended load and bed sediment and the water temperature. Because observed data are used in this method it is considered the most reliable of the methods available for discharge of unmeasured load.

The Colby (1957) method of estimating sediment discharge requires only the mean velocity of the stream, its width, the mean suspended sediment concentration and concentration of suspended bed sediment. It has the advantage of being simple although it may not give as reliable results as the more elaborate Modified Einstein method. Both the Modified Einstein and Colby methods are given in ASCE (1975).

6. Evaluation of Formulas

Formulas can be evaluated by comparing measured sediment discharge corrected for unmeasured load with that calculated by formula. Examples of one way to make such comparisons are shown in Figs. 10 to 12. These figures are plots of measured data against calculated data. The lines parallel to the line of perfect agreement show values that are 0.5 and 2.0 times the values on the line of perfect agreement.

Figure 10 compares data for 184 flume experiments and 67 sets of river measurements with values calculated by the formula of Chang et al. (1967). The authors report that the error in the sediment discharge calculated by the formula exceeds 100% in only 43% of the cases.

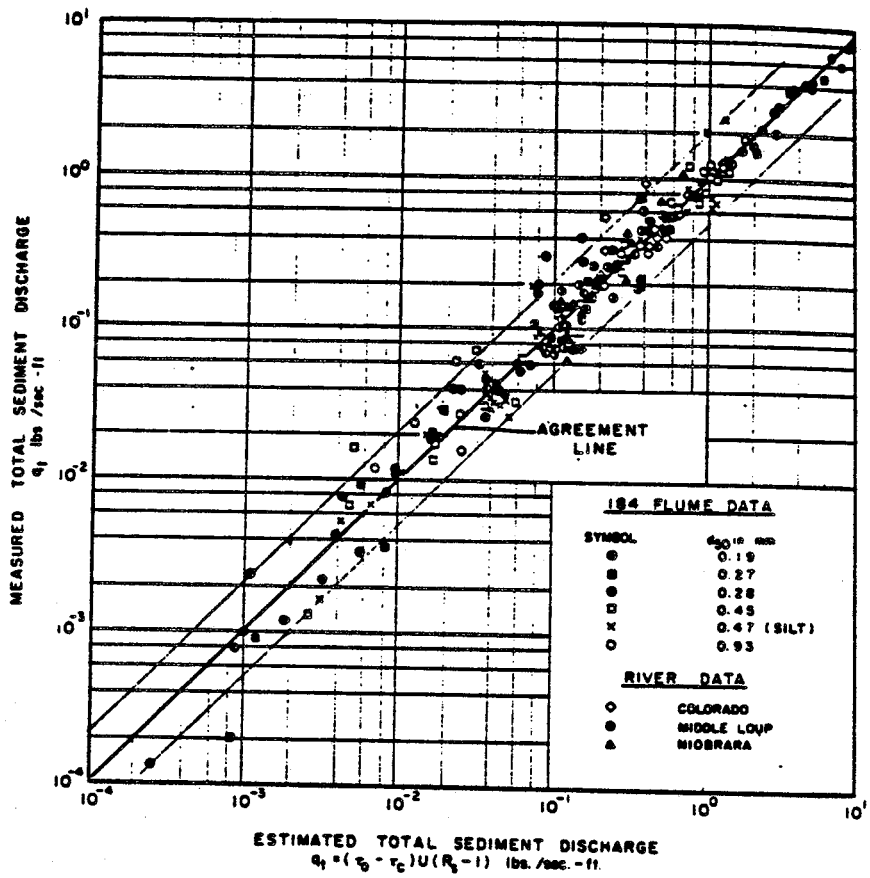

Fig. 10 Comparison of Measured Sediment Discharge in Flumes and Rivers with Values Calculated by the Formula of Chang et al. (1967). Upper and lower lines represent values that are 0.5 and 2.0 times these on the "agreement line".

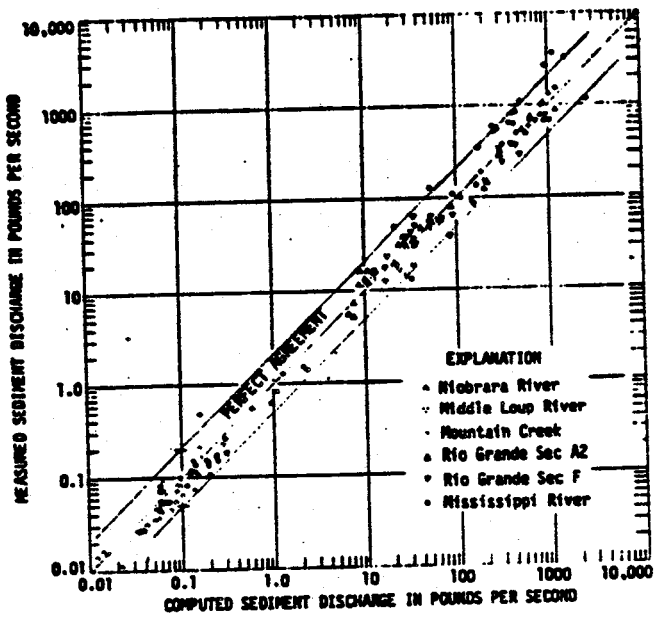

Fig. 11 Comparison of Observed Sediment Discharge in Six Rivers with Those Calculated by the Formula of Yang and Stall (1976). (The upper and lower lines represent values that are 2.0 and 0.5, respectively times the values on the line of perfect agreement.)

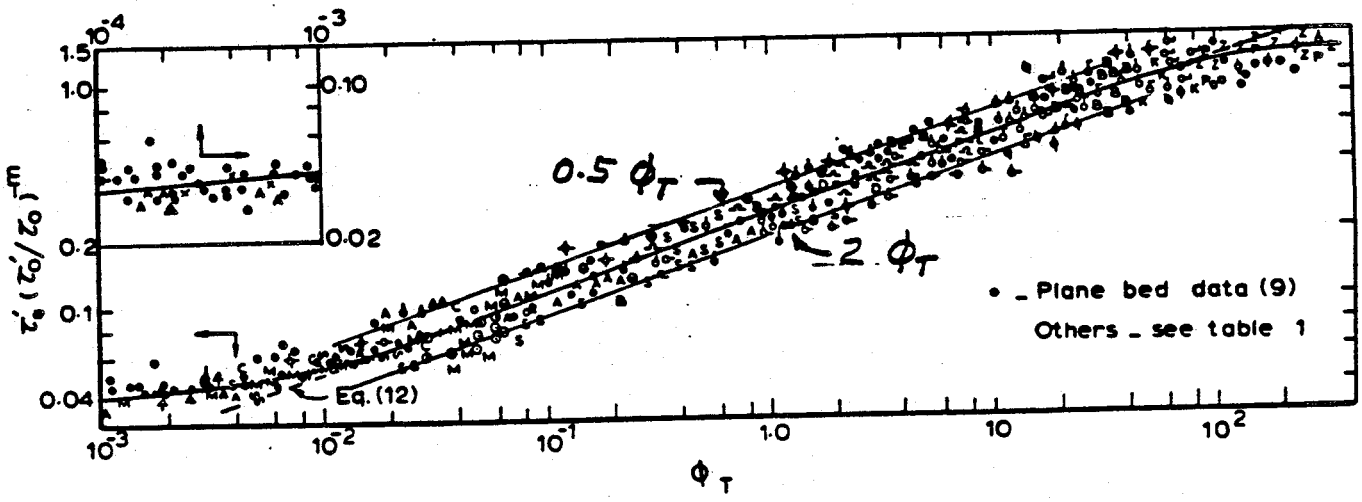

Fig. 12 Sediment Transport Relation by Ranga Raju, Garde and Bardway (1981) for Flat, Ripple and Dune Beds. (The Quantity ϕ is Proportional to Sediment Discharge.)

Figure 11 shows a graph in which measured sediment discharge in six rivers is compared with estimates calculated by the formula of Yang (1973). Again the lines of 0.50 and 2.0 times the values indicated by the line of perfect agreement are shown. Most of the data fall within these lines. Figure 12 shows a comparison of measured values and values calculated by the formula of Ranga Raju et al. (1981). The quantity ϕ_T is proportional to the total transport rate and is a function of the value of the ordinate of the curve. The data plotted in Fig. 12 are taken from flume experiments with 47 different sands by various workers and measurements on seven rivers.

White et al. (1973) compared observed sediment discharge concentrations from flume and field measurements with those calculated by 15 formulas. One thousand sets of flume measurements were used in the analysis. These included experiments with sands and with lightweight sediments. The field data used were taken from 270 sets of measurements on 11 rivers. The results were presented as histograms of the ratio of calculated concentration to measured concentration, $\frac{C(calc)}{C(meas)}$. The histograms are shown in Fig. 13. Three formulas with best ratings are those of Ackers-White (1972), Engelund-Hansen (1967) and Rottner (1959). As shown in Fig. 13 the percent of the calculated concentrations that fell between one half and twice the observed values were 64% for the Ackers-White formula, 58% for the Engelund-Hansen formula and 53% for the Rottner formula.

The comparison of 14 formulas by Brownlie (1982) is shown in Fig. 14. The bars show the 16th and 84th percentile of the values of C(calc)/(C)measured for flume data (solid lines) and field data (dotted lines). The median value is indicated by "x". The formulas of Ackers-White (no. 1), Engelund-Hansen (no. 6) and Rottner (no. 10) rate well as they did in Fig. 13. The coefficients in the Brownlie formula were determined from the data used in the

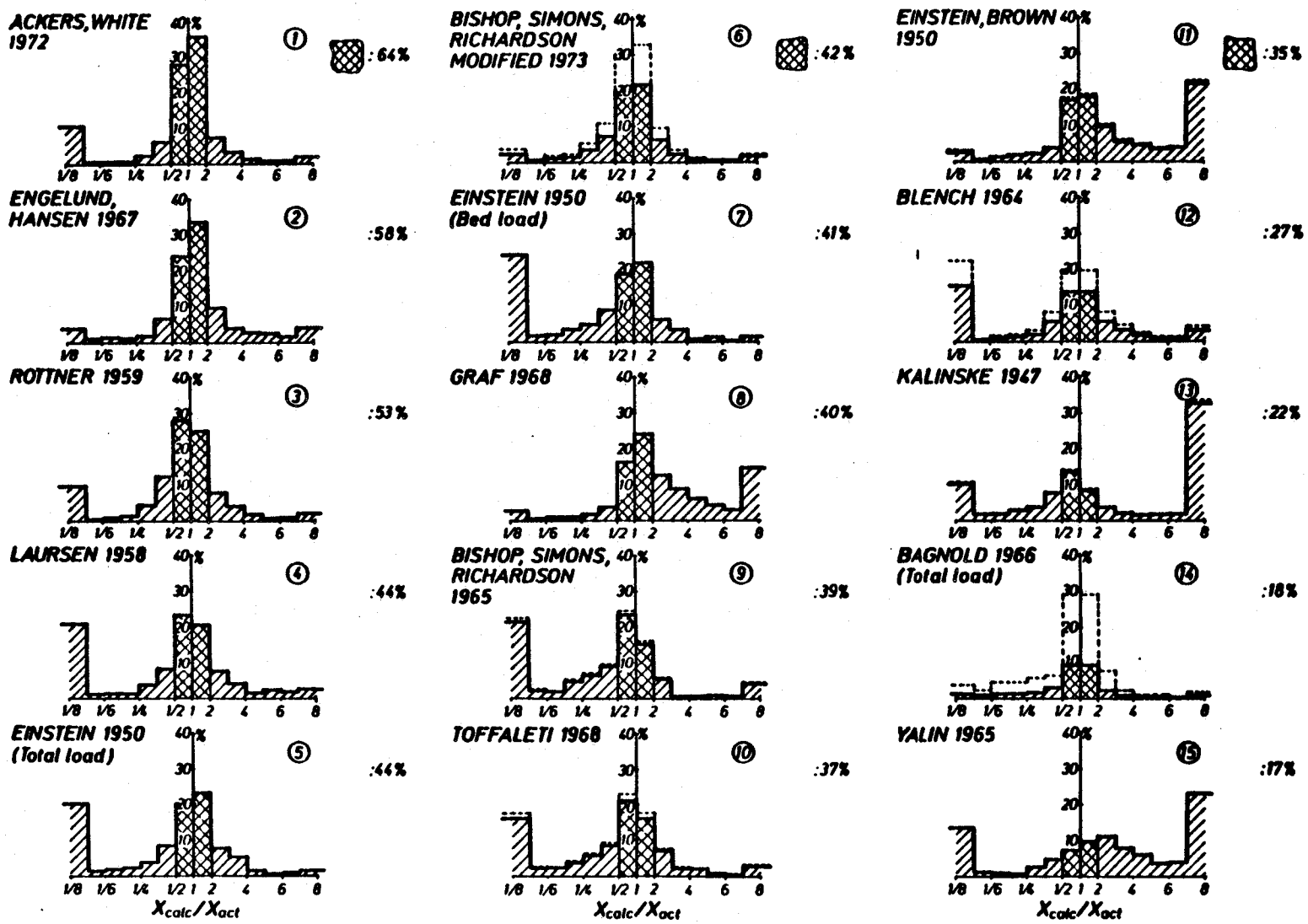

Fig. 13 Histograms of X_{calc}/X_{act} in which X_{calc} = sediment discharge concentration calculated by formula and X_{act} = measured concentration. The bars indicate the percent of the data in the range of concentration ratios indicated. Values for 15 formulas are compared.

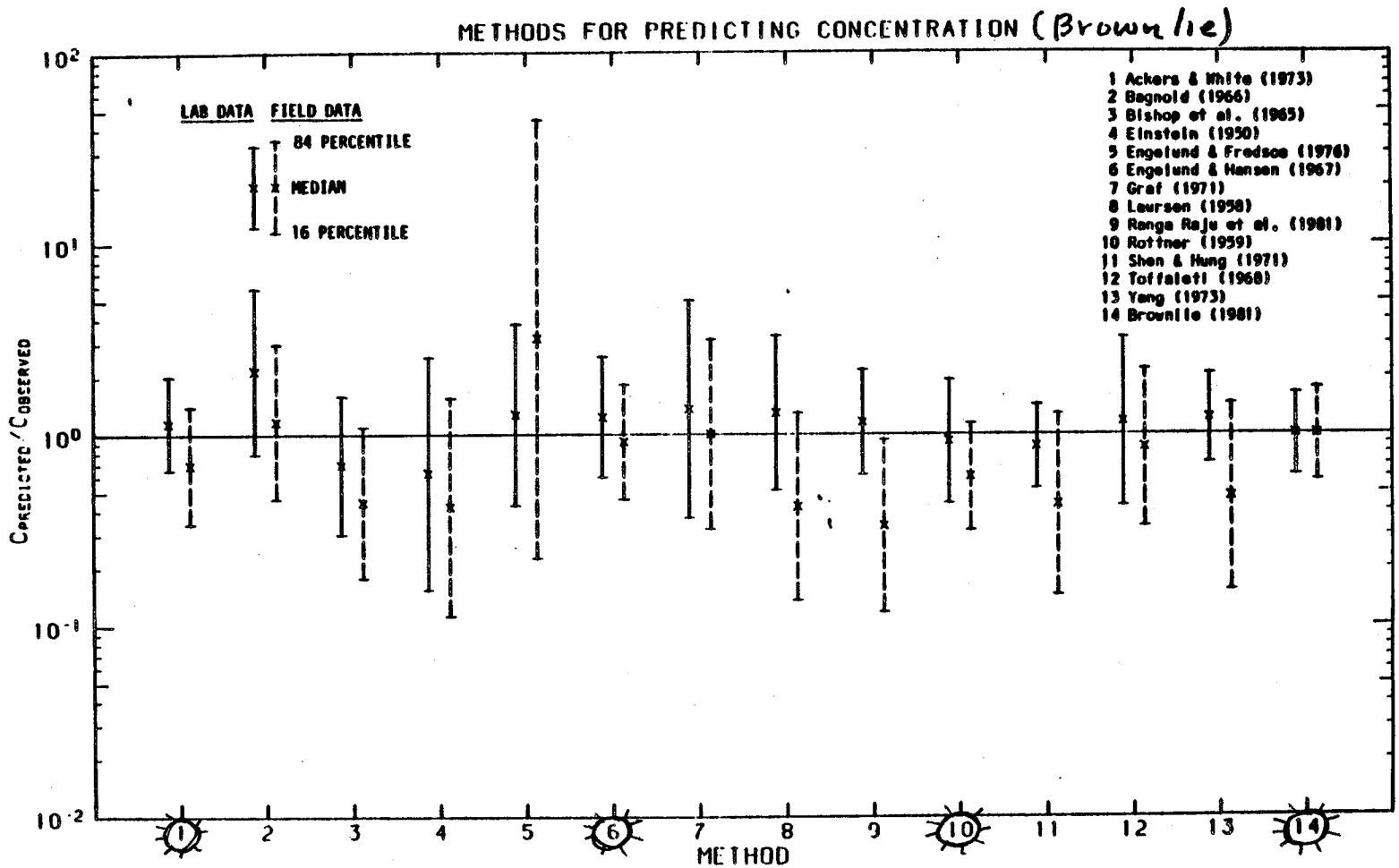

Figure 14 Comparison of methods for predicting sediment concentration. Median and 16 and 84 percentile values are based on the approximation of a log-normal distribution of errors.

comparisons of Fig. 14. Therefore the bars in Fig. 14 show how well the formula fits the data and cannot be considered as a rating of the formula.

The rating of the formulas of Ackers-White, Engelund-Hansen and Rottner by three different workers are shown in Table 2. This table also shows the rating of the Yang formula by himself and Brownlie. Each author used a different set of data in his comparisons shown on Table 2.

Table 2. Comparison of Sediment Discharge Formulas.

Formula	Number of Data Sets		Workers doing Evaluation	Percent of data for which (C)calc/(C)meas fall between 1/2 and 2		
	flume	field		flume	field	all data
Ackers-White (1972)	1000	270	White et al. (1973)	--	--	64
	1091	156	Yang (1973)	--	--	68
	480	519	Brownlie (1982)	76	61	68
Engelund-Hansen (1967)	1000	270	White et al. (1973)	--	--	58
	1091	156	Yang (1973)	--	--	63
	480	519	Brownlie (1982)	64	69	67
Rottner (1959)	1000	270	White et al. (1973)	--	--	53
	1091	156	Yang (1973)	--	--	56
	480	519	Brownlie (1982)	65	59	62
Yang (1973)	1091	156	Yang (1976)	91	92	91
	480	519	Brownlie (1982)	77	51	63

7. Selection of Formulas

The results presented above show clearly that one cannot expect precise predictions of sediment discharge from formulas. Furthermore, results of formulas vary greatly from each other. This makes it very difficult for an engineer to select a formula for analyzing a particular problem. Unfortunately it is not possible to recommend one or more formulas for use under any given set of conditions.

If one has some measurements of sediment discharge and flow rate for the stream under investigation these should be used to select a formula which fits them. If enough measurements are available to construct a sediment transport curve this curve should be used in preference to one derived by formula. In the absence of data one should be guided by data from comparable streams.

If one is forced to use the results of formulas to study a project one must keep in mind that the result so obtained are probably only rough estimates. When the problem requires that relative amount of sediment discharge be estimated the results will be more reliable than the values of the sediment discharge estimated by formula.

II. Velocity-Depth Relations for Alluvial Streams

1. Sand Bed Streams

A number of methods for predicting the depth and velocity of alluvial streams have appeared in the technical literature (see ASCE, 1975). Figure 15 is a graph of mean velocity against depth for the Colorado River showing observed values and values calculated by several methods. The calculated relations show a wide range of values and do not inspire confidence in them. The observed velocity and depth data also scatter widely and correlate poorly. Some of the scatter of data in Fig. 15 may be due to the large range in water temperature which was from 48°F to 80°F.

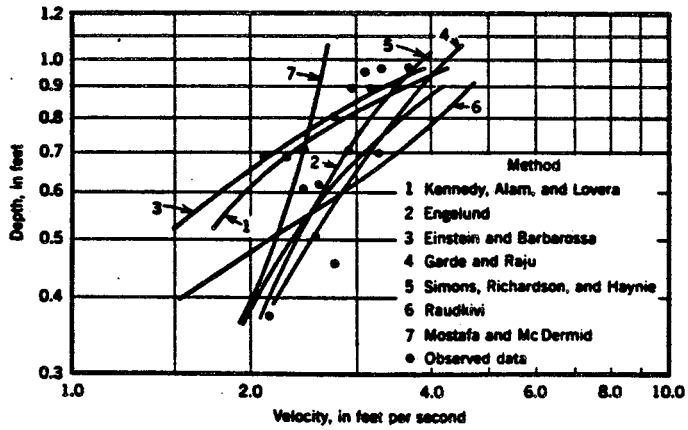

FIG. 15 —Comparison of Predicted and Observed Depth-Velocity Relations for Colorado River

Figure 16 shows a plot of Manning's "n" against water temperature for the Middle Loup River (Colby & Scott, 1965). The friction factor fell as water temperature dropped and as the bed dunes became lower and longer as shown by Fig. 17. The values of the Manning friction factor "n" corresponding to the data on Fig. 17 varied from 0.023 to .035 and had an average value of 0.029 which is a common value for sand bed rivers.

The wide variation in values of velocity and depth predicted by the seven methods for the Colorado River illustrates the difficulty of predicting the relation for any given case. Again as in the case of predicting sediment discharge one should rely strongly on observed depth-velocity data if available. Lacking data one should seek data for comparable cases. Channels are comparable when the bed forms are comparable. Several predictors of bed form are available, e.g., ASCE (1975) p. 165 and Vanoni (1974). These predictors indicate bed form in terms of slope, depth, velocity, bed sediment size and water viscosity.

2. Gravel Bed Streams

Bray (1979) fitted relations for friction factors to data from 67 gravel-bed rivers. The flow rates in the rivers ranged from 195 to 290,000 cu ft per sec, depths varied from 2.5 to 23 ft and median size of the bed sediment varied from 19 to 140 mm.

Hey (1979) developed a relation for flow velocity in a gravel stream which took account of the shape of the channel as well as the size of gravel on the bed.

The relations fitted to the data by Bray were of two forms: 1) Strickler type and 2) Keuligan type. The Strickler type equation gives the Manning friction factor "n" in terms of a characteristic size K_s of the bed sediment,

$$n = a\, K_s^{1/6} \qquad (14)$$

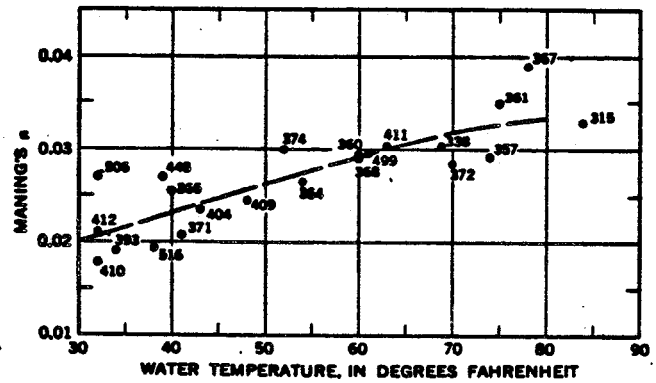

Fig. 16 Plot of Manning "n" against water temperature for Middle Loup River at Dunning, Nebraska after Colby and Scott, 1965. (Numbers by points indicate discharge in cu ft per sec.)

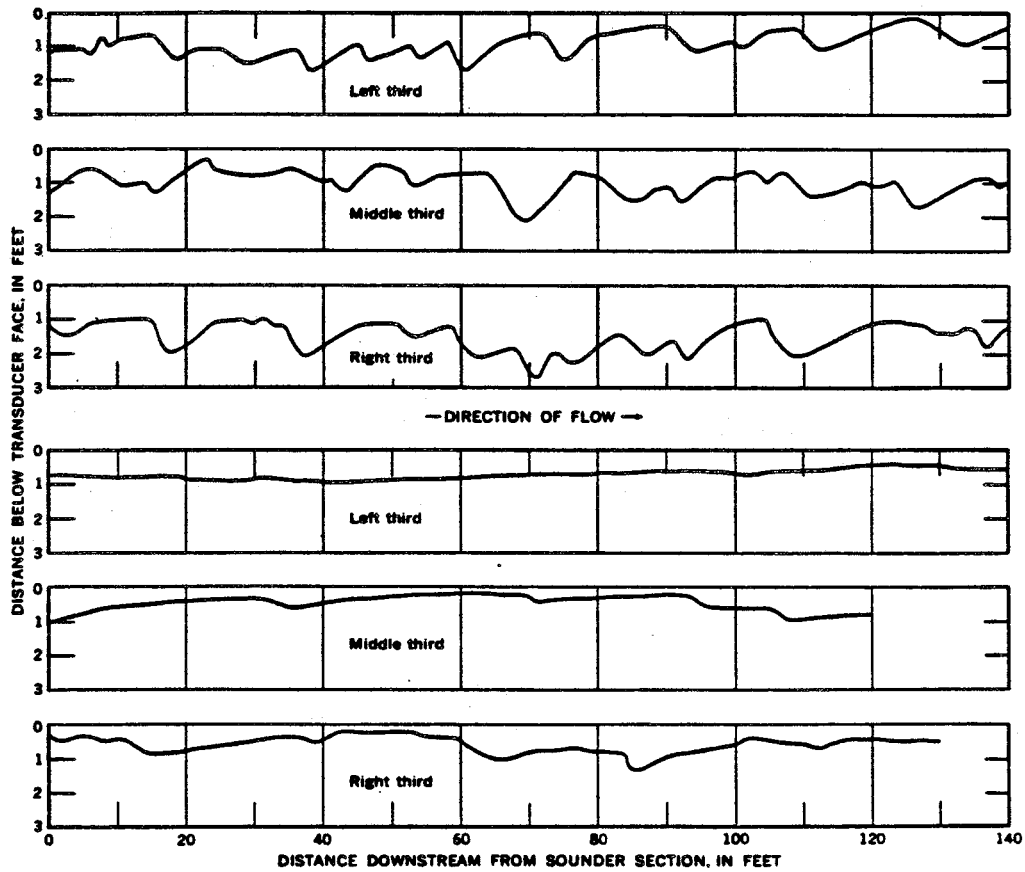

Fig. 17 Two sets of three longitudinal profiles each of bed of Middle Loup River at Dunning, Nebraska showing effect of water temperature on bed form, after Colby and Scott (1965). (Temperature for upper profiles = 83°F and for lower profiles = 39°F; discharge for upper and lower profiles = 350 and 360 cu ft per sec respectively.)

The Keuligan relation is,

$$\frac{V}{\sqrt{gRS}} = 6.25 + 5.75 \text{ Log } \left(\frac{R}{K_s}\right) \tag{15}$$

in which R = hydraulic radius of the channel, S = channel slope, g = acceleration of gravity, V = mean velocity and K_s = characteristic bed sediment size.

The Keuligan equation can be manipulated to give the Manning "n" by introducing the Manning equation,

$$V = \frac{1}{n} R^{2/3} S^{1/2} \tag{16}$$

This gives,

$$n = \frac{0.113 \; R^{1/6}}{2.21 + 2.03 \log \frac{R}{K_s}} \tag{17}$$

In Eqs. 16 and 17, R and K_s are in meters and V is in meters per sec. The Limerinos (1970) equation for n is,

$$n = \frac{0.113 \; R^{1/6}}{1.16 + 2.00 \log \left(\frac{R}{D_{84}}\right)} \tag{18}$$

in which R = hydraulic radius in meters and D_{84} is the grain size of the bed sediment for which 84 percent of the total number of grains on the bed are finer. Note that this size differs from the usual one which is based on weight percent instead of number percent.

Bray compared values of observed velocities in 67 rivers with those calculated by the Manning equation (Eq.16) with "n" values given by the Strickler, Keuligan and Limerinos equations. To calculate n by Eq.(14) the following forms were used,

$$n = 0.041 \; D_{50}^{1/6} \tag{19}$$

$$n = 0.038\ D_{90}^{1/6} \tag{20}$$

Values of n were calculated with the Keuligan equation (Eq.17) with $K_s = D_{50}$, D_{65} and D_{90}. The sediment sizes were expressed in meters and based on percent by number.

Bray found that the Limerinos equation (Eq.18) gave the smallest mean error and standard deviation of errors in the calculated velocity. He also compared results obtained with relations by Cowan and Lacey and developed equations of the Strickler and Limerinos form with constants which best fit the data for the 67 rivers.

III. Stability of Granular Sediments

1. Granular sediment on a stream bed

Figure 18 is a diagram showing the forces acting on a grain in a bed of other grains. When critical conditions exist and the grain is on the verge of moving and the moment due to the shear stress τ_c about the point of support is just equal to that of the weight of the grain. Equating these moments gives:

$$\tau_c = \frac{c_1 a_1}{c_2 a_2} (\gamma_s - \gamma) d_s \cos\phi (\tan\theta - \tan\phi) \tag{21}$$

in which γ_s = specific weight of sediment grains, γ = specific weight of water, d_s = diameter of grains, ϕ is the slope angle of the stream, θ = the angle of repose of the sediment, c_1 and c_2 are dimensionless constants and a_1 and a_2 are lengths as shown in Fig. 18. Any consistent set of units may be used in Eq. 21 for example the ft, lb (force) and sec system.

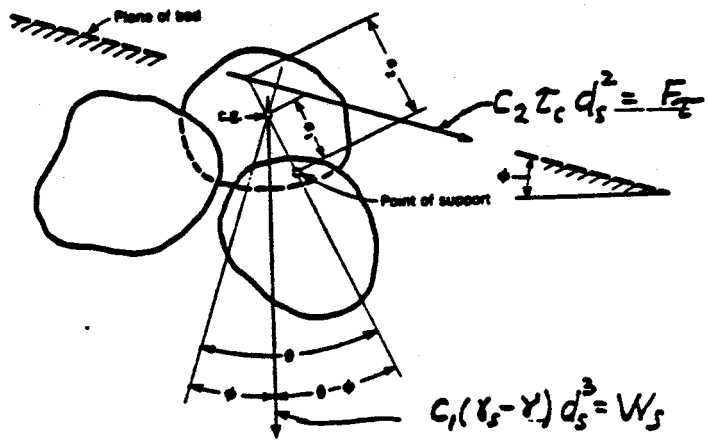

FIG. 18 .—FORCES ON SEDIMENT GRAIN IN BED OF SLOPING STREAM (J. Hyd. Div. ASCE Mar '66)

Fig. 18

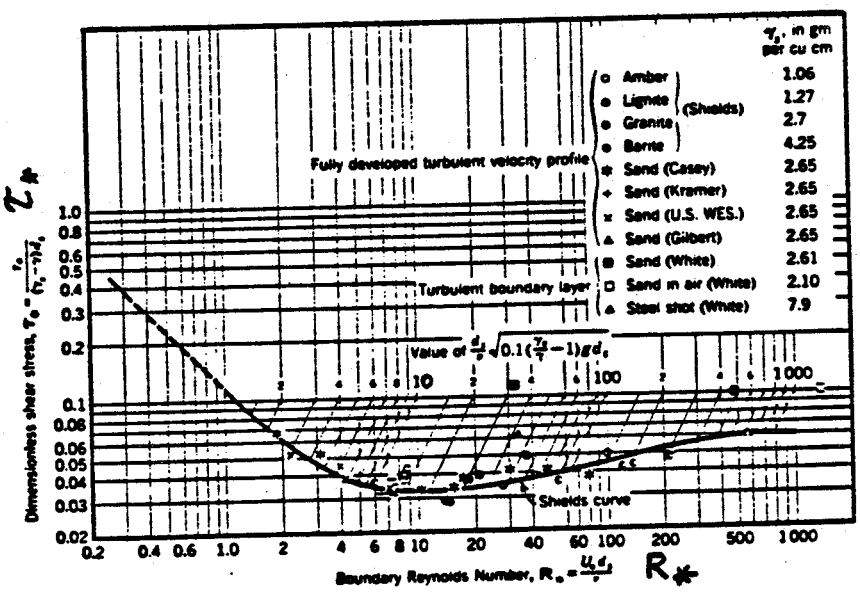

Fig. 19 Shields Diagram for Calculating Critical Shear Stress τ_c (Jour. of Hyd. Div. ASCE Mar 1966).

Equation 21 cannot be used to give τ_c because the factors c_1, c_2, a_1 and a_2 are not known. Therefore the relation between the pertinent quantities is expressed by dimensional analysis and the actual relation is determined from experimental data. Figure 19 is such a relation first presented by Shields (1936) and carries his name. The curve is expressed by dimensionless combinations of critical shear stress τ_c, sediment and water specific weights γ_s and γ, sediment size d_s, critical shear velocity $u_* = \sqrt{\tau_c}/\rho$ and kinematic viscosity of water ν. These quantities can be expressed in any consistent set of units.

The Shields curve is awkward to use because τ_c and d_s occur in both coordinates of the curve. These coordinates can be rearranged into more convenient combinations to facilitate calculation. One such set of coordinates is shown in Fig. 20. In this formulation the shear stress τ_c has been eliminated from the abscissa and a straightforward solution for τ_c can be made when d_s, and properties of the water and sediment grains are given.

The Shields values of τ_c are used commonly to denote conditions under which bed sediments are stable but on the verge of being entrained. Not all workers agree with the results given by the Shield curve. For example, some workers give $\tau_{*c} = 0.047$ for the dimensionless critical shear stress for values of R_* in excess of 500 instead of 0.06 as shown in Fig. 19. Taylor and Vanoni (1972) reported that small but finite amounts of sediment were transported in flows with values of τ_c given by the Shields curve.

The value of τ_c to be used in design depends on the particular case at hand. If the situation is such that grains that are moved can be replaced by others moving from upstream some motion can be tolerated and the Shields values may be used. On the other hand if grains removed

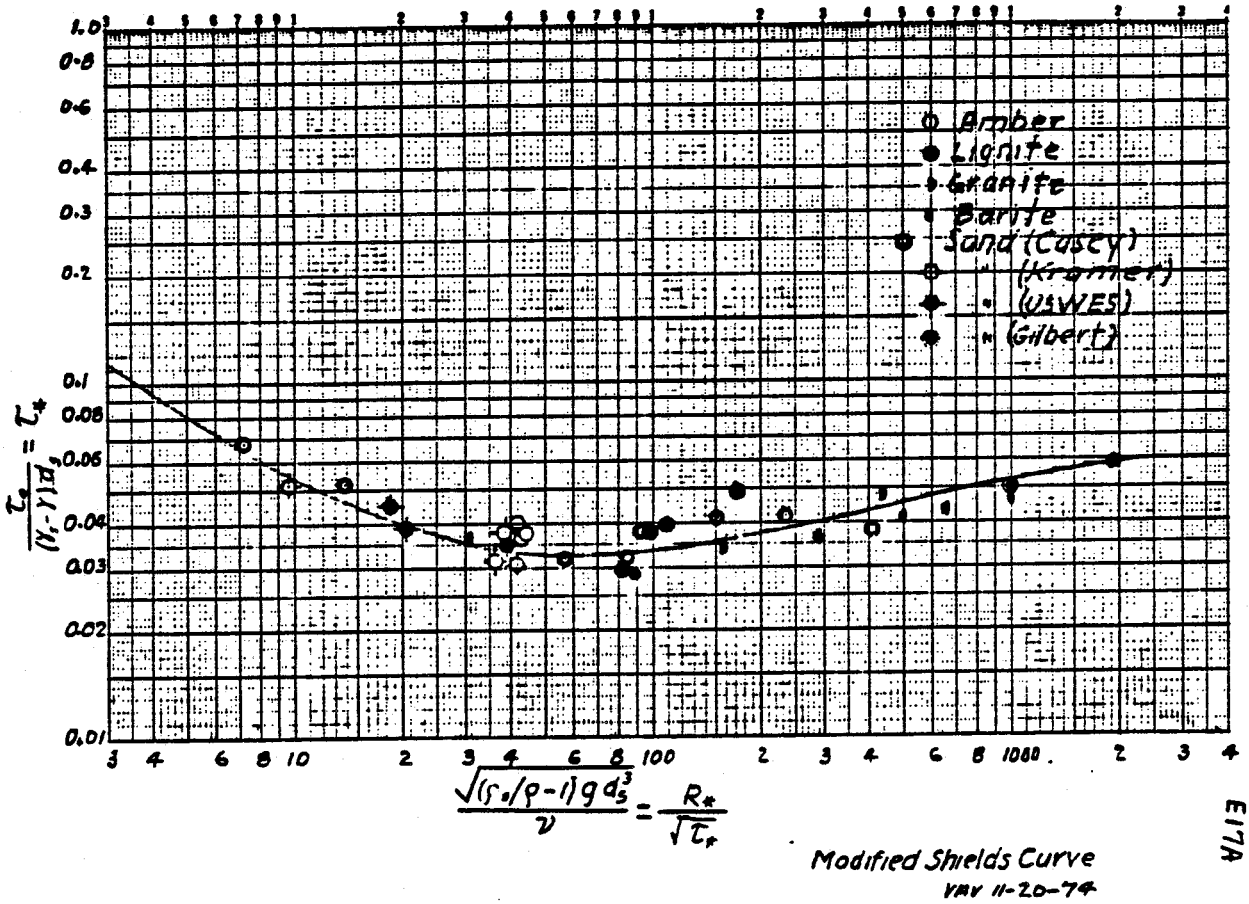

Fig. 20 Shields Curve Modified so Direct Calculation Can Be Made for Critical Shear Stress in Terms of Sediment Size d_s, Fluid Properties ρ and ν and Sediment Properties ρ_s and γ_s (unpublished).

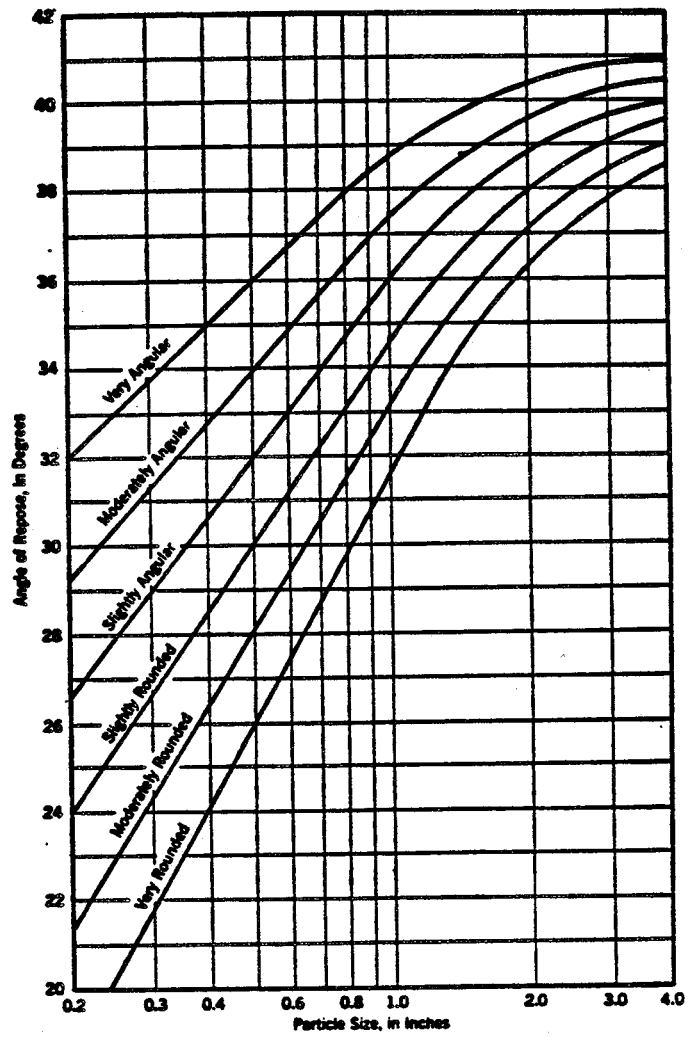

Fig. 21. Angle of Repose of Noncohesive Sediment after Lane (1955).

cannot be replaced as on a stream bank, the Shields values of τ_c are too large and should be reduced.

The value of bed shear stress τ_o for a wide rectangular channel is given by $\tau_o = \gamma dS$ in which γ = specific weight of water, d is flow depth and S = channel slope. The average bed shear stress for any channel is given by $\tau_o = \gamma rs$ in which r = the hydraulic radius of the channel cross-section.

2. Granular Sediment on Bank

A sediment grain on a bank is less stable than one on the bed because the gravity force tends to move it downward. The ratio of the critical shear stress τ_{wc} for a particle on a bank to that for the same particle on the bed τ_c as given by Lane (1955):

$$\frac{\tau_{wc}}{\tau_c} = \cos\phi_1 \sqrt{1 - \left(\frac{\tan\phi_1}{\tan\theta}\right)^2} \tag{22}$$

in which ϕ_1 is the slope of the bank and θ is the angle of repose for the sediment. Values of θ are given by Lane (1955) and Simons and Senturk (1976).

3. Granular Sediment on Sloping Bed

Equation 21 shows that τ_c diminishes as the slope angle ϕ increases. For very small ϕ τ_c is:

$$\tau_c = \frac{c_1 a_1}{c_2 a_2} (\gamma_s - \gamma) d_s \tan\theta \tag{23}$$

We can now write:

$$\frac{(\tau_c)\phi = \phi}{(\tau_c)\phi = 0} = \cos\phi \left(1 - \frac{\tan\phi}{\tan\theta}\right) \tag{24}$$

$(\tau_c)\phi = \phi$ is the critical shear stress for sediment on a bed with a slope angle ϕ and $(\tau_c)\phi = 0$ in the critical shear stress for a bed with very small slope. The value of $(\tau_c)\phi = o$ can be found from the Shields diagram or by other means. Equations (21-24) are for positive ϕ which is positive for downward sloping beds. For beds with adverse slope ϕ is negative and the term $\tan\phi/\tan\theta$ in Eq. (24) is positive.

IV. References

A. Technical Papers

1. Ackers, P. and White, W. R. (1973) - Sediment Transport: New Approach and Analysis, J. Hyd. Div., ASCE, Vol. 99, No. HY11, Nov. 1973, pp. 2041-2060.
2. ASCE (1975) Sedimentation Engineering, Manual on Engineering Practice No. 54, Amer. Soc. of Civ. Engrs.
3. Bagnold, R. A. (1966) An Approach to the Sediment Transport Problem from General Physics, U.S. Geological Survey, Professional Paper 462I.
4. Bray, D. I. (1979) Estimating Average Velocity in Gravel Bed Rivers, J. Hyd. Div. ASCE, Sept. 1979, pp. 1103-1122.
5. Brooks, N. H. (1958) Mechanics of Streams with Movable Beds of Fine Sand, Trans. ASCE, Vol. 123, pp. 526-594.
6. Chang, Feng-Ming, Simons, D. B. and Richardson, E. V. (1967), Total Bed-Material Discharge in Alluvial Channels, Proceedings Twelfth Congress of the International Assoc. for Hydraulic Research, Fort Collins, Colo., Vol. No. 1, pp. 132-140.
7. Colby, B. R. (1957) Relationship of Unmeasured Sediment Discharge to Mean Velocity - Trans. American Geophysical Union, Vol. 38, No. 5, Oct. 1957, pp. 707-717.
8. Colby, B. R. (1964) Practical Computations of Bed Material Discharge, J. Hyd. Div. ASCE, Vol. 90, March 1964, Part 1, pp. 217-246.
9. Colby, B. R. and Hembree, C. H. (1955) U. S. Geological Survey Water-Supply Paper 1357.
10. Colby, B. R. and Scott, C. H. (1965) Effects of Water Temperature on the Discharge of Bed Material, U.S. Geological Survey Professional Paper 462-G.
11. Cook, H. L. (1935) Outline of Energetics of Stream Transportation of Solids - Trans. Amer. Geophysical Union, Vol. II, pp. 456-463.
12. Einstein, H. A. (1950) The Bed Load Function for Sediment Transportation in Open Channels, U.S. Dept. of Agriculture Technical Bulletin No. 1026.

13. Einstein, H. A. and Barbarossa, N. (1952) River Channel Roughness, Trans. ASCE, vol. 117, pp. 1121-1146.

14. Emmett, W. W. (1979) A Field Calibration of the Sediment-Trapping Characteristics of the Helley-Smith Bedload Sampler, U.S. Geological Survey Open-File Report 79-411, Denver, Colo.

15. Guy, H. P., Simons, D. B. and Richardson, E. V. (1966) Summary of Alluvial Channel Data from Flume Experiments 1956-61, U.S. Geological Survey Professional Paper 462-I.

16. Hey, R. D. (1979) Flow Resistance in Gravel-Bed Rivers, J. Hyd. Div. ASCE, Vol. 105, April 1979, pp. 365-379.

17. Knapp, R. T. (1938) Energy Balance in Stream-Flows Carrying Suspended Load, Trans. Amer. Geophysical Union, 19th Annual Meeting, Apr. 27-30, 1938.

18. Lane, E. W., Carlson, E. J. and Hanson, O. S. (1949) Low Temperature Increases Sediment Transportation in Colorado River, Civil Engineering, Vol. 19, No. 9, Sept. 1949, pp. 45-46.

19. Lane, E. W. (1955) Design of Stable Channels, Trans. ASCE, Vol. 120, pp. 1234-1279.

20. Limerinos, J. T. (1970) Determination of the Manning Coefficient from Measured Bed Roughness in Natural Channels, U.S. Geological Survey Water Supply Paper 1898B.

21. Maddock, T. Jr. (1970) Indeterminate Hydraulics of Alluvial Channels, J. Hyd. Div. ASCE, Vol. 96, No. HY11, Nov. 1970, pp. 2309-2323.

22. Shields (1936) Geschiebebewegung der Aenlichkeitsmechanik und der Turbulenzforschung auf die Geshiebewegung (see ASCE, 1975, p. 96).

23. Shen, H. W. and Hung, C. S. (1972) An Engineering Approach to Total Bed-Material Load by Regression Analysis, Sedimentation Symposium to Honor Prof. H. A. Einstein, pp. 14-1 to 14-17, Published By H. W. Shen, Fort Collins, Colo.

24. Stein, R. A. (1965) Laboratory Studies of the Total Load and Apparent Bed Load, J. Geophysical Research, Vol. 70, No. 8, pp. 1831-1842.

25. Taylor, B. D. and Vanoni, V. A. (1972) Temperature Effects in Low-Transport Flat-Bed Flows, J. of Hyd. Div. ASCE, Vol. 98, No. HY8, Aug. 1972, pp. 1427-1445.

26. U.S. Army Corps of Engineers (1969) Missouri River Channel Regime Studies, Omaha District MRD Sediment Series No. 13B, Nov. 1969 (see also ASCE, 1975, pp. 186-187).

27. Vanoni, V. A. (1978) Predicting Sediment Discharge in Alluvial Channels, Water Supply and Management, pp. 399-417, Pergamon Press.

28. Vanoni, V. A. (1974) Factors Determining Bed Forms of Alluvial Streams, J. Hyd. Div. ASCE, Vol. 100, No. HY3, March 1974, pp. 363-377.

29. Yang, C. T. and Stall, J. B. (1976) Applicability of Unit Stream Power Equation, J. Hyd. Div. ASCE, Vol. 98, No. HY10, Oct. 1972, pp. 1805-1826.

30. Nordin, C. F. Jr. (1963) A Preliminary Study of Sediment Transport Parameters Rio Puerco Near Bernardo, New Mexico. U.S. Geological Survey Professional Paper 462-C.

31. Guy, H.P., Simons, D. B. and Richardson, E. V. (1966) Summary of Alluvial Channel Data from Flume Experiments 1956-61, Prof. Paper 462-I, U.S. Geological Survey.

32. Yang, C. T. (1973) Incipient Motion and Sediment Transport, Journal of the Hydraulics Division, ASCE, Vol. 99, No. HY10, Oct. 1973, pp. 1679-1704.

33. Rottner, J. (1959) A Formula for Bed Load Transport. La Houille Blanche, No. 3, pp. 301-307.

34. White, W. R., Milli, H. and Crabbe, A. D. (1973) Sediment Transport: An Appraisal of Available Methods. Vol. 1 Summary of Existing Theories. Vol. 2 Performance of Theoretical Methods When Applied to Flume and Field Data. Report INT 119 Hydraulic Research Station, Wallingsford, England.

B. Text Books and Summaries

Brown, C. B., Chapter XIV Fluid Mechanics for Hydraulic Engineers, Edited by Hunter Rouse, John Wiley & Sons, 1950, pp. 327-350.

Lelliavsky, S., An Introduction to Fluvial Hydraulics, Constable & Co., 1955.

Anderson, A. G., Section 18, Handbook of Fluid Dynamics, Edited by Victor L. Streeter, McGraw-Hill Co., 1961.

Einstein, H. A., River Sedimentation, Section 17-II, Handbook of Applied Hydrology, Edited by V. T. Chow, McGraw-Hill Co., pp. 35-67, 1964.

Blench, T., Mobile Bed Fluviology, T. Blench and Assoc., Ltd., Edmonton, Alberta, Canada, 1966.

Henderson, F. M., Open Channel Flow, Chapter 10, The MacMillan Co., N.Y., 1966.

Raudkivi, A. J., Loose Boundary Hydraulics, Pergamon Press, 1967.

Graf, W. H., Hydraulics of Sediment Transportation, McGraw-Hill, 1970.

Rouse, H., Elementary Mechanics of Fluids, John Wiley and Sons, 1946.

Sedimentation Engineering, Edited by Vito A. Vanoni, ASCE Manuals on Engineering Practice No. 54, 1975, 745 pp.

Garde, R. J. and Ranga Raju, K. G., Mechanics of Sediment Transportation and Alluvial Stream Problems, Wiley Eastern Limited, New Delhi, 1977.

Yalin, M. Selim, Mechanics of Sediment Transport, Pergamon Press, 1972.

Simons, D. B. and Senturk, F., Sediment Transport Technology, Water Resources Publications, Fort Collins, Colorado, 1976.

OVERVIEW OF DESIGN METHODS

FOR ALLUVIAL CHANNELS

by

Howard H. Chang

TABLE OF CONTENTS

Page

1. INTRODUCTION 1
2. ALLUVIAL CHANNELS SUBJECT TO SCOUR BUT NOT SILT 1
   A. Permissible Velocity Method 2
   B. Tractive Force Method 3
3. ALLUVIAL CHANNELS SUBJECT TO BOTH SCOUR AND SILT 4
   A. Alluvial Canals 4
   B. Rivers and Flood Control Channels 11

1. INTRODUCTION

Alluvial channels are designed to provide proper conveyance for the discharge while objectionable scour and deposition need to be avoided. According to the function, alluvial channels may be classified as canals and flood control channels (or rivers). Canals that are used to convey water for irrigation, navigation, etc. are usually designed for a constant discharge. Flood control channels, on the other hand, are for the purpose of carrying a design flood of specified frequency; the discharge varies significantly during the flood. While a canal usually has a steady uniform flow, a flood control channel has an unsteady and varied flow. For this reason, the hydraulics of flow for the latter may not be computed directly from the uniform flow equation such as the Manning's equation.

Two basic types of alluvial channels may be classified; namely, those subject to scour but not deposition and those subject to both scour and deposition. The distinction between them lies in the bed load. When bed-load sediment is not present, the channel is subject to scour but not deposition; therefore, one is concerned with providing proper channel protection so that objectionable scour can be avoided. On the other hand, if bed-load sediment is present, the channel is subject to both scour and deposition; therefore, it needs to be so designed that the dynamic equilibrium of sediment transport and channel stability are maintained. Design methods for these two types of channels are quite different, as described below separately:

2. ALLUVIAL CHANNELS SUBJECT TO SCOUR BUT NOT SILT

When water is drawn from a storage reservoir, it is normally

free of bed-load sediment, and the basic criterion in designing a stable channel is to prevent scour of the material from the channel boundary. Based upon the scour criterion, two different design methods are generally used, namely, the permissible velocity method and the tractive force method. Maximum permissible velocities and corresponding values of the tractive force for different channel materials are given in Table 1; permissible velocities for channels lined with grass are given in Table 2. Similar criteria can be found in different design manuals.

A. Permissible Velocity Method

Under the permissible velocity method, an alluvial channel is so designed that the cross-sectionally averaged velocity does not exceed the permissible velocity. Since this method does not consider the bank's configuration, it must be selected separately with consideration given to bank stability. This method, however, proves to be useful for flood-control channels with gradually varied flow for which the water-surface profile and velocity can be computed using a fixed-bed computer model such as the HEC-2 model. The peak discharge should be used in channel design. The final channel configuration can be obtained using a trial-and-error procedure through repeated adjustments starting from an initial configuration. For each selected channel configuration, the water-surface profile and velocity are obtained using the computer program. The configuration is adjusted repeatedly until the computed water-surface profile and velocity satisfy the design requirements. To stay within the permissible velocity, the channel slope may need to be reduced. In such a case, drop structures are usually used.

Examples of channel design using this approach include the Mission Valley Flood Control Channel in the City of San Diego (see Figure 1) and the Salt River Flood Control Channel at Scottsdale, Arizona. In both cases, bed-load sediment is not a major factor, and grass lining is used to maintain channel stability. The Mission Valley Flood Control Channel is designed to carry the 100-year flood at the maximum velocity of 6 to 7 feet per second. The natural channel slope is reduced by three drop structures which also serve as road crossings for the river. The final configuration of the channel with the drop structures was obtained by repeated trials. For each trial configuration, the water-surface profile and the velocity at each cross section were computed using the HEC-2 program. The computed results for each configuration also provided the needed adjustments for that configuration. The final configuration so obtained satisfies the requirements for flood control and channel stability.

B. Tractive Force Method

Tractive force exerted on the channel boundary is a drag force acting in the direction of flow. For a wide channel, the unit tractive force is expressed as

$$\tau = \gamma DS \tag{1}$$

in which τ = tractive force in lbs/ft^2; γ = specific weight of water; D = flow depth; and S = slope or energy gradient. For trapezoidal channels with different width-depth ratios, the unit tractive force is shown in Figure 2.

The permissible tractive force is related to the channel material as shown in Table 1. For canals in noncohesive materials, the permissible unit tractive force may be obtained from Figure 3. Similar relationships are provided by different design manuals. Materials on channel banks are also under the action of gravitation in addition to the tractive force exerted by the flowing water; the permissible tractive force is multiplied by a factor K (K < 1) defined as

$$K = \cos\theta \left(1 - \frac{\tan^2\theta}{\tan^2\phi} \right)^{\frac{1}{2}} \qquad (2)$$

in which θ = angle of the bank slope and ϕ = angle of repose of the bank material. For sinuous channels, the permissible tractive force needs to be reduced; a recommended reduction to allow for channel sinuosity is given in Table 3.

The tractive force method is usually used for channels of a uniform flow; it is also applied to determine the size of riprap for bank protection. In either case, the tractive force needs to be computed first, then this tractive force is compared with the permissible tractive force. Channel configuration and channel materials are usually obtained in such a way that the tractive force stays within the permissible tractive force. While the channel slope is usually designed to follow the natural terrain, it may also be reduced by using drop structures.

3. ALLUVIAL CHANNELS SUBJECT TO BOTH SCOUR AND DEPOSITION

A. Alluvial Canals

Alluvial channels carrying a certain amount of bed load are

subject to both scour and deposition. A stable alluvial channel maintains the equilibrium not only in sediment transport but also in its geometry. For an unlined canal, the channel geometry has three degrees of freedom in its width, depth, and slope. In addition, the bank slope needs to be selected in consideration of the bank material. Field experience from stable alluvial canals shows that the straight alignment of such canals can be maintained within a certain range. The stability of the straight alignment is described in a separate chapter.

Traditional methods used in the design of stable alluvial canals are based upon the regime concept. A channel in regime is defined as having zero net erosion and deposition over an operating cycle. Previous regime methods have been developed using the empirical approach; that is, regime relationships for the channel width, depth, and slope are based upon measurement from existing stable irrigation canals. Examples are those developed by Lacey, Inglis, Blench, Simons, etc. Each method usually consists of three formulas for the width, depth, and slope.

Lacey's Regime Method - The regime method by Lacey may be summarized by three equations. First, the resistance to flow equation

$$V = 16\ R^{2/3}\ S^{1/3} \tag{3}$$

in which V = mean velocity in feet per second; R = hydraulic radius; and S = channel slope. This equation is similar to the Manning's equation in form; the difference between them suggests that alluvial bed roughness (or bed form) is related to the flow condition. The

second equation by Lacey has the form

$$P = 2.67 \sqrt{Q} \tag{4}$$

in which P = wetted perimeter and Q = bankfull discharge. This equation may be interpreted as the relation for the regime width of canals, since the wetted perimeter of a canal is directly proportional to the width. It is interesting to point out that, based upon this relationship, the channel width is essentially a function of the discharge alone. This relation is in sharp contrast to certain rivers for which the width is strongly dependent upon the slope in addition to the discharge. Explanations are given in the chapter on the analysis of alluvial streams.

The third equation by Lacey is for the channel slope, i.e.

$$S = \frac{f^{5/3}}{1750\ Q^{1/6}} \tag{5}$$

in which f = silt factor = $\sqrt{d}$; and d = sediment size in inches. For the given bankfull discharge and sediment size, the three independent equations by Lacey provide the required stable channel width, depth, and slope. No specific relation is given for the bank slope of the channel.

<u>Blench's Regime Method</u> - Since the appearance of Lacey's method, much more development work has been done, particularly by Blench. His regime method consists of three independent conditions, i.e. the bed factor, the side factor, and the slope equation as given below:

$$F_b = \frac{V^2}{D} \tag{6}$$

$$F_s = \frac{V^3}{B} \tag{7}$$

and

$$\frac{V^2}{gDS} = 3.63\ (1 + aC)\ \left(\frac{VB}{\nu}\right)^{\frac{1}{4}} \tag{8}$$

in which F_b = bed factor; D = depth of flow; F_s = side factor; B = average width; a = an empirical coefficient having the value of 1/233; C = bed load concentration in parts per 100,000 by weight; ν = kinematic viscosity.

Empirical value for the bed factor and side factor as provided by Blench are

$$F_b = 1.9\ \sqrt{d}\ (1 + 0.12\ C) \tag{9}$$

$$\begin{aligned} F_s &= 0.1 \text{ for slightly cohesive banks} \\ &= 0.2 \text{ for medium cohesive banks} \\ &= 0.3 \text{ for highly cohesive banks} \end{aligned} \tag{10}$$

in which d = median sediment size in mm. Now, the three independent conditions represented by Equations 6, 7, and 8 can be solved to obtain the channel width, depth, and slope, and one has

$$B = \left(\frac{F_b Q}{F_s}\right)^{1/2} \tag{11}$$

$$D = \left(\frac{F_s Q}{F_b^{\,2}}\right)^{1/3} \tag{12}$$

and

$$S = \frac{F_b^{\,5/6}\ F_s^{\,1/12}\ \nu^{1/4}}{3.63\ (1 + aC)\ gQ^{1/6}} \tag{13}$$

These three equations provide the dimensions of a stable canal under given conditions of the design discharge, sediment concentration, sediment size, and bank cohesiveness. By introducing the side factor, this method accounts for the effect of bank cohesiveness on the channel geometry. Based upon this method, the stable channel width decreases, while the depth increases with an increase in bank cohesiveness. Physically, cohesiveness of the bank material has the effect on the bank slope in that steeper bank slopes usually develop in the form of a berm in cohesive materials.

Simons and Albertson's Regime Method - The design method by Blench is limited to canals with a sand bed and cohesive banks. The method developed by Simons and Albertson has extended this scope to canals of different characteristics. Based upon a large collection of data, they classified canals into the following five types: (1) sand bed and banks, (2) sand bed and cohesive banks, (3) cohesive bed and banks, (4) coarse noncohesive material, and (5) same as (2) but with heavy sediment loads, 2,000-8,000 ppm. Regime equations by Simons and Albertson may be classified into three groups. The first group of equations is for the stable width; these equations are

$$P = K_1 \, Q^{\frac{1}{2}} \tag{14}$$

$$B = 0.9 \, P \tag{15}$$

and

$$B = 0.92 \, T - 2.0 \tag{16}$$

in which K_1 = a coefficient related to the canal type and T = surface width. The second group of equations provides the channel depth; they are

$$R = K_2 \, Q^{0.36} \tag{17}$$

$$D = 1.21 \, R \qquad \text{for } R \leqq 7 \text{ feet} \tag{18}$$

and

$$D = 2 + 0.93 \, R \qquad \text{for } R > 7 \text{ feet} \tag{19}$$

in which K_2 = a coefficient. The third group of equations is for the channel slope; these are

$$V = K_3 \, (R^2 \, S)^m \tag{20}$$

and

$$\frac{V^2}{gDS} = K_4 \left(\frac{VB}{\nu}\right)^{0.37} \tag{21}$$

in which m = an exponent and K_3, K_4 = coefficients. Coefficients and exponents for these equations are tabulated below.

	CHANNEL TYPE				
Coefficient	1	2	3	4	5
K_1	3.5	2.6	2.2	1.75	1.7
K_2	0.52	0.44	0.37	0.23	0.34
K_3	13.9	16.0	---	17.9	16.0
K_4	0.33	0.54	0.87	---	---
m	0.33	0.33	---	0.29	0.29

This method reflects the effects of bed and bank material on the stable channel geometry in addition to the discharge. For the same materials, the width and depth are in direct proportion to the discharge, and they are essentially independent of the slope. For the same discharge, canals with cohesive banks are smaller in width, deeper in depth, and flatter in slope than those with noncohesive banks. This comparison is attributed to the fact that cohesive banks are generally steeper than noncohesive ones.

A rational method for stable alluvial canal design has recently been developed by Chang. This method and design charts pertaining to sand-bed canals and gravel canals are described in a separate chapter. The rational method provides the stable channel geometry and conditions for which the straight alignment can be maintained.

B. Rivers and Flood Control Channels

Natural rivers and flood control channels are usually subject to both scour and silt. The fundamental difference between these channels and canals is that the discharge is not controlled in natural rivers. For this reason, a hydrograph is used as the basis of channel design or channel improvement. Since flood flow in a river is classified as gradually varied unsteady flow, the evaluation of such flow in an erodible channel must consider the hydraulics of flood and sediment routing and associated river-channel changes.

An alluvial river is the author of its own geometry; therefore, it will respond to any design scheme for river control or regulation through self-adjustments, i.e., river channel changes. The evaluation of the flood level and other impacts resulting from any design project requires a model for erodible channels. Two types of model are used to evaluate the channel-related project, namely the physical model and the mathematical model. Detailed descriptions of a mathematical model and its applications are given in a separate chapter.

TABLE 1

MAXIMUM PERMISSIBLE VELOCITIES RECOMMENDED BY FORTIER AND SCOBEY AND THE CORRESPONDING UNIT-TRACTIVE-FORCE VALUES CONVERTED BY THE U.S. BUREAU OF RECLAMATION. (For straight channels of small slope, after aging)

Material	n	Clear Water		Water transporting colloidal silts	
		V fps	τ_o lb/ft^2	V fps	τ_o lb/ft^2
Fine sand, colloidal	0.020	1.50	0.027	2.50	0.075
Sandy Loam, noncolloidal	0.020	1.75	0.037	2.50	0.075
Silt loam, noncolloidal	0.020	2.00	0.048	3.00	0.11
Alluvial silts, noncolloidal	0.020	2.00	0.048	3.50	0.15
Ordinary firm loam	0.020	2.50	0.075	3.50	0.15
Volcanic ash	0.020	2.50	0.075	3.50	0.15
Stiff clay, very colloidal	0.025	3.75	0.26	5.00	0.46
Alluvial silts, colloidal	0.025	3.75	0.26	5.00	0.46
Shales and hardpans	0.025	6.00	0.67	6.00	0.67
Fine gravel	0.020	2.50	0.075	5.00	0.32
Graded loam to cobbles when noncolloidal	0.030	3.75	0.38	5.00	0.66
Graded silts to cobbles when colloidal	0.030	4.00	0.43	5.50	0.80
Coarse gravel, noncolloidal	0.025	4.00	0.30	6.00	0.67
Cobbles and shingles	0.035	5.00	0.91	5.50	1.10

TABLE 2

PERMISSIBLE VELOCITIES FOR CHANNELS LINED WITH GRASS

	Slope range, %	Permissible velocity, fps	
		Erosion-resistant soils	Easily eroded soils
Bermuda grass	0-5	8	6
	5-10	7	5
	>10	6	4
Buffalo grass, Kentucky bluegrass, smooth brome, blue grama	0-5	7	5
	5-10	6	4
	>10	5	3
Grass mixture	0-5	5	4
	5-10	4	3
	Do not use on slopes steeper than 10%		
Lespedeza sericea, weeping love grass, ischaemum (yellow bluestem) kudzu, alfalfa, crabgrass	0-5	3.5	2.5
	Do not use on slopes steeper than 5%, except for side slopes in a combination channel		
Annuals--used on mild slopes or as temporary protection until permanent covers are established, common lespedeza, Sudan grass	0-5	3.5	2.5
	Use on slopes steeper than 5% is not recommended		

TABLE 3

INFLUENCE OF BENDS ON PERMISSIBLE TRACTIVE FORCE

Degree of sinuosity	Relative limiting tractive force
Straight canals	1.00
Slightly sinuous canals	0.90
Moderately sinuous canals	0.75
Very sinuous canals	0.66

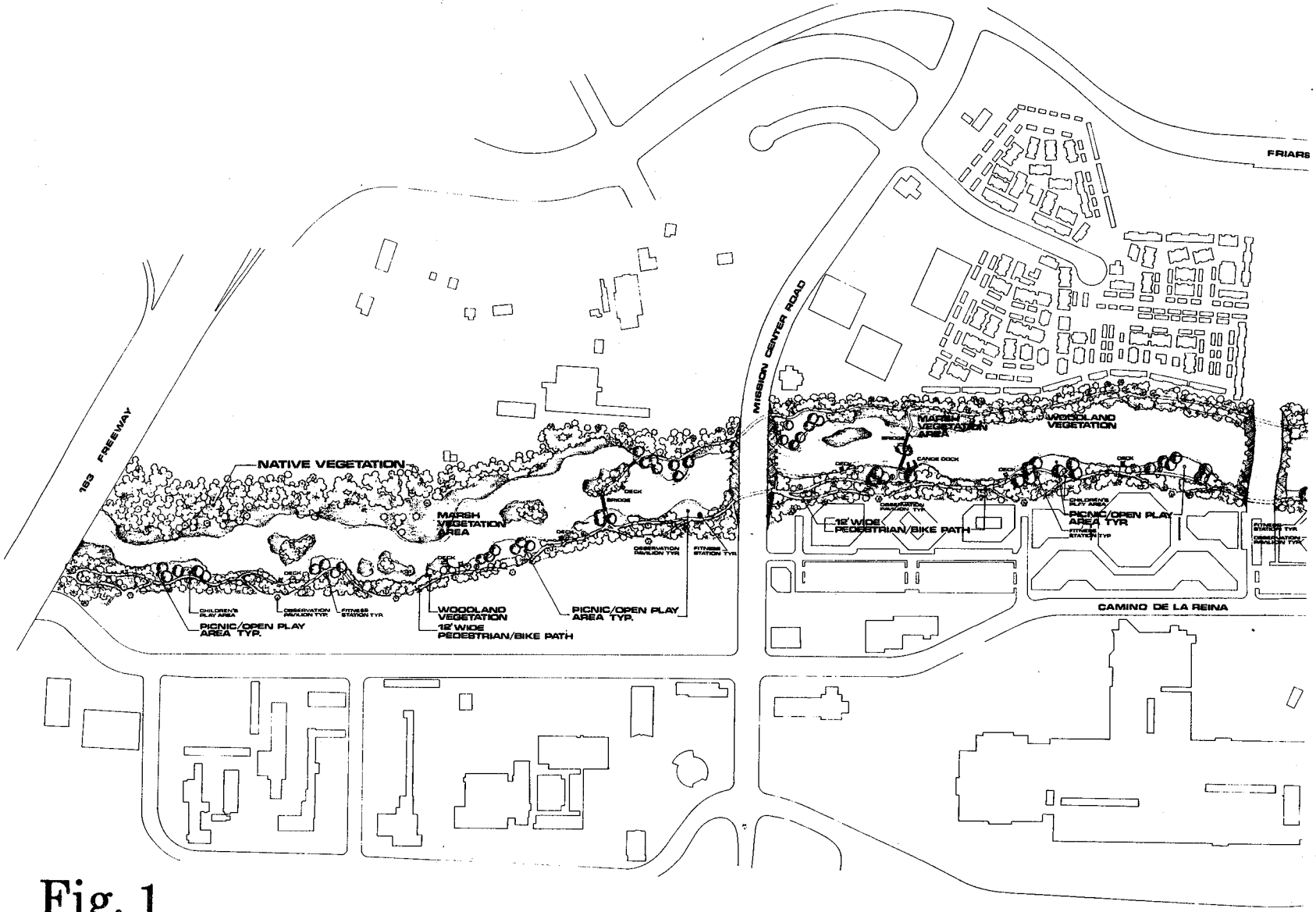

Fig. 1

LANDSCAPE DEVELOPMENT PLAN
SAN DIEGO RIVER FLOODWAY PROJECT

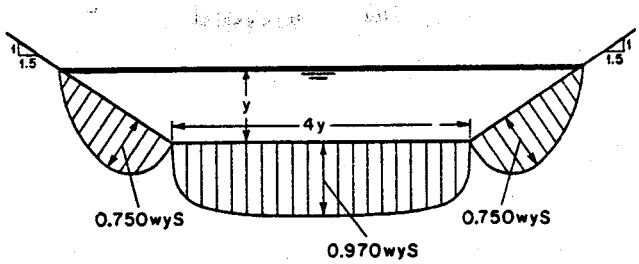

FIG. 7-6. Distribution of tractive force in a trapezoidal channel section.

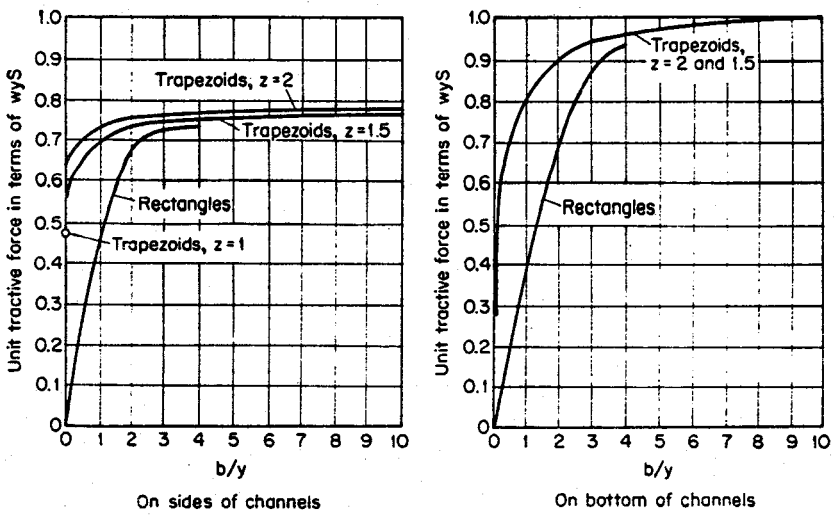

FIG. 2. Maximum unit tractive forces in terms of *wyS*.

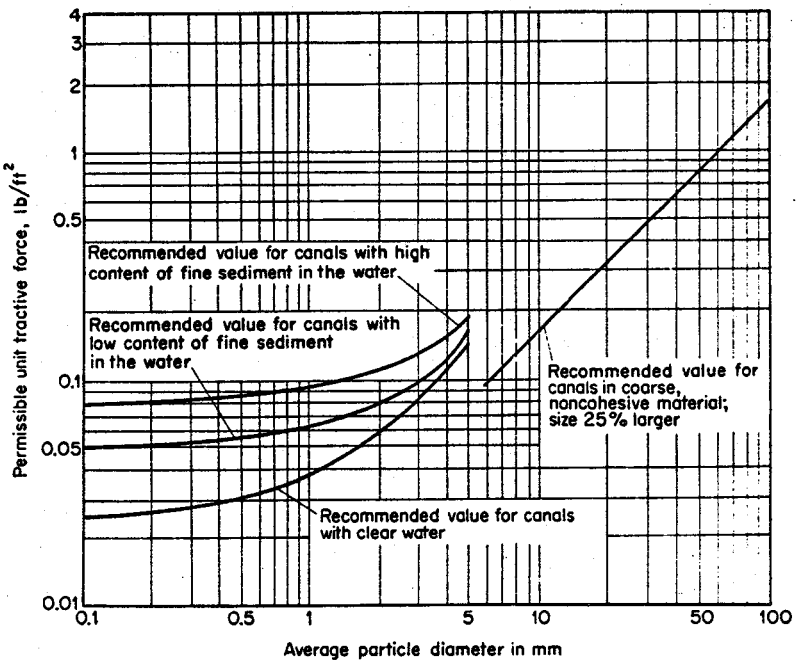

FIG. 3. Recommended permissible unit tractive forces for canals in noncohesive material. (*U.S. Bureau of Reclamation.*)

STABLE ALLUVIAL CANAL DESIGN

By Howard H. Chang[1], M.ASCE

INTRODUCTION

Steady uniform flow in an open channel with a movable boundary (alluvial channel) can only be described with a set of three independent equations. For any given water discharge and sediment discharge conveyed through an alluvial channel, the flow will establish its width, depth, and slope over a period of time. For the design of canals, regime formulas have been developed by many investigators, notably by Lacey, Inglis, Blench, Simons, etc. Most regime formulas consist of three independent equations to solve for the three degrees of freedom in channel width, depth and slope. For a channel in regime, the water discharge, sediment discharge, channel geometry and slope are in equilibrium. The regime researchers obtained data from regime channels, relating the variables considered pertinent in various combinations and thereby to discover what relations hold among the hydraulic and sediment parameters obtained in these channels.

Among the independent relations for alluvial channels, the flow resistance formula and sediment transport formula have been studied by many investigators. Assuming that formulas for flow resistance and sediment transport may be selected for application under appropriate conditions, only one additional condition will be needed to describe an alluvial channel.

In searching for this third condition, the equilibrium state of alluvial channels will be considered. The regime channel described above

---

1. Professor and Chairman, Civil Engineering Dept., San Diego State University, San Diego, CA.

as well as graded streams (11) studied by geologists are alluvial channels in equilibrium. In this paper, the equilibrium condition will be related to the condition of minimum stream power for an alluvial channel and thereby applied to obtain the equilibrium configuration. Some canal data are used for experimental substantiation.

In a previous study, Chang and Hill (2) applied these three conditions to compute the variation of the stream geometry on a delta. The delta stream, being more or less unconstrained in its width and depth, may be concentrated or braided in flow pattern depending on the width-depth ratio of the cross-section. Using these three conditions for the delta stream in dynamic equilibrium, the width, depth, and slope were computed and compared favorably with measured data.

MINIMUM STREAM POWER

Stream power represents the energy consumption per unit time of the stream flow. For a unit channel length, the stream power is given by γQS, where γ = specific weight of flow; Q = flow discharge; and S = slope or energy gradient. Before describing minimum stream power as it applies to alluvial channels, one may recall the minimum energy principle in thermodynamics (1) and the principle of least work in solid mechanics (10). Similarities among them may be observed.

The hypothesis of minimum stream power for a hydraulic system may be derived from the principle of virtual work for a mechanical system. The principle of virtual work as defined by Langhaar (10) is given as follows:

> For an unchecked mechanical system, the necessary and sufficient condition for equilibrium is
>
> $\delta W \equiv 0$
>
> provided that δW exists. (1)

In this statement, δW is the virtual work done by the forces (external and internal) that act on the system caused by a virtual displacement consistent with the constraints. The sign $\equiv$ signifies that the equality holds for all admissible virtual displacements. A system is said to be unchecked if the forces change continuously when a virtual displacement is executed.

This principle may be generalized immediately to apply to systems that translate at constant velocity, since uniform translation such as channel flow in a moving frame is equivalent to a static system. It may also be applied to a fixed control volume in a flow field as long as the mass inside remains constant. Also, the work or energy may be replaced by power when the rate of energy is of interest. Now, consider a control volume of steady uniform flow in a channel with a unit length. With the introduction of a virtual displacement per unit time (virtual velocity) to the control volume, the change in forces is continuous for every admissible path subject to the constraints. Therefore, under the equilibrium condition, the virtual stream power δp caused by a virtual velocity must satisfy the condition

$$\delta p \equiv 0 \tag{2}$$

which represents an extremum. Since a maximum has no meaning, therefore, it represents a minimum. The hypothesis of minimum stream power for an alluvial channel is given as follows:

> For an alluvial channel, the necessary and sufficient condition for equilibrium is when the stream power is a minimum subject to given constraints. Hence, an alluvial channel with given water discharge and sediment inflow tends to establish its width, depth and slope such that the stream power or slope is a minimum.

It should be pointed out that this definition is different from the hypothesis of minimum unit stream power proposed by Yang (19, 20) in that he uses the unit stream power VS instead of QS. The difference is the cross-sectional area of flow A which is a variable; therefore, minimizing QS will not give the same result as minimizing VS.

According to the above definition for minimum stream power, a stable alluvial channel has the cross-sectional shape for best hydraulic efficiency subject to the constraints. Therefore, as the sediment load approaches zero for a stable alluvial channel, its cross-section should approach the best hydraulic section for rigid boundary channels as demonstrated later in the paper.

BASIC RELATIONS FOR ALLUVIAL CHANNELS

In the long term field situation for stable alluvial channels, the water discharge Q and sediment discharge Q_s are independent variables while slope, depth, and width are the three dependent variables as pointed out by Mackin (11), Kennedy and Brooks (7), Maddock (12), and others. This means that an alluvial channel will establish its velocity, slope and channel geometry subject to the Q and Q_s provided. For a given set of Q and Q_s, the three dependent variables may be determined using the three conditions of a flow resistance formula, a sediment discharge formula and the minimum condition of γQS or S. Before describing the procedures for computation, the flow resistance and sediment discharge formulas are described below separately:

Flow Resistance Formula

This formula provides the stage-discharge relationship in a channel when the resistance coefficient is known. A simple flow resistance

formula is the Manning formula

$$V = \frac{1.486}{n} R^{2/3} S^{1/2} \tag{3}$$

where V = mean velocity; n = resistance coefficient or the Manning coefficient; and R = hydraulic radius. While this equation is widely used in rigid boundary channels, its accuracy for alluvial channels is limited since the roughness coefficient also depends on the bed form and other variables. According to Chow (3), the value of n in clean straight earth channels is in the range of 0.016 to 0.025 for sand bed and in the range of 0.022 to 0.030 for gravel bed.

Among the regime formulas, perhaps the most widely acknowledged and well known are those developed by Lacey (8). The flow resistance formulas by Lacey have the form

$$V = \frac{1.346}{N_a} D^{1/4} R^{1/2} S^{1/2} \tag{4}$$

in which, N_a = absolute rugosity; D = mean bed depth; and

$$N_a = 0.0225 f^{1/4} \tag{5}$$

$$f = 1.6\sqrt{d} \tag{6}$$

where f = Lacey's silt factor; and d = median bed material size in mm. According to Lacey, this equation is applicable within the ranges of bed material size between 0.15 to 0.40mm and discharge between 5 to 5000 cfs in an alluvial channel with non-cohesive bed material. In addition, the bed load has to be small and the bed form had to be in the lower flow regime of ripples and small dunes but not in the upper regime of waves. Under the ranges specified above, this equation is applicable to most of the regime canals.

Engelund and Hansen (4) expressed the total roughness in terms of the grain roughness and bedform roughness; the following relation was obtained:

$$\Theta = \Theta' + \Theta'' \tag{7}$$

In which, Θ, Θ' and Θ'' = dimensionless total shear stress, shear stress due to grain roughness, and shear stress due to bedform roughness. Among them, Θ and Θ' are defined as follows:

$$\Theta = \frac{\gamma DS}{(\gamma_s - \gamma)d} \tag{8}$$

$$\Theta' = \frac{\gamma D'S}{(\gamma_s - \gamma)d} \tag{9}$$

In which, γ_s = specific weight of sediment grains; D = flow depth; D' = depth of flow due to grain roughness, and d = size of particle. Using the flume data reported by Guy, Simons, and Richardson (6), Engelund and Hansen obtained the following relationship for lower regime flow with a dune bed.

$$\Theta' = 0.06 + 0.4\,\Theta^2 \tag{10}$$

For upper regime flow with standing waves and flat bed, the relationship is

$$\Theta = \Theta' \tag{11}$$

They also suggested the following logarithmic resistance formula for D'

$$\frac{V}{\sqrt{gD'S}} = 6 + 2.5\,ln\,\frac{D'}{2.5d} \tag{12}$$

In which, g = acceleration of gravity.

Other resistance to flow formulas for alluvial channels consider additional hydraulic and sediment variables, such as the relationships developed by Einstein, Shen, Simons, Senturk, etc. An excellent summary and comparison of these relationships are given in Reference 16. These formulas are applicable to more general cases of flow in alluvial channels not restricted by those of the regime formulas. However, these

formulas require the gradation of the bed material as a part of the input in addition to the median sediment size.

Sediment Discharge Formula

Numerous formulas are available for predicting the sediment load in an alluvial channel. To account for the shear stress distribution in a canal as described later, the type of formulas selected for this application is stated in terms of the shear stress. Specifically, the Duboys formula (16, 18), the Einstein-Brown formula (16, 18), and the Engelund-Hansen formula (4) were used because the canal data used herein contain the required information for these formulas. Among them, the first two are for the bedload while the third one is for the bed material load.

The DuBoys formula has the form:

$$q_s = \frac{0.173}{d^{3/4}} \tau_o [\tau_o - \tau_c] \tag{13}$$

where q_s = sediment load per unit width and time in cfs per foot; τ_o = shear stress in psf; and τ_c = critical shear stress = 0.0125 + 0.019d.

The Einstein-Brown formula has the form

$$0.465\Phi = e^{-0.391\Psi} \qquad \Psi > 5.5 \tag{14}$$

$$\Phi = C \left(\frac{1}{\Psi}\right)^3 \qquad \Psi \leq 5.5 \tag{15}$$

in which

$$\Phi = \frac{q_s}{\gamma_s F \sqrt{g \frac{\gamma_s}{\gamma} - 1 \; d^3}} \tag{16}$$

$$\Psi = \frac{\left(\gamma_s - \gamma\right) d}{\tau_o} \tag{17}$$

$$F = \sqrt{\frac{2}{3} + \frac{36\nu^2}{gd^3\left(\frac{\gamma_s}{\gamma} - 1\right)}} - \sqrt{\frac{36\nu^2}{gd^3\left(\frac{\gamma_s}{\gamma} - 1\right)}} \tag{18}$$

and C = a numerical constant having a mean value of 40; γ_s = specific weight of sediment in lbs/ft^3; ν = kinematic viscosity of water in ft^2/sec; and g = gravitational acceleration in ft/sec^2.

In an effort to rationalize Lacey's regime flow equations, Gill (5) developed a flow equation from the Einstein-Brown formula which verifies the exponential form of all the Lacey's equation, excepting the width equation which was not examined. Using the Gilbert's and Simons-Richardson data, Gill observed a departure of the Einstein-Brown formula from the data in the zone of low shear stress when τ_o and τ_c are of the same order of magnitude. To correct the departure, he suggested the following modification

$$\Phi = C\left(\frac{\tau_o}{\tau_c} - 1\right)^3 \tag{19}$$

At high values of shear stress, this equation reduces to the Einstein-Brown formula. At low shear stress, this equation bears resemblance to the DuBoys formula which was calibrated mainly using the Gilbert data. In the threshold condition of bed movement, the term $\tau_o - \tau_c$ in DuBoys formula and the $\tau_o/\tau_c - 1$ term in the above Gill formula become significant. As pointed out by Gill, this may explain why regime equations apply only to those channels which are actively mobile but not in the low shear stress region.

The Engelund-Hansen formula is

$$q_s = 0.05\gamma_s V^2 \sqrt{\frac{d}{g\left(\frac{\gamma_s}{\gamma} - 1\right)}} \left[\frac{\tau_o}{(\gamma_s - \gamma)d}\right]^{3/2} \tag{20}$$

where V = mean velocity in fps.

These formulas will be applied, one at a time, to compute the geometry of the stable canals. For the computing procedures described later, only the functional relationships represented by the formulas are used in determining the canal geometry.

The above sediment formulas predict the sediment discharge per unit width; the total amount of sediment discharge in a channel may be obtained by integration. For a canal, the transport of bed material is limited essentially to the bed and therefore

$$Q_s = \int_b q_s db \tag{21}$$

where Q_s = sediment discharge of the canal in lbs/sec; b = bed width of canal in feet. Since the unit sediment discharge q_s is related to the shear stress τ_o in the above sediment discharge formulas, therefore, in computing Q_s, one needs to consider the shear stress distribution. In a wide canal, τ_o is given by γDS, where D is the mean bed depth. In a trapezoidal section, the shear stress distribution declines toward the banks depending upon the bank slope z and width-depth ratio b/D (9), as shown in Fig. 1. Numerical integration will be employed to evaluate the integral in Eq. 21 for each shear stress distribution.

THE COMPUTER PROGRAM AND SAMPLE RESULTS

The computer program FLUVIAL-7 has been developed to predict the geometry of stable alluvial channels. For the given parameters of water dis-

charge, sediment load, bank slope, bed material and temperature, it computes the width, depth and slope of the channel by solving the three simultaneous equations. The results obtained satisfy the flow resistance formula, the sediment discharge formula and the minimum stream power condition.

The flow diagram showing major steps of the computation for the program is given in Fig. 2, in which nested iterations are employed to search for the unknowns since they are implicit variables. These iteration loops are described below separately:

1. The first iteration -- with the given values of Q, Q_s, d, z, ν, this iteration is used to search for the channel with B at which the slope is a minumum. The computation is carried to an accuracy of 1.5% of the width.
2. The second iteration --for each value of B within the first iteration, the second iteration is employed to solve for the values of D and S such that Q is equal to the given value. A trial-and-error procedure, based upon the IBM Scientific Subroutine RTMI (17), is used for this purpose. At each value of D, the value of S is computed based upon the sediment transport formula and then the value of Q is computed using the flow resistance formula. In the trial-and-error solution, the computation is carried to an accuracy of 0.001 foot for D.

To demonstrate the variations of stream power and other flow parameters with the channel configuration some sample calculations are shown in Fig. 3. In which, S, γQS, D, B/D, n and Froude number are shown as functions of the channel width B for the specified input of Q, Q_s, d, and z. The value of S has its minimum of 0.00095 at the width of 72 feet and the depth of 7.6 feet; these values are taken as the solutions of the stable canal for the specified input parameters.

Field experience from the India-Pakistan Canals has demonstrated that the stability of canals may be maintained if they are in the lower flow regime and that meandering and bank erosion often develop as upper regime flow is reached. Canal designers often use the Froude number as a criterion for the flow regime; its value is usually kept at about 0.2 and never above 0.3 in the canals. The graphical relation representing the upper limit for lower regime flow developed by Athaullah and Simons as described in References 16 may be approximated by the equation

$$Fr = 4.388 \left(\frac{R}{d}\right)^{-0.31} \tag{22}$$

where R = hydraulic radius. This relation is employed herein as the upper limit for canal analysis.

DESIGN CHART FOR STABLE ALLUVIAL CANALS

A design chart for stable alluvial canals has been constructed as shown in fig. 4, using the computer program developed herein. While this chart is for the sediment size of 0.3 mm and the 2 to 1 side slope, similar charts may also be obtained for other combinations of sediment size and side slope. The variations of velocity and sediment discharge are shown in Fig. 5. With a given set of Q, S, d, z, the values of B, B/D, V, and Q_s may be obtained directly from the appropriate design charts. The region of analytical prediction as shown in the figure has its lower limit at the threshold for sediment motion, and its upper limit specified by Equation 22 above which canals are known to have meandering tendency as described previously.

Since the design chart was constructed based upon the condition of minimum stream power, the channel configuration as shown represents that of best hydraulic efficiency for the water and sediment discharges imposed. Therefore, as the sediment discharge approaches zero, the canal configuration must approach that of the best hydraulic section for rigid channels. For the 2 to 1 side slope, the best hydraulic section has the width-depth ratio of 2.47.

Except in the region of low shear stress for incipient sediment motion, the analytical relationships represented by the design chart generally agree with other regime formulas. As stated previously, most regime formulas fail in the flow region of low shear stress.

The flow resistance and sediment discharge formulas as desribed previously were used in producing different design charts each of them was then compared with the canal data to determine the accuracy. Based upon the three sets of canal data which will be described later in the paper, the flow resistance formula by Engelund and Hansen was found to be slightly more accurate than the Lacey formula and it was therefore adopted for application. The applicability of each sediment discharge formula was also investigated. Except in the flow region of low shear stress, analytical results obtained based upon the Engelund-Hansen formula are somewhat better than the Einstein-Brown formula and the DuBoys formula. For the reasons given by Gill, the Einstein-Brown formula is inadequate in the low shear stress region. This fact is verified as it does not produce the best hydraulic section as the sediment discharge approaches zero. Similarly, the sediment discharge formula by Engelund and Hansen is also found inadequate in the low shear stress region. That is not surprising because this formula, developed

based upon the similarity principle, is not supposed to be used in the low shear stress region of plane bed.

The Gill and DuBoys sediment formulas have been found to generate reasonable results in the low shear stress region. Since the DuBoys formula is applicable in the entire flow region under consideration, it was therefore used in constructing the design chart.

Analytical predictions of stable canal configuration in relation to the sediment size and side slope and shown in Figs. 6 and 7 respectively. For a constant discharge and side slope, the channel width and width-depth ratio are shown to vary inverse proportionally to the sediment size. That is, stable canals of finer materials are wider and shallower than those of coarser materials when other conditions are equal. For a constant discharge and sediment size, the channel width and width-depth ratio are shown to vary proportionally to the side slope; they are also quite sensitive to the changes in side slope, especially at steeper slopes. That is, a wider and shallower section is associated with a flatter side slope when other conditions are equal. While the finer sediment size produces a wider and shallower canal section, canals with fine materials often have steeper side slopes due to higher concentration of cohesive material which affect the canal slope in the opposite direction.

COMPARISON WITH CANAL DATA

To verify the analytical method developed herein, four sets of regime canal data are used for comparison with the analytical prediction. The canal data include both field data and laboratory data. Here, the field data (14) include the Simons and Bender data, the Punjab Canal data, and

the Sind Canal data; the laboratory data are those reported by Ranga Raju, et al. in a recent publication (13). A summary of the canal data pertaining to their respective ranges in discharge, slope, depth, average width, bank slope and sediment size are shown in Table 1. Typical of the regime canals, most of the field data are for canals with a low Froude number, a small sediment discharge, and a bed form in the lower regime of plain bed, ripples or small dunes.

The Punjab Canal data are plotted directly on the design chart as shown in Fig. 5 for comparison with the analytical prediction. Other field data are not plotted because they cover greater ranges of sediment size and side slope; that is especially true for the Simons and Bender data.

As shown in the sample design chart in Fig. 5, the analytical width and width-depth ratio may be obtained for a given set of water discharge and slope. In the following comparisons, the given discharge and channel slope for each canal are used to obtain the analytical channel width and width-depth ratio which are then compared with the measured values. However, the sediment discharge is required as an input parameter and the slope is an output parameter using the computing procedures shown in Fig. 2. Since the sediment discharge is an unknown, it is determined by trial-and-error such that the minimum slope it produces equals the given slope.

To facilitate the computation, canal cross sections are approximated as trapezoids, some examples are shown in Fig. 8. The trapezoidal section is selected so that it has the same A, B, D, and P (wetted perimeter) as the original canal. The bank slope of the trapezoid may be obtained from the given B, D, and P values according to the following calculation. Referring to the figure, one has the geometric relationships

$$P = b + 2\sqrt{1 + z^2}\, D \tag{23}$$

and $$z = \frac{B - b}{D} \tag{24}$$

Solving for z from the above two equations, one obtains

$$z = \frac{k + 2\sqrt{k^2 - 3}}{3} \tag{25}$$

where $k = (P - B)/D$ which is obtainable from the data. The bank slope represented by z is required as an input parameter in the computer program. The Simons and Bender data contains the cross-sectional profile of all canals from which more accurate bank slope may sometimes be obtained, see Fig. 8.

In their study of stable canals, Simons and Albertson (15) distinguished five types of canals, namely, canals with sand bed and banks; canals with sand bed and cohesive banks; canals with cohesive bed and banks; canals with coarse non-cohesive material; and canals with sand bed and cohesive banks with heavy sediment loads (2,000 $\sim$ 8,000 ppm). Different bank materials are associated with different bank slopes and therefore, the bank slope is used herein as an indication of the bank material.

Each of the sediment discharge formulas described previously was used in the computer program and the results generated were compared with the canal data. Except in the zone of low shear stress, the Engelund-Hansen formula produced results somewhat better than the Einstein-Brown and the DuBoys formula and it was therefore selected for application. For the reasons given previously, the DuBoys and the Gill formulas in Eq. 19 are more accurate in the region of low shear when τ_o and τ_c are of the

same order of magnitude. The DuBoys equation was used in this region since it produced slightly better results.

For the Punjab Canal data and the Sind Canal data, the comparison between computed and measured widths is shown in Fig. 9, and that between computed and measured width-depth ratios is shown in Fig. 10. The comparisons for the Simons and Bender data are shown in Figs. 11 and 12, in which the third parameter is the bank slope related to the type of bank material. In general, non-cohesive banks have flatter bank slopes with the value of z in the range of 2.0 to 3.1. For moderately cohesive banks, z is in the range of 0.9 to 1.5; and for cohesive banks, z is between 1.4 to 2.0. As the figure shows, the width-depth ratio of a canal is sensitive to the bank slope. This figure also illustrates the fact that a flat bank slope usually associates with a large width-depth ratio, as recognized by Simons and Albertson and some other regime researchers.

The experimental data by Ranga Raju et al. was obtained in a recirculating sand tray at a constant discharge using sand of medium size 0.27 mm. They compared the measured geometric parameters with the regime relations by Lacey, Simons and Albertson and Engelund-Hansen. The experimental canal was generally wider and shallower than predicted from these regime relations due to the non-cohesive bank material. However, using the computer model developed herein, good comparison between the analytical prediction and experimental data is observed, see Figs. 9 and 10.

CONCLUSIONS

This paper demonstrates the application of the minimum stream power method to stable alluvial canals. Using the minimum stream power hypothesis together with flow resistance and sediment discharge formulas,

a computer program has been developed which may be used to obtain the width, depth, and either slope or sediment discharge or stable canals. The hypothesis of minimum stream power provides a condition for alluvial channels in equilibrium with which the degree of indeterminacy may now be reduced by one. While additional verification of this hypothesis is necessary, it may prove to be a useful tool for a variety of problems in fluvial hydraulics. Other conclusions are outlined below:

1. The minimum stream power hypothesis states that, subject to the given constraints, the necessary and sufficient condition for equilibrium of alluvial channels is when the stream power is a minimum. Therefore, an alluvial channel with given water and sediment discharges tends to establish its width, depth and slope such that the stream power (or slope) is a minimum. The equilibrium configuration corresponds to the condition of best hydraulic efficiency subject to the constraints.

2. Except in the flow region of low shear stress, the results of the computer model on stable canals obtained based upon the Engelund-Hansen sediment formula are somewhat better than the Einstein-Brown formula and the DuBoys formula. Both the Engelund-Hansen formula and Einstein-Brown formula are inadequate for flow in the low shear stress region in which Lacey's regime equations also fail. However, the DuBoys formula and the Gill formula are found adequate for canals with low shear stress corresponding to incipient sediment movement.

3. Using the computer model to obtain the stable configuration of a canal, the width-depth ratio of the canal is sensitive to the bank slope. In general, a large width-depth ratio is associated with a flat bank slope. The bank slope may be used adequately to describe the type of bank material of the canal.

4. In addition to the field canals, the computer model has been found applicable to small experimental canals in non-cohesive sand, for which other regime formulas were found inadequate.

5. The stable alluvial channel configuration obtained using the minimum stream power method represents that of best hydraulic efficiency under the given conditions. Therefore, as the sediment discharge approaches zero, the channel configuration approaches that of the best hydraulic section for rigid boundary channels. The sediment discharge in a canal approaches zero in the flow region of incipient sediment motion in which most regime formulas fail.

ACKNOWLEDGEMENTS

The writer gratefully acknowledges the suggestions from Professors P. E. Johnson and F. E. Stratton of San Diego State University and Mr. J. Magee of the County of San Diego.

APPENDIX I.--REFERENCES

1. Callen, H. B., Thermodynamics, John Wiley and Sons, Inc., 1960, 376 pp.

2. Chang, H. H., and Hill, J. C., "Minimum Stream Power for Rivers and Deltas," Journal of the Hydraulics Division, Proc. ASCE, Vol. 102, No. HY10, October, 1976, pp. 1461-1477.

3. Chow, V. T., Open Channel Hydraulics, McGraw-Hill Book Co., Inc., 1971.

4. Engelund, F., and Hansen, E., "A Monograph on Sediment Transport in Alluvial Streams," Teknisk Vorlag, Copenhagen, Denmark, 1967.

5. Gill, M. A., "Rationalization of Lacey's Regime Flow Equations," Journal of the Hydraulics Division, ASCE, Vol. 94, No. HY4, Proc. Paper 6039, July, 1968, pp. 983-995.

6. Guy, H.P., Simons, D. B., and Richardson, E.V., "Summary of Alluvial Channel Data from Flume Experiments, 1956-61, "U.S. Geological Survey Professional Paper 462-I, 1966, 96pp.

7. Kennedy, J.F. and Brooks, N.H., "Laboratory Study of Alluvial Streams at Constant Discharge," Proc. of the Federal Inter-Agency Sedimentation Conference, Misc. Publication No. 970, Agricultural Research Service, 1963, pp. 320-330.

8. Lacey, G., "Flow in Alluvial Channels with Sandy Mobile Beds," Proc., Institute of Civil Engineers, London, Vol. 9, discussion, Vol. 11, 1958.

9. Lane, E. W., "Design of Stable Channels," Proceedings, ASCE, Vol. 120, Separate No. 280, September, 1953, pp. 1234-1260.

10. Langhaar, H. L., Energy Methods in Applied Mechanics, John Wiley and Sons, Inc. 1962, 350 pp.

11. Mackin, J. H., "Concept of the Graded River," Bull. of the Geological Society of America, Vol. 59, 1948, pp. 463-512.

12. Maddock. T., Jr., "Equations for Resistance to Flow and Sediment Transport in Alluvial Channels," Water Resources Research, Vol. 12, No. 1, Feb., 1976, pp. 11-21.

13. Ranga Raju, K. G., Dhandapani, K. R., and Kondap, D. M., "Effect of Sediment Load on Stable Sand Canal Dimensions," Journal of the Waterway, Port, Coastal and Ocean Division, ASCE, Vol. 103, No. WW2, Proc. Paper 12931, May, 1977, pp. 241-249.

14. Simons, D.B. "Theory and Design of Stable Channels in Alluvial Material," Ph.D. Dissertation, Dept. of Civil Engineering, Colorado State University, Ft. Collins, Colorado, 1957.

15. Simons, D. B., and Albertson, M. L., "Uniform Water Conveyance Channels in Alluvial Material," Proc., ASCE, Vol. 86, No. HY5, May 1960.

16. Simons, D. B., and Senturk, F., Sediment Transport Technology, Water Resources Publications, Ft. Collins, Colorado, 1977.

17. System Scientific 360 Subroutine Package, International Business Machines, Corp., Armank, New York, 5th ed., August, 1970.

18. Vanoni, V. A., Editor, Sedimentation Engineering, ASCE M & R No. 54, 1975.

19. Yang, C. T., "Potential Energy and Stream Morphology," Water Resources Research, Vol. 7, No. 2, April, 1971, pp. 311-322.

20. Yang, C. T., "Minimum Unit Stream and Fluvial Hydraulics," Journal of the Hydraulics Division, ASCE, Vol. 102, No. HY7, Proc. Paper 12238, July, 1976, pp. 919-934.

APPENDIX II.--NOTATION

The following symbols are used in this paper:

A = cross-sectional area of flow;

B = average width of a channel;

b = bed width of a channel;

C = numerical constant;

D = average bed depth;

D' = depth of flow due to grain roughness;

d = median size of sediment;

f = Lacey's silt factor;

g = gravitational acceleration;

n = Manning's roughness coefficient;

N_a = Lacey's roughness coefficient or absolute rugosity;

P = wetted perimeter;

p = power;

Q = water discharge;

Q_s = sediment discharge;

q_s = sediment discharge per unit channel width;

R = hydraulic radius;

S = slope;

V = mean velocity;

W = work;

x = distance;

z = ratio of horizontal distance to one unit vertically;

γ = Specific weight of water;

γ_s = specific weight of sediment;

ν = kinematic viscosity;

τ_o = shear stress;

τ_c = critical shear stress.

Table 1. Summary of canal data used

Name	No. of canals	Q cfs	$S \times 10^3$	B feet	D feet	z	d mm.
Simons & Bender data	24	43 ~ 1039	0.058 ~ 0.388	10.5 ~ 72.8	2.63 ~ 8.50	0.9 ~ 3.1	0.029 ~ 7.60
Punjab Canal data	42	5.8 ~ 9005	0.12 ~ 0.33	2.0 ~ 264.0	1.75 ~ 10.90	1.2 ~ 3.1	0.15 ~ 0.43
Sind Canal data	28	305 ~ 9057	0.0592 ~ 0.0831	41.0 ~ 259.4	4.67 ~ 13.14	1.2 ~ 3.0	0.021 ~ 0.196
Laboratory data by Ranga Raju et al.	6	0.632 ~ 0.696	0.75 ~ 2.83	3.6 ~ 4.5	0.24 ~ 0.37	2.1 ~ 2.7	0.27

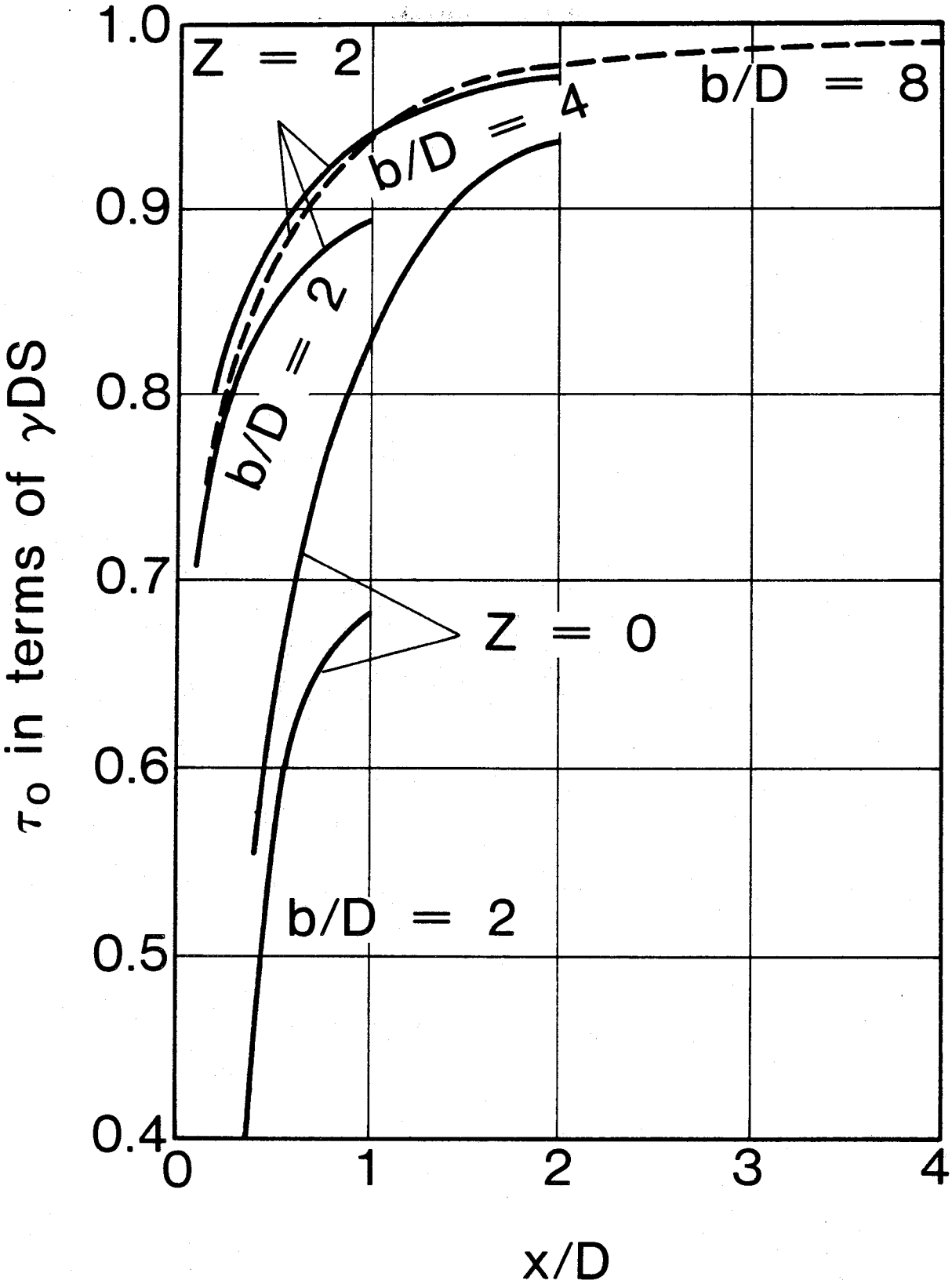

Figure 1 Shear stress distributions in trapezoidal channels, after Lane

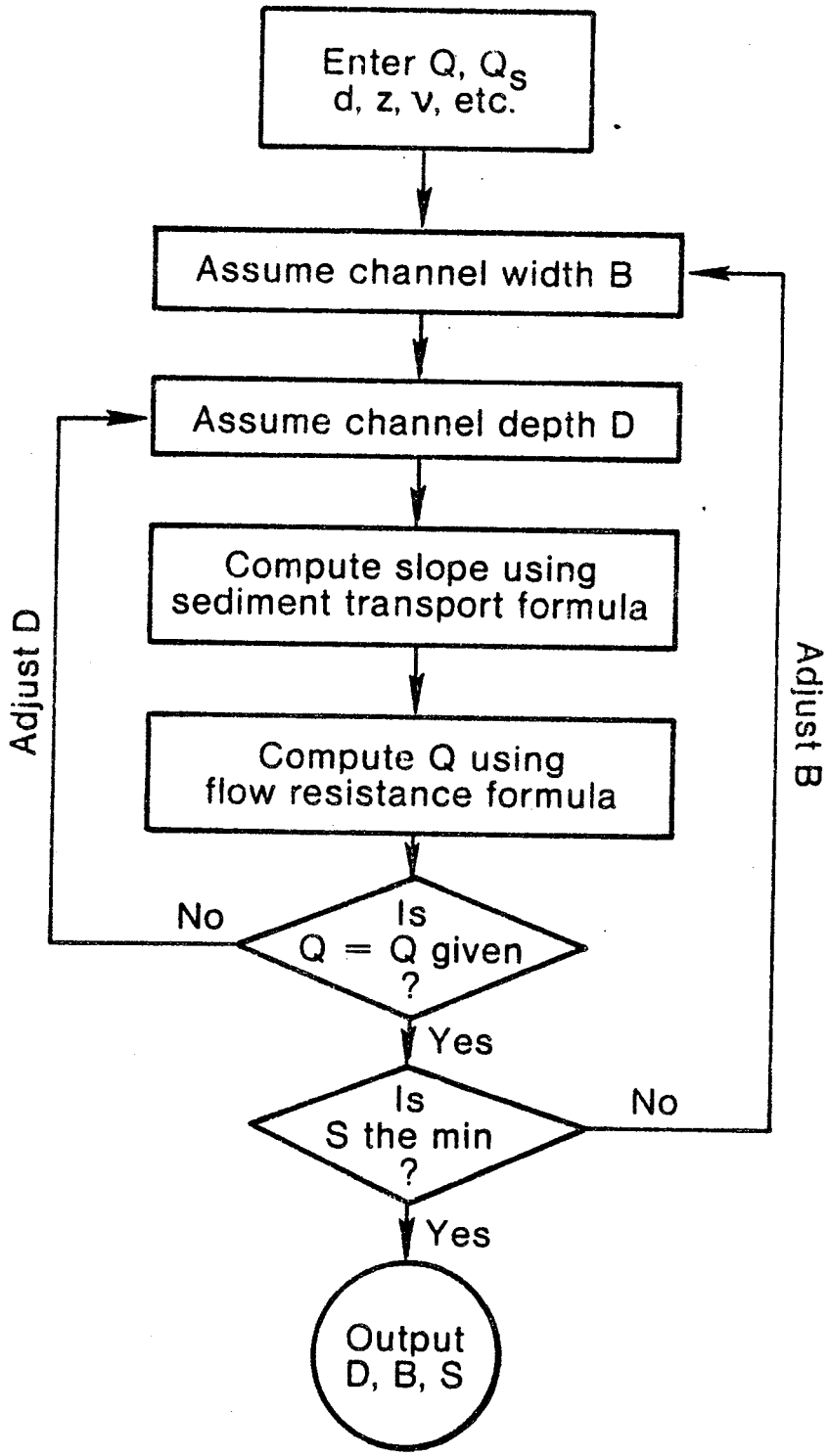

Figure 2 Flow diagram showing major steps of computation

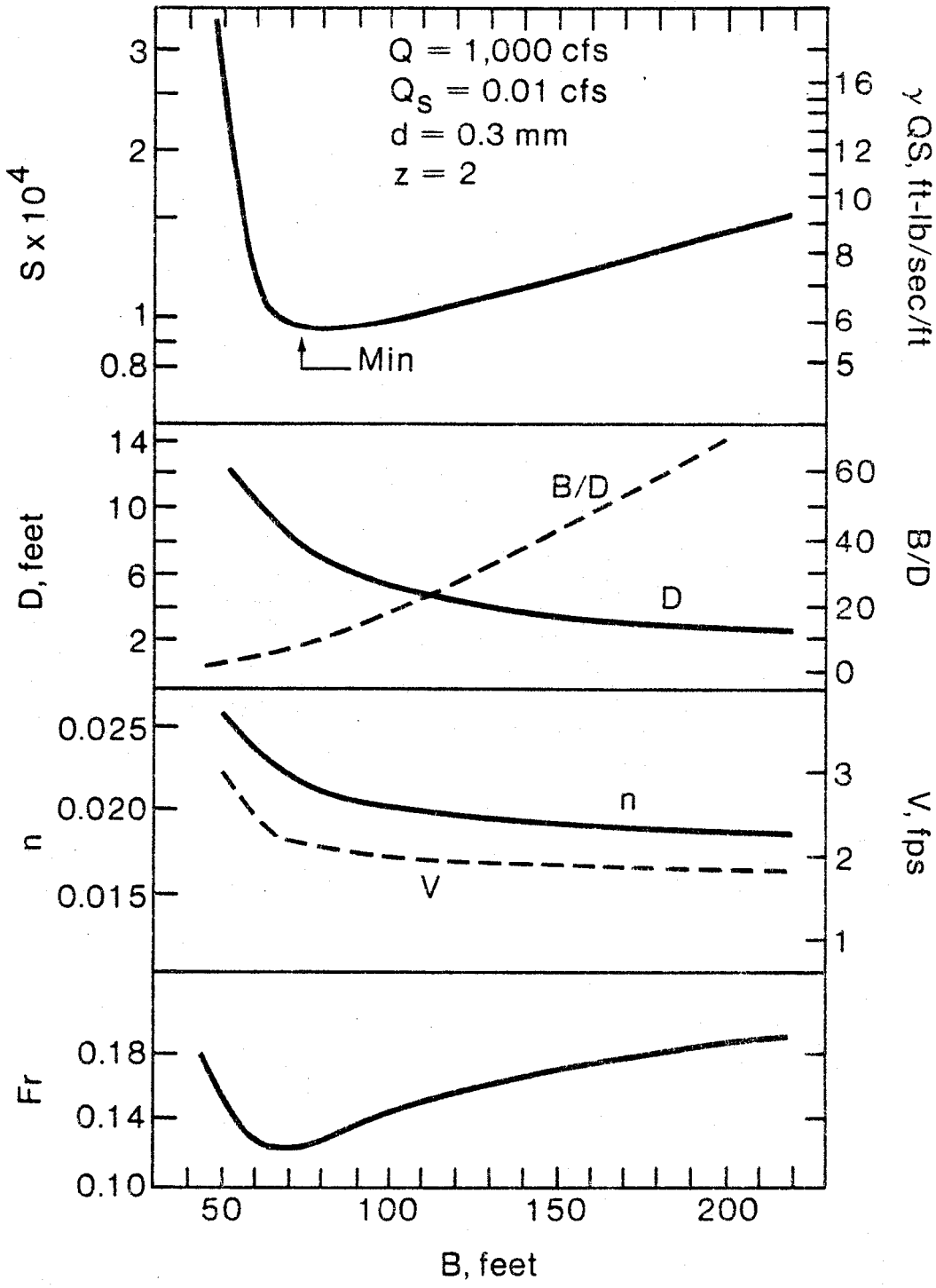

Figure 3 Variations of computed parameters with channel width for specified water and sediment discharges

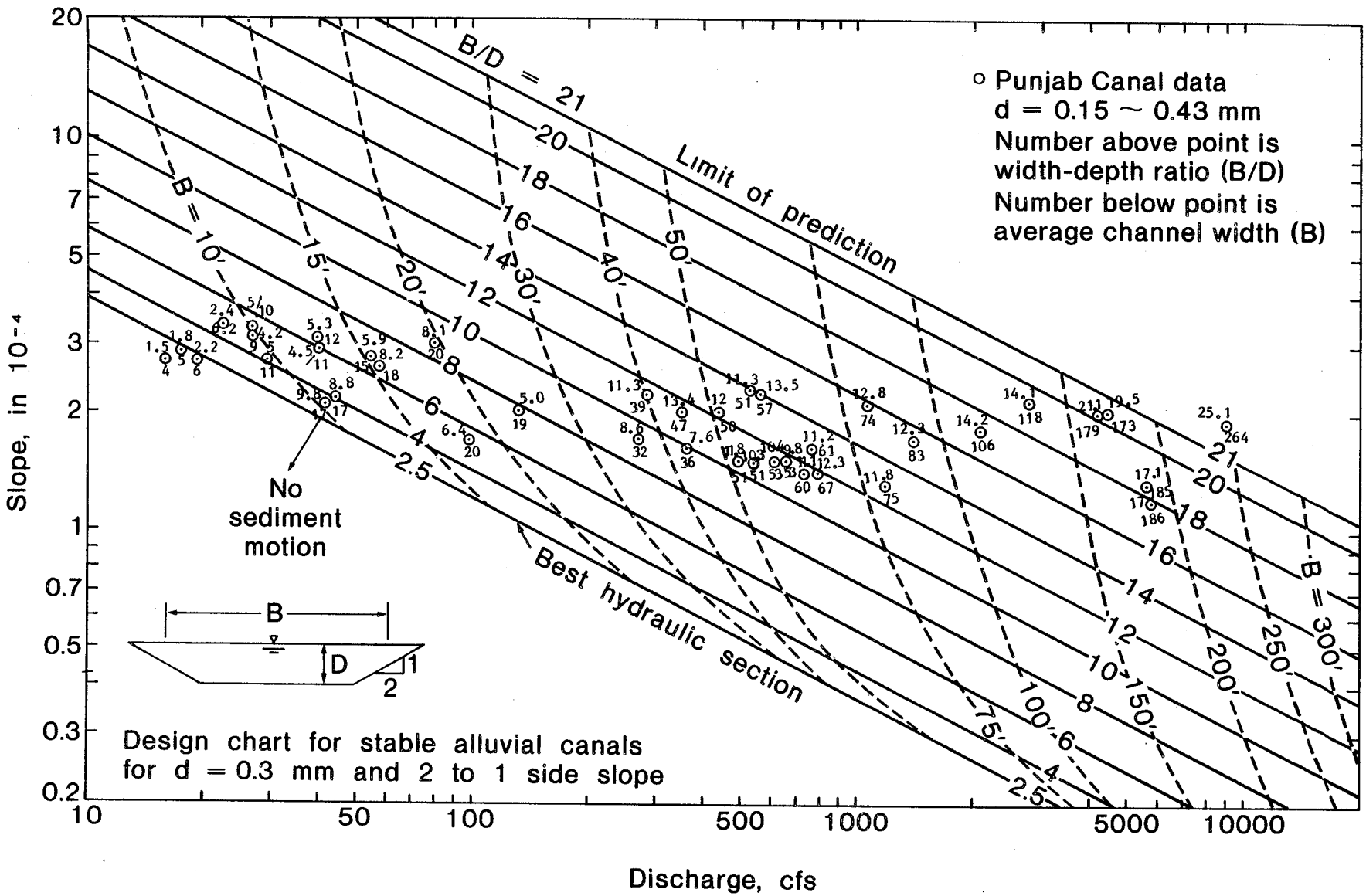

Figure 4 Design chart for stable alluvial canals for specified sediment size and side slope

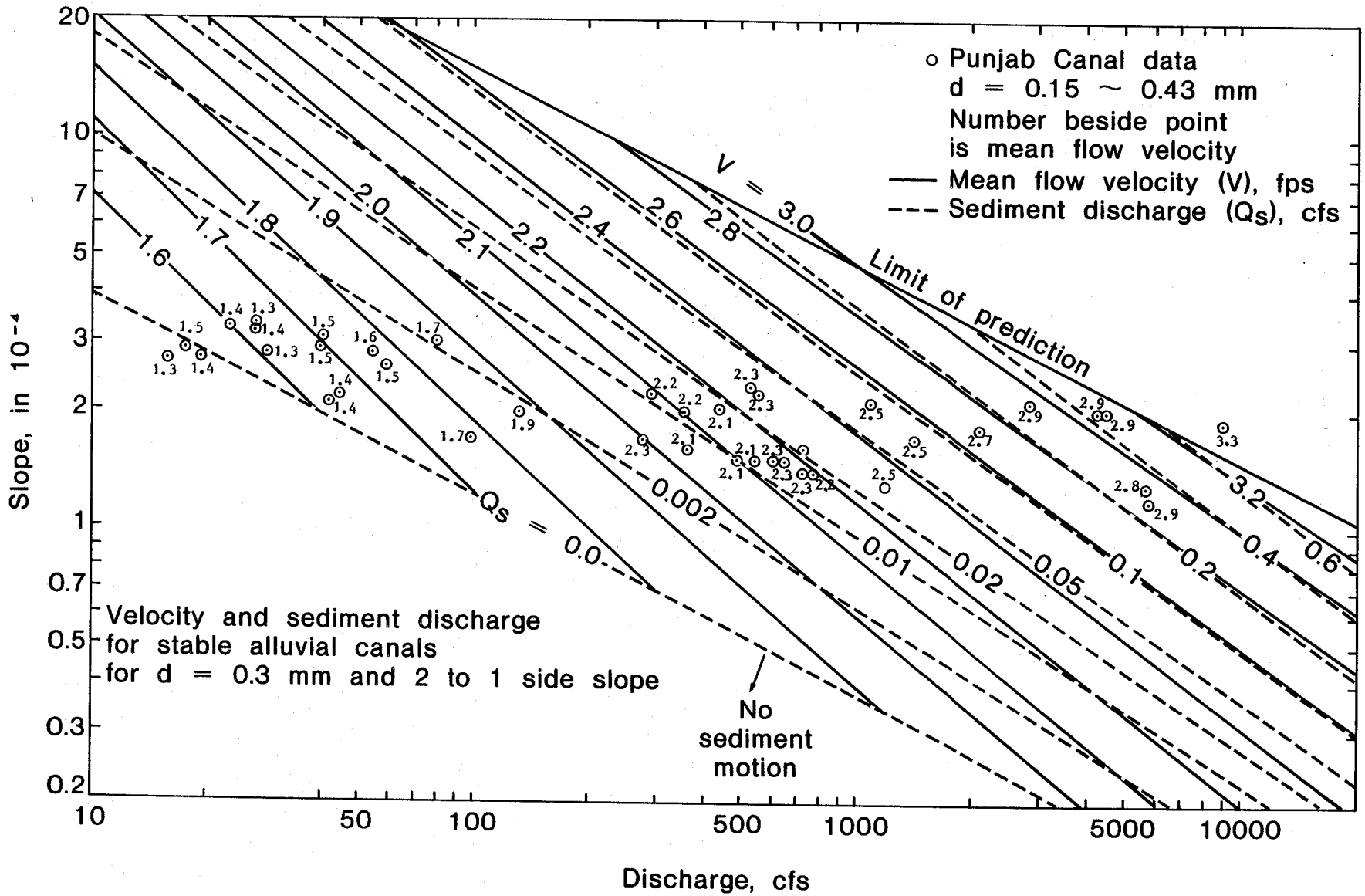

Figure 5 Velocity and sediment discharge for stable alluvial canals for specified sediment size and side slope

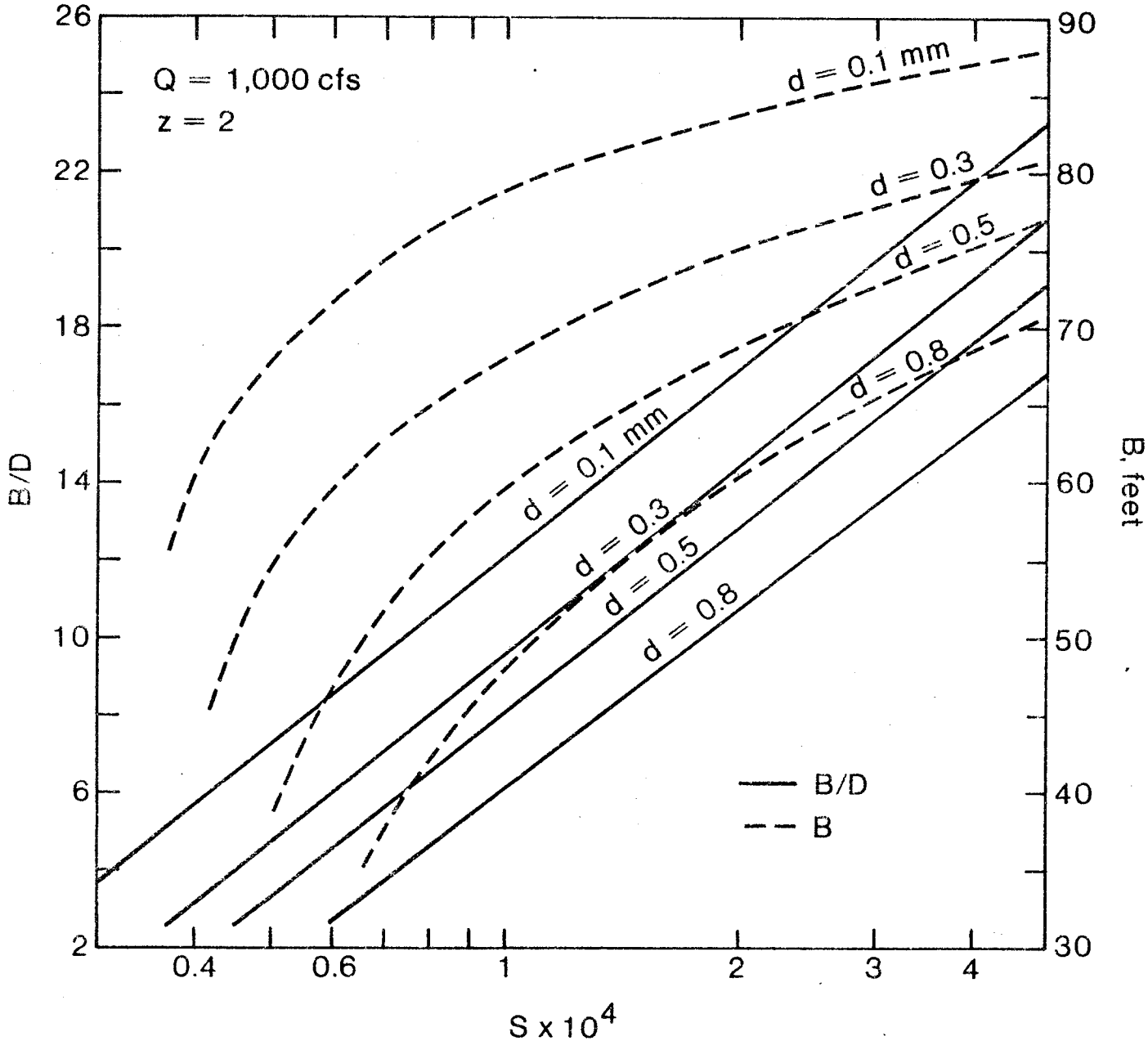

Figure 6 Channel geometry as functions of sediment size and channel slope for specified water discharge and side slope

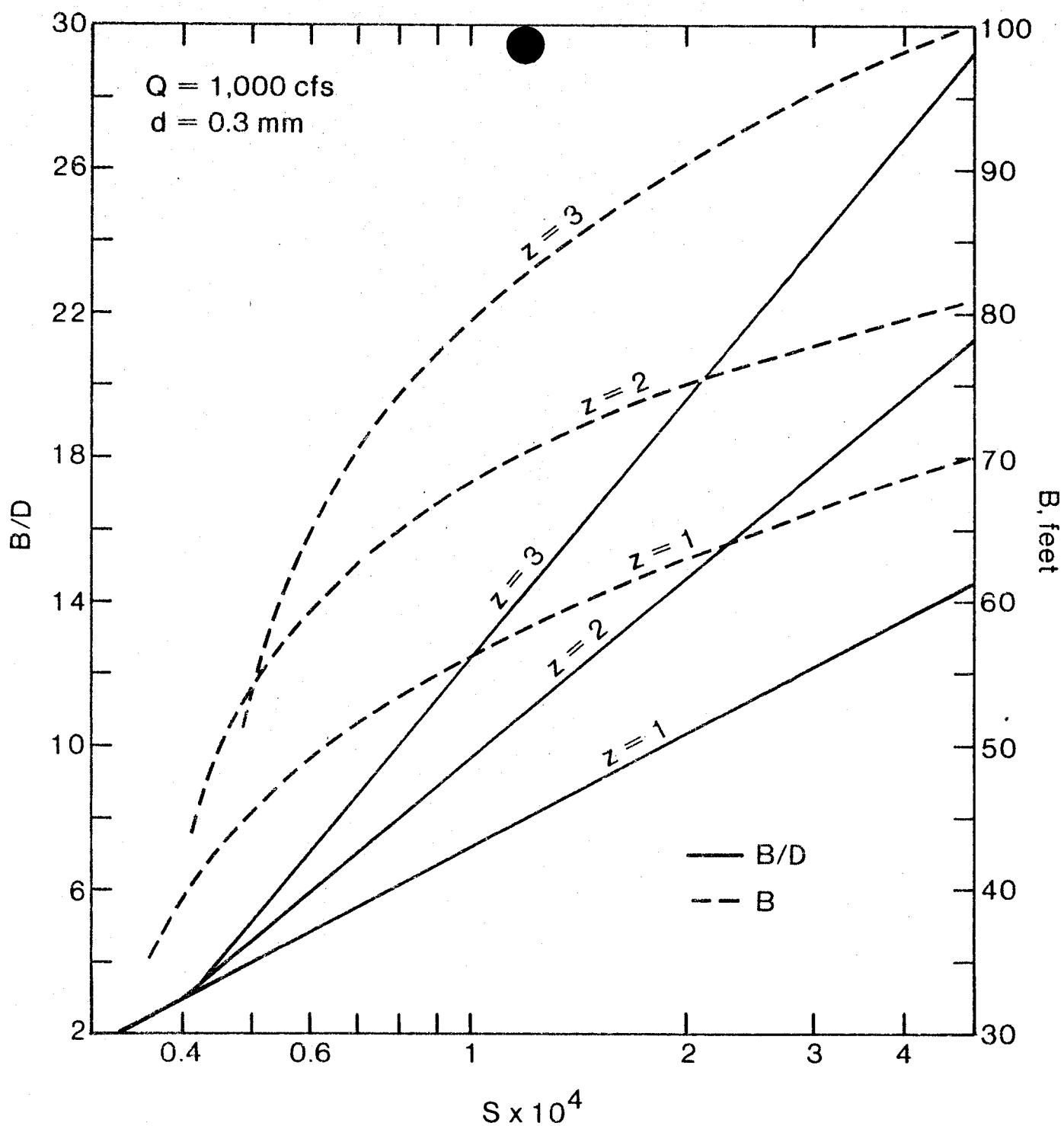

Figure 7 Channel geometry as functions of side slope and channel slope for specified water discharge and sediment size

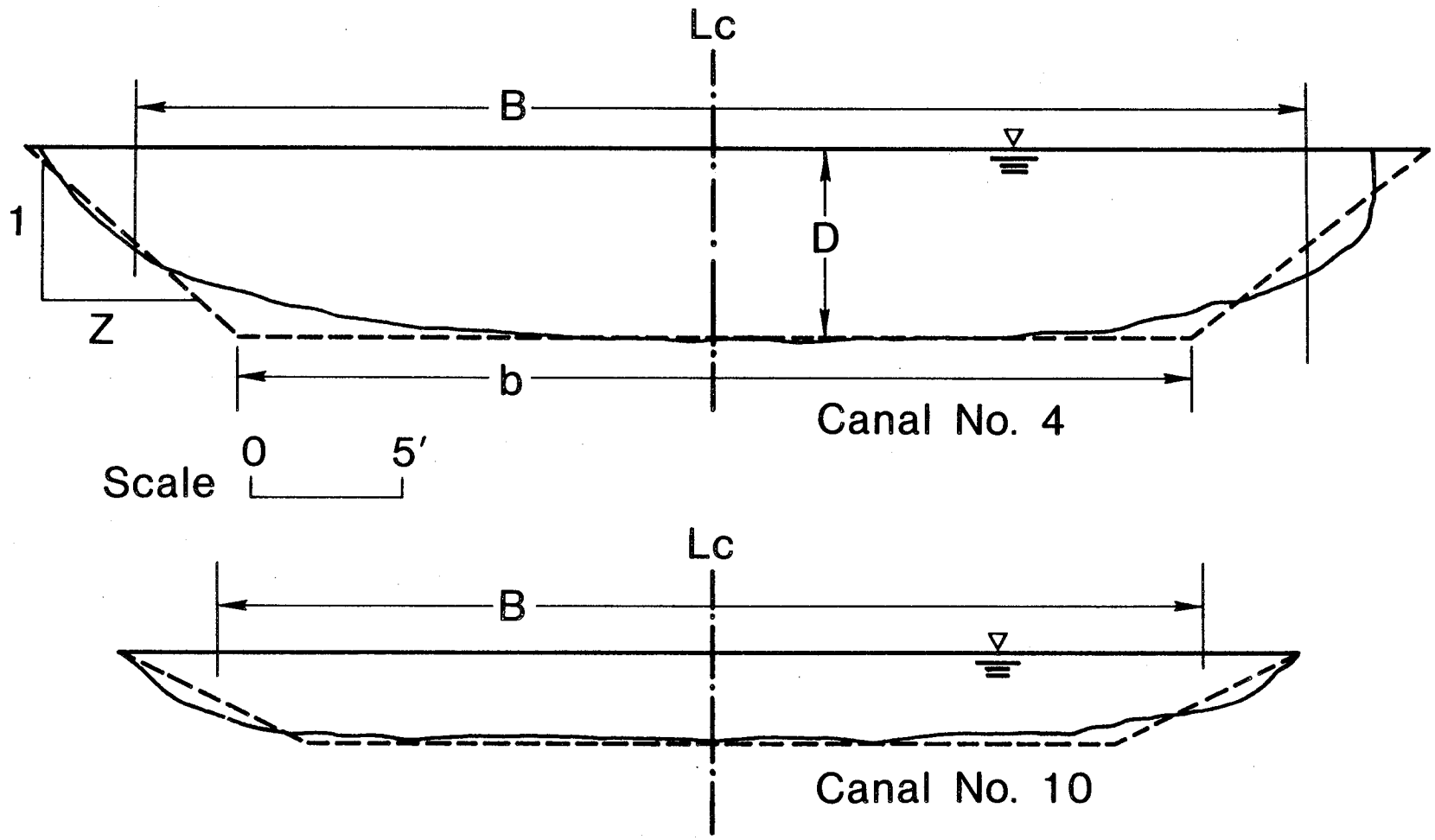

Figure 8 Sample canals and their trapezoidal approximation, Simons and Bender data

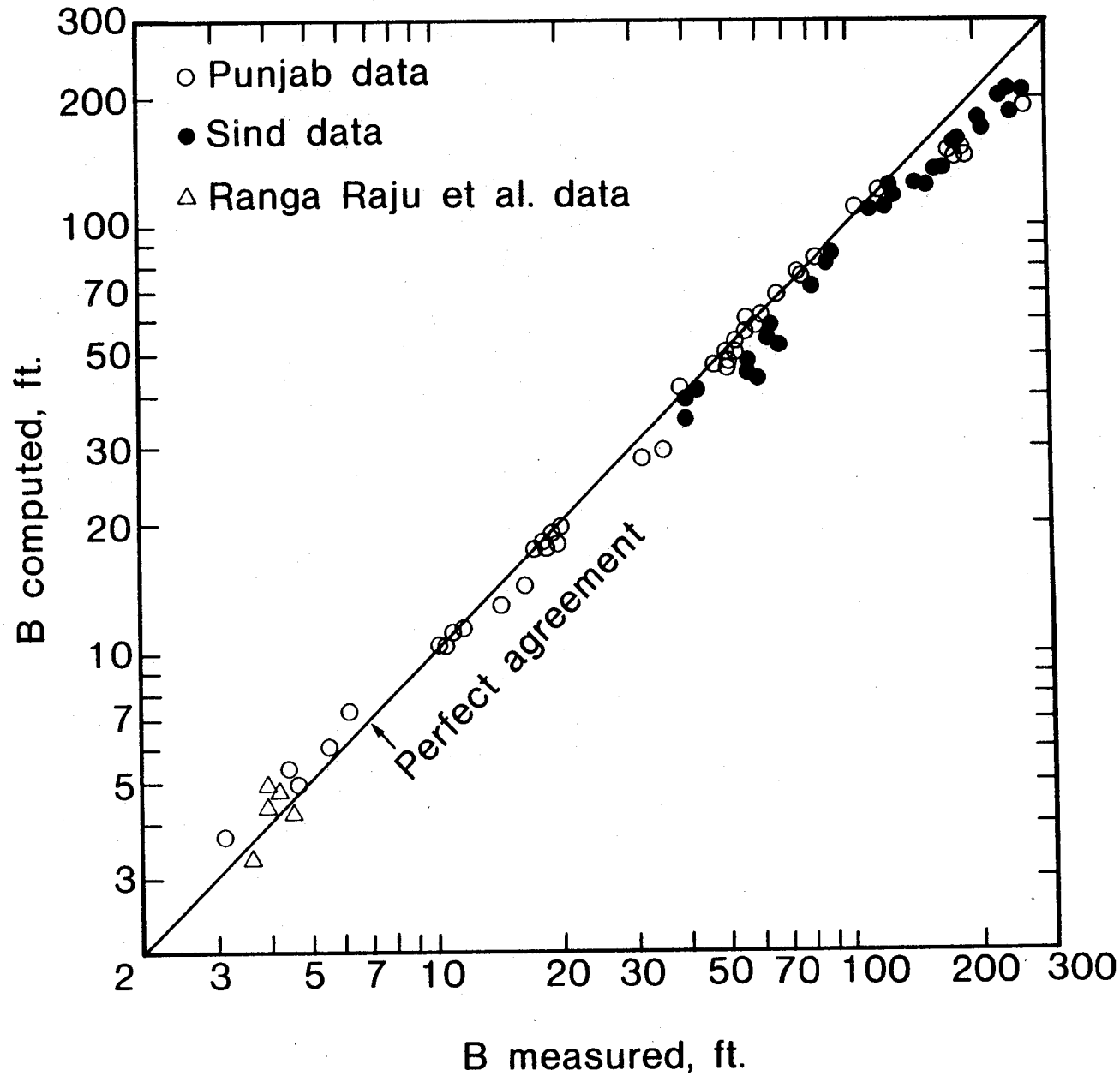

Figure 9 Comparison of computed channel width with measured width

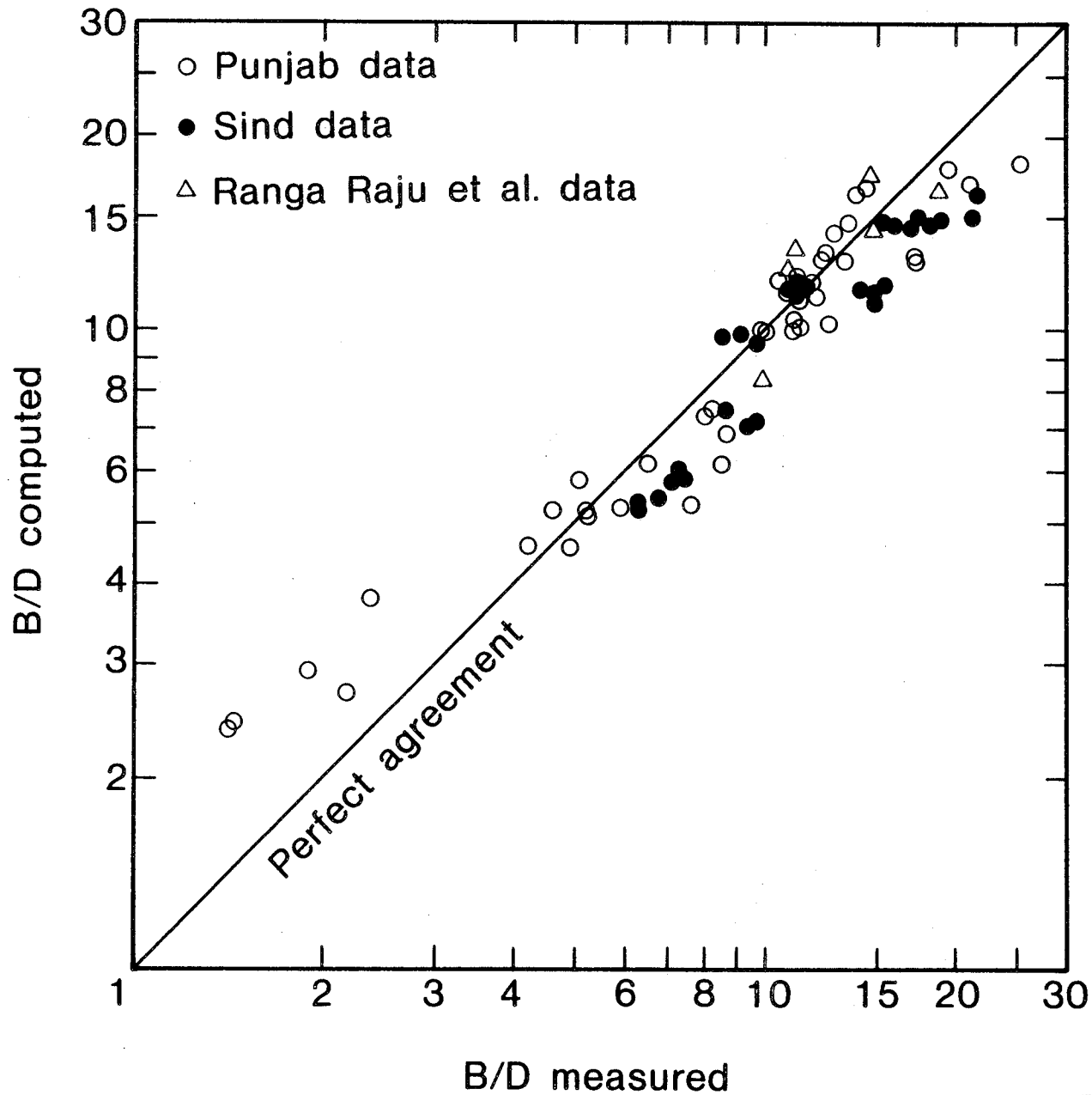

Figure 10 Comparison between computed and measured width-depth ratios

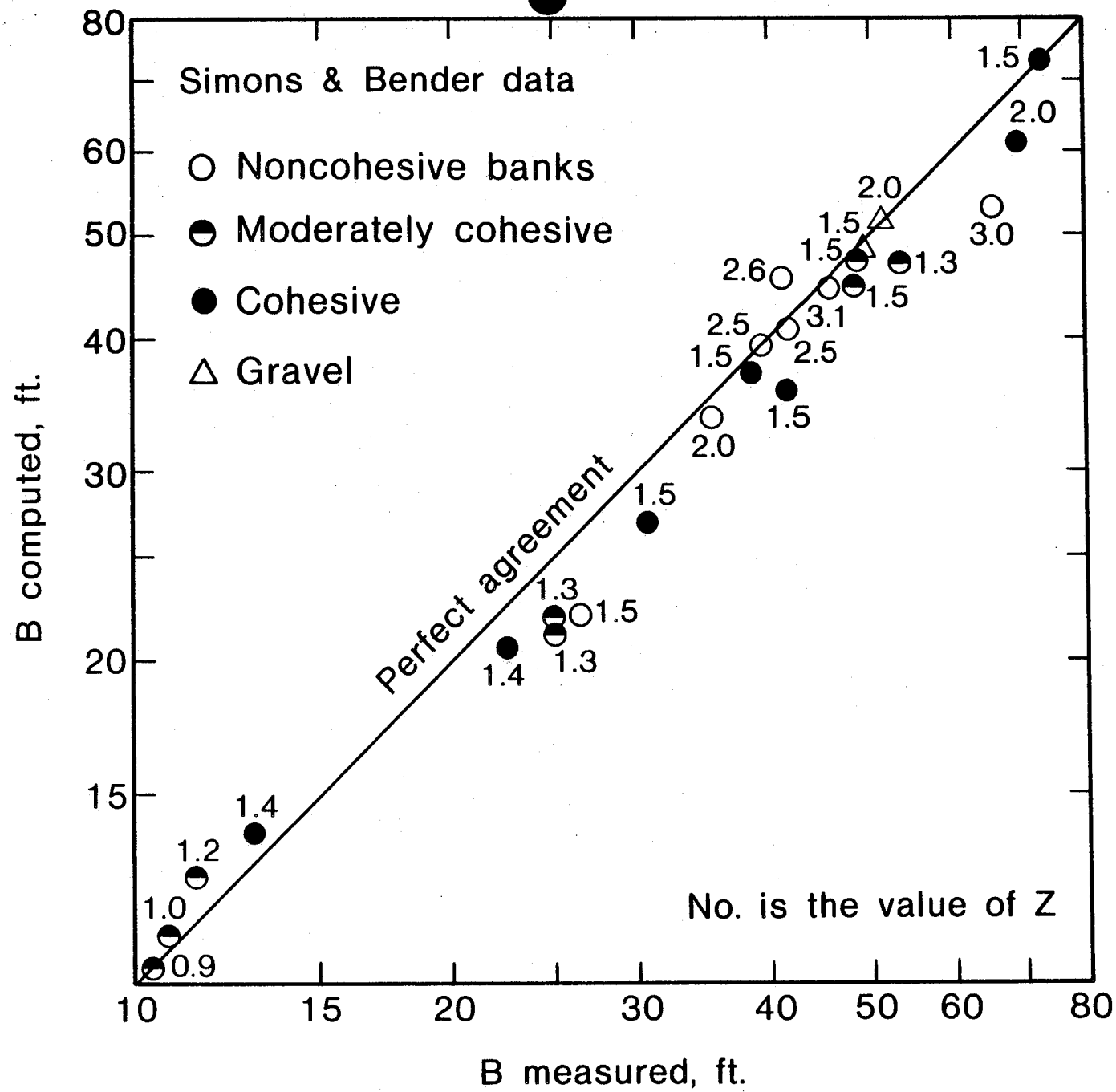

Figure 11 Comparison of computed channel width with measured width

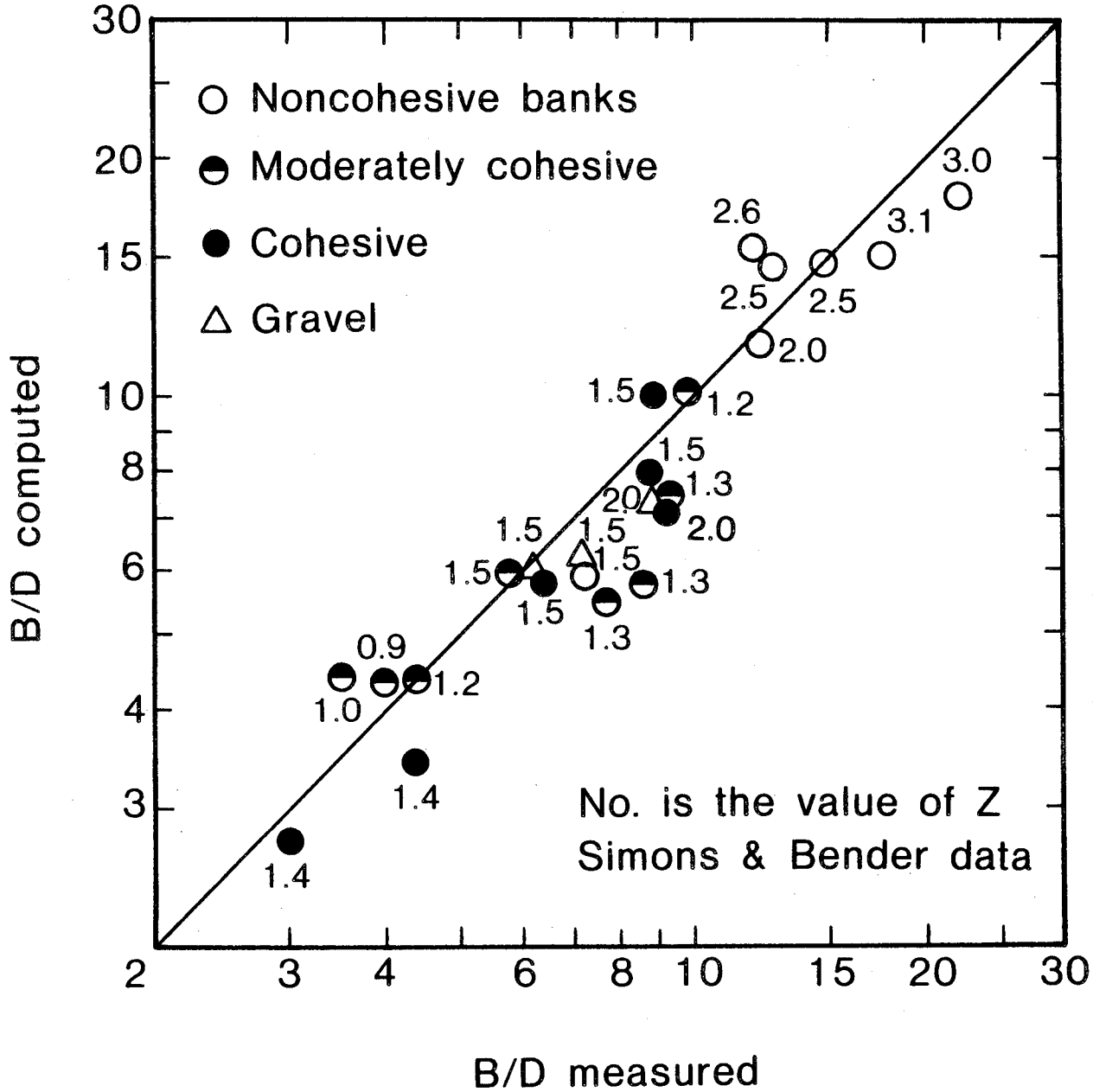

Figure 12 Comparison between computed and measured width-depth ratios

RIVER MORPHOLOGY AND THRESHOLDS

by Howard H. Chang[1], M. ASCE

ABSTRACT

The regime geometry and channel patterns of alluvial rivers are analyzed using an energy approach together with physical relationships of flow continuity, flow resistance, and sediment transport. Because of the discontinuity in flow resistance, i.e., in power expenditure, between lower and upper flow regimes, the adjustment in river regime consists of sudden changes in channel geometry, channel pattern and sometimes silt-clay content, when such a discontinuity is crossed. Thresholds or discontinuities in river morphology are obtained in the analysis. In accordance with such thresholds, rivers of distinct morphological features are classified into four regions based upon the bankfull discharge, channel slope, and median size of bed sediment. Their respective features are described and certain regime relationships for channel width and depth are established. The predicted channel geometry are compared with river data.

INTRODUCTION

The scientific and engineering literature is replete with regime relationships for alluvial rivers. The quasi equilibrium channel geometry is usually related to the slope, discharge, and sediment properties, etc. (14,15,26). However, such relationships are by no means continuous because there exist several apparent thresholds or discontinuities between pattern states; therefore, regime adjustment

[1] Professor of Civil Engineering, San Diego State University, San Diego, California 92182

involving a small change in slope may lead to a large change in channel pattern if the slope is close to a critical value (30,31). It is clear that a large change in channel pattern is accompanied by a significant change in channel geometry.

Based upon experimental and field data, threshold slopes as functions of discharge (mean annual discharge or mean annual flood) separating meandering rivers from steeper braided ones have been obtained by Lane (14) and Leopold and Wolman (16). Such a threshold has also been observed in experiments by Friedkin (11) and Schumm and Khan (29). Ackers and Charlton (1) and Schumm and Khan have also observed a lower threshold slope between meandering and straight streams in experiments, with meandering streams above the threshold. For a given discharge, there should be another lower slope at the threshold for bedload movement, below which river channel formation ceases (30). In addition, it appears that there exists some threshold for the silt-clay (sediments smaller than 0.074mm) content in the channel perimeter as Schumm (26,27,28,31) has found certain distinct channel features associated with the variation in channel silt-clay content.

The development of regime relationships for alluvial rivers is complicated by the existence of thresholds, yet the thresholds and different morphological features separated by them are obviously important parts of our knowledge in river engineering. Stability analysis has been employed to determine channel patterns and thresholds. For example, Parker (21) obtained a relation for meandering and a relation differentiating between meandering and braided regimes. This paper presents an analysis of river morphology and thresholds for sand-bed rivers using an energy approach. Certain quantitative relationships

pertaining to channel geometry and channel patterns in different regions separated by thresholds are obtained. The analysis is also correlated with channel geometry and silt-clay content using field data.

Rivers may be classified according to channel pattern or channel type. Three major channel patterns are those of straight (or sinuous), meandering, and braided rivers (16,17). Brice and Blodgett (2) classified alluvial streams into four major types as shown in Fig. 1. In the order of increasing channel slope, they are: equiwidth point-bar streams, wide-bend point-bar streams, braided point-bar streams, and braided streams without point bars. Equiwidth point-bar streams are relatively narrow and deep; the width is not sensitive to changes in channel slope. The widths of other types of streams vary in direct relation to the slope and are sensitive to changes in slope. The threshold conditions for which these channel patterns and channel types occur are analyzed herein. It will be demonstrated that morphological features predicated by the analysis are, to a large extent, coherent with those of the four major types.

Meandering rivers analyzed in a previous paper (8) are limited to equiwidth point-bar streams, characterized by flat slopes and flow resistance in the lower flow regime. For other types of steeper streams, there exist possibilities for flow resistance of both lower and upper flow regimes. The sudden change in flow resistance between these two flow regimes (34) should be matched by responses in river morphology. The analysis will demonstrate that the adjustment in flow resistance and its associated power transformation in part account for the characteristic geometry associated with each channel pattern.

ANALYSIS

This analysis is an extension of the previous analysis (8) which is limited to equiwidth point-bar streams. The sketch of a point-bar stream with riffles and pools is shown in Fig. 2. It represents a wide-bend point-bar stream if it is nonbraided; otherwise, it is a braided point-bar stream. Transverse flow distribution is uneven at the pool section with most of the flow concentrated in the pool. The effective width at the pool section is defined as that portion of the total width which provides power expenditure of the section in excluding the dead-water spaces at the channel margins from the calculations. This definition for effective width is equivalent to that given by Cherkauer (9). He noted that the effective width more closely approaches the total channel width in riffles than in pools. Thus, although the total width may be constant, effective width oscillates from narrow pools to wide riffles (9,24).

For the purpose of this analysis, each channel cross-section is approximated as a trapezoid or, for braided channels, a number of trapezoids separated by islands. If a section is in a curved channel, the base of the trapezoid is replaced by the transverse bed slope S_t. For a set of channel width B (or effective width) and center depth D, the maximum transverse bed slope occurs when the sloping bed extends to the water surface on the convex bank (see Fig. 2). Since S_t is directly related to the channel curvature (19), the maximum S_t occurs under the maximum curvature (or minimum radius of curvature) for the given conditions.

In the following, variables and physical conditions used in the analysis are outlined; the case of straight and nonbraided channel is

first considered; then the effects of channel curvature and braided channels on power expenditure and on channel geometry are analyzed.

Variables and Physical Conditions. - River channel formation is governed by such independent variables as the water discharge, sediment load, and sediment properties that are imposed upon the river from the drainage basin (13,14,17,18). Since the regime condition is the state of equilibrium toward which each river evolves, river channel formation involves delicate adjustments in channel width, depth, slope, roughness, etc., so that the inflow quantities of water and sediment are balanced by the river's ability to transport. In the analysis, the independent variables consist of the bankfull (channel-forming) discharge Q, the bedload Q_s, and the median size of bed sediment d. The dependent variables include channel width, depth, slope, velocity, and channel curvature. Note that channel roughness and transverse bed slope in a curved channel are not additional variables because they can be related to other variables. Valley slope is treated as another independent variable since the time scale for its formation is much longer than that for the river channel. Bank slope, z, is another dependent variable. While a steeper bank slope is hydraulically more efficient, it, nevertheless, is constrained by the erodibility of bank materials. Cohesive banks which have a higher silt-clay content can be steeper than noncohesive ones. This analysis does not consider such heterogeneities as bedrocks, trees and vegetation, etc.

River flow can be analyzed by the physical conditions of flow continuity, bedload transport, and resistance relation among the discharge, depth, width, channel roughness, and curvature. While these physical

conditions are employed in the analysis, they are insufficient to provide a complete solution because there exist more dependent variables or unknowns. Recent studies in river morphology have verified that a regime alluvial channel is adjusted so that the inflow quantities of water and sediment are transported with the minimum stream power per unit channel length (3,4) and equal stream power per unit length along the channel reach (5,6). These concepts are also given in earlier literature (17). Theoretical proof of minimum rate of energy dissipation has been made by Yang and Song (35). Stream power per unit length is expressed as γQS, in which γ is the specific weight of water and S is channel slope or energy gradient. The power associated with sediment transport is usually negligible. Since Q is a given independent variable, minimum γQS is equivalent to minimum S. These two energy related conditions, minimum S at a cross section and equal S along the reach, are also employed in the analysis. In addition, physical relationships for curved channels pertaining to power expenditure, transverse bed slope, etc., are also used. Since all these physical conditions are described in previous papers (3,4,7,8), their details are not repeated.

Straight and Nonbraided Case. - With a set of given independent variables and constraints, the physical conditions are employed to obtain the dependent variables. As a first step, three of the physical conditions consisting of the flow continuity equation, flow resistance relation, and bedload equation are solved to obtain the mean velocity, depth, and energy gradient at a series of incremental widths. Procedures for solving the three unknowns using the three physical conditions are given in Fig. 3 under the case of no channel curvature. Some sample

results are shown in Figs. 4 and 5, in which each graphical relation showing the variation of energy gradient S (or power expenditure per unit channel length γQS) with channel width (or effective width) for the given set of independent variables is called a stream power diagram. The water discharge of 1,000 cfs, sediment size of 0.3 mm, and various bedloads are used as the independent variables in the sample calculations. These diagrams are first examined before remaining physical conditions are applied to obtain the channel geometry.

For small values of Q_s, e.g., curves a or b in Fig. 4, the stream power diagram has a unique minimum in S. The flow is in the lower regime with ripples or dunes. With a higher Q_s, the stream power diagram has two minima, one in the lower flow regime (Min. 1) and the other in the upper flow regime (Min. 2), as illustrated by curves c-g in Fig. 4. The minimum energy gradients at Min. 1 and Min. 2 are designated S_1 and S_2, respectively. From computed results shown in Fig. 5, the channel represented at Min. 1 (riffle) is wider and shallower and has a lower velocity than the channel at Min. 2 (pool).

The computed results in Fig. 5 show greater sediment efficienty, i.e., less power expenditure, associated with a higher degree of channel roughness in terms of Manning's n. The existence of Min. 1 is attributed to the greater channel roughness of the lower flow regime. With a decrease in width from this point, the flow begins to transform into the upper flow regime through the transition. Since this development is associated with a significant decrease in roughness (34), thus it is also accompanied by rapid increase in power expenditure.

From the condition of minimum stream power per unit channel length, the channel width at the minimum energy gradient S_1 or S_2 is a stable

width. Other variables associated with this energy gradient and width, including the depth, velocity, width-depth ratio are directly obtained as results of the computation. For example, such values for the sample calculation shown in Fig. 5 for the straight and nonbraided case are as follows:

	Section 1	Section 2
	Riffle	Pool
Minimum energy gradient (S)	0.00119	0.00119
Effective width (B), feet	121	44.5
Center depth (D), feet	2.1	4.2
Average velocity (V), fps	3.7	6.5
Effective width-depth ratio (B/D)	57.6	10.6

If a stream power diagram has a unique minimum in S, a unique channel geometry is obtained. However, if a diagram has two minima, the same water discharge and bedload may be transported by two stable channel geometries. From the condition of minimum stream power for a river reach, gradually varied flow of the riffle-and-pool pattern may develop along the reach if power expenditures per unit channel length for these sections are equal; that is, if S_1 equals S_2. If they are unequal, the lesser of the two is more stable.

Whether a stream power diagram may have two equal minima is now investigated. The minimum energy gradients S_1 and S_2 are also functions of the bank slope using the trapezoidal approximation for the cross-sectional shape. Under the same independent variables, the value of S_1 or S_2 decreases as the bank slope steepens; it reaches a minimum when the bank slope angle equals 60° or $z = 1/\sqrt{3}$. Note that this is the bank

slope for the best hydraulic section. While a steeper bank slope within the limit of $1/\sqrt{3}$ is associated with greater efficiency, the bank slope nevertheless is constrained by the stability of bank materials. In consideration of possible cohesive materials on channel banks, the maximum bank slope is assumed to be 60°. Within this constraint for bank slope, the values of z for these sections may be adjusted so as to equalize S_1 and S_2, if possible. In the present analysis, the 2-to-1 bank slope is assumed for the riffle section, i.e., the value of z is 2, while it is adjusted within the range of $1/\sqrt{3}$ to 2 for the pool section. For stream power diagrams c and d in Fig. 4, S_2 is greater than S_1 even when the maximum bank slope is used for S_2. Therefore, channel geometry represented at Min. 1 is more stable. For diagrams e and f, S_1 and S_2 can be equalized if a steeper bank slope is used for S_2. For diagram g, S_2 is equal to S_1 when the same 2-to-1 bank slope is used for both S_1 and S_2. Therefore, multiple channel geometries may coexist in the same reach for rivers represented by stream power diagrams e, f, and g in Fig. 4.

Effects of Channel Curvature. - Channel curvature contributes to the transverse bed slope and increased power expenditure associated with transverse currents; it also affects sediment transport as described previously (8). For a set of independent variables Q, Q_s, and d, the physical conditions of flow continuity, flow resistance, bedload transport, and those pertaining to curved channels are employed to solve for the center depth, mean velocity, energy gradient, and transverse bed slope S_t (or center radius of curvature r_c) at a series of incremental widths. Major steps of computation are shown in Fig. 3 under the cases

of maximum curvature and any intermediate curvature. Note that the energy gradient at a curved channel section, S, is partitioned into the components of S' and S", of which S' is due to longitudinal resistance and S" is associated with the transverse loss as detailed in previous papers (7,8). The value of S_t is related to r_c and other variables according to the relationship developed by Odgaard (19).

Sample results for the pool section at the maximum channel curvature are shown in Fig. 5. With the z value of 1.4 for the bank slope, the minimum energy gradient of this section is equal to that for the straight case. Other variables, including the effective width, center depth, and velocity, are similar for both cases. Similar results have also been obtained for the pool section under intermediate channel curvatures. Therefore, it may be concluded that the pool section can be equally stable under different channel curvatures within its maximum value. Under the maximum curvature, the radius of curvature for this case is obtained to be 2.9 times the width of the riffle section which more closely approximates the channel width (see Fig. 2). For different sets of independent variables, the ratio of radius of curvature to channel width under the maximum curvature is found to be nearly constant with a value of about 3. Because it is obtained using conditions of minimum stream power, it therefore represents the maximum curvature for which a river does the least work in turning.

The conclusion regarding the effects of channel curvature on the pool does not apply to the riffle section. Because of the smaller depth and lower velocity, power expended through transverse currents is less at the riffle section (7,25). But, under the maximum curvature or any

intermediate curvature, the change in channel roughness due to transverse bed slope is such that it reduces the sediment efficiency thereby increasing the power expenditure as illustrated in Fig. 5. This result concurs with previous findings by Onishi, Jain, and Kennedy (20) for wide curved channels. It may therefore be concluded that, for a wide riffle section, the straight channel pattern is more stable.

Effects of Braided Channels. - The water discharge and bedload are subdivided among the anabranches at a braided river section. Formation of braided channels reflects in part a river's adjustment in power expenditure which, in turn, affects the channel stability. The effects of braided channels on channel stability are illustrated in Fig. 5 by the variations of energy gradient S (or power expenditure γQS) with channel width or effective width. Graphical relations as shown are for two equal braided channels and the total width is the combined widths of the anabranches. It shows that for the pool section, which has a small width-depth ratio, braiding results in significant increase in power expenditure. Therefore, the nonbraided channel is more stable for the pool. For the riffle section which has a large width-depth ratio, the braided condition is associated with slightly greater power expenditure and channel width. Since braiding has little effect on the power expenditure for riffles, the braided and nonbraided patterns are approximately equal in stability under this situation. In reality, wide streams are usually braided because of high sediment rates, bank erosion, physical heterogeneity, etc., (16,17).

CHANNEL GEOMETRY, CHANNEL PATTERNS, AND THRESHOLDS

Based upon characteristics of these stream power diagrams, rivers are classified into four regions (Regions 1, 2, 3, and 4) separated by thresholds. Results pertaining to regime channel geometry for these regions are shown in Fig. 6. While this graphical relationship is obtained using a 2-to-1 bank slope (for Min. 1), similar relationships using other values may be obtained. In constructing this figure, different sets of independent variables Q, Q_s and d in the sand-size range were used to produce the width, depth, and slope as illustrated by the sample given in Fig. 5. Then, channel width and average center depth are plotted in Fig. 6 as functions of Q, S and d. Note that, in the case of riffle-and-pool patterns, channel width as shown is the width of the riffle section as it more closely approximates the channel width (see Fig. 2).

Several thresholds or discontinuities for channel geometry designated as Lines I to IV are also shown in Figs. 4 and 6. From the bottom, the first threshold (Line I) which corresponds to the critical slope for bedload movement, S_c, is represented by the equation (4)

$$\frac{S_c}{\sqrt{d}} = 0.00238\ Q^{-0.51} \qquad (1)$$

This equation is obtained in the computation using the critical shear for incipient bedload developed by Straub (32). The equation for the second threshold (Line II) is obtained from Fig. 6 as

$$\frac{S}{\sqrt{d}} = 0.05\ Q^{-0.55} \qquad (2)$$

and the third threshold (Line III) is represented by

$$\frac{S}{\sqrt{d}} = 0.047\ Q^{-0.51} \qquad (3)$$

There should also be a fourth threshold, represented by the dashed line (Line IV) at the lower boundary for steep braided streams. The precise location of this threshold is not determined in this analysis.

In the following, regime channel geometry and its associated channel pattern and channel type for each region are described.

Region 1. This region has its lower threshold at incipient motion for bedload (Line I) and its upper threshold at Line II in Figs. 4 and 6. A regime channel in this region is characterized by a flat slope, low velocity, small bedload, and flow resistance in the lower regime of ripples and dunes. The channel is relatively deep and narrow, with a width-depth ratio generally ranging from 4 to 20. It is interesting to find that all man-made stable canals are within this region. Each of these canals has constant width, depth, and long straight reaches. Natural rivers in this region are usually meandering in channel pattern. Previous analysis (8) has shown that, for such rivers, the channel width and center depth stay approximately the same along the meandering channel; therefore, they are equiwidth point-bar streams.

Graphical relations for channel geometry as shown in Fig. 6 can be expressed in mathematical forms. The surface width varies with Q, S and d, i.e.,

$$B = 3.49 \left[\frac{S}{\sqrt{d}} - \frac{S_c}{\sqrt{d}}\right]^{0.02} Q^{0.47} \qquad (4)$$

Therefore, the width is primarily a function of the discharge; its dependence on S and d is not significant. The following equation for

the center depth is obtained from the figure

$$D = 0.51\ Q^{0.47}\ \exp[-0.38(S/S_c - 1)^{0.4}] \qquad (5)$$

Empirical relations for stable canals are in general agreement with these relations (12,33).

While most natural rivers in this region have a meandering channel pattern, a straight channel pattern for which the channel slope equals the valley slope may also be maintained as long as constant inflows of Q and Q_s are in balance with the channel's capacity for transport. Field evidences from stable canals indicate that the straight channel pattern can be maintained with periodic minor repairs. However, if the discharge or slope of a canal is large enough such that the canal crosses the threshold into Region 2 or 3, then rapid bank erosion starts to occur as experienced from canals in Pakistan (23).

Region 2. - This small region represented by stream power diagrams c and d is between Lines II and III in Figs. 4 and 6. Each diagram has two unequal minima of which S_1 is smaller and hence it is the global minimum. This means that the channel geometry represented at Min. 2 is less stable and hence unlikely to develop. In other words, rivers in this region are more likely to assume a unique channel geometry represented at Min. 1. Figs. 4 and 6 show that the channel geometry is sensitive to the slope in that an increase in slope is accompanied by a rapid increase in channel width and a rapid decrease in depth. Because the width-depth ratio is usually large, rivers in this region are quite often braided. A river with a unique channel geometry, which has a large width-depth ratio, is usually straight in channel pattern since

meandering development is inhibited by the large width.

Existing literature describing rivers possessing these characteristics is limited. This may be because this region is small in range, especially at lower bankfull discharges. Perhaps the most interesting study was made by Lane (14). He classified a group of rivers as straight, braided rivers, including 12 river reaches of the upper Mississippi, the lower Nile, the lower Yangtze, etc. With bankfull discharges ranging from 40,000 to 500,000 cfs, these rivers all fall within or near Region 2 (3). These data points are not plotted in Fig. 6 due to the lack of measured channel geometry.

Region 3. - This region is between Lines III and IV in Figs. 4 and 6. A stream power diagram in this region, e.g., e or f in Fig. 4, has two minima of which S_1 is for the riffle section and S_2 is for the pool section. For the same bank slope, S_1 is less than S_2 and hence it represents a more stable condition. However, S_1 and S_2 can be equalized since S_2 can be associated sith a steeper bank slope. Under this situation, the riffle and pool sections may coexist in the same reach according to the condition of equal stream power along a river reach. Both channel width and depth are sensitive to the slope, a fact in sharp contrast to rivers in Region 1. The strong dependence of width on the slope has been addressed by previous researchers (14,17,31). Since an increase in slope is accompanied by rapid increase in width and decrease in depth, rivers in this region may be braided; the extent of braiding is in direct relation to the slope.

Graphical relations for channel width and depth in Fig. 6 may be written in mathematical forms. The width B is a function of both

channel slope and bankfull discharge, i.e.,

$$B = 33.2\ Q^{0.93} \left(\frac{S}{\sqrt{d}}\right)^{0.84} \tag{6}$$

The equation for the average center depth D is

$$D = \left(0.015 - 0.025\ \ln Q - 0.049\ \ln\frac{S}{\sqrt{d}}\right) Q^{0.45} \tag{7}$$

The width-depth ratio is generally between 25 and 100 in this region.

When the discharge is less than the bankfull discharge, a river in this region may move into Region 2 or 1. Therefore, it may have quite different channel characteristics at lower discharges.

The relation of channel slope to valley slope determines the channel pattern. As a general rule, the channel slope cannot be steeper than the valley slope under the equilibrium state. If S_1 is equal to the valley slope, then the river has a straight pattern. With a unique channel geometry which is wide and shallow, it is usually a braided stream. The extent of braiding increases with the channel slope. If S_1 is flatter than the valley slope, then S_1 and S_2 can be equal to allow the coexistence of riffle and pool sections along the same channel reach. As described previously, a river does less work in turning through the pool than through the riffle; therefore, channel bends usually form at pools. The resulting alternating riffle-pool pattern allows the channel to stay in dynamic equilibrium on a steeper valley slope. A river of these characteristics is a wide-bend point-bar stream or a braided point-bar stream. The latter which have steeper slopes are usually wider. The large width associated with a braided pattern may inhibit the concentration of flow for the formation of pools; hence, pools may be absent in certain reaches of such wide streams. For this

reason, braided point-bar streams are less sinuous than wide-bend point-bar streams.

Region 4. - Rivers in this region are similar to those in Region 3 in that the stream power diagram may have two equal minima for riffles and pools but those in this region are steeper in slope. No clear division between these two regions is delineated but an approximate line of separation (Line IV) is shown in Fig. 6. Since the width-depth ratio represented at Min. 1 is very large, rivers in this region are usually highly braided. The width-depth ratio is usually greater than 100. While there exists another possible stable channel geometry represented at Min. 2 for the pool, this geometry can be equally stable only if it is nonbraided. Since concentration of flow in the pool is usually physically prevented by the large width, the pool section is usually missing in such rivers. In the absence of the pool section, the braided channel pattern is usually straight although some of the anabranches may be sinuous.

COMPARISON WITH RIVER DATA

Different data for sand-bed rivers are used for comparison with the analysis. These include stable canal data from Punjab Canals (23) and All-American Canals (22), river data of Midwestern United States compiled by Schumm (28), and the Mississippi River data (10).

In addition to channel geometry, the Midwestern river data also contain information on meander sinuosity (ratio of valley slope to channel slope) and silt-clay content in the channel perimeter. These data as plotted in Fig. 7 indicate a distinct discontinuity near the

second threshold, with rivers above this line having less sinuosity and silt-clay content. This discontinuity correlates remarkably well with the sudden change in channel geometry shown in Fig. 6. While the silt-clay content should be related to the supply of such materials from the watershed, it also appears to be related to the channel characteristics. The variation of silt-clay content shown in Fig. 7 is consistent with the findings by Scumm (31), because the lower silt-clay content is associated with steeper and wider rivers.

Channel width data are plotted in Fig. 6 for comparison. At the same discharge, rivers that are plotted above Line II are considerably wider; the discontinuity of measured widths is in general agreement with the analysis. In addition to the comparison shown in Fig. 6, measured and predicted channel widths and depths are compared separately in Figs. 8 and 9. Because of the high silt-clay content associated with the Midwestern rivers in Region 1, the 1-to-1 bank slope is assumed in generating the predicted widths and depths for these natural rivers shown in Figs. 8 and 9.

While there is general agreement between measured and predicted channel geometry, variations are significant for certain rivers. These variations may be attributed to such heterogeneties as vegetation, bedrocks, sediment distribution, etc., that are not considered in the analysis.

SUMMARY AND CONCLUSIONS

The regime geometry and channel patterns of sand-bed rivers are analyzed using an energy approach. On the basis of the adjustment in flow resistance and associated power transformation, rivers of distinct

characteristics are obtained and classified into four regions separated by thresholds (see Fig. 6).

A river in Region 1 is characterized by a flat slope, a relatively small and uniform width, and a small width-depth ratio. The regime width which is insensitive to the slope is essentially only a function of bankfull discharge. While most natural rivers belonging to this region are meandering in channel pattern, stability of straight channel pattern may also be maintained as evidenced by stable alluvial canals. While such natural rivers may have various degrees of meander sinuosity, very sinuous rivers are found in this region. Rivers in Region 2 have fairly flat slopes, but steeper than those in Region 1. The regime width is fairly wide and highly sensitive to the slope. Such rivers are characterized by a usually braided and fairly straight channel pattern, an example being the lower Nile. Rivers in Region 3 have slopes ranging from moderately steep to fairly steep, characterized by the alternating riffles and pools at bankfull stage. The regime width is very sensitive to the slope. Rivers that exist on moderately steep slopes are usually less braided but more sinuous, and are classified as wide-bend point-bar streams. Those on fairly steep slopes are usually more braided and less sinuous; they are classified as braided point-bar streams. Rivers in Region 4 exist on steep slopes, characterized by a highly braided but fairly straight channel pattern.

From the data of some Midwestern U.S. rivers, there appears to be a threshold for channel silt-clay content right above the boundary of Region 1. With an increase in slope across this line, the significant decrease in silt-clay content is associated with distinct increase in channel width and decreases in depth and meander sinuosity for such

natural rivers.

ACKNOWLEDGEMENTS

This paper is a part of the research on mathematical modelling of alluvial rivers sponsored by the National Science Foundation under Grant No. CEE-8209029.

APPENDIX I - REFERENCES

1. Ackers, P., and Charlton, F.G., "The Geometry of Small Meandering Channels," Proc. Inst. Civil Engineers, Paper 73285, 1970, pp. 289-317.

2. Brice, J.C., and Blodgett, J.C., "Countermeasures for Hydraulic Problems at Bridges, Vol. 1, Analysis and Assessment," Federal Highway Administration, Washington, D.C., Rept. No. FHWA-RD-78-162, 1978, 169 pp.

3. Chang, H.H., "Minimum Stream Power and River Channel Patterns," Journal of Hydrology, Vol. 41, Elsevier Scientific Publishing Co., Amsterdam, Netherlands, 1979, pp. 303-327.

4. Chang, H.H., "Stable Alluvial Canal Design," Journal of the Hydraulics Division, ASCE, Vol. 105, No. HY5, Proc. Paper 15420, May 1980, pp. 873-891.

5. Chang, H.H., "A Mathematical Model for Erodible Channels," Journal of the Hydraulics Division, ASCE, Vol. 108, No. HY5, Proc. Paper 17062, May 1982, pp. 678-689.

6. Chang, H.H., "Fluvial Hydraulics of Deltas and Alluvial Fans," Journal of the Hydraulics Division, ASCE, Vol. 108, No. HY11, November, 1982, pp. 1282-1295.

7. Chang, H.H., "Energy Expenditure in Curved Open Channels," Journal of Hydraulic Engineering, ASCE, Vol. 109, No. 7, July, 1983, pp. 1012-1022.

8. Chang, H.H., "Analysis of River Meanders," Journal of Hydraulic Engineering, ASCE, Vol. 109, No. 12, December, 1983, (in press).

9. Cherkauer, D.S., "Minimization of Power Expenditure in a Riffle-Pool Alluvial Channel," Water Resources Research, Vol. 9, No. 6, December, 1973, pp. 1613-1628.

10. Chitale, S.V., "Theories and Relationships of River Channel Patterns," Journal of Hydrology, Vol. 19, 1973, pp. 285-308.

11. Friedkin, J.F., "A Laboratory Study of the Meandering of Alluvial Rivers," U.S. Waterways Experiment Station, Vicksburg, Miss., May 1945, 43 pp.

12. Henderson, F.M., Open Channel Flow, The Macmillan Company, New York, 1966, 522 pp.

13. Kennedy, J.F., and Brooks, N.H., "Laboratory Study of Alluvial Streams at Constant Discharge," Proceedings, Federal Interagency Sedimentation Conference, Miscellaneous Publication No. 970, Agricultural Research Service, 1963, pp. 320-330.

14. Lane, E.W., "A Study of the Shape of Channels formed by Natural Streams Flowing in Erodible Material," U.S. Army Eng. Division, Missouri River, Corps of Engineers, Omaha, Nebraska, M.R.D. Sediment Series No. 9, 1957.

15. Leopold, L.B., and Maddock, T., "The Hydraulic Geometry of Stream Channels and Physiographic Implications," USGS Professional Paper 252, 1953, 57pp.

16. Leopold, L.B., and Wolman, M.G., "River Channel Patterns: Braided, Meandering and Straight," USGS Professional Paper 282-B, 1957, pp. 45-62.

17. Leopold, L.B., Wolman, M.G., and Miller, J.P., Fluvial Processes in Geomorphology, W.H. Freeman and Co., San Francisco, 1964, 522 pp.

18. Mackin, J.H., "Concept of the Graded River," Geological Society of America Bulletin, Vol. 59, May, 1948, pp. 463-512.

19. Odgaard, A.J., "Transverse Bed Slope in Alluvial Channel Bends," Jouranl of the Hydraulics Division, ASCE, Vol. 107, No. HY12, December, 1981, pp. 1677-94.

20. Onishi, Y., Jain, S.C., and Kennedy, J.F., "Effects of Meandering in Alluvial Streams," Journal of the Hydraulics Division, ASCE, Vol. 107, No. HY7, Proc. Paper 12248, July, 1976, pp. 899-917.

21. Parker, G., "On the Cause and Characteristic Scales of Meandering and Braiding in Rivers," Journal of Fluid Mechanics, Vol. 76, Part 3, 1976, pp. 457-480.

22. Personal communication with D.A. Twogood, Imperial Irrigation District, El Centro, Calif.

23. Punjab Irrigation Research Institute, "Report for the Year Ending April 1941," Lahore, Punjab, Superintendent of Government Printing, 1943, 234 pp.

24. Richards, K.S., "Channel Width and Riffle-Pool Sequence," Geological Society of America Bulletin, Vol. 87, June 1976, pp. 883-890.

25. Rozovskii, I.L., "Flow of Water in Bends of Open Channels," Israel Program for Scientific Translations, Jerusalem, Israel, 1961 (available from Office of Technical Services, U.S. Department of Commerce, Washington, D.C., PST Catalog No. 363, OTS 60-51133).

26. Schumm, S.A., "The Shape of Alluvial Channels in Relation to Sediment Type," USGS Professional Paper 352B, 1960, pp. 17-30.

27. Schumm, S.A., "Sinuosity of Alluvial Rivers on the Great Plains," Geological Society of America Bulletin, Vol. 74, September, 1963, pp.1089-1100.

28. Schumm, S.A., "River Adjustments to Altered Hydrologic Regimen-Murrumbidgee River and Paleochannels, Australia," U.S. Geological Survey Professional Paper 598, 1968, 65 pp.

29. Schumm, S.A., and Khan, H.R., "Experimental Study of Channel Patterns," Geological Society of America Bulletin, Vol. 83, 1972, pp. 1755-1770.

30. Schumm, S.A., "Geomorphic Thresholds and Complex Response of Drainage Systems," in Fluvial Geomorphology, Morisawa, M., Editor, State University of New York, Binghamton, New York, 1974, pp. 299-310.

31. Schumm, S.A., The Fluvial System, John Wiley and Sons, New York, N.Y., 1977, 338 pp.

32. Sedimentation Engineering, Manual No. 54, ASCE, 1975.

33. Simons, D.B., and Albertson, M.L., "Uniform Water-Conveyance Channels in Alluvial Material," Journal of the Hydraulics Division, ASCE, Vol. 86, No. HY5, Proc. Paper 2484, May, 1960, pp.33-71.

34. Simons, D.B., and Richardson, E.V., "Resistance to Flow in Alluvial Channels," U.S. Geological Survey Professional Paper 422-J, 1966.

35. Yang, C.T., and Song, C.S., "Theory of Minimum Rate of Energy Dissipation," Journal of the Hydraulics Division, ASCE, Vol. 105, No. HY7, Proc. Paper 14677, July, 1979, pp. 769-784.

APPENDIX II. - NOTATION

The following symbols are used in this paper:

B = surface width or effective width of channel in feet;

D = flow depth at center of channel, also average center depth of channel reach in feet;

d = median size of bed sediment in mm;

n = Manning's coefficient;

Q = bankfull discharge in cfs;

Q_s = bedload discharge in cfs;

r_c = center radius of curvature in feet;

S = slope or energy gradient;

S' = longitudinal energy gradient;

S'' = transverse energy gradient;

S_1 = slope or energy gradient at Min. 1;

S_2 = slope or energy gradient at Min. 2;

S_c = slope for incipient bedload;

S_t = transverse bed slope;

V = mean velocity of cross section in fps;

z = bank slope of channel as defined in Fig. 2; and

γ = specific weight of water.

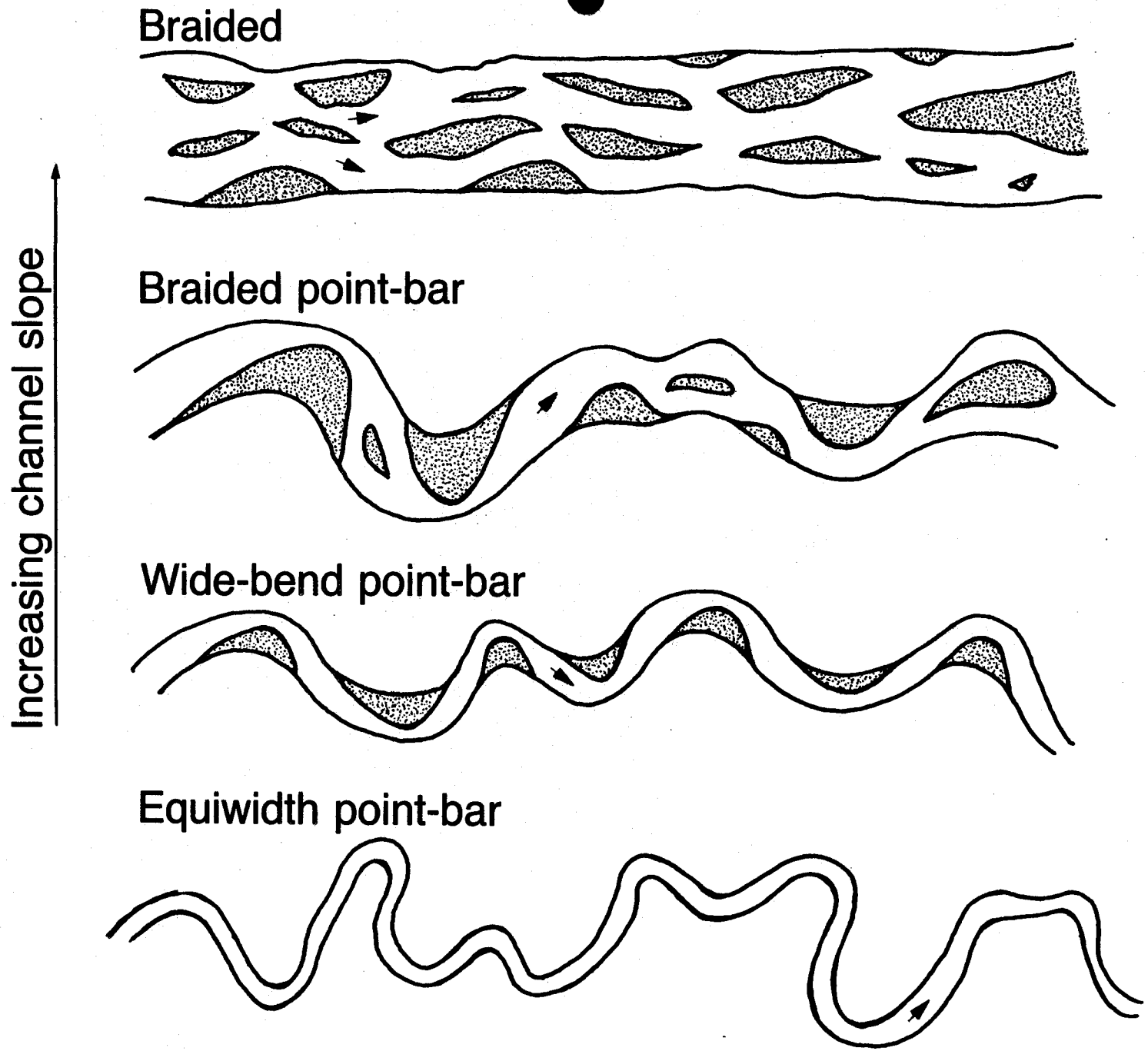

Figure 1. Classification of channel types [after Brice and Blodgett(2)]

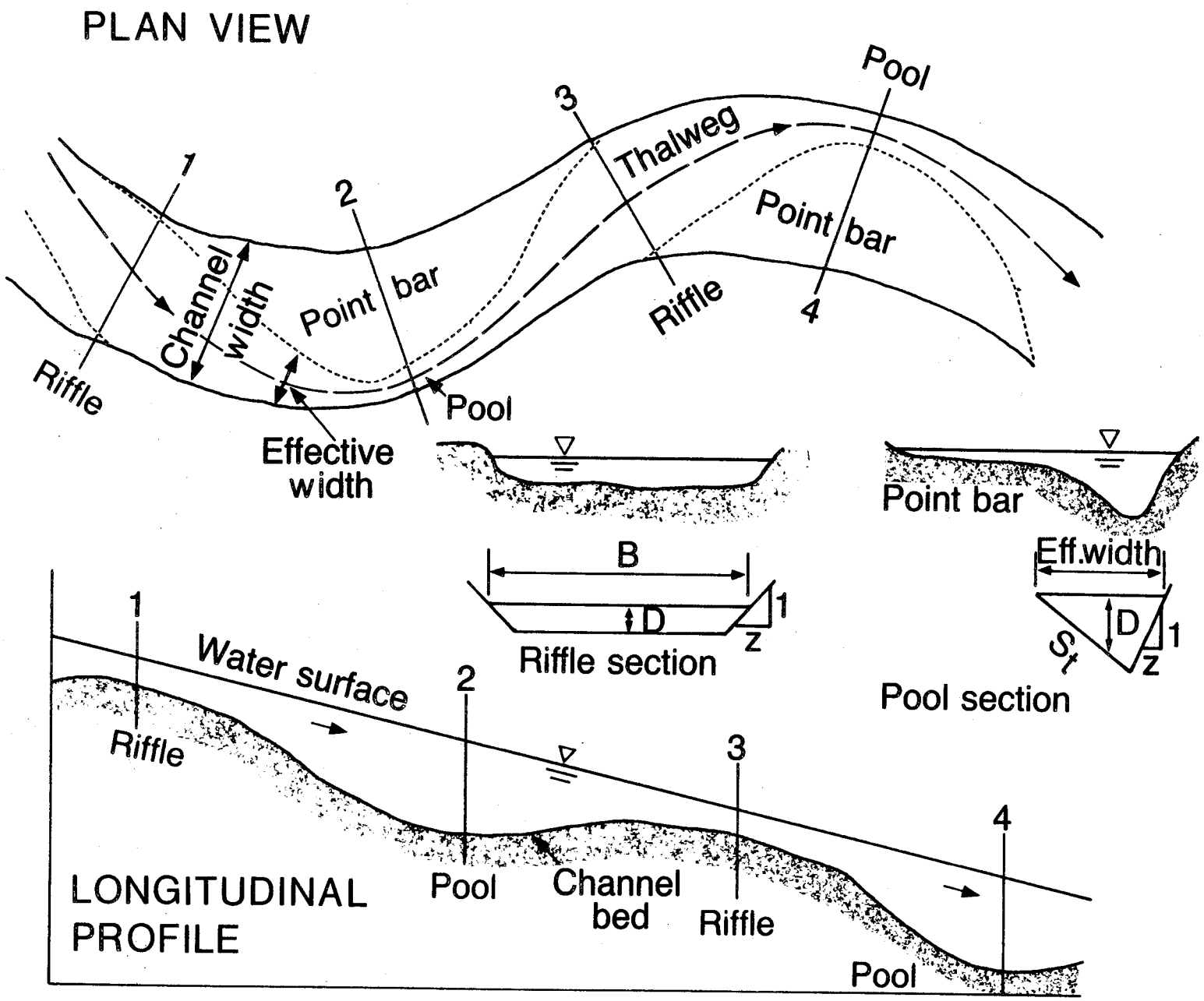

Figure 2. Schematic drawing of wide-bend point-bar stream

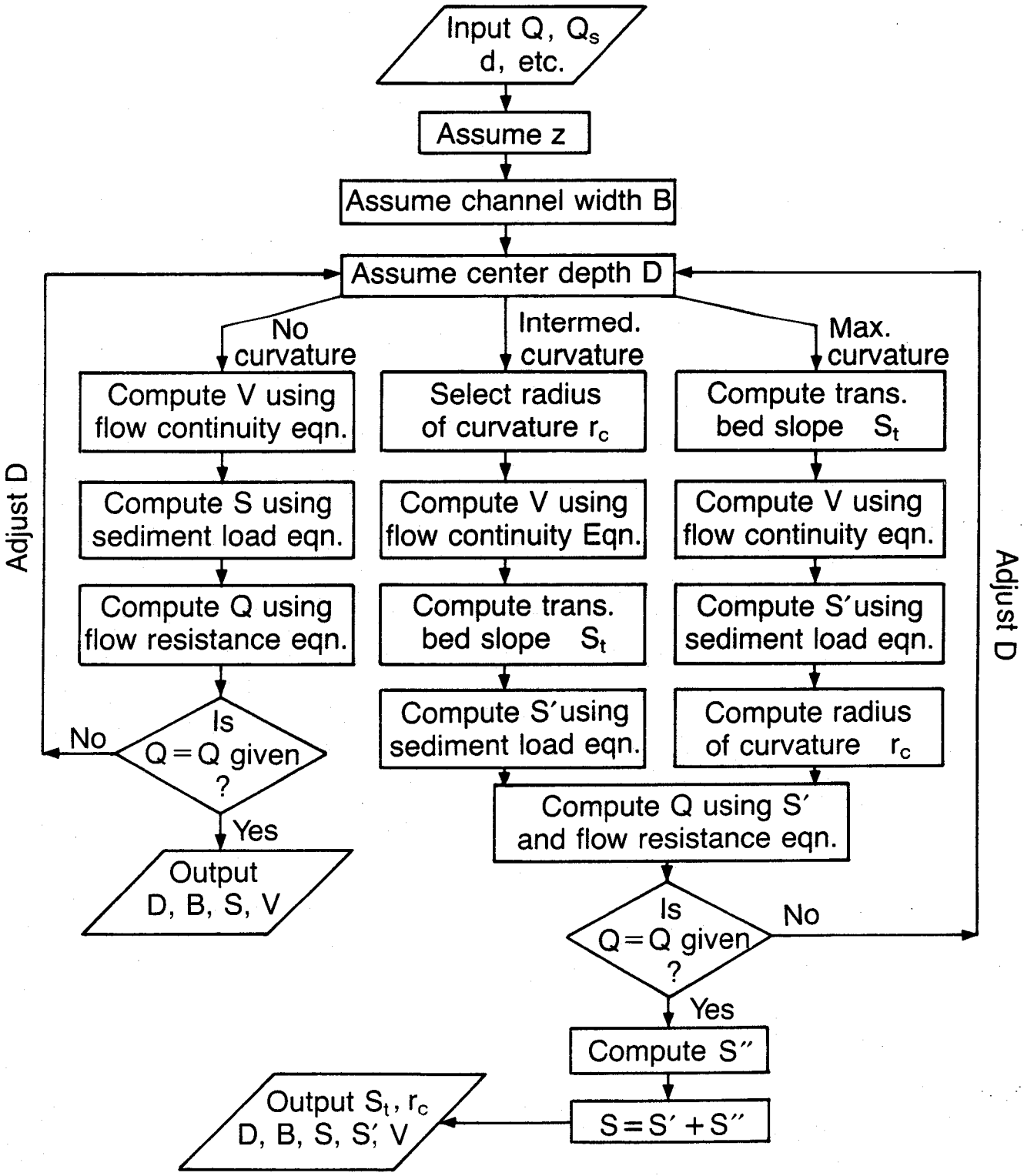

Figure 3. Flow diagram showing major steps of computation

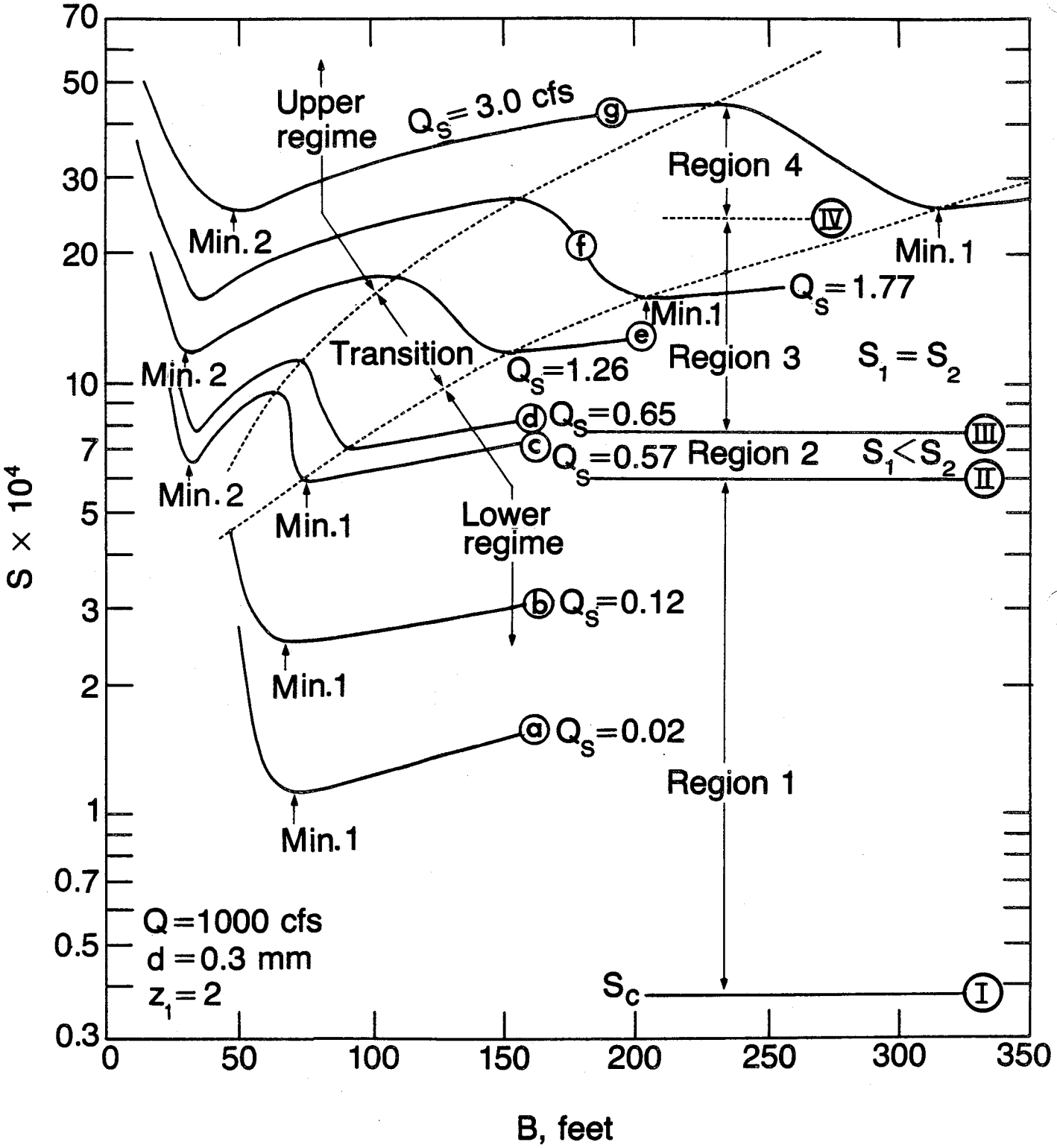

Figure 4. Stream power diagrams

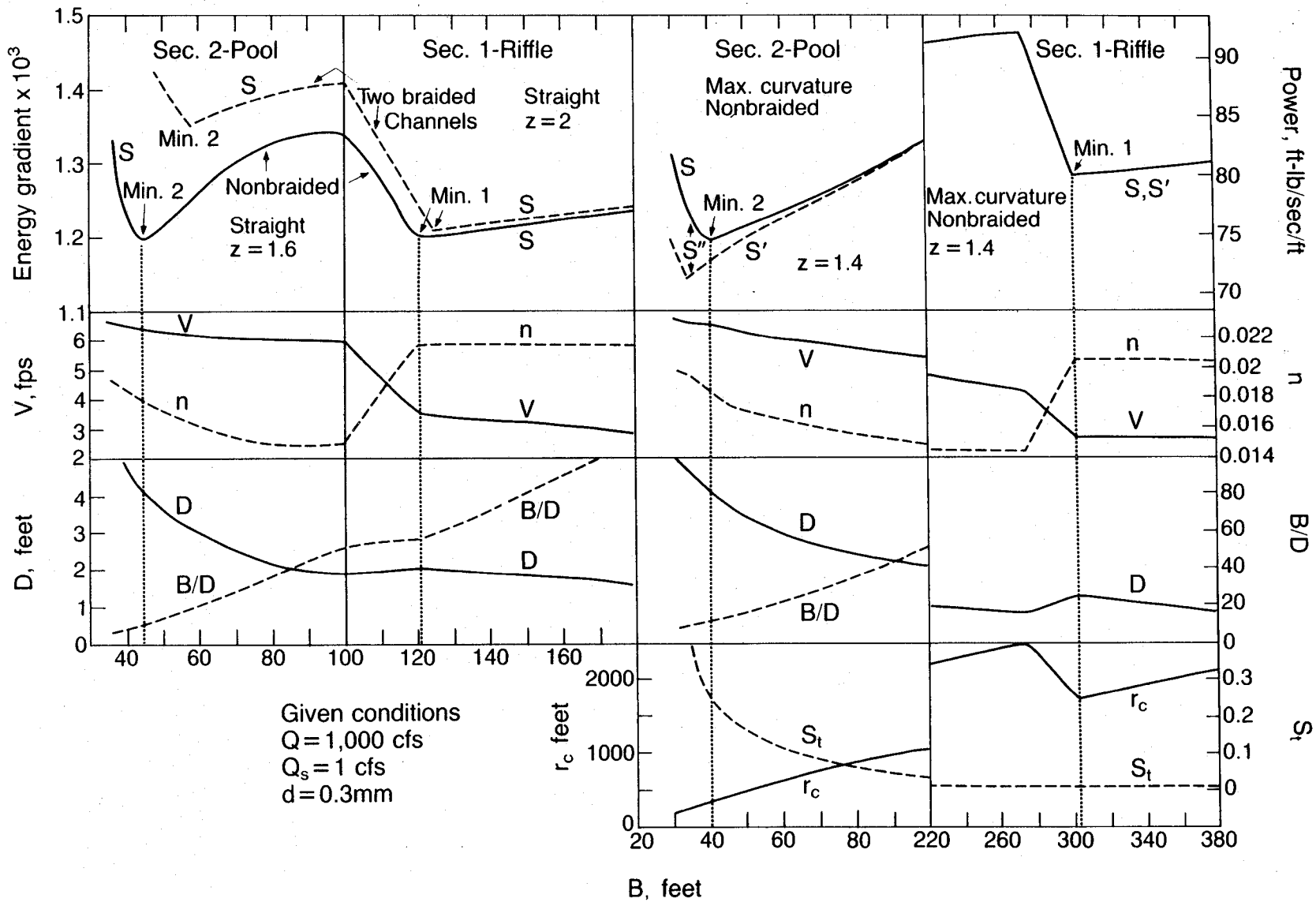

Figure 5. Variations of computed variables with channel width or effective width

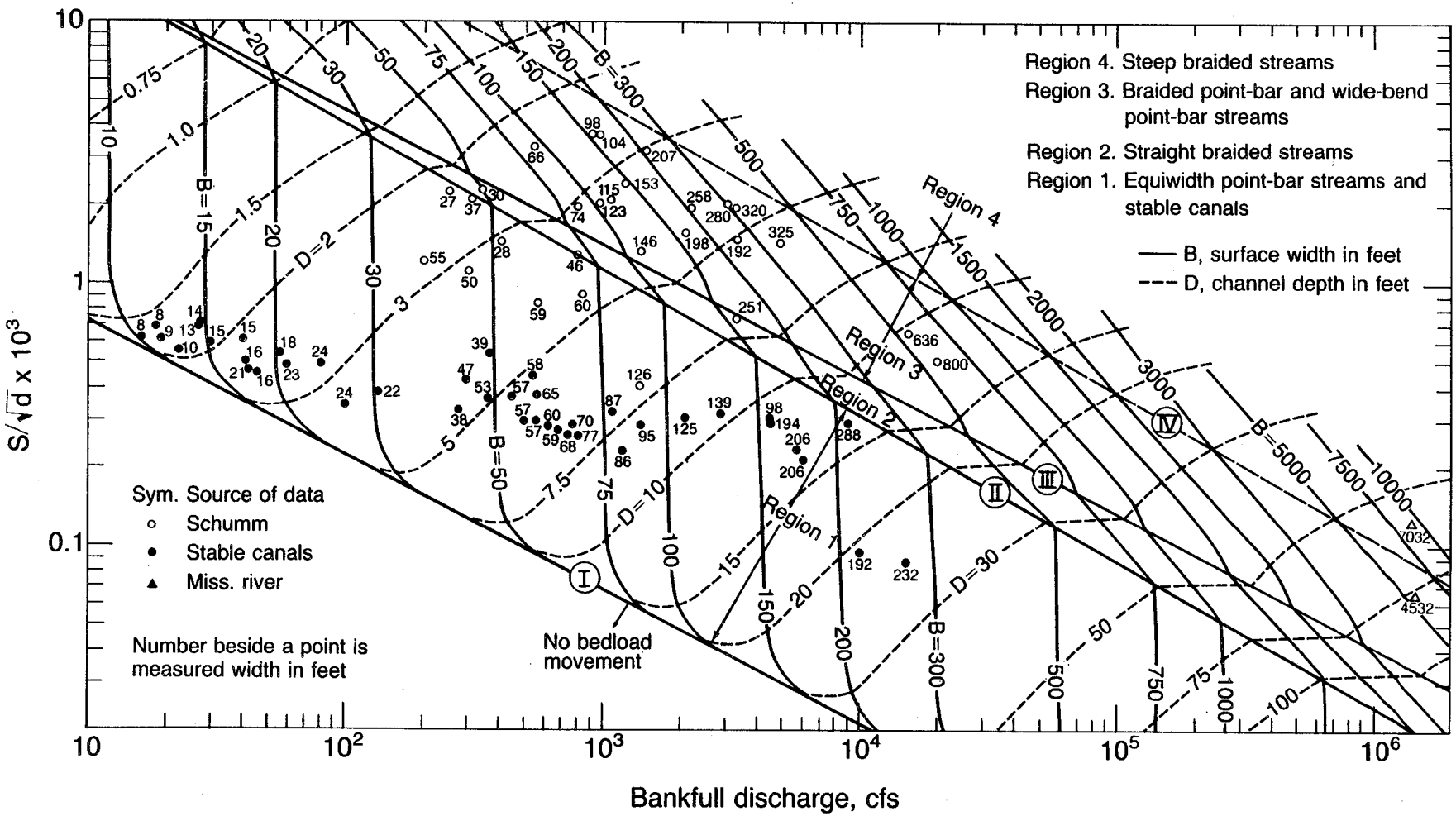

Figure 6. Regime channel geometry for sand-bed rivers

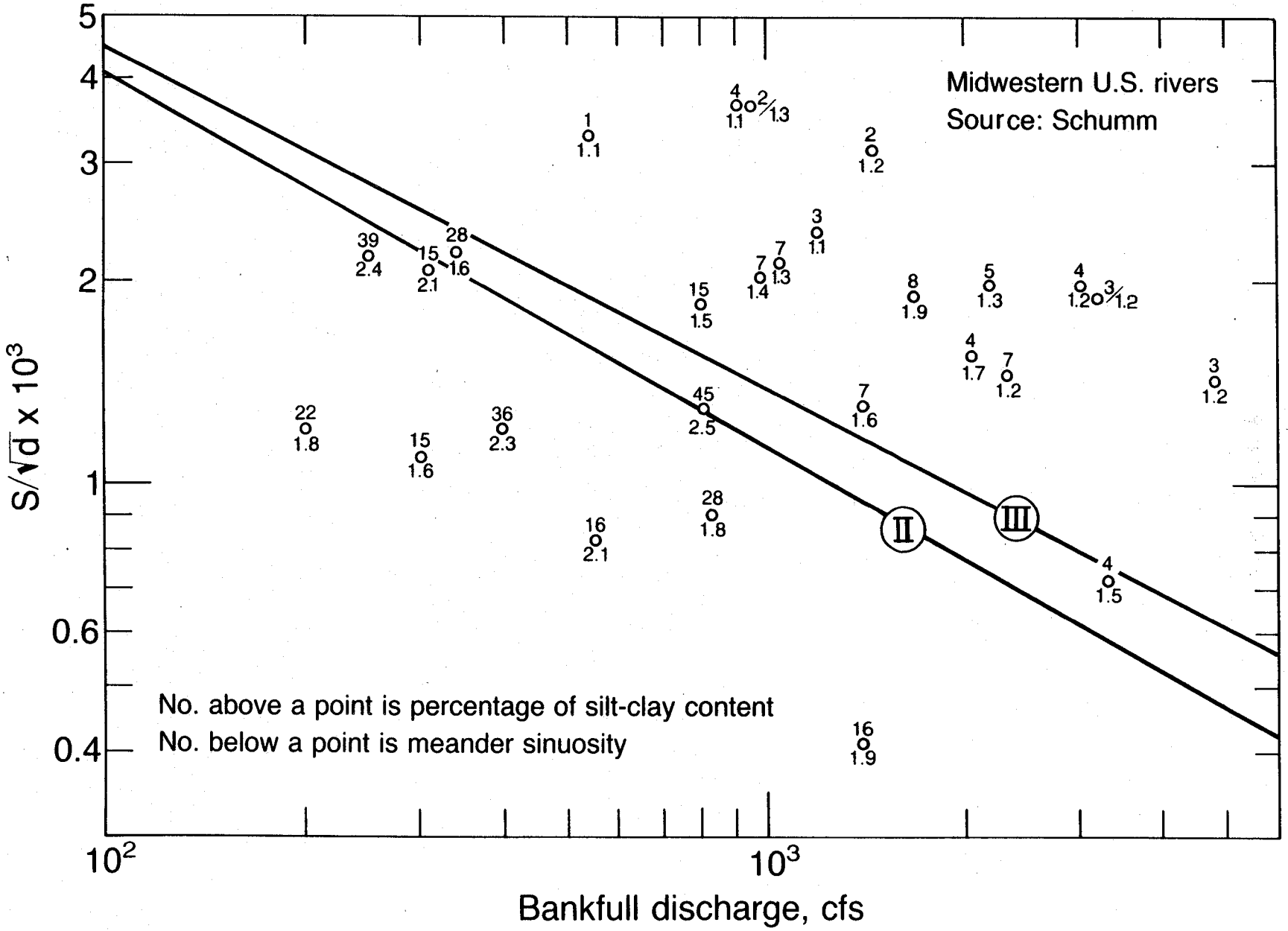

Figure 7. Variations of channel silt-clay content and meander sinuosity near Thresholds II and III

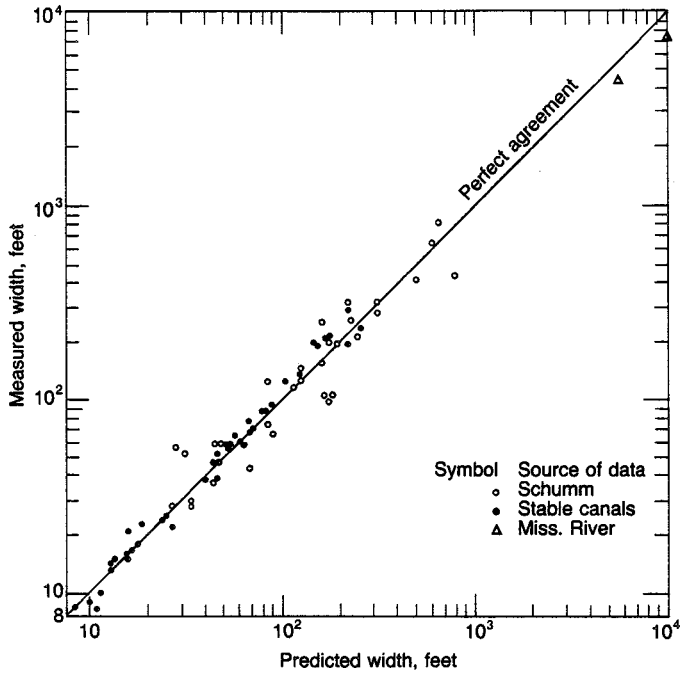

Figure 8. Comparison of predicted and measured widths

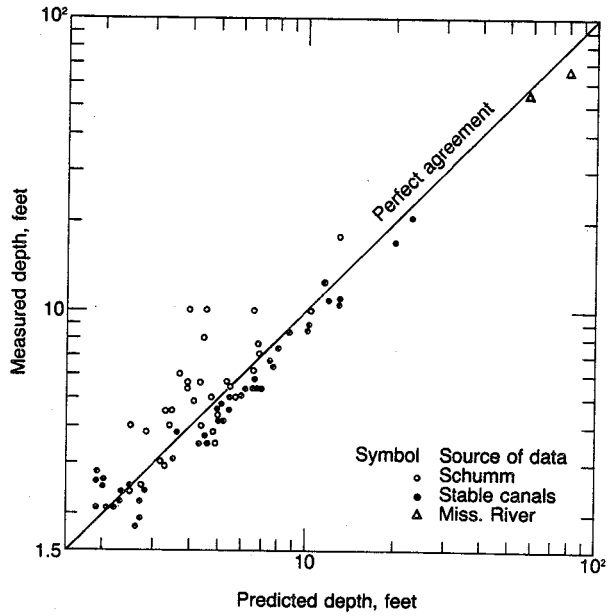

Figure 9. Comparison of predicted and measured depths

A MATHEMATICAL MODEL FOR ERODIBLE CHANNELS

by Howard H. Chang,[1] M. ASCE

INTRODUCTION

Natural streams are self-regulatory in that they adjust their characteristics in response to any change in the environment. These environmental changes may occur naturally or may be results of such human activities as development, sand mining, bridge and highway construction, and river regulation. Such changes distort the natural quasi-equilibrium of streams; in the process of restoring the equilibrium, either aggradation or degradation, or both, usually occur. Channel width variations usually occur in an aggrading or degrading stream. Generally speaking, a degrading stream tends to assume a narrower width while an aggrading stream tends to widen itself by flooding adjoining areas (4, 7, 8, 10). Many case histories of stream adjustment involving substantial width changes can be found in the literature (4, 7, 8, 10). Since changes in channel width and channel-bed elevation are closely interrelated, modeling of aggradation and degradation must also take width changes into account.

This paper presents a mathematical model which computes not only aggradation and degradation but also width changes for erodible channels with gradually varied unsteady flow. It represents an extension of existing models which consider only aggradation and degradation (3, 11). This model employs the techniques for water and sediment routing. To compute the width variation, an additional condition based upon a stream power approach is used. This approach has been applied as a width predictor for alluvial streams in the past (4, 5);

---

[1]Professor of Civil Engineering, San Diego State University, San Diego, Calif.

its application is extended herein to compute width changes at any number of cross-sections in a stream reach. While this model is applicable to alluvial streams with erodible bed and banks, physical constraints such as rigid banks, bedrock outcrops, check dams can also be specified as given conditions.

STREAM POWER APPLICATION

For a gradually varied flow, the total stream power or the rate of total energy expenditure of a stream reach is given as

$$P = \int_L \gamma Q S \, dx \tag{1}$$

in which P = total stream power in energy per time; L = reach length; γ = specific weight of flow; Q = discharge; S = energy gradient; and x = distance along the flow direction. The concept of minimum stream power for a gradually varied flow may be stated that the stream adjusts itself in such a way that its total stream power is minimized subject to certain physical constraints. With a never ceasing tendency to attain equilibrium, a stream with constant inflows of water and sediment will eventually establish its uniform flow. Under this situation, Equation 1 reduces to a constant as

$$P = \gamma Q \Delta H \tag{2}$$

in which ΔH = drop in elevation for the stream reach. It will be verified later that, in minimizing the total stream power, the adjustment in a stream with varied flow is toward that of a uniform flow. In addition, the stream power for a uniform flow represents an eventual minimum for the given conditions.

In the application of the concept of minimum stream power as a width predictor, a set of conditions are available for a reach defined by multiple cross-sections, that is

$$\frac{\partial P}{\partial B_i} = 0 \tag{3}$$

in which, B = channel width; i = the number of a cross-section counted from the upstream end. These conditions are equal in number to the cross-sections and hence sufficient to predict their respective width changes. However, the width of a section does not change freely; the rate of width change is usually subject to certain limitations and the extent of width change may be subject to certain physical constraints. In this model, the limitation for the rate of width change is related to the rate of sediment deposition or removal along the banks. Non-erodible portions of a cross-section, such as rigid banks, bedrock outcrops, abutments, etc., are treated as physical constraints.

ANALYTICAL DEVELOPMENT

This mathematical model has three major components: (1) water routing; (2) sediment routing; and (3) changes in channel width and bed profile. The third component, due to its length, will be described in a separate section. This model employs a space-time domain in which the space domain is represented by the discrete cross-sections along the reach and the time domain is represented by discrete time increments. In water routing, the time and spatial variations of the discharge and stage are obtained by an iterative procedure. Since the sediment movement and changes in channel geometry are slow in comparison to the flow velocity and changes in discharge and stage, they are corrected separately for each time increment. The components of water and sediment routing are described below:

Water Routing -- Basic equations for water routing include the continuity and momentum equation of flow, these are

$$\frac{\partial Q}{\partial x} + \frac{\partial A}{\partial t} - q = 0 \tag{4}$$

$$g\frac{\partial H}{\partial x} + \frac{1}{A}\frac{\partial Q}{\partial t} + \frac{1}{A}\frac{\partial}{\partial x}\left(\frac{Q^2}{A}\right) + gS - \frac{Q}{A^2}q = 0 \tag{5}$$

in which A = cross-sectional area of flow; t = time; q = lateral inflow rate per unit length; g = gravitational acceleration; H = stage or water surface elevation; and S = energy gradient computed using the Manning equation.

Equations 4 and 5 constitute a system of partial differential equations; they may be written as difference equations at a number of discrete points in the space-time domain. With the prescribed initial and boundary conditions, water discharge Q and stage H at each cross-section at an instant may be obtained as solutions of Equations 4 and 5. The time variations of Q and H along the reach may be obtained by an iterative procedure. This technique for water routing can be found in existing literature (1, 2, 4, 9).

Sediment Routing — The sediment routing component has two major features: (1) numerical solution of the continuity equation for sediment; and (2) computation of bed material load using a formula suitable for the physical conditions. Sediment routing is used to compute the change in channel boundary at a section for each time increment. This change may occur at the bed and/or the banks as described in the following sections.

Now, consider the continuity equation for sediment

$$(1 - \lambda) \frac{\partial A_c}{\partial t} + \frac{\partial Q_s}{\partial x} - q_s = 0 \tag{6}$$

in which, λ = porosity of bed material; A_c = cross-sectional area of channel bed within some arbitrary frame; Q_s = volumetric sediment rate; and q_s = lateral inflow rate of sediment per unit length. Using this equation, the correction in cross-sectional area of channel bed, ΔA_c, for a time increment can be written as

$$\Delta A_c = - \frac{\Delta t}{1-\lambda} \left(\frac{\partial Q_s}{\partial x} - q_s\right) \tag{7}$$

At a section i, the lateral sediment inflow may be written as

$$q_{s_i} = \frac{1}{2}\left(q^j_{s_i} + q^{j+1}_{s_i}\right)$$

in which the superscripts j and j + 1 designate the times at t and $t + \Delta t$ respectively. Using a backward difference in the x and a centered difference in t for the partial derivative $\partial Q_s/\partial x$ in Eq. 10 as suggested by Chang and Hill (3), one has

$$\left(\frac{\partial Q_s}{\partial x}\right)_i = \frac{1}{\Delta x_{i-1}}\left(\frac{Q^j_{s_i} + Q^{j+1}_{s_i}}{2} - \frac{Q^j_{s_{i-1}} + Q^{j+1}_{s_{i-1}}}{2}\right) \tag{8}$$

in which Δx_{i-1} = distance between Sections i-1 and i. With this relationship for $\partial Q_s/\partial x$ in Eq. 7, the change in cross-sectional area of channel bed at a section i depends on sediment rates at this section and its upstream section i-1; it is independent of the sediment rate at the downstream section. In other words, it is under upstream control. In contrast to this, the stage at a section in subcritical flow depends on the downstream stage and is independent of the upstream stage, i.e., the stage is under downstream control in a subcritical flow.

Different equations for sediment load may be used in the model. The selection of a suitable sediment equation depends on the physical conditions (12, 13).

CHANGES IN CHANNEL WIDTH AND BED PROFILE

The change in cross-sectional area ΔA_c obtained in water and sediment routing represents the correction for a time increment Δt that needs to be applied to the bed and banks. With ΔA_c being the total correction, it is possible for both the bed and banks to have deposition or erosion; it is also possible to have deposition along the banks but erosion in the bed and vice

versa. Generally speaking, deposition in the bed is often accompanied by channel widening while channel-bed erosion is usually associated with a reduction in channel width. These types of channel adjustment follow the path of minimum stream power toward the direction of new equilibrium for the reach.

The amount of sediment deposition or removal along the banks directly affects the width change. When the concept of minimum stream power is applied to predict the new widths, the width changes at all the cross-sections are such that the total stream power of the reach is minimized. However, these changes must be limited by the rate of sediment deposition or removal and other factors. For this reason, the limitations for width change need to be evaluated. These limitations define the maximum amounts of width adjustment for a time increment. Since the limitations for width adjustment are usually very small, the new width at each section may be obtained using a search procedure within its limitations.

Before describing the search procedure, the limitations for width adjustment are first described.

Limitations for Width Adjustment -- For a time increment, the maximum amount (the limitation) of width change depends on the sediment rate, the bank configuration and the rate of change in stage. The slope of an erodible bank is limited by the angle of repose of the material. For the same sediment rate, width adjustment at a tall bank is not as rapid as that at a low bank. The limitations for width adjustment for width increase and width decrease are somewhat different as described below separately.

An increase in width at a channel section depends on sediment removal from the bank areas and/or a change in stage. The maximum amount of widening occurs when sediment inflow from the upstream section does not reach the banks of this

section. Therefore, the limitation for bank retreat at a section can be obtained using the local sediment removal rate, the rate of stage variation and the bank configuration at this section, or

$$\Delta B_i = E_i(q_{b_i}, \frac{\Delta H_i}{\Delta t}, \text{bank configuration})\Delta t \tag{9}$$

in which ΔB = limitation for bank retreat for the time increment Δt; E = a function; and q_b = local sediment rate along the bank. The values of ΔB may be different for different banks at a section.

A decrease in channel width is accomplished by sediment deposition along the banks and/or a change in stage. For practical reasons, deposition does not exceed the stage in the model. The maximum amount (the limitation) of width reduction at a section occurs when sediment inflow from the upstream section $Q_{s_{i-1}}$, is spread out at this section and the sediment removal from the bank areas at this section is zero, that is

$$\Delta B_i' = E_i'(Q_{s_{i-1}}, \frac{\Delta H_i}{\Delta t}, \text{bank configuration})\Delta t \tag{10}$$

<u>Determination of New Channel Width</u> -- The channel width at time $t + \Delta t$ may be obtained using the width at time t and a search procedure such that the total stream power at $t + \Delta t$ is a minimum subject to the limitations and constraints described previously. Written in finite difference form, Equation 1 for total stream power becomes

$$P = \sum_{i=1}^{N-1} \frac{1}{2} \gamma (Q_i S_i + Q_{i+1} S_{i+1}) \Delta x_i \tag{11}$$

in which N = total number of cross-sections for the reach. Although width changes are subject to the limitations which are small for each Δt, it is still time consuming to search for the new widths that provide the minimum stream power. This is because, with the possibilities for either an increase or a decrease in width, different combinations of width changes at all sections need to be evaluated. However, this search procedure for new widths becomes greatly simplified after certain patterns for width adjustment have been discovered and applied in the model. It has been found, using the initial search procedure, that the total stream power of a reach is minimized if the widths are so adjusted that the variations in energy gradient among the adjacent sections are reduced. Also, an increase in width at a section usually causes an increase in its energy gradient but decreases in velocity and sediment load when the roughness coefficient remains unchanged. On the other hand, a decrease in width is usually associated with a decrease in energy gradient but increases in velicity and sediment load. For a subcritical flow, an increase in energy gradient at a section tends to decrease the energy gradient at its next upstream section and vice versa. Its impact does not extend very far upstream for a small change in width.

Using these guidelines, a simplified search procedure for new widths has been developed. In this procedure, the minimum total stream power of the reach can be attained rapidly when the widths are so adjusted that the variations in energy gradient for adjacent sections are reduced using the following simple rule. For a section i, the weighted average energy gradient of its adjacent sections is

$$\bar{S}_i = \frac{S_{i-1}\Delta X_{i-1} + S_{i+1}\Delta X_i}{2(\Delta X_{i-1} + \Delta X_i)} \tag{12}$$

in which $\overline{S}_i$ = weighted average energy gradient. The actual energy gradient at Section i, S_i, is compared with the weighted average. If the actual energy gradient is higher, channel width at this section is reduced so as to decrease the energy gradient. On the other hand, if the actual energy gradient is lower, channel width is increased so as to increase the energy gradient. These changes are subject to the limitations for width adjustment and physical constraints described previously. If any adjustment in width reverses the energy gradient variation, it is reduced accordingly.

Change in Channel Bed Profile -- After the banks are adjusted, the remaining correction for ΔA_c needs to be applied to the bed. Erosion and deposition at a cross-section is not necessarily uniform. Generally speaking, deposition tends to be more uniformly distributed in that it tends to build up the channel bed in horizontal layers. This process of deposition is often accompanied by channel widening. On the other hand, channel-bed erosion tends to be more confined with greater erosion in the thalweg. This process is usually associated with a reduction in width. These types of channel adjustment follow the path of minimum stream power toward the direction of new equilibrium for the reach. In the model, deposition at an aggrading section is assumed to start from the lowest point and it is assumed to build up the channel bed in horizontal layers. For a degrading section, the change in area is distributed in proportion to the effective tractive force, $\tau - \tau_{cr}$, along the bed, where τ is the local tractive force and τ_{cr} is the critical tractive force.

MODEL DESCRIPTION

The mathematical model FLUVIAL-14 has been developed; its input data, computing procedures and output parameters are described below:

Input Data -- Input to the model include the initial cross-sections, channel roughness, Δt, sediment characteristics, inflow hydrograph, downstream stage-discharge relationship and physical constraints such as bedrock outcrops, check dams and rigid banks. The cross-sectional data are identical to the HEC-2 (14) input except that non-erodible parts of a cross-section are flagged.

Computing Procedures -- The following steps are outlined for the computing procedures:

1. Enter input data.

2. Evaluate initial flow conditions. The standard-step method for water surface computation is used.

3. Set $t = t + \Delta t$.

4. Evaluate new flow conditions by solving simultaneous equations for water routing.

5. Determine changes in cross-sectional area of channel bed using sediment routing equations.

6. Compute changes in channel widths so that the total stream power is minimized subject to the limitations for width change and physical constraints

7. Obtain new bed profiles at all sections.

After step 7, the computation returns to Step 3 for another time step. The iteration continues until the required time period is covered.

Output Parameters -- These parameters may be requested for any selected time interval during the flow period, including the stage, discharge, width, depth, sediment discharge, energy gradient, Froude number and cross-sectional profile for each of the cross-sections.

CASE STUDY

Physical Changes -- Significant changes in channel width and bed profile occurred in the San Diego River near Highway 67 in Lakeside, California, during the March 1978 flood (see Figures 1 and 4). These changes have been documented by the County of San Diego and the California Department of Transportation. The natural channel configuration had been altered primarily by sand mining before the flood. The two large borrow pits created on each side of the bridge left a sand ridge between them. The river-bed profile including the borrow pits and the sand ridge is shown in Figures 4a and 4b. The downstream borrow pit, with an average width of 350 feet at the bottom, is between Secs. 72 and 79. The upstream borrow pit, shaped like an inverted cone, is between Secs. 80 and 82.

A gully was cut through the sand ridge as shown in Figure 2 by a small flood in February 1978; it was subsequently backfilled in order to protect the bridge footings. The sequence of events during the March 1978 flood can be separated into four phases as described below:

Phase 1. At the beginning of the flood, the sand ridge acted as a dam, ponding water and sediment in the upstream channel and borrow pit.

Phase 2. After overtopping, the sand ridge was eroded in the shape of a deep narrow gully similar to that shown in Figure 2. The backwater effect of the sand ridge continued to pond water in the upstream borrow pit. The spatial variation of channel width was uneven due to the narrow

gully and the resulting backwater effect. Considerable aggradation occurred in the borrow pits.

Phase 3. As the flood flow continued through the sand ridge, significant changes took place. The initial narrow and deep gully through the ridge was replaced by a wider and shallower section. While aggradation continued in the borrow pits, degradation also developed in certain parts of the upstream channel.

Phase 4. As the flood flow receded, the initially uneven channel profile was replaced by a smoother profile as shown in Figure 1.

Simulated Results — The mathematical model FLUVIAL-14 was employed to simulate the changes in this reach of the San Diego River during the March 1978 flood. The hydrograph established by the County of San Diego is shown in Figure 3(6). A total of 16 cross-sections, as shown in Figure 4, were employed to represent the river-bed geometry. Roughness in terms of Manning's n was found to be 0.03 in the channel based upon several measurements; it was estimated to be 0.035 at the bridge crossing. The bed material consisted of sand with a median diameter of 0.8 mm; its size showed no significant change before and after the flood. Graf's equation for sediment load was used in the model. The 35 hour flood was computed using 1200 time increments.

Simulated results using the mathematical model are presented in Figures 4 and 5. Time and spatial variations of the width, bed elevation, water-surface elevation, velocity, energy gradient, and sediment load along the reach are shown in Figure 4; cross-sectional profiles and flood stages for the channel at the H-67 bridge crossing (Sec. 79) are shown in Figure 5. Measurements of the channel-bed made after the flood are also plotted for comparison with the simulated results.

Changes at the bridge crossing as shown in these figures are characterized by the initial gully formation through the sand ridge and its gradual widening. The maximum depth of channel-bed scour is predicted to occur in the initial gully followed by gradual widening and a decrease in scour depth.

Changes in the width of flow as shown in Figure 4a are characterized by a rather uneven initial width variation along the reach followed by the gradual formation of a smoother channel. Since the initial width of flow through the gully between Secs. 79 and 80 is confined, it also causes a higher stage and a wider channel in its upstream sections. This backwater effect is gradually relieved with the removal of the sand ridge.

Changes in the channel-bed profile as shown in Figure 4b may be described by degradation at higher grounds and aggradation in the borrow pits. The initial uneven variation along the channel-bed is gradually reduced to form a smooth profile during the flood. Changes in the velocity, energy gradient, and sediment load as shown respectively in Figures 4d, 4e, and 4f follow the same pattern in that their initial uneven variations are gradually reduced during the flood. During the initial interval, the high velocity and sediment load occur in the gully through the sand ridge.

The channel changes are rapid during the initial interval and then slow down gradually. With sufficient flow duration, a stream will eventually establish a new equilibrium with a more or less uniform flow.

SUMMARY AND CONCLUSIONS

A mathematical model for predicting morphological changes of erodible channels has been formulated, developed and tested with field data. A significant feature of the model is its ability to account for changes in both

channel width and channel-bed profile of aggrading and degrading streams. This model employs the techniques for water and sediment routing; an additional condition based upon the concept of minimum stream power is used as the width predictor.

Analysis using the model shows that the total stream power of a reach is reduced if the widths at all cross-sections are so adjusted as to reduce the variation in energy gradients at these sections. When this model is applied, a varied flow will eventually develop into a uniform flow for which the stream power is an eventual minimum. The model as substantiated with field data provides a verification of the concept of minimum stream power as a physical principle governing the morphology of alluvial streams. It also provides a basic understanding of the adjustment of streams in response to various hydraulic and environmental parameters. Such understanding is of fundamental importance in river control and channel design.

ACKNOWLEDGMENTS

The writer wishes to thank P.E. Johnson, J.C. Hill, and V.M. Ponce for their suggestions on the manuscript.

APPENDIX I. - REFERENCES

1. Amein, M., and Chu, H.L., "Implicit Numerical Modeling for Unsteady Flows," Journal of the Hydraulics Division, ASCE, Vol. 101, No. HY6, June, 1975, pp. 717-732.
2. Amein, M., and Fang, C.S., "Implicit Flood Routing in Natural Channels," Journal of the Hydraulics Division, ASCE, Vol. 96, No. HY12, December, 1970, pp. 2481-2500.

3. Chang, H.H., and Hill, J.C., "Computer Modeling of Erodible Flood Channels and Deltas," Journal of the Hydraulics Division, ASCE, Vol. 102, No. HY10, Proc. Paper 12485, October, 1976, pp. 1461-1477.

4. Chang, H.H., and Hill, J.C., "Minimum Stream Power for Rivers and Deltas," Journal of the Hydraulics Division, ASCE, Vol. 103, No. HY12, Proc. Paper 13394, Dec., 1977, pp. 1375-1389.

5. Chang, H.H., "Stable Alluvial Canal Design," Journal of the Hydraulics Division, ASCE, Vol. 106, No. HY5, Proc. Paper 15420, May, 1980, pp. 873-891.

6. "Lakeside Storm Report , March 5-6, 1978," Dept. of Sanitation and Flood Control, County of San Diego, 1978.

7. Lane, E.W., "A Study of the Shape of Channels Formed by Natural Streams Flowing in Erodible Material," United States Army Engineer Division, Missouri River, Corps of Engineers, Omaha, Neb., M.R.D. Sediment Series No. 9, 1957.

8. Leopold, L.B., Wolman, M.G., and Miller, J.P., Fluvial Processes in Geomorphology, W.H. Freeman and Co., San Francisco, Calif., 1964.

9. Ponce, V.M., Indlekofer, H., and Simons, D.B., "Convergence of Four-Point Implicit Water Wave Models," Journal of the Hydraulics Division, ASCE, Vol. 104, No. HY7, July, 1978.

10. Schumm, S.A., The Fluvial System, John Wiley and Sons, 1977.

11. Scour and Deposition in Rivers and Reservoirs," Hydrologic Engineering Center, U.S. Army Corps of Engineers, January, 1974.

12. Sedimentation Engineering, Manual No. 54, ASCE, 1975.

13. Simons, D.B., and Senturk, F., Sediment Transport Technology, Water Resources Publications, Ft. Collins, Colo., 1977.

14. "Water Surface Profiles, HEC-2," Hydrological Engineering Center, U.S. Army Corps of Engineers, Nov., 1976.

APPENDIX II - NOTATION

The following symbols are used in this paper:

A = cross-sectional area of flow;

A_c = channel cross-sectional area within reference frame;

B, B' = surface widths of channel;

E, E' = functions;

g = gravitational acceleration;

H = stage or water-surface elevation;

i = number of cross-section counted from upstream to downstream;

j = time t;

$j+i$ = time $t + \Delta t$;

L = length of stream reach;

N = total number of cross-sections for stream reach;

n = Manning's roughness coefficient;

P = total stream power of river reach;

Q = flow discharge;

q = discharge of lateral inflow;

Q_s = sediment discharge at cross-section;

q_b = sediment discharge per unit channel width;

q_s = lateral inflow of sediment;

S = energy gradient;

t = time;

x = distance along flow direction;

γ = specific weight of flow;

λ = porosity;

τ = tractive force

τ_{cr} = critical tractive force

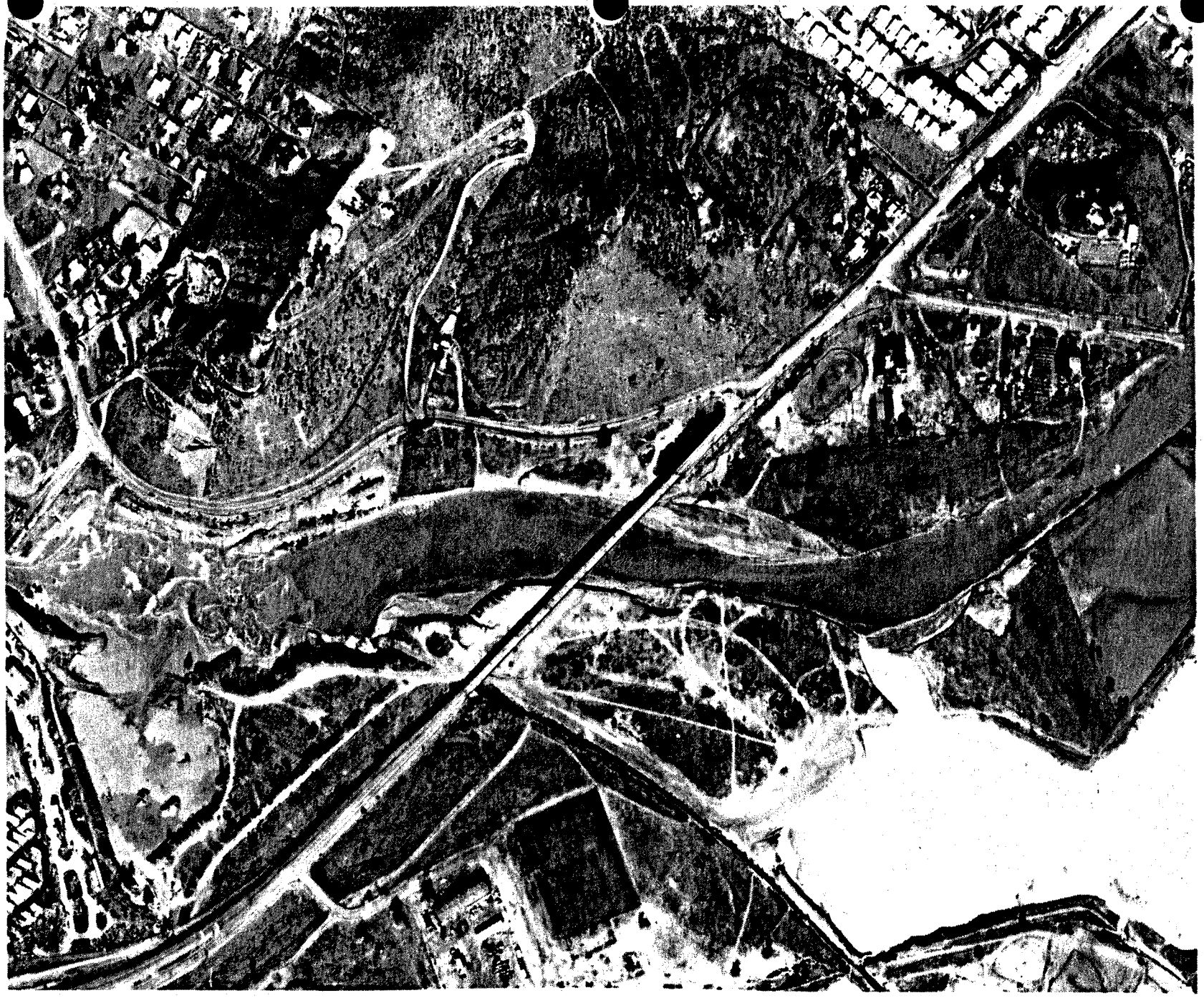

Figure 1. Aerial view of the River when flood was receding

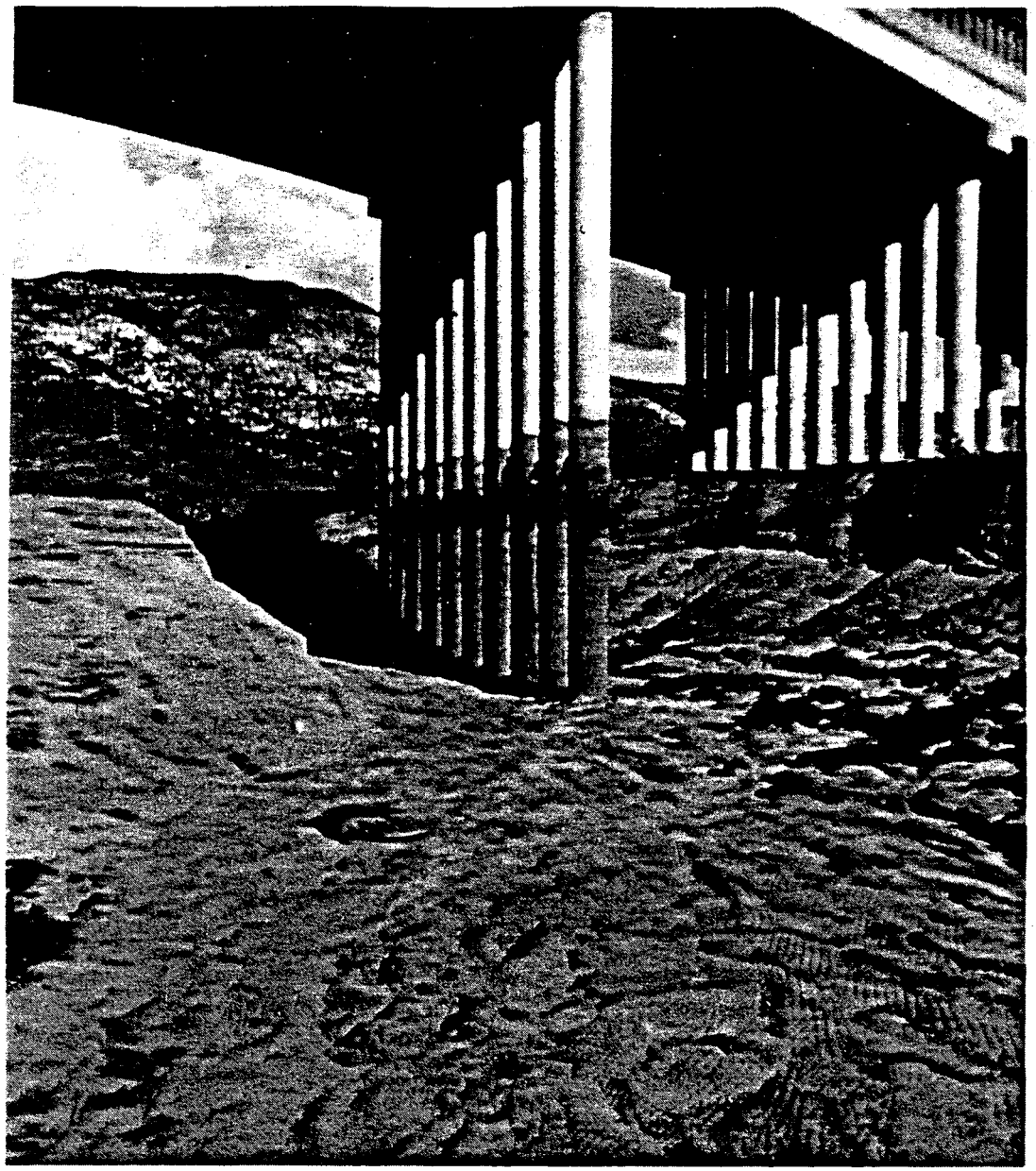

Figure 2. Gully formation through the sand ridge at H-67 bridge crossing. This gully was formed by a small flood in February, 1978. It was backfilled before the March 1978 flood.

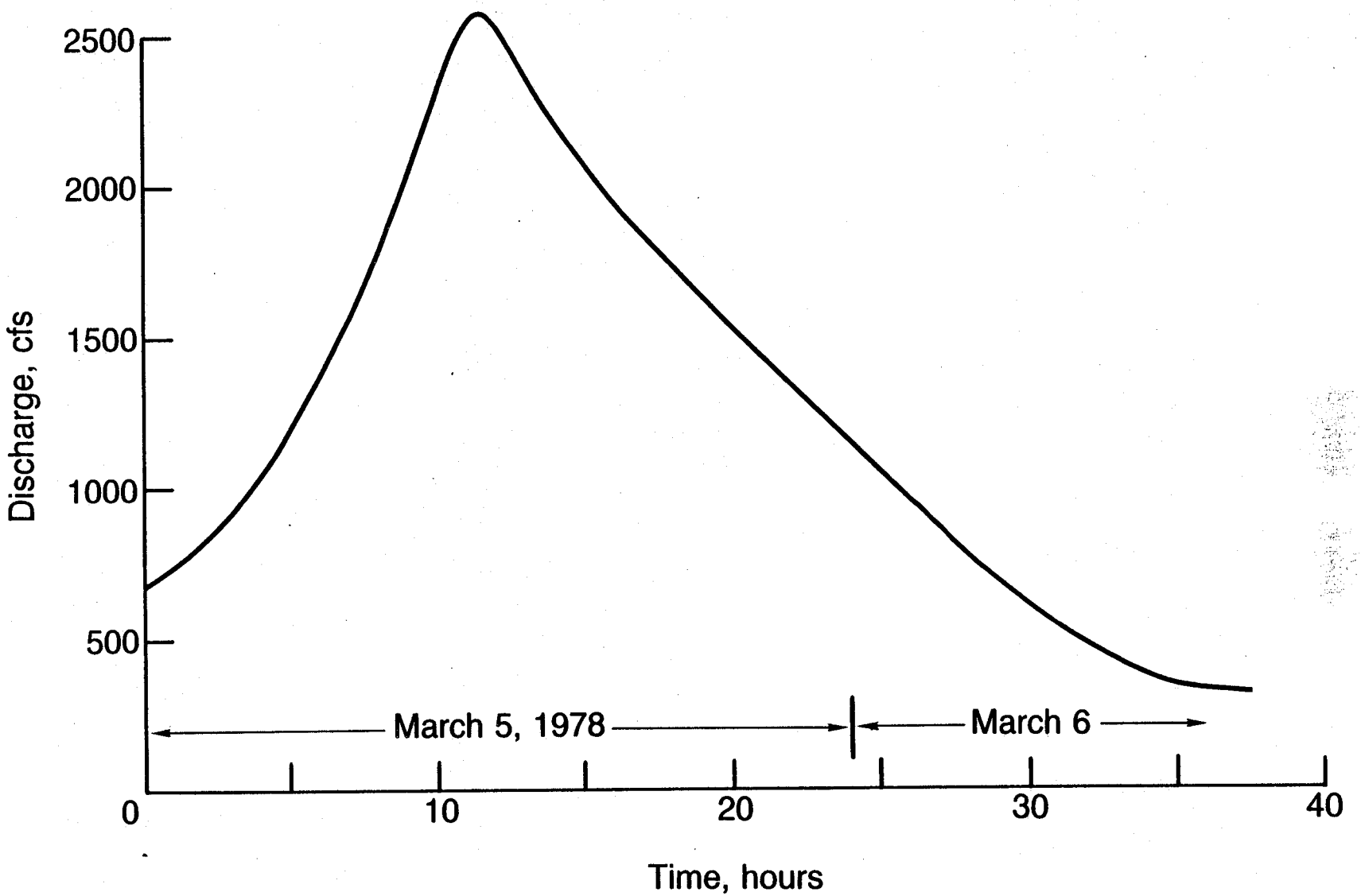

Figure 3. Hydrograph of March 1978 flood

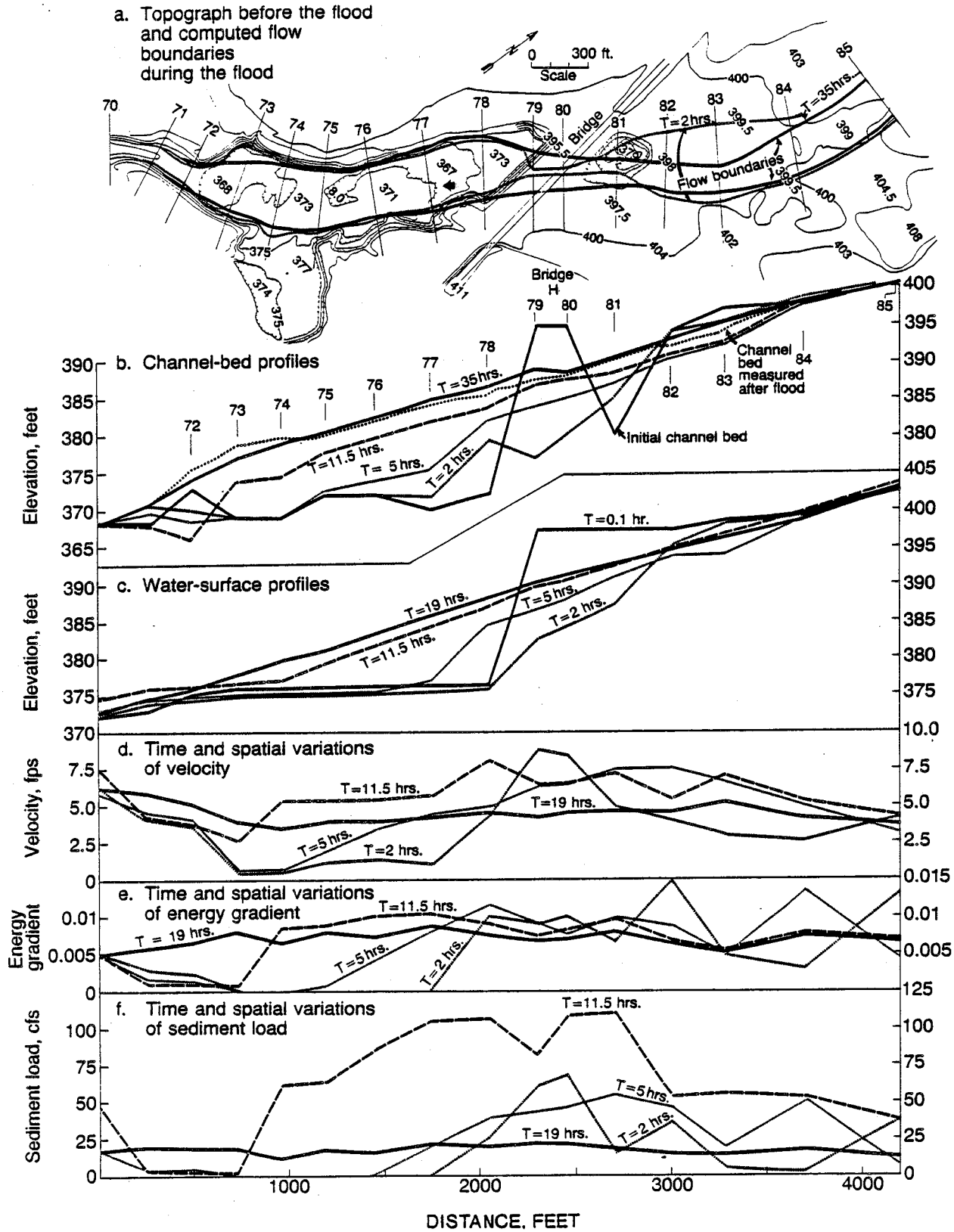

Figure 4. Computed and measured parameters

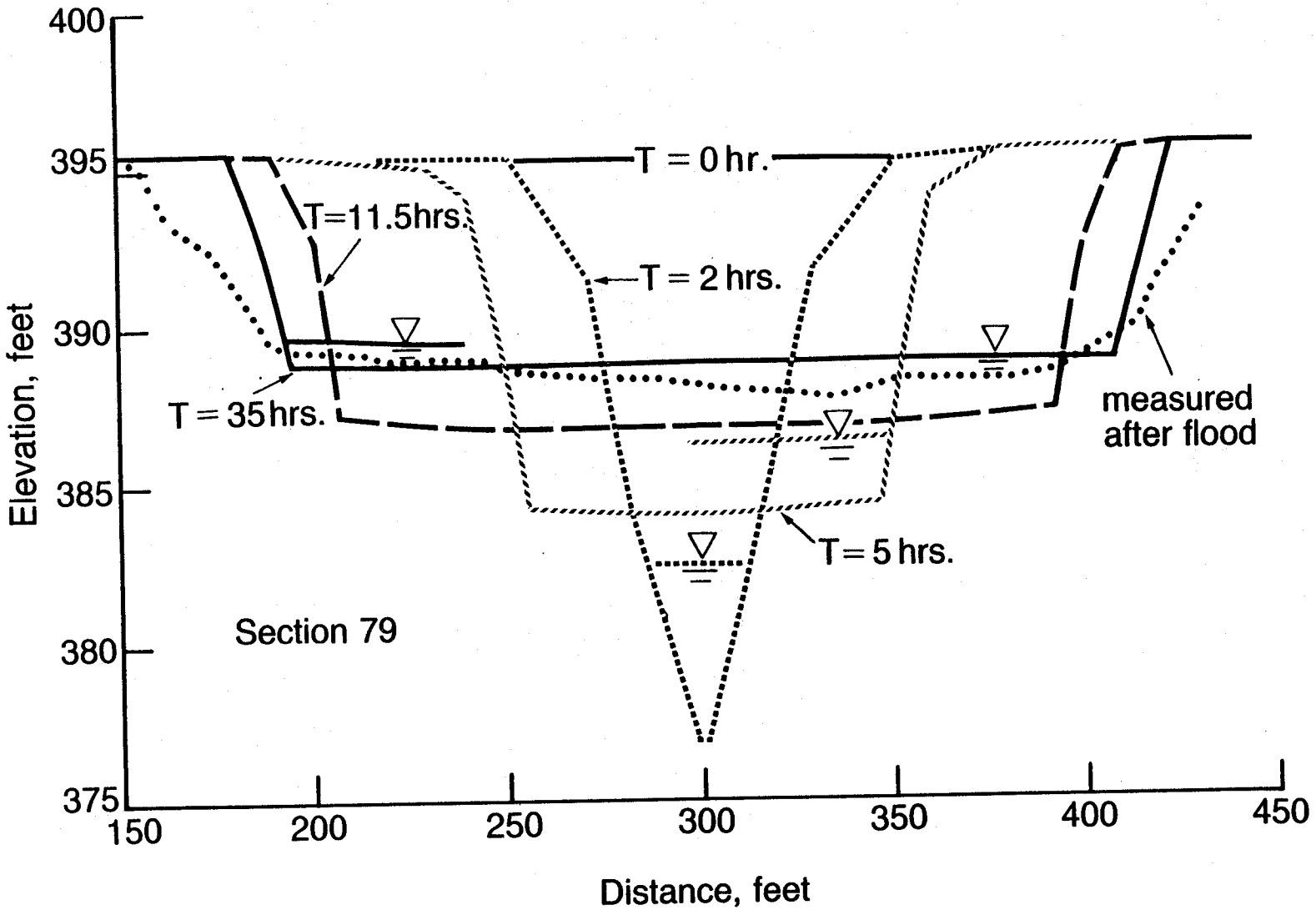

Figure 5. Cross-sectional profiles at different time intervals at H-67 bridge crossing

MODELLING RIVER-CHANNEL CHANGES USING ENERGY APPROACH

by Howard H. Chang,[1] Joseph C. Hill[2], M. ASCE

ABSTRACT

A computer-based flood- and sediment-routing model which simulates river-channel changes is described. As the change in channel width reflects the river's adjustment in resistance--that is, in energy expenditure; it is therefore simulated using the energy approach. This model has been applied to study river-channel changes of the San Dieguito River; predicted results using this model are supported by field measurements. Changes in channel widths, while closely interrelated to the changes in channel-bed elevation and other variables, reflect the river's tendency to seek equal power expenditure along the channel.

INTRODUCTION

River channel changes generally include channel-bed aggradation and degradation, width variation, and laterial migration in channel bends. These changes may occur naturally or as a result of a change in the environment. Man is also regarded as a geomorphic agent with certain activities such as sand and gravel mining, bridge construction, river control schemes, etc. having contributed to river channel changes. Langbein and Leopold maintain that the equilibrium channel represents a state of balance with a minimum rate of energy expenditure or an equal rate of energy expenditure along the channel (10). Changes induced by nature or men's activities distort the channel equilibrium and therefore result in river-channel changes.

The three types of river channel changes in channel-bed elevation, channel width, and lateral migration are closely interrelated to each other and may occur concurently. Changes in channel-bed elevation are often inseparable from width variation because a channel tends to become narrower during degradation, and it tends to widen during aggradation. Earlier versions of the FLUVIAL model have considered channel-bed aggradation and degradation (2,3,4) and width variation (3,4). The current version FLUVIAL-11 which simulates all three types of changes has been formulated, developed and applied in a case study. This paper describes this model and its application

---

[1] Professor of Civil Engineering, San Diego State University, San Diego, CA

[2] Principal Civil Engineering, County of San Diego

in the case study. Special attention is given to the lateral migration and to the nature of energy (or power) transformation in alluvial rivers associated with river-channel changes.

ANALYTICAL BACKGROUND

This mathematical model has five major components: 1) water routing; 2) sediment routing; 3) changes in channel width; 4) changes in channel-bed profile; and 5) lateral migration of the channel. This model employs a space-time domain in which the space domain is represented by the discrete cross-sections along the reach and the time domain is represented by discrete time steps. In water routing, the time and spatial variations of the discharge, stage, velocity, energy gradient, etc., along the reach are obtained by an iterative procedure. At each time step, sediment discharge at each cross-section is computed; changes in channel width, channel-bed profile and lateral migration are obtained and applied to each cross-section. The bed-material composition is updated at each time step. Since changes in channel geometry and bed-material composition are slow in comparison to water routing, corrections for them are made separately for each time step. The component on width changes is related to the energy expenditure as described below:

Changes in Channel Width--Simulation of width variation is based upon the concept of minimum stream power. At a time step, width corrections for all cross-sections are such that the total stream power (or rate of energy expenditure) for the reach is minimized; these corrections are subject to the physical constraint of rigid banks and limited by the amount of sediment removal or deposition along the banks within the time step. Total stream power of a channel reach is

$$P = \int_L \gamma Q S dx \qquad (1)$$

in which P = total stream power of the reach: L = length of the reach; Q = discharge; S = energy gradient; γ = specific weight of water and sediment mixture; and x = distance in the flow direction. Written in finite difference form, this equation becomes

$$P = \sum_{i=1}^{N-1} \frac{1}{2} \gamma (Q_i S_i + Q_{i+1} S_{i+1}) \Delta x_i \qquad (2)$$

in which N = total number of cross-sections for the reach; i = number of a cross-section; and Δx_i = distance between Sections i and i + 1. Previous studies have established that minimum stream power for an alluvial river is equivalent to equal power expenditure per unit channel length, that is, constant γQS along the reach (4,9,10). A river channel undergoing changes usually has uneven spatial distribution in power expenditure or γQS. Usually the spatial variation in Q is small but that in S is pronounced. Total stream power of a reach is reduced with the reduction in spatial variation in QS or S along the reach. Adjustments in channel widths are made in such a way that the spatial variation of QS is minimized subject to the constraints and limitations stated above. An adjustment in width

reflects the river's adjustment in flow resistance--that is, in power expenditure. A reduction in width at a cross-section is usually associated with a decrease in energy gradient for the section whereas an increase in width is accompanied by an increase in energy gradient. Using these guidelines, a technique for width correction has been developed as described in a previous publication (4).

Width changes in alluvial rivers are characterized by the formation of small widths at degrading reaches and widening at aggrading reaches (3,4,7,9,10,11). This type of width formation represents the river's adjustment in resistance to seek equal power expenditure along its course. A degrading reach usually has a higher channel-bed elevation and energy gradient than its adjacent sections. Formation of a narrower and deeper channel at the degrading reach decreases its energy gradient due to reduced boundary resistance. On the other hand, an aggrading reach is usually lower in channel-bed elevation and energy gradient. Widening at the aggrading reach increases its energy gradient due to increased boundary resistance. These adjustments in channel width reduce the spatial variation in energy gradient and total power expenditure of the channel. Since the sediment discharge is proportional to the stream power (1), these adjustments favor the establishment of channel's equilibrium.

A CASE HISTORY OF RIVER CHANNEL CHANGES

The San Dieguito River at Rancho Santa Fe, California, experienced significant changes in a two-mile reach (see Figure 1) during recent floods. Documentation of river channel changes and flood hydrographs were made by the County of San Diego (5,12), providing a valuable set of field data for river studies.

Physical Conditions -- The study reach is about four miles from the ocean and about five miles below Lake Hodges Dam. The channel has a wide and flat natural configuration; the natural slope and bed-material size decrease significantly in the downstream direction. Bed material of the study reach varies from coarse sand (d_{50} = 0.85 mm) at the upstream end to find sand (d_{50} = 0.24 mm) downstream.

The natural channel configuration was distorted prior to recent flood events by men's activities including sand mining and construction of the Via de Santa Fe Road and bridge as shown in Figure 1. As a result of sand mining, several large borrow pits with a depth as great as 25 feet were created. The natural wide channel is encroached upon by the road embankment on each side of the bridge (Section 51). While the river channel has an erodible bed and banks, the banks, however, are constrained by the hills at the south bank of Section 51 and along the north banks of Section 60 to 63 and by bank protections at the north banks of Sections 51 and 58.

Two floods passed through the river, one in March, 1978 (peak flow = 4,400 cfs), and another in February, 1980 (peak flow = 22,000 cfs), when Lake Hodges spilled. Hydrographs of these floods are shown in Figure 2. Prior to these events, Lake Hodges had not spilled for 26 years.

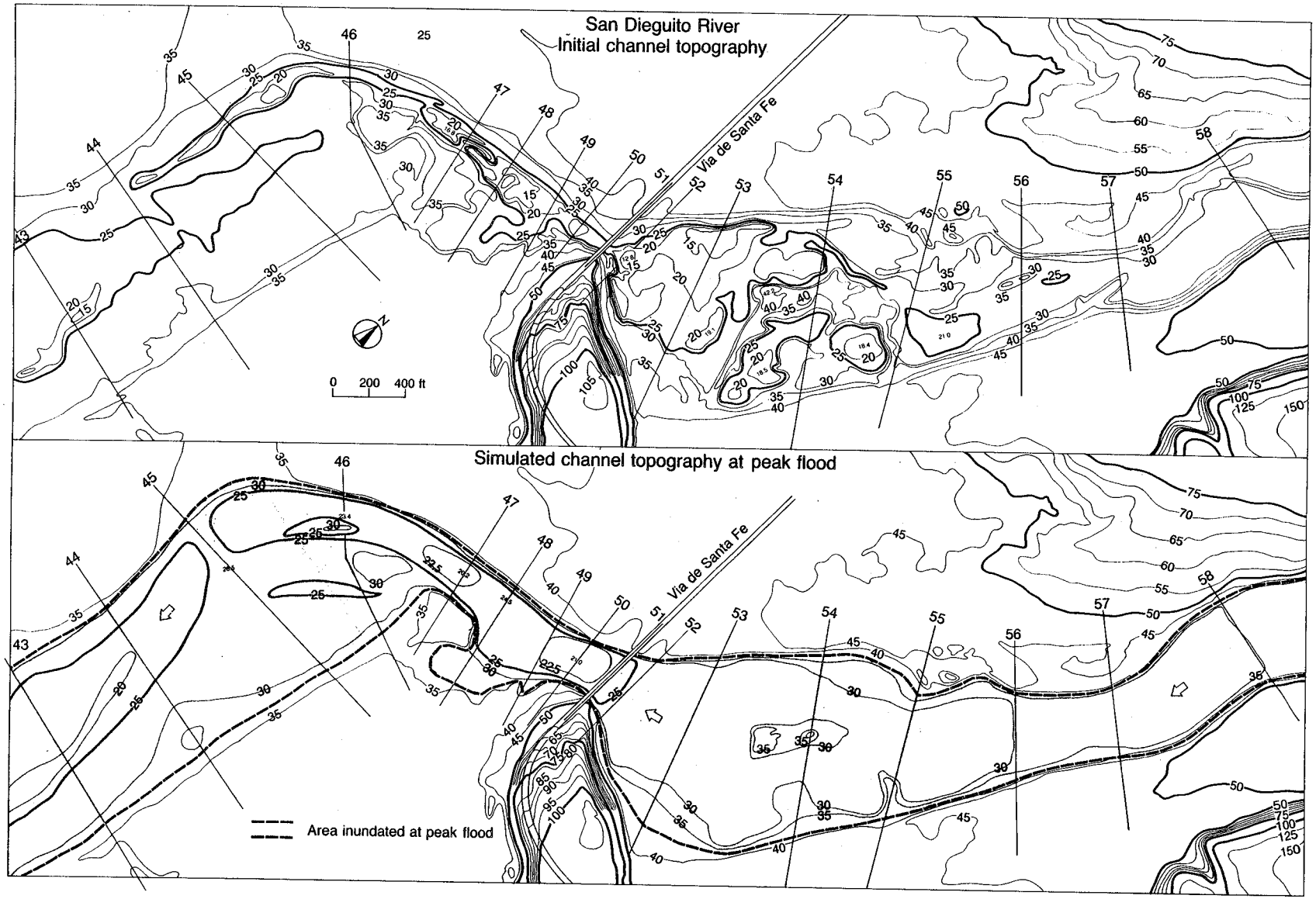

Figure 1. Topographies and cross-section locations

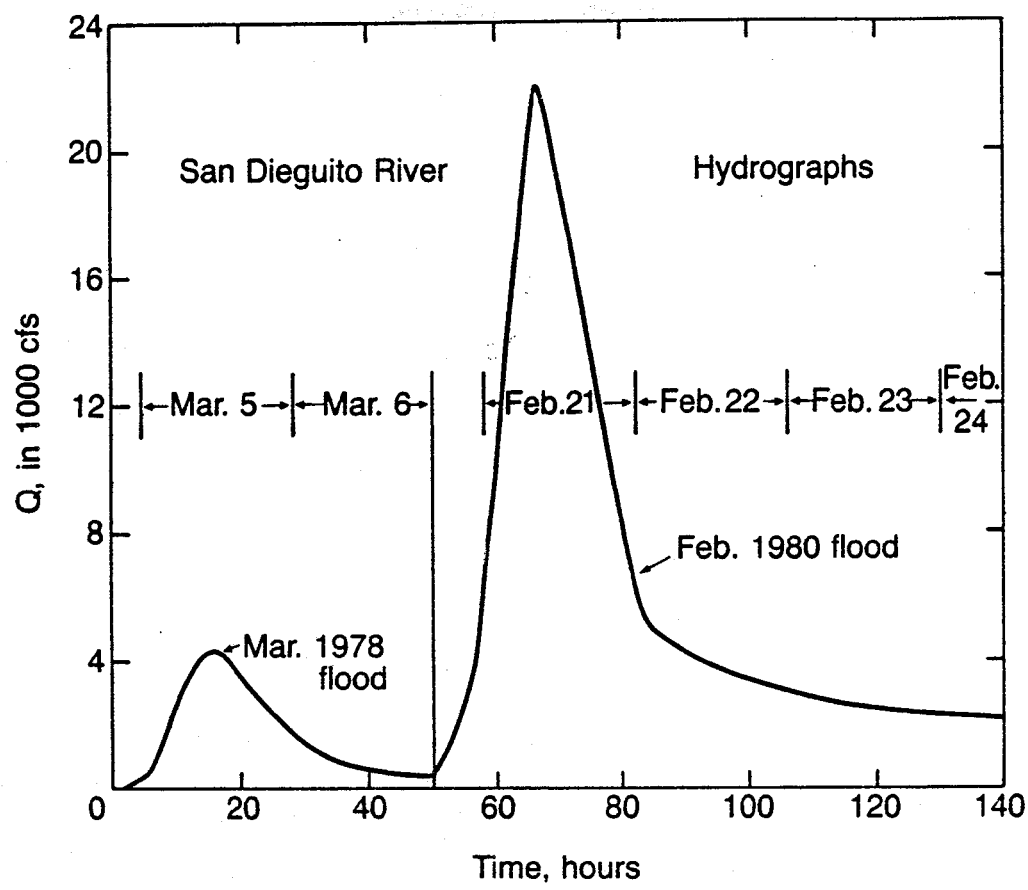

Figure 2. Flood hydrographs

River Channel Changes -- Significant changes in the river channel were observed after the March, 1978, flood. Channel-bed scour occurred near borrow pits and notably at the bridge crossing where measurements were made as shown in Figure 3 for Section 51. Deposition was observed in the borrow pits. With limited flood discharge and duration, these borrow pits were only partially refilled.

Major changes in the river channel occurred during the greater February, 1980, flood. These changes included channel-bed aggradation and degradatin, width variation, and lateral migration of the channel are described below. These changes were recorded by a high water mark at Section 52, by channel-bed measurements at selected cross-sections after the flood as shown in Figure 3, and by photographs taken during the flood as shown in Figures 4, 5, and 6.

SIMULATION AND RESULTS

The mathematical model FLUVIAL-11 was used to simulate river channel changes in the San Dieguito River during the 1978 and 1980 floods. Graf's equation (6) for bed-material load was used in computing the sediment movement. Channel roughness in terms of Manning's n was

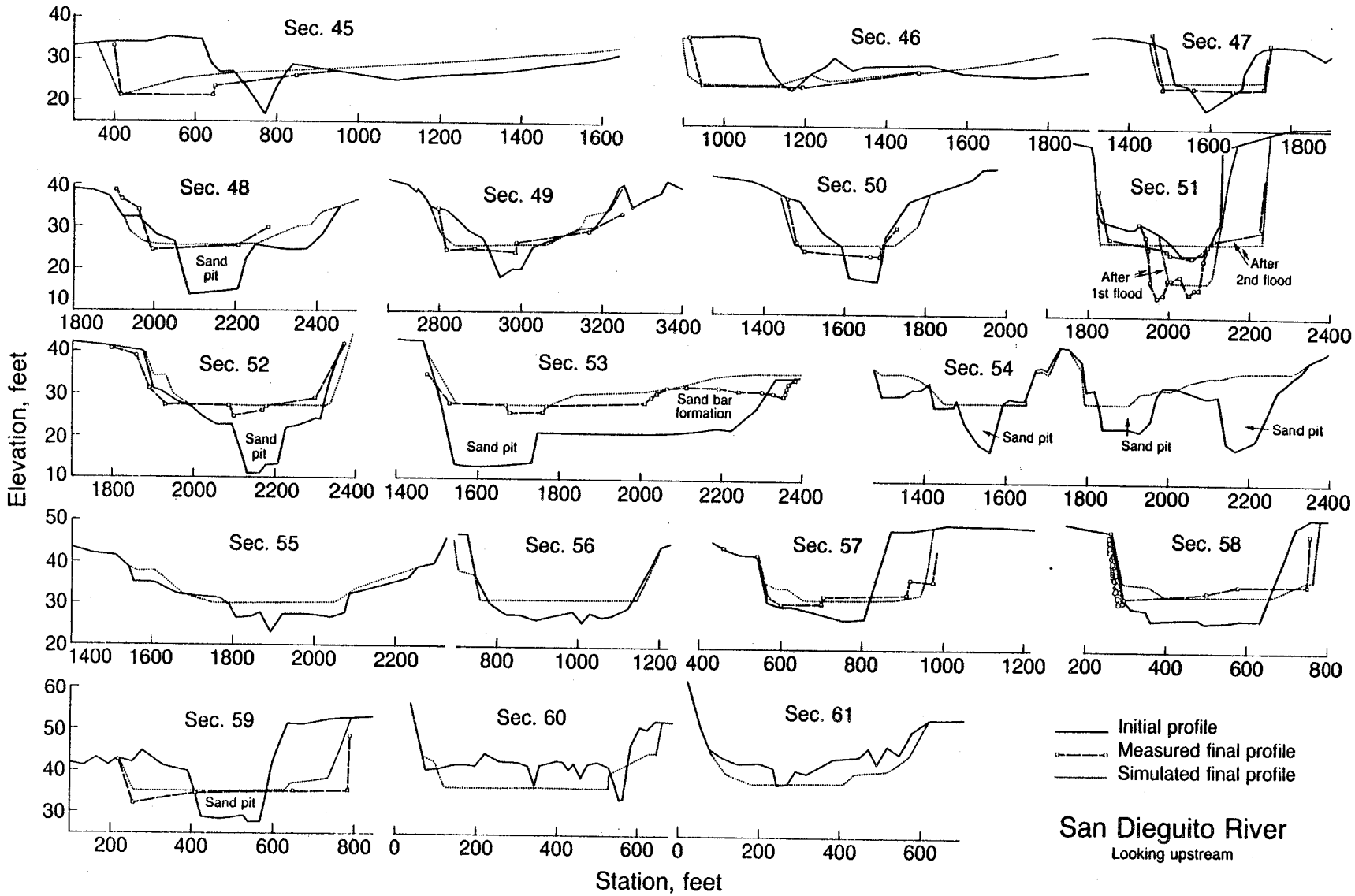

Figure 3. Simulated and measured cross-sectional changes

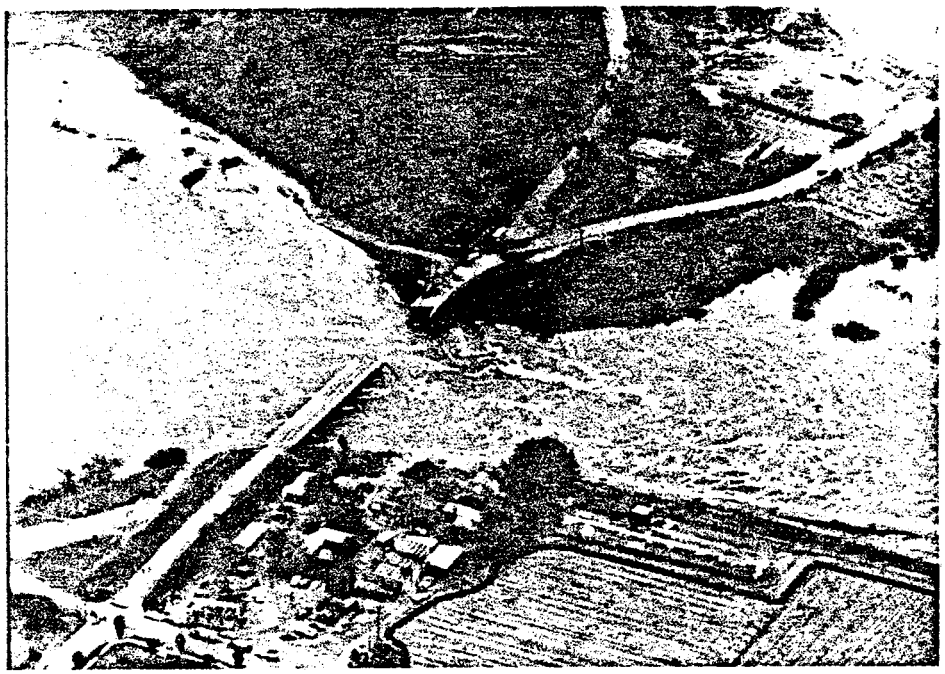

Figure 4. San Dieguito River on February 21, 1980
(Looking toward south)

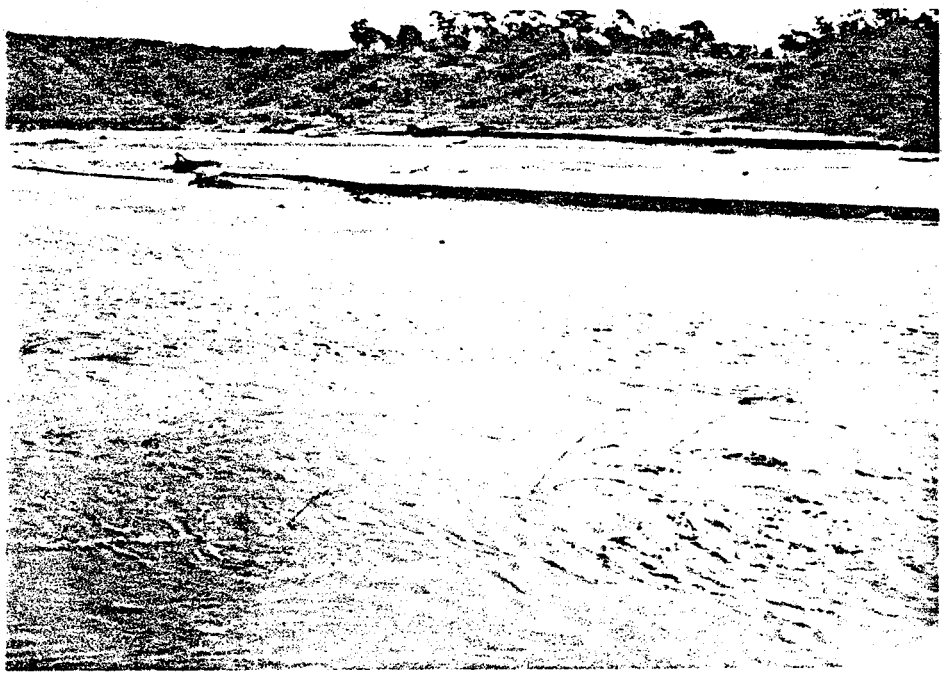

Figure 5. Sand bar formation near Section 53
(Looking toward south)

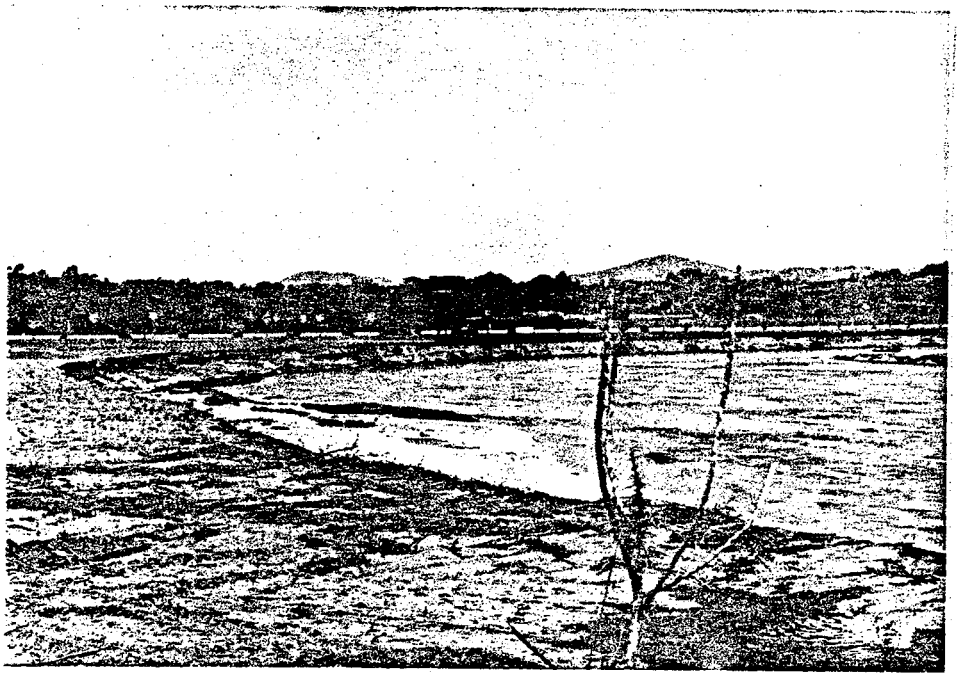

Figure 6. Channel bank scour near Sections 45 and 46
(Looking toward north)

selected to be 0.035 in consideration of the channel irregularity and minor vegetation growth; it was estimated to be 0.04 at the bridge crossing. The combined duration of 140 hours for these two floods was computed using 2,000 time steps.

Simulated results as presented in Figures 1, 3, and 7 are described below.

Changes in River Channel Configuration -- River channel changes, including those in channel-bed profile, channel width, and lateral migration, as simulated by the computer model, are described herein. Changes in the longitudinal channel-bed profile (see Figure 7) are characterized by aggradation in the borrow pits, erosion at higher grounds, and the gradual formation of a more or less smooth channel-bed profile at the end of the flood. In that process, considerable variation in the longitudinal channel-bed elevation through the downstream portion of the river reach is predicted at the peak flood as shown in Figures 1 and 7. The higher channel-bed elevations at Sections 45, 46, and 48 are associated with large channel widths while the lower elevations at Sections 47 and 50 are due to their small widths.

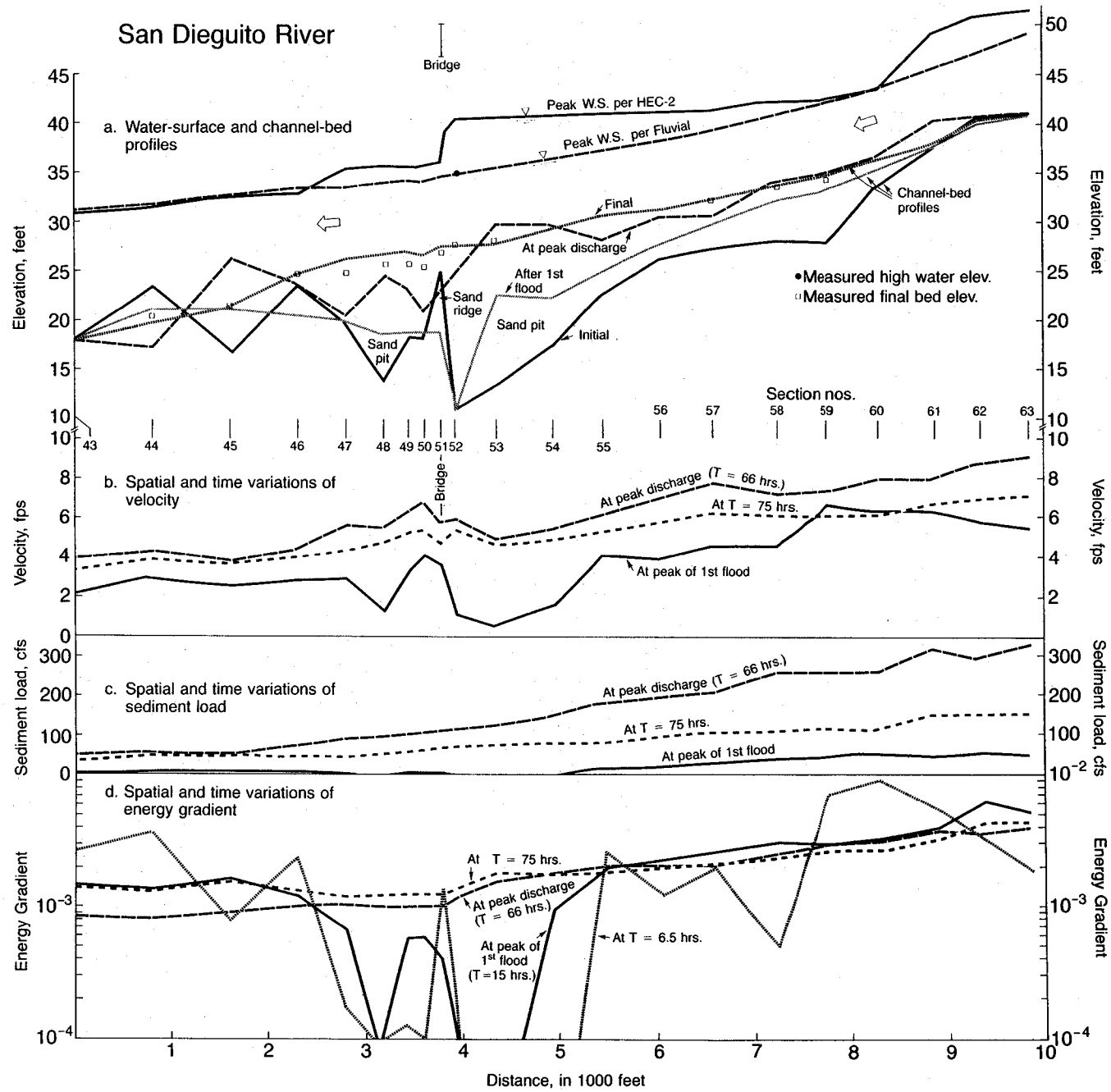

Figure 7. Simulated and measured results

Changes in channel width which occur concurrently with variations in channel-bed elevation and lateral migration are simulated. Width changes are characterized by the gradual widening at those initially narrow sections, notably at Sections 47, 49, 50, 51, 57, 58 and 59 and reductions in width at initially wide sections, notably at Sections 53 and 54. Initial and simulated final cross-sectional profiles of these sections are shown in Figure 3 together with some measured profiles. Simulated channel width at the peak flood (shown in Figure 1) is highly uneven in its spatial variation along the river. This variation is gradually reduced during the flood as reflected by the simulated final cross-sectional profiles in Figure 3. By comparing the initial and final channel-bed profiles, one finds that widening at a section is through bank erosion and that the reduction in width is usually through sand-bar formation along the bank(s). Simulated variation of the cross-sectional profile for Section 53 illustrates the sand-bar formation and the associated reduction in channel width. A picture of this sand bar taken at the end of the flood is shown in Figure 5.

That changes in channel width and channel-bed elevation are closely related may be illustrated by the simulated time variation of the cross-sectional profile at Section 51 (see Figure 9). Initially Section 51 is on a sand ridge with borrow pits existing on both sides. Gully formation through this sand ridge during the first flood is simulated followed by gradual widening and lessening of the gully depth during the second flood. The maximum scour depth is predicted to occur in the initial gully. The simulated results correlate well with measurements at this section shown in Figure 3, in which the uneven final channel-bed profile as measured is related to the removal of several piers during the flood (see Figure 4).

Lateral migration of the channel at Sections 44, 45, and 46 in the river bend as simulated is illustrated by the variation of the cross-sectional profile at Section 46. Lateral migration is through gradual erosion of the concave bank and deposition on the convex bank. A picture of the eroded concave bank is shown in Figure 6.

RIVER-CHANNEL CHANGES IN RELATION TO POWER EXPENDITURE

Changes in river-channel configuration are accompanied by changes in flow resistance and hence the rate of energy (or power) expenditure. The γQS product represents the rate of energy expenditure per unit channel length. Since the spatial variation of Q is small, the spatial variation of γQS may be represented by the spatial variation of the energy gradient S shown in Figure 7.

Simulated river channel changes are associated with the gradual reduction of the spatial variation of energy gradient along the channel subject to the physical constraint of rigid banks. That the adjustment in river-channel configuration is closely related to the change in power expenditure can be illustrated by the sequential changes of cross-sectional profile at Section 51 as shown in Figure 3. Because it is initial sand ridge (see Figure 7), the energy

gradient at this section is initially much greater than those of its adjacent sections. This pronounced spatial variation in energy gradient is reduced through gully formation at this section and deposition at the adjacent sections. The gully which is small in width and has a low channel-bed elevation provides the least possible flow resistance and hence lowest energy gradient at this section; it also reduces the back-water effect on the upstream section and thereby increases its energy gradient. At subsequent time intervals, the energy gradient at Section 51 becomes less than its adjacent sections. Cross-sectional changes at this section then include widening in channel width and aggradation in the gully. These changes are accompanied by increases in boundary resistance and energy gradient at this section, favoring the establishment of equal energy gradient along the reach. This pattern of river channel changes characterized by the formation of narrow channel width during channel-bed degradation and widening during aggradation, is evident in nature and has been reported in the literature (3,4,7,8,9,10,11).

SUMMARY AND CONCLUSIONS

The mathematical model FLUVIAL-11 has been formulated and developed; it has been employed to simulate flood- and sediment-routing and associated river channel changes in the San Dieguito River near the Via de Santa Fe bridge. Simulated results using this model are supported by field observations and measurements.

An alluvial river is the author of its own geometry; therefore it will respond to any change imposed upon by nature or by men through self adjustments. River channel changes may include channel-bed aggradation and degradation, width variation, and lateral migration in channel bends. These changes are interretated as they may occur concurrently. Therefore, a mathematical model for erodible channels must include these variables.

River channel changes in the San Dieguito River are characterized by the trend toward a more uniform configuration from the initially distorted configuration. In this process, the river channel tends to become narrower during channel-bed degradation and it tends to widen during aggradation. This pattern of adjustment reflects the river's tendency to seek equal power expenditure along the channel. River channel changes provide a mechanism with which the river seeks to establish the dynamic equilibrium in sediment transport, that is equal sediment load along the reach.

In erodible channels, flood-level computation using a fixed-bed model may be limited in accuracy. Improved accuracy for flood-level determination in such channels may be provided by an erodible-bed model.

APPENDIX I. REFERENCES

1. Bagnold, R. A., "An Approach to Sediment Transport Problem from General Physics," U.S. Geological Survey Professional Paper 422-I, Washington, D.C., 1966, 137 pp.

2. Chang, H. H. and Hill, J. C., "Computer Modeling of Erodible Flood Channels and Deltas," Journal of the Hydraulics Division, ASCE, Vol. 102, No. HY10, October 1976, pp. 1461-75.

3. Chang, H. H. and Hill, J. C., "Minimum Stream Power for Rivers and Deltas," Journal of the Hydraulics Division, ASCE, Vol. 103, No. HY12, December 1977, pp. 1375-89.

4. Chang, H. H., "Mathematical Model for Erodible Channels," Journal of the Hydraulics Division, ASCE, Vol. 108, No. HY5, Proc. Paper 17062, May 1982.

5. "Flood Plain Changes During Major Floods," Department of Sanitation and Flood Control, Community Services Agency, County of San Diego, 1979.

6. Graf, W. H., Hydraulics of Sediment Transport, McGraw-Hill Book Co., 1971, 509 pp.

7. Gregory, K. J., Editor, River Channel Changes, John Wiley and Sons, 1977, 448 pp.

8. Lane, E. W., "A Study of the Shape of Channels Formed by Natural Streams Flowing in Erodible Material," Missouri River Division Sediment Series No. 9, U.S. Army Engineer Division, Missouri River Corps of Engineers, Omaha, Nebraska, 1957.

9. Langbein, W. B. and Leopold, L. B., "River Meanders, Theory of Minimum Variance," U.S. Geol. Survey Prof. Paper 282-B, 1957.

10. Leopold, L. B., Wolman, M. G., and Miller, J. P., Fluvial Processes in Geomorphology, W. H. Freeman and Co., San Francisco, 1964, 522 pp.

11. Schumm, S. A., The Fluvial System, Wiley-Interscience, 1977, 338 pp.

12. "Storm Report, February 1980," San Diego County Flood Control District, 26 pp.

INPUT/OUTPUT DESCRIPTIONS FOR FLUVIAL PROGRAMS

I. INPUT DESCRIPTION

The HEC-2 format for input data is used in all versions of the FLUVIAL model. Data cards for HEC-2 pertaining to cross-sectional geometry (X1 and GR), job title (T1, T2, and T3), and end of job (EJ), are used in the FLUVIAL model. If a HEC-2 data deck is available, it is not necessary to delete the unused cards except that the information they contain are not used in the computation. For the purpose of flood- and sediment-routing, additional data pertaining to sediment characteristics, flood hydrograph, etc., are required and supplied by other data cards. Sequential arrangements of data cards are shown in the following table.

Cards	Description of Card Type
T1, T2, T3	Title Cards
G1	General use Card
G2	General Use Cards for Hydrographs
G3	General Use Card for Downstream Boundary Condition
GS	General Use Cards for Initial Sediment Compositions
X1	Cross-sectional card
G4	Card for Specifying Non-erodible Portions of a Cross section
GR	Card for Ground Profile of a Cross section
EJ	End of Job Card

Variable locations for each input card are shown by the field number. Each card has an input format of (A2, F6.0, 9F8.0). Field 0 occupying columns 1 and 2 are reserved for the required card identification characters. Field 1 occupies columns 3 to 8; Fields 2 to 10 occupy 8 columns each. The data cards are first tabulated and then described in the following pages.

T1, T2, T3 Cards

These three cards are title cards for output title; all three cards are required for each job.

Field	Variable	Value	Description
0	IA	T1	Card identification character.
1-10	None		Numbers and alphameric characters for title.

G1 Card

This card is required for each job, used to enter the general parameters.

Field	Variable	Value	Description
0	IA	G1	Card identification characters
1	TYME	+	Starting time of computation on the hydrograph, in hours.
2	ETIME	+	Ending time of computation on the hydrograph, in hours.
3	DTMAX	+	Maximum time increment Δt allowed, in seconds.
4	ISED	1	Graf's sediment load equation is used.
		2	Yang's unit stream power equation for bed material load is used.
		3	Other sediment load equation is used. The equation selected needs to be supplied to the program.
5	DFB	+	Median sediment size of the bank material, in mm.
6	PHI	+	Angle of repose of bed-material, in degrees.
7	ANN	+	Manning's "n" value for the reach. This value is used for a section unless otherwise specified by Field 8 of the X1 card.
8	PTIME1	+	Starting time of the period in which output are printed at a greater frequency.
9	PTIME2	+	Ending time of the period in which output are printed at a greater frequency.

10	KPFNM	+	Frequency of printing the output, in number of time steps.

G2 Cards

These cards are required for each job, used to define the flood hydrograph(s) in the channel reach. The first G2 card is used to define the spatial variation in flood discharge along the reach; the succeeding ones are employed to define the time variation(s) of the flood discharge.

Field	Variable	Value	Description
First G2 Card			
0	IA	G2	Card identification characters.
1	IHP1	+	Number of last section using the first hydrograph. The number of section is counted from downstream to upstream with the downstream section being one.
2	NP1	+	Number of points connected by straight segments used to approximate the first hydrograph. The maximum value is 10.
3	IHP2	+ 0	Number of last section using the second hydrograph if any. Otherwise leave it blank.
4	NP2	+ 0	Number of points used to approximate the second hydrograph. The maximum value is 10.
5	IHP3	+ 0	Number of last section using the third hydrograph if any. Otherwise leave it blank.
6	NP3	+ 0	Number of points used to approximate the third hydrograph. The maximum value is 5.
Succeeding G2 card(s)			
1	Q1(1), Q2(1) Q3(1)	+	Discharge coordinate of point 1 for each hydrograph, in cfs.
2	TM1(1), TM2(1), TM3(1)	+	Time coordinate of point 1 for each hydrograph, in hours.
3	Q1(2), Q2(2)	+	Discharge coordinate of point 2 for

	Q3(2)		each hydrograph, in cfs.
4	TM1(2), TM2(2) TM3(2)	+	Time coordinate of point 2 for each hydrograph, in hours.

Continue with additional discharge and time coordinates.

G3 Card

This is a required card for each job, used to define the channel slope at the downstream section. This slope is required for the stage-discharge relation at the section; it should be measured from the topographic map.

Field	Variable	Value	Description
0	IA	G3	Card identification characters.
1	S11	+	Slope of the downstream section.
2	ZMIN1	±	Minimum elevation (invert elevation) at the downstream section contained in the GR card, in feet.
3	DSOP	0	Downstream slope is allowed to vary during flow.
		1	Downstream slope is a constant as S11.

GS Card

Two GS cards are required for each job, used to specify initial sediment compositions in the channel at the upstream and downstream cross sections. Sediment composition at each section is represented by five size fractions.

Field	Variable	Value	Description
0	IA	GS	Card identification characters.
1	DFF(1)	+	Median diameter of bed materials for the smallest size fraction in mm.
2	PC(1)	+	Fraction of bed materials in this size range.

Continue for other DFF's and PC's.

X1 Card

This card is required for each cross section (50 cross sections can be used for each channel reach); it is used to specify the cross-sectional geometry and program options applicable to that cross-section.

Field	Variable	Value	Description
0	IA	X1	Card identification characters.
1	SECNO(I)	+	Original section number from the map.
2	NP(I)	+	Total number of stations or points on the next GR cards for cross section I.
3	STCHL(I)	+	Station of the left bank of the channel. Must be equal to one of the Y(I,J) on next GR cards.
4	STCHR(I)	+	Station of the right bank of the channel. Must be equal to one of the Y(I,J) one next GR cards.
7	DX(I)	+	Length of reach between current cross section I and the next downstream cross section I-1 for the channel, in feet.
8	AN(I)	0	Channel roughness is the same as the reach.
		+	Manning's "n" value for this section.
9	CPC(I)	0	Center of thalweg coincides with the channel invert.
		+	Horizontal coordinate of the center of thalweg, in feet.
10	IRC(IC)	0	Regular erodible cross section.
		+	Rigid or non-erodible cross section such as a drop structure or a road crossing.

G4 Card

This is an optional card used to specify non-erodible portions of a cross section.

Field	Variable	Value	Description
0	IA	G4	Card identification character.
1	YC1(I)	0	Regular erodible left bank.
		+	Station of rigid left bank, to the left of which channel is non-erodible.
2	YC2(I)	0	Regular erodible right bank.
		+	Station of rigid right bank, to the right of which channel is non-erodible.

GR Card

This card specifies the elevation and station of each point for a digitized cross section; it is required for each X1 card.

Field	Variable	Value	Description
0	IA	GR	Card identification characters.
1	Z(I,1)	±	Elevation of point 1 at station Y(I,1), in feet. May be positive or negative.
2	Y(I,1)	+	Station of point 1, in feet.
3	Z(I,2)	±	Elevation of point 2 at station Y(I,2), in feet.
4	Y(I,2)	+	Station of point 2, in feet.

Continue with additional GR cards using up to 25 points to describe the cross section. Stations should be in increasing order. Cross section number I is counted from downstream to upstream with the number of the downstream section as 1.

EJ Card

This card is required following the last cross section for each job. Each group of cards beginning with a T1 card is considered as a job.

Field	Variable	Value	Description
0	IA	EJ	Card identification characters.
1-10			Not used.

II. OUTPUT DESCRIPTION

Output of the model include initial bed-material compositions, time and spatial variations of the water-surface profile, channel width, flow depth, flood discharge, velocity, energy gradient, roughness coefficient, median sediment size, and bed-material load. In addition, cross-sectional profiles are printed at different time intervals.

Symbols used in the output are generally descriptive, some of them are defined below:

SEC NO	Number of a cross-section.
TIME	Time on the hydrograph.
DT	Size of the time step or Δt.
W.S.ELEV	Water-surface elevation.
WIDTH	Width of channel flow.
DEPTH	Depth of flow measured from channel invert to the water-surface elevation.
Q	Discharge of flow.
V	Mean velocity at a cross-section.
SLOPE	Energy gradient.
N VALUE	Composite roughness in terms of Manning's "n" for a cross-section.
D50	Median bed-material size of d_{50} in the active layer.
QS	Bed-material load for all sediment-size fractions.
QS1	Bed-material load for the first (finest) size fraction.
QS2	Bed-material load for the second size fraction.
QS3	Bed-material load for the third size fraction.
QS4	Bed-material load for the fourth size fraction.
QS5	Bed-material load for the fifth size fraction.
WSEL	Water-surface elevation, in feet.
Z	Vertical coordinate (elevation) of a point on channel boundary of a cross-section, in feet.

Y	Horizontal coordinate (station) of a point on channel boundary of a cross-section, in feet.
DZ	Change in elevation during the current time step, in feet.
TDZ	Total or accumulated change in elevation, in feet.

Estimating Erosion and Sediment Yield on Field-Sized Areas

G. R. Foster, L. J. Lane, J. D. Nowlin, J. M. Laflen, R. A. Young

MEMBER ASAE — MEMBER ASAE — MEMBER ASAE

ABSTRACT

A model for field-sized areas was developed to evaluate sediment yield under various management practices. The model provides a tool for evaluating sediment yield on a storm-by-storm basis for control of erosion and sediment yield from farm fields. The model incorporates fundamental principles of erosion, deposition, and sediment transport. The procedures allow parameter values to change along complex overland flow profiles and along waterways to represent both spatial variability and variations that occur from storm to storm. Many of the model parameter values are obtained from topographic maps or directly from the Universal Soil-Loss Equation (USLE). Thus we feel that the model has immediate applications without extensive calibration.

Individual components of the model were tested using experimental data from studies of overland flow, erodible channels, and small impoundments. These results suggest that the model produces reasonable estimates of erosion, sediment transport, and deposition under a variety of conditions common to field-sized areas. The procedures developed here can be used to evaluate alternative management practices such as conservation tillage, terracing, and contouring.

INTRODUCTION

Estimates of erosion and sediment yield on field-sized areas are needed so that best management practices (BMPs) can be selected to control erosion for maintaining soil productivity and to control sediment yield for preventing excessive degradation of water quality. The field is typically the management unit used by most farmers to select management practices. For several years, soil conservationists have used the Universal Soil-Loss Equation (USLE) (Wischmeier and Smith, 1978) to select erosion control practices tailored for a given farmer and his fields. If sediment yield tolerances for maintenance of water quality are established for local areas, a model is needed to select BMPs based on a farmer's site specific conditions, his needs, and tolerable loading rates for streams in his area.

On a given field, sediment yield is controlled by either sediment detachment or sediment transport capacity (Ellison, 1947; Meyer and Wischmeier, 1969), depending on factors such as topography, soil, cover, and rainfall/runoff characteristics. The effects of these factors change from season to season and from storm to storm. The need to consider detachment and transport processes on a storm-by-storm basis limits the accuracy of lumped equations such as the USLE (an erosion equation), or Williams' (1975) modified USLE (a flow transport sediment yield equation) on field-sized areas.

Several detailed models (Beasley et al., 1980; Donigian and Crawford, 1976; Li, 1977) compute erosion and sediment transport at various times over a runoff event. Although these models are powerful, their considerable use of computer time prohibits the practical simulation of long periods of record on many fields to select a BMP for specific fields.

The purpose of this paper is to describe a model that, while simply constructed and usable over a broad range of situations at reasonable cost, embodies the latest knowledge on the fundamentals of erosion mechanics. The model may be used without calibration or collection of data to determine parameter values. It can be linked to hydrologic and chemical transport models, and was developed for that specific purpose as a component of CREAMS, a field scale model for Chemicals, Runoff, and Erosion from Agricultural Management Systems (USDA, 1980).

BASIC CONCEPTS

The basis of this model is that USLE storm erosivity, EI, and the peak runoff rate at the watershed outlet can be used to characterize a storm's rainfall, runoff, and sediment yield. Quasi-steady state is assumed. Thus, sediment movement downslope obeys continuity expressed by:

$$dq_s/dx = D_L + D_F \quad [1]$$

where q_s = sediment load (mass/unit width/unit time), x = distance, D_L = lateral inflow of sediment (mass/unit area/ unit time), and D_F = detachment or deposition by flow (mass/unit area/unit time). Mathematically, detachment and deposition differ only in sign; detachment is positive, deposition is negative.

Hydrologically and hydraulically, a typical watershed may be divided into areas or elements of overland flow, channel flow, or impounded runoff. Each type of flow is

Article was submitted for publication in September 1980; reviewed and approved for publication by the Soil and Water Division of ASAE in March 1981.

Contribution from USDA-SEA-AR in cooperation with the Purdue Agricultural Experiment Station, Purdue Journal No. 8111.

The authors are: G. R. FOSTER, Hydraulic Engineer, USDA, and Associate Professor, Agricultural Engineering Dept., Purdue University, Lafayette, IN; L. J. LANE, Hydrologist, USDA, Tucson, AZ; J. D. NOWLIN, Computer Programmer, USDA, Agricultural Engineering Dept., Purdue University, Lafayette, IN; J. M. LAFLEN, Agricultural Engineer, USDA, Ames, IA; and R. A. YOUNG, Agricultural Engineer, USDA, Morris, MN.

Acknowledgements: The erosion-sediment yield model described herein is a component of CREAMS, a comprehensive field-scale model including hydrologic, erosion, pesticide, and nutrient components developed by USDA-SEA-AR scientists under the leadership of W. G. Knisel, Jr. Complete documentation on the comprehensive model is given by USDA (1980). Additional support for this project, including computer programming by V. A. Ferreira, was provided by K. G. Renard, Research Leader, Southwest Rangeland Watershed Research Center, USDA-SEA-AR, Tucson, AZ; W. C. Moldenhauer, Research Leader, Erosion Research Unit, USDA-SEA-AR, Lafayette, IN; and G. W. Isaacs, Head, Agricultural Engineering Dept., Purdue University, W. Lafayette, IN.

This article is reprinted from the TRANSACTIONS of the ASAE (Vol. 24, No. 5, pp. 1253-1262, 1981)

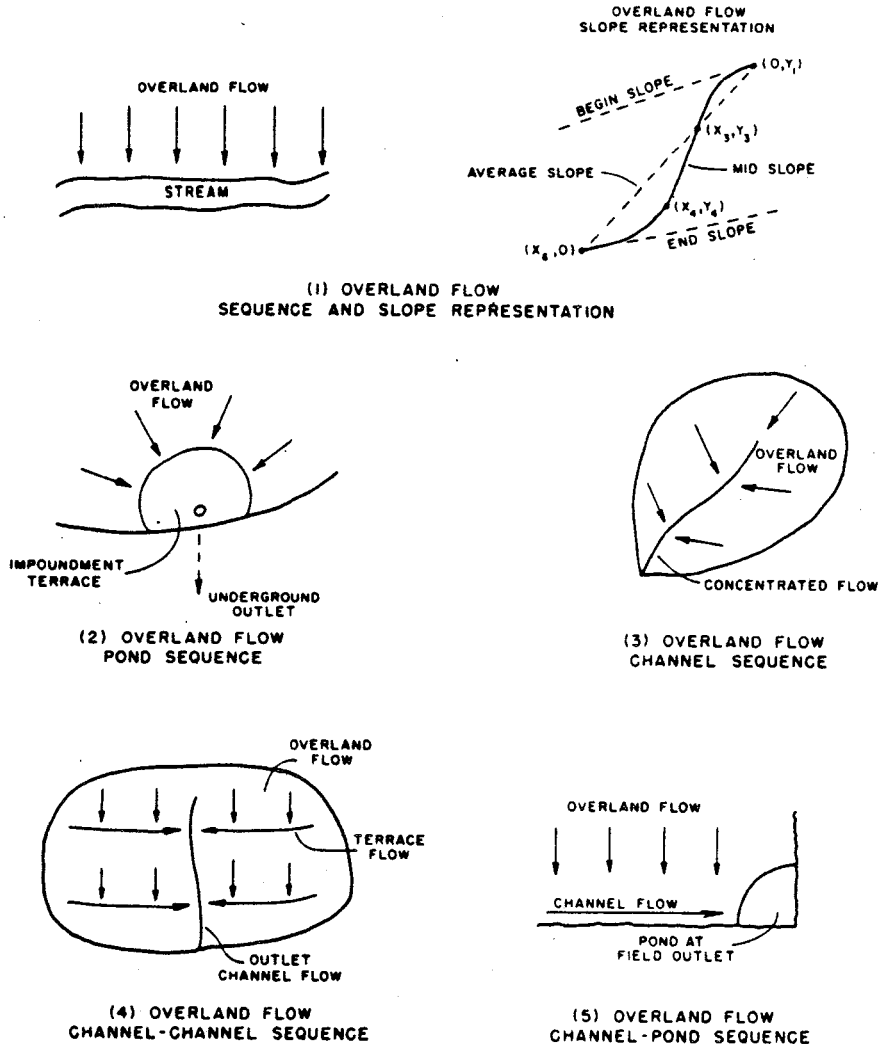

FIG. 1 Schematic representation of typical field systems in the field-scale erosion/sediment yield model.

treated in the model with a specific set of equaions for that type of flow. Lateral sediment inflow is from interrill erosion on overland flow areas, or from overland flow (or channels if a set of channels drain into a main channel) for the channel areas. Overland flow or channels, but not both, may drain directly into an impoundment according to the model's structure. Flow in rills on overland flow areas or in channels transports all sediment downstream. Lateral sediment inflow to runoff in rills or channels is assumed regardless of whether the flow is detaching or depositing.

The watershed is represented by selecting a combination of elements from a typical overland flow profile, a main channel, a set of channels draining into a main channel, or a small impoundment as illustrated in Fig. 1. The selected combination of elements depends on the site being analyzed. Overland flow and channel elements are divided into segments along their length. Computations proceed downstream segment by segment and element by element. The computational sequence is shown in Fig. 2.

For an overland flow or channel segment, the model computes a potential sediment load which is the sum of the sediment load from the immediate upslope segment plus that added by lateral inflow within the segment. If the potential load is less than the sediment transport capacity of the flow, detachment occurs either at the detachment capacity of the flow or at the rate that will just fill transport capacity, whichever is less. Sediment detachment by rainfall or flow adds sediment having a given size and density distribution. No sorting is allowed during detachment.

If potential sediment load is greater than transport capacity, deposition is assumed to occur at the rate of (Foster and Meyer, 1975):

$$D_d = \alpha (T_c - q_s) \quad [2]$$

where D_d = deposition rate (mass/unit area/unit time), α = a first order reaction coefficient (length $^{-1}$), and T_c = transport capacity (mass/unit width/unit time). The coefficient α is given by:

$$\alpha = \xi V_s/q_w \quad [3]$$

where ξ = 0.5 for overland flow (Davis, 1978), and 1.0 for channel flow (Einstein, 1968), V_s = particle fall velocity, and q_w = discharge per unit width (volume/unit width/unit time). Fall velocity is computed using standard relationships and drag coefficients for a sphere falling in still water.

The assumption that dT_c/dx is constant over a segment permitted use of analytical solutions to equations [1] and [2] where deposition occurred. Where deposition did not occur, sediment load was calculated from:

$$q_s = (D_u + D_l)\Delta x/2 + D_L \Delta x + q_{su} \quad [4]$$

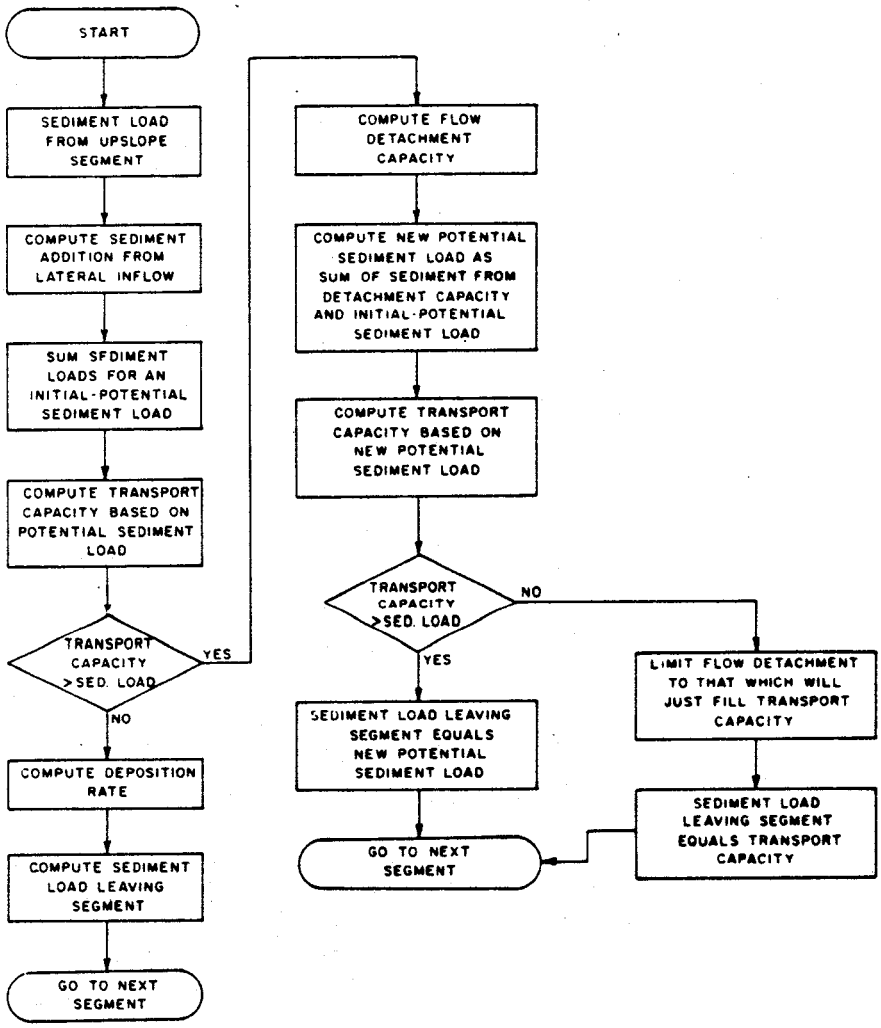

FIG. 2 Flow chart for detachment-transport-deposition computations within a segment of an overland flow or channel element.

where D_u and D_l respectively, rates of detachment by flow at the upper and lower ends of the segment or its portion where detachment by flow is occurring, Δx = length of the segment or its portion where detachment by flow is occurring, and q_{su} = sediment load at the upper end of the segment or its portion where detachment by flow is occurring.

The Yalin sediment transport equation was modified (Yalin, 1963; Foster and Meyer, 1972; Davis, 1978; and Khaleel et al., 1979) to describe sediment transport capacity for various particle sizes and densities. A particle type is a class of particles represented by a given diameter and specific gravity. If transport capacity exceeds availability for one particle type while it is less for another, excess transport capacity is shifted from the particle type having the excess to the one having the deficit. Furthermore, simultaneous deposition and detachment of particles by flow is not allowed. Equations [1 - 4] are solved for each particle type within these constraints.

OVERLAND FLOW ELEMENT

Detachment on interrill and rill areas and transport and deposition by flow in rills are the important erosion-transport processes on overland flow areas. Detachment is described by a modified USLE written as (Foster et al., 1977):

$$D_{Li} = 4.57\ EI\ (s_o + 0.014) K\Phi P\ (\sigma_p/V_u) \quad [5]$$

and

$$D_{Fr} = (6.86 \times 10^6)\ \eta\ v_u \sigma_p^{1/3}\ (x/22.1)^{\eta-1}\ K\Phi P\ (\sigma_p/V_u) \quad [6]$$

where D_{Li} = interrill detachment rate (g/m² of land surface/s), D_{Fr} = capacity rate for rill detachment (g/m² of land surface/s), EI = rainfall erosivity (energy times maximum 30-min intensity) (N/h)*, x = distance downslope (m), s_o = sine of slope angle, η = slope length exponent for rill erosion, K = USLE soil erodibility factor* [g h/ (N m²)], Φ = USLE cover-management soil-loss ratio, P = USLE contouring factor, V_u = runoff amount [volume/unit area (m)], and σ_p = peak runoff rate [volume/unit area/unit time (m/s)]. The term σ_p/V_u converts a total soil loss for a storm to an average rate for the storm. Only the contouring part of the USLE P factor is used. The model is structured to directly account for other supporting conservation practices like terraces and stripcropping.

For downslope distances less than 50 m, η is set to 2.0, but for slopes longer than 50 m, η is limited by:

$$\eta = 1.0 + 3.912/\ln x \quad [7]$$

*The units on the K factor from the USLE must be carefully noted. Multiplication of the K in U. S. customary units by 131.7 gives a metric K having units of gh/(Nm²). Foster, G. R., D. K. McCool, K. G. Renard and W. C. Moldenhauer, 1981. Conversion of the Universal Soil-Loss Equation (USLE) to metric SI units. Accepted by J. Soil and Water Conservation. Manuscript available from senior author.

This limit avoids apparent excessive rill erosion for very long slopes (Foster et al., 1977). Equation [7] limits the effective slope length exponent for rill and interrill erosion combined to 1.67 so far as it is a function of length. The effective exponent is also a function of slope and runoff erosivity relative to rainfall erosivity.

The detachment equations [5] and [6] (except for the σ_p/V_u term) as originally developed (Foster et al., 1977) were on a storm basis, whereas the transport equation is on an instantaneous rate basis. The two were combined by assuming that the computed sediment concentrations are average concentrations for the runoff event.

Cover and management effects on detachment are described with the USLE soil loss ratios (Wischmeier and Smith, 1978). Cover and management affect transport by their reduction of σ_p and V_u (estimated outside of the model) and by reducing the flow's shear stress acting along the soil-water interface. The concept (Graf, 1971) of dividing shear between form roughness (cover like mulch or vegetation) and grain roughness (soil) is used to estimate the proportion of total shear stress acting on the soil. The shear stress acting on the soil, τ_{soil}, is estimated by:

$$\tau_{soil} = \gamma y s_o (n_{bov}/n_{cov})^{9/10} \quad [8]$$

where Y = weight density of water, y = flow depth for bare, smooth soil, n_{bov} = Manning's n for bare soil, and n_{cov} = Manning's n for rough, mulch, or vegetative covered soil. Flow depth is estimated by the Manning equation as:

$$y = [q_w n_{bov}/s^{1/2}]^{3/5} \quad [9]$$

where q_w = discharge rate per unit width. Although the Darcy-Weisbach equation with a varying friction factor for laminar flow might be more accurate in some cases for y, most users are better acquainted with estimating Manning's n. Values for Manning's n may be selected from Foster et al. (1980a) and Lane et al. (1975).

Segments along the overland flow profile are established by the model. The overland flow profile may be uniform, convex, concave, or a combination of these shapes. Input data requirements are slope length, average slope steepness, location of the end points of a uniform section at midslope, slope at the upper end of the profile, and slope at the lower end of the profile. A quadratic curve is fitted to curved portions of the slope so that it passes through an end point of the uniform segment at midslope and is tangent to the profile near each of its ends. Convex portions of a profile are divided into three equal length segments while concave portions are divided into ten equal length segments because calculation of deposition on concave slopes is quite sensitive to the number of segments, and accurate computation of the location of the beginning of deposition is important. Uniform portions of a profile are single segments. Additional segment ends are designated by the model where K, Φ, P, or n_{cov} change.

CHANNEL ELEMENT

The channel element describes detachment, transport, and deposition by flow in terrace channels, diversions, natural waterways, grassed waterways, row middles or graded rows, tailwater ditches, and other similar channels where topography has caused overland flow to converge. The channel element does not describe erosion in gullies or large streams.

The same basic concepts are used in both the channel and overland flow elements. Discharge along the channel is assumed to vary directly with upstream drainage area. An initial discharge is permitted at the upper end of a channel to account for upland contributing areas. Changes in controlling variables like slope and cover along the channel are allowed.

Flow in most channels in fields is spatially varied, with discharge increasing along the channel. The model approximates the energy gradeline along the channel assuming a triangular channel section and steady flow at the characteristic peak discharge from a set of polynomial curves fitted to solutions of the normalized spatially varied flow equation (Chow, 1959). This feature approximates either drawdown or backwater at a channel outlet like at the edge of a field where vegetation may hinder runoff. As an alternative in the model, the slope of the energy gradeline can be assumed equal to the channel slope. After the slope of the energy gradeline is estimated, a triangular, rectangular, or "naturally eroded" section is selected at the user's option to compute flow hydraulics and channel erosion and sediment transport.

In the spring immediately after planting, concentrated flow from intense rains on a freshly prepared seedbed may erode through the finely tilled layer to the depth of secondary tillage. If the soil is susceptible to erosion by flow when tilled, the flow may erode deeper to the depth of primary tillage. Often the soil is much less erodible at this level and downcutting will stop here. Before the channel reaches a nonerodible layer, its width is a function of the flow's shear stress and the soil's critical shear stress. Once the flow reaches a relatively nonerodible layer, the channel widens. As it widens, the erosion rate decreases until it approaches zero as the channel approaches a maximum width. The maximum width depends on the flow's shear stress and the soil's critical shear stress. Data from rill erosion studies (Meyer et al., 1975; Lane and Foster, 1980) suggest that erosion by flow over a tilled, loose seedbed may be described by:

$$D_c = K_{ch} (1.35\bar{\tau} - \tau_{cr})^{1.05} \quad [10]$$

where D_c = erosion rate in a channel (mass/unit area of wetted perimeter/unit time), K_{ch} = soil erodibility factor for a channel erosion $\bar{\tau}$ = average shear of the flow at a channel section, and τ_{cr} = a critical shear stress below which erosion is negligible. Critical shear stress of the surface layer of soil seems to increase greatly over the year as the soil consolidates (Graf, 1971; Foster et al., 1980a).

The shear stress acting on the soil is the shear stress used to compute detachment and sediment transport capacity. Grass and mulch reduce this stress. Total shear is divided into that acting on the vegetation, mulch, or large scale roughness and that acting on the soil using sediment transport theory (Graf, 1971).

Shear stress at a channel location varies with time as runoff rises and falls. The model assumes that shear stress is triangularly distributed in time during the runoff event to estimate the time t_b that shear stress exceeds the critical shear stress. Shear stress is assumed constant and equal to shear stress computed from the characteristic peak discharge for this time period. This tends to overestimate total erosion for the storm. The derivation and

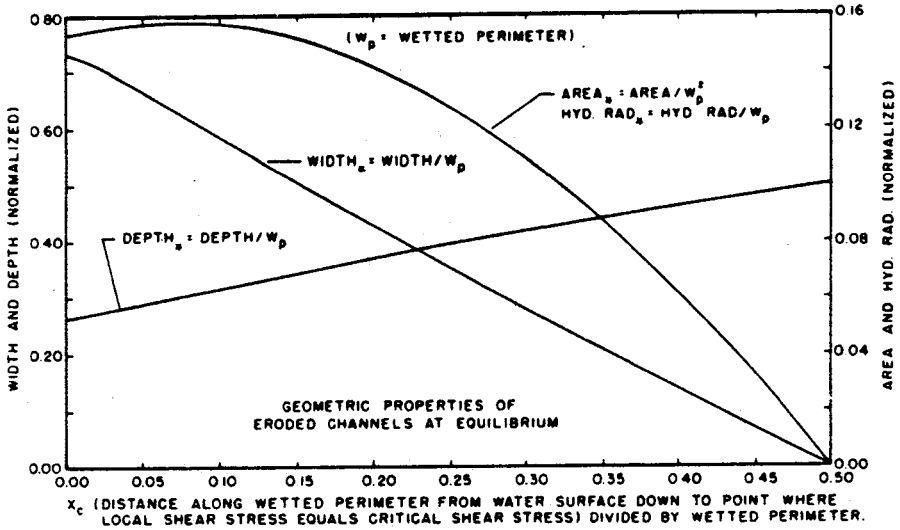

FIG. 3 Geometric properties of an eroding channel at equilibrium.

validation of the equations for channel erosion discussed below were described by Lane and Foster (1980).

Until the channel reaches the nonerodible layer, an active channel is assumed to be rectangular with the width obtained by Fig. 3 and 4 and equations [11] and [12]. The solution requires that a value for x_c be found. Given the discharge Q, Manning's n, and friction slope S_f, a value $g(x_c)$ is calculated from:

$$g(x_c) = (Qn/S_f^{1/2})^{3/8} (\gamma S_f/\tau_{cr}) \quad [11]$$

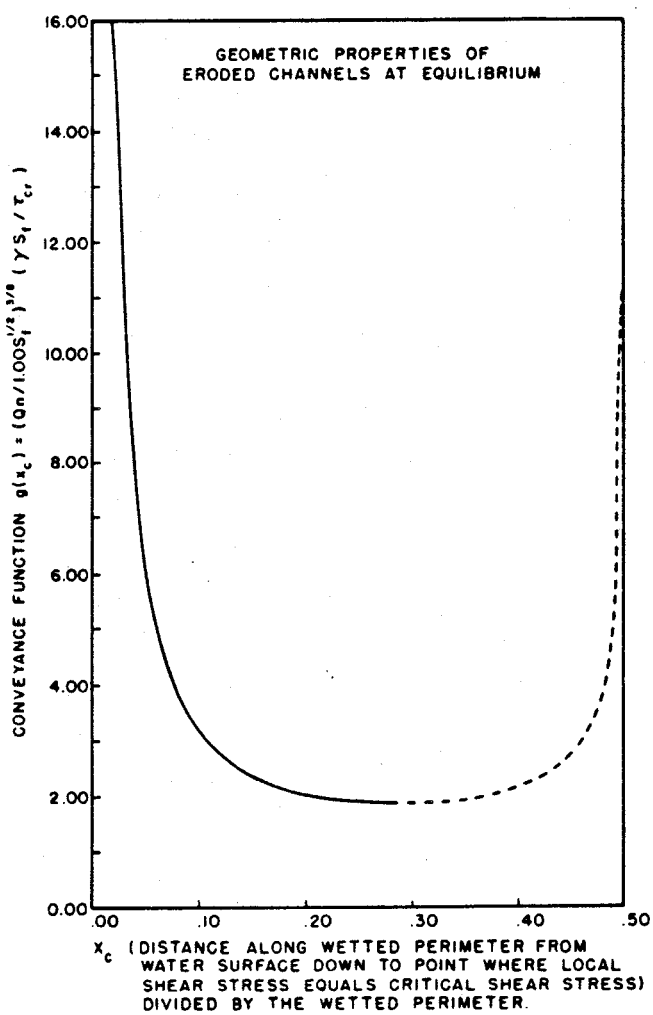

FIG. 4 Function $g(x_c)$ for an eroding channel at equilibrium.

Given a particular value $g(x_c)$, a value of x_c is obtained from Fig. 3. Having determined x_c, a value for $R_* =$ hydraulic radius/wetted perimeter and $W_* =$ width /wetted perimeter is read from Fig. 4. The width of the channel before it reaches the nonerodible layer is then calculated from:

$$W_{ac} = (Qn/S_f^{1/2})^{3/8} \; W_*/R^{5/8}) \quad [12]$$

The channel moves downward at the rate d_{ch}:

$$d_{ch} = D_c/\rho_{soil} = K_{ch} (1.35\tau - \tau_{cr})^{1.05}/\rho_{soil} \quad [13]$$

where ρ_{soil} = mass density of the soil in place. The erosion rate in the channel is:

$$E_{ch} = W_{ac} K_{ch} (1.35 \tau - \tau_{cr})^{1.05} t_b \quad [14]$$

where E_{ch} is the soil loss per unit channel length for the storm (mass/unit length).

Erosion rate e_p (mass/unit area of wetted perimeter/unit time) normal to the wetted perimeter at a point is assumed equal to:

$$e_p = K_{ch} (\tau_x - \tau_{cr})^{1.05} \quad [15]$$

where τ_x = the shear stress at a given point along the wetted perimeter. In order for a channel to be eroding downward in an equilibrium shape at an equilibrium rate, the vertical component of the erosion rates, e_p, must be equal at all points along the wetted perimeter. Equations [10 - 13] and Figs. 3 and 4 are based on this condition. The 1.35 factor is the ratio of the shear stress in the center of the channel to the average shear stress for the cross section.

Once the channel reaches the nonerodible boundary, erosion rate decreases with time as the channel widens. The rate decreases even if discharge rate remains constant. The width W of the channel at any time after the channel has eroded to the nonerodible layer is estimated by:

$$W_* = [1-\exp(-t_*)] \quad [16]$$

where:

$$W_* = (W - W_i)/(W_f - W_i) \quad [17]$$

$$t_* = (t - t_i)\,(dW/dt)_i/(W_f - W_i) \quad [18]$$

where W = width at t, W_i = width at t_i, W_f = final eroded width for $t \rightarrow \infty$ and the given Q, t = time, and $(dW/dt)_i$ = rate that channel widens at $t = t_i$. The initial widening rate is given by:

$$(dW/dt)_i = 2K_{ch}\,(\tau_b - \tau_{cr})^{1.05}/\rho_{soil} \quad [19]$$

where τ_b is given by:

$$f(x_b) = \left(\tau_b/\bar{\tau}\right) = \exp\,[0.127 - 0.516 \ln x_b - 0.408 (\ln x_b)^2 - 0.0344 (\ln x_b)^3] \qquad x_b \geq 0.02 \quad [20]$$

or

$$f(x_b) = \left(\tau_b/\bar{\tau}\right) = 0.13\, x_b/0.02 \qquad x_b < 0.02 \quad [21]$$

where x_b = flow depth/wetted perimeter.

The final width W_f is determined by finding the x_{cf} that gives:

$$(Qn/S_f^{1/2})^{3/8}\,(\gamma S_f/\tau_{cr}) = \left\{[x_{cf}(1 - 2x_{cf})]^{3/8}\, f(x_{cf})\right\}^{-1} \quad [22]$$

where $f(x_{cf})$ is the function given by equation [20] or [21] and evaluated at x_{cf}. The final width is:

$$W_f = \left\{(Qn/S_f^{1/2})\,[(1 - 2x_{cf})/x_{cf}^{5/3}]\right\}^{3/8} \quad [23]$$

Equations [16 - 23] are based on the assumption that in a rectangular channel on a nonerodible layer, the channel widens at the rate that the flow erodes the channel wall at the nonerodible layer. Widening ceases when the shear stress at the nonerodible boundary equals the critical shear stress.

Channel erosion after the channel reaches the nonerodible layer is:

$$E_{ch} = \Delta W\, H_{sw}\rho_{soil} \quad [24]$$

where ΔW = the change in width calculated from equations [16 - 23] and H_{sw} = the height of the channel sidewall.

IMPOUNDMENT ELEMENT

The impoundment element describes deposition behind impoundment terraces and other small structures that drain between storms through a pipe near the bottom of the impoundment where an orifice controls discharge.

Deposition is the main sedimentation process occurring in impoundments. Since transport capacity in impoundments is essentially nonexistent, the amount of sediment trapped in an impoundment depends primarily on time available for sediment to settle to the bottom of the impoundment before flow can carry the particles from the impoundment. The equations for the impoundment element were developed from regression analyses where relationships were fitted to simulate the data from a more complex model (Laflen et al., 1978). That model had previously been validated with field data (Laflen et al., 1972.

The fraction of a given particle type that passes through the impoundment is:

$$F_{pi} = A_p \exp(B_p\, d_{epi}) \quad [25]$$

where F_{pi} = fraction passing through the impoundment for particle type i, A_p and B_p = coefficients given below, and d_{eqi} = the equivalent sand diameter in microns of particle tipe i. Equation [25] is integrated over a particle class interval to obtain the total discharge for the particle class.

The coefficients A_p and B_p are given by:

$$A_p = 1.136 \exp(Z_s) \quad [26]$$

$$B_p = -0.152 \exp(Y_s) \quad [27]$$

with Z_s and Y_s in turn given by:

$$Z_s = (-6.68 \times 10^{-6})\, f\,(0.3048)^{B-2} - 0.0903B + (1.19 \times 10^{-4})C_{or} - (1.21 \times 10^{-4})V_{in} - 0.0185I \quad [28]$$

$$Y_s = (3.28 \times 10^{-5})\, f\,(0.3048)^{B-2} + 0.123B - (2.4 \times 10^{-4})C_{or} + (2.86 \times 10^{-4})\, V_{in} - 0.0108I \quad [29]$$

where f and B = coefficient and exponent in the power equation relating surface area to depth $S_a = fY_d^B$, Y_d = depth in the impoundment (m), S_a = surface area (m^2), V_{in} = volume of runoff reaching the impoundment (m^3), and I = infiltration rate in the impoundment (mm/h). The coefficient C_{or} related to the orifice in the pipe outlet is given by:

$$C_{or} = 0.15\, d_{or}^2 \quad [30]$$

where d_{or} = diameter of the orifice (mm).

Less water leaves the impoundment than entered it because of infiltration through the boundary of the impoundment. The volume leaving is estimated by:

$$V_{out} = 0.95\, V_{in} \exp(Z_r) \quad [31]$$

where V_{out} = volume of runoff discharged, and Z_r is given by:

$$Z_r = (-9.29 \times 10^{-6})\, f\,(0.3048)^{B-2} + 0.0282B + (1.25 \times 10^{-4})C_{or} - (1.09 \times 10^{-4})\, V_{in} - 0.0304I \quad [32]$$

In addition:

$$\text{If } I = 0.0,\ V_{out} = V_{in} \quad [33]$$

$$\text{If } V_{out} > V_{in},\ V_{out} = V_{in} \quad [34]$$

are additional constraints on V_{out} from equation [31] because 0 and V_{in} are not lower and upper limits for equations [31] and [32].

ERODED SEDIMENT CHARACTERISTICS

Sediment eroded from field-sized areas is often a mixture of primary particles and aggregates. The size and density distribution of these particles as they are detached is a function of soil properties, soil management, and rainfall and runoff characteristics. If deposition changes the distribution, usually the coarse and dense particles are deposited first, leaving a mixture of finer sediment. The initial particle input to the model is the distribution of the sediment as it is detached; the model calculates a new distribution when it calculates the occurrence of deposition. No selectivity is assumed in detachment of particles.

TABLE 1. TYPICAL SEDIMENT CHARACTERISTICS OF DETACHED SEDIMENT BEFORE DEPOSITION FOR A MIDWESTERN SOIL.*

Particle type	Diameter	Specific gravity	Fraction of total
	mm		mass basis
Primary clay	0.002	2.60	0.05
Primary silt	0.010	2.65	0.08
Small aggregate	0.030	1.80	0.50
Large aggregate	0.500	1.60	0.31
Primary sand	0.200	2.65	0.06

*Particle distribution in soil mass: Clay = 25%, Silt = 60%, Sand = 15%.

Based on a survey of existing data, values given in Table 1 are typical of some midwestern soils. If the particle distribution is unknown, the model estimates the distribution from the primary particle size distribution of the soil mass using the following equations:

$$PSA = SAO\,(1.0 - CLO)^{2.49} \quad [35]$$

$$PSI = 0.13\ SIO \quad [36]$$

$$PCL = 0.2\ CLO \quad [37]$$

$$SAG = 2\ CLO \qquad CLO < 0.25 \quad 38]$$

$$SAG = 0.28\,(CLO - 0.25) + 0.5 \qquad 0.25 \leqslant CLO \leqslant 0.50 \quad [39]$$

$$SAG = 0.57 \qquad 0.5 < CLO \quad [40]$$

$$LAG = 1.0 - PSA - PS - PCL - SAG \quad 41]$$

if LAG < 0.0, multiply PSA, PS, PCL, and SAG by same ratio to make:

$$LAG = 0.0 \quad [42]$$

The variables, CLO, SIO, SAO, PCL, PSI, PSA, SAG, and LAG, are respectively, fractions for primary clay, silt, and sand in the original soil mass, and primary clay, silt, sand, and small and large aggregates in the sediment at the point of detachment. The diameters for the particles are defined as:

$$DPCL = 0.002\ mm \quad [43]$$

$$DPSI = 0.010\ mm \quad [44]$$

$$DPSA = 0.200\ mm \quad [45]$$

$$DSAG = 0.03\ mm \qquad CLO < 0.25 \quad [46]$$

$$DSAG = 0.20\,(CLO - 0.25) + 0.03\ mm \qquad 0.25 \leqslant CLO \leqslant 0.60 \quad [47]$$

$$DSAG = 0.1\ mm \qquad 0.60 < CLO \quad [48]$$

$$DLAG = 2\ CLO\ mm \quad [49]$$

where DPCL, DPSI, DPSA, DSAG, and DLAG are, respectively, the diameters of the primary clay, silt, and sand, and the small and large aggregates in the sediment. The assumed specific gravities are shown in Table 1. The primary particle composition of the aggregates is estimated from:

$$CLSAG = SAG\,[CLO/(CLO + SIO)] \quad [50]$$

$$SISAG = SAG\,[SIO/(CLO + SIO)] \quad [51]$$

$$SASAG = 0.0 \quad [52]$$

$$CLLAG = CLO - PCL - CLSAG \quad [53]$$

$$SILAG = SIO - PSI - SISAG \quad [54]$$

$$SALAG = SAO - PSA \quad [55]$$

where CLSAG, SISAG, and SASAG = fractions of the total for the sediment of, respectively, primary clay, silt, and sand in the small aggregates in the sediment load, and CLLAG, SILAG, and SALAG are corresponding fractions for the large aggregates.

If the fraction of clay in the large aggregate based on the mass of the large aggregate and not on the total mass of sediment is less than 0.5 times CLO, the distribution of the particle types is recomputed. A sum of Γ is computed whereby:

$$\Gamma = PCL + PSI + PSA \quad [56]$$

The fractions PSA, PSI, and PCL are not changed. The new SAG is:

$$SAG = (0.3 + 0.5\,\Gamma)\,(CLO + SIO)/([1 - 0.5(CLO + SIO)] \quad [57]$$

Equation [57] is derived given (i) previously determined values for PCL, PSI, and PSA; (ii) the assumption that the sum of primary clay fractions for the total sediment is 1; and (iii) the assumption that the fraction of primary clay in LAG equals one half of the primary clay in the original soil.

The model also computes an enrichment ratio using values for specific surface area of organic matter, clay, silt, and sand. Organic matter is distributed among the particle types based on the proportion of primary clay in each type. The enrichment ratio is the ratio of total specific surface area of the sediment to that for the original soil.

DISCUSSION

The model gave reasonable results, when compared with data from concave plots under simulated rainfall, single terrace watersheds, small watersheds with impoundment terraces, and a small watershed under conservation tillage. The simulations were made using measured rainfall and runoff values.

Concave Plots

Three concave plots 10.7 m long were carefully shaped in uniform soil so that slope along the plots continuously decreased from 18 percent at the upper end to 0 percent at the lower end (Foster et al., 1980b). Simulated rainfall at 64 mm/h was applied to one of the plots and deposi-

TABLE 2. COMPARISON OF OBSERVED SOIL LOSS FROM CONCAVE FIELD PLOTS WITH THAT COMPUTED BY THE MODEL.

	Plot length	Slope at lower end	Sediment yield	Particle distribution in size class				
				0.002	0.03	0.3	0.75	1.5 mm
	m	%	kg/m	Fraction				
Observed*	7.0	6	8.6	0.05	0.36	0.15	0.17	0.27
Observed	8.8	3	3.9	0.07	0.48	0.12	0.12	0.21
Computed			6.5	0.08	0.58	0.24	0.10	0.01
Observed	10.7	0	3.0	0.10	0.85	0.02	0.01	0.02
Computed			3.0	0.19	0.80	0.01	0.00	0.00

*These data were used to calibrate soil erodibility factor, Manning's n, and particle distribution of sediment reaching deposition area. Source of data: Foster et al. (1980b).

tion began at 7 m from the upper end. Plot ends were installed at 7.0 m and 8.8 m on the other two plots. The measured particle distribution of the sediment entering the deposition area was used, and the soil erodibility factor and Manning's n were adjusted in the model to give the observed soil loss and particle distribution for the 7.0 m plot. The results shown in Table 2 for the 8.8 and 10.7 m plots were obtained using these calibrated values and the approximate slope shape curves in the model rather than the actual slope shape.

Single Terrace Watersheds

Soil loss was simulated for eight years of data, about 53 runoff producing storms, from small, single terrace watersheds at Guthrie, Oklahoma (Daniel et al., 1943). The simulations were made without calibration using instructions in the user manual for the model (Foster et al., 1980a). Table 3 gives computed and measured results.

Impoundment Terraces

Soil loss was simulated under a range of rainfall and runoff characteristics for six selected storms at the Charles City, and Guthrie Center, Iowa, and for five storms at Eldora, Iowa. Data were taken from an impoundment terrace study (Laflen et al., 1972). The model was run using the user manual instruction without calibration. Table 4 gives the results.

Small Watershed

Simulations were run without calibrating for approximately 2½ years of data, about 35 runoff producing storms, from the P2 watershed at Watkinsville, Georgia in conservation tillage systems for corn (Smith et al., 1978). Deposition in the backwater from the flume at the watershed outlet was modeled. Deposition measured in the flume backwater was about equal to the measured sediment yield on a similar, nearby watershed (Langdale et al., 1979). The computed sediment yield total for the period of record was 1.47 kg/m², while the measured value was 1.95 kg/m².

TABLE 3. COMPUTED AND OBSERVED SOIL LOSS FOR 8 YEARS OF DATA FROM SINGLE TERRACE WATERSHEDS AT GUTHRIE, OKLAHOMA*.

Terrace	Total soil loss for period per unit area of watershed	
	Observed	Computed
	kg/m²	kg/m²
Uniform grade of 0.0017, 457 m long	4.8	4.6
Uniform grade of 0.005, 457 m long	12.1	10.6
Variable grade, 0.005 at outlet to 0 at upper end, 871 m long	13.8	11.9
Variable grade, 0.0033 at outlet to 0 at upper end, 773 m long	12.2	6.4

*Source of data: Daniel et al. (1943)

Overland Flow Detachment

The relationships for detachment used in the overland flow element gave good results for a watershed at Treynor, Iowa. Estimates were better than those from the USLE using storm EI (Foster et al., 1977) and those obtained using the USLE and runoff volume and peak discharge (Onstad et al., 1977) as measures of erosivity. These results were confirmed by Lombardi (1979) for data from natural rainfall on uniform slopes. On long-term simulation, the model should produce results similar to those of the USLE for uniform slopes.

Overland Flow Sediment Transport

As the results in Table 2 indicate, estimates of sediment transport by overland flow may be in error by a factor of two. The Yalin equation was selected to describe sediment transport by overland flow after studies showed that it gave better results than did several other widely used equations (Alonso, 1980; Neibling and Foster, 1980). However, overland flow conditions are outside the range of most sediment transport equations developed for stream flow. Many give results greatly in error for overland flow.

Channel Detachment

The relationships for channel erosion are the ones most likely to be in error, because data for flow concentrations 300 mm wide from the studies (Meyer et al., 1975; Lane and Foster, 1980) where the relationships were derived may not apply to 2 m wide channels. Also, parameter values for channel soil erodibility and critical shear stress are not readily available. Few models except that of Bruce et al. (1975) consider the decay in erosion with time due to previous erosion. This component of the model may require calibration.

TABLE 4. SIMULATED AND OBSERVED SOIL LOSS FOR IMPOUNDMENT TERRACES IN IOWA.

Location	Total soil loss per unit area of watershed for selected storms	
	Observed	Computed
	kg/m²	kg/m²
Eldora	0.115	0.069
Charles City	0.043	0.016
Guthrie Center	0.050	0.050

SUMMARY

An erosion-sediment yield model for field-sized areas was developed for use on a storm-by-storm basis. The overall objective was to develop a model incorporating fundamental erosion-sediment transport relationships for use in evaluating best management practices for control of erosion and sediment yield from farm fields. The procedure allows parameters to change along the overland flow profile and along waterways to represent both spatial variability and the variations that occur from storm-to-storm. Many of the model parameters are directly from the Universal Soil-Loss Equation (USLE) and other similar, process-type relationships. For this reason, we feel that the model has immediate applications without extensive calibration.

Individual components of the model were tested using experimental data from studies of overland flow, erodible channels, and impoundments. Testing suggests that the model gives reasonable results and may be a useful tool for analyzing the influence of alternate management practices on erosion and sediment yield from field-sized-areas.

References

1 Alonso, C. V. 1980. Selecting a formula to estimate sediment transport in nonvegetated channels. In: CREAMS - A Field Scale Model for Chemicals, Runoff, and Erosion from Agricultural Management Systems. Vol III: Supporting Documentation. Conservation Research Report No. 26. USDA, Sci. and Educ. Admin. Chpt. 5. pp. 426-439.

2 Beasley, D. B., E. J. Monke, and L. F. Huggins. 1980. ANSWERS: A model for watershed planning. TRANSACTIONS of the ASAE. 23(4):839-944.

3 Bruce, R. R., L. A. Harper, R. A. Leonard, W. M. Snyder, and A. W. Thomas. 1975. A model for runoff of pesticides from small upland watersheds. J. Environ. Qual. 4(4):541-548.

4 Chow, V. T. 1959. Open-Channel Hydraulics. McGraw-Hill Book Co. New York, NY. 680 pp.

5 Davis, S. S. 1978. Deposition of nonuniform sediment by overland flow on concave slopes. M. S. Thesis. Purdue Univ., W. Lafayette, IN.

6 Daniel, H. A., H. M. Elwell and M. B. Cox. 1943. Investigations in erosion control and reclamation of eroded land at the Red Plains Conservation Experiment Station, Guthrie, OK, 1930-40. USDA-Tech. Bull. No. 837. 94 pp.

7 Donigian, A. S., Jr. and N. H. Crawford. 1976. Modeling nonpoint source pollution from the land surface. EPA-600/3-76-083. U. S. Environ. Protection Agency. 279 pp.

8 Einstein, H. A. 1968. Deposition of suspended particles in a gravel bed. J. Hydr. Div. ASCE. 94(HY5):1197-1205.

9 Ellison, W. D. 1947. Soil erosion studies. AGRICULTURAL ENGINEERING 28:145-146, 127-201, 245-248, 297-300, 349-351, 402-405, 442-444.

10 Foster, G. R., L. J. Lane, and J. D. Nowlin. 1980a. A model to estimate sediment yield from field sized areas: Selection of parameter values: In: CREAMS - A Field Scale Model for Chemicals, Runoff, and Erosion from Agricultural Management Systems. Vol. II: User Manual. Conservation Research Report No. 26. USDA, Sci. and Educ. Admin. Chpt. 2. pp. 193-281.

11 Foster, G. R., W. H. Neibling, S. S. Davis, and E. E. Alberts. 1980b. Modeling particle segregation during deposition by overland flow. In: Proc. Hydrologic Transport Modeling Symposium. ASAE Publ. 4-80. pp. 184-195.

12 Foster, G. R. and L. D. Meyer. 1972. Transport of soil particles by shallow flow. TRANSACTIONS of the ASAE 15(1):99-102.

13 Foster, G. R. and L. D. Meyer. 1975. Mathematical simulation of upland erosion by fundamental erosion mechanics. In: Present and Prospective Technology for Predicting Sediment Yields and Sources. ARS-S-40. USDA, Agric. Research Ser. pp. 190-207.

14 Foster, G. R., L. D. Meyer, and C. A. Onstad. 1977. A runoff erosivity factor and variable slope length exponents for soil loss estimates. TRANSACTIONS of the ASAE 20(4):683-687.

15 Graf, W. H. 1971. Hydraulics of Sediment Transport. McGraw-Hill Book Co. New York, NY. 544 pp.

16 Khaleel, R., G. R. Foster, K. R. Reddy, M. R. Overcash and P. W. Westerman. 1979. A nonpoint source model for land areas receiving animal wastes: III. A conceptual model for sediment and manure transport. TRANSACTIONS of the ASAE 22(5):1353-1361.

17 Laflen, J. M., H. P. Johnson, and R. O. Hartwig. 1978. Sedimentation modeling of impoundment terraces. TRANSACTIONS of the ASAE 21(6):1131-1135.

18 Laflen, J. M., H. P. Johnson, and R. C. Reeves. 1972. Soil loss from tile outlet terraces. J. Soil and Water Conserv. 27(2):74-77.

19 Lane, L. J. and G. R. Foster. 1980. Concentrated flow relationships. In: CREAMS - A Field Scale Model for Chemicals, Runoff, and Erosion from Agricultural Management Systems. Vol. III: Supporting Documentation. Conservation Research Report No. 26. USDA, Sci. and Educ. Admin. Chpt. 10. pp. 474-485.

20 Lane, L. J., D. A. Woolhiser, and V. Yevjevich. 1975. Influence of simplification in watershed geometry in simulation of surface runoff. Hydrology Paper No. 81. Colorado State Univ., Fort Collins. 50 pp.

21 Langdale, G. W., A. P. Barnett, R. A. Leonard, and W. G. Fleming. 1979. Reduction of soil erosion by no-till systems in the Southern Piedmont. TRANSACTIONS of the ASAE 22(1):82-86, 92.

22 Li, R. M. 1977. Water and sediment routing from watersheds. In: Proc. River Mechanics Institute. Colorado State Univ., Fort Collins. Chpt. 9.

23 Lombardi, F. 1979. Universal Soil Loss Equation (USLE), runoff erosivity factor, slope length exponent, and slope steepness exponent for individual storms. Ph.D. Thesis. Purdue Univ., W. Lafayette, IN. 128 pp.

24 Meyer, L. D., G. R. Foster, and S. Nikolov. 1975. Effect of flow rate and canopy on rill erosion. TRANSACTIONS of the ASAE 18(5):905-911.

25 Meyer, L. D. and W. H. Wischmeier. 1969. Mathematical simulation of the process of soil erosion by water. TRANSACTIONS of the ASAE12(6):754-758, 762.

26 Neibling, W. H. and G. R. Foster. 1980. Sediment transport capacity of overland flow. In: CREAMS - A Field Scale Model for Chemicals, Runoff, and Erosion from Agricultural Management Systems. Vol. III: Supporting Documentation. Conservation Research Report No. 26. USDA, Sci. and Educ. Admin. Chpt. 10. pp. 463-473.

27 Onstad, C. A., R. F. Piest, and K. E. Saxton. 1976. Watershed erosion model validation for Southwest Iowa. In: Proc. of the Third Federal Inter-Agency Sedimentation Confer. Water Resources Council. Washington, DC. Chpt. 1. pp. 23-24.

28 Smith, C. N., R. A. Leonard, G. W. Langdale, and G. W. Bailey. 1978. Transport of agricultural chemicals from small upland Piedmont watersheds. EPA-600/3-78-056. U. S. Environ. Protection Agency. 364 pp.

29 U. S. Department of Agriculture (USDA), 1980. CREAMS - A Field Scale Model for Chemicals, Runoff, and Erosion from Agricultural Management Systems. Conservation Research Report No. 26. Sci. and Educ. Admin. 643 pp.

30 Williams, J. R. 1975. Sediment-yield prediction with universal equation using runoff energy factor. In: Present and Prospective Technology for Predicting Sediment Yields and Sources. ARS-S-40. USDA, Agric. Research Ser. pp. 244-253.

31 Wischmeier, W. H. and D. D. Smith. 1978. Predicting Rainfall Erosion Losses. Agricultural Handbook No. 537. USDA, Sci. and Educ. Admin. 58 pp.

32 Yalin, Y. S. 1963. An expression for bed-load transportation. J. Hydr. Div. ASCE. 89(HY3):221-250.

LIST OF SYMBOLS

A_p	Coefficient in equation for deposition in an impoundment
B	Exponent in surface area - depth relationship for an impoundment
B_p	Exponent in equation for deposition in an impoundment
CLLAG	Clay content of large aggregates, fraction of total sediment
CLO	Fraction of original soil made up of primary clay
CLSAG	Clay content of small aggregates, fraction of total sediment
C_{or}	Orifice coefficient for drainage from impoundment
d_{ch}	Rate that channel erodes downward, (depth/time)
d_{eq}	Equivalent sand diameter of a sediment particle
d_{or}	Diameter of orifice in an impoundment drain
D_c	Rate of sediment detachment by flow in channels (mass/area/time)
D_d	Rate of deposition by flow (mass/area/time)
D_F	Rate of detachment or deposition by flow (mass/area/time)
D_{Fr}	Rate of sediment detachment by rill erosion, (mass/area/time)

D_l	Rate of detachment by flow at lower end of a segment, (mass/area/time)
D_L	Rate of lateral inflow of sediment, (mass/area or length/time)
D_{Li}	Rate of sediment from interrill areas (mass/area/time)
D_u	Rate of detachment by flow at upper end of a segment, (mass/area/time)
DLAG	Diameter of large aggregate sediment particles
DPCL	Diameter of primary clay sediment particles
DPSA	Diameter of primary sand sediment particles
DPSI	Diameter of primary silt sediment particles
DSAG	Diameter of small aggregate sediment particles
E_p	Erosion rate normal to channel boundary, (mass/area/time)
E_{ch}	Erosion rate per unit length of channel, (mass/length of channel)
EI	Rainfall erosivity, total storm energy times maximum 30-min intensity
f	Coefficient in surface area-depth relationship for impoundment
$f(x_b)$	Shear stress distribution around a channel
F_{pi}	Fraction of a particular particle class deposited in an impoundment
$g(x_c)$	Conveyance function for flow in an eroding channel at equilibrium
H_{rw}	Height of channel sidewall
i	Particle class index
I	Infiltration rate through boundary of an impoundment
K	Soil erodibility factor for the USLE
K_{ch}	Soil erodibility factor for channel erosion
LAG	Fraction of sediment made up of large aggregates
n	Manning's n
n_{bov}	Manning's n for bare, smooth, overland flow surface
n_{cov}	Manning's n for a covered or rough overland flow surface
P	Contouring component of USLE supporting practices factor
PCL	Fraction of sediment made up of primary clay
PSA	Fraction of sediment made up of primary sand
PSI	Fraction of sediment made up of primary silt
q_s	Sediment load, (mass/width/time)
q_{su}	Sediment load at upper end of segment, (mass/width/time)
q_w	Rate of runoff discharge per unit width (volume/time /width)
Q	Discharge rate, (volume/time)
R_*	Ratio of hydraulic radius to wetted perimeter
s_o	Sine of angle of slope
S_a	Surface area in an impoundment
S_f	Friction slope for flow hydraulics in a channel
SAG	Fraction of sediment made up of small aggregates
SALAG	Fraction of sand in large aggregates, fraction of total sediment
SAO	Fraction of original soil made up of primary sand
SASAG	Fraction of sand in small aggregates, fraction of total sediment
SILAG	Fraction of silt in large aggregates, fraction of total sediment
SIO	Fraction of original soil made up of primary silt
SISAG	Fraction of silt in small aggregates, fraction of total sediment
t	Time
t_b	Time that shear stress exceeds critical shear stress
t_*	Normalized time for channel erosion
t_i	Initial time
T_c	Transport capacity, (mass/area/time)
V_{in}	Runoff volume into impounment
V_{out}	Runoff volume out of impoundment
V_s	Particle fall velocity
V_u	Runoff volume per unit area, (depth)
W	Channel width
W_*	Normalized channel width
W_{ec}	Width of an eroding channel at equilibrium
W_f	Final eroded channel width
W_i	Initial channel width
x	Distance
x_b	Normalized distance around wetted perimeter to nonerodible boundary
x_c	Normalized distance around wetted perimeter to location where $\tau=\tau_{cr}$ for an eroding channel at equilibrium
x_{cf}	Normalized distance around wetted perimeter to location where $\tau=\tau_{cr}$ at nonerodible boundary
y	Flow depth
Y_d	Depth in impoundment
Y_s	Exponent in deposition equation for an impoundment
Z_r	Exponent in equation for runoff reduction by an impoundment.
Z_s	Exponent in equation for deposition in impoundment
α	Reaction coefficient for deposition by flow, length^{-1}
γ	Weight density of water
Γ	Sum of PCL, PSI, and PSA
Δx	Segment length
ΔW	Change in channel width
η	Slope length exponent for rill erosion
ε	Coefficient in deposition equation
ρ_{soil}	Mass density of soil in place
σ_p	Peak runoff rate, (depth/time)
$\bar{\tau}$	Average shear stress around wetted perimeter
τ_b	Shear stress in channel at a nonerodible boundary
τ_{cr}	Critical shear stress
τ_{soil}	Shear stress acting on soil
τ_x	The shear stress at a given point along the wetted perimeter.
Φ	Soil loss ratio from USLE

Leonard J. Kane

PREDICTING RAINFALL EROSION LOSSES

A GUIDE TO CONSERVATION PLANNING

Supersedes Agriculture Handbook No. 282, "Predicting Rainfall-Erosion Losses From Cropland East of the Rocky Mountains"

Science and Education Administration
United States Department of Agriculture
in cooperation with
Purdue Agricultural Experiment Station

USDA policy does not permit discrimination because of age, race, color, national origin, sex, or religion. Any person who believes he or she has been discriminated against in any USDA-related activity should write immediately to the Secretary of Agriculture, Washington, D.C. 20250.

December 1978

ABSTRACT

Wischmeier, W. H., and Smith, D.D. 1978. Predicting rainfall erosion losses—a guide to conservation planning. U.S. Department of Agriculture, Agriculture Handbook No. 537.

The Universal Soil Loss Equation (USLE) enables planners to predict the average rate of soil erosion for each feasible alternative combination of crop system and management practices in association with a specified soil type, rainfall pattern, and topography. When these predicted losses are compared with given soil loss tolerances, they provide specific guidelines for effecting erosion control within specified limits. The equation groups the numerous interrelated physical and management parameters that influence erosion rate under six major factors whose site-specific values can be expressed numerically. A half century of erosion research in many States has supplied information from which at least approximate values of the USLE factors can be obtained for specified farm fields or other small erosion prone areas throughout the United States. Tables and charts presented in this handbook make this information readily available for field use. Significant limitations in the available data are identified.

The USLE is an erosion model designed to compute longtime average soil losses from sheet and rill erosion under specified conditions. It is also useful for construction sites and other nonagricultural conditions, but it does not predict deposition and does not compute sediment yields from gully, streambank, and streambed erosion.

Keywords: Conservation practices, conservation tillage, construction sites, crop canopy, crop sequence, delivery ratios, erosion factors, erosion index, erosion prediction, erosion tolerances, erosivity, gross erosion, minimum tillage, no-till, rainfall characteristics, rainfall data, residue mulch, runoff, sediment, sediment delivery, slope effect, water quality, soil erodibility.

For sale by the Superintendent of Documents, U.S. Government Printing Office
Washington, D.C. 20402

Stock Number 001-000-03903-2

CONTENTS

Purpose of handbook 1
History of soil loss equations 1
Soil loss tolerances 2
Soil loss equation 3
Rainfall and runoff factor (**R**) 5
  Rainfall erosion index 5
  R values for thaw and snowmelt 7
Soil erodibility factor (**K**) 8
  Definition of factor **K** 8
  Values of **K** for specific soils 8
  Soil erodibility nomograph 10
Topographic factor (**LS**) 12
  Slope-effect chart 12
  Slope-length effect 14
  Percent slope 15
  Irregular slopes 16
  Changes in soil type or cover along the slope 16
  Equation for soil detachment on successive segments of a slope 17
Cover and management factor (**C**) 17
  Definition of factor **C** 17
  Cropstage periods 18
  Quantitative evaluations of crop and management effects 18
  Soil loss ratios 20
  Erosion index distribution data 21
  Procedure for deriving local **C** values 28
Support practice factor (**P**) 34
  Contouring 34
  Contour stripcropping 36
  Terracing 37
Applying the soil loss equation 40
  Predicting cropland soil losses 40
  Determining alternative land use and treatment combinations 42
  Construction sites 44
  Estimating upslope contributions to watershed sediment yield 45
  Accuracy of USLE predictions 47
References 48
Appendix 50
  Estimating percentages of canopy and mulch covers 50
  Probability values of **EI** in the United States 50
  Computing the erosion index from recording-rain gage records 50
  Conversion to metric system 51

TABLES

1.—Computed **K** values for soils on erosion research stations 9
2.—Approximate values of the soil erodibility factor, **K**, for 10 benchmark soils in Hawaii 9
3.—Values of the topographic factor, **LS**, for specific combinations of slope length and steepness 12
4.—Estimated relative soil losses from successive equal-length segments of a uniform slope 15
5.—Ratio of soil loss from cropland to corresponding loss from continuous fallow 22
5—A.—Approximate soil loss ratios for cotton 25
5—B.—Soil loss ratios for conditions not evaluated in table 5 26
5—C.—Soil loss ratios (percent) for cropstage 4 when stalks are chopped and distributed without soil tillage 26
5—D.—Factors to credit residual effects of turned sod 26
6.—Percentages of the average annual **EI** which normally occurs between January 1 and the indicated dates. Computed for the geographic areas shown in figure 9 . . 28
7.—Monthly distribution of **EI** at selected rain gage locations 29
8.—Sample working table for derivation of a rotation **C** value 30
9.—Mulch factors and length limits for construction slopes 31
10.—Factor **C** value for permanent pasture, range, and idle land 32
11.—Factor **C** values for undisturbed forest land 33
12.—Factor **C** for mechanically prepared woodland sites 34
13.—**P** values and slope-length limits for contouring 35
14.—**P** values, maximum strip widths, and slope-length limits for contour stripcropping 36
15.—**P** values for contour-farmed terraced fields 37
16.—Maximum permissible **C** values (**T/RKLS**) for **R** = 180, **K** = 0.32, **and T** = 5 43
17.—Observed range and 50-, 20-, and 5 percent probability values of erosion index at each of 181 key locations 52
18.—Expected magnitudes of single-storm **EI** index values 54
19.—Kinetic energy of rainfall expressed in foot-tons per acre per inch of rain 56
20.—Kinetic energy of rainfall expressed in metric ton-meters per hectare per centimeters of rain . 56

FIGURES

1.—Average annual values of the rainfall erosion index (map) . . . . . between pages 6 and 7
2.—Estimated average annual values of the rainfall erosion index in Hawaii 7
3.—The soil erodibility nomograph 11
4.—Slope-effect chart (topographic factor, **LS**) 13
5.—Influence of vegetative canopy on effective **EI** values 19
6.—Combined mulch and canopy effects when average fall distance of drops from canopy to the ground is about 40 inches 19
7.—Combined mulch and canopy effects when average fall distance of drops from canopy to the ground is about 20 inches 19
8.—Typical **EI**-distribution curves for three rainfall patterns 27
9.—Key map for selection of applicable **EI**-distribution data from table 6 27
10.—Relation of percent cover to dry weight of uniformly distributed residue mulch 50
11.—Slope-effect chart for metric system 58

PREDICTING RAINFALL EROSION LOSSES— A GUIDE TO CONSERVATION PLANNING

Walter H. Wischmeier and Dwight D. Smith[1]

PURPOSE OF HANDBOOK

Scientific planning for soil and water conservation requires knowledge of the relations between those factors that cause loss of soil and water and those that help to reduce such losses. Controlled studies on field plots and small watersheds have supplied much valuable information regarding these complex factor interrelations. But the greatest possible benefits from such research can be realized only when the findings are converted to sound practice on the numerous farms and other erosion prone areas throughout the country. Specific guidelines are needed for selecting the control practices best suited to the particular needs of each site.

The soil loss prediction procedure presented in this handbook provides such guidelines. The procedure methodically combines research information from many sources to develop design data for each conservation plan. Widespread field experience for more than two decades has proved it highly valuable as a conservation planning guide.

The procedure is founded on an empirical soil loss equation that is believed to be applicable wherever numerical values of its factors are available. Research has supplied information from which at least approximate values of the equation's factors can be obtained for specific farm fields or other small land areas throughout most of the United States. Tables and charts presented in this handbook make this information readily available for field use.

This revision of the 1965 handbook (*64*) updates the content and incorporates new material that has been available informally or from scattered research reports in professional journals. Some of the original charts and tables are revised to conform with additional research findings, and new ones are developed to extend the usefulness of the soil loss equation. In some instances, expanding a table or chart sufficiently to meet the needs for widespread field application required projection of empirical factor relationships appreciably beyond the physical limits of the data from which the relationships were derived. Estimates obtained in this manner are the best information available for the conditions they represent. However, the instances are identified in the discussions of the specific erosion factors, tables, and charts. Major research needs are suggested by these discussions and were recently summarized in an available publication by Stewart and others (*42*).

HISTORY OF SOIL LOSS EQUATIONS

Developing equations to calculate field soil loss began about 1940 in the Corn Belt. The soil loss estimating procedure developed in that region between 1940 and 1956 has been generally referred to as the slope-practice method. Zingg (*64*)[2] published an equation in 1940 relating soil loss rate to length and percentage of slope. The following year, Smith (*38, 39*) added crop and conservation practice factors and the concept of a specific soil loss limit, to develop a graphical method for

[1] Retired. Former research statistician (water management), Science and Education Administration (SEA), and professor emeritus, agricultural engineering, Purdue University, West Lafayette, Ind.; and agricultural engineer, SEA, Beltsville, Md.

[2] Numbers in parentheses refer to References p. 48.

determining conservation practices on Shelby and associated soils of the Midwest. Browning and associates (*6*) added soil and management factors and prepared a set of tables to simplify field use of the equation in Iowa. Research scientists and operations personnel of the Soil Conservation Service (SCS) in the North Central States worked together in developing the slope-practice equation for use throughout the Corn Belt.

A national committee met in Ohio in 1946 to adapt the Corn Belt equation to cropland in other regions. This committee reappraised the Corn Belt factor values and added a rainfall factor. The resulting formula, generally known as the Musgrave Equation (*31*), has been widely used for estimating gross erosion from watersheds in flood abatement programs. A graphical solution of the equation was published in 1952 (*19*) and used by the SCS in the Northeastern States.

The soil loss equation presented in this handbook has become known as the Universal Soil Loss Equation (USLE). Regardless of whether the designation is fully accurate, the name does distinguish this equation from the *regionally* based soil loss equations. The USLE was developed at the National Runoff and Soil Loss Data Center established in 1954 by the Science and Education Administration (formerly Agricultural Research Service) in cooperation with Purdue University. Federal-State cooperative research projects at 49 locations[3] contributed more than 10,000 plot-years of basic runoff and soil loss data to this center for summarizing and overall statistical analyses. After 1960, rainfall simulators (*23*) operating from Indiana, Georgia, Minnesota, and Nebraska were used on field plots in 16 states to fill some of the gaps in the data needed for factor evaluation.

Analyses of this large assembly of basic data provided several major improvements for the soil loss equation (*53*): (a) a rainfall erosion index evaluated from local rainfall characteristics; (b) a quantitative soil erodibility factor that is evaluated directly from soil property data and is independent of topography and rainfall differences; (c) a method of evaluating cropping and management effects in relation to local climatic conditions; and (d) a method of accounting for effects of interactions between crop system, productivity level, tillage practices, and residue management.

Developments since 1965 have expanded the use of the soil loss equation by providing techniques for estimating site values of its factors for additional land uses, climatic conditions, and management practices. These have included a soil erodibility nomograph for farmland and construction areas (*58*); topographic factors for irregular slopes (*12, 55*); cover factors for range and woodland (*57*); cover and management effects of conservation tillage practices (*54*); erosion prediction on construction areas (*61, 24, 25*); estimated erosion index values for the Western States and Hawaii (*5, 21, 55*); soil erodibility factors for benchmark Hawaii soils (*9*); and improved design and evaluation of erosion control support practices (*17, 36*).

Research is continuing with emphasis on obtaining a better understanding of the basic principles and processes of water erosion and sedimentation and development of fundamental models capable of predicting specific-storm soil losses and deposition by overland flow (*10, 11, 22, 26, 32*). The fundamental models have been helpful for understanding the factors in the field soil loss equation and for interpreting the plot data.

SOIL LOSS TOLERANCES

The term "soil loss tolerance" denotes the maximum level of soil erosion that will permit a high level of crop productivity to be sustained economically and indefinitely.

[3] The data were contributed by Federal-State cooperative research projects at the following locations: Batesville, Ark.; Tifton and Watkinsville, Ga.; Dixon Springs, Joliet, and Urbana, Ill.; Lafayette, Ind.; Clarinda, Castana, Beaconsfield, Independence, and Seymour, Iowa; Hays, Kans.; Baton Rouge, La.; Presque Isle, Maine; Benton Harbor and East Lansing, Mich.; Morris, Minn.; Holly Springs and State College, Miss.; Bethany and McCredie, Mo.; Hastings, Nebr.; Beumerville, Marlboro, and New Brunswick, N.J.; Ithaca, Geneva, and Marcellus, N.Y.; Statesville and Raleigh, N.C.; Coshocton and Zanesville, Ohio; Cherokee and Guthrie, Okla.; State College, Pa.; Clemson and Spartanburg, S.C.; Madison, S.Dak.; Knoxville and Greeneville, Tenn.; Temple and Tyler, Tex.; Blacksburg, Va.; Pullman, Wash.; LaCrosse, Madison, and Owen, Wis.; and Mayaguez, P.R.

The major purpose of the soil loss equation is to guide methodical decisionmaking in conservation planning on a site basis. The equation enables the planner to predict the average rate of soil erosion for each of various alternative combinations of crop system, management techniques, and control practices on any particular site. When these predicted losses can be compared with a soil loss tolerance for that site, they provide specific guidelines for effecting erosion control within the specified limits. Any cropping and management combination for which the predicted erosion rate is less than the tolerance may be expected to provide satisfactory erosion control. From the satisfactory alternatives indicated by this procedure, the one best suited to a particular farm or other enterprise may then be selected.

Soil loss tolerances ranging from 5 to 2 t/A/year for the soils of the United States were derived by soil scientists, agronomists, geologists, soil conservationists, and Federal and State research leaders at six regional workshops in 1961 and 1962. Factors considered in defining these limits included soil depth, physical properties and other characteristics affecting root development, gully prevention, on-field sediment problems, seeding losses, soil organic matter reduction, and plant nutrient losses. A deep, medium-textured, moderately permeable soil that has subsoil characteristics favorable for plant growth has a greater tolerance than soils with shallow root zones or high percentages of shale at the surface. Widespread experience has shown these soil loss tolerances to be feasible and generally adequate for sustaining high productivity levels indefinitely. Some soils with deep favorable root zones may exceed the 5-t tolerance without loss of sustained productivity.

Soil loss limits are sometimes established primarily for water quality control. The criteria for defining field soil loss limits for this purpose are not the same as those for tolerances designed to preserve cropland productivity. Soil depth is not relevant for offsite sediment control, and uniform limits on erosion rates will allow a range in the quantities of sediment per unit area that are delivered to a river. Soil material eroded from a field slope may be deposited in the field boundaries, in terrace channels, in depressional areas, or on flat or vegetated areas traversed by the overland flow before it reaches a river. The erosion damages the cropland on which it occurs, but sediment deposited near its place of origin is not directly relevant for water quality control.

If the soil loss tolerance designed for sustained cropland productivity fails to attain the desired water quality standard, flexible limits that consider other factors should be developed rather than uniformly lowering the soil loss tolerance. These factors include distance of the field from a major waterway, the sediment transport characteristics of the intervening area, sediment composition, needs of the particular body of water being protected, and the probable magnitude of fluctuations in sediment loads (*42*). Limits of sediment yield would provide more uniform water quality control than lowering the limits on soil movement from field slopes. They would also require fewer restrictions on crop system selection for fields from which only small percentages of the eroded soil become off-farm sediment.

SOIL LOSS EQUATION

The erosion rate at a given site is determined by the particular way in which the levels on numerous physical and management variables are combined at that site. Physical measurements of soil loss for each of the large number of possible combinations in which the levels of these variable factors can occur under field conditions would not be feasible. Soil loss equations were developed to enable conservation planners to project limited erosion data to the many localities and conditions that have not been directly represented in the research.

The USLE is an erosion model designed to predict the longtime average soil losses in runoff from specific field areas in specified cropping and management systems. Widespread field use has substantiated its usefulness and validity for this purpose. It is also applicable for such nonagricultural conditions as construction sites.

With appropriate selection of its factor values, the equation will compute the average soil loss for a multicrop system, for a particular crop year in a rotation, or for a particular cropstage period within a crop year. It computes the soil loss for a given

site as the product of six major factors whose most likely values at a particular location can be expressed numerically. Erosion variables reflected by these factors vary considerably about their means from storm to storm, but effects of the random fluctuations tend to average out over extended periods. Because of the unpredictable short-time fluctuations in the levels of influential variables, however, present soil loss equations are substantially less accurate for prediction of specific events than for prediction of longtime averages.

The soil loss equation is

$$A = R\,K\,L\,S\,C\,P \qquad (1)$$

where

A is the computed soil loss per unit area, expressed in the units selected for **K** and for the period selected for **R**. In practice, these are usually so selected that they compute **A** in tons per acre per year, but other units can be selected.

R, the rainfall and runoff factor, is the number of rainfall erosion index units, plus a factor for runoff from snowmelt or applied water where such runoff is significant.

K, the soil erodibility factor, is the soil loss rate per erosion index unit for a specified soil as measured on a unit plot, which is defined as a 72.6-ft length of uniform 9-percent slope continuously in clean-tilled fallow.

L, the slope-length factor, is the ratio of soil loss from the field slope length to that from a 72.6-ft length under identical conditions.

S, the slope-steepness factor, is the ratio of soil loss from the field slope gradient to that from a 9-percent slope under otherwise identical conditions.

C, the cover and management factor, is the ratio of soil loss from an area with specified cover and management to that from an identical area in tilled continuous fallow.

P, the support practice factor, is the ratio of soil loss with a support practice like contouring, stripcropping, or terracing to that with straight-row farming up and down the slope.

The soil loss equation and factor evaluation charts were initially developed in terms of the English units commonly used in the United States. The factor definitions are interdependent, and direct conversion of acres, tons, inches, and feet to metric units would not produce the kind of integers that would be desirable for an expression of the equation in that system. Therefore, only the English units are used in the initial presentation of the equation and factor evaluation materials, and their counterparts in metric units are given in the Appendix under **Conversion to Metric System.**

Numerical values for each of the six factors were derived from analyses of the assembled research data and from National Weather Service precipitation records. For most conditions in the United States, the approximate values of the factors for any particular site may be obtained from charts and tables in this handbook. Localities or countries where the rainfall characteristics, soil types, topographic features, or farm practices are substantially beyond the range of present U.S. data will find these charts and tables incomplete and perhaps inaccurate for their conditions. However, they will provide guidelines that can reduce the amount of local research needed to develop comparable charts and tables for their conditions.

The subsection on **Predicting Cropland Soil Losses**, page 40 illustrates how to select factor values from the tables and charts. Readers who have had no experience with the soil loss equation may wish to read that section first. After they have referred to the tables and figures and located the values used in the sample, they may move readily to the intervening detailed discussions of the equation's factors.

The soil loss prediction procedure is more valuable as a guide for selection of practices if the user has a general knowledge of the principles and factor interrelations on which the equation is based. Therefore, the significance of each factor is discussed before presenting the reference table or chart from which local values may be obtained. Limitations of the data available for evaluation of some of the factors are also pointed out.

RAINFALL AND RUNOFF FACTOR (R)

Rills and sediment deposits observed after an unusually intense storm have sometimes led to the conclusion that the significant erosion is associated with only a few storms, or that it is solely a function of peak intensities. However, more than 30 years of measurements in many States have shown that this is not the case (*51*). The data show that a rainfall factor used to estimate average annual soil loss must include the cumulative effects of the many moderate-sized storms, as well as the effects of the occasional severe ones.

The numerical value used for **R** in the soil loss equation must quantify the raindrop impact effect and must also provide relative information on the amount and rate of runoff likely to be associated with the rain. The rainfall erosion index derived by Wischmeier (*49*) appears to meet these requirements better than any other of the many rainfall parameters and groups of parameters tested against the assembled plot data. The local value of this index generally equals **R** for the soil loss equation and may be obtained directly from the map in figure 1. However, the index does not include the erosive forces of runoff from thaw, snowmelt, or irrigation. A procedure for evaluating **R** for locations where this type of runoff is significant will be given under the topic **R Values for Thaw and Snowmelt.**

Rainfall Erosion Index

The research data indicate that when factors other than rainfall are held constant, storm soil losses from cultivated fields are directly proportional to a rainstorm parameter identified as the **EI** (defined below) (*49*). The relation of soil loss to this parameter is linear, and its individual storm values are directly additive. The sum of the storm **EI** values for a given period is a numerical measure of the erosive potential of the rainfall within that period. The average annual total of the storm **EI** values in a particular locality is the rainfall erosion index for that locality. Because of apparent cyclical patterns in rainfall data (*33*), the published rainfall erosion index values were based on 22-year station rainfall records.

Rain showers of less than one-half inch and separated from other rain periods by more than 6 hours were omitted from the erosion index computations, unless as much as 0.25 in of rain fell in 15 min. Exploratory analyses showed that the **EI** values for such rains are usually too small for practical significance and that, collectively, they have little effect on monthly percentages of the annual **EI.** The cost of abstracting and analyzing 4,000 location-years of rainfall-intensity data was greatly reduced by adopting the 0.5-in threshold value.

EI Parameter

By definition, the value of **EI** for a given rainstorm equals the product, total storm energy (**E**) times the maximum 30-min intensity (I_{30}), where **E** is in hundreds of foot-tons per acre and I_{30} is in inches per hour (in/h). **EI** is an abbreviation for energy-times-intensity, and the term should not be considered simply an energy parameter. The data show that rainfall energy, itself, is not a good indicator of erosive potential. The storm energy indicates the volume of rainfall and runoff, but a long, slow rain may have the same **E** value as a shorter rain at much higher intensity. Raindrop erosion increases with intensity. The I_{30} component indicates the prolonged-peak rates of detachment and runoff. The product term, **EI,** is a statistical interaction term that reflects how total energy and peak inensity are combined in each particular storm. Technically, it indicates how particle detachment is combined with transport capacity.

The energy of a rainstorm is a function of the amount of rain and of all the storm's component intensities. Median raindrop size increases with rain intensity (*62*), and terminal velocities of free-falling waterdrops increase with increased dropsize (*13*). Since the energy of a given mass in motion is proportional to velocity-squared, rainfall energy is directly related to rain intensity. The relationship is expressed by the equation,

$$E = 916 + 331 \log_{10} I, \qquad (2)$$

where **E** is kinetic energy in foot-tons per acre-inch and **I** is intensity in inches per hour (*62*). A limit of 3 in/h is imposed on **I** by the finding that median dropsize does not continue to increase when intensities exceed 3 in/h (*7, 15*). The energy

of a rainstorm is computed from recording-rain gage data. The storm is divided into successive increments of essentially uniform intensity, and a rainfall energy-intensity table derived from the above formula (app., table 19) is used to compute the energy for each increment. (Because the energy equation and energy-intensity table have been frequently published with energy expressed in foot-tons per acre-inch, this unit was retained in table 19. However, for computation of **EI** values, storm energy is expressed in hundreds of foot-tons per acre. Therefore, energies computed by the published formula or table 19 must be divided by 100 before multiplying by I_{30} to compute **EI**.)

Isoerodent Maps

Local values of the rainfall erosion index may be taken directly from the isoerodent maps, figures 1 and 2. The plotted lines on the maps are called isoerodents because they connect points of equal rainfall erosivity. Erosion index values for locations between the lines are obtained by linear interpolation.

The isoerodent map in the original version of this handbook (*64*) was developed from 22-year station rainfall records by computing the **EI** value for each storm that met the previously defined threshold criteria. Isoerodents were then located between these point values with the help of published rainfall intensity-frequency data (*47*) and topographic maps. The 11 Western States were omitted from the initial map because the rainfall patterns in this mountainous region are sporadic and not enough long-term, recording-rain gage records were available to establish paths of equal erosion index values.

The isoerodent map was extended to the Pacific Coast in 1976 by use of an estimating procedure. Results of investigations at the Runoff and Soil Loss Data Center at Purdue University showed that the known erosion index values in the Western Plains and North Central States could be approximated with reasonable accuracy by the quantity 27.38 $P^{2.17}$, where **P** is the 2-year, 6-h rainfall amount (*55*). This relationship was used with National Weather Service isopluvial maps to approximate erosion index values for the Western States. The resulting isoerodents are compatible with the few point values that had been established within the 11 Western States and can provide helpful guides for conservation planning on a site basis. However, they are less precise than those computed for the 37-State area, where more data were available and rainfall patterns are less erratic. Also, linear interpolations between the lines will not always be accurate in mountain regions because values of the erosion index may change rather abruptly with elevation changes. The point values that were computed directly from long-term station rainfall records in the Western States are included in table 7, as reference points.

Figure 2 was developed by computing the erosion index for first-order weather stations in Hawaii and deriving the relation of these values to National Weather Service intensity-frequency data for the five major islands. When the present short-term, rainfall-intensity records have been sufficiently lengthened, more point values of the index should be computed by the standard procedure.

Figure 1 shows that local, average-annual values of the erosion index in the 48 conterminous States range from less than 50 to more than 500. The erosion index measures the combined effect of rainfall and its associated runoff. If the soil and topography were exactly the same everywhere, average annual soil losses from plots maintained in continuous fallow would differ in direct proportion to the erosion index values. However, this potential difference is partially offset by differences in soil, topography, vegetative cover, and residues. On fertile soils in the high rainfall areas of the Southern States, good vegetal cover protects the soil surface throughout most of the year and heavy plant residues may provide excellent cover also during the dormant season. In the regions where the erosion index is extremely low, rainfall is seldom adequate for establishing annual meadows and the cover provided by other crops is often for relatively short periods. Hence, serious soil erosion hazards exist in semiarid regions as well as in humid.

Frequency Distribution

The isoerodent maps present 22-year-average annual values of **EI** for the delineated areas. However, both the annual and the maximum-storm values at a particular location vary from year to year. Analysis of 181 station rainfall records showed that they tend to follow log-normal frequency distributions that are usually well defined by contin

R values

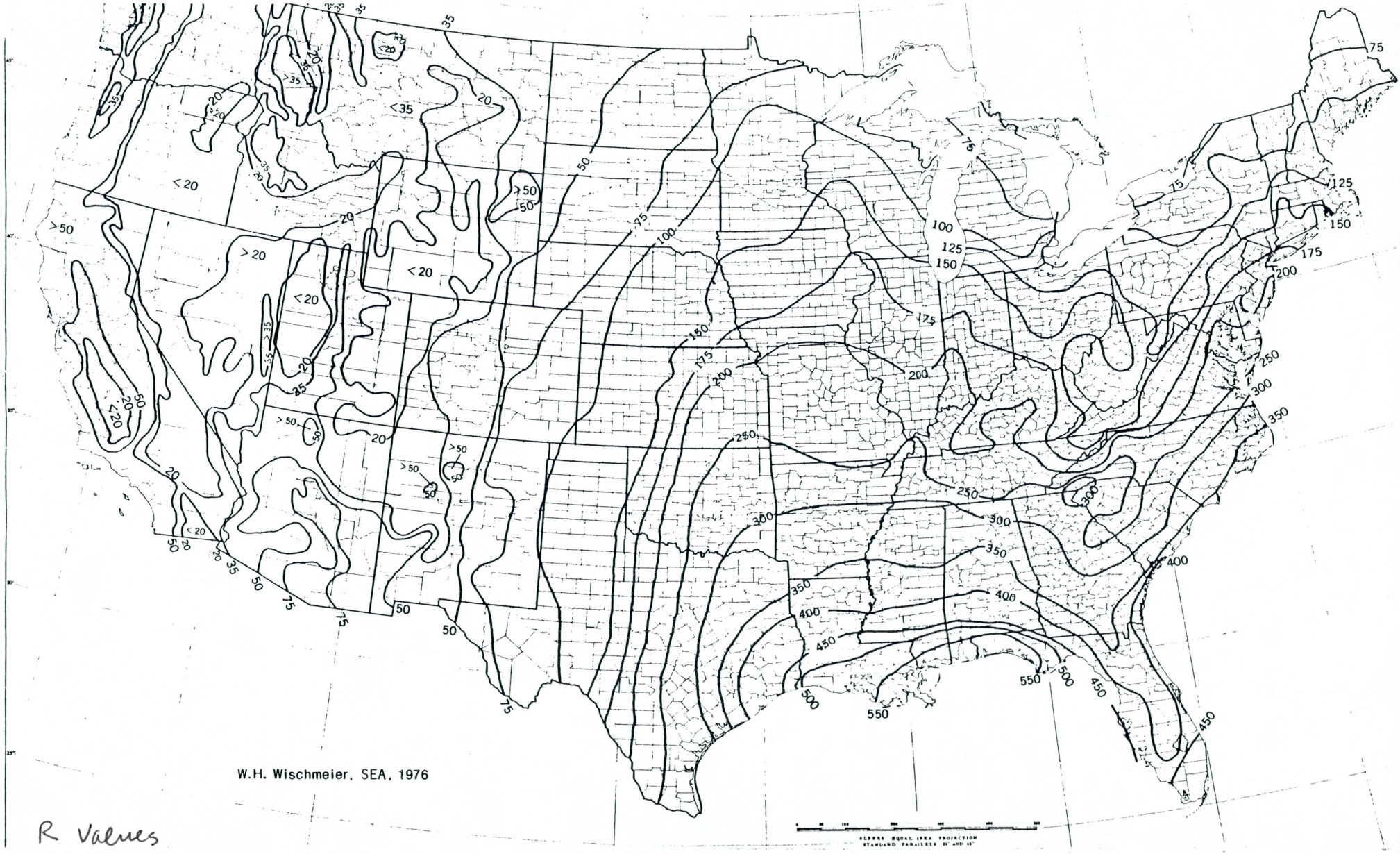

R Values

ous records of from 20 to 25 years (*49*). Tables of specific probabilities of annual and maximum-storm **EI** values at the 181 locations are presented in the appendix (tables 17 and 18).

R Values for Thaw and Snowmelt

The standard rainfall erosion index estimates the erosive forces of the rainfall and its directly associated runoff. In the Pacific Northwest, as much as 90 percent of the erosion on the steeply rolling wheatland has been estimated to derive from runoff associated with surface thaws and snowmelt. This type of erosion is not accounted for by the rainfall erosion index but is considered either predominant or appreciable in much of the Northwest and in portions of the central Western States. A linear precipitation relationship would not account for peak losses in early spring because as the winter progresses, the soil becomes increasingly more erodible as the soil moisture profile is being filled, the surface structure is being broken down by repeated freezing and thawing, and puddling and surface sealing are taking place. Additional research of the erosion processes and means of control under these conditions is urgently needed.

In the meantime, the early spring erosion by runoff from snowmelt, thaw, or light rain on frozen soil may be included in the soil loss computations by adding a subfactor, $\mathbf{R}_s$, to the location's erosion index to obtain **R**. Investigations of limited data indicated that an estimate of $\mathbf{R}_s$ may be obtained by taking 1.5 times the local December-through-March precipitation, measured as inches of water. For example, a location in the North-

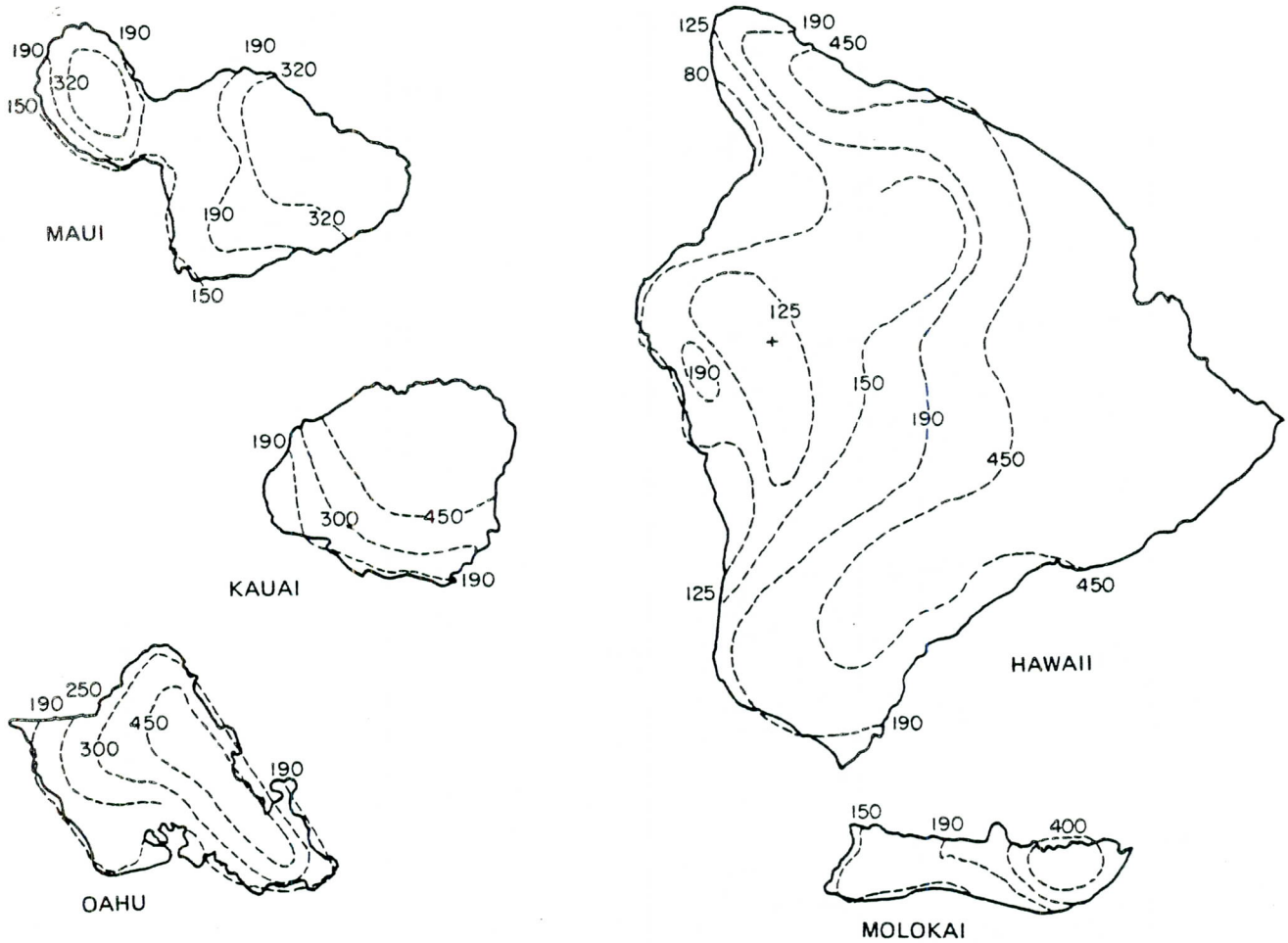

FIGURE 2.—Estimated average annual values of the rainfall erosion index in Hawaii.

that has an erosion index of 20 (fig. 1) and averages 12 in of precipitation between December 1 and March 31 would have an estimated average annual **R** of 1.5(12) + 20, or 38.

This type of runoff may also be a significant factor in the northern tier of Central and Eastern States. Where experience indicates this to be the case, it should be included in **R** and also in the erosion index distribution curves as illustrated on page 27.

SOIL ERODIBILITY FACTOR (K)

The meaning of the term "soil erodibility" is distinctly different from that of the term "soil erosion." The rate of soil erosion, **A**, in the soil loss equation, may be influenced more by land slope, rainstorm characteristics, cover, and management than by inherent properties of the soil. However, some soils erode more readily than others even when all other factors are the same. This difference, caused by properties of the soil itself, is referred to as the soil erodibility. Several early attempts were made to determine criteria for scientific classifications of soils according to erodibility (*6, 18, 28, 35*), but classifications used for erosion prediction were only relative rankings.

Differences in the natural susceptibilities of soils to erosion are difficult to quantify from field observations. Even a soil with a relatively low erodibility factor may show signs of serious erosion when it occurs on long or steep slopes or in localities with numerous high-intensity rainstorms. A soil with a high natural erodibility factor, on the other hand, may show little evidence of actual erosion under gentle rainfall when it occurs on short and gentle slopes, or when the best possible management is practiced. The effects of rainfall differences, slope, cover, and management are accounted for in the prediction equation by the symbols **R**, **L**, **S**, **C**, and **P**. Therefore, the soil erodibility factor, **K**, must be evaluated independently of the effects of the other factors.

Definition of Factor K

The soil erodibility factor, **K**, in the USLE is a quantitative value experimentally determined. For a particular soil, it is the rate of soil loss per erosion index unit as measured on a "unit" plot, which has been arbitrarily defined as follows:

A unit plot is 72.6 ft long, with a uniform lengthwise slope of 9 percent, in continuous fallow, tilled up and down the slope. Continuous fallow, for this purpose, is land that has been tilled and kept free of vegetation for more than 2 years. During the period of soil loss measurements, the plot is plowed and placed in conventional corn seedbed condition each spring and is tilled as needed to prevent vegetative growth and severe surface crusting. When all of these conditions are met, **L**, **S**, **C**, and **P** each equal 1.0, and **K** equals **A**/**EI**.

The 72.6 ft length and 9 percent steepness were selected as base values for **L**, **S**, and **K** because they are the predominant slope length and about the average gradient on which past erosion measurements in the United States had been made. The designated management provides a condition that nearly eliminates effects of cover, management, and land use residual and that can be duplicated on any cropland.

Direct measurements of **K** on well-replicated, unit plots as described reflect the combined effects of all the soil properties that significantly influence the ease with which a particular soil is eroded by rainfall and runoff if not protected. However, **K** is an average value for a given soil, and direct measurement of the factor requires soil loss measurements for a representative range of storm sizes and antecedent soil conditions. (See **Individual Storm Soil Losses** under **APPLYING THE SOIL LOSS EQUATION**.) To evaluate **K** for soils that do not usually occur on a 9-percent slope, soil loss data from plots that meet all the other specified conditions are adjusted to this base by **S**.

Values of K for Specific Soils

Representative values of **K** for most of the soil types and texture classes can be obtained from tables prepared by soil scientists using the latest available research information. These tables are available from the Regional Technical Service Centers or State offices of SCS. Values for the exact

TABLE 1.—*Computed* **K** *values for soils on erosion research stations*

Soil	Source of data	Computed K
Dunkirk silt loam	Geneva, N.Y.	[1]0.69
Keene silt loam	Zanesville, Ohio	.48
Shelby loam	Bethany, Mo.	.41
Lodi loam	Blacksburg, Va.	.39
Fayette silt loam	LaCrosse, Wis.	[1].38
Cecil sandy clay loam	Watkinsville, Ga.	.36
Marshall silt loam	Clarinda, Iowa	.33
Ida silt loam	Castana, Iowa	.33
Mansic clay loam	Hays, Kans.	.32
Hagerstown silty clay loam	State College, Pa.	[1].31
Austin clay	Temple, Tex.	.29
Mexico silt loam	McCredie, Mo.	.28
Honeoye silt loam	Marcellus, N.Y.	[1].28
Cecil sandy loam	Clemson, S.C.	[1].28
Ontario loam	Geneva, N.Y.	[1].27
Cecil clay loam	Watkinsville, Ga.	.26
Boswell find sandy loam	Tyler, Tex.	.25
Cecil sandy loam	Watkinsville, Ga.	.23
Zaneis fine sandy loam	Guthrie, Okla.	.22
Tifton loamy sand	Tifton, Ga.	.10
Freehold loamy sand	Marlboro, N.J.	.08
Bath flaggy silt loam with surface stones > 2 inches removed	Arnot, N.Y.	[1].05
Albia gravelly loam	Beemerville, N.J.	.03

[1] Evaluated from continuous fallow. All others were computed from rowcrop data.

soil conditions at a specific site can be computed by use of the soil erodibility nomograph presented in the next subsection.

Usually a soil type becomes less erodible with decrease in silt fraction, regardless of whether the corresponding increase is in the sand fraction or the clay fraction. Overall, organic matter content ranked next to particle-size distribution as an indicator of erodibility. However, a soil's erodibility is a function of complex interactions of a substantial number of its physical and chemical properties and often varies within a standard texture class.

Values of **K** determined for 23 major soils on which erosion plot studies under natural rain were conducted since 1930 are listed in table 1. Seven of these values are from continuous fallow. The others are from row crops averaging 20 plot-years of record and grown in systems for which the cropping effect had been measured in other studies. Other soils on which valuable erosion studies have been conducted[4] were not included in the table because of uncertainties involved in adjustments of the data for effects of cropping and management.

Direct measurement of the erodibility factor is both costly and time consuming and has been feasible only for a few major soil types. To achieve a better understanding of how and to what extent each of various properties of a soil affects its erodibility, an interregional study was initiated in 1961. The study included the use of field-plot rainfall simulators in at least a dozen States to obtain comparative data on numerous soils, laboratory determinations of physical and chemical properties, and operation of additional fallow plots under natural rain. Several empirical erodibility equations were reported (*3, 60*). A soil erodibility nomograph for farmland and construction sites (*58*) provided a more generally applicable working tool. Approximate **K** values for 10 benchmark soils in Hawaii are listed in table 2.

[4] See footnote 3, p. 2.

TABLE 2.—*Approximate values of the soil erodibility factor,* **K**, *for 10 benchmark soils in Hawaii*

Order	Suborder	Great group	Subgroup	Family	Series	K
Ultisols	Humults	Tropohumults	Humoxic Tropohumults	Clayey, kaolinitic, isohyperthermic	Waikane	0.10
Oxisols	Torrox	Torrox	Typic Torrox	Clayey, kaolinitic, isohyperthermic	Molokai	.24
Oxisols	Ustox	Eutrustox	Tropeptic Eutrustox	Clayey, kaolinitic, isohyperthermic	Wahiawa	.17
Vertisols	Usterts	Chromusterts	Typic Chromusterts	Very fine, montmorillonitic, isohyperthermic	Lualualei	.28
					Kawaihae	.32
Aridisols	Orthids	Camborthids	Ustollic Camborthids	Medial, isohyperthermic	(Extremely stony phase)	
Inceptisols	Andepts	Dystrandepts	Hydric Dystrandepts	Thixotropic, isothermic	Kukaiau	.17
Inceptisols	Andepts	Eutrandepts	Typic Eutrandepts	Medial, isohyperthermic	Naolehu (Variant)	.20
Inceptisols	Andepts	Eutrandepts	Entic Eutrandepts	Medial, isohyperthermic	Pakini	.49
Inceptisols	Andepts	Hydrandepts	Typic Hydrandepts	Thixotropic, isohyperthermic	Hilo	.10
Inceptisols	Tropepts	Ustropepts	Vertic Ustropepts	Very fine, kaolinitic, isohyperthermic	Waipahu	.20

SOURCE: El-Swaify and Dangler (*9*).

Soil Erodibility Nomograph

The soil loss data show that very fine sand (0.05-0.10 mm) is comparable in erodibility to silt-sized particles and that mechanical-analysis data are much more valuable when expressed by an interaction term that describes the proportions in which the sand, silt, and clay fractions are combined in the soil. When mechanical analysis data based on the standard USDA classification are used for the nomograph in figure 3, the percentage of very fine sand (0.1-0.05 mm) must first be transferred from the sand fraction to the silt fraction. The mechanical analysis data are then effectively described by a particle-size parameter **M**, which equals percent silt (0.1-0.002 mm) times the quantity 100-minus-percent-clay. Where the silt fraction does not exceed 70 percent, erodibility varies approximately as the 1.14 power of this parameter, but prediction accuracy is improved by adding information on organic matter content, soil structure, and profile permeability class.

For soils containing less than 70 percent silt and very fine sand, the nomograph (fig. 3) solves the equation:

$$K = 2.1\, M^{1.14} (10^{-4}) (12 - a) + 3.25 (b - 2) + 2.5 (c - 3) \quad (3)$$

where

M = the particle-size parameter defined above,
a = percent organic matter,
b = the soil-structure code used in soil classification, and
c = the profile-permeability class.

The intersection of the selected percent-silt and percent-sand lines computes the value of **M** on the unidentified horizontal scale of the nomograph. (Percent clay enters into the computation as 100 minus the percentages of sand and silt.)

The data indicate a change in the relation of **M** to erodibility when the silt and very fine sand fraction exceeds about 70 percent. This change was empirically reflected by inflections in the percent-sand curves at that point but has not been described by a numerical equation.

Readers who would like more detail regarding the data and relationships underlying the nomograph equation may obtain this from journal articles (*58, 60*).

Nomograph Solution

With appropriate data, enter the scale at the left and proceed to points representing the soil's percent sand (0.10-2.0 mm), percent organic matter, structure code, and permeability class as illustrated by the dotted line on the nomograph. The horizontal and vertical moves must be made in the listed sequence. Use linear interpolations between plotted lines. The structure code and permeability classes are defined on the nomograph for reference.

Many agricultural soils have both fine granular topsoil and moderate permeability. For these soils, **K** may be read from the scale labeled "first approximation of **K**," and the second block of the graph is not needed. For all other soils, however, the procedure must be completed to the soil erodibility scale in the second half of the graph.

The mechanical analysis, organic matter, and structure data are those for the topsoil. For evaluation of **K** for desurfaced subsoil horizons, they pertain to the upper 6 in of the new soil profile. The permeability class is the profile permeability. Coarse fragments are excluded when determining percentages of sand, silt, and clay. If substantial, they may have a permanent mulch effect which can be evaluated from the upper curve of the chart on mulch and canopy effects (p. 19, fig. 6) and applied to the number obtained from the nomograph solution.

Confidence Limits

In tests against measured **K** values ranging from 0.03 to 0.69, 65 percent of the nomograph solutions differed from the measured **K** values by less than 0.02, and 95 percent of them by less than 0.04. Limited data available in 1971 for mechanically exposed **B** and **C** subsoil horizons indicated about comparable accuracy for these conditions. However, more recent data taken on desurfaced high-clay subsoils showed the nomograph solution to lack the desired sensitivity to differences in erodibilities of these soil horizons. For such soils the content of free iron and aluminum oxides ranks next to particle-size distribution as an indicator of erodibility (*37*). Some high-clay soils form what has been called irreversible aggregates on the surface when tilled. These behave like larger primary particles.

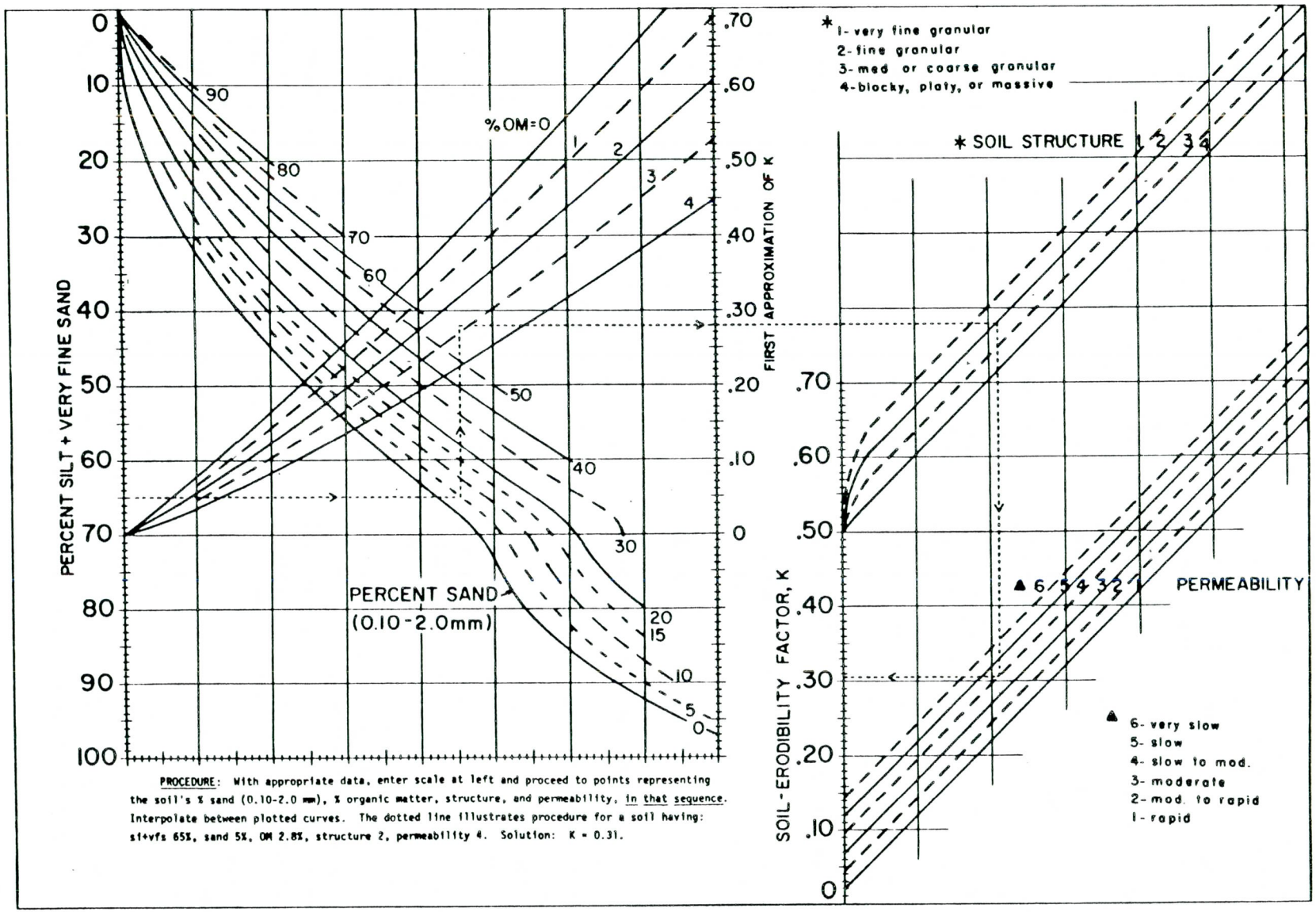

FIGURE 3.—The soil-erodibility nomograph. Where the silt fraction does not exceed 70 percent, the equation is $100\ K = 2.1\ M^{1.14}\ (10^{-4})\ (12 - a) + 3.25\ (b - 2) + 2.5\ (c - 3)$ where M = (percent si + vfs) (100 — percent c), a = percent organic matter, b = structure code, and c = profile permeability class.

TOPOGRAPHIC FACTOR (LS)

Both the length and the steepness of the land slope substantially affect the rate of soil erosion by water. The two effects have been evaluated separately in research and are represented in the soil loss equation by **L** and **S**, respectively. In field applications, however, considering the two as a single topographic factor, **LS**, is more convenient.

Slope-Effect Chart

LS is the expected ratio of soil loss per unit area from a field slope to that from a 72.6-ft length of uniform 9-percent slope under otherwise identical conditions. This ratio for specified combinations of field slope length and uniform gradient may be obtained directly from the slope-effect chart (fig. 4). Enter on the horizontal axis with the field slope length, move vertically to the appropriate percent-slope curve, and read **LS** on the scale at the left. For example, the **LS** factor for a 300-ft length of 10-percent slope is 2.4. Those who prefer a table may use table 3 and interpolate between listed values.

To compute soil loss from slopes that are appreciably convex, concave, or complex, the chart **LS** values need to be adjusted as indicated in the section **LS Values for Irregular Slopes**. Figure 4 and table 3 assume slopes that have essentially uniform gradient. The chart and table were derived by the equation

$$\mathbf{LS} = (\lambda/72.6)^{m}\ (65.41\ \sin^2\theta + 4.56\ \sin\theta + 0.065) \quad (4)$$

where λ = slope length in feet;
θ = angle of slope; and
m = 0.5 if the percent slope is 5 or more, 0.4 on slopes of 3.5 to 4.5 percent, 0.3 on slopes of 1 to 3 percent, and 0.2 on uniform gradients of less than 1 percent.

The basis for this equation is given in the subsection discussing the individual effects of slope length and steepness. However, the relationships expressed by the equation were derived from data obtained on cropland, under natural rainfall, on slopes ranging from 3 to 18 percent in steepness and about 30 to 300 ft in length. How far beyond these ranges in slope characteristics the relationships derived from the data continue to be accurate has not been determined by direct soil loss measurements.

The Palouse Region of the Northwest represents

TABLE 3.—*Values of the topographic factor,* **LS**, *for specific combinations of slope length and steepness*[1]

Percent slope	Slope length (feet)											
	25	50	75	100	150	200	300	400	500	600	800	1,000
0.2	0.060	0.069	0.075	0.080	0.086	0.092	0.099	0.105	0.110	0.114	0.121	0.126
0.5	.073	.083	.090	.096	.104	.110	.119	.126	.132	.137	.145	.152
0.8	.086	.098	.107	.113	.123	.130	.141	.149	.156	.162	.171	.179
2	.133	.163	.185	.201	.227	.248	.280	.305	.326	.344	.376	.402
3	.190	.233	.264	.287	.325	.354	.400	.437	.466	.492	.536	.573
4	.230	.303	.357	.400	.471	.528	.621	.697	.762	.820	.920	1.01
5	.268	.379	.464	.536	.656	.758	.928	1.07	1.20	1.31	1.52	1.69
6	.336	.476	.583	.673	.824	.952	1.17	1.35	1.50	1.65	1.90	2.13
8	.496	.701	.859	.992	1.21	1.41	1.72	1.98	2.22	2.43	2.81	3.14
10	.685	.968	1.19	1.37	1.68	1.94	2.37	2.74	3.06	3.36	3.87	4.33
12	.903	1.28	1.56	1.80	2.21	2.55	3.13	3.61	4.04	4.42	5.11	5.71
14	1.15	1.62	1.99	2.30	2.81	3.25	3.98	4.59	5.13	5.62	6.49	7.26
16	1.42	2.01	2.46	2.84	3.48	4.01	4.92	5.68	6.35	6.95	8.03	8.98
18	1.72	2.43	2.97	3.43	4.21	3.86	5.95	6.87	7.68	8.41	9.71	10.9
20	2.04	2.88	3.53	4.08	5.00	5.77	7.07	8.16	9.12	10.0	11.5	12.9

[1] $\mathbf{LS} = (\lambda/72.6)^{m}\ (65.41\ \sin^2\theta + 4.56\ \sin\theta + 0.065)$ where λ = slope length in feet; **m** = 0.2 for gradients < 1 percent, 0.3 for 1 to 3 percent slopes, 0.4 for 3.5 to 4.5 percent slopes, 0.5 for 5 percent slopes and steeper; and θ = angle of slope. (For other combinations of length and gradient, interpolate between adjacent values or see fig. 4.)

SLOPE LENGTH (FEET)

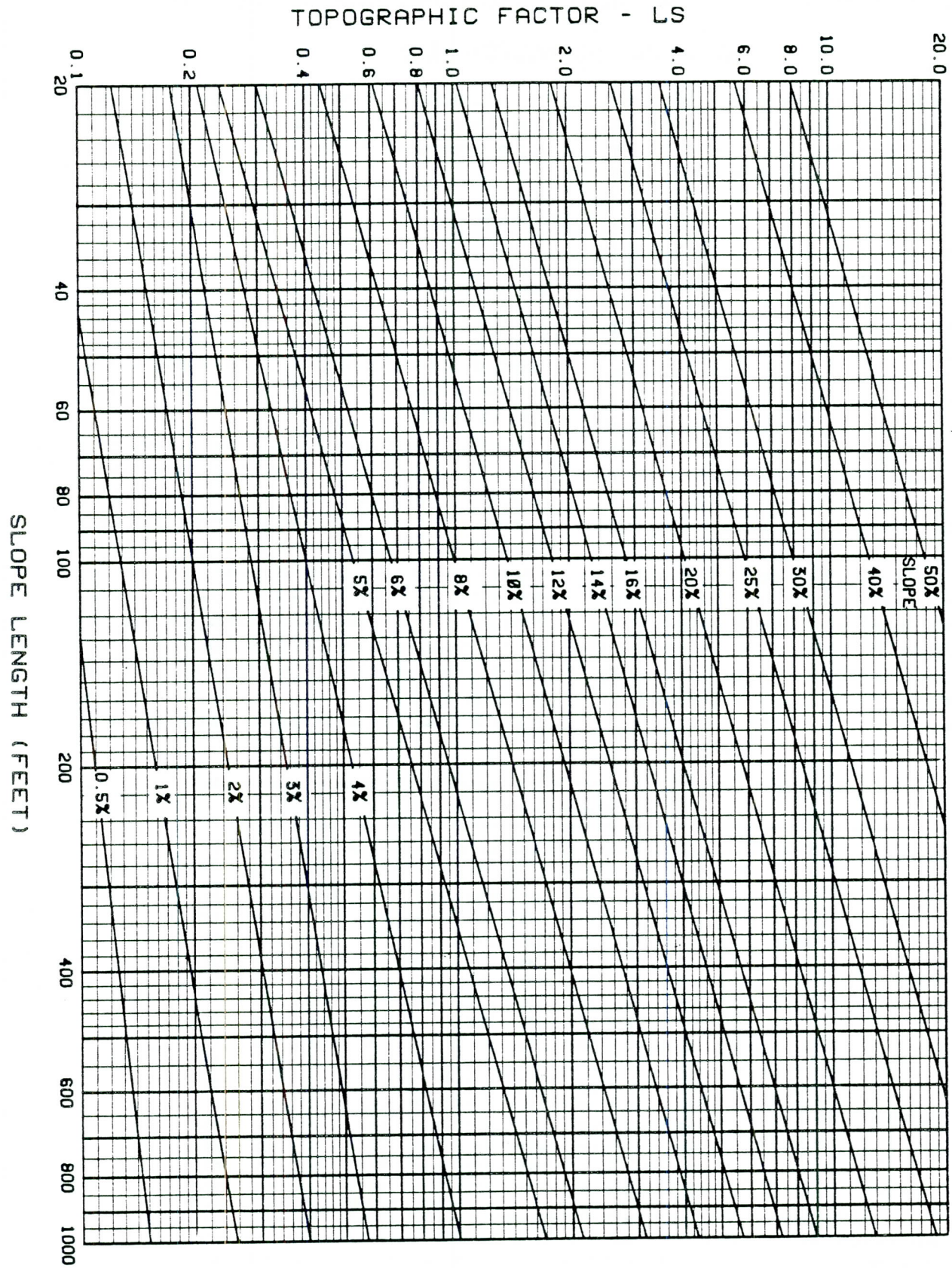

FIGURE 4.—Slope-effect chart (topographic factor, LS). $LS = (\lambda/72.6)^m (65.41 \sin^2\theta + 4.56 \sin\theta + 0.065)$ where λ = slope length in feet; θ = angle of slope; and $m = 0.2$ for gradients < 1 percent, 0.3 for 1 to 3 percent slopes, 0.4 for 3.5 to 4.5 percent slopes, and 0.5 for slopes of 5 percent or steeper.

a different situation. The rainfall erosion index is quite low because most of the rain comes as small drops and at low intensities. But many of the cropland slopes are long or steep, and substantial erosion occurs because of runoff from snowmelt or light rains over saturated soil surfaces. Limited erosion data from this region, mostly observational, strongly indicate that for this type of runoff (not accompanied by raindrop impact) the effects of percent and length of slope are of lower magnitude than indicated by the humid region data. Investigations designed to develop a more accurate **LS** equation for this region are underway at Pullman, Wash. (*21*). In the meantime, the researchers are temporarily recommending using a modified equation which computes **LS** values that are close to those that would be calculated by the equation given above if $\sin^{1.5}\theta$ were substituted for $\sin^{2}\theta$ and the length-exponent, **m**, were assumed to equal 0.3. Intuitively, these changes seem reasonable for the conditions under which about 90 percent of the erosion in this region occurs.

Slope-Length Effect

Slope length is defined as the distance from the point of origin of overland flow to the point where either the slope gradient decreases enough that deposition begins, or the runoff water enters a well-defined channel that may be part of a drainage network or a constructed channel (*40*). A change in land cover or a substantial change in gradient along a slope does not begin a new slope length for purposes of soil loss estimation.

The effect of slope length on annual *runoff* per unit area of cropland may generally be assumed negligible. In some of the studies runoff per unit area was slightly lower on the longer slopes during the growing season and slightly higher during the dormant season, but the differences were relatively small and neither of the relationships was consistent (*52*).

However, the *soil loss* per unit area generally increases substantially as slope length increases. The greater accumulation of runoff on the longer slopes increases its detachment and transport capacities.

The plot data showed average soil loss per unit area to be proportional to a power of slope length. Because **L** is the ratio of field soil loss to the corresponding loss from 72.6-ft slope length, its value may be expressed as $L = (\lambda/72.6)^m$, where λ is the field slope length in feet, and **m** assumes approximately the values given in the **LS** equation in the preceding section. These are average values of **m** and are subject to some variability caused by interaction effects which are not now quantitatively predictable.

The existing field plot data do not establish a general value greater than 0.5 for **m** on slopes steeper than 10 percent, as was suggested in 1965 (*64*). Although apparent values up to 0.9 were observed in some of the data (*63*), the higher values appear to have been related to soil, crop, and management variables rather than to greater slope steepness. However, basic modeling work has suggested that **m** may appreciably exceed 0.5 on steep slopes that are highly susceptible to rilling, like some construction slopes (*10*). Additional research data are greatly needed to quantify the significant interaction effects so that specific site values of **m** can be more precisely computed. Subdividing erosion between interrill (or sheet) erosion and rill erosion, being done in recent modeling work (*10, 11, 22*), promises to be quite helpful for solving this problem.

Some observations have indicated that the values of the length exponent that were derived from the plot data may overestimate soil loss when applied to lengths in the range of a quarter of a mile or more. This is logical because slopes of such lengths would rarely have a constant gradient along their entire length, and the slope irregularities would affect the amount of soil movement to the foot of the slope. By the definition of slope length quoted earlier, such slopes would usually consist of several lengths, between points where deposition occurs.

Slope length is difficult to determine for long slopes with an average gradient of less than 1 percent, unless they are precisely formed with a land leveler. On flat slopes, reflecting both the erosion and the deposition accurately by a length factor may not be possible. However, on a nearly zero-percent slope, increased length would have minor effect on runoff velocity, and the greater depths of accumulated runoff water would cushion the raindrop impact. An exponent of 0.2 for gradients of less than 1 percent is compatible with the

scarce data available for such slopes and was used to derive figure 4 and table 3.

Distribution of Length Effect

LS values from figure 4 or table 3 predict the *average* erosion over the entire slope. But this erosion is not evenly distributed over the entire length. The rate of soil loss per unit of area increases as the mth power of the distance from the top of the slope, where **m** is the length exponent in the preceding equation.

An equation by Foster and Wischmeier (*12*) estimates the relative amounts of soil loss from successive segments of a slope under conditions where there is no deposition by overland flow. When the gradient is essentially uniform and the segments are of equal length, the procedure can be shortened (*55*). Table 4, derived by this procedure, shows the proportionate amounts of soil detachment from successive equal-length segments of a uniform slope.

Table 4 is entered with the total number of equal-length segments, and the fraction of the soil loss for each segment is read beneath the applicable value of **m**. For example, three equal-length segments of a uniform 6-percent slope would be expected to produce 19, 35, and 46 percent, respectively, of the loss from the entire slope.

TABLE 4.—*Estimated relative soil losses from successive equal-length segments of a uniform slope*[1]

Number of segments	Sequence number of segment	Fraction of soil loss		
		m = 0.5	m = 0.4	m = 0.3
2	1	0.35	0.38	0.41
	2	.65	.62	.59
3	1	.19	.22	.24
	2	.35	.35	.35
	3	.46	.43	.41
4	1	.12	.14	.17
	2	.23	.24	.24
	3	.30	.29	.28
	4	.35	.33	.31
5	1	.09	.11	.12
	2	.16	.17	.18
	3	.21	.21	.21
	4	.25	.24	.23
	5	.28	.27	.25

[1] Derived by the formula:

$$\text{Soil loss fraction} = \frac{i^{m+1} - (i-1)^{m+1}}{N^{m+1}}$$

where **i** = segment sequence number; **m** = slope-length exponent (0.5 for slopes $\geq$ 5 percent, 0.4 for 4 percent slopes, and 0.3 for 3 percent or less); and **N** = number of equal-length segments into which the slope was divided.

Four segments would produce 12, 23, 30, and 35 percent, respectively. Segment No. 1 is always at the top of the slope.

Percent Slope

Runoff from cropland generally increases with increased slope gradient, but the relationship is influenced by such factors as type of crop, surface roughness, and profile saturation. In the natural rain slope-effect studies, the logarithm of runoff from row crops was linearly and directly proportional to percent slope. With good meadow sod and with smooth bare surfaces, the relationship was insignificant. The effect of slope on runoff decreased in extremely wet periods.

Soil loss increases much more rapidly than runoff as slopes steepen. The slope-steepness factor, **S**, in the soil loss equation is evaluated by the equation

$$S = 65.41 \sin^2 \theta + 4.56 \sin \theta + 0.065 \qquad (5)$$

where θ is the angle of slope.

This equation was used to develop the slope-effect chart. The values reflect the average effect of slope steepness on soil loss in the plot studies. The relation of percent slope to soil loss is believed to to be influenced by interactions with soil properties and surface conditions, but the interaction effects have not been quantified by research data. Neither are data available to define the limits on the equation's applicability.

This equation can be derived from the formerly published equation for **S**. Expressing the factor as a function of the sine of the angle of slope rather than the tangent is more accurate because raindrop-impact forces along the surface and runoff shear stress are functions of the sine. Substituting 100 sin θ for percent slope, which is 100 tan θ, does not significantly affect the initial statistical derivation or the equation's solutions for slopes of less than 20 percent. But as slopes become steeper, the difference between the sine and the tangent becomes appreciable and projections far beyond the range of the plot data become more realistic. The numerator was divided by the constant denominator for simplification.

Irregular Slopes

Soil loss is also affected by the shape of a slope. Many field slopes either steepen toward the lower end (convex slope) or flatten toward the lower end (concave slope). Use of the average gradient to enter figure 4 or table 3 would underestimate soil movement to the foot of a convex slope and would overestimate it for concave slopes. Irregular slopes can usually be divided into segments that have nearly uniform gradient, but the segments cannot be evaluated as independent slopes when runoff flows from one segment to the next.

However, where two simplifying assumptions can be accepted, **LS** for irregular slopes can be routinely derived by combining selected values from the slope-effect chart and table 4 (*55*). The assumptions are that (1) the changes in gradient are not sufficient to cause upslope deposition, and (2) the irregular slope can be divided into a small number of equal-length segments in such a manner that the gradient within each segment for practical purposes can be considered uniform.

After dividing the convex, concave, or complex slope into equal-length segments as defined ear- the procedure is as follows: List the segment gradients in the order in which they occur on the slope, beginning at the upper end. Enter the slope-effect chart with the total slope length and read **LS** for each of the listed gradients. Multiply these by the corrresponding factors from table 4 and add the products to obtain **LS** for the entire slope. The following tabulation illustrates the procedure for a 400-ft convex slope on which the upper third has a gradient of 5 percent; the middle third, 10 percent; and the lower third, 15 percent:

Segment	*Percent slope*	*Table 3*	*Table 4*	*Product*
1	5	1.07	0.19	0.203
2	10	2.74	.35	.959
3	15	5.12	.46	2.355
				LS = 3.517

For the concave slope of the same length, with the segment gradients in reverse order, the values in the third column would be listed in reverse order. The products would then be 0.973, 0.959, and 0.492, giving a sum of 2.42 for **LS**.

Research has not defined just how much gradient change is needed under various conditions for deposition of soil particles of various sizes to begin, but depositional areas can be determined by observation. When the slope breaks are sharp enough to cause deposition, the procedure can be used to estimate **LS** for slope segments above and below the depositional area. However, it will not predict the total sediment moved from such an interrupted slope because it does not predict the amount of deposition.

Changes in Soil Type or Cover Along the Slope

The procedure for irregular slopes can include evaluation of changes in soil type within a slope length (*55*). The products of values selected from table 3 or figure 4 and table 4 to evaluate **LS** for irregular slopes are multiplied by the respective values of **K** before summing. To illustrate, assume the **K** values for the soils in the three segments of the convex slope in the preceding example were 0.27, 0.32, and 0.37, respectively. The average **KLS** for the slope would be obtained as follows:

Segment No.	*Table 3*	*Table 4*	K	*Product*
1	1.07	0.19	0.27	0.055
2	2.74	.35	.32	.307
3	5.12	.46	.37	.871
				KLS = 1.233

Within limits, the procedure can be further extended to account for changes in cover along the slope length by adding a column of segment **C** values. However, it is not applicable for situations where a practice change along the slope causes deposition. For example, a grass buffer strip across the foot of a slope on which substantial erosion is occurring induces deposition. The amount of this deposition is a function of transport relationships (*10*) and cannot be predicted by the USLE.

Equation for Soil Detachment on Successive Segments of a Slope

This procedure is founded on an equation (12) that can be applied also when the slope segments are not of equal length. Concepts underlying this equation include the following:

Sediment load at a location on a slope is controlled either by the transport capacity of the runoff and rainfall or by the amount of detached soil material available for transport. When the amount of detached material exceeds the transport capacity, deposition occurs and the sediment load is determined primarily by the transport capacity of the runoff at that location. Where upslope detachment has not equaled the transport capacity, sediment load at a given location is a function of erosion characteristics of the upslope area and can be computed by the USLE. Soil loss from a given segment of the slope can then be computed as the difference between the sediment loads at the lower and upper ends of the segment.

Foster and Wischmeier (12) present a procedure for using this equation to evaluate **LS** for irregular slopes and to account for the effects of the soil or coverage changes along a slope, so long as the changes do not cause deposition to occur.

COVER AND MANAGEMENT FACTOR (C)

Cover and management effects cannot be independently evaluated because their combined effect is influenced by many significant interrelations. Almost any crop can be grown continuously, or it can be grown in rotations. Crop sequence influences the length of time between successive crop canopies, and it also influences the benefits obtained from residual effects of crops and management. The erosion control effectiveness of meadow sod turned under before a row crop depends on the type and quality of the meadow and on the length of time elapsed since the sod was turned under. Seedbeds can be clean tilled, or they can be protected by prior crop residues. They can be left rough, with much available capacity for surface storage and reduction of runoff velocity, or they can be smoothed by secondary tillage.

Crop residues can be removed, left on the surface, incorporated near the surface, or plowed under. When left on the surface, they can be chopped or dragged down, or they can be allowed to remain as left by the harvesting operation. The effectiveness of crop residue management will depend on the amount of residue available. This, in turn, depends on the amount and distribution of rainfall, on the fertility level, and on the management decisions made by the farmer.

The canopy protection of crops not only depends on the type of vegetation, the stand, and the quality of growth, but it also varies greatly in different months or seasons. Therefore, the overall erosion-reducing effectiveness of a crop depends largely on how much of the erosive rain occurs during those periods when the crop and management practices provide the least protection.

Definition of Factor C

Factor **C** in the soil loss equation is the ratio of soil loss from land cropped under specified conditions to the corresponding loss from clean-tilled, continuous fallow. This factor measures the combined effect of all the interrelated cover and management variables.

The loss that would occur on a particular field if it were continuously in fallow condition is computed by the product of **RKLS** in the soil loss equation. Actual loss from the cropped field is usually much less than this amount. Just how much less depends on the particular combination of cover, crop sequence, and management practices. It also depends on the particular stage of growth and development of the vegetal cover at the time of the rain. **C** adjusts the soil loss estimate to suit these conditions.

The correspondence of periods of expected highly erosive rainfall with periods of poor or good plant cover differs between regions or locations. Therefore, the value of **C** for a particular cropping system will not be the same in all parts of the country. Deriving the appropriate **C** values for a given locality requires knowledge of how the erosive rainfall in that locality is likely to be distributed through the 12 months of the year and

how much erosion control protection the growing plants, crop residues, and selected management practices will provide at the time when erosive rains are most likely to occur. A procedure is presented for deriving local values of **C** on the basis of available weather records and research data that reflect effects of crops and management in successive segments of a rotation cycle. The cropping and weather data needed for this purpose appear in reference form in the subsections entitled, **Soil Loss Ratios** and **Erosion Index Distribution Data**.

Cropstage Periods

The change in effectiveness of plant cover within the crop year is gradual. For practical purposes, the year is divided into a series of cropstage periods defined so that cover and management effects may be considered approximately uniform within each period.

Initially, five periods were used, with the seedling and establishment periods defined as the first and second months after crop seeding (*50*). Because of the existing ranges in soil fertility, row spacing, plant population, and general growing conditions, however, soil loss prediction accuracy is improved when the cropstage periods are defined according to percentage of canopy cover rather than for uniform time periods. The lengths of the respective periods will then vary with crop, climate, and management and will be determined by conditions in a particular geographic area.

The soil loss ratios presented in the next subsection for computation of **C** were evaluated for six cropstage periods defined as follows:

Period F (rough fallow)—Inversion plowing to secondary tillage.

Period SB (seedbed)—Secondary tillage for seedbed preparation until the crop has developed 10 percent canopy cover.

Period 1 (establishment)—End of *SB* until crop has developed a 50 percent canopy cover. (Exception: period 1 for cotton ends at 35 percent canopy cover.)

Period 2 (development)—End of period 1 until canopy cover reaches 75 percent. (60 percent for cotton.)

Period 3 (maturing crop)—End of period 2 until crop harvest. This period was evaluated for three levels of final crop canopy.

Period 4 (residue or stubble)—Harvest to plowing or new seeding.

Quantitative Evaluations of Crop and Management Effects

More than 10,000 plot-years of runoff and soil loss data from natural rain,[5] and additional data from a large number of erosion studies under simulated rainfall, were analyzed to obtain empirical measurements of the effects of cropping system and management on soil loss at successive stages of crop establishment and development. Soil losses measured on the cropped plots were compared with corresponding losses from clean-tilled, continuous fallow to determine the soil loss reductions ascribable to effects of the crop system and management. The reductions were then analyzed to identify and evaluate influential subfactors, interactions, and correlations. Mathematical relationships observed for one crop or geographic region were tested against data from other research sites for consistency. Those found compatible with all the relevant data were used to compute soil loss reductions to be expected from conditions not directly represented in the overall plot studies.

The value of **C** on a particular field is determined by many variables, one of which is weather. Major variables that can be influenced by management decisions include crop canopy, residue mulch, incorporated residues, tillage, land use residual, and their interactions. Each of these effects may be treated as a subfactor whose numerical value is the ratio of soil loss with the effect to corresponding loss without it (*57*). **C** is the product of all the pertinent subfactors.

Crop Canopy

Leaves and branches that do not directly contact the soil have little effect on amount and velocity of *runoff* from prolonged rains, but they reduce the effective rainfall energy by intercepting falling raindrops. Waterdrops falling from the canopy may regain appreciable velocity but usually less than the terminal velocities of free-falling

[5] See footnote 3, p. 2.

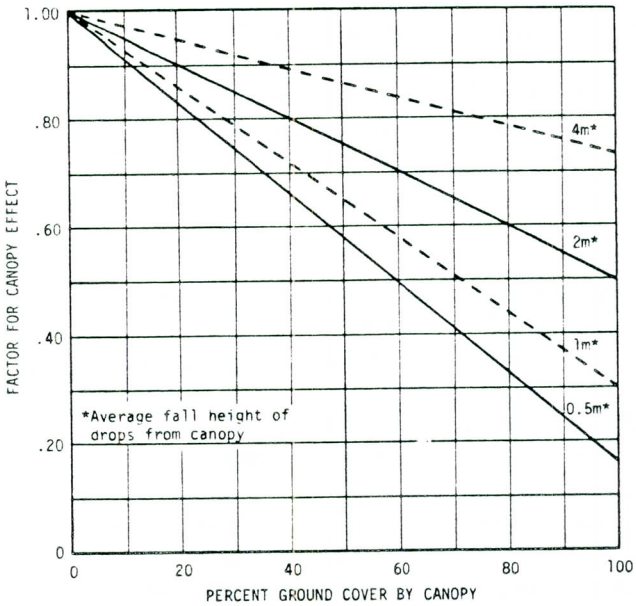

FIGURE 5.—Influence of vegetative canopy on effective EI values. Canopy factor is a subfactor of C.

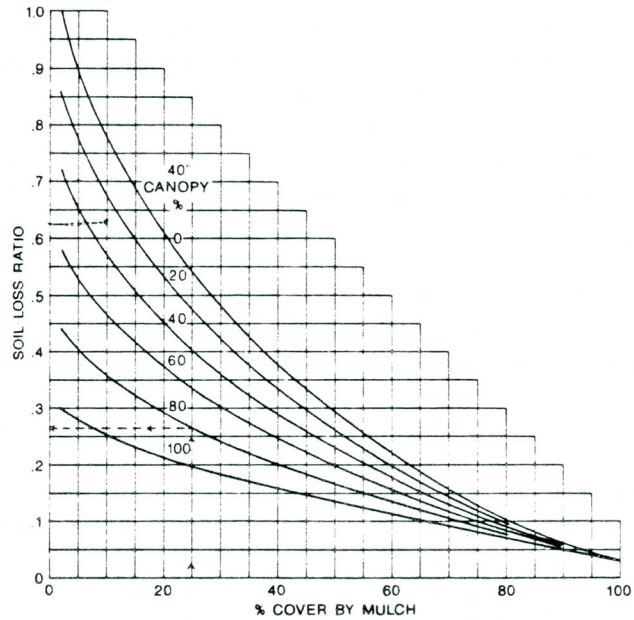

FIGURE 6.—Combined mulch and canopy effects when average fall distance of drops from canopy to the ground is about 40 inches (1 m).

raindrops. The amount by which energy expended at the soil surface is reduced depends on the height and density of the canopy. The subfactor for canopy effect can be estimated for specified conditions by reference to figure 5.

Residue Mulch

Residue mulches and stems from close-growing vegetation are more effective than equivalent percentages of canopy cover. Mulches intercept falling raindrops so near the surface that the drops regain no fall velocity, and they also obstruct runoff flow and thereby reduce its velocity and transport capacity. Measurements of the effectiveness of several types and rates of mulch have been published (*1, 2, 20, 27, 43*). Average subfactors for specific percentages of surface cover by plant materials at the soil surface are given by the upper curve of figure 6. Guides for estimating percent cover are given in the appendix.

If the cover includes both canopy and mulch, the two are not fully additive; the impact energy of drops striking the mulch is dissipated at that point regardless of whether canopy interception has reduced its velocity. The expected effects of mulch and canopy combinations have been computed and are given in figures 6 and 7. Figure 6 applies to corn, sorghum, and cotton in the maturing stage. Figure 7 applies to small grain, soybeans, potatoes, and the establishment period for taller row crops. Enter either figure 6 or 7 along the horizontal scale, move vertically to the appro-

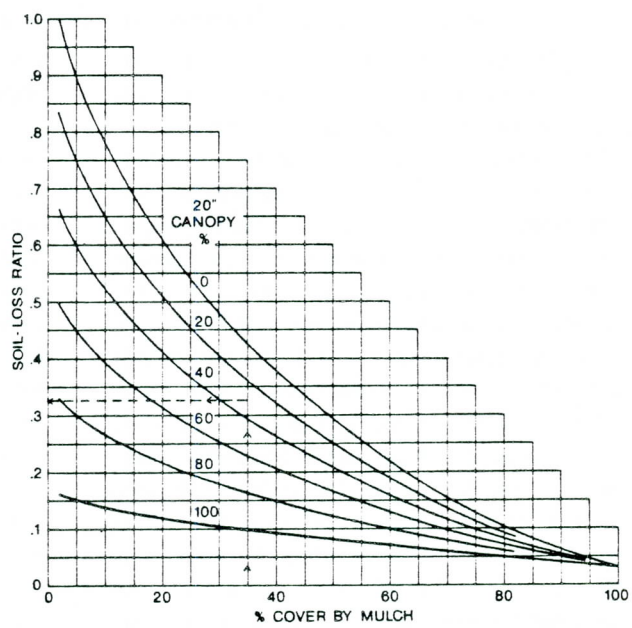

FIGURE 7.—Combined mulch and canopy effects when average fall distance of drops from canopy to the ground is about 20 inches (0.5 m).

priate percent-canopy curve, and read at the left the soil loss ratio from cover effect. This ratio is a subfactor that may be combined with other pertinent subfactors to account for the cropstage soil loss of table 5 or to estimate others.

Incorporated Residues

The plot data indicate that, at least during the seedbed and establishment periods, the erosion-reducing effectivensss of residues mixed into the upper few inches of soil by shallow tillage is appreciably greater than the residual effect of long-term annual incorporation with a moldboard plow. However, the incorporated residues are less effective than if left on the surface.

Tillage

The type, frequency, and timing of tillage operations influence porosity, roughness, cloddiness, compaction, and microtopography. These, in turn, affect water intake, surface storage, runoff velocity, and soil detachability, all of which are factors in potential erosion. These effects are highly correlated with cropland residual effects.

Land Use Residuals

These include effects of plant roots; long-term residue incorporation by plowing; changes in soil structure, detachability, density, organic matter content, and biological activity; and probably other factors. The residual effects are most apparent during seedbed and establishment periods.

Some residual effect will be apparent on nearly any cropland, but the magnitude of its erosion-reducing effectiveness will differ substantially with crops and practices. Tillage and land use residuals are influenced by so many factor interrelations that development of charts like those for canopy and mulch has not been feasible. However, apparent values of these subfactors for some situations were derived from the data and used for expansion of the soil loss ratio table to include conditions somewhat different from those directly represented in the plot studies.

Plowing residues down is far less effective than leaving them on the surface but better than burning them or removing them from the land. After several years of turning the crop residues under with a moldboard plow before row crop seeding in plot studies under natural rainfall, both runoff and soil loss from the row crops were much less than from similar plots from which cornstalks and grain straw were removed at harvesttimes (*52, 54, 59*).

Short periods of rough fallow in a rotation will usually lose much less soil than the basic, clean-tilled, continuous fallow conditions for which **C** = 1. This is largely because of residual effects and is also partly because of the roughness and cloddiness.

The most pronounced residual effect is that from long-term sod or forest. The effect of a grass-and-legume rotation meadow turned under diminishes gradually over about 2 years. In general, the erosion-reducing effectiveness of sod residual (from grass or grass-and-legume meadows) in the plot studies was directly proportional to hay yields. Site values of the subfactor for sod residuals in rotations can be obtained from soil loss ratio table 5-D. The effectiveness of virgin sod and of long periods of alfalfa in which grass became well established was longer lasting. Mixtures of grasses and legumes were more effective than legumes alone.

Residual effectiveness of winter cover crops plowed under in spring depends largely on the type and quality of the crop and its development stage at the time it is plowed under. The effectiveness of grass-and-legume catch crops turned under in spring was less and of shorter duration than that of full-year rotation meadows. Covers such as vetch and ryegrass seeded between corn or cotton rows before harvest and turned under in April were effective in reducing erosion during the winter and showed some residual effect in the following seedbed and establishment periods. Small grain seeded alone in corn or cotton residues showed no residual effect under the next crop. Small grain or vetch on fall-plowed seedbed and turned at spring planting time lost more soil than adjacent plots with undisturbed cotton residues on the surface.

Soil Loss Ratios

Factor **C** is usually given in terms of its average annual value for a particular combination of crop system, management, and rainfall pattern. To derive site values of **C**, soil loss ratios for the indi-

vidual cropstage periods must be combined with erosion-index distribution data, as demonstrated later. Ratios of soil losses in each cropstage period of specified cropping and management systems to corresponding losses from the basic long-term fallow condition were derived from analysis of about a quarter million plot soil loss observations. The ratios are given in table 5 as percentages.

The observed soil loss ratios for given conditions often varied substantially from year to year because of influences of unpredictable random variables and experimental error. The percentages listed in table 5 are the best available averages for the specified conditions. To make the table inclusive enough for general field use, expected ratios had to be computed for cover, residue, and management combinations that were not directly represented in the plot data. This was done by using empirical relationships of soil losses to the subfactors and interactions discussed in the preceding subsection. The user should recognize that the tabulated percentages are subject to appreciable experimental error and could be improved through additional research. However, because of the large volume of data considered in developing the table, the listed values should be near enough to the true averages to provide highly valuable planning and monitoring guidelines. A ratio derived locally from 1-year rainfall simulator tests on a few plots would not necessarily represent the true average for that locality more accurately. Small samples are more subject to bias by random variables and experimental error than larger samples.

Table for Cropland

Table 5, with its supplements 5A, B, C, and D, replaces tables 2, 3, and 4 in the 1965 edition. The supplements had to be separated from the main table to accommodate changes in format requirements. The ratios are expressed as percentages in the tables to eliminate decimal points.

More than half the lines in table 5 are for conditions associated with conservation tillage practices (65), which were not included in the 1965 edition. Also, it provides a direct means of crediting effects of faster and more complete canopy development by improved fertility, closer row spacing, and greater plant population. Because the table includes several times as many specific conditions as the table in the 1965 edition and defines applicable field conditions more accurately, some simplicity has been sacrificed. However, it is not intended for direct use by each field technician or farmer.

Table 5 as presented here is designed to provide the details needed by a trained agronomist to develop simple handbook tables of **C** values for conditions in specific climatic areas. It is designed for use of the revised definitions of cropstage periods given in the preceding section. The agronomist will first determine, for the particular climatic area, the number of weeks normally required for the crop canopies to attain 10, 50, and 75 percent surface cover, respectively. The table will then be used as illustrated in the next major section. Linear interpolation between ratios listed in the table is recommended where appropriate.

Semiarid Regions

Water erosion is a serious problem also in subhumid and semiarid regions. Inadequate moisture and periodic droughts reduce the periods when growing plants provide good soil cover and limit the quantities of plant residue produced. Erosive rainstorms are not uncommon, and they are usually concentrated within the season when cropland is least protected. Because of the difficulty of establishing rotation meadows and the competition for available soil moisture, sod-based rotations are often impractical. One of the most important opportunities for a higher level of soil and moisture conservation is through proper management of available residues. The effects of mulch-tillage practices in these areas can be evaluated from lines 129 to 158 of table 5 and item 12 of 5-B.

Erosion Index Distribution Data

The rainfall factor, **R**, in the soil loss equation does not completely describe the effects of local differences in rainfall pattern on soil erosion. The erosion control effectiveness of a cropping system on a particular field depends, in part, on how the year's erosive rainfall is distributed among the six cropstage periods of each crop included in the system. Therefore, expected monthly distribution

TABLE 5.—*Ratio of soil loss from cropland to corresponding loss from continuous fallow*

Line No.	Cover, crop sequence, and management[1]	Spring residue[2]	Cover after plant[3]	Soil loss ratio[4] for cropstage period and canopy cover[5]							
				F	SB	1	2	3:80	90	96	4L[6]
		Lb	*Pct*	*Pct*	*Pct*	*Pct*	*Pct*	*Pct*	*Pct*	*Pct*	*Pct*
	CORN AFTER C, GS, G OR COT IN MEADOWLESS SYSTEMS										
	Moldboard plow, conv till:										
1	RdL, sprg TP	4,500	—	31	55	48	38	—	—	20	23
2		3,400	—	36	60	52	41	—	24	20	30
3		2,600	—	43	64	56	43	32	25	21	37
4		2,000	—	51	68	60	45	40 33	26	22	47
5	RdL, fall TP	HP[2]	—	44	65	53	38	—	—	20	—
6		GP	—	49	70	57	41	—	24	20	—
7		FP	—	57	74	61	43	32	25	21	—
8		LP	—	65	78	65	45	32	26	22	—
9	RdR, sprg TP	HP	—	66	74	65	47	—	—	22	56
10		GP	—	67	75	66	47	—	27	23	62
11		FP	—	68	76	67	48	35	27	—	69
12		LP	—	69	77	68	49	35	—	—	74
13	RdR, fall TP	HP	—	76	82	70	49	—	—	22	—
14		GP	—	77	83	71	50	—	27	23	—
15		FP	—	78	85	72	51	35	27	—	—
16		LP	—	79	86	73	52	35	—	—	—
17	*Wheeltrack pl, RdL, TP[8]*	4,500	—	—	31	27	25	—	—	18	23
18		3,400	—	—	36	32	30	—	22	18	30
19		2,600	—	—	43	36	32	29	23	19	37
20		2,000	—	—	51	43	36	31	24	20	47
21	*Deep off-set disk or*	4,500	10	—	45	38	34	—	—	20	23
22	*disk plow*	3,400	10	—	52	43	37	—	24	20	30
23		2,600	5	—	57	48	40	32	25	21	37
24		2,000	—	—	61	51	42	33	26	22	47
25	*No-till plant in crop residue[9]*	6,000	95	—	2	2	2	—	—	2	14
26		6,000	90	—	3	3	3	—	—	3	14
27		4,500	80	—	5	5	5	—	—	5	15
28		3,400	70	—	8	8	8	—	8	6	19
29		3,400	60	—	12	12	12	12	9	8	23
30		3,400	50	—	15	15	14	14	11	9	27
31		2,600	40	—	21	20	18	17	13	11	30
32		2,600	30	—	26	24	22	21	17	14	36
	Chisel, shallow disk, or fld cult, as only tillage:										
33	On moderate slopes	6,000	70	—	8	8	7	—	—	7	17
34			60	—	10	9	8	—	—	8	17
35			50	—	13	11	10	—	—	9	18
36			40	—	15	13	11	—	—	10	19
37			30	—	18	15	13	—	—	12	20
38			20	—	23	20	18	—	—	16	21
39	Do.	4,500	70	—	9	8	7	—	—	7	18
40			60	—	12	10	9	—	—	8	18
41			50	—	14	13	11	—	—	9	19
42			40	—	17	15	13	—	—	10	20
43			30	—	21	18	15	—	—	13	21
44			20	—	25	22	19	—	—	16	22
45	Do.	3,400	60	—	13	11	10	—	10	8	20
46			50	—	16	13	12	—	12	9	24

Line No.	Cover, crop sequence, and management[1]	Spring residue[2]	Cover after plant[3]	Soil loss ratio[4] for cropstage period and canopy cover[5]							
				F	SB	1	2	3:80	90	96	4L[6]
		Lb	*Pct*	*Pct*	*Pct*	*Pct*	*Pct*	*Pct*	*Pct*	*Pct*	*Pct*
	CORN AFTER WC OF RYEGRASS OR WHEAT SEEDED IN C STUBBLE										
	WC reaches stemming stage:										
79	No-till pl in killed WC	4,000	—	—	7	7	7	—	7	6	([13])
80		3,000	—	—	11	11	11	11	9	7	
81		2,000	—	—	15	15	14	14	11	9	
82		1,500	—	—	20	19	18	18	14	11	
	Strip till one-fourth row space										
83	Rows U/D slope	4,000	—	—	13	12	11	—	11	9	([13])
84		3,000	—	—	18	17	16	16	13	10	
85		2,000	—	—	23	22	20	19	15	12	
86		1,500	—	—	28	26	24	22	17	14	
87	Rows on contour[11]	4,000	—	—	10	10	10	—	10	8	([13])
88		3,000	—	—	15	15	15	15	12	9	
89		2,000	—	—	20	20	19	19	15	12	
90		1,500	—	—	25	24	23	22	17	14	
91	TP, conv seedbed	4,000	—	36	60	52	41	—	24	20	([13])
92		3,000	—	43	64	56	43	31	25	21	
93		2,000	—	51	68	60	45	33	26	22	
94		1,500	—	61	73	64	47	35	27	23	
	WC succulent blades only:										
95	No-till pl in killed WC	3,000	—	—	11	11	17	23	18	16	([13])
96		2,000	—	—	15	15	20	25	20	17	
97		1,500	—	—	20	20	23	26	21	18	
98		1,000	—	—	26	26	27	27	22	19	
99	Strip till one-fourth row space	3,000	—	—	18	18	21	25	20	17	([13])
100		2,000	—	—	23	23	25	27	21	18	
101		1,500	—	—	28	28	28	28	22	19	
102		1,000	—	—	33	33	31	29	23	20	
	CORN IN SOD-BASED SYSTEMS										
	No-till pl in killed sod:										
103	3 to 5 tons hay yld	—	—	—	1	1	1	—	1	1	1
104	1 to 2 tons hay yld	—	—	—	2	2	2	2	2	2	2
	Strip till, 3-5 ton M:										
105	50 percent cover, tilled strips	—	—	—	2	2	2	—	2	2	4
106	20 percent cover, tilled strips	—	—	—	3	3	3	—	3	3	5
	Strip till, 1-2 ton M:										
107	40 percent cover, tilled strips	—	—	—	4	4	4	4	4	4	6
108	20 percent cover, tilled strips	—	—	—	5	5	5	5	5	5	7
	Other tillage after sod:			([14])	([14])	([11])	([14])	([14])	([14])	([14])	([11])
	CORN AFTER SOYBEANS										
109	*Sprg TP, conv till*	HP	—	40	72	60	48	—	—	25	29
110		GP	—	47	78	65	51	—	30	25	37
111		FP	—	56	83	70	54	40	31	26	44
112	*Fall TP, conv till*	HP	—	47	75	60	48	—	—	25	—
113		GP	—	53	81	65	51	—	30	25	—
114		FP	—	62	86	70	54	40	31	26	—
115	Fall & sprg chisel or cult	HP	[15]30	—	40	35	29	—	—	23	29
116		GP	25	—	45	39	33	—	27	23	37

45	Do.	3,400	60	—	13	11	10	—	10	8	20	
46			50	—	16	13	12	—	12	9	24	
47			40	—	19	17	16	—	14	11	25	
48			30	—	23	21	19	—	17	14	26	
49			20	—	29	25	23	—	21	16	27	
50			10	—	36	32	29	—	24	20	30	
51	Do.	2,600	50	—	17	16	15	15	13	10	29	
52			40	—	21	20	19	19	15	12	30	
53			30	—	25	23	22	22	18	14	32	
54			20	—	32	29	28	27	22	17	34	
55			10	—	41	36	34	32	25	21	37	
56	Do.	2,000	40	—	23	21	20	20	15	12	37	
57			30	—	27	25	24	23	19	15	39	
58			20	—	35	32	30	28	22	18	42	
59			10	—	46	42	38	33	26	22	47	
	On slopes > 12 percent.											
60	Lines 33-59 times factor of:	—	—	—	1.3	1.3	1.1	1.0	1.0	1.0	1.0	
	Disk or harrow after spring chisel or fld cult:											
	Lines 33-59 times factor of:											
61	On moderate slopes	—	—	—	1.1	1.1	1.1	1.0	1.0	1.0	1.0	
62	On slopes > 12 percent	—	—	—	1.4	1.4	1.2	1.0	1.0	1.0	1.0	
	Ridge plant:[10]											
	Lines 33-59 times factor of:											
63	Rows on contour[11]	—	—	—	.7	.7	.7	.7	.7	.7	.7	
64	Rows U/D slope < 12 percent	—	—	—	.7	.7	1.0	1.0	1.0	1.0	1.0	
65	Rows U/D slope > 12 percent	—	—	—	.9	.9	1.0	1.0	1.0	1.0	1.0	
	Till plant:											
	Lines 33-59 times factor of:											
66	Rows on contour[11]	—	—	—	.7	.85	1.0	1.0	1.0	1.0	1.0	
67	Rows U/D slope < 7 percent	—	—	—	1.0	1.0	1.0	1.0	1.0	1.0	1.0	
	Strip till one-fourth of row spacing:											
68	Rows on contour[11]	4,500	[12]60	—	12	10	9	—	—	8	23	
69		3,400	50	—	16	14	12	—	11	10	27	
70		2,600	40	—	22	19	17	17	14	12	30	
71		2,000	30	—	27	23	21	20	16	13	36	
72	Rows U/D slope	4,500	[12]60	—	16	13	11	—	—	9	23	
73		3,400	50	—	20	17	14	—	12	11	27	
74		2,600	40	—	26	22	19	17	14	12	30	
75		2,000	30	—	31	26	23	20	16	13	36	
	Vari-till:											
76	Rows on contour[11]	3,400	40	—	13	12	11	—	—	11	22	
77		3,400	30	—	16	15	14	14	13	12	26	
78		2,600	20	—	21	19	19	19	16	14	34	

115	Fall & sprg chisel or cult	HP	[13]30	—	40	35	29		—	23	29	
116		GP	25	—	45	39	33		27	23	37	
117		GP	20	—	51	44	39	34	27	23	37	
118		FP	15	—	58	51	44	36	28	23	44	
119		LP	10		67	59	48	36	28	23	54	
120	*No-till pl in crop res'd*	HP	[13]40	—	25	20	19	—	14	11	26	
121		GP	30	—	33	29	25	22	18	14	33	
122		FP	20		44	38	32	27	23	18	40	
	BEANS AFTER CORN											
123	*Sprg TP, RdL, conv till*	HP	—	33	60	52	38	—	20	17	([16])	
124		GP	—	39	64	56	41	—	21	18		
125		FP	—	45	68	60	43	29	22	—		
126	*Fall TP, RdL, conv till*	HP	—	45	69	57	38	—	20	17	([16])	
127		GP	—	52	73	61	41	—	21	18		
128		FP	—	59	77	65	43	29	22	—		
	Chisel or fld cult:			([17])	([17])	([17])	([17])	([17])	([17])	([17])	([16])	
	BEANS AFTER BEANS			([18])	([18])	([18])	([18])	([18])	([18])	([18])	([16])	
	GRAIN AFTER C, G, GS, COT[19]											
129	*In disked residues:*	4,500	70	—	12	12	11	7	4	2	([20])	
130		3,400	60	—	16	14	12	7	4	2		
131			50	—	22	18	14	8	5	3		
132			40	—	27	21	16	9	5	3		
133			30	—	32	25	18	9	6	3		
134			20	—	38	30	21	10	6	3		
135	Do.	2,600	40	—	29	24	19	9	6	3	([20])	
136			20	—	43	34	24	11	7	4		
137			10	—	52	39	27	12	7	4		
138	Do.	2,000	30	—	38	30	23	11	7	4	([20])	
139			20	—	46	36	26	12	7	4		
140			10	—	56	43	30	13	8	5		
141	*In disked stubble, RdR*	—	—	—	79	62	42	17	11	6	([20])	
142	*Winter G after fall TP, RdL*	HP	—	31	55	48	31	12	7	5	([20])	
143		GP	—	36	60	52	33	13	8	5		
144		FP	—	43	64	56	36	14	9	5		
145		LP	—	53	68	60	38	15	10	6		
	GRAIN AFTER SUMMER FALLOW											
146	*With grain residues*	200	10	—	70	55	43	18	13	11	([21])	
147		500	30	—	43	34	23	13	10	8		
148		750	40	—	34	27	18	10	7	7		
149		1,000	50	—	26	21	15	8	7	6		
150		1,500	60	—	20	16	12	7	5	5		
151		2,000	70	—	14	11	9	7	5	5		
152	*With row crop residues*	300	5	—	82	65	44	19	14	12	([21])	
153		500	15	—	62	49	35	17	13	11		
154		750	23	—	50	40	29	14	11	9		
155		1,000	30	—	40	31	24	13	10	8		
156		1,500	45	—	31	24	18	10	8	7		
157		2,000	55	—	23	19	14	8	7	5		
158		2,500	65	—	17	14	12	7	5	4		
	POTATOES											
159	*Rows with slope*	—	—	43	64	56	36	26	19	16		
	Contoured rows, ridged when canopy cover is about											
160	*50 percent*[11]	—		43	64	56	18	13	10	8		

See footnotes, p. 24.

Footnotes for table 5.

---

[1] Symbols: B, soybeans; C, corn; conv till, plow, disk and harrow for seedbed; cot, cotton; F, rough fallow; fld cult, field cultivator; G, small grain; GS, grain sorghum; M, grass and legume meadow, at least 1 full year; pl, plant; RdL, crop residues left on field; RdR, crop residues removed; SB, seedbed period; sprg, spring; TP, plowed with moldboard; WC, winter cover crop; —, insignificant or an unlikely combination of variables.

[2] Dry weight per acre after winter loss and reductions by grazing or partial removal: 4,500 lbs represents 100 to 125 bu corn; 3,400 lbs, 75 to 99 bu; 2,600 lbs, 60 to 74 bu; and 2,000 lbs, 40 to 59 bu; with normal 30-percent winter loss. For RdR or fall-plow practices, these four productivity levels are indicated by HP, GP, FP and LP, respectively (high, good, fair, and low productivity). In lines 79 to 102, this column indicates dry weight of the winter-cover crop.

[3] Percentage of soil surface covered by plant residue mulch *after* crop seeding. The difference between spring residue and that on the surface after crop seeding is reflected in the soil loss ratios as residues mixed with the topsoil.

[4] The soil loss ratios, given as percentages, assume that the indicated crop sequence and practices are followed consistently. One-year deviations from normal practices do not have the effect of a permanent change. Linear interpolation between lines is recommended when justified by field conditions.

[5] Cropstage periods are as defined on p. 18. The three columns for cropstage 3 are for 80, 90, and 96 to 100 percent canopy cover at maturity.

[6] Column 4L is for all residues left on field. Corn stalks partially standing as left by some mechanical pickers. If stalks are shredded and spread by picker, select ratio from table 5-C. When residues are reduced by grazing, take ratio from lower spring-residue line.

[7] Period 4 values in lines 9 to 12 are for corn stubble (stover removed).

[8] Inversion plowed, no secondary tillage. For this practice, residues must be left and incorporated.

[9] Soil surface and chopped residues of *matured* preceding crop undisturbed except in narrow slots in which seeds are planted.

[10] Top of old row ridge sliced off, throwing residues and some soil into furrow areas. Reridging assumed to occur near end of cropstage 1.

[11] Where lower soil loss ratios are listed for rows on the contour, this reduction is in addition to the standard field contouring credit. The *P* value for contouring is used with these reduced loss ratios.

[12] Field-average percent cover; probably about three-fourths of percent cover on undisturbed strips.

[13] If again seeded to WC crop in corn stubble, evaluate winter period as a winter grain seeding (lines 132 to 148). Otherwise, see table 5-C.

[14] Select the appropriate line for the crop, tillage, and productivity level and multiply the listed soil loss ratios by sod residual factors from table 5-D.

[15] Spring residue may include carryover from prior corn crop.

[16] See table 5-C.

[17] Use values from lines 33 to 62 with appropriate dates and lengths of cropstage periods for beans in the locality.

[18] Values in lines 109 to 122 are best available estimates, but planting dates and lengths of cropstages may differ.

[19] When meadow is seeded with the grain, its effect will be reflected through higher percentages of cover in cropstages 3 and 4.

[20] Ratio depends on percent cover. See table 5-C.

[21] See item 12, table 5-B.

TABLE 5

Expected fi
Estimated i
stalks
Practice
Number
COTTON A
1....No
2....Ch
3....Fa
4....Ch
5....Be
6....Bec
7....Hip
8....Hip
9....Cor
COTTON AF
For the
meadow ha
lines above
COTTON AF
Select v
See footn

TABLE 5-A.—*Approximate soil loss ratios for cotton*

Practice Number	Tillage operation(s)	Soil loss ratio[1]		
	Expected final canopy percent cover:	65	80	95
	Estimated initial percent cover from defoliation + stalks down:	30	45	60
	COTTON ANNUALLY:	*Percent*		
1	*None:*			
	Defoliation to Dec. 31	36	24	15
	Jan. 1 to Feb. or Mar. tillage:			
	Cot Rd only	52	41	32
	Rd & 20 percent cover vol veg[2]	32	26	20
	Rd & 30 percent cover vol veg	26	20	14
2	*Chisel plow soon after cot harvest:*			
	Chiseling to Dec. 31	40	31	24
	Jan. 1 to sprg tillage	56	47	40
3	*Fall disk after chisel:*			
	Disking to Dec. 31	53	45	37
	Jan. 1 to sprg tillage	62	54	47
4	*Chisel plow Feb-Mar, no prior tillage:*			
	Cot Rd only	50	42	35
	Rd & 20 percent vol veg	39	33	28
	Rd & 30 percent vol veg	34	29	25
5	*Bed ("hip") Feb-Mar, no prior tillage:*			
	Cot Rd only	100	84	70
	Rd & 20 percent vol veg	78	66	56
	Rd & 30 percent vol veg	68	58	50
	Split ridges & plant after hip, or Disk & plant after chisel (SB):			
	Cot Rd only	61	54	47
	Rd & 20 percent vol veg	53	47	41
	Rd & 30 percent vol veg	50	44	38
	Cropstage 1:			
	Cot Rd only	57	50	43
	Rd & 20 percent vol veg	49	43	38
	Rd & 30 percent vol veg	46	41	36
	Cropstage 2	45	39	34
	Cropstage 3	40	27	17
6	*Bed (hip) after 1 prior tillage:*			
	Cot Rd only	110	96	84
	Rd & 20 percent veg	94	82	72
	Rd & 30 percent veg	90	78	68
	Split ridges after hip (SB):			
	Cot Rd only	66	61	52
	Rd & 20 to 30 percent veg	61	55	49
	Cropstage 1:			
	Cot Rd only	60	56	49
	Rd & 20 to 30 percent veg	56	51	46
	Cropstage 2	47	44	38
	Cropstage 3	42	30	19
7	*Hip after 2 prior tillages:*			
	Cot Rd only	116	108	98
	Rd & 20-30 percent veg	108	98	88
	Split ridges after hip (SB)	67	62	57
8	*Hip after 3 or more tillages:*	120	110	102
	Split ridges after hip (SB)	68	64	59
9	*Conventional moldboard plow and disk:*			
	Fallow period	42	39	36
	Seedbed period	68	64	59
	Cropstage 1	63	59	55
	Cropstage 2	49	46	43
	Cropstage 3	44	32	22
	Cropstage 4 (See practtices 1, 2, and 3)			

COTTON AFTER SOD CROP:

For the first or second crop after a grass or grass-and-legume meadow has been turnplowed, multiply values given in the last five lines above by sod residual factors from table 5-D.

COTTON AFTER SOYBEANS:

Select values from above and multiply by 1.25.

See footnotes at right.

of erosive rainfall at a particular location is an element in deriving the applicable value of cover and management, **C**.

Central and Eastern States

A location's erosion index is computed by summing **EI** values of individual rainstorms over periods from 20 to 25 years. Thus, the expected monthly distribution of the erosion index can be computed from the same data. For each rainfall record abstracted for development of the isoerodent map, the monthly **EI** values were computed and expressed as percentages of the location's average annual erosion index. When the monthly percentages are plotted cumulatively against time, they define **EI** distribution curves such as illustrated in figure 8 for three locations. The three contrasting curves are presented to demonstrate how drastically the normal **EI** distribution can differ among climatic regions.

On the basis of observed seasonal distributions of **EI**, the 37 States east of the Rocky Mountains were divided into the 33 geographic areas delineated in figure 9. The changes in distribution are usually gradual transitions from one area to the next, but the average distribution within any one of the areas may, for practical purposes, be considered applicable for the entire area. The **EI** distributions in the 33 areas, expressed as cumulative percentages of annual totals, are given in table 6. The area numbers in the table correspond to those in figure 9. The data in the table were

[1] *Alternate procedure for estimating the soil loss ratios:*

The ratios given above for cotton are based on estimates for reductions in percent cover through normal winter loss and by the successive tillage operations. Research is underway in Mississippi to obtain more accurate residue data in relation to tillage practices. This research should provide more accurate soil loss ratios for cotton within a few years.

Where the reductions in percent cover by winter loss and tillage operations are small, the following procedure may be used to compute soil loss ratios for the preplant and seedbed periods: Enter figure 6 with the percentage of the field surface covered by residue mulch, move vertically to the upper curve, and read the mulch factor on the scale at the left. Multiply this factor by a factor selected from the following tabulation to credit for effects of land-use residual, surface roughness and porosity.

Productivity level	No tillage	Rough surface	Smoothed surface
High	0.66	0.50	0.56
Medium	.71	.54	.61
Poor	.75	.58	.65

Values for the bedded period on slopes of less than 1 percent should be estimated at twice the value computed above for rough surfaces.

[2] Rd, crop residue; vol veg, volunteer vegetation.

TABLE 5-B.—*Soil loss ratios for conditions not evaluated in table 5*

COTTON:
See table 5-A.

CROPSTAGE 4 FOR ROWCROPS:
Stalks broken and partially standing: Use col. 4L.
Stalks standing after hand picking: Col. 4L times 1.15.
Stalks shredded without soil tillage: See table 5-C.
Fall chisel: Select values from lines 33-62, seedbed column.

CROPSTAGE 4 FOR SMALL GRAIN:
See table 5-C.

DOUBLE CROPPING:
Derive annual C value by selecting from table 5 the soil loss percentages for the successive cropstage periods of each crop.

ESTABLISHED MEADOW, FULL-YEAR PERCENTAGES:

Grass and legume mix,	3 to 5 t hay	0.4
Do.	2 to 3 t hay	.6
Do.	1 t hay	1.0
Sericea, after second year		1.0
Red clover		1.5
Alfalfa, lespedeza, and second-year sericea		2.0
Sweetclover		2.5

MEADOW SEEDING WITHOUT NURSE CROP:
Determine appropriate lengths of cropstage periods SB, 1, and 2 and apply values given for small grain seeding.

PEANUTS:
Comparison with soybeans is suggested.

PINEAPPLES:
Direct data not available. Tentative values derived analytically are available from the SCS in Hawaii or the Western Technical Service Center at Portland, Oreg. (Reference 5).

SORGHUM:
Select values given for corn, on the basis of expected crop residues and canopy cover.

SUGARBEETS:
Direct data not available. Probably most nearly comparable to potatoes, without the ridging credit.

SUGARCANE:
Tentative values available from sources given for pineapples.

SUMMER FALLOW IN LOW-RAINFALL AREAS, USE GRAIN OR ROW CROP RESIDUES:
The approximate soil loss percentage after each successive tillage operation may be obtained from the following tabulation by estimating the percent surface cover after that tillage and selecting the column for the appropriate amount of initial residue. The given values credit benefits of the residue mulch, residues mixed with soil by tillage, and the crop system residual.

Percent cover by mulch	Initial residue (lbs/A)			
	>4,000	3,000	2,000	1,500
90	4	—	—	—
80	8	[1]8	—	—
70	12	13	[1]14	—
60	16	17	[1]18	[1]19
50	20	22	24	[1]25
40	25	27	30	32
30	29	33	37	39
20	35	39	44	48
10	47	55	63	68

[1] For grain residue only.

WINTER COVER SEEDING IN ROW CROP STUBBLE OR RESIDUES:
Define cropstage periods based on the cover seeding date and apply values from lines 129 to 145.

TABLE 5-C.—*Soil loss ratios (percent) for cropstage when stalks are chopped and distributed without so tillage*

Mulch cover[1]	Corn or Sorghum: Tilled seedbed[2]	Corn or Sorghum: No-till	Soybeans: Tilled seedbed[2]	Soybeans: No-till in corn rd[3]	Grain Stubble
20	48	34	60	42	48
30	37	26	46	32	37
40	30	21	38	26	30
50	22	15	28	19	22
60	17	12	21	16	17
70	12	8	15	10	12
80	7	5	9	6	7
90	4	3	—	—	4
95	3	2	—	—	3

[1] Part of a field surface directly covered by pieces of residue mulc

[2] This column applies for all systems other than no-till.

[3] Cover after bean harvest may include an appreciable number stalks carried over from the prior corn crop.

[4] For grain with meadow seeding, include meadow growth in percei cover and limit grain period 4 to 2 mo. Thereafter, classify as estal lished meadow.

abstracted from the published **EI** distributio curves.

The percentage of the annual erosion index thc is to be expected within each cropstage perio may be obtained by reading from the appropriat line of table 6, the values for the last and firs date of the period, and subtracting. Interpolat

TABLE 5-D.—*Factors to credit residual effects of turne sod*[1]

Crop	Hay yield	Factor for cropstage period: F	SB and 1	2	3	4
	Tons					
First year after mead:						
Row crop or grain . . .	3-5	0.25	0.40	0.45	0.50	0.6
	2-3	.30	.45	.50	.55	.6
	1-2	.35	.50	.55	.60	.7
Second year after mead:						
Row crop	3.5	.70	.80	.85	.90	.9
	2-3	.75	.85	.90	.95	1.
	1-2	.80	.90	.95	1.0	1.
Spring grain	3-5	—	.75	.80	.85	.9
	2-3	—	.80	.85	.90	1.
	1-2	—	.85	.90	.95	1.
Winter grain	3-5	—	.60	.70	.85	.9
	2-3	—	.65	.75	.90	1.
	1-2	—	.70	.85	.95	1.

[1] These factors are to be multiplied by the appropriate soil loss per centages selected from table 5. They are directly applicable for sod forming meadows of at least 1 full year duration, plowed not mor than 1 month before final seedbed preparation.

When sod is fall plowed for spring planting, the listed values for al cropstage periods are increased by adding 0.02 for each additiona month by which the plowing precedes spring seedbed preparation. Fo example, September plowing would precede May disking by 8 month and 0.02(8—1), or 0.14, would be added to each value in the table. Fo nonsod-forming meadows, like sweetclover or lespedeza, multiply th factors by 1.2. When the computed value is greater than 1.0, use as 1.0

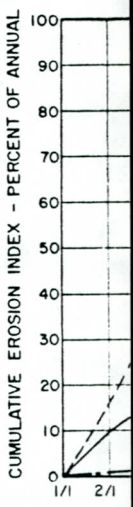

FIGURE 8.—Ty

between v
sired dates

Weste

Normal
States ofte
tance. Figu
States bec
available
daries of
tributions
abstracted

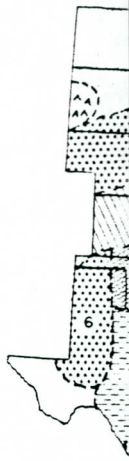

FIGURE 9.—Ke

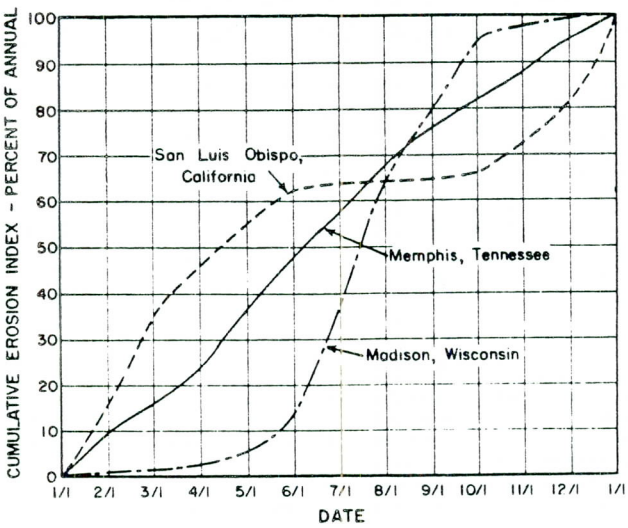

FIGURE 8.—Typical EI-distribution curves for three rainfall patterns.

between values in the selected line when the desired dates are not listed.

Western States, Hawaii, and Puerto Rico

Normal rainfall patterns in these mountainous States often change abruptly within a short distance. Figure 9 was not extended to include these States because long-term intensity data were not available for enough locations to delineate boundaries of homogeneous areas. However, **EI** distributions indicated by station records that were abstracted are given in table 7 for reference.

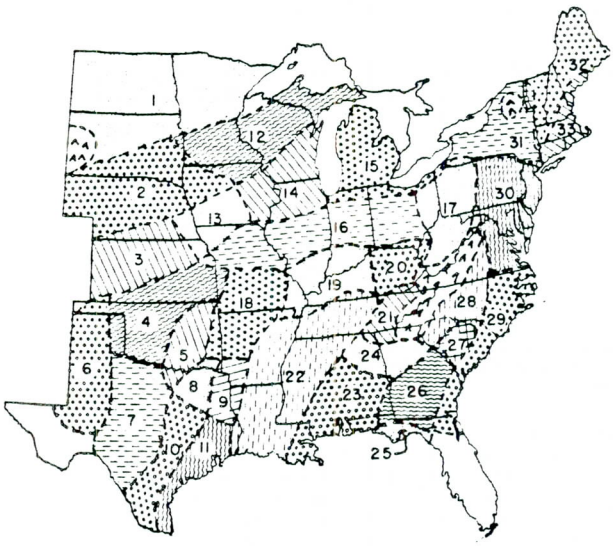

FIGURE 9.—Key map for selection of applicable EI-distribution data from table 6.

Winter Periods

Site **EI** values reflect only rain falling at erosive intensities. Where the winter precipitation comes as snow or light rain, **EI** distribution curves may show insignificant percentages for several winter months. Yet, snowmelt and low intensity rains on frozen soil may cause appreciable runoff that is erosive even though the associated maximum 30-minute rainfall intensity is extremely low or zero. The section on **Isoerodent Maps** pointed out that where this type of runoff is significant its erosive force must be reflected in an $\mathbf{R}_s$ value that is added to the **EI** value to obtain **R**. This additional erosive force must also be reflected in the *monthly distribution* of **R**. Otherwise, poor management during the winter period will not be reflected in the USLE estimate of annual soil loss because a zero crop-stage **R** value would predict zero soil loss regardless of the relevant soil loss ratio.

Soil erosion by thaw runoff is most pronounced in the Northwest, where $\mathbf{R}_s$ values often exceed the average annual **EI**. However, it may also be significant in other Northern States. Probable amounts of thaw runoff were not available for inclusion in the calculations of the **EI** distributions given in tables 6 and 7, but the significance and probable time of occurrence of such runoff can be estimated by local people. The procedure for adjusting table 6 cumulative percentages to include this erosive potential will be illustrated.

Based on the previously described estimating procedure, $\mathbf{R}_s$ values in area No. 1, figure 9, appear to equal about 8 percent of the annual **EI**. Assuming that the thaw runoff in that area normally occurs between March 15 and April 15, the percentage in table 6 for April 1 is increased by 4, the April 15 and all subsequent readings are increased by 8, and all the adjusted readings are then divided by 1.08. This procedure corrects the data given in line 1, table 6, for dates April 1 to September 1 to the following cumulative percentages listed in chronological sequence: 5, 9, 10, 13, 18, 29, 41, 53, 66, 79, 91. The other values are unchanged. Such adjustments in monthly distribution of **R** where thaw runoff is significant will be particularly helpful when the USLE is used to estimate seasonal distribution of sediment from agricultural watersheds.

LE 6.—*Percentage of the average annual* **EI** *which normally occurs between January 1 and the indicated dates.*[1] *Computed for the geographic areas shown in figure 9*

Area No.	Jan.		Feb.		Mar.		Apr.		May		June		July		Aug.		Sept.		Oct.		Nov.		Dec.	
	1	15	1	15	1	15	1	15	1	15	1	15	1	15	1	15	1	15	1	15	1	15	1	15
1	0	0	0	0	0	0	1	2	3	6	11	23	36	49	63	77	90	95	98	99	100	100	100	100
2	0	0	0	0	1	1	2	3	6	10	17	29	43	55	67	77	85	91	96	98	99	100	100	100
3	0	0	0	0	1	1	2	3	6	13	23	37	51	61	69	78	85	91	94	96	98	99	99	100
4	0	0	1	1	2	3	4	7	12	18	27	38	48	55	62	69	76	83	90	94	97	98	99	100
5	0	1	2	3	4	6	8	13	21	29	37	46	54	60	65	69	74	81	87	92	95	97	98	99
6	0	0	0	0	1	1	1	2	6	16	29	39	46	53	60	67	74	81	88	95	99	99	100	100
7	0	1	1	2	3	4	6	8	13	25	40	49	56	62	67	72	76	80	85	91	97	98	99	99
8	0	1	3	5	7	10	14	20	28	37	48	56	61	64	68	72	77	81	86	89	92	95	98	99
9	0	2	4	6	9	12	17	23	30	37	43	49	54	58	62	66	70	74	78	82	86	90	94	97
10	0	1	2	4	6	8	10	15	21	29	38	47	53	57	61	65	70	76	83	88	91	94	96	98
11	0	1	3	5	7	9	11	14	18	27	35	41	46	51	57	62	68	73	79	84	89	93	96	98
12	0	0	0	0	1	1	2	3	5	9	15	27	38	50	62	74	84	91	95	97	98	99	99	100
13	0	0	0	1	1	2	3	5	7	12	19	33	48	57	65	74	82	88	93	96	98	99	100	100
14	0	0	0	1	2	3	4	6	9	14	20	28	39	52	63	72	80	87	91	94	97	98	99	100
15	0	0	1	2	3	4	6	8	11	15	22	31	40	49	59	69	78	85	91	94	96	98	99	100
16	0	1	2	3	4	6	8	10	14	18	25	34	45	56	64	72	79	84	89	92	95	97	98	99
17	0	1	2	3	4	5	6	8	11	15	20	28	41	54	65	74	82	87	92	94	96	97	98	99
18	0	1	2	4	6	8	10	13	19	26	34	42	50	58	63	68	74	79	84	89	93	95	97	99
19	0	1	3	6	9	12	16	21	26	31	37	43	50	57	64	71	77	81	85	88	91	93	95	97
20	0	2	3	5	7	10	13	16	19	23	27	34	44	54	63	72	80	85	89	91	93	95	96	98
21	0	3	6	10	13	16	19	23	26	29	33	39	47	58	68	75	80	83	86	88	90	92	95	97
[illegible]	0	3	6	9	13	17	21	27	33	38	44	49	55	61	67	71	75	78	81	84	86	90	94	97
[illegible]	0	3	5	7	10	14	18	23	27	31	35	39	45	53	60	67	74	80	84	86	88	90	93	95
24	0	3	6	9	12	16	20	24	28	33	38	43	50	59	69	75	80	84	87	90	92	94	96	98
25	0	1	3	5	7	10	13	17	21	24	27	33	40	46	53	61	69	78	89	92	94	95	97	98
26	0	2	4	6	8	12	16	20	25	30	35	41	47	56	67	75	81	85	87	89	91	93	95	97
27	0	1	2	3	5	7	10	14	18	22	27	32	37	46	58	69	80	89	93	94	95	96	97	99
28	0	1	3	5	7	9	12	15	18	21	25	29	36	45	56	68	77	83	88	91	93	95	97	99
29	0	1	2	3	4	5	7	9	11	14	17	22	31	42	54	65	74	83	89	92	95	97	98	99
30	0	1	2	3	4	5	6	8	10	14	19	26	34	45	56	66	76	82	86	90	93	95	97	99
31	0	0	0	1	2	3	4	5	7	12	17	24	33	42	55	67	76	83	89	92	94	96	98	99
32	0	1	2	3	4	5	6	8	10	13	17	22	31	42	52	60	68	75	80	85	89	92	96	98
33	0	1	2	4	6	8	11	13	15	18	21	26	32	38	46	55	64	71	77	81	85	89	93	97

[1] For dates not listed in the table, interpolate between adjacent values.

Procedure for Deriving Local C Values

Factor **C** in the USLE measures the combined effect of all the interrelated cover and management variables and is defined as the ratio of soil loss from land cropped under specified conditions to the corresponding loss from clean-tilled continuous fallow. It is usually expressed as an annual value for a particular cropping and management system. Soil loss ratios, as used in table 5, express a similar ratio for a short time interval within which cover and management effects are [illegible]tively uniform. The cropstage soil loss ratios must be combined in proportion to the applicable percentages of **EI** to derive annual **C** values.

To compute the value of **C** for any particular crop and management system on a given field, one needs first to determine the most likely seeding and harvest dates, rate of canopy development, and final canopy cover. Also, the system to be evaluated must be carefully defined with regard to crop and residue management details. Within the broad limits of tables 5 and 6, these tables then supply the research data needed to complete

TABLE 7.—*Monthly distribution of* **EI** *at selected raingage locations*

Location[1]	Average percentage of annual EI occurring from 1/1 to:											
	2/1	3/1	4/1	5/1	6/1	7/1	8/1	9/1	10/1	11/1	12/1	12/31
California												
Red Bluff (69)	18	36	47	55	62	64	65	65	67	72	82	100
San Luis Obispo (51)	19	39	54	63	65	65	65	65	65	67	83	100
Colorado												
Akron (91)	0	0	0	1	18	33	72	87	98	99	100	100
Pueblo (68)	0	0	0	5	14	23	40	82	84	100	100	100
Springfield (98)	0	0	1	4	26	36	60	94	96	99	100	100
Hawaii												
Hilo (770)	9	23	34	44	49	51	55	60	65	72	87	100
Honolulu (189)	19	33	43	51	54	55	56	57	58	62	81	100
Kahului (107)	14	32	49	62	67	68	69	70	71	76	86	100
Lihue (385)	19	29	36	41	44	45	48	51	56	64	80	100
Montana												
Billings (18)	0	0	1	6	22	49	86	88	96	100	100	100
Great Falls (17)	1	1	2	6	20	56	74	93	98	99	100	100
Miles City (28)	0	0	0	1	10	32	65	93	98	100	100	100
New Mexico												
Albuquerque (15)	1	1	2	4	10	21	52	67	89	98	99	100
Roswell (52)	0	0	2	7	20	34	55	71	92	99	99	100
Oregon												
Pendleton (6)	8	12	15	22	56	64	67	67	74	87	96	100
Portland (43)	15	27	35	37	40	45	46	47	54	65	81	100
Puerto Rico												
Mayaguez (600)	1	2	3	6	15	31	47	63	80	91	99	100
San Juan (345)	5	8	11	17	33	43	53	66	75	84	93	100
Washington												
Spokane (8)	5	9	11	15	25	56	61	76	84	90	94	100
Wyoming												
Casper (11)	0	0	1	6	32	44	70	90	96	100	100	100
Cheyenne (32)	0	1	2	5	17	42	73	90	97	99	100	100

[1] Numbers in parentheses are the observed average annual **EI**.

the computation of **C**. The procedure will be explained by an example that, for illustration purposes, was selected to include many changes in field conditions.

Problem. Evaluate **C** for a 4-year rotation of wheat-meadow-corn-corn on moderately sloping land in Central Illinois or Indiana, assuming the following management details and dates: Wheat is seeded October 15 in a 40-percent cover of disked corn residue, and a grass and legume meadow mix is seeded with the wheat. The wheat would normally develop a 10-percent cover by November 1, 50 percent by December 1, 75 percent by April 15, and nearly 100 percent in the maturing stage. It is harvested July 15, leaving an 80-percent surface cover of straw and small grass. The sod developed under 1 full year of meadow, yielding more than 3 t of hay, is turned under in April. The field is disked May 5 and is harrowed and planted to corn May 10. The first-year corn, harvested October 15, is followed by fall chiseling about November 15 and spring disking for second-year corn. Residue cover is 50 percent after fall chiseling and 30 percent after corn planting on May 10. Fertility, row spacing, and plant population for both corn years are such that 10, 50, and 75 percent canopy covers will be developed in 20, 40, and 60 days, respectively, from planting, and final canopy cover is more than 95 percent.

Procedure. Set up a working table similar to the one illustrated in table 8, obtaining the needed information as follows:

Column 1. List in chronological sequence all the land-cover changes that begin new cropstage periods, as previously defined.

Column 2. List the date on which each cropstage period begins.

Column 3. Select the applicable area number

TABLE 8.—*Sample working table for derivation of a rotation* **C** *value*

(1) Event	(2) Date	(3) Table 6, area 16	(4) Crop-stage period	(5) EI in period	(6) Soil loss ratio[1]	(7) Sod Factor	(8) Cropstage C value	(9) Crop year
Pl W[2]	10/15	92	SB	0.03	0.27(132)	0.95	0.0077	
10 percent c	11/1	95	1	.03	.21	.95	.0060	
50 percent c	12/1	98	2	.12	.16	1.0	.0192	
75 percent c	4/15	10	3	.46	.03		.0138	
Hv W	7/15	56	4	.28	.07(5C)		.0196	0.066
Meadow	9/15	84		1.26	.004(5B)	1.0	.0050	.005
TP	4/15	10	F	.05	.36(2)	.25	.0045	
Disk	5/5	15	SB	.10	.60	.40	.0240	
Pl C	5/10	—						
10 percent c	6/1	25	1	.13	.52	.40	.0270	
50 percent c	6/20	38	2	.14	.41	.45	.0258	
75 percent c	7/10	52	3	.40	.20	.50	.0400	
Hv C	10/15	92	4L	.05	.30	.60	.0090	.130
Chisel	11/15	97	4c	.17	.16(46)	.60	.0163	
Disk	5/1	14	SB	.11	.25(48 & 61)	.80	.0220	
Pl C	5/10	—						
10 percent c	6/1	25	1	.13	.23	.80	.0239	
50 percent c	6/20	38	2	.14	.21	.85	.0250	
75 percent c	7/10	52	3	.40	.14(48)	.90	.0504	.138
Hv C & pl W	10/15	92						
Rotation totals				4.0			0.3392	
Average annual C value for rotation							.085	

[1] Numbers in parentheses are line numbers in table 5.

[2] Abbreviations: c, canopy cover; C, corn; hv, harvest; pl, plant; TP, moldboard plow; W, wheat.

from figure 9, and from the line in table 6 having the corresponding area number (in this case, 16), read the cumulative percentage of **EI** for each date in column 2. Values for the corn planting dates were omitted in table 8 because the seedbed periods had begun with the spring diskings. The **EI** percentage for May 5 was obtained by interpolating between readings from May 1 and 15.

Column 4. Identify the cropstage periods.

Column 5. Subtract the number in column 3 from the number in the next lower line. If the cropstage period includes a year end, subtract from 100 and add the number in the next lower line. The differences are percentages and may be pointed off as hundredths.

Column 6. Obtain from table 5. Enter the table with crop and management, pounds of spring residue or production level, and percent mulch cover after planting, in that sequence. The data in the selected line are percentages and are used as hundredths in the computation of **C**. For cropstage 3, use the column whose heading corresponds with expected final canopy. For conditions not listed in the primary table, consult supplements 5-A to D. Lines used for the examples are given in parentheses in column 6.

Column 7. From table 5-D.

Column 8. The product of values in columns 5, 6 and 7. The sum of these products is the value of **C** for the entire rotation. Because **C** is usually desired as an average annual value, this sum is divided by the number of years in the rotation.

Column 9. The subtotals in this column are **C** values for the individual crop-years. They also show the relative contributions of the four crops to the rotation **C** value.

Changes in geographic area or in planting dates would affect the **C** value by changing columns 3 and 5. Changes in amount or disposition of residues, tillage practices, or canopy development would change column 6. Thus **C** can vary substantially for a given crop system.

Values of **C** for one-crop systems are derived by the same procedure but would require only a few lines. Also, column 7 is omitted for meadowless systems.

C-Value Tables for Cropland

It will rarely, if ever, be necessary for a field technician or farmer to compute values of **C**. Persons experienced in the procedures outlined above have prepared **C** value tables for specific geographic areas. Such a table will list all the one-crop and multicrop systems likely to be found within the designated area and will list the **C** values for each system for each of the combinations of management practices that may be associated with it. They are usually listed in ascending or descending order of magnitude of the **C** values. The user can then quickly determine all the potential combinations of cropping and management that have **C** values smaller than any given threshold value. Persons in need of **C** values for a particular locality can usually obtain a copy of the applicable table from the nearest SCS state office.

C Values for Construction Areas

Site preparations that remove all vegetation and also the root zone of the soil not only leave the surface completely without protection but also remove the residual effects of prior vegetation. This condition is comparable to the previously defined continuous fallow condition, and **C** = 1. Roots and residual effects of prior vegetation, and partial covers of mulch or vegetation, substantially reduce soil erosion. These reductions are reflected in the soil loss prediction by **C** values of less than 1.0.

Applied mulches immediately restore protective cover on denuded areas and drastically reduce **C** (*1, 2, 20, 27, 43*). Soil loss ratios for various percentages of mulch cover on field slopes are given by the upper curve of figure 6. Where residual effects are insignificant, these ratios equal **C**. The percentage of surface cover provided by a given rate of uniformly spread straw mulch may be estimated from figure 10 (appendix).

Straw or hay mulches applied on steep construction slopes and not tied to the soil by anchoring and tacking equipment may be less effective than equivalent mulch rates on cropland. In Indiana tests on a 20 percent slope of scalped subsoil, a 2.3-t rate of unanchored straw mulch allowed soil loss of 12 t/A when 5 in of simulated rain was applied at 2.5 in/h on a 35-ft plot (*61*). There was evidence of erosion from flow beneath the straw. Mulches of crushed stone at 135 or more t/A, or wood chips at 7 or more t/A, were more effective. (Broadcast seedings of grass after the tests gave good stands on the plots mulched with 135 or 240 t crushed stone, 70 t road gravel, 12 t wood chips, or 2.3 t straw. Stands were poor on the no-mulch and the 15-t rate of crushed stone mulch.)

Table 9 presents approximate **C** values for straw, crushed stone, and woodchip mulches on construction slopes where no canopy cover exists, and also shows the maximum slope lengths on which these values may be assumed applicable.

Soil loss ratios for many conditions on construc-

TABLE 9.—*Mulch factors and length limits for construction slopes*[1]

Type of mulch	Mulch Rate	Land Slope	Factor C	Length limit[2]
	Tons per acre	*Percent*		*Feet*
None	0	all	1.0	—
Straw or hay,	1.0	1-5	0.20	200
tied down by	1.0	6-10	.20	100
anchoring and				
tacking	1.5	1-5	.12	300
equipment[3]	1.5	6-10	.12	150
Do.	2.0	1-5	.06	400
	2.0	6-10	.06	2[illegible]
	2.0	11-15	.07	150
	2.0	16-20	.11	100
	2.0	21-25	.14	75
	2.0	26-33	.17	50
	2.0	34-50	.20	35
Crushed stone,	135	<16	.05	200
¼ to 1½ in	135	16-20	.05	150
	135	21-33	.05	100
	135	34-50	.05	75
Do.	240	<21	.02	300
	240	21-33	.02	200
	240	34-50	.02	150
Wood chips	7	<16	.08	75
	7	16-20	.08	50
Do.	12	<16	.05	150
	12	16-20	.05	100
	12	21-33	.05	75
Do.	25	<16	.02	200
	25	16-20	.02	150
	25	21-33	.02	100
	25	34-50	.02	75

[1] From Meyer and Ports (*24*). Developed by an interagency workshop group on the basis of field experience and limited research data.

[2] Maximum slope length for which the specified mulch rate is considered effective. When this limit is exceeded, either a higher application rate or mechanical shortening of the effective slope length is required.

[3] When the straw or hay mulch is not anchored to the soil values on moderate or steep slopes of soils having K values gre than 0.30 should be taken at double the values given in this table.

tion and developmental areas can be obtained from table 5 if good judgment is exercised in comparing the surface conditions with those of agricultural conditions specified in lines of the table. Time intervals analogous to cropstage periods will be defined to begin and end with successive construction or management activities that appreciably change the surface conditions. The procedure is then similar to that described for cropland.

Establishing vegetation on the denuded areas as quickly as possible is highly important. A good sod has a **C** value of 0.01 or less (table 5-B), but such a low **C** value can be obtained quickly only by laying sod on the area, at a substantial cost. When grass or small grain is started from seed, the probable soil loss for the period while cover is developing can be computed by the procedure outlined for estimating cropstage-period soil losses. If the seeding is on topsoil, without a mulch, the soil loss ratios given in line 141 of table 5 are appropriate for cropstage **C** values. If the seeding is on a desurfaced area, where residual effects of prior vegetation are no longer significant, the ratios for periods SB, 1 and 2 are 1.0, 0.75 and 0.50, respectively, and line 141 applies for cropstage 3. When the seedbed is protected by a mulch, the pertinent mulch factor from the upper curve of figure 6 or table 9 is applicable until good canopy cover is attained. The combined effects of vegetative mulch and low-growing canopy are given in figure 7. When grass is established in small grain, it can usually be evaluated as established meadow about 2 mo after the grain is cut.

C Values for Pasture, Range, and Idle Land

Factor **C** for a specific combination of cover conditions on these types of land may be obtained from table 10 (*57*). The cover characteristics that must be appraised before consulting this table are defined in the table and its footnotes. Cropstage periods and **EI** monthly distribution data are generally not necessary where perennial vegetation has become established and there is no mechanical disturbance of the soil.

Available soil loss data from undisturbed land were not sufficient to derive table 10 by direct comparison of measured soil loss rates, as was done for development of table 5. However, analyses of the assembled erosion data showed that the research information on values of **C** can be extended to completely different situations by combining subfactors that evaluate three separate and distinct, but interrelated, zones of influence: (a) vegetative cover in direct contact with the soil surface, (b) canopy cover, and (c) residual and tillage effects.

Subfactors for various percentages of surface cover by mulch are given by the upper curve of

TABLE 10.—*Factor* **C** *for permanent pasture, range, and idle land*[1]

Vegetative canopy			Cover that contacts the soil surface					
			Percent ground cover					
Type and height[2]	Percent cover[3]	Type[4]	0	20	40	60	80	95+
No appreciable canopy		G	0.45	0.20	0.10	0.042	0.013	0.003
		W	.45	.24	.15	.091	.043	.011
Tall weeds or short brush with average drop fall height of 20 in	25	G	.36	.17	.09	.038	.013	.003
		W	.36	.20	.13	.083	.041	.011
	50	G	.26	.13	.07	.035	.012	.003
		W	.26	.16	.11	.076	.039	.011
	75	G	.17	.10	.06	.032	.011	.003
		W	.17	.12	.09	.068	.038	.011
Appreciable brush or bushes, with average drop fall height of 6½ ft	25	G	.40	.18	.09	.040	.013	.003
		W	.40	.22	.14	.087	.042	.011
	50	G	.34	.16	.08	.038	.012	.003
		W	.34	.19	.13	.082	.041	.011
	75	G	.28	.14	.08	.036	.012	.003
		W	.28	.17	.12	.078	.040	.011
Trees, but no appreciable low brush. Average drop fall height of 13 ft	25	G	.42	.19	.10	.041	.013	.003
		W	.42	.23	.14	.089	.042	.011
	50	G	.39	.18	.09	.040	.013	.003
		W	.39	.21	.14	.087	.042	.011
	75	G	.36	.17	.09	.039	.012	.003
		W	.36	.20	.13	.084	.041	.011

[1] The listed **C** values assume that the vegetation and mulch are randomly distributed over the entire area.

[2] Canopy height is measured as the average fall height of water drops falling from the canopy to the ground. Canopy effect is inversely proportional to drop fall height and is negligible if fall height exceeds 33 ft.

[3] Portion of total-area surface that would be hidden from view by canopy in a vertical projection (a bird's-eye view).

[4] G: cover at surface is grass, grasslike plants, decaying compacted duff, or litter at least 2 in deep.

W: cover at surface is mostly broadleaf herbaceous plants (as weeds with little lateral-root network near the surface) or undecayed residues or both.

TABLE 11.—*Factor* **C** *for undisturbed forest land*[1]

Percent of area covered by canopy of trees and undergrowth	Percent of area covered by duff at least 2 in deep	Factor C[2]
100-75	100-90	.0001-.001
70-45	85-75	.002-.004
40-20	70-40	.003-.009

[1] Where effective litter cover is less than 40 percent or canopy cover is less than 20 percent, use table 6. Also use table 6 where woodlands are being grazed, harvested, or burned.

[2] The ranges in listed **C** values are caused by the ranges in the specified forest litter and canopy covers and by variations in effective canopy heights.

figure 6. Subfactors for various heights and densities of canopy cover are given in figure 5. The subfactor for residual effects of permanent pasture, range, idle land, or grazed or harvested woodland has been estimated to vary from 0.45 to 0.10 (*57*). Major influences on this subfactor are plant roots, organic matter buildup in the topsoil, reduced soil compaction, and surface stabilization after long periods without soil disturbance. The **C** values given in table 10 were derived by combining subfactors for specified combinations of type, height, and density of canopy cover; type and density of cover at the soil surface; and probable residual effects of longtime existence of the specified cover on the land. They are compatible with the rather scarce existing soil loss data from undisturbed land areas.

C Values for Woodland

Three categories of woodland are considered separately: (1) undisturbed forest land; (2) woodland that is grazed, burned, or selectively harvested; and (3) forest lands which have had site preparation treatments for re-establishment after harvest.

In undisturbed forests, infiltration rates and organic matter content of the soil are high, and much or all of the surface is usually covered by a layer of compacted decaying forest duff or litter several inches thick. Such layers of duff shield the soil from the erosive forces of runoff and of drop impact and are extremely effective against soil erosion. Where cover by trees and litter is incomplete, the spots with little or no litter cover are partially protected by undergrowth canopy. Factor **C** for undisturbed forest land may be obtained from table 11. These estimated **C** values are supported by the quite limited existing data and also by the subfactor-evaluation procedure discussed in the preceding subsection.

Woodland that is grazed or burned, or has been recently harvested, does not merit the extremely low **C** values of table 11. For these conditions, **C** is obtained from table 10. However, the buildup of organic matter in the topsoil under permanent woodland conditions is an added factor that should be accounted for by a reduction in the **C** value read from table 10. An earlier publication (*57*) recommended a factor of 0.7 for this purpose.

Site preparation treatments for re-establishing trees on harvested forest land usually alter the erosion factors substantially. Canopy effect is initially greatly reduced or lost entirely, and its restoration is gradual. Some of the forest litter is incorporated in the soil, and it may be entirely removed from portions of the area. A surface roughness factor is introduced. Windrowed debris, if across slope, may function as terraces by reducing effective slope length and inducing deposition above and in the windrows. The amount of residual effect retained depends on the amount and depth of surface scalping. Some of the changes are analogous to cropland situations. Some of the relationships available from tables 5 and 10 can be used to evaluate **C** for these conditions, but neither table is directly applicable.

Table 12 presents **C** values computed for Southern Pine Forests that have had site preparation treatments after harvesting. This table was jointly developed (in 1977) by representatives of SEA, SCS, and Forest Service, using factor relationships from tables 5, 10, and 11 as basic guides. Its application on forest lands in other climatic regions may require some modifications of factor values. Research designed to refine and improve tables 10, 11, and 12 is underway.

Tree plantings on converted cropland should, in the initial years, be evaluated similarly to cropland because the forest residual effect which underlies tables 10 to 12 will not be applicable. The subfactor for residual effects may be estimated by selecting from lines 1 to 16 of table 5 the line that most nearly describes the condition of the converted cropland and assuming a residual subfactor equal to the seedbed-period value given in that line. If the cropland has most recently been in

TABLE 12.—*Factor* **C** *for mechanically prepared woodland sites*

Site preparation	Mulch cover[1]	Soil condition[2] and weed cover[3]							
		Excellent		Good		Fair		Poor	
		NC	WC	NC	WC	NC	WC	NC	WC
	Percent								
Disked, raked, or bedded[4]	None	0.52	0.20	0.72	0.27	0.85	0.32	0.94	0.36
	10	.33	.15	.46	.20	.54	.24	.60	.26
	20	.24	.12	.34	.17	.40	.20	.44	.22
	40	.17	.11	.23	.14	.27	.17	.30	.19
	60	.11	.08	.15	.11	.18	.14	.20	.15
	80	.05	.04	.07	.06	.09	.08	.10	.09
Burned[5]	None	.25	.10	.26	.10	.31	.12	.45	.17
	10	.23	.10	.24	.10	.26	.11	.36	.16
	20	.19	.10	.19	.10	.21	.11	.27	.14
	40	.14	.09	.14	.09	.15	.09	.17	.11
	60	.08	.06	.09	.07	.10	.08	.11	.08
	80	.04	.04	.05	.04	.05	.04	.06	.05
Drum chopped[5]	None	.16	.07	.17	.07	.20	.08	.29	.11
	10	.15	.07	.16	.07	.17	.08	.23	.10
	20	.12	.06	.12	.06	.14	.07	.18	.09
	40	.09	.06	.09	.06	.10	.06	.11	.07
	60	.06	.05	.06	.05	.07	.05	.07	.05
	80	.03	.03	.03	.03	.03	.03	.04	.04

[1] Percentage of surface covered by residue in contact with the soil.

[2] *Excellent* soil condition—Highly stable soil aggregates in topsoil with fine tree roots and litter mixed in.

Good—Moderately stable soil aggregates in topsoil or highly stable aggregates in subsoil (topsoil removed during raking), only traces of litter mixed in.

Fair—Highly unstable soil aggregates in topsoil or moderately stable aggregates in subsoil, no litter mixed in.

Poor—No topsoil, highly erodible soil aggregates in subsoil, no litter mixed in.

[3] NC—No live vegetation.

WC—75 percent cover of grass and weeds having an average drop fall height of 20 in. For intermediate percentages of cover, interpolate between columns.

[4] Modify the listed C values as follows to account for effects of surface roughness and aging:

First year after treatment: multiply listed C values by 0.40 for rough surface (depressions >6 in); by 0.65 for moderately rough; and by 0.90 for smooth (depressions <2 in).

For 1 to 4 years after treatment: multiply listed factors by 0.7.

For 4+ to 8 years: use table 6.

More than 8 years: use table 7.

[5] For first 3 years: use C values as listed.

For 3+ to 8 years after treatment: use table 6.

More than 8 years after treatment: use table 7.

meadow, the selected seedbed soil loss ratio is multiplied by a factor from table 5-D. If mulch is applied, a subfactor read from the upper curve of figure 6 is multiplied by the residual subfactor to obtain **C**. When canopy develops, a canopy subfactor from figure 5 is also included.

SUPPORT PRACTICE FACTOR (P)

In general, whenever sloping soil is to be cultivated and exposed to erosive rains, the protection offered by sod or close-growing crops in the system needs to be supported by practices that will slow the runoff water and thus reduce the amount of soil it can carry. The most important of these supporting cropland practices are contour tillage, stripcropping on the contour, and terrace systems. Stabilized waterways for the disposal of excess rainfall are a necessary part of each of these practices.

By definition, factor **P** in the USLE is the ratio of soil loss with a specific support practice to the corresponding loss with up-and-down-slope culture. Improved tillage practices, sod-based rotations, fertility treatments, and greater quantities of crop residues left on the field contribute materially to erosion control and frequently provide the major control in a farmer's field. However, these are considered conservation cropping and management practices, and the benefits derived from them are included in **C**.

Contouring

The practice of tillage and planting on the contour, in general, has been effective in reducing erosion. In limited field studies, the practice provided almost complete protection against erosion from storms of moderate to low intensity, but it provided little or no protection against the occasional severe storms that caused extensive breakovers of the contoured rows. Contouring appears to be the most effective on slopes in the 3- to 8-percent range. As land slope decreases, it approaches equality with contour row slope, and the soil loss ratio approaches 1.0. As slope increases, contour row capacity decreases and the soil loss ratio again approaches 1.0.

Effectiveness of contouring is also influenced by the slope length. When rainfall exceeds infiltration and surface detention in large storms, breakovers of contour rows often result in concentrations of runoff that tend to become progressively greater with increases in slope length. Therefore, on slopes exceeding some critical length the amount of soil moved from a contoured field may approach or exceed that from a field on which each row carries its own runoff water down the slope. At what slope length this could be expected to occur would depend to some extent on gradient, soil properties, management, and storm characteristics.

P Values for Contouring

A joint SEA and SCS workshop group, meeting at Purdue University in 1956, adopted a series of contour **P** values that varied with percent slope. The **P** values were based on available data and field observations supplemented by group judgment. Subsequent experience indicated only a few minor changes. Current recommendations are given in table 13. They are average values for the factor on the specified slopes. Specific-site values may vary with soil texture, type of vegetation, residue management, and rainfall pattern, but data have not become available to make the deviations from averages numerically predictable.

Full contouring benefits are obtained only on fields relatively free from gullies and depressions other than grassed waterways. Effectiveness of this practice is reduced if a field contains numerous small gullies and rills that are not obliterated by normal tillage operations. In such instances, land smoothing should be considered before contouring. Otherwise, a judgment value greater than shown in table 13 should be used when computing the benefits for contouring.

TABLE 13.—**P** *values and slope-length limits for contouring*

Land slope percent	P value	Maximum length[1]
		Feet
1 to 2	0.60	400
3 to 5	.50	300
6 to 8	.50	200
9 to 12	.60	120
13 to 16	.70	80
17 to 20	.80	60
21 to 25	.90	50

[1] Limit may be increased by 25 percent if residue cover after crop seedlings will regularly exceed 50 percent.

Slope-Length Limits

After the 1956 workshop, the SCS prepared reference tables for use with the Corn Belt slope-practice procedure. They included guides for slope-length limits for effective contouring, based largely on judgment. These limits, as modified with later data and observations (*16*, *42*), are also given in table 13. Data to establish the precise limits for specific conditions are still not available. However, the **P** values given in table 13 assume slopes short enough for full effectiveness of the practice. Their use for estimating soil loss on unterraced slopes that are longer than the table limits specified is speculative.

Contour Listing

Contour listing, with corn planted in the furrows, has been more effective than surface planting on the contour (*29*). However, the additional effectiveness of the lister ridges applies only from the date of listing until the ridges have been largely obliterated by two corn cultivations. Therefore, it can be more easily credited through **C** than through **P**. This is done by a 50-percent reduction in the soil loss ratios (table 5) that apply to the time interval during which the ridges are intact. The standard **P** value for contouring is applicable in addition to the **C** value reduction.

Potato rows on the contour present a comparable condition from lay-by time until harvest. However, this ridging effect has been already credited in table 5, line 160, and should not be duplicated.

Controlled-Row Grade Ridge Planting

A method of precise contouring has been developed that provides effective conservation on farm fields where the land slope is nearly uniform, either naturally or by land smoothing, and runoff from outside the field can be diverted. The practice uses ridge planting with undiminished channel capacity to carry water maintained throughout the year. It is being studied in Texas (*36*), Arkansas, Mississippi (*8*), and Iowa (*30*). In Texas, the channel cross section, with 40-in row spacing, was nearly 0.5 ft^2, and row grades varied from nearly zero at the upper end to 1 percent at the lower end

of a 1,000-ft length. Measured soil loss compared favorably with that from an adjacent terraced watershed. Soil loss measurements in Mississippi and Iowa showed similar effectiveness during the test periods.

Because each furrow functions as an individual terrace, **P** values similar to those for terracing seem appropriate. Slope-length limits for contouring would then not apply, but the length limits would be applicable if the channel capacity were only sufficient for a 2-year design storm.

Contoured-Residue Strips

Contoured strips of heavy crop-residue mulch, resembling contour stripcropping without the sod, may be expected to provide more soil loss reduction than contouring alone. **P** values equal to about 80 percent of those for contouring are recommended if fairly heavy mulch strips remain throughout the year. If the strips are maintained only from harvest until the next seedbed preparation, the credit should be applied to the soil loss ratio for cropstage 4 rather than the **P** value.

Contour Stripcropping

Stripcropping, a practice in which contoured strips of sod are alternated with equal-width strips of row crops or small grain, is more effective than contouring alone. Alternate strips of grain and meadow year after year are possible with a 4-year rotation of corn-wheat with meadow seeding-meadow-meadow. This system has the added advantage of a low rotation **C** value. A stripcropped rotation of corn-corn-wheat-meadow is less effective. Alternate strips of winter grain and row crop were effective on flat slopes in Texas (*14*), but alternate strips of spring-seed grain and corn on moderate to steep slopes have not provided better erosion control than contouring alone.

Observations from stripcrop studies showed that much of the soil eroded from a cultivated strip was filtered out of the runoff as it was slowed and spread within the first several feet of the adjacent sod strip. Thus the stripcrop factor, derived from soil loss measurements at the foot of the slope, accounts for off-the-field soil movement but not for all movement within the field.

P Values, Strip Widths, and Length Limits

Recommended **P** values for contour stripcropping are given in table 14. The system to which each column of factors applies is identified in the table footnotes. The strip widths given in column 5 are essentially those recommended by the 1956 slope-practice workshop and are to be considered approximate maximums. Reasonable adjustments to accommodate the row spacing and row multiple of the planting and harvesting equipment are permissible. Slope-length limit is generally not a critical factor with contour stripcropping except on extremely long or steep slopes. The lengths given in column 6 are judgment values based on field experience and are suggested as guides.

Buffer Stripcropping

This practice consists of narrow protective strips alternated with wide cultivated strips. The location of the protective strips is determined by the width and arrangement of adjoining strips to be cropped in the rotation and by the location of steep, severely eroded areas on slopes. Buffer strips usually occupy the correction areas on sloping land and are seeded to perennial grasses and legumes. This type of stripcropping is not as effective as contour stripcropping (*4*).

TABLE 14.—**P** *values, maximum strip widths, and slope-length limits for contour stripcropping*

Land slope percent	P values[1]			Strip width[2]	Maximum length
	A	B	C		
				Feet	*Feet*
1 to 2	0.30	0.45	0.60	130	800
3 to 5	.25	.38	.50	100	600
6 to 8	.25	.38	.50	100	400
9 to 12	.30	.45	.60	80	240
13 to 16	.35	.52	.70	80	160
17 to 20	.40	.60	.80	60	120
21 to 25	.45	.68	.90	50	100

[1] **P** values:

A For 4-year rotation of row crop, small grain with meadow seeding, and 2 years of meadow. A second row crop can replace the small grain if meadow is established in it.

B For 4-year rotation of 2 years row crop, winter grain with meadow seeding, and 1-year meadow.

C For alternate strips of row crop and small grain.

[2] Adjust strip-width limit, generally downward, to accommodate widths of farm equipment.

Terracing

The most common type of terrace on gently sloping land is the broadbase, with the channel and ridge cropped the same as the interterrace area. The steep backslope terrace is most common on steeper land. Difficulty in farming point rows associated with contoured terraces led to developing parallel terracing techniques (*16*). Underground outlets, landforming, and variable channel grades help establish parallel terraces. The underground outlets are in the low areas along the terrace line. The ridge is constructed across these areas. Another type of terrace, using a level and broad channel with either open or closed ends, was developed to conserve moisture in dryland farming areas.

Terraces with underground outlets, frequently called impoundment terraces, are highly effective for erosion control. Four-year losses from four such terrace systems in Iowa (*17*) averaged less than 0.4 t/A/year, which was less than 5 percent of the calculated soil movement to the channel. Comparable losses were measured from installations in Nebraska.

Terracing combined with contour farming and other conservation practices is more effective than those practices without the terraces because it positively divides the slope into segments equal to the horizontal terrace interval. The horizontal terrace interval for broadbase terraces is the distance from the center of the ridge to the center of the channel for the terrace below. For steep backslope terraces with the backslope in sod, it is the distance from the point where cultivation begins at the base of the ridge to the base of the frontslope of the terrace below (*44*). With terracing, the slope length is this terrace interval; with stripcropping or contouring alone, it is the entire field slope length.

P Values

Values of **P** for contour farming terraced fields are given in table 15. These values apply to contour farmed broadbase, steep backslope, and level terraces. However, recognize that the erosion control benefits of terraces are much greater than indicated by the **P** values. As pointed out earlier, soil loss per unit area on slopes of 5 percent or steeper is approximately proportional to the square root of slope length. Therefore, dividing a field slope into **n** approximately equal horizontal terrace intervals divides the average soil loss per unit area by the square root of **n**. This important erosion control benefit of terracing is not included in **P** because it is brought into the USLE computation through a reduced **LS** factor obtained by using the horizontal terrace interval as the slope length when entering figure 4 or table 3.

Erosion control between terraces depends on the crop system and other management practices evaluated by **C**. The total soil movement within a contour-farmed terrace interval may be assumed equal to that from the same length of an identical slope that is contoured only. Therefore, if a control level is desired that will maintain soil movement between the terraces within the soil loss tolerance limit, the **P** value for a contour-farmed terraced field should equal the contour factor (col. 2, table 15), and use of these values for farm planning purposes is generally recommended.

With contour stripcropping, the soil deposited in the grass strips is not considered lost because it remains on the field slope. With terraces, most of the deposition occurs in the terrace channels, but research measurements have shown that this deposition may equal 80 percent of the soil moved from the contour-farmed slopes between the terraces (*67*). Use of the contour factor as the **P** value for terracing assumes that all of the eroded soil deposited in the terrace channels is lost from the productive areas of the field. With broadbase terraces, the channels and ridges are cropped the same as

TABLE 15.—**P** *values for contour-farmed terraced fields*[1]

Land slope (percent)	Farm planning		Computing sediment yield[3]	
	Contour factor[2]	Stripcrop factor	Graded channels sod outlets	Steep backslope underground outlets
1 to 2	0.60	0.30	0.12	0.05
3 to 6	.50	.25	.10	.05
9 to 12	.60	.30	.12	.05
13 to 16	.70	.35	.14	.05
17 to 20	.80	.40	.16	.06
21 to 25	.90	.45	.18	.06

[1] Slope length is the horizontal terrace interval. The listed values are for contour farming. No additional contouring factor is used in the computation.

[2] Use these values for control of interterrace erosion within specified soil loss tolerances.

[3] These values include entrapment efficiency and are used for control of offsite sediment within limits and for estimating the field's contribution to watershed sediment yield.

the interterrace slopes, and some of the material deposited in the channels is moved to the ridges in terrace maintenance. The 1956 slope-practice group felt that some of the deposition should be credited as soil saved and recommended use of a terracing practice factor equal to the stripcrop factor (*64*). However, the more conservative values given in column 2 are now commonly used in conservation planning.

When the USLE is used to compute a terraced field's contribution to offsite sediment or watershed gross erosion, the substantial channel deposition must be credited as remaining on the field area. For this purpose, the **P** values given in the last two columns of table 15 are recommended unless an overland flow deposition equation based on transport relationships is used with the USLE.

With widespread use of large multirow equipment, farming with field boundaries across nonparallel terraces is not uncommon in some regions. When terraces are not maintained and overtopping is frequent, **P** = 1 and the slope length is the field slope length. However, if the terraces are periodically maintained so that overtopping occurs only during the most severe storms, **LS** is based on the horizontal terrace interval. If farming across terraces is at an angle that approximates contour farming, **P** values less than 1.0 but greater than the contour factors would be appropriate.

Soil Loss Terrace Spacing

Traditionally, terrace spacing has been based on slope gradient; however, some recent spacing guides have included modifying factors for severity of rainfall and for favorable soil and tillage combinations. A major objective of cropland conservation planning is to hold the productive topsoil in place. Extending this objective to terrace system design suggests limiting slope lengths between terraces sufficiently so that specified erosion tolerances will not be exceeded. Using the USLE in developing spacing guides will make this possible.

The USLE may be written as **LS = T/RKCP**, where **T** is the tolerance limit. If **T/RKP = Z**, then **LS = Z/C**, and **C = Z/LS**. The values **T**, **R**, **K** and **P** are constant for a given location and can be obtained from handbook tables and charts as illustrated in the section **Predicting Cropland Soil Losses**. Factor **C** can be selected as the **C** value of the most erosion-vulnerable crop system that a farmer is likely to use on the terraced field. **LS** can be computed by solving the equation as written above and, with the percent slope known, the maximum allowable length can be read from the slope-effect chart, figure 4.

To illustrate the procedure, assume a 6-percent slope at a location where **R** = 175, **K** = 0.32, **T** = 5, **P** = 0.5, and the most erodible crop expected to occur on the field has a **C** value of 0.24. (An assumption that the field will always be in a sod based rotation or that the operator will always make the best possible use of the crop residues would be too speculative to serve as a guide for terrace spacing.) With these assumptions, **Z** = 5/175 (0.32)(0.5) = 0.179 and **LS** = 0.179/0.24, or 0.744. Enter the slope-effect chart, figure 4, on the **LS** scale with a value of 0.744, move horizontally to intersect the 6 percent-slope line and read the corresponding slope length, 120 ft, on the horizontal scale. Add to this value the width of the terrace frontslope and compute the vertical interval: $\left(\frac{120 + 12}{100}\right)6 = 7.9$ ft. However, the horizontal interval should not exceed the slope-length limit for effectiveness of contouring. From table 13 the length limit for contouring on a 6-percent slope is 200 ft, so the computed terrace interval is satisfactory. A small modification in spacing may be made to adjust to an even multiple of machinery width.

The maximum **C** value that will allow a horizontal terrace spacing equal to the length limit for effective contouring on the given slope can also be determined by using figure 4 and table 13. For the conditions in the illustration above, **C** = 0.179/**LS**. The maximum acceptable length for contouring is 200 ft. From figure 4, the **LS** value for a 200-ft length of 6-percent slope is 0.95. Therefore, the maximum allowable **C** = 0.179/0.95, which is 0.188. With terraces spaced at 200-ft intervals, any cropping and management system with a **C** value of less than 0.188 should provide the level of conservation prescribed by the assumed soil loss tolerance limit of 5 t/A/year.

One additional consideration is important. For a terrace to function satisfactorily, the channel

capacity must be sufficient to carry the runoff safely to a stabilized outlet without excessive channel scour or overtopping of the ridge. SCS engineering practice standards specify a capacity sufficient to control the runoff from a 10-year-frequency, 24-hour storm without overtopping. Some SCS practice standards may require a shorter terrace interval than would be indicated by the foregoing procedure.

The discussion of the topographic factor pointed out that the erosion rate increases as slope length increases. Table 4 lists the relative soil losses for successive equal-length increments of a uniform slope divided into 2, 3, 4, or 5 segments. The third column of table 4 shows that if a uniform 6-percent slope were controlled at a tolerance of 5 t average soil loss, the average loss per unit area from the lower third of the slope would exceed the tolerance by about 38 percent. Soil loss from the upper third would be 43 percent less than the tolerance limit. To have an average rate of 5 t from the lower third, the **T** values used in the spacing calculation would need to be 1/1.38 times the 5-t tolerance, or 3.6 t. This is an approach that can be used to calculate terrace spacings for a higher level of conservation.

Effect of Terraces on Amount and Composition of Offsite Sediment

By reducing runoff velocity and inducing deposition of sediment in the channels, terraces have a profound effect on the amount and composition of offsite sediments from cultivated fields. The type of terrace, the channel grade, and the type of outlet influence the magnitude of the effect.

The greatest reduction in sediment is attained with the impoundment type terrace systems that use underground outlets. With the outlets in the lower areas of the field and terrace ridges built across these areas, temporary ponds are created around the risers of the outlet tile. The outlets are designed to drain the impounded runoff in 1 to 2 days. Thus, the ponds provide a maximum stilling effect, and only the smallest and lightest soil particles are carried off the field in the runoff water. The increased time for infiltration also reduces runoff.

Sediments collected from four impoundment terrace systems over 4 years in Iowa (*17*) showed the following percentages of fine materials:

Soil type	< 0.002 mm	< 0.008 mm
	Percent	*Percent*
Fayette silt loam	78	91
Sharpsburg silty clay loam	68	96
Floyd loam	31	82
Clarion loam	35	78

Sediment concentrations in the runoff ranged from about 1,300 p/m on the Fayette soil to 6,300 p/m on the Clarion. Average annual sediment from the outlets was less than 800 lb/A for all four systems.

Farm chemical losses in runoff vary with type and formulation, amount, placement, and time of rainfall in relation to time of application, as well as with the usual runoff and erosion factors. Principal chemicals are the fertilizers, insecticides, fungicides, and herbicides. Losses are by solution and by suspension of chemical granules or adsorption on soil particles suspended in the runoff water.

Terracing exerts its greatest influence in reducing offsite pollution from those chemicals that are adsorbed on soil particles. Examples of these are the phosphates, organic nitrogen, and persistent organochlorine insecticides. Reductions in offsite *sediment* by terrace systems with contouring are estimated to range from 82 to 95 percent. However, the reductions in chemical transport are generally not proportional to reductions in soil loss because of an enrichment process that applies to the suspensions. The nutrient content of sediments is often 50 percent greater than that of the soil. Offsite delivery of sediment is also affected by watershed characteristics, particularly size of the drainage area. This reduction is measured by a "delivery ratio" that ranges from 0.33 for an area of one-half square mile to 0.08 for a 200-mi^2 area (*45*).

Terracing has the least effect on offsite pollution from those chemicals transported primarily in solution. Annual runoff reductions by terracing and contour farming, at 21 locations throughout the United States, have been estimated to vary only from 9 to 37 percent (*42*). Examples of farm chemicals transported primarily in solution are the nitrates and some herbicides such as 2,4-D ((2,4-dichlorophenoxy) acetic acid). The predominate transport modes for an extensive list of pesticides are listed in volumes 1 and 2 of "Control of Water Pollution From Cropland" (*42*).

APPLYING THE SOIL LOSS EQUATION

The major purpose of the soil loss prediction procedure is to supply specific and reliable guides for selecting adequate erosion control practices for farm fields and construction areas. The procedure is also useful for computing the upland erosion phase of sediment yield as a step in predicting rates of reservoir sedimentation or stream loading, but the USLE factors are more difficult to evaluate for large mixed watersheds. Specific applications of the soil loss equation are discussed and illustrated below.

Predicting Cropland Soil Losses

The USLE is designed to predict longtime-average soil losses for specified conditions. This may be the average for a rotation or for a particular crop year or cropstage period in the rotation. Where the term "average loss" is used below, it denotes the average for a sufficient number of similar events or time intervals to cancel out the plus and minus effects of short-time fluctuations in uncontrolled variables.

Rotation Averages

To compute the average annual soil loss from a particular field area, the first step is to refer to the charts and tables discussed in the preceding sections and select the values of **R**, **K**, **LS**, **C**, and **P** that apply to the specific conditions on that field. For example, assume a field on Russell silt loam soil in Fountain County, Ind. The dominant slope is about 8 percent with a length of 200 ft. Fertility and crop management on this field are such that crop yields are rarely less than 85 bu corn, 40 bu wheat, or 4 t alfalfa-brome hay. The probability of meadow failure is slight.

Factor **R** is taken from the isoerodent map (fig. 1). Fountain County, in west-central Indiana, lies between isoerodents of 175 and 200. By linear interpolation, **R** = 185. **K** is taken from a table of **K** values that were derived either by direct research measurement or by use of the soil erodibility nomograph (fig. 3). For the Russell silt loam soil, **K** = 0.37. The slope-effect chart, figure 4, shows that an 8 percent slope 200 ft long has an **LS** of 1.41. If the field were continuously in clean-tilled fallow, the average annual soil loss from the dominant slope would equal the product **RKLS**; that is, 185(0.37)(1.41) = 96.5 t/A.

Next, we need to know the effect of the cropping and management system and support practices existing on the field. This effect is represented by factors **C** and **P**. The **C** value for the field may either be derived by the procedure previously presented, using data from tables 5 and 6, or it may be obtained from a centrally prepared **C** value table available from the SCS. For convenience, assume the same crop system and management as were assumed for the problem illustrating the derivation of locality **C** values. From table 8, **C** then equals 0.085. If rows and tillage are in the direction of the land slope, factor **P** = 1.0. The computed average soil loss is then 96.5(0.085)(1.0) = 8.2 t/A/year.

From table 13, contour farming on 8 percent slopes not exceeding 200 ft in length has a **P** value of 0.5. Therefore, if farming were on the contour, the computed average soil loss for the field would be 96.5(0.085)(0.5) = 4.1 t. If the length of 8-percent slope was appreciably greater than 200 ft, the effectiveness of contouring could not be assumed, and the **P** value of 0.5 would not be applied unless the slope length was broken by terraces or diversions. Any change in either the crop sequence or the management practices would likely increase or decrease soil loss. This would be reflected in the USLE solution through a change in the **C** value.

When **C** is used at its average annual value for a rotation that includes a sod crop, as was done in the example given in table 8, the heavier losses experienced during row crop years are diluted by trivial losses in the meadow year(s). For holding longtime-average soil losses below some prescribed tolerance limit, this dilution poses no problem. But from the viewpoint of offsite water quality, it may not be desirable. The USLE may also be used to compute the average soil loss for each crop in the rotation or for a particular cropstage period.

Crop-Year Averages

The subtotals in column 9 of table 8 show that

with the assumed management system, **C** for the first-year corn would be 0.130 and for the second-year, 0.138. For the second-year corn, without contouring, the expected average soil loss would equal 185(0.37)(1.41)(0.138), or 13.3 t. If, in the same crop system, the corn residues were plowed down in fall, the **C** value for second-year corn would be 0.29, and the soil loss would average 28 t. On the other hand, no-till planting the second-year corn in a 70-percent cover of shredded cornstalks would reduce the **C** value for this crop to 0.08 and the soil loss to about 8 t. This would also reduce the rotation average for straight row farming to 7 t. Killing the meadow instead of turning it under, and no-till planting, would reduce the **C** value for the first-year corn to 0.01 and the soil loss to less than 1 t. Thus, crop-year **C** values can be helpful for sediment control planning.

Cropstage Averages

Additional information can be obtained by computing the average annual soil loss for each cropstage period. First, the computed cropstage soil losses will show in which portions of the crop year (or rotation cycle) improved management practices would be most beneficial. Second, they provide information on the probable seasonal distribution of sediment yields from the field. When a tabulation like table 8 has been prepared, the values in column 8 will be directly proportional to the cropstage soil losses. They can be converted to tons per acre for a specific field by multiplying them by the product of factors **R**, **K**, **LS**, and **P**.

To estimate the average soil loss for a particular cropstage when such a table has not been prepared, the cropstage soil loss ratio from table 5 is used as **C**. The annual **EI** fraction that is applicable to the selected period is obtained from table 6 and is multiplied by the location's annual erosion index value (fig. 1) to obtain the relevant **R** value. **K**, **LS**, and **P** will usually be assumed to have the same values as for computation of average annual soil losses.

Suppose, for example, that one wishes to predict the average soil loss for the seedbed and establishment periods of corn that is conventionally planted about May 15 on spring plowed soybean land in southwestern Iowa (area No. 13, fig. 9). Suppose also that the corn is on a field for which the combined value of factors **K**, **LS**, and **P** is 0.67 and the fertility and crop management are such that corn planted by May 15 usually develops a 10 percent canopy cover by June 5, 50 percent by June 25, and a final canopy cover of more than 95 percent. Interpolating between values in line 13 of table 6 shows cumulative **EI** percentages of 12, 23, and 43 for these three dates. Therefore, on the average, 11 percent of the annual **EI** would occur in the seedbed period, and 20 percent would occur in the establishment period. From line 109 of table 5, the soil loss ratios for these two cropstage periods under the assumed management are 0.72 and 0.60. From figure 1, the average annual **EI** is 175. The soil loss would be expected to average 0.11(175)(0.72)(0.67) = 9.3 t/A in the seedbed period and 0.20(175)(0.60)(0.67) = 14 t in the establishment period. The cropping assumed for this example represents an extremely erodible condition. For second-year corn with good residue management, the applicable soil loss ratios and the predicted soil losses would be much lower.

Individual Storm Soil Losses

The USLE factors derived from tables and charts presented herein compute longtime-average soil losses for specified cover and management on a given field. The USLE is not recommended for prediction of specific soil loss events.

If it is applied to a specific rainstorm, using the storm **EI** for **R** and the relevant cropstage soil loss ratio for **C**, it will estimate the *average* soil loss for a large number of storms of this size occurring on that field and in that cropstage period. However, the soil loss from any one of these events may differ widely from this average because of interactions with variables whose values fluctuate randomly over time (*56*).

When rain falls on relatively dry, freshly tilled soil, most of the water may infiltrate before runoff begins, resulting in a low-average soil loss per unit of **EI** for that storm. When rain falls on presaturated soil, runoff begins quickly, and most of the rain becomes runoff. Such rains usually produce above-average soil loss per **EI** unit. Some rains are accompanied by high winds that increase the impact energy of raindrops; others occur in a fairly calm atmosphere. Some storms begin with a high intensity and seal the surface quickly so that trailing lower intensities encounter a low infiltration rate. In other storms the moderate intensities

precede the high ones. In some seasons the soil is cultivated when wet and remains cloddy; in other seasons it is cultivated when soil moisture is ideal for fine pulverization. A claypan or fragipan subsoil may substantially influence permeability in early spring or in a wet growing season and yet have no significant effect on infiltration rates during intense thunderstorms on dry soil.

The soil loss ratios of table 5 are averages for cropstage periods that cover several weeks to several months. Early in a cropstage period, the ratio will usually be higher than the average because the development of cover is gradual. Later in the period it will be lower than average. In a poor growing season the ratio will be above average because cover and water use by transpiration are below normal. In a favorable growing season, the ratio will be below average. Cover effect in a specific year may be substantially influenced by abnormal rainfall. A crop canopy or conservation tillage practice may delay the start of runoff long enough to be 100 percent effective for moderate storms on a given field and yet allow substantial erosion by prolonged runoff periods.

The irregular fluctuations in these and other variables can greatly influence specific-storm soil losses. However, they do not invalidate the USLE for predicting long-term-average soil losses for specific land areas and management conditions. Their positive and negative effects tend to balance over a longtime period, and their average effects are reflected in the factor-evaluation tables and charts.

Two recent research reports are recommended references for those who find it necessary to estimate specific-storm soil losses (*34, 10*). The authors present modifications of **R** and **LS** that are designed to account for some random effects discussed.

Specific-Year Soil Losses

In any given year, both the annual **EI** and its monthly distribution may differ substantially from the location averages. Therefore, **R** values from figure 1 and **EI** distribution data from table 6 will not correctly reflect specific-year values of these variables. The most accurate procedure is to compute the **EI** value for each storm from a recording-rain gage record for the location and year by the method given in the appendix. The storm values are summed for each cropstage period, and the subtotals are combined with soil loss ratios from table 5 to estimate the soil loss for each cropstage period. The sum of the cropstage soil losses then reflects the effects of possible abnormal **EI** distribution, as well as the corrected **R** value for the specific year. However, the irregular fluctuations in variables discussed in the preceding subsection are often related to abnormalities in rainfall. The plus and minus effects on soil loss may not average out within 1 year but may appreciably bias specific-year soil losses. These biases will not be evaluated by the USLE. Therefore, specific-year estimates of soil loss will be less accurate than USLE estimates of long-term, crop-year averages.

Soil Loss Probabilities

Soil loss probabilities are a function of the combination of the probabilities for annual **EI**, seasonal distribution of the erosive rains, abnormal antecedent soil moisture conditions, favorable or unfavorable conditions for soil tillage and crop development, and other factors. The section on the **Rainfall Erosion Index** pointed out that a location's annual and maximum storm **EI** values tend to follow log-normal frequency distributions and that specific probability values are listed in tables 17 and 18 for 181 key locations. When these probabilities of **EI** are used for **R** in the USLE, the equation will estimate the soil loss that would occur if all the other factors were at their normal levels. However, the seasonal distribution of erosive rains, and the surface conditions in the field, may also be abnormal in years of rainfall extremes. Deriving probable relationships of these variables to extremes in annual **EI** would require longer records than were available.

Stochastic modeling techniques (*66*) are available that could be used to generate synthetic data having the same statistical properties as historical data. Such data could be used to estimate the probable range in specific-year soil losses in a particular rainfall area.

Determining Alternative Land Use and Treatment Combinations

The soil loss prediction procedure supplies the practicing conservationist with concise reference tables from which he can ascertain, for each particular situation encountered, which specific land

use and management combinations will provide the desired level of erosion control. A number of possible alternatives are usually indicated. From these, the farmer will be able to make a choice in line with his desires and financial resources.

Management decisions generally influence erosion losses by affecting the factor **C** or **P** in the erosion equation. **L** is modified only by constructing terraces, diversions, or contour furrows with sufficient capacity throughout the year to carry the runoff water from the furrow area above. **R**, **K**, and **S** are essentially fixed as far as a particular field is concerned.

When erosion is to be limited within a predetermined tolerance, **T**, the term **A** in the equation is replaced by **T**, and the equation is rewritten in the form **CP** = **T/RKLS**. Substituting the site values of the fixed factors in this equation and solving for **CP** give the maximum value that the product **CP** may assume under the specified field conditions. With no supporting practices, **P** = 1, and the most intensive cropping plan that can be safely used on the field is one for which **C** just equals this value. When a supporting practice like contouring or stripcropping is added, the computed value of **T/RKLS** is divided by the practice factor, **P**, to obtain the maximum permissible cover and management factor value. Terracing increases the value of **T/RKLS** by decreasing the value **L**.

A special USLE calculator, originally designed in Tennessee (*41*) and recently updated, enables rapid and systematic calculation of either average annual soil loss or **T/RKLS** for any specific situation.

Many practicing conservationists prefer to use handbook tables. **C**-value tables for specific geographic areas (fig. 9) are centrally prepared by persons who are experienced in the procedures outlined in a preceding section and who obtain the needed data from tables 5 and 6. Values of **T/RKLS** are also centrally computed and arranged in two-way classification as illustrated in table 16 for **R** = 180, **K** = 0.32, and **T** = 5. Similar tables are prepared for other combinations of **R**, **K**, and **T**.

A conservationist working in the field usually carries a pocket-sized handbook which includes the **R** value(s), **T** and **K** soil values, applicable tables of **T/RKLS** values, and a table of **C** values for the area. These items will provide all the information needed to use this procedure as a guide

TABLE 16.—*Maximum permissible* **C** *values (***T/RKLS***) for* **R** = *180,* **K** = *0.32 and* **T** = *5*

Gradient percent	Values for slope lengths (feet)							
	50	75	100	150	200	250	300	400
	STRAIGHT ROW							
2	0.53	0.47	0.43	0.38	0.35	0.33	0.31	0.28
4	.29	.24	.22	.18	.16	.15	.14	.12
6	.18	.15	.13	.11	.091	.082	.074	.064
8	.12	.10	.087	.072	.062	.055	.050	.044
10	.090	.073	.063	.052	.045	.040	.037	.032
12	.068	.056	.048	.039	.034	.030	.028	.024
14	.054	.044	.038	.031	.027	.024	.022	.019
16	.043	.035	.030	.025	.022	.019	.018	.015
	CONTOURED[1]							
2	0.89	0.78	0.72	0.64	0.58	0.55	0.52	0.47
4	.57	.49	.43	.37	.33	.30	.28	.25
6	.36	.30	.26	.21	.18	.16	([2])	—
8	.25	.20	.17	.14	.12	.11	—	—
10	.15	.12	.11	.086	([2])	—	—	—
12	.11	.093	.080	.065	—	—	—	—
14	.077	.062	.054	([2])	—	—	—	—
16	.062	.050	.044	—	—	—	—	—

[1] The values for contour farming are **T/RKLSP**, where **P** is dependent on percent slope (see table 13).

[2] Omission of values indicates that the slope-lengths exceed the limits for effectiveness of contouring. Use corresponding values from upper half of table.

for selecting conservation practices in each field. Solving the equation or performing field computations rarely will be necessary.

Example. The first step is to ascertain the soil type, percent slope, and slope length for the field being planned. From his handbook data, the conservationist can then obtain the values of **R**, **K**, and **T**. To complete the illustration, assume that **R** = 180, **K** = 0.32, **T** = 5, and the field slope is 400 ft long with a nearly uniform gradient of 6 percent. For this combination, the **T/RKLS** table shows a value of 0.064 for straight-row farming with the land slope (table 16). This is the maximum **C** value that will hold the average annual soil loss from that field within the 5-t tolerance limit, if no supporting practices are used. Consulting the **C** value table will show that a **C** as low as 0.064 can be attained only with well-managed, sod-based crop systems, or with no-till planting in residue covers of at least 70 percent.

A logical improvement is to add contouring. Table 13 shows a slope-length limit of 200 ft (250 ft if residue cover after seeding exceeds 50 percent) for contouring on 6-percent slope. Therefore,

the **P** value of 0.5 for contouring will not be applicable on the 400-ft slope without terracing. Construction of three, equally spaced terraces across the slope would divide it into four 100-ft slope lengths. Shortening the slope lengths to 100 ft will assure contour effectiveness and will also reduce the site value of **L**. For a 100-ft length of 6-percent slope farmed on the contour, table 16 shows a **T/RKLSP** value of 0.26. Any combination of cropping and management practices having a **C** value less than 0.26 will now be acceptable. Consulting the table of **C** values will show that with the terraces and contouring, the conservationist can recommend a range of possibilities for land use and management. If a system with a **C** value appreciably less than 0.26 is selected, a higher level of conservation will be attained than required by the 5-t tolerance limit.

Had the slope length in the example been only 200 ft, the contour **P** value of 0.5 (table 13) would have been applicable without the terraces. Table 16 shows that this combination would have permitted use of any system having a **C** value less than 0.18.

Thus, by this procedure a conservationist can list all the alternative crop system and management combinations that would control erosion on a field at an acceptable level. Study of this list will show how an erosion control program can be improved and still increase crop yields or decrease labor and fuel costs. In making a selection from this list, practices needed for control of nutrient and pesticide losses in the runoff (*42*) should also be considered.

Construction Sites

Procedures and data have been presented for predicting erosion losses from specific cropland areas and logically determining alternative ways in which the losses from each field may be held below given tolerance limits. These procedures and data can also be adapted to conditions on highway, residential, and commercial developing areas. The USLE will show under which development plan the area will produce the least sediment, and it will also show about how much sediment the developer will need to trap in sediment basins (*46*) during construction to prevent excessive soil movement to streams or reservoirs.

Evaluating the erosion factors for construction site conditions is discussed below. However, those primarily concerned with this particular phase of sediment control should also read the preceding discussions of the USLE factors and the procedures for predicting cropland soil losses.

Factor R. For a construction project extending over several years, the average annual **R** value for the site is obtained directly from figure 1. Probabilities of **EI** values greater than average are given in table 17. Using **EI** probabilities for **R** was discussed in the subsection **Soil Loss Probabilities.**

For construction periods of less than 1 year, the procedure outlined for predicting cropland soil losses for specific cropstage periods is appropriate. The portion of the annual **R** value that is applicable to the construction period is obtained from table 6 illustrated on p. 41 for cropstage averages.

Factor K. Because the soil surface is often unprotected during construction, this factor assumes even greater importance than for cropland. The soil erodibility nomograph (fig. 3) can be especially helpful for sediment prediction and erosion control planning on construction sites because it can predict the changes in erodibility when various subsoil horizons are exposed in the reshaping process. Some subsoils are substantially more erodible than the original topsoil, and others are less erodible. The planner can usually obtain a detailed description of the successive horizons of his soil from published soil survey data. By using the data for each soil horizon separately to follow the steps of the nomograph solution, the **K** value can be determined after various depths of desurfacing. Soil losses from the successive soil horizons, if exposed on similar slopes, would be directly proportional to the horizon **K** values. Information on the subsoil **K** values not only shows the depths of cut that would result in the most or the least soil erosion but also indicates whether return of stockpiled topsoil on the exposed subsoil would be profitable on the particular site.

When a chemical soil additive is used that stabilizes the soil and makes it less erodible, the **K** value is the nomograph solution times a factor for the effectiveness of the chemical additive.

Factor LS. Within limits, the **LS** value for a given length and steepness of uniform slope can be obtained directly from figure 4 or table 3. When the

slope is concave or convex, the figure 4 value needs to be adjusted by the procedure outlined for irregular slopes in the section on **The Topographic Factor.**

Development planning may include measures designed to reduce sediment yield by lowering **LS.** The effect of shortening slope lengths by diversions or stabilized drainageways is credited by entering figure 4 with the reduced slope length. A slope graded to flatten toward the bottom (concave) will lose less soil than an equivalent uniform slope whereas one that steepens toward the bottom (convex) will lose more. Reduction or increase in soil loss can be predicted by the procedure illustrated in the subsection **Irregular Slopes.**

Data are not available to evaluate **LS** on very steep slopes, like 2:1 and 3:1 roadbank slopes, in relation to soil and rainstorm characteristics. The best presently available estimates of **LS** for these slopes can be obtained by the **LS** equation presented earlier. However, values projected by this equation for steep slopes are speculative because the equation was derived from data obtained on slopes of less than 20 percent.

Factor C. Procedures for selecting **C** values for construction sites were given in the **Cover and Management Factor** section.

Factor P. This factor as used for soil conservation planning on cropland would rarely have a counterpart during construction on development areas, and **P** will usually equal 1.0. Erosion-reducing effects of shortening slopes or reducing slope gradients are accounted for through the **LS** factor.

If the lower part of a grass or woodland slope on a development area can be left undisturbed while the upper part is being developed, the procedure outlined for computing the value of **LSC** on irregular slopes is applicable, and sediment deposition on the undisturbed strip must be accounted for separately. For prolonged construction periods, buffer strips of grass, small grain, or high rates of anchored mulch may also be feasible to induce deposition within the area. Such deposition is important for water quality or offsite sediment control, but it should be evaluated from soil-transport factors rather than by a **P** factor.

Alternative plans. When appropriate numerical values of the six erosion factors are combined, their product is the soil loss estimate for the particular area in tons per acre and for the time interval for which **R** was evaluated. With the information supplied by the tables and charts in this handbook, the six factor values can be derived for each feasible alternative plan. Successive solutions of the equation will then provide comparative soil loss estimates to help guide decisions by the developer.

Estimating Upslope Contributions to Watershed Sediment Yield

The importance of predicting watershed sediment yields and identifying the major sediment sources was increased by the Federal Water Pollution Control Act Amendments of 1972, Public Law 92-500. Sources, causes, and potentials of sediment, nutrient, and pesticide losses from cropland, and measures that may be necessary to control these pollutants, are dealt with in depth in a two-volume manual developed by SEA and the Environmental Protection Agency (EPA) (*42*). Volume II, "An Overview," also includes an extensive list of other relevant publications. Only sediment yield prediction will be considered here.

Estimates show that about one-fourth of the amount of sediment moved by flowing water in the United States annually reaches major streams (*42*). The USLE can be used to compute average sheet and rill erosion in the various parts of a watershed, but deposition and channel-type erosion must be estimated by other means. A fully tested equation for sediment transport to use on agricultural land is not now available. One presented by Neibling and Foster (*32*) is perhaps the best now available for use with the USLE. It estimates transport capacity for sand and large silt-sized particles and does not consider the transport of clay particles.

Of the several methods now used for estimating sediment yield, the Gross Erosion-Sediment Delivery Method uses the USLE. A brief description of this method follows. More details are available from the SCS National Engineering Handbook (*45*). The equation is

$$Y = E(DR)/W_s \qquad (6)$$

where **Y** is sediment yield per unit area,

E is the gross erosion,

DR is the sediment delivery ratio, and

W_s is the area of the watershed above the point for which the sediment yield is being computed.

Gross Erosion

Gross erosion is the summation of erosion from all sources within the watershed. It includes sheet and rill erosion from tilled cropland, meadows, pastures, woodlands, construction sites, abandoned acreages, and surface-mined areas; gully erosion from all sources; and erosion from streambeds and streambanks. The relative importance of each of these sources of gross erosion will vary between watersheds.

The USLE can be used to estimate the sediment generated by sheet and rill erosion that is usually, but not always, the major portion of a watershed's gross erosion. Sediment from gully, streambank and streambed erosion, and from uncontrolled roadsides must be added to the USLE estimates. Methods for estimating sediment yields from these sources are discussed in Section 3 of the SCS National Engineering Handbook (*45*).

For small areas like farm fields or construction sites, the six USLE factors can usually be evaluated directly from the information presented in this handbook. For a large heterogeneous watershed, the factors are more difficult to define. Several methods of computing the average slope length and gradient for a large drainage area are available. Using **LS** values based on such averages, together with estimated watershed-average soil and cover factors, simplifies the computing procedure, but the saving in time is at the expense of substantial loss in accuracy. Erosion hazards are highly site specific. The parameters that determine the USLE factor values vary within a large watershed, and the variations are often not interrelated. Combining overall averages in the equation does not reflect the particular way in which the factors are actually combined in different parts of the watershed. Neither does it show which portions of the drainage area are contributing most of the sediment.

A more accurate procedure is to divide the heterogeneous drainage area into subareas for which representative soil type, slope length, gradient, cover, and erosion-control practice factors can be defined. The USLE is then used to compute the sheet and rill erosion on each subarea. For this purpose, eroded soil that is entrapped within the field area by terrace systems is not soil loss. An estimate of the entrapped sediment can be excluded from the USLE soil loss estimates by using values from the last two columns of table 15 as the **P** values. An alternate procedure is to estimate the channel deposition by sediment-transport relationships and subtract this amount from the soil loss computed by using the standard terracing factor (col. 2, table 15) in the USLE. By this procedure, the subarea soil loss computations identify the portions of the drainage area that contribute most of the sediment and also show how much of the sediment derives from tracts that receive heavy applications of agricultural chemicals.

Procedures for computing soil losses from cropped, idle, pasture, range, or wooded areas and from construction or development areas were outlined in the preceding sections. Factor values derived by the prescribed procedures are assumed applicable also for surface-mined areas. However, the effect of mining processes on soil erodibility, **K**, has not been determined. Length and percent slope and deposition within the area also are hard to determine for rugged strip mine spoils. Sometimes nearly all the sediment may be trapped within the bounds of the area. The USLE can be quite useful for predicting the effectiveness of each feasible reclamation plan for such areas.

Sediment Delivery Ratio

Eroded soil materials often move only short distances before a decrease in runoff velocity causes their deposition. They may remain in the fields where they originated or may be deposited on more level slopes that are remote from the stream system. The ratio of sediment delivered at a given location in the stream system to the gross erosion from the drainage area above that location is the sediment delivery ratio for that drainage area. A general equation for computing watershed delivery ratios is not yet available, but the ratios for some specific drainage areas have been computed directly from local data. Helpful guides for estimating this factor for other drainage areas were published by SCS in Section 3 of their National Engineering Handbook (*45*), and most of these guides were also included in a publication by SEA and EPA (*42*). Therefore, the relationships involved will be only briefly summarized here.

Available watershed data indicate that the delivery ratio varies approximately as the 0.2 power of drainage-area size, with representative values of about 0.33 for 0.5 mi^2; 0.18 for 10 mi^2; and 0.10 for 100 mi^2. There were indications that the exponent in this relationship may be as small as 0.1 for very large areas. But the ratio may vary substantially for any given size of drainage area. Other important factors include soil texture, relief, type of erosion, sediment transport system, and areas of deposition within the watershed. Fine soil texture, high channel density, and high stream gradients generally indicate delivery ratios that are above average for the drainage-area size.

A substantial reduction in sediment delivered to a stream may sometimes result in a compensatory increase in channel erosion. Channel erosion produces sediment that is immediately available to the transport system and that may remain in motion as bedload and suspended sediment. The composition of sediment derived from channel erosion will usually differ substantially from that derived from cropland erosion. This is particularly important from the viewpoint of transported chemical pollutants.

With reference to a field-sized area, the delivery ratio can closely approach 1.0 if the runoff drains directly into a lake or stream system with no intervening obstructions or flattening of the land slope. On the other hand, a substantial width of forest litter or dense vegetation below the eroding area may cause deposition of essentially all the sediment except colloidal material. Anything that reduces runoff velocity (such as reduction in gradient, physical obstructions, vegetation, and ponded water) reduces its capacity to transport sediment. When the sediment load exceeds the transport capacity of the runoff, deposition occurs.

From analysis of runoff and soil loss data from small single-cropped watersheds, Williams (*48*) concluded that the need for a sediment delivery ratio could be eliminated by using the watershed runoff times peak rate as the storm **R** value in the USLE.

Accuracy of USLE Predictions

Soil losses computed with the USLE are best available estimates, not absolutes. They will generally be most accurate for medium-textured soils, slope lengths of less than 400 ft, gradients of 3 to 18 percent, and consistent cropping and management systems that have been represented in the erosion plot studies. The farther these limits are exceeded, the greater will be the probability of significant extrapolation error.

An indication of the accuracy of the equation, tables, and charts presented herein was obtained by using them to compute longtime average soil losses for plots in past erosion studies and comparing these with the actually measured losses on each plot. About 53 percent of the differences were less than 1 t/A, 84 percent were less than 2 t, and 5 percent were as much as 4.6 t (*53*). The mean annual soil loss for this 2,300 plot-year sample was 11.3 t. Of those differences that exceeded 1 t/A, 67 percent were from comparisons with plot records whose duration was less than half of a normal 22-year rainfall cycle (*33*). Such short records are subject to bias by cyclical effects and random fluctuations in uncontrolled variables whose effects are averaged in the USLE factor values (*56*). Testing the complete equation against the assembled plot data was statistically valid because the equation for each factor, as a function of several parameters, was independently derived from only selected portions of the data.

The accuracy of a predicted soil loss will depend on how accurately the physical and management conditions on the particular piece of land are described by the parameter values used to enter the factor-evaluation tables and charts. An error in the selection of a factor value will produce an equivalent percentage error in the soil loss estimate. Large-scale averaging of parameter values on mixed drainage areas will usually also reduce accuracy. For reasons previously pointed out and discussed in depth in another publication (*56*), specific-storm or specific-year soil losses and short-term averages may differ substantially from the longtime average predicted by the USLE for the specified physical and management conditions.

REFERENCES

(1) Adams, J. E. 1966. Influence of mulches on runoff, erosion, and soil moisture depletion. Soil Science Society of America Proceedings 30:110-114.

(2) Barnett, A. P., Diseker, E. G., and Richardson, E. C. 1967. Evaluation of mulching methods for erosion control on newly prepared and seeded highway backslopes. Agronomy Journal 59:83-85.

(3) ——— and Rogers, J. S. 1966. Soil physical properties related to runoff and erosion from artificial rainfall. American Society of Agricultural Engineers Transactions 9:123-125.

(4) Blakely, B. D., Coyle, J. J., and Steele, J. G. 1957. Erosion on cultivated land. *In* Soil, Yearbook of Agriculture, pp. 290-306.

(5) Brooks, F. L. 1976. Use of the universal soil loss equation in Hawaii. *In* Soil Erosion: Prediction and Control. Soil Conservation Society of America, pp. 29-30.

(6) Browning, G. M., Parish, C. L., and Glass, J. A. 1947. A method for determining the use and limitation of rotation and conservation practices in control of soil erosion in Iowa. Soil Science Society of America Proceedings 23:246-249.

(7) Carter, C. E., Greer, J. D., Braud, H. J., and Floyd, J. M. 1974. Raindrop characteristics in South Central United States. American Society of Agricultural Engineers Transactions 17:1033-1037.

(8) ——— and Carreker, J. R. 1969. Controlling water erosion with graded furrows. American Society of Agricultural Engineers Transactions 12:677-680.

(9) El-Swaify, S. A., and Dangler, E. W. 1976. Erodibility of selected tropical soils in relation to structural and hydrological parameters. *In* Soil Erosion: Prediction and Control, Soil Conservation Society of America, pp. 105-114.

(10) Foster, G. R., Meyer, L. D., and Onstad, C. A. 1977. A runoff erosivity factor and variable slope length exponents for soil loss estimates. American Society of Agricultural Engineers Transactions 20:683-687.

(11) ——— Meyer, L. D., and Onstad, C. A. 1977. An erosion equation derived from basic erosion principles. American Society of Agricultural Engineers Transactions 20:678-682.

(12) ——— and Wischmeier, W. H. 1974. Evaluating irregular slopes for soil loss prediction. American Society of Agricultural Engineers Transactions 17:305-309.

(13) Gunn, R., and Kinzer, G. D. 1949. The terminal velocity of fall for water droplets. Journal Met. 6:243-248.

(14) Hill, H. O., Peevy, W. J., McCall, A. G., and Bell, F. G. 1944. Investigations in erosion control and reclamation of eroded land at the Blackland Conservation Experiment Station, 1931-41. U.S. Department of Agriculture, Technical Bulletin 859, 109 pp.

(15) Hudson, N. W. 1971. Raindrop size. *In* Soil Conservation: Cornell University Press, Ithaca, New York, pp. 50-56.

(16) Jamison, V. C., Smith, D. D., and Thornton, J. F. 1968. Soil and Water research on a claypan soil. U.S. Department of Agriculture, Technical Bulletin 1379.

(17) Laflen, J. M., and Johnson, H. P. 1976. Soil and water loss from impoundment terrace systems. 3d Federal Inter-Agency Sedimentation Conference Proceedings 2:20-41.

(18) Lillard, J. H., Rogers, H. T., and Elson, Jesse. 1941. Effects of slope, character of soil, rainfall, and cropping treatments on erosion losses from Dunmore silt loam. Virginia Agricultural Experiment Station Technical Bulletin 72, 32 pp.

(19) Lloyd, C. H., and Eley, G. W. 1952. Graphical solution of probable soil loss formula for Northeastern Region. Journal of Soil and Water Conservation 7:189-191.

(20) Mannering, J. V., and Meyer, L. D. 1963. Effects of various rates of surface mulch on infiltration and erosion. Soil Science Society of America Proceedings 27:84-86.

(21) McCool, D. K., Papendick, R. I., and Brooks, F. L. 1976. The universal soil loss equation as adapted to the Pacific Northwest. 3d Federal Inter-Agency Sedimentation Conference Proceedings 2:135-147.

(22) Meyer, L. D., Foster, G. R., and Romkens, M. J. M. 1975. Source of soil eroded by water from upland slopes. Sediment Prediction Workshop Proceedings, Oxford, Miss. ARS-S-40:177-189.

(23) ——— and McCune, D. L. 1958. Rainfall simulator for runoff plots. Agricultural Engineering 39:644-648.

(24) ——— and Ports, M. A. 1976. Prediction and control of urban erosion and sedimentation. National Symposium on Urban Hydrology, Hydraulics, and Sedimentation Proceedings, University of Kentucky, Lexington, Bulletin 111, pp. 323-331.

(25) ——— and Romkens, M. J. M. 1976. Erosion and sediment control on reshaped land. 3d Federal Inter-Agency Sedimentation Conference Proceedings 2:65-72.

(26) ——— and Wischmeier, W. H. 1969. Mathematical simulation of the process of soil erosion by water. American Society of Agricultural Engineers Transactions 12:754-758, 762.

(27) ——— Wischmeier, W. H., and Foster, G. R. 1970. Mulch rates required for erosion control on steep slopes. Soil Science Society of America Proceedings 34:928-931.

(28) Middleton, H. E., Slater, C. S., and Byers, H. G. 1932-1934. Physical and chemical characteristics of the soils from the erosion experiment stations. U.S. Department of Agriculture, Technical Bulletin No. 316 and 430.

(29) Moldenhauer, W. C., and Wischmeier, W. H. 1960. Soil and water losses and infiltration rates on Ida silt loam as influenced by cropping systems, tillage practices and rainfall characteristics. Soil Science Society of America Proceedings 24:409-413.

(30) ——— Lovely, W. G., Swanson, N. P., and Currence, H. D. 1971. Effect of row grades and tillage systems on soil and water losses. Journal of Soil and Water Conservation 26(5): 193-195.

(31) Musgrave, G. W. 1947. The quantitative evaluation of factors in water erosion, a first approximation. Journal of Soil and Water Conservation 2(3):133-138.

(32) Neibling, W. H., and Foster, G. R. 1977. Estimating deposition and sediment yield from overland flow processes. 1977 International Symposium on Urban Hydrology, Hydraulics, and Sediment Control Proceedings, University of Kentucky, Lexington.

(33) Newman, J. E. 1970. Climate in the 1970's. American Society of Agronomy, Crops and Soils 22(4):9-12.

(34) Onstad, C. A., and Foster, G. R. 1975. Erosion modeling on a watershed. American Society of Agricultural Engineers Transactions 18:288-292.

(35) Peele, T. C., Latham, E. E., and Beale, O. W. 1945. Relation of the physical properties of different soil types to erodibility. South Carolina Agricultural Experiment Station Bulletin No. 357.

(36) Richardson, C. W. 1973. Runoff, erosion and tillage efficiency on graded furrows and terraced watersheds. Journal of Soil and Water Conservation 28(4):162-164.

(37) Roth, C. B., Nelson, D. W., and Romkens, M. J. M. 1974. Prediction of subsoil erodibility using chemical, mineralogical and physical parameters. U. S. Environmental Protection Agency Report No. 660/2-74-043. 111 pp.

(38) Smith, D. D. 1941. Interpretation of soil conservation data for field use. Agricultural Engineering 22:173-175.

(39) ——— and Whitt, D. M. 1947. Estimating soil losses from field areas of claypan soils. Soil Science Society of America Proceedings 12:485-490.

(40) ——— and Wischmeier, W. H. 1957. Factors affecting sheet and rill erosion. American Geophysical Union Transactions 38:889-896.

(41) Springer, D. L., Breinig, C. B., and Springer, M. E. 1963. Predicting soil losses in Tennessee. Journal of Soil and Water Conservation 18(4):157-158.

(42) Stewart, B. A., Wischmeier, W. H., Woolhiser, and others. 1975. Control of water pollution from cropland: Vol. I, a manual for guideline development; Vol. II, an overview. U.S. Department of Agriculture, ARS-H-5-1 and ARS-H-5-2.

(43) Swanson, N. P., Dedrick, A. R., Weakley, H. E., and Haise, H. R. 1965. Evaluation of mulches for water-erosion control. American Society of Agricultural Engineers Transactions 8: 438-440.

(44) U.S. Department of Agriculture. 1977. Terracing Code 600. *In* National Engineering Handbook. U.S. Department of Agriculture, Soil Conservation Service.

(45) ——— 1971. Sediment sources, yields and delivery ratios. *In* National Engineering Handbook, Section 3, Sedimentation. U.S. Department of Agriculture,Soil Conservation Service.

(46) ——— 1975. Standards and specifications for soil erosion and sediment control in developing areas, approved by Maryland Water Resources Administration. U.S. Department of Agriculture, Soil Conservation Service. 200 pp.

(47) U. S. Weather Bureau. 1958. Rainfall intensity-frequency regime. Technical Paper No. 29, 5 parts.

(48) Williams, J. R. 1975. Sediment-yield prediction with the universal equation using a runoff energy factor. U.S. Department of Agriculture, ARS-S-40:244-252.

(49) Wischmeier, W. H. 1959. A rainfall erosion index for a universal soil-loss equation. Soil Science Society of America Proceedings 23:246-249.

(50) ——— 1960. Cropping-management factor evaluations for a universal soil-loss equation. Soil Science Society of America Proceedings 23:322-326.

(51) ——— 1962. Storms and soil conservation. Journal of Soil Water and Conservation 17(2):55-59.

(52) Wischmeier, W. H. 1966. Relation of field-plot runoff to management and physical factors. Soil Science Society of America Proceedings 30:272-277.

(53) ——— 1972. Upslope erosion analysis. *In* Environmental Impact on Rivers. Water Resources Publications, Fort Collins, Colo.

(54) ——— 1973. Conservation tillage to control water erosion. National Conservation Tillage Conference Proceedings, Soil Conservation Society of America, pp. 133-141.

(55) ——— 1974. New developments in estimating water erosion. 29th Annual Meeting of the Soil Conservation Society of America Proceedings, pp. 179-186.

(56) ——— 1976. Use and misuse of the universal soil loss equation. Journal of Soil and Water Conservation 31(1): 5-9.

(57) ——— 1975. Estimating the soil loss equation's cover and management factor for undisturbed areas. Sediment Yield Workshop Proceedings, Oxford, Miss. U.S. Department of Agriculture, ARS-S-40.

(58) ——— Johnson, C. B., and Cross, B. V. 1971. A soil erodibility nomograph for farmland and construction sites. Journal of Soil and Water Conservation 26:189-193.

(59) ——— and Mannering, J. V. 1965. Effect of organic matter content of the soil on infiltration. Journal of Soil and Water Conservation 20:150-152.

(60) ——— and Mannering, J. V. 1969. Relation of soil properties to its erodibility. Soil Science Society of America Proceedings 33:131-137.

(61) ——— and Meyer, L. D. 1973. Soil erodibility on construction areas. Highway Research Board, National Academy of Science Special Report 135:20-29.

(62) ——— and Smith, D. D. 1958. Rainfall energy and its relationship to soil loss. American Geophysical Union Transactions 39:285-291.

(63) ——— Smith, D. D., and Uhland, R. E. 1958. Evaluation of factors in the soil loss equation. Agricultural Engineering 39:458-462, 474.

(64) ——— and Smith, D. D. 1965. Predicting rainfall-erosion losses from cropland east of the Rocky Mountains—Guide for selection of practices for soil and water conservation. Agricultural Handbook No. 282.

(65) Witmuss, H. D., Triplett, G. B., Jr., and Creb, B. W. 1973. Concepts of conservation tillage systems using surface mulches. National Conservation Tillage Conference Proceedings, Soil Conservation Society of America 5-12.

(66) Woolhiser, D. G. 1975. Simulation of unsteady overland flow. *In* Unsteady Flow in Open Channels. Water Resources Publications, Fort Collins, Colo. Vol. II, Ch. 12, pp. 485-508.

(67) Zingg, R. W. 1940. Degree and length of land slope as it affects soil loss in runoff. Agricultural Engineering 21:59-64.

APPENDIX

Estimating Percentages of Canopy and Mulch Covers

"Percent canopy cover" is the percentage of the field area that could not be hit by vertically falling raindrops because of canopy interception. It is the portion of the soil surface that would be covered by shadows if the sun were directly overhead. Because the blades from adjacent rows intertwine does not necessarily indicate 100 percent canopy cover.

"Percent mulch cover" is the percentage of the field area that is covered by pieces of mulch lying on the surface. Researchers in Indiana attempted to relate percent cover to mulch rate by photographing numerous small, equal-sized areas in harvested corn fields. The residues on the photographed areas were carefully picked up, dried, and weighed to measure mulch rates, and the photographs were projected on grids to determine percent cover. The indicated average relation of percent cover to dry weight of well-distributed corn stover mulch is shown by the solid-line curve in figure 10. However, observed differences between samples were appreciable. The average relation of percent cover to dry weight of straw mulch uniformly distributed over research plots is shown by the broken-line curve.

A simple method of estimating percent mulch cover on a field is with a cord, preferably not shorter than 50 ft, that has 100 equally spaced knots or other readily visible markings. The cord is stretched diagonally across several rows, and the knots that contact a piece of mulch are counted. This procedure is repeated at randomly selected spots on the field, and the data are averaged to obtain a representative value for the field.

Probability Values of EI in the United States

The annual and maximum-storm values of **EI** at any given location differ substantially from year to year. The observed ranges and 50 percent, 20 per[illegible] and 5 percent probabilities of annual **EI** values from 22-year precipitation records at 181 locations in 44 States are listed in table 17. Other probabilities can be derived by plotting the 50 percent and 5 percent values on log-probability paper and joining the two points by a straight line. Annual maxima storm probabilities for the same locations are given in table 18.

Computing the Erosion Index from Recording-Rain Gage Records

Soil loss prediction by the method presented in this handbook does not require computation of **EI** values by application personnel, but the procedure is included here for the benefit of those who may wish to do so.

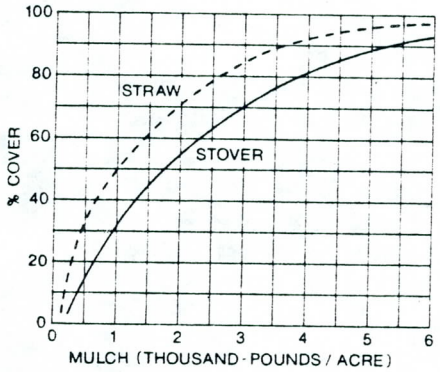

FIGURE 10.—Relation of percent cover to dry weight of uniformly distributed residue mulch.

The kinetic energy of a given amount of rain depends on the sizes and terminal velocities of the raindrops, and these are related to rainfall intensity. The computed energy per inch of rain at each intensity is shown in table 19. The energy of a given storm depends on all the intensities at which the rain occurred and the amount that occurred at each intensity. A recording-rain gage record of the storm will provide this information. Clock time and rain depth are read from the chart at each point where the slope of the pen line changes and are tabulated as shown in the first two columns of the sample computation below. Clock times (col. 1) are subtracted to obtain the time intervals given in column 3, and the depths (col. 2) are subtracted to obtain the incremental amounts tabulated in column 4. The intensity for each increment (col. 5) is the incremental amount times 60, divided by column 3.

Chart readings		For each increment			Energy	
Time	Depth (inch)	Duration (minute)	Amount (inch)	Intensity (in/hr)	Per inch	Total
4:00	0					
:20	0.05	20	0.05	0.15	643	32
:27	.12	7	.07	.60	843	59
:36	.35	9	.23	1.53	977	225
:50	1.05	14	.70	3.00	1074	752
:57	1.20	7	.15	1.29	953	143
5:05	1.25	8	.05	.38	777	39
:15	1.25	20	0	0	0	0
:30	1.30	15	.05	.20	685	34
Totals		90	1.30			1,284

Kinetic energy of the storm = $1{,}284(10^{-2}) = 12.84$

The energy per inch of rain in each interval (col. 6) is obtained by entering table 19 with the intensity given in column 5. The incremented energy amounts (col. 7) are products of columns 4 and 6. The total energy for this 90-minute rain is 1,284 foot-tons per acre. This is multiplied by a constant factor of 10^{-2} to convert the storm energy to the dimensions in which **EI** values are expressed.

The maximum amount of rain falling within 30 consecutive minutes was 1.08 in, from 4:27 to 4:57. I_{30} is twice 1.08, or 2.16 in/h. The storm **EI** value is 12.84(2.16) = 27.7. When the duration of a storm is less than 30 minutes, I_{30} is twice the amount of the rain.

The **EI** for a specified time is the sum of the computed values for all significant rain periods within that time. The average annual erosion index for a specific locality, as given in figures 1 and 2, is the sum of all the significant storm **EI** values over 20 to 25 years, divided by the number of years. For erosion index calculations, 6 h or more with less than 0.5 in of precipitation was defined as a break between storms. Rains of less than 0.5 in, separated from other showers by 6 h or more, were omitted as insignificant unless the maximum 15-min intensity exceeded 0.95 in/h.

Recent studies showed that the median dropsize of rain does not continue to increase for intensities greater than about 2.5 to 3 in/h (*7, 15*). Therefore, energy per unit of rainfall also does not continue to increase, as was assumed in the derivation of the energy-intensity table published in 1958 (*62*). The value given in table 19 for rain at 3 in/h (7.6 cm/h in table 20) should be used for all greater intensities. Also, analysis of the limited soil loss data available for occasional storms with 30-min intensities greater than 2.5 in/h showed that placing a limit of 2.5 in (6.35 cm)/h on the I_{30} component of **EI** improved prediction accuracy for these storms. Both of these limits were applied in the development of figure 1. They slightly lowered previously computed erosion index values in the Southeast, but average-annual **EI** values for the U.S. mainland other than the Southeast were not significantly affected by the limits because they are rarely exceeded.

Conversion to Metric System

Metric equivalents were not included in the procedures and tables presented in this handbook because direct conversion of each English unit would produce numbers that would be awkward and undesirable. Converting the USLE as a whole is more appropriate. Metric units can then be selected so that each of the interdependent factors will have a metric counterpart whose values will be expressed in numbers that are easy to visualize and to combine in computations.

A convenient unit for measuring cropland soil losses is metric tons per hectare per year. **EI** values of convenient magnitude can be obtained by expressing rainfall energy in metric ton-meters per hectare, expressing intensities in centimeters per hour, and retaining the constant factor of 10^{-2} that has been used consistently for **EI** calculations in English units. Factor **K** will then be in metric tons per hectare per metric **EI** unit. If 22 meters is taken as the basic slope length and 9 percent is retained as the basic slope gradient, the **LS** factor will not be significantly affected. Using these units is recommended and is assumed in the following paragraphs.

The USLE factors will normally be derived directly in these units by procedures outlined below. However, the following conversion factors will facilitate comparisons of the metric factor values with the English values published in this handbook. Factors expressed in the recommended metric units are identified by the subscript, **m**.

Text continues on page 56.

TABLE 17.—*Observed range and 50-, 20-, and 5- percent probability values of erosion index at each of 181 key locations*

Location	Values of erosion index (*EI*)			
	Observed 22-year range	50-percent probability	20-percent probability	5-percent probability
Alabama:				
Birmingham	179-601	354	461	592
Mobile	279-925	673	799	940
Montgomery	164-780	359	482	638
Arkansas:				
Fort Smith	116-818	254	400	614
Little Rock	103-625	308	422	569
Mountain Home	98-441	206	301	432
Texarkana	137-664	325	445	600
California:				
Red Bluff	11-240	54	98	171
San Luis Obispo	5-147	43	70	113
Colorado:				
Akron	8-247	72	129	225
Pueblo	5-291	44	93	189
Springfield	4-246	79	138	233
Connecticut:				
Hartford	65-355	133	188	263
New Haven	66-373	157	222	310
District of Columbia	84-334	183	250	336
Florida:				
Apalachicola	271-944	529	663	820
Jacksonville	283-900	540	693	875
Miami	197-1225	529	784	1136
Georgia:				
Atlanta	116-549	286	377	488
Augusta	148-476	229	308	408
Columbus	215-514	336	400	473
Macon	117-493	282	357	447
Savannah	197-886	412	571	780
Watkinsville[1]	182-544	278	352	441
Illinois:				
Cairo	126-575	231	349	518
Chicago	50-379	140	212	315
Dixon Springs[1]	89-581	225	326	465
Moline	80-369	158	221	303
Rantoul	73-286	152	201	263
Springfield	38-315	154	210	283
Indiana:				
Evansville	104-417	188	263	362
Fort Wayne	60-275	127	183	259
Indianapolis	60-349	166	225	302
South Bend	43-374	137	204	298
Terre Haute	81-413	190	273	389
Iowa:				
Burlington	65-286	162	216	284
Charles City	39-308	140	205	295
Clarinda[1]	75-376	162	220	295
Des Moines	30-319	136	198	284
Dubuque	54-389	175	251	356
Sioux City	56-336	135	205	308
Rockwell City	40-391	137	216	335
Kansas:				
Burlingame	57-447	176	267	398
Coffeyville	66-546	234	339	483
Concordia	38-569	131	241	427
Dodge City	16-421	98	175	303
Goodland	10-166	76	115	171
Hays[1]	66-373	116	182	279
Wichita	42-440	188	292	445
Kentucky:				
Lexington	54-396	178	248	340
Louisville	84-296	168	221	286
Middlesboro	107-301	154	197	248
Louisiana:				
Lake Charles	200-1019	572	786	1063
New Orleans	273-1366	721	1007	1384
Shreveport	143-707	321	445	609
Maine:				
Caribou	26-120	58	79	106
Portland	36-241	91	131	186
Skowhegan	39-149	78	108	148
Maryland:				
Baltimore	50-388	178	263	381
Massachusetts:				
Boston	39-366	99	159	252
Washington	65-229	116	153	198
Michigan:				
Alpena	14-124	57	85	124
Detroit	56-179	100	134	177
East Lansing	35-161	86	121	166
Grand Rapids	33-203	84	123	178
Minnesota:				
Alexandria	33-301	88	147	240
Duluth	7-227	84	127	189
Fosston	22-205	62	108	184
Minneapolis	19-173	94	135	190
Rochester	46-338	142	207	297
Springfield	37-290	96	154	243
Mississippi:				
Meridian	216-820	416	557	737
Oxford	131-570	310	413	543
Vicksburg	165-786	365	493	658
Missouri:				
Columbia	98-419	214	297	406
Kansas City	28-361	170	248	356
McCredie[1]	64-410	189	271	383
Rolla	105-415	209	287	387
Springfield	97-333	199	266	352
St. Joseph	50-359	178	257	366
St. Louis	59-737	168	290	488
Montana:				
Billings	2-82	12	26	50
Great Falls	3-62	13	24	44
Miles City	1-101	21	40	72
Nebraska				
Antioch	18-131	60	86	120
Lincoln	44-289	133	201	299
Lynch	34-217	96	142	205
North Platte	14-236	81	136	224
Scribner	69-312	154	205	269
Valentine	4-169	64	100	153

See footnote at end of table.

TABLE 17.—*Observed range and 50-, 20-, and 5- percent probability values of erosion index at each of 181 key locations*—Continued

Location	Values of erosion index (*EI*)			
	Observed 22-year range	50-percent probability	20-percent probability	5-percent probability
New Hampshire:				
Concord	52-212	91	131	187
New Jersey:				
Atlantic City	71-318	166	229	311
Marlboro[1]	58-331	186	254	343
Trenton	37-382	149	216	308
New Mexico:				
Albuquerque	0-46	10	19	35
Roswell	5-159	41	73	128
New York:				
Albany	40-172	81	114	159
Binghamton	20-151	76	106	146
Buffalo	20-148	66	96	139
Geneva[1]	33-180	73	106	152
Marcellus[1]	24-241	74	112	167
Rochester	22-180	66	101	151
Salamanca	31-202	70	106	157
Syracuse	8-219	83	129	197
North Carolina:				
Asheville	76-238	135	175	223
Charlotte	113-526	229	322	443
Greensboro	102-357	184	244	320
Raleigh	152-569	280	379	506
Wilmington	196-701	358	497	677
North Dakota:				
Bismarck	9-189	43	73	120
Devils Lake	21-171	56	90	142
Fargo	5-213	62	113	200
Williston	4-71	30	45	67
Ohio:				
Cincinnati	66-352	146	211	299
Cleveland	21-186	93	132	185
Columbiana	29-188	96	129	173
Columbus	45-228	113	158	216
Coshocton[1]	72-426	158	235	343
Dayton	56-245	125	175	240
Toledo	32-189	83	120	170
Oklahoma:				
Ardmore	100-678	263	395	582
Cherokee[1]	49-320	167	242	345
Guthrie[1]	69-441	210	316	467
McAlester	105-741	272	411	609
Tulsa	19-584	247	347	478
Oregon:				
Pendleton	2-28	4	8	16
Portland	16-80	40	56	77
Pennsylvania:				
Erie	11-534	96	181	331
Franklin	50-228	97	135	184
Harrisburg	48-232	105	146	199
Philadelphia	72-361	156	210	282
See footnote at end of table.				
Pittsburgh	43-201	111	148	194
Reading	84-308	144	204	285
Scranton	52-198	104	140	188
Puerto Rico:				
San Juan	203-577	345	445	565
Rhode Island:				
Providence	53-225	119	167	232
South Carolina:				
Charleston	174-1037	387	559	795
Clemson[1]	138-624	280	384	519
Columbia	81-461	213	298	410
Greenville	130-589	249	350	487
South Dakota:				
Aberdeen	19-295	74	129	219
Huron	18-145	60	91	136
Isabel	16-141	48	78	125
Rapid City	10-140	37	64	108
Tennessee:				
Chattanooga	163-468	269	348	445
Knoxville	64-370	173	239	325
Memphis	139-595	272	384	536
Nashville	116-381	198	262	339
Texas:				
Abilene	27-554	146	253	427
Amarillo	33-340	110	184	299
Austin	59-669	270	414	624
Brownsville	46-552	267	386	549
Corpus Christi	124-559	237	330	451
Dallas	93-630	263	396	586
Del Rio	19-405	121	216	374
El Paso	4-85	18	36	67
Houston	176-1171	444	674	1003
Lubbock	17-415	82	158	295
Midland	35-260	82	139	228
Nacogdoches	153-769	401	571	801
San Antonio	77-635	220	353	556
Temple[1]	81-644	261	379	542
Victoria	108-609	265	385	551
Wichita Falls	79-558	196	298	447
Vermont:				
Burlington	33-270	72	114	178
Virginia:				
Blacksburg[1]	81-245	126	168	221
Lynchburg	64-366	164	232	324
Richmond	102-373	208	275	361
Roanoke	78-283	129	176	237
Washington:				
Pullman[1]	1-30	6	12	21
Spokane	1-19	7	11	17
West Virginia:				
Elkins	43-223	118	158	209
Huntington	56-228	127	173	233
Parkersburg	69-303	120	165	226
Wisconsin:				
Green Bay	17-148	77	107	147
LaCrosse[1]	61-385	153	228	331
Madison	38-251	118	171	245
Milwaukee	31-193	93	139	202
Rice Lake	24-334	122	202	327
Wyoming:				
Casper	1-24	9	15	26
Cheyenne	8-66	28	43	66

[1] Computations based on SEA rainfall records. All others are based on Weather Bureau records.

TABLE 18.—*Expected magnitudes of single-storm erosion index values*

Location	Index values normally exceeded once in—				
	year 1	years 2	years 5	years 10	years 20
Alabama:					
Birmingham	54	77	110	140	170
Mobile	97	122	151	172	194
Montgomery	62	86	118	145	172
Arkansas:					
Fort Smith	43	65	101	132	167
Little Rock	41	69	115	158	211
Mountain Home	33	46	68	87	105
Texarkana	51	73	105	132	163
California:					
Red Bluff	13	21	36	49	65
San Luis Obispo	11	15	22	28	34
Colorado:					
Akron	22	36	63	87	118
Pueblo	17	31	60	88	127
Springfield	31	51	84	112	152
Connecticut:					
Hartford	23	33	50	64	79
New Haven	31	47	73	96	122
District of Columbia	39	57	86	108	136
Florida:					
Apalachicola	87	124	180	224	272
Jacksonville	92	123	166	201	236
Miami	93	134	200	253	308
Georgia:					
Atlanta	49	67	92	112	134
Augusta	34	50	74	94	118
Columbus	61	81	108	131	152
Macon	53	72	99	122	146
Savannah	82	128	203	272	358
Watkinsville	52	71	98	120	142
Illinois:					
Cairo	39	63	101	135	173
Chicago	33	49	77	101	129
Dixon Springs	39	56	82	105	130
Moline	39	50	89	116	145
Rantoul	27	39	56	69	82
Springfield	36	52	75	94	117
Indiana:					
Evansville	26	38	56	71	86
Fort Wayne	24	33	45	56	65
Indianapolis	29	41	60	75	90
South Bend	26	41	65	86	111
Terre Haute	42	57	78	96	113
Iowa:					
Burlington	37	48	62	72	81
Charles City	33	47	68	85	103
Clarinda	35	48	66	79	94
Des Moines	31	45	67	86	105
Dubuque	43	63	91	114	140
Rockwell City	31	49	76	101	129
Sioux City	40	58	84	105	131
Kansas:					
Burlingame	37	51	69	83	100
Coffeyville	47	69	101	128	159
Concordia	33	53	86	116	154
Dodge City	31	47	76	97	124
Goodland	26	37	53	67	80
Hays	35	51	76	97	121
Wichita	41	61	93	121	150
Kentucky:					
Lexington	28	46	80	114	151
Louisville	31	43	59	72	85
Middlesboro	28	38	52	63	73
Louisiana:					
New Orleans	104	149	214	270	330
Shreveport	55	73	99	121	141
Maine:					
Caribou	14	20	28	36	44
Portland	16	27	48	66	88
Skowhegan	18	27	40	51	63
Maryland:					
Baltimore	41	59	86	109	133
Massachusetts:					
Boston	17	27	43	57	73
Washington	29	35	41	45	50
Michigan:					
Alpena	14	21	32	41	50
Detroit	21	31	45	56	68
East Lansing	19	26	36	43	51
Grand Rapids	24	28	34	38	42
Minnesota:					
Duluth	21	34	53	72	93
Fosston	17	26	39	51	63
Minneapolis	25	35	51	65	78
Rochester	41	58	85	105	129
Springfield	24	37	60	80	102
Mississippi:					
Meridian	69	92	125	151	176
Oxford	48	64	86	103	120
Vicksburg	57	78	111	136	161
Missouri:					
Columbia	43	58	77	93	107
Kansas City	30	43	63	78	93
McCredie	35	55	89	117	151
Rolla	43	63	91	115	140
Springfield	37	51	70	87	102
St. Joseph	45	62	86	106	126
Montana:					
Great Falls	4	8	14	20	26
Miles City	7	12	21	29	38
Nebraska:					
Antioch	19	26	36	45	52
Lincoln	36	51	74	92	112
Lynch	26	37	54	67	82
North Platte	25	38	59	78	99
Scribner	38	53	76	96	116
Valentine	18	28	45	61	77

TABLE 18.—*Expected magnitudes of single-storm erosion index values*—Continued

Location	Index values normally exceeded once in— year 1	years 2	years 5	years 10	years 20
New Hampshire:					
Concord	18	27	45	62	79
New Jersey:					
Atlantic City	39	55	77	97	117
Marlboro	39	57	85	111	136
Trenton	29	48	76	102	131
New Mexico:					
Albuquerque	4	6	11	15	21
Roswell	10	21	34	45	53
New York:					
Albany	18	26	38	47	56
Binghamton	16	24	36	47	58
Buffalo	15	23	36	49	61
Marcellus	16	24	38	49	62
Rochester	13	22	38	54	75
Salamanca	15	21	32	40	49
Syracuse	15	24	38	51	65
North Carolina:					
Asheville	28	40	58	72	87
Charlottte	41	63	100	131	164
Greensboro	37	51	74	92	113
Raleigh	53	77	110	137	168
Wilmington	59	87	129	167	206
North Dakota:					
Devils Lake	19	27	39	49	59
Fargo	20	31	54	77	103
Williston	11	16	25	33	41
Ohio:					
Cincinnati	27	36	48	59	69
Cleveland	22	35	53	71	86
Columbiana	20	26	35	41	48
Columbus	27	40	60	77	94
Coshocton	27	45	77	108	143
Dayton	21	30	44	57	70
Toledo	16	26	42	57	74
Oklahoma:					
Ardmore	46	71	107	141	179
Cherokee	44	59	80	97	113
Guthrie	47	70	105	134	163
McAlester	54	82	127	165	209
Tulsa	47	69	100	127	154
Oregon:					
Portland	6	9	13	15	18
Pennsylvania:					
Franklin	17	24	35	45	54
Harrisburg	19	25	35	43	51
Philadelphia	28	39	55	69	81
Pittsburgh	23	32	45	57	67
Reading	28	39	55	68	81
Scranton	23	32	44	53	63
Puerto Rico:					
San Juan	57	87	131	169	216
Rhode Island:					
Providence	23	34	52	68	83
South Carolina:					
Charleston	74	106	154	196	240
Clemson	51	73	106	133	163
Columbia	41	59	85	106	132
Greenville	44	65	96	124	153
South Dakota:					
Aberdeen	23	35	55	73	92
Huron	19	27	40	50	61
Isabel	15	24	38	52	67
Rapid City	12	20	34	48	64
Tennessee:					
Chattanooga	34	49	72	93	114
Knoxville	25	41	68	93	122
Memphis	43	55	70	82	91
Nashville	35	49	68	83	99
Texas:					
Abilene	31	49	79	103	138
Amarillo	27	47	80	112	150
Austin	51	80	125	169	218
Brownsville	73	113	181	245	312
Corpus Christi	57	79	114	146	171
Dallas	53	82	126	166	213
Del Rio	44	67	108	144	182
El Paso	6	9	15	19	24
Houston	82	127	208	275	359
Lubbock	17	29	53	77	103
Midland	23	35	52	69	85
Nacogdoches	77	103	138	164	194
San Antonio	57	82	122	155	193
Temple	53	78	123	162	206
Victoria	59	83	116	146	178
Wichita Falls	47	63	86	106	123
Vermont:					
Burlington	15	22	35	47	58
Virginia:					
Blacksburg	23	31	41	48	56
Lynchburg	31	45	66	83	103
Richmond	46	63	86	102	125
Roanoke	23	33	48	61	73
Washington:					
Spokane	3	4	7	8	11
West Virginia:					
Elkins	23	31	42	51	60
Huntington	18	29	49	69	89
Parkersburg	20	31	46	61	76
Wisconsin:					
Green Bay	18	26	38	49	59
LaCrosse	46	67	99	125	154
Madison	29	42	61	77	95
Milwaukee	25	35	50	62	74
Rice Lake	29	45	70	92	119
Wyoming:					
Casper	4	7	9	11	14
Cheyenne	9	14	21	27	34

$$
\begin{aligned}
1\ t/ha &= 2.242 \text{ tons per acre} \\
1\ t\text{-}m/ha/cm &= 0.269 \text{ ft-tons per acre per inch} \\
1\ E_m &= 0.683\ E \\
1\ I_{30m} &= 2.54\ I_{30} \\
1\ (EI)_m &= 1.735\ EI \\
1\ K_m &= 1.292\ K
\end{aligned}
\tag{7}
$$

Factor R. The procedure for computing $(\mathbf{EI})_m$ for a given rain period is similar to that described in the preceding section for computation of **EI**, but the input data will be in different units. If the rain gage chart used for the preceding example had been calibrated in millimeters, the computation would have been as follows:

Chart readings		Storm increments			Energy	
Time	Depth (mm)	Duration (min)	Amount (cm)	Intensity (cm/h)	Per cm	For increment
4:00	0					
:20	1.2	20	0.12	0.36	175	21
:27	3.0	7	.18	1.54	226	41
:36	8.8	9	.58	3.87	263	153
:50	26.6	14	1.78	7.68	289	514
:57	30.4	7	.38	3.26	256	97
5:05	31.7	8	.13	.98	220	29
:15	31.7	10	0	0	0	0
:30	33.0	15	.13	.52	184	24
Totals		90	3.30			879

Kinetic energy of the storm = $879(10^{-2}) = 8.79$

TABLE 19.—*Kinetic energy of rainfall expressed in foot-tons per acre per inch of rain*[1]

Intensity inch per hour	0.00	0.01	0.02	0.03	0.04	0.05	0.06	0.07	0.08	0.09
0	—	254	354	412	453	485	512	534	553	570
0.1	585	599	611	623	633	643	653	661	669	677
.2	685	692	698	705	711	717	722	728	733	738
.3	743	748	752	757	761	765	769	773	777	781
.4	784	788	791	795	798	801	804	807	810	814
.5	816	819	822	825	827	830	833	835	838	840
.6	843	845	847	850	852	854	856	858	861	863
.7	865	867	869	871	873	875	877	878	880	882
.8	884	886	887	889	891	893	894	896	898	899
.9	901	902	904	906	907	909	910	912	913	915
	0	0.1	0.2	0.3	0.4	0.5	0.6	0.7	0.8	0.9
1	916	930	942	954	964	974	984	992	1000	1008
2	1016	1023	1029	1036	1042	1048	1053	1059	1064	1069
3	[2]1074									

[1] Computed by the equation, $E = 916 + 331 \log_{10} I$, where E = kinetic energy in foot-tons per acre per inch of rain, and I = rainfall intensity in inches per hour.

[2] The 1074 value also applies for all intensities greater than 3 in/h (see text).

TABLE 20.—*Kinetic energy of rainfall expressed in metric ton-meters per hectare per centimeter of rain*[1]

Intensity cm/h	.0	0.1	0.2	0.3	0.4	0.5	0.6	0.7	0.8	0.9
0 ..	0	121	148	163	175	184	191	197	202	206
1 ..	210	214	217	220	223	226	228	231	233	235
2 ..	237	239	241	242	244	246	247	249	250	251
3 ..	253	254	255	256	258	259	260	261	262	263
4 ..	264	265	266	267	268	268	269	270	271	272
5 ..	273	273	274	275	275	276	277	278	278	279
6 ..	280	280	281	281	282	283	283	284	284	285
7 ..	286	286	287	287	288	288	[2]289			

[1] Computed by the equation $E = 210 + 89 \log_{10} I$,
where E = kinetic energy in metric-ton meters per hectare per centimeter of rain, and
I = rainfall intensity in centimeters per hour.

[2] The 289 value also applies for all intensities greater than 7.6 cm/h.

Values for column 6 are obtained by entering table 20 with the intensities listed in column 5, and their sum, 879, is the kinetic energy ($\mathbf{E}_m$) of the 3.30 cm of rain expressed in metric ton-meters per hectare. The constant factor of 10^{-2} used for the English system should be applied here also so that storm $(\mathbf{EI})_m$ values will usually not exceed 100. The maximum amount of rain in any 30-minute period was 2.74 cm, from 4:27 to 4:57. Therefore $\mathbf{I}_{30m} = 2(2.74 = 5.48$ cm/h. $(\mathbf{EI})_m = 8.79(5.48) = 48.17$

The procedure for combining storm **EI** values for local erosion index values was fully described in the preceding section. For predicting average annual soil losses from rainfall and its associated runoff, **R** equals the erosion index. Where runoff from thaw, snowmelt, or irrigation is significant, an $\mathbf{R}_s$ factor must be added to the **EI** value as previously discussed.

Where adequate rainfall intensity data are not available, the erosion index cannot be estimated solely from annual precipitation data. It is a function of the sizes and intensities of the individual rainstorms, and these are not closely related to annual precipitation. Therefore a given annual rainfall will indicate only a broad range of possible values of the local erosion index. However, the United States data indicate that the range of likely values can be somewhat narrowed by knowledge of the general climatic conditions in the particular geographic area.

In the U.S. Northern and Northeastern States, the winter precipitation generally comes as snow and low-intensity rains, but erosive intensities occur during the spring and summer. There, the local erosion index values, $(\mathbf{EI})_m$, have ranged from **2P**-52 to 2.6**P**, where **P** is the average annual precipitation expressed in centimeters. In several Northwestern States, where rain intensities rarely exceed 2.5 cm/h, the annual $(\mathbf{EI})_m$ is generally less than **P**, but $\mathbf{R}_s$ values are high. Near the Gulf of Mexico and along the southern half of the Atlantic Coast, the rainfall characteristics are substantially influenced by coastal storms, 24-h rainfall exceeds 10 cm at least once in 2 years, on the average, and erosive rains occur in nearly every month of the year. There, erosion index values range between 4.2**P** and 6.7**P**. Values computed from the few long-term, recording-raingage records available for the islands of Hawaii and Puerto Rico were also within this range. In the large region between the northern and southern extremes mentioned above, the annual $(\mathbf{EI})_m$ values range from 2.5**P** to 4.5**P**. Brief, high-intensity thunderstorms are common in this region during the summer months, but general rains of longer duration also occur.

Where data are adequate to determine 2-year probabilities of 6-hour rainfall, these probabilities may provide more specific estimates of the local erosion index values. In the U.S. data, local erosion index values were approximately equal to the quantity $27.38\ \mathbf{P}^{2.17}$, where **P** = the 2-year, 6-hour precipitation in inches. Converted to the recommended metric units, $(\mathbf{EI})_m$ equals approximately $6.28\mathbf{P}^{2.17}$, where **P** is expressed in centimeters. However, this estimating procedure should not be substituted for the standard erosion index calculation procedure where adequate intensity data are available.

Factor K. This factor is the average soil loss in metric tons per hectare per unit of $(\mathbf{EI})_m$, measured on unit plots of the given soil. A unit plot is a 22-m length of uniform 9 percent slope that has been in clean fallow for more than 2 years and is tilled to prevent vegetative growth and surface crusting during the period of soil loss measurement. If a gradient other than 9 percent must be used, the data are adjusted by an **LS** factor available from figure 11. If the soil-erodibility nomograph (fig. 3) is used to evaluate $\mathbf{K}_m$, the **K** value read from the nomograph is multiplied by a conversion factor of 1.292.

The most accurate direct measurement of **K** for a given soil is obtained by measuring soil losses from unit plots under natural rain for at least 5 years, beginning 2 years after the clean-fallow condition was established. This permits averaging the interactions of soil erodibility with antecedent soil moisture, storm size, and other randomly distributed variables. The fallow plots receive the same annual tillage as conventionally tilled row crops.

Using rainfall simulators to evaluate **K** is quicker and less costly, but it requires caution. A one-time simulator test, even though replicated on several plots, measures soil loss from only one storm size and rain intensity, on one set of antecedent conditions, and these may or may not represent natural rainfall patterns. When simulated rainfall is used to evaluate **K**, measuring the soil losses for four or five successive 30-minute periods is helpful so that the segmented data can be rearranged to represent small, intermediate, and large storms beginning at various antecedent soil moisture levels. These can be weighted according to their probability of occurrence in natural rainfall (58).

Factor LS. Selecting 22 m as the basic slope length and retaining 9 percent as the basic slope gradient leaves the **LS** values essentially unchanged from those used in the English system of units. For uniform slopes, **LS** may be obtained by entering figure 11 with the field slope length expressed in meters. For concave or convex slopes, the value read from figure 11 should be modified by the procedure given in the subsection **Irregular Slopes.**

Factors C and P. Soil loss ratios (table 5) and **P** values (tables 13, 14, 15) are not affected by the units selected for the other factors. However, in countries where crops and farming techniques are different from those reflected in table 5, measurements of soil loss reductions attainable with feasible changes in crop system, tillage methods, and residue management may merit priority over establishing **EI** and **K** values.

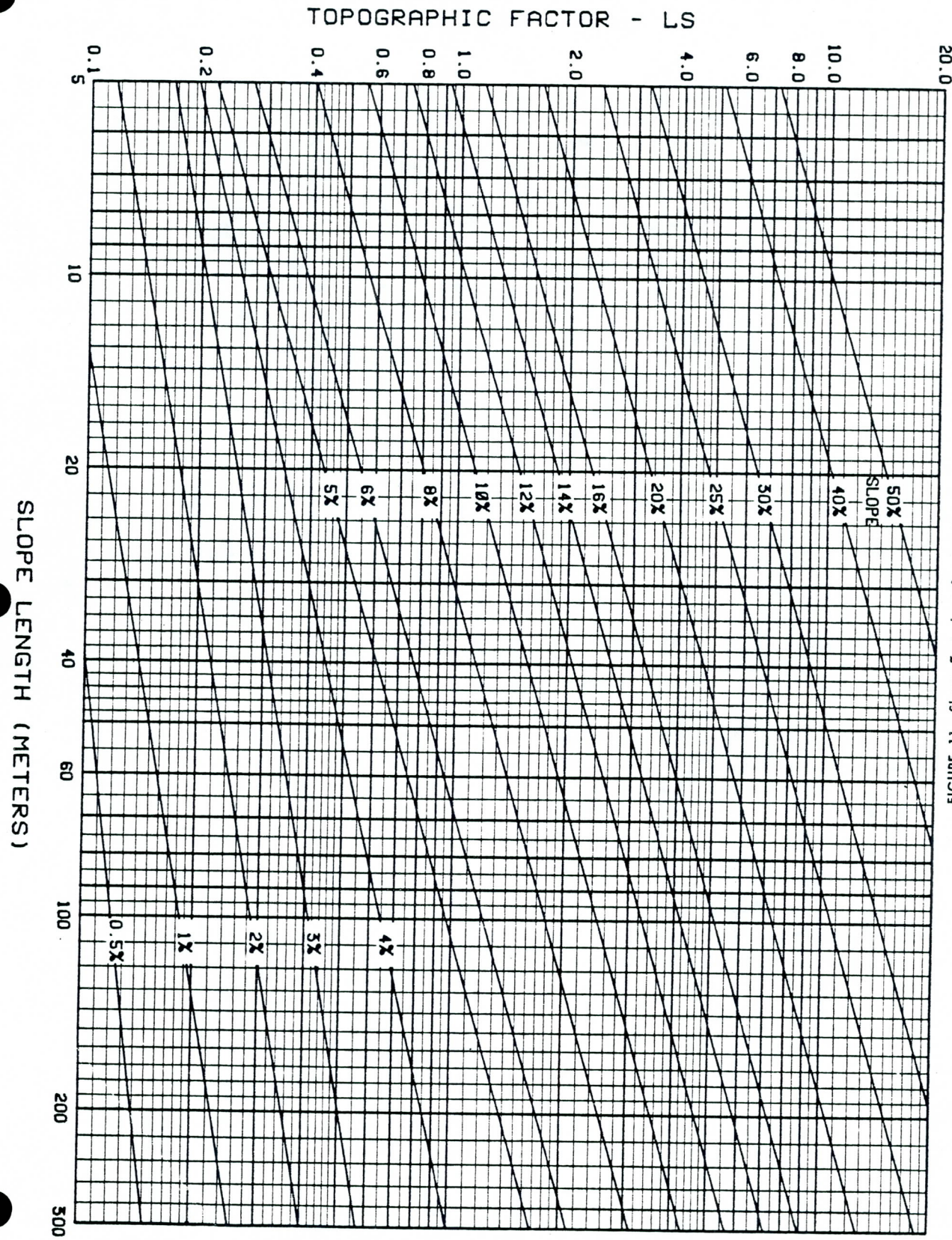

FIGURE 11.—Slope-effect chart for metric system.

☆U.S. GOVERNMENT PRINTING OFFICE: 1978 O— 278-995/6583

AH-537, PREDICTING RAINFALL EROSION LOSSES—A GUIDE TO CONSERVATION PLANNING

ERRATA

The following corrections and minor additions should be made with pen and ink in existing desk copies of AH-537. Corrected words or numbers have been identified by underlining. Additional footnotes that were added to clarify original content can be inserted in the lower margins of the indicated pages.

Page

4 Insert footnote symbol [4] after the definitions of **R** and **K** in column 1 and add footnote:

[4] The erosion index values in figures 1 and 2 and the EI values used in the text have the dimension 100 (foot-ton inch)/(acre hour). K values in tables 1 and 2 and figure 3 are in tons per acre per EI unit and have the dimensions 0.01 (ton acre hour)/(acre foot-ton inch).

---

5 Equation (2) $\underline{e} = 916 + 331 \log_{10} \underline{i}$,

where e is kinetic energy in foot-tons per acre-inch and i is intensity in in/h (62). A limit of 3 in/h is imposed on i . . .

---

9 column 2. Change footnote number from [4] to [5].

---

18 column 1. Change footnote number from [5] to [6].

---

19 column 1, last sentence. Insert footnote symbol [7] after "The expected effects of mulch and canopy combinations" and add footnote in lower margin:

[7] Figures 6 and 7 and table 5 assume that slope-length limits for full effectiveness of residue mulches at the stated rates are not exceeded. Beyond these limits, the subfactor for mulch effect approaches 1.0. The length limits vary inversely with mulch rate, runoff depth and velocity, but have not been precisely defined by research.

FIGURE 6 and 7. Change the ordinate labels from "SOIL-LOSS RATIO" to SUBFACTOR FOR EFFECT OF COVER.

---

23 TABLE 5, line 160. Change 50 percent to 10 percent and reduce the ratio for cropstage 1 from 56 to 28.

---

24 Add to footnote [4]: *See also* footnote [7], page 19.

Change footnote 13 to: Divide the winter-cover period into cropstages for the seeded cover and use lines 132-145.

---

32 TABLE 10. Corrected title: *Factor* **C** *for permanent pasture, range, idle land, or grazed woodland*[1]

Change second category of vegetative canopy to: Tall grass, weeds or bushes with average drop fall height of less than 3 ft.[5]

Footnote [1]: The listed C values assume that the vegetation and mulch are randomly distributed over the entire area.

For grazed woodland with high buildup of organic matter in the topsoil under permanent forest conditions, multiply the table values by 0.7.

For areas that have been mechanically disturbed by root plowing, implement traffic or other means, use table 5 or 12.

Footnote [4], G: cover at surface is grass, grasslike plants, or decaying compacted duff. (Delete "or litter at least 2 in deep")

Add footnote [6]: [6] The portion of a grass or weed cover that contacts the soil surface during a rainstorm and interferes with water flow over the soil surface is included in "cover at the surface." The remainder is included in canopy cover. Use table 5-B for nearly complete grass covers.

---

33 TABLE 11.

Second column heading: Delete "at least 2 in deep."

Footnote [1]: The references to table 6 should be to table 10, and the following may be added: For sites that are mechanically treated following harvest, use table 12.

---

34 TABLE 12, footnotes [4] and [6]. The references to tables 6 and 7 should be to tables 10 and 11, respectively.

---

35 TABLE 13, footnote [1]. Change the word "seedlings" to plantings.

---

36 TABLE 14, footnote [1]. C For alternate strips of row crop and winter grain.

---

51 column 2, line 6. 0.5 should be 0.05 in of precipitation . . .

centered heading. Insert footnote symbol [8] after **Conversion to Metric System** and add footnote in lower margin:

[8] See supplement for a recommended metrication of the USLE in the International System of Units (SI), which may be substituted for this section.

---

56 TABLES 19 and 20, footnotes. Change E to e and I to i in the energy equations.

Below the footnotes for table 20, insert the note: The table values multiplied by 9.81 would equal kilojoules of energy in the SI system.

UNITED STATES DEPARTMENT OF AGRICULTURE

AGRICULTURE HANDBOOK NUMBER 537

PREPARED BY SCIENCE AND EDUCATION ADMINISTRATION

Washington, D.C. January 1981

☆U.S. Government Printing Office: 1981—340-939/96